PHYSICAL REVIEW

VOLUME 86 [illegible] NUMBER [illegible]

MAY 15, 1952

[illegible]

AMERICAN PHYSICAL SOCIETY

[illegible]

THE PHYSICAL REVIEW

A journal [illegible] and theoretical physics established by E. L. Nichols in 1893

Published by the American [illegible]
for the
AMERICAN PHYSICAL [illegible]

Officers

President

J. H. VAN VLECK
Harvard University
Cambridge, Massachusetts

Vice-President

ENRICO FERMI
Institute for Nuclear Studies
University of Chicago
Chicago 37, Illinois

Secretary

K. K. DARROW
Bell Telephone Laboratories
Office:
Columbia University
New York 27, New York

Treasurer

G. B. PEGRAM
Columbia University
New York 27, New York

Local Secretaries for the Pacific Coast

J. KAPLAN
University of California
Los Angeles
Los Angeles, California

Managing Editor

S. A. GOUDSMIT
Brookhaven National Laboratory
Upton, Long Island
New York

BOARD OF EDITORS

Editor

S. A. Goudsmit

Associate Editors

[illegible]	M. GOLDHABER	W. P. [illegible]
J. F. CARLETT	R. HOFSTADTER	E. G. [illegible]
C. L. CRITCHFIELD	A. W. LAWSON	W. B. [illegible]
L. DAUNTSEY	A. PAIS	[illegible]
T. H. JOHNSON	R. SERBER	H. W. [illegible]
Bruno Rossi	C. H. TOWNES	[illegible]

Manuscripts for publication should be submitted to S. A. Goudsmit, Brookhaven National Laboratory, Upton, Long Island, New York. [illegible] authors' institutions are requested to pay a publication charge of $10 per page which, if honored, entitles them to 100 free reprints. Illustrations will be sent with galley proofs.

Proof and all correspondence concerning papers in the process of publication should be addressed to the Publication Manager, American Institute of Physics, 57 East 55 Street, New York 22, New York.

Subscription Price

United States and Canada..... $12.00
Elsewhere..... $15.00

Back Numbers*

Yearly back number rate (plus complete year in combination):
Prior to 1940: $20.00
Thereafter: $27.50
Single copies: $2.50 each, prior to July, 1929;
$1.00 each, July, 1929–December, 1945;
$2.00 each, January, 1946–December, 1948;
$3.00 each, January, 1949–December, 1948;
$5.00 each, thereafter.
Bound [illegible], 1893–1929: $4.00.

Subscriptions, renewals, and orders for back numbers should be addressed to the American Institute of Physics, 57 East 55 Street, New York 22, New York.

Changes of address in the case of members of the American Physical Society should be addressed to the Treasurer; in the case of other subscribers to the American Institute of Physics.

*Pan-American Institute of Fluvial Engineering, Catholic University, Washington, D. C.

[illegible] manuscript as Physical Review, Lancaster, Pennsylvania
[illegible], 1927, at the Post Office in Lancaster, Pennsylvania, under the Act of [illegible]
[illegible] granted for in Section 34.40, P. L. & R. of 1948, authorized [illegible]

Entered as second-class matter [illegible]
Acceptance for mailing at special rate [illegible]

THE
PHYSICAL REVIEW

A journal of experimental and theoretical physics established by E. L. Nichols in 1893

SECOND SERIES, VOL. 86, NO. 4 MAY 15, 1952

Pion-Proton Scattering and the Strong Coupling Meson Theory

G. WENTZEL
Institute for Nuclear Studies and Department of Physics, University of Chicago, Chicago, Illinois
(Received January 31, 1952)

From the pseudoscalar charge-symmetric strong coupling meson theory, scattering cross sections are derived for meson energies well below resonance and at resonance with an excited nucleon state.

RECENT experimental findings on pion-proton interactions have been interpreted as indicating the existence of an excited nucleon state of the kind predicted by the strong coupling meson theory. According to Fujimoto and Miyazawa[1] the comparatively large cross section for the photoproduction of neutral pions in hydrogen[2] may be explained as being a result of a magnetic dipole transition into an excited state providing a broad resonance level. Such a resonance may also be responsible for the large cross sections observed for the scattering of pions in hydrogen.[3] Brueckner[4] has pointed out that the isotopic spin $\frac{3}{2}$ of the isobar state makes the resonance roughly three times more effective for positive than for negative pion scattering in hydrogen (including charge exchange), and this ratio 3:1 is most strikingly confirmed by the experiments.[3,5]

It is true, as was emphasized by Anderson *et al.*,[3] that the experiments so far fail to establish a resonance beyond doubt. Other mechanisms may be thought of providing a strong pion-nucleon interaction particularly in states of isotopic spin $\frac{3}{2}$. To ascertain the existence of proton-isobars, experiments with even higher meson energies will be needed. They may reveal, for instance, inelastic (Raman) scattering events, followed by the emission of a second pion of roughly constant energy.

Notwithstanding such doubts, the new developments have revived the interest in the strong coupling meson theory. Further exploration of this theory and comparison with the new data seem worthwhile. However, it should also be remembered that the strong coupling method cannot be expected to provide a very good approximation. Its failure to explain quantitatively the magnetic moments of the nucleons[6,7] and the neutron-proton mass difference[7] indicates that the Yukawa coupling cannot be really strong. Yet, a qualitative validity is not excluded and deserves further testing.

In the present note we want to summarize briefly some results derivable from the strong coupling theory, pseudoscalar charge-symmetric version, in the approximation so far achieved,[6,7] with regard to the pion-nucleon scattering. Obviously, the assumption of charge symmetry cannot be rigorously valid since charged and neutral pions are known to have different masses. Furthermore, we are dealing with a "static" approximation neglecting nucleon recoils and nucleon pair creation. This implies that only in P states ($l=1$) will pseudoscalar mesons interact with nucleons. For mesons of 100–200-Mev kinetic energy, however, no serious error will result from these simplifying assumptions. Finally, we recall that the theory involves two parameters *a priori* unknown, namely, the coupling parameter g and the "nucleon radius" a ($1/a$ is the cut-off momentum). In principle g may be determined from the nuclear forces (which are $\sim g^2$) and a from the isobar excitation energy ($\sim ag^{-2}$). The expansion into falling powers of g yields a good approximation if $g \gg a$ (in the notation of reference 7).

[1] Y. Fujimoto and H. Miyazawa, Prog. Theoret. Phys. **5**, 1052 (1950), H. Miyazawa (preprint). See also K. A. Brueckner and K. M. Case, Phys. Rev. **83**, 1141 (1951).
[2] Steinberger, Panofsky, and Steller, Phys. Rev. **78**, 802 (1950).
[3] Anderson, Fermi, Long, Lundby, Martin, and Yodh (preprints). See also Lundby *et al.* and Nagle *et al.*, Bull. Am. Phys. Soc. **27**, No. 1, 28 (1952).
[4] K. A. Brueckner (preprint).
[5] At lower energies the ratio seems to be smaller (~1.6 at 60 Mev as measured by J. Steinberger and quoted by Brueckner (see reference 4)).
[6] W. Pauli and S. M. Dancoff, Phys. Rev. **63**, 400 (1943).
[7] A. Houriet, Helv. Phys. Acta **18**, 473 (1945). See also G. Wentzel, Revs. Modern Phys. **19**, 1 (1947) where various arguments against "strong coupling" are summarized (in Sec. 4).

In the one-nucleon case the Hamiltonian obtained from the strong coupling expansion comprises the following leading terms:

(1) The isobar energy or energy of the physical nucleon (bare nucleon plus bound mesons)

$$H_I=(\epsilon/3)j(j+1), \quad j=\tfrac{1}{2}, \tfrac{3}{2}, \cdots.$$

In this notation the excitation energy of the lowest isobar state ($j=\frac{3}{2}$) is ϵ. Each state j has the total spin j and also isotopic spin j; the degree of degeneracy is $(2j+1)^2$.

(2) The free meson energy

$$H_M=\sum_k \omega_k N_k, \quad \omega_k=(\mu^2+k^2)^{\frac{1}{2}}, \quad N_k=0, 1, 2, \cdots.$$

(3) The interaction energy whose leading term H_{sc} (independent of g and proportional to a) describes a "true" scattering of the mesons by the nucleon, and also meson pair creation processes. Terms describing emission and absorption of single mesons appear in higher order approximations, but they have so far not been calculated. These terms are, of course, important in the resonance region ($\omega_k \approx \epsilon$). On the other hand, if the coupling were really strong, the resonance width should be narrow, and therefore we might imagine that there is an energy interval, well below resonance, where the true scattering predominates. Adopting this point of view, we first consider the scattering caused by H_{sc} alone, disregarding the absorption and re-emission processes. We also ignore the virtual creation of meson pairs as seems legitimate in this low energy region.

A set of variables most suitable for the representation of H_{sc} in the pseudoscalar charge-symmetric theory is the following: k = magnitude of meson momentum; l = orbital angular momentum, but $(l|H_{sc}|l')=0$ except for $l=l'=1$, as aforementioned; j = spin and isotopic spin of the nucleon, but we are concerned only with the elastic scattering: $j=j'=\frac{1}{2}$; J = total angular momentum of meson and nucleon (eigenvalues $\frac{3}{2}$ and $\frac{1}{2}$); $M=J_z$; I = total isotopic spin of meson and nucleon (eigenvalues $\frac{3}{2}$ and $\frac{1}{2}$); and $N=I_3$ (= total charge $-\frac{1}{2}$). The matrix H_{sc}, then, is diagonal in J, M, I, N, and the Schrödinger equation of the scattering problem reduces to

$$(-E+\omega_k)F_{JMIN}(k) + \int_0^\infty dk'(k|H_{sc,JI}|k')F_{JMIN}(k')=0. \quad (1)$$

Normalizing the probability amplitudes according to

$$\int_0^\infty dk\,|F(k)|^2=1,$$

one obtains from previously derived expressions for H_{sc},[8]

$$(k|H_{sc,JI}|k')=\alpha A_{2J,2I}(kk')^2(\omega_k\omega_{k'})^{-\frac{1}{2}}u(k)u^*(k'), \quad (2)$$

where α is a constant of the order a [viz. $\alpha=(g/\Gamma)^2/8\pi^2$ in Houriet's[7] notation]; $u(k)$ is a form factor which cuts down the contributions of high momenta ($k \gg 1/a$) but may be replaced by unity in the case of "real" meson momenta ($\lesssim$300 Mev).

$$A_{11}=0, \quad A_{13}=A_{31}=1, \quad A_{33}=\tfrac{1}{2}, \quad (3)$$

The solutions of (1) which correspond to stationary P waves are obtained by setting

$$F(k)=\lim_{\zeta\to+0}\frac{k^2u(k)}{\omega_k^{\frac{1}{2}}}\left(\frac{\gamma_1}{\omega_k-E+i\zeta}-\frac{\gamma_2}{\omega_k-E-i\zeta}\right),$$

where the first and second term represent the ingoing and outgoing wave, respectively. For the coefficients γ_1, γ_2 one obtains from (1)

$$\gamma_1/\gamma_2=e^{2i\delta},$$

$$\tan\delta_{2J,2I}=\frac{\pi k_E^3}{E^2}\left[(\alpha A_{2J,2I})^{-1} + \mathrm{P}\int_0^\infty \frac{dk}{\omega_k-E}\frac{k^4|u(k)|^2}{\omega_k^3}\right]^{-1}. \quad (4)$$

P indicates "principal value" (with respect to the singularity at $\omega_k=E$), and k_E is the momentum corresponding to the energy $E(k_E^2=E^2-\mu^2)$. Transforming to wave functions in ordinary space one verifies easily that the δ's are the P wave phase shifts as they are commonly used in the analysis of scattering problems. Then, by standard transformations, the cross sections for the scattering of charged pions by protons are found to be (ϑ = scattering angle, $\eta=e^{i\delta}\sin\delta$)[9]

$P+\pi^+\to P+\pi^+$ (only $I=\frac{3}{2}$ contributes),

$$\frac{d\sigma}{d\Omega}=\frac{1}{k^2}[\cos^2\vartheta\,|2\eta_{33}+\eta_{13}|^2+\sin^2\vartheta\,|\eta_{33}-\eta_{13}|^2]; \quad (5a)$$

$P+\pi^-\to P+\pi^-$,

$$\frac{d\sigma}{d\Omega}=\frac{1}{9k^2}[\cos^2\vartheta\,|2\eta_{33}+\eta_{13}+4\eta_{31}+2\eta_{11}|^2 + \sin^2\vartheta\,|\eta_{33}-\eta_{13}+2\eta_{31}-2\eta_{11}|^2]; \quad (5b)$$

[8] Unfortunately, Pauli's and Dancoff's calculations[6] presuppose $\omega_k \gg \epsilon$ (including inelastic scattering) and are therefore not easily applicable to low energy scattering. My own work, based on a slightly different method (making use of canonical variables throughout), has been published in full only for the scalar and vector meson theories [Helv. Phys. Acta **13**, 269 (1940), **14**, 633 (1941), **16**, 551 (1943)], but a condensed account of the pseudoscalar theory is given in Houriet's paper (reference 7, Sec. 2.) In Houriet's Hamiltonian K, his Eq. (2,51), the last term is our H_{sc}; the coefficients λ there are defined by (2,41) and (2,26). The matrix elements of $S_{ip}S_{jq}$ for all nucleon transitions can be calculated from the formulas given by M. Fierz, Helv. Phys. Acta **17**, 181 (1944); see his Eqs. (II, 13).

[9] According to a general theorem proved by Heitler for a charge-symmetric theory, the cross section for the process $P+\pi^0\to P+\pi^0$ is given by $\frac{1}{2}[(5a)+(5b)-(5c)]$. See W. Heitler, Proc. Irish Acad. **51**, 33 (1946).

$P+\pi^-\rightarrow N+\pi^0$ ("charge exchange"),

$$\frac{d\sigma}{d\Omega}=\frac{2}{9k^2}[\cos^2\vartheta\,|2\eta_{33}+\eta_{13}-2\eta_{31}-\eta_{11}|^2 +\sin^2\vartheta\,|\eta_{33}-\eta_{13}-\eta_{31}+\eta_{11}|^2]. \quad (5c)$$

According to (4), $\tan\delta$ [excepting δ_{11} which is zero, see (3)] has the order of magnitude ak_R^3/E^2 and can therefore hardly be large enough to account for the large cross sections actually observed (above 100 Mev) which then must be attributed to a resonance. Moreover, since η_{31} is not small compared with η_{13} and η_{33} [see (3)], the ratio of the three cross sections, as derived from H_{sc} alone, would be quite at variance with what is known experimentally.

Before turning to the resonance case an observation should be made regarding the low energy limit $k_R\rightarrow 0$. Because all δ's tend to zero in this limit, one might expect to come back to the well-known formulas of the weak coupling theory.[10] Actually, there is no resemblance at all, even if one neglects the reaction term (*viz.*, the principal value integral) in (4).

In order to include the case of resonance, one may introduce probability amplitudes F_{mn}' for the nucleon isobar states $j=\frac{3}{2}(|m|,\ |n|\leqslant\frac{3}{2})$ with no free mesons present. Because all these states belong to $J=I=\frac{3}{2}$, the amplitudes $F_{JMIN}(k)$ with $J=I=\frac{3}{2}$ only can be affected by the resonance; for the other three J,I-combinations the Eqs. (1)–(4) remain unaltered. For $J=I=\frac{3}{2}$, (1) will be replaced by

$$(-E+\omega_k)F_{MN}(k) +\int_0^\infty dk'(k\,|H_{sc}\,|k')F_{MN}(k')+B(k)F_{MN}'=0,$$

$$(-E+\epsilon)F_{MN}'+\int_0^\infty dkB^*(k)F_{MN}(k)=0.$$

Elimination of F' leads to an equation of type (1), with H_{sc} replaced by

$$(k\,|H_{sc}'\,|k')=(k\,|H_{sc}\,|k')+B(k)B^*(k')(E-\epsilon)^{-1}. \quad (6)$$

The function $B(k)$ being as yet unknown, we want to make the simplifying assumption (which cannot seriously falsify the result)

$$|B(k)|=k^2\omega_k^{-1}|u(k)|\,b,\quad b\approx\text{const.} \quad (7)$$

Then, comparing (6) with (2), one sees that in (4) αA_{33} should be replaced by $\alpha A_{33}+b^2(E-\epsilon)^{-1}$. The resulting formula for δ_{33} may be rewritten by just multiplying the right-hand side of (4) with $(E-\epsilon')/(E-\epsilon'')$,

$$\tan\delta_{33}=(\tan\delta_{33})_{\text{true}}\times(E-\epsilon')/(E-\epsilon''), \quad (8)$$

where

$$\epsilon'=\epsilon-b^2(\alpha A_{33})^{-1},$$
$$\epsilon''=\epsilon'+b^2[\alpha A_{33}(1+\alpha A_{33}P\textstyle\int\cdots)]^{-1}.$$

$P\int\cdots$ stands for the same principal value integral as occurs in (4). $A_{33}=\frac{1}{2}$ according to (3).

Full resonance occurs at $E=\epsilon''(\delta_{33}=\pm\pi/2,\ \eta_{33}=i)$. Since the other phases δ_{13}, δ_{31} are small, the terms $\sim|\eta_{33}|^2$ in (5) will strongly predominate, leading to an angular distribution $\sim(1+3\cos^2\vartheta)$ for each of the three scattering types and to the approximate ratio 9:1:2 for the cross sections (5a, b, c). The total cross section of negative pions (i.e., the sum of (5b) and (5c)), integrated over all directions is $8\pi/3k^2$ at $E=\epsilon''$ or rather somewhat larger owing to a small real value of $\eta_{13}=\eta_{31}$.

To obtain agreement with the presently known experimental facts[3] it is only necessary to assume that the resonance width is large enough to cover essentially the kinetic energy range between, say, 80 and 240 Mev. For very strong coupling, of course, the resonance would be narrow ($b^2/\alpha\ll\epsilon$ although ϵ becomes small, too), but we know already that the coupling cannot be really strong. An actual calculation of b or rather $B(k)$ in terms of g and a will be necessary to find out whether the resonance level and width, together with the strength of the nuclear forces, can be properly adapted to match the experimental data, at least roughly in consistency with the strong coupling condition. This program, however, requires pushing the strong coupling theory to higher approximations which shall not be attempted here. It goes without saying that detail features of the theory, like the angular distribution $\sim(1+3\cos^2\vartheta)$ at resonance or the vanishing of δ_{33} at $E=\epsilon'$ [see (8)], afford crucial items for experimental tests.

Note added in proof:—The recent Chicago experiments [Fermi, Anderson, and Nagle (to be published in Phys. Rev.)] on the angular distribution of pions scattered in hydrogen have revealed a strong asymmetry, in the sense that backward scattering ($\vartheta>\pi/2$) is favored (at kinetic energies between 100 and 140 Mev). Obviously, it was an oversimplification to disregard the S scattering ($l=0$) which, in the theory here discussed, occurs via virtual nucleon pair formation (term $\sim\psi^*\gamma_5\tau_\rho\psi\varphi_\rho$ in the interaction Lagrangian, "pseudovector" coupling). Considering the S scattering as weak, on account of the large energy denominators appearing in the second-order perturbation scheme, one finds, in the same representation as used above in (1) and (2), the following scattering Hamiltonian for S waves:

$$(k\,|H_{sc,\,II}\,|k')=-C_{2I}kk'(\omega_k\omega_{k'})^{\frac{1}{2}}u(k)u^*(k'),$$
$$C_3=g^2(2\pi)^{-3}(2M-\omega_k)^{-1},$$
$$C_1=C_3[1-3\omega_k(2M+\omega_k)^{-1}]. \quad (9)$$

The negative sign of the matrix element, together with the positive sign of (2), (3) [at least for $E<\epsilon'$, see (8)], leads to an $S-P$ interference which favors backward scattering.

But even with this amendment the theory appears to be at variance with some of the experimental data. For instance, according to (9), C_1 is not much (only 40 percent) smaller than C_3, which would make the charge-exchange S scattering much weaker than is indicated by the phase shift analysis of the observational data.

[10] This has been postulated by Brueckner in his half-phenomenological scattering theory (see reference 4) as a rather stringent condition for the determination of his parameters.

Microwave Spectrum of BrCN at Six Millimeters*

S. J. TETENBAUM
Sloane Physics Laboratory, Yale University, New Haven, Connecticut
(Received January 28, 1952)

69 lines of the $J=5\rightarrow6$ pure rotational spectrum have been measured. Lines were found due to the following molecules in their normal isotopic abundances; $Br^{79}C^{12}N^{14}$, $Br^{81}C^{12}N^{14}$, $Br^{79}C^{13}N^{14}$, $Br^{81}C^{13}N^{14}$, $Br^{79}C^{12}N^{15}$, and $Br^{81}C^{12}N^{15}$. Transitions have been found in the vibrational states (0 0 0), (0 1^1 0), (1 0 0), (0 2^0 0), (0 2^2 0), and (1 1^1 0). The apparatus is described and experimental results are compared with those of previous investigators. Fermi resonance effects have been observed and analyzed. A dependence of the l-type doubling constant on the bromine quadrupole field has been found. Quadrupole coupling constants have been determined for the first excited vibrational states in $Br^{79}C^{12}N^{14}$ and $Br^{81}C^{12}N^{14}$.

I. INTRODUCTION

THE microwave spectrum of the linear molecule BrCN was first observed in the $J=2\rightarrow3$ pure rotational transition by Townes, Holden, and Merritt.[1] Since then, additional work has been done on the $J=2\rightarrow3$ transition,[2,3] as well as on the transitions $J=3\rightarrow4$,[4] and $J=8\rightarrow9$, and $J=9\rightarrow10$.[5,6] These spectra have been interpreted satisfactorily, using the modified first-order quadrupole theory of Casimir,[7] the second-order quadrupole theory of Bardeen and Townes,[8] the two-quadrupole theory of Bardeen and Townes,[9] and the l-type doubling theory of Nielsen and Shaffer.[10]

Neglecting hyperfine structure, the rotation-vibration energy levels of a linear XYZ molecule are given by Nielsen[11] as

$$\begin{aligned}E/hc&=E_{\text{rot}}/hc+E_{\text{vib}}/hc\\&=[J(J+1)-l^2]B_v-[J(J+1)-l^2]^2D_v+\cdots\\&\quad+\omega_1(v_1+\tfrac{1}{2})+\omega_2(v_2+1)+\omega_3(v_3+\tfrac{1}{2})\\&\quad+x_{11}(v_1+\tfrac{1}{2})^2+x_{22}(v_2+1)^2+x_{33}(v_3+\tfrac{1}{2})^2\\&\quad+x_{12}(v_1+\tfrac{1}{2})(v_2+1)+x_{13}(v_1+\tfrac{1}{2})(v_3+\tfrac{1}{2})\\&\quad+x_{23}(v_2+1)(v_3+\tfrac{1}{2})+x_{ll}l^2+\cdots,\end{aligned}\quad(1)$$

where J is the total extranuclear angular momentum quantum number; l is the projection of J on the internuclear axis and is the result of vibration in a bending mode; B_v and D_v are, respectively, the reciprocal moment of inertia and centrifugal distortion coefficient in the vibrational state v; the ω_i are the vibrational frequencies; x_{ij} the anharmonicity constants; and the v_i the vibrational quantum numbers.

A pure rotational absorption transition obeys the selection rules

$$\Delta v_i=0,\ i=1,2,3;\quad \Delta|l|=0;\quad \Delta J=+1.\quad(2)$$

The effective reciprocal moment of inertia in a given vibrational state may be expressed to first order of approximation as

$$B_{v_1v_2v_3}=B_e-\alpha_1(v_1+\tfrac{1}{2})-\alpha_2(v_2+1)-\alpha_3(v_3+\tfrac{1}{2}),\quad(3)$$

where B_e is the equilibrium reciprocal moment of inertia and the α's are the rotation-vibration constants. The splitting due to l-type doubling in $|l|=1$ states is usually taken into account by the addition of the term $\pm\frac{1}{2}q_l(v_2+1)$ to the right-hand side of (3). The lower frequency line resulting from this splitting is designated by l_1 and the higher frequency line by l_2. q_l will be called the l-type doubling constant. The splitting for $|l|>1$ is negligible, except for very high J states and has not yet been observed experimentally.

II. APPARATUS

A block diagram of the apparatus is shown in Fig. 1. 6-mm power is obtained as the second harmonic from a silicon-tungsten crystal excited by a 2K33 klystron oscillator. These crystals were made with very light contact pressures using electrolytically etched points of 0.002-in. diameter tungsten wire and silicon blocks from similar crystals described by Beringer.[12] The crystal capsules were used in a coaxial wave-guide circuit, similar to that described.[12] With this arrangement, second harmonic power 15 db down from the fundamental has been obtained. Powers of about 250 microwatts are not uncommon. Because of this relatively large amount of power, the spectroscope can be used at higher harmonics with only slight modifications.

The same crystal capsules were used as detectors of the 6-mm power. No correlation was found with these home-made crystals between harmonic efficiency and 6-mm detection efficiency. Some crystals were excellent for both uses, while others only for one or the other of these applications.

The absorption cell consists of a silverplated brass cylinder 11 inches in height, with an outer diameter of

* Assisted by the ONR.
[1] Townes, Holden, and Merritt, Phys. Rev. **71**, 64 (1947).
[2] Townes, Holden, Bardeen, and Merritt, Phys. Rev. **71**, 644 (1947).
[3] Townes, Holden, and Merritt, Phys. Rev. **74**, 1113 (1948).
[4] Gordy, Smith, Smith, and Ring, Phys. Rev. **72**, 259 (1947); Smith, Ring, Smith, and Gordy, Phys. Rev. **74**, 370 (1948).
[5] Smith, Gordy, Simmons, and Smith, Phys. Rev. **75**, 260 (1948).
[6] J. W. Simmons and W. E. Anderson, Phys. Rev. **80**, 338 (1950).
[7] H. Casimir, Physica **2**, 719 (1935).
[8] J. Bardeen and C. H. Townes, Phys. Rev. **73**, 627, 1204 (1948).
[9] J. Bardeen and C. H. Townes, Phys. Rev. **73**, 97 (1948).
[10] H. H. Nielsen, and W. H. Shaffer, J. Chem. Phys. **11**, 140 (1943); also, see note by H. H. Nielsen, Phys. Rev. **75**, 1961 (1949).
[11] A. H. Nielsen, J. Chem. Phys. **11**, 160 (1943).
[12] R. Beringer, Phys. Rev. **70**, 53 (1946).

5¾ inches and a ⅛-inch wall thickness, having a rectangular thread 0.170 in.×0.420 in. cut into its outer surface. A long strip of copper was soldered to the outside of the thread to complete the wave guide. Input and output wave guides were attached to the top and bottom of the cylinder, and the cell is placed in a five-gallon gasoline can. Commercial diatomaceous earth is poured between the cylinder and the walls of the can for thermal insulation. A brass plate is soldered to the bottom of the cylinder. The cylinder is cooled by filling it with dry ice or liquid air. The top of the can is covered with "magnesia block" insulation. The cell wave guide has an over-all length of 25½ feet from input to output mica windows.

Reflections introduced by the cell system produce signals which appear on the screen of the oscilloscope. However, it is relatively easy to distinguish them from true absorption signals and, in any small frequency region, they can be eliminated by proper tuning adjustments.

The 110 kc/sec source modulation system effectively differentiates an absorption line without preserving phase, and in the absence of reflections produces a double-peaked signal on the oscilloscope.

The 110 kc/sec output from the 6-mm detector is amplified by a low noise cascode preamplifier similar in design to that described by Good.[13]

The sensitivity of this spectrometer is approximately 5×10^{-7} cm^{-1}. This value was determined by comparison with lines whose absolute intensities were calculated from the formula[14]

$$\alpha_{max}=2.19\times10^{-15}\mu^2\nu^3 \text{ cm}^{-1}, \quad (4)$$

where μ is the electric dipole moment in Debye units and ν is the frequency in Mc/sec. This approximate formula for linear molecules neglects hyperfine structure, and assumes a temperature of 300°K and a half-width at half-intensity of 25 Mc/sec for a pressure of 1 mm of Hg. This formula has previously been verified, within experimental error, by measurements on a $Br^{81}C^{12}N^{14}$ line as well as on lines in other linear molecules.[3]

The resolution is approximately 0.3 Mc/sec at 50 kMc/sec. Except for the weakest lines, frequency measurements were made to an accuracy of ±0.1 Mc/sec. Pressures of approximately 1 micron were used.

The marker system is shown in the upper part of Fig. 1. Frequency-swept 1.2-cm power, 3.5-cm power from a Pound-stabilized 723A/B klystron, and 270-Mc/sec and 30-Mc/sec signals from a frequency standard are fed into a 1N26 crystal. Beats from the third harmonic of the 3.5-cm signal, the fundamental of the 1.2-cm power, and a harmonic combination of the 270-Mc/sec and 30-Mc/sec signals, are amplified and used to provide markers on the oscilloscope spaced 60

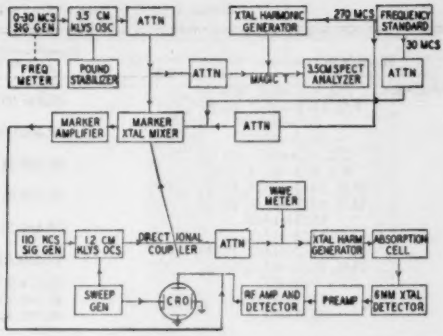

FIG. 1. Block diagram of spectrometer.

Mc/sec apart. Their approximate frequencies are determined by the 1.2-cm cavity wavemeter. The exact frequency of the stabilized 3.5-cm signal is determined by using a spectrum analyzer. Fixed pips 30 Mc/sec apart are produced on the screen of the analyzer by exciting a 1N23 crystal with 270-Mc/sec and 30-Mc/sec signals. By producing FM sidebands on the 3.5-cm signal with a variable 0- to 30-Mc/sec signal generator, one can superimpose a given sideband on a known pip, thus accurately determining the frequency of the 3.5-cm signal. The 0- to 30-Mc/sec frequency is measured with a BC-221 frequency meter. The FM sidebands also appear on the main oscilloscope but can be made very small.

The most important inaccuracies of this frequency measuring system are in the superposition of the marker on the exact center of the spectral line, and in the absolute accuracy of the 100-kc/sec oscillator from which all the frequencies of the frequency standard originate. The probable error due to the former is less than 0.1 Mc/sec. The 100th harmonic of the 100-kc/sec oscillator is heterodyned with the 10-Mc/sec signal of *WWV* in a communication receiver, and the beat over a period of weeks was always less than 1 cps. Thus, the absolute error at 50 kMc/sec due to the frequency standard is negligible.

III. RESULTS

Tables I and II list the ground vibrational state lines measured. Table III lists the 1st bending mode lines and Table IV the lines in the vibrational states (1 0 0), (0 2^0 0), and (0 2^2 0). The superscript on the bending mode quantum number v_2 gives the absolute value of l. Table V lists those lines which were identified as belonging to the (1 1^1 0) state. These lines are very small and were not measured to as high an accuracy as the others. More than 20 other very small lines were observed but were not identified.

In Table VI is given the experimentally determined q_l values for different F transitions in the 1st excited

[13] W. E. Good, "New Techniques in Microwave Spectroscopy," Scientific Paper No. 1538 (Westinghouse Research Laboratories, East Pittsburgh, Pennsylvania).

[14] P. Kisliuk and C. H. Townes, J. Research Natl. Bur. Standards 44, 611 (1950).

TABLE I. (0 0 0) lines of $J=5\rightarrow6$ transition of $Br^{79}CN$.

Molecule and transition		Experimental frequency in Mc/sec	Calculated frequency in Mc/sec[a]	Calculated intensity at 300°K in 10^{-8} cm^{-1}
$Br^{79}C^{13}N^{14}$	7/2, 9/2→9/2, 9/2 9/2, 11/2→11/2, 11/2	49,445.65±0.15	49,445.59	4.7
	7/2→9/2 [b] 9/2→11/2	49,446.90±0.10	49,446.74	342
	7/2, 7/2→9/2, 7/2 9/2, 9/2→11/2, 9/2	49,448.31±0.15	49,448.13	4.7
	11/2, 13/2→13/2, 13/2 13/2, 15/2→15/2, 15/2	49,438.01±0.15	49,437.75	3.5
	11/2→13/2 13/2→15/2	49,439.12±0.10	49,438.98	492
	11/2, 11/2→13/2, 11/2 13/2, 13/2→15/2, 13/2	49,440.40±0.15	49,440.39	3.5
	9/2→9/2	49,274.99±0.10	49,275.11	9.3
	11/2→11/2	49,398.90±0.10	49,398.86	12.1
	13/2→13/2	49,610.43±0.15	49,610.55	9.3
$Br^{79}C^{13}N^{15}$	7/2→9/2 9/2→11/2	48,884.82±0.10	48,884.84	3.8
	11/2→13/2 13/2→15/2	48,877.11±0.10	48,877.09	5.5
$Br^{79}C^{13}N^{15}$	7/2→9/2 9/2→11/2	47,342.44±0.10	47,342.52	1.3
	11/2→13/2 13/2→15/2	47,334.84±0.10	47,334.76	1.9

[a] Using molecular constants listed under $J=5\rightarrow6$ in Table VII except for D_0 and $(eqQ)_{N^{14}}$ which were taken from *c* and *a* of Table VII.
[b] Only the initial and final values of F_1 are given since the hyperfine components are all within 0.1 Mc/sec of each other. See reference 9 for the two-quadrupole notation used.

bending mode. There is a linear relationship between q_l and the bromine quadrupole correction which can be seen graphically in Fig. 2. A similar dependence has been found in the ICN molecule.[15]

Vibrational states which have nearly the same energy and are of the same symmetry type (i.e., belong to the same electronic state and have the same value of *l*) perturb each other. This effect was first recognized by

TABLE II. (0 0 0) lines of $J=5\rightarrow6$ transition of $Br^{81}CN$.

Molecule and transition		Experimental frequency in Mc/sec	Calculated frequency in Mc/sec[a]	Calculated intensity at 300°K in 10^{-8} cm^{-1}
$Br^{81}C^{13}N^{14}$	7/2, 9/2→9/2, 9/2 9/2, 11/2→11/2, 11/2	49,163.82±0.15	49,163.90	4.6
	7/2→9/2 [b] 9/2→11/2	49,165.10±0.10	49,165.05	333
	7/2, 7/2→9/2, 7/2 9/2, 9/2→11/2, 9/2	49,166.56±0.15	49,166.44	4.6
	11/2, 13/2→13/2, 13/2 13/2, 15/2→15/2, 15/2	49,157.27±0.15	49,157.35	3.4
	11/2→13/2 13/2→15/2	49,158.64±0.10	49,158.58	479
	11/2, 11/2→13/2, 11/2 13/2, 13/2→15/2, 13/2	49,159.85±0.15	49,159.99	3.4
	9/2→9/2	49,021.91±0.10	49,021.92	9.1
	11/2→11/2	49,125.04±0.10	49,125.06	11.9
	13/2→13/2	49,301.67±0.10	49,301.68	9.1
$Br^{81}C^{13}N^{14}$	7/2→9/2 9/2→11/2	48,598.93±0.10	48,598.89	3.7
	11/2→13/2 13/2→15/2	48,592.37±0.10	48,592.41	5.3
$Br^{81}C^{13}N^{15}$	7/2→9/2 9/2→11/2	47,064.86±0.15	47,064.74	1.3
	11/2→13/2 13/2→15/2	47,058.19±0.10	47,058.26	1.9

[a] Using molecular constants listed under $J=5\rightarrow6$ in Table VIII except for D_0 and $(eqQ)_{N^{14}}$ which were taken from *c* and *a* of Table VIII.
[b] Only the initial and final values of F_1 are given since the hyperfine components are all within 0.1 Mc/sec of each other. See reference 9 for the two-quadrupole notation used.

[15] C. H. Townes (private communication).

TABLE III. (0 1 0) lines in the $J=5\rightarrow6$ transition of BrCN.

Molecule and transition		Experimental frequency in Mc/sec	Calculated frequency in Mc/sec[a]	Calculated intensity at 300°K in 10^{-9} cm^{-2}
$Br^{79}C^{12}N^{14}$	$7/2\rightarrow9/2;\ l_1$	49,558.32±0.10	49,558.39	27.4
	l_2	49,605.29±0.10	49,605.36	27.4
	$9/2\rightarrow11/2;\ l_1$	49,563.28±0.10	49,563.20	32.6
	l_2	49,610.43±0.15	49,610.35	32.6
	$11/2\rightarrow13/2;\ l_1$	49,557.49±0.10	49,557.50	38.9
	l_2	49,604.35±0.10	49,604.36	38.9
	$13/2\rightarrow15/2;\ l_1$	49,552.62±0.10	49,552.63	46.3
	l_2	49,599.57±0.10	49,599.58	46.3
	$9/2\rightarrow9/2;\ l_1$	49,403.74±0.15	49,403.84	1.6
	l_2	49,452.59±0.15	49,452.69	1.6
	$11/2\rightarrow11/2;\ l_1$	49,520.03±0.15	49,520.10	2.1
	l_2	49,567.45±0.15	49,567.52	2.1
	$13/2\rightarrow13/2;\ l_1$	49,712.00±0.15	49,712.04	1.6
	l_2	49,757.39±0.15	49,757.43	1.6
$Br^{81}C^{12}N^{14}$	$7/2\rightarrow9/2;\ l_1$	49,276.54±0.10	49,276.50	26.7
	l_2	49,323.03±0.10	49,322.99	26.7
	$9/2\rightarrow11/2;\ l_1$	49,280.69±0.10	49,280.63	31.9
	l_2	49,327.08±0.10	49,327.02	31.9
	$11/2\rightarrow13/2;\ l_1$	49,275.67±0.10	49,275.74	38.0
	l_2	49,322.08±0.10	49,322.15	38.0
	$13/2\rightarrow15/2;\ l_1$	49,271.73±0.10	49,271.70	45.2
	l_2	49,318.15±0.10	49,318.12	45.2
	$9/2\rightarrow9/2;\ l_1$	49,147.47±0.15	49,147.44	1.5
	l_2	49,195.39±0.15	49,195.36	1.5
	$11/2\rightarrow11/2;\ l_1$	49,244.47±0.15	49,244.50	2.0
	l_2	49,291.25±0.15	49,291.27	2.0
	$13/2\rightarrow13/2;\ l_1$	49,404.69±0.15	49,404.77	1.5
	l_2	49,449.98±0.15	49,450.06	1.5

[a] Using molecular constants of Table VI and those listed under $J=5\rightarrow6$ in Tables VII and VIII except for D_0 and $(eqQ)_{N^{14}}$ which were taken from c and a of Tables VII and VIII.

TABLE IV. $J=5\rightarrow6$ spectrum of BrCN in (1 0 0), (0 2^0 0) and (0 2^2 0) vibrational states.

Molecule and transition		Experimental frequency in Mc/sec	Calculated frequency in Mc/sec[a]	Calculated intensity at 300°K in 10^{-9} cm^{-2}
$Br^{79}C^{12}N^{14}(1\ 0\ 0)$	$7/2\rightarrow9/2$	49,310.06±0.10	49,310.04	21.7
	$9/2\rightarrow11/2$			
	$11/2\rightarrow13/2$	49,302.27	49,302.28	30.8
	$13/2\rightarrow15/2$			
$Br^{81}C^{12}N^{14}(1\ 0\ 0)$	$7/2\rightarrow9/2$	49,028.32	49,028.36	21.2
	$9/2\rightarrow11/2$			
	$11/2\rightarrow13/2$	49,021.91	49,021.88	30.1
	$13/2\rightarrow15/2$			
$Br^{79}C^{12}N^{14}(0\ 2^0\ 0)$	$7/2\rightarrow9/2$	49,673.93	49,673.92	10.5
	$9/2\rightarrow11/2$			
	$11/2\rightarrow13/2$	49,666.19	49,666.20	14.9
	$13/2\rightarrow15/2$			
$Br^{81}C^{12}N^{14}(0\ 2^0\ 0)$	$7/2\rightarrow9/2$	49,391.95	49,391.94	10.3
	$9/2\rightarrow11/2$			
	$11/2\rightarrow13/2$	49,385.48	49,385.49	14.6
	$13/2\rightarrow15/2$			
$Br^{79}C^{12}N^{14}(0\ 2^2\ 0)$	$7/2\rightarrow9/2$	49,709.00	49,708.93	25.8
	$13/2\rightarrow15/2$			
	$9/2\rightarrow11/2$	49,728.46	49,728.54	25.0
	$11/2\rightarrow13/2$			
$Br^{81}C^{12}N^{14}(0\ 2^2\ 0)$	$7/2\rightarrow9/2$	49,427.87	49,427.88	25.2
	$13/2\rightarrow15/2$			
	$9/2\rightarrow11/2$	49,444.30	49,444.29	24.5
	$11/2\rightarrow13/2$			

[a] Using molecular constants listed under $J=5\rightarrow6$ in Tables VII and VIII except for D_0 and $(eqQ)_{N^{14}}$ which were taken from c and a of Tables VII and VIII.

TABLE V. (1 1^1 0) lines of the $J=5\rightarrow6$ transition of BrCN.

Molecule and transition		Observed frequency in Mc/sec	Calculated intensity at 300°K in 10^{-6} cm^{-1}
$Br^{79}C^{12}N^{14}$	$7/2\rightarrow 9/2; l_2$	49,496.11±0.20	1.7
	$9/2\rightarrow11/2; l_2$	49,501.09±0.20	2.0
	$11/2\rightarrow13/2; l_1$	49,448.31±0.20	2.4
	$13/2\rightarrow15/2; l_1$	49,443.83±0.20	2.8

TABLE VI. Relationship between l-type doubling constant and bromine quadrupole corrections.

Br^{79} transition	Quadrupole correction in Mc/sec[a]	q_l in Mc/sec
$7/2\rightarrow 9/2$	+1.49	3.914±0.01
$9/2\rightarrow11/2$	+6.39	3.929±0.02
$11/2\rightarrow13/2$	+0.55	3.905±0.01
$13/2\rightarrow15/2$	−4.27	3.912±0.01
$9/2\rightarrow 9/2$	−152.12	4.071±0.02
$11/2\rightarrow11/2$	−36.57	3.952±0.02
$13/2\rightarrow13/2$	+154.35	3.783±0.02
Br^{81} transition	Quadrupole correction in Mc/sec[b]	q_l in Mc/sec
$7/2\rightarrow 9/2$	+1.26	3.874±0.01
$9/2\rightarrow11/2$	+5.34	3.866±0.01
$11/2\rightarrow13/2$	+0.46	3.868±0.01
$13/2\rightarrow15/2$	−3.57	3.868±0.01
$9/2\rightarrow 9/2$	−127.07	3.993±0.02
$11/2\rightarrow11/2$	−30.60	3.898±0.02
$13/2\rightarrow13/2$	+128.93	3.774±0.02

[a] $(eqQ)_{Br^{79}} = +682.84$ Mc/sec.
[b] $(eqQ)_{Br^{81}} = +570.44$ Mc/sec.

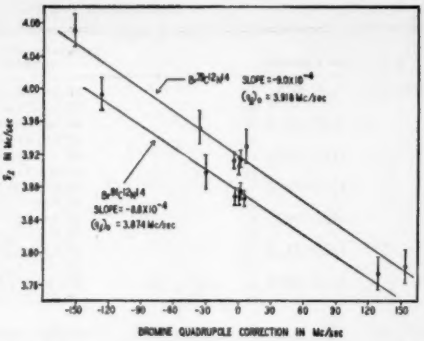

FIG. 2. Dependence of the l-type doubling constant q_l on the bromine quadrupole correction. Data is taken from Table VI.

Fermi in the band spectrum of CO_2,[16] and is called Fermi resonance. A discussion of Fermi resonance is given by Herzberg.[17] Because of this effect, the use of Eq. (3) to calculate the α's from vibrational states, one of which is perturbed, will lead to incorrect results. Fermi resonance effects in pure rotational transitions have been observed in OCS, OCSe, and ICN.[18]

Most of the pairs of levels which perturb each other are those with quantum numbers $(v_1, v_2^{|l|}, v_3)$ and $(v_1-1, v_2+2^{|l|}, v_3)$. Such a pair of levels will be designated, respectively, by the subscripts 1 and 2. The first pair of perturbing levels in BrCN are (1 0^0 0) and (0 2^0 0). It can be shown [19] that

$$W_{12}=k\{v_1[(v_2+2)^2-l^2]\}^{\frac{1}{2}}, \qquad (6)$$

TABLE VII. Molecular parameters of $Br^{79}CN$.

Molecule	Constant	$J=5\rightarrow6$ value	Previous values
$Br^{79}C^{12}N^{14}$	B_0	4120.198±0.009 Mc/sec	4120.206±0.02 Mc/sec[a] 4120.254[b] 4120.230±0.02[c]
	D_0	——[d]	0.91±0.09 kc/sec[e]
	α_2 (from 0 0 0 and 0 1 0)	−11.564±0.012 Mc/sec	−11.49±0.02 Mc/sec[a]
	α_2 (from 0 0 0 and 0 2^2 0)	−11.528±0.006	
	α_1	15.54±0.04 Mc/sec[a]	
	$W_{12}[v_1=1; v_2=0, l=0]$	61.5 cm^{-1} [f]	
	$(eqQ)_{000}$	686.06±0.45 Mc/sec[g]	686.5±0.5 Mc/sec[a] 686[b]
	$(eqQ)_{010}$	682.84±0.21 Mc/sec	
	$(eqQ)_{N^{14}}$	——	−3.83±0.08 Mc/sec[a]
	$(q_l)_0$	3.918 Mc/sec[h]	3.912±0.02 Mc/sec[a]
$Br^{79}C^{13}N^{14}$	B_0	4073.373±0.007 Mc/sec	4073.384 Mc/sec[b]
$Br^{79}C^{12}N^{15}$	B_0	3944.846±0.009 Mc/sec	

[a] $J=2\rightarrow3$; Townes, Holden, and Merritt, Phys. Rev. **74**, 1113 (1948).
[b] $J=3\rightarrow4$; Smith, Ring, Smith, and Gordy, Phys. Rev. **74**, 370 (1948).
[c] $J=8\rightarrow9$; James W. Simmons and Wallace E. Anderson, Phys. Rev. **80**, 338 (1950).
[d] The value of D_0 given in note c is used in calculations on all Br^{79} isotopic molecules and all vibrational states.
[e] Calculated using $\alpha_2 = -11.54\pm0.02$ Mc/sec.
[f] Calculated using a separation between unperturbed levels of $\delta=156$ cm^{-1}.
[g] This value used for ground state coupling in other Br^{79} isotopic molecules. In higher vibrational states calculations are based on $(eqQ)=684$ Mc/sec.
[h] Taken from graph in Fig. 2.

[16] E. Fermi, Z. Physik **71**, 250 (1931).
[17] G. Herzberg, *Infrared and Raman Spectra of Polyatomic Molecules* (D. Van Nostrand Company, Inc., New York, 1945), pp. 215–219, 378.
[18] W. Low and C. H. Townes, Phys. Rev. **79**, 224 (1950).
[19] The author is indebted to Professor C. H. Townes for making available an unpublished analysis of Fermi resonance in linear triatomic molecules.

TABLE VIII. Molecular parameters of $Br^{81}CN$.

Molecule	Constant	$J=5\rightarrow6$ value	Previous values
$Br^{81}C^{12}N^{14}$	B_0	4096.788±0.007 Mc/sec	4096.775±0.02 Mc/sec[a] 4096.823[b] 4096.804±0.02[c]
	D_0	——[d]	0.81±0.09 kc/sec[c]
	α_2 (from 0 0 0 and 0 1 0)	−11.486±0.009 Mc/sec	−11.49±0.02 Mc/sec[a]
	α_2 (from 0 0 0 and 0 2^2 0)	−11.462±0.005	
	α_1	15.48±0.03 Mc/sec[e]	
	$W_{12}[v_1=1; v_2=0, l=0]$	60.5 cm^{-1} [f]	
	$(eqQ)_{000}$	572.27±0.09 Mc/sec[g]	573.5±0.5 Mc/sec[a] 573[b]
	$(eqQ)_{010}$	570.44±0.17 Mc/sec	
	$(eqQ)_{N^{14}}$	——	−3.83 ±0.08 Mc/sec[a]
	$(q)_0$	3.874 Mc/sec[h]	3.845±0.02 Mc/sec[a]
$Br^{81}C^{13}N^{14}$	B_0	4049.608±0.007 Mc/sec	4049.632 Mc/sec[b]
$Br^{81}C^{13}N^{15}$	B_0	3921.787±0.010 Mc/sec	

[a] $J=2\rightarrow3$; Townes, Holden and Merritt. Phys. Rev. 74, 1113 (1948).
[b] $J=3\rightarrow4$; Smith, Ring, Smith, and Gordy, Phys. Rev. 74, 370 (1948).
[c] $J=8\rightarrow9$; James W. Simmons and Wallace E. Anderson, Phys. Rev. 80, 338 (1950).
[d] The value of D_0 in note c is used in the calculations on all Br^{81} isotopic molecules and all vibrational states.
[e] Calculated using $\alpha_2=-11.47\pm0.01$ Mc/sec.
[f] Calculated using a separation between unperturbed levels of $\delta=156$ cm^{-1}.
[g] This value used for ground state coupling in other Br^{81} isotopic molecules. In higher vibrational states calculations are based on $(eqQ)=571$ Mc/sec.
[h] Taken from graph in Fig. 2.

where W_{12} is the interaction energy and k is a constant for a given molecule.

We can express the perturbed wave functions in terms of the unperturbed ones. Thus

$$\psi_1=a\psi_1^0-b\psi_2^0, \quad \psi_2=b\psi_1^0+a\psi_2^0, \tag{7}$$

where

$$a=\left(\frac{[\delta^2+4|W_{12}|^2]^{\frac{1}{2}}+\delta}{2[\delta^2+4|W_{12}|^2]^{\frac{1}{2}}}\right)^{\frac{1}{2}}, \qquad b=\left(\frac{[\delta^2+4|W_{12}|^2]^{\frac{1}{2}}-\delta}{2[\delta^2+4|W_{12}|^2]^{\frac{1}{2}}}\right)^{\frac{1}{2}}. \tag{8}$$

δ is the separation of the unperturbed levels; using $\omega_1=580$ cm^{-1} and $\omega_2=368$ cm^{-1},[20] it is taken equal to 156 cm^{-1}.

The actual B values of the interacting levels are given by

$$B_1=a^2B_1^0+b^2B_2^0, \quad B_2=b^2B_1^0+a^2B_2^0. \tag{9}$$

Since $a^2+b^2=1$,

$$B_1+B_2=B_1^0+B_2^0. \tag{10}$$

Table IX shows the effects of Fermi resonance in BrCN. Perturbed states are bracketed together. The unperturbed value of α_2 can be obtained by use of Eq. (3) and the experimental B values in the states (0 0 0), (0 1^1 0), and (0 2^2 0). The value of α_2 obtained using the (0 0 0) and (0 1^1 0) states is slightly different from that obtained using the (0 0 0) and (0 2^2 0) states. This is due to Eq. (3) being a 1st-order approximation. In our analysis an average value of α_2 is used. This value, in conjunction with the experimental B values in the (1 0^0 0) and (0 2^0 0) states, and Eq. (10) enables one to calculate the unperturbed α_1. a^2 and b^2 can then be calculated from Eq. (9) and W_{12} obtained using Eq. (8). B values in other pairs of perturbed levels can be calculated using Eq. (6) and reversing the above process.

Tables VII and VIII list the calculated molecular parameters of BrCN and compare them with previously determined values. 1st- and 2nd-order bromine quadrupole theory is used in the calculation. For $|l|>0$, it is assumed that the molecule behaves like a symmetric top with $K=l$. No detailed experimental analysis was made on the effects of the N^{14} quadrupole. The general

TABLE IX. Fermi resonance perturbations in the $J=5\rightarrow6$ rotational spectrum of BrCN.

Molecule	Vibrational state v_1, $v_2^{|l|}$, v_3	Experimental B values in Mc/sec (center of gravity of l-type doublet when present)	Correction to rotational frequency due to perturbations in Mc/sec[a]
$Br^{79}C^{12}N^{14}$	0 0 0	4120.198±0.009	0
	0 1^1 0	4131.762±0.007	0
	0 2^2 0	4143.254±0.008	0
	1 0^0 0	4108.807±0.007	+49.75
	0 2^0 0	4139.132±0.007	−49.75
	1 1^1 0	4122.67 ±0.02[b]	+77.00
	0 3^1 0	——[b]	−77.00
$Br^{81}C^{13}N^{14}$	0 0 0	4096.788±0.007	0
	0 1^1 0	4108.264±0.006	0
	0 2^2 0	4119.701±0.006	0
	1 0^0 0	4085.339±0.007	+48.37
	0 2^0 0	4115.697±0.007	−48.37
	1 1^1 0	——[b]	+75.26
	0 3^1 0	——[b]	−75.26

[a] Calculated using values $\delta=156$ cm^{-1}, $W_{12}[v_1=1; v_2=0, l=0]=61.5$ cm^{-1} and 60.5 cm^{-1}, respectively, for $Br^{79}CN$ and $Br^{81}CN$, $\alpha_2=15.54$ Mc/sec and 15.48 Mc/sec for $Br^{79}CN$ and $Br^{81}CN$, and $\alpha_2=-11.54$ Mc/sec and −11.47 Mc/sec, respectively, for $Br^{79}CN$ and $Br^{81}CN$.
[b] Calculated values are 4122.618 Mc/sec and 4148.401 Mc/sec for $Br^{79}CN$ (1 1^1 0) and (0 3^1 0), respectively, and 4099.042 Mc/sec and 4124.926 for $Br^{81}CN$ (1 1^1 0) and (0 3^1 0), respectively.

[20] G. Herzberg, reference 17, p. 174.

features of the resulting hyperfine structure are that the center of gravity of a given line does not change significantly and that two small satellites appear, one on either side of the main line. Their intensity is about 1/100 of that of the main line and hence they were observed only for the four most intense lines.

The B_0 values agree most closely with those given in reference 3. The value of the quadrupole coupling constants are slightly smaller than those previously reported, and the corresponding coupling constants in the 1st excited bending mode are smaller than those in the ground state by about 1 part in 250. The value of the l-type doubling constant compared to that in the $J=2\rightarrow3$ transition shows the slight J dependence previously reported for OCS and HCN.[21]

I wish to thank Professor Robert Beringer for his very helpful advice and criticism throughout the course of this work.

[21] R. G. Shulman and C. H. Townes, Phys. Rev. **77**, 421 (1950).

PHYSICAL REVIEW VOLUME 86, NUMBER 4 MAY 15, 1952

Neutrino Recoils Following the Capture of Orbital Electrons in A^{37}*

GEORGE W. RODEBACK† AND JAMES S. ALLEN
Department of Physics, University of Illinois, Urbana, Illinois

(Received January 21, 1952)

The energy spectrum of the recoil nuclei resulting from orbital electron capture in A^{37} has been determined by a time-of-flight measurement of the recoil ions. A^{37} disintegrations occurred within a gas-filled source volume, where the total pressure was approximately 10^{-4} mm of Hg. The time-of-flight distribution, as measured by a multichannel delayed-coincidence technique, has a definite maximum time limit. Furthermore, the shape and extent of the distribution correspond to that expected from monoenergetic recoils, originating in an extended source and having an energy of 9.7 ev as predicted by the single neutrino hypothesis. Zero and short time coincidences were observed in addition to the above distribution. Further measurements indicate these to be the result of electron scattering associated with A^{37} decays not originating in the source volume.

I. INTRODUCTION

THE measurement of the energy of the recoil nucleus associated with orbital electron capture in an isotope in gaseous form should provide an answer to the question of whether or not single neutrinos are emitted in this type of radioactive decay, as was pointed out by Crane.[1] This experiment was an attempt at such a measurement in which radioactive A^{37} was used.

The isotope A^{37} has properties which make it well suited for a recoil energy determination by a time-of-flight measurement. First of all, the expected recoil velocity results in a time-of-flight of the order of a few microseconds for a drift distance of several centimeters. In addition, the excited atom, following orbital electron capture, returns to its ground state primarily by the emission of one or more Auger electrons of less than 3000-ev energy. The detection of these low energy electrons with an electron multiplier provides a means of initiating the time measurement. Since the low velocity recoil atoms which emit the Auger electrons are either singly or multiply ionized, they can be accelerated through an electric field to an energy which renders them easily detectable with an electron multiplier.

The primary experimental requirements for this measurement were to continuously maintain a gaseous source of constant and suitable strength and to record the data in a reliable fashion for long periods of time. The geometry finally employed proved to be a compromise between good velocity resolution and high coincidence counting rates.

II. PROPERTIES OF A^{37}

Assuming the emission of a single neutrino, the orbital-electron capture disintegration of A^{37} is represented by the equation

$$A^{37}+e_{K,L}\rightarrow Al^{37}+\nu+Q,$$

where $e_{K,L}$ is the captured orbital electron, ν the emitted neutrino, and Q is the disintegration energy. If the neutrino has zero rest mass, the Q of the above reaction is given by the $A^{37}-Cl^{37}$ mass difference. A value of 816 ± 4 kev for this mass difference has been obtained from a recent $Cl^{37}(p,n)A^{37}$ threshold measurement[2] together with a n-p mass difference[3] of 782 ± 1 kev. If the entire disintegration energy is carried away

* This investigation was supported jointly by the AEC and ONR.

† Now at North American Aviation Company, Downey, California. The material in this paper was submitted by G.W.R. to the University of Illinois in partial fulfillment of the requirements for the Doctor of Philosophy degree.

[1] H. R. Crane, Revs. Modern Phys. **20**, 295 (1948).

[2] Richards, Smith, and Browne, Phys. Rev. **80**, 524 (1950).

[3] Taschek, Jarvis, Argo, and Hemmendinger, Phys. Rev. **75**, 1268 (1949).

by the single neutrino and the recoiling nucleus and if we assume that linear momentum is conserved between the neutrino and the recoiling nucleus, the energy of the nuclear recoil should be 9.67 ± 0.08 ev corresponding to a velocity of 0.711 ± 0.004 cm/μsec. The contribution of the binding energy of the orbital electron to the reaction energy is negligible, and has been omitted in the above computations.

A^{37} decays entirely by orbital electron capture with a half-life of 34 days.[4] About 93 percent of the disintegrations result from K capture with about 90 percent of this fraction resulting in emission of Auger electrons; the remainder is K x-ray emission. The other 7 percent of the total number of disintegrations result from L capture as was first reported by Pontecorvo *et al.*[5] Using the proportional counter technique, this group measured the spectrum of energies due to the emission of Auger electrons and x-rays[6] and confirmed the existence of Auger electron energies of about 2400, 2600, and 200 ev corresponding to $K-L^2$, $K-LM$, and $L-M^2$ converted electrons. These energies are in agreement with the values computed from the known critical absorption wavelengths of chlorine.[7]

According to Morrison and Schiff,[8] about 0.05 percent of the disintegrations should result from radiative orbital electron capture. In this radiative capture process the available energy is shared between a neutrino, a γ-quantum, and the recoiling nucleus. An almost continuous spread of recoil momenta should result from this type of disintegration. However, this effect was not observed in the present experiment since the expected counting rate was much smaller than the chance coincidence rate. Maeder and Preiswerk[9] have recently shown that radiative electron capture does occur in Fe^{55}.

III. RECOIL CHAMBER AND METHOD OF RECORDING DATA

Figure 1 shows a schematic cross section of the chamber in which the time-of-flight measurements were made. During the run the total pressure of the gases in the chamber, including that of the A^{37}, was maintained at about 10^{-5} mm Hg. This corresponds to a mean free path of about 500 cm for argon atoms. The shaded trapizoidal cross section indicates the effective source volume which was defined by baffles and also by the region seen simultaneously by both detectors. The necessary baffles, shields, and wire gauze grids (denoted by dotted lines) were all maintained at ground potential with the exception of grid 3 which was maintained at approximately -4500 volts with respect to ground. A

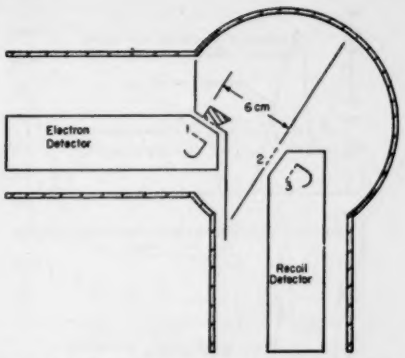

FIG. 1. Schematic of A^{37} time-of-flight apparatus. The effective source volume is indicated by the shaded trapezoidal cross section in front of the grid 1. The recoil Cl^{37} ions resulting from a disintegration within the source volume traverse a field free path to grid 2 and then enter the ion counter after an acceleration through a potential difference of 4.5 kv.

delayed coincidence was recorded for an A^{37} disintegration occurring within the source volume when the resulting Auger electron passed through grid 1 into the electron detector and when, in addition, the ionized chlorine atom traversed the field free distance to grid 2 and was counted by the recoil detector. Both detectors were Allen-type electron multipliers.[10]

Delayed coincidences of the recoil detector output with respect to the electron detector output were recorded by a 20-channel delayed coincidence circuit. The outputs of the two multipliers were fed through two identical channels consisting of preamplifiers, linear pulse amplifiers, and discriminators. The final output of the electron detector channel emerged from a pulse shaper circuit and initiated the delayed coincidence circuit. The final output of the recoil detector channel also was shaped and fed into the multichannel coincidence circuit. Time calibration of the entire delayed-coincidence circuit, including measurement of resolving times and total delays for individual channels, was accomplished by the introduction at the preamplifier inputs of two pulses separated by a precisely known time interval.

The 20 delayed coincidence channels follow consecutively in time and usually the adjacent channels overlap by as much as 10 percent of the time width of an individual channel. During the period of a run the total counts for each channel are recorded and chance counts for each channel are computed on the basis of its resolving time and the measured singles counts from both detectors. The true counts are given by the difference between the total coincidence counts and the calculated chance counts. What is plotted, however, is the number of true counts per channel of unit time

[4] Weimer, Kurbatov, and Pool, Phys. Rev. **66**, 209 (1944).
[5] Pontecorvo, Kirkwood, and Hanna, Phys. Rev. **75**, 982 (1949).
[6] Kirkwood, Pontecorvo, and Hanna, Phys. Rev. **74**, 497 (1948).
[7] A. H. Compton and S. K. Allison, *X-Rays in Theory and Experiment* (D. Van Nostrand Company, Inc., New York, 1935), p. 792.
[8] P. Morrison and L. I. Schiff, Phys. Rev. **58**, 24 (1940).
[9] D. Maeder and P. Preiswerk, Phys. Rev. **84**, 595 (1951).
[10] J. S. Allen, Rev. Sci. Instr. **18**, 739 (1947).

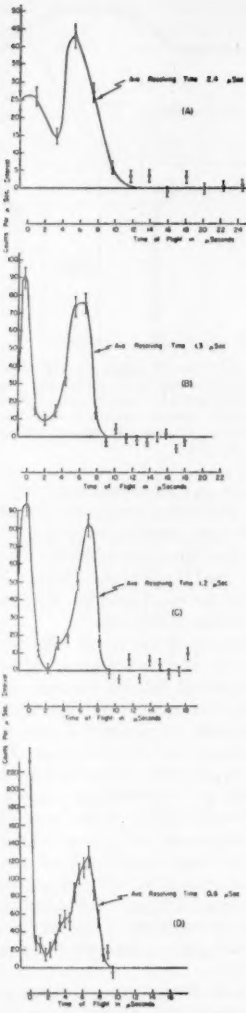

FIG. 2. Time-of-flight distributions obtained with a geometry similar to that of Fig. 1. The mean time-of-flight path was 5 cm. The average channel width of the time recorder was progressively decreased in order to yield increasingly greater details of the distribution.

width (i.e., true counts divided by resolving time) as a function of the total elapsed time to the midpoint of a coincidence channel. The plot then represents an experimental determination of the differential time distribution of the recoils coming from the source volume.

The relative statistical accuracy in the number of true counts can be defined as the ratio of true counts to the probable statistical error in the observed number of counts. An expression for this ratio in terms of the constants of the counting arrangement can be obtained. Assuming an extended source which emits monoenergetic recoils, it can be shown that this ratio is proportional to $(\tau T)^{\frac{1}{2}}$ where τ is the resolving time of a channel and T is the total elapsed counting time. Therefore, when the details of the time of flight spectrum are desired (implying that the resolving time be shorter than the time spread expected for the recoils coming from the extended source volume), increased resolution is obtained at the expense of the statistical accuracy, and this loss can be compensated for only by increasing the counting time. For most of the experiments to be described below, the source strength was adjusted to produce a true to chance ratio greater than unity. The statistical accuracy in the number of coincidences per channel then was determined by the length of the observation period.

IV. RESULTS

Figure 2 shows several time-of-flight distributions obtained for a geometry similar to that of Fig. 1 with a mean traversal distance for the recoil ions of about 5 cm. The conditions for each run were similar, except that the resolving times of the coincidence channels were successively decreased, thus yielding increasingly greater detail of the distribution. The statistical accuracy was made nearly the same for each plot by controlling the time duration of each run.

The peak at about 7 μsec is the result of the recoils originating in the source volume. The abrupt cessation of the time-of-flight distribution at about 9 μsec, with no further coincidences indicated out to at least 35 μsec, indicates the absence of recoils with velocities less than the expected value of 0.711 cm/μsec. This sharp cutoff, together with the fact that the distribution has the general shape expected for monoenergetic recoils from the source volume, is interpreted as experimental verification of the unique energy of the recoil atoms. This explanation assumes that the zero and short time counts of the distribution can be satisfactorily explained.

Following the runs shown in Fig. 2, the apparatus was altered slightly to give a better defined source volume. Figure 3 shows the resulting distribution. The dashed curve is the predicted distribution based on the shape and location of the source volume and the assumed value of recoil velocity which gives the best fit.

The far edge of the measured distribution was used to calculate an experimental value for the recoil velocity based on the time for a singly ionized Cl^{37} atom to traverse the maximum field-free distance from the source volume to grid 2 of Fig. 1. The following considerations entered into the calculation of the delay time to be used:

1. The ideal time-of-flight distribution is modified

due to the thermal velocities of the A^{37} atoms in the source. The root-mean-square velocity at room temperature is about 0.04 cm/μsec and results in a spreading at the base of the ideal distribution. The expected spread is very similar to the observed far edge of the distribution in Fig. 3. Therefore, the intercept of the dotted curve at 7.8 μsec is taken as the observed time-of-flight corresponding to the maximum recoil distance. However, further corrections must be made to this value based on the following:

2. The time required for a singly ionized Cl^{37} atom to be accelerated between grids 2 and 3 (Fig. 1) and thence to travel at constant velocity to the sensitive region of the first dynode is calculated to be 0.3 μsec.

3. The field between grids 2 and 3 (Fig. 1) was found to have penetrated the supposedly field-free region between the source volume and grid 2. This field distribution was subsequently measured, and calculations based on this show that the traversal time in this region for a singly ionized atom is decreased by 1.0 μsec. For doubly ionized atoms this is 1.4 μsec. With the above corrections for a singly ionized atom the corrected maximum time is $7.8-0.3+1.0=8.5$ μsec. The maximum distance is 6.0 cm, resulting in a recoil velocity determination of 0.71×0.06 cm/μsec, which is in excellent agreement with the expected value of 0.711×0.004 cm/μsec.

The following two additional corrections are negligible compared to the uncertainties of this experiment:

1. Time of flight of Auger electrons from source volume to electron detector.

2. The momentum of the recoiling nucleus is equal in magnitude and opposite in direction to the vector sum of the momenta of the neutrino and the Auger electron, since the electron emission occurs before the recoil has moved through an appreciable distance. When the recoil atom and electron are at 90° as in the present arrangement, the maximum change expected in the recoil momentum is 0.2 percent.

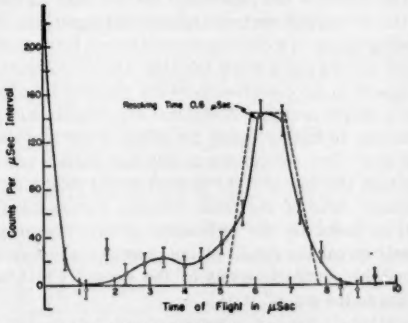

FIG. 3. Time-of-flight distribution obtained with improved definition of the source volume. The dashed curve is the distribution expected for monoenergetic recoils coming from the source volume. The tail of the solid curve in the region of 8 μsec is due to the thermal velocities of the A^{37} atoms in the gaseous source.

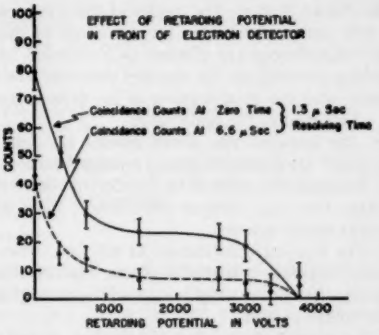
EFFECT OF RETARDING POTENTIAL IN FRONT OF ELECTRON DETECTOR
Coincidence Counts At Zero Time
Coincidence Counts At 6.6 μ Sec
1.3 μ Sec Resolving Time
COUNTS
RETARDING POTENTIAL IN VOLTS

FIG. 4. Curves showing the effect of retarding potentials on the electrons entering the electron counter.

Based on the geometry and estimated counting efficiencies, the probability of an A^{37} disintegration in the source volume resulting in a coincidence count is about 10^{-5}. Calculations indicate that during the above run the specific activity in the source volume was about 200 disintegrations per sec per cm^3.

By imposing a retarding potential on the left side of grid 2 in Fig. 1 and noting the effect on the time-of-flight distribution as this potential is varied, it should be possible to determine the relative degrees of ionization of the recoil atoms. Due to instrumental difficulties it was possible only to verify that a retarding potential of 16.5 volts eliminated the distribution of delayed counts from the source volume.

V. ORIGIN OF ZERO AND SHORT TIME COUNTS

A series of measurements were made in an attempt to explain the origin of the zero time peak and the other coincidences occurring at times shorter than those of the main time-of-flight peak. Zero time coincidences were recorded for two separate runs made under identical conditions except that the first was made with no ion accelerating field in front of the ion detector (first dynode at ground) while the second run was made under the normal conditions for a time-of-flight measurement. It was found that there were 20 percent as many zero time coincidences without the accelerating field as with it. Therefore, at least 80 percent of the zero time coincidences are to be associated with the presence of the 4500-volt difference of potential between grids 2 and 3. It is likely that some of the coincidences measured without the field can be detected only under this condition and may be due to x-ray electron or electron-electron coincidences resulting from cascade Auger processes in the Cl^{37} atom.

A series of runs were made to determine the effect of an electron retarding potential in front of the electron detector. Grid 1 together with the first dynode of the electron detector (Fig. 1) was maintained at a negative potential with respect to the grounded source volume

baffle. Figure 4 shows the results of these runs where the zero time and 6.6-μsec (at maximum of delayed peak) coincidences are plotted as a function of the retarding potential at the electron detector. For each of these runs the total number of ion detector counts was maintained at the same value.

On the basis of the above results the following conclusions are made concerning a normal run:

1. The electrons counted by the electron detector for the zero time and delayed coincidences have nearly identical energy spectra.

2. The delayed coincidences at 6.6 μsec, when the electron retarding potential is greater than 2800 volts, probably are due to x-ray ion coincidences originating in the source volume.

3. No appreciable number of zero time coincidences originate in the source volume. Probably the best evidence for this is the fact that as mentioned in Sec. IV a retarding potential of 16.5 volts eliminated the delayed coincidences at 6.6 μsec. This indicates the absence of high energy positive ions which would be necessary for an essentially zero time of flight over a path of 5 cm.

4. Most of the zero and short time counts are believed to be due to disintegrations occurring in or near the region between grids 2 and 3. The coincidence would be between the recoil ion and an Auger electron which undergoes an elastic scattering process with the baffle structure surrounding the source volume and subsequently enters the electron detector. The acceleration of electrons by the field between grids 2 and 3 will aid this process. This is indicated by Fig. 4, where appreciable zero time counts are recorded for electron energies above the maximum Auger electron energy.

5. A few zero time counts may originate from those secondary electrons emitted at the first dynode of the ion detector which escape outwards and after acceleration between grids 3 and 2 are elastically scattered into the electron detector.

6. According to the above explanations a number of delayed coincidences involving scattered Auger electrons are to be expected from disintegrations occurring in the region between the source volume and grid 2. From solid angle considerations a peak in the number of coincidences should occur near the source volume, and going toward grid 2, this number should at first fall to a minimum and finally increase rapidly as grid 2 is approached. The general shape of the time of flight distribution (Fig. 3) below 5 μsec seems to agree with these predictions.

VI. METHOD OF PROVIDING SOURCE

The A^{37} used for these measurements was initially obtained from the Oak Ridge reactor, where it was prepared by neutron bombardment of Ca^{40}. The radioisotope arrived mixed with a small amount of air. Preceding a run, the oxygen and nitrogen were removed from approximately 1 millicurie of the 30 millicurie source by exposure to outgassed metallic calcium heated to 565°C. The remaining gas was then introduced into the high pressure side of a three-stage diffusion and booster pump combination after the fore pump had been sealed off from the system. The resulting pressure was a few microns of Hg. The calcium purifier was now operated at 300°C and adequately performed the functions of the usual fore pump and, in addition, removed the impurities from the A^{37}. With this arrangement the recoil chamber could be kept evacuated to less than 10^{-6} mm of Hg.

During a run the A^{37} in the reservoir at the rough vacuum side of the pumps was allowed to leak into the recoil chamber through a needle valve at a rate giving a suitable counting rate for the experiment. A steady state was very quickly reached and the recycling process could be steadily maintained for over twelve hours. The best source used resulted in a total pressure of about 10^{-5} mm of Hg in the recoil chamber. A relative measure of the source strength present in the reservoir was continuously provided by a monitor. This monitor was a thin window mica Geiger counter which was exposed to the gaseous source and responded to the small percentage of Cl^{37} recoils emitting K radiation. The high absorptivity of charcoal at liquid air temperatures was utilized for storage of the A^{37} between runs. All but a very small fraction of the source in the reservoir could be collected and sealed off in a cooled tube containing outgassed charcoal powder. This made it possible to use the same source sample many times.

VII. CONCLUSIONS

The results of this experiment indicate that for most of the A^{37} orbital electron capture disintegrations, the missing energy of a disintegration is shared between the recoil nucleus and a single neutrino. Linear momentum is shown to be conserved between the recoil nucleus and a single neutrino. Additional experiments will be necessary to further clarify the origin of the zero time and short time coincidence counts, and further refinements in the time of flight method should yield a more accurate value of the recoil velocity. Future investigations based on the techniques of this experiment should reveal the details of the processes which occur when the electronic levels of the excited Cl^{37} atom return to the ground state.

A Re-Investigation of the Double Beta-Decay from Sn^{124}

E. L. FIREMAN AND D. SCHWARZER
Brookhaven National Laboratory, Upton, New York
(Received February 5, 1952)

Radiations from natural tin and tin enriched with the 124 isotope are examined in a magnetic field with a helium filled cloud chamber that is triggered by internal counters. Only three pictures out of more than four thousand photographs are pictures of two electrons coming out of the same point in the tin and entering the counters, and even these may be pictures of multiply scattered electrons passing through the tin. However, one may set a lower limit to the half-life of double beta-decay from Sn^{124} as 10^{17} years. This is a decay rate less than one-tenth of a value previously reported by one of the authors.

INTRODUCTION

THEORIES of the neutrino predict different properties for the double beta-decay process. Some[1] predict that two neutrinos accompany the two electrons. Others[2–5] require no neutrinos. Therefore, the deciding point between the two types of theories is the sum of the energies of the two electrons. This sum is either constant and equal to the mass difference or has a distribution of values. The two types of theories also predict different half-lives for the process; however, the fourth power of the nuclear matrix element enters into the half-life calculation. This matrix element must be less than one; otherwise its magnitude is quite uncertain. Therefore, a measurement of a minimum half-life for the process is not a conclusive way of distinguishing between the theories.

Attempts[6–9] have been made to detect double beta-decay from various isotopes. In the main these have given negative results, i.e., minimum half-lives for the process. In a previous letter one of the authors[6] had interpreted a slight coincidence activity from a Sn^{124} sample as a possible double beta-activity. It was therefore decided to re-investigate Sn^{124} with the present apparatus, which is more sensitive for detecting rare coincidence electrons than the previous apparatus. The present apparatus also measures the energies of the electrons.

DESCRIPTION OF APPARATUS[10]

A cylindrical cloud chamber of 12¾-in. inside diameter and 4⅝-in. depth is filled with helium and ethyl alcohol at 108-cm pressure at 20°C temperature. The tin sample is placed across the center of the chamber. This sample acts both as a source and as the chamber clearing field. Three different samples were used in the experiment: a sheet of tin of normal isotopic constitution 10½ in. long, 4 in. high, and 0.003 in. thick; another sheet of the same tin rolled to 0.0008-in. thickness; and a tin sample enriched in the 124 isotopes of 2.2205-g weight, and 0.0015-in. thickness. The enriched sample was obtained from Oak Ridge[11] and contained the 124 isotope in 95.04 percent abundance.

On either side of the sample is a counter. Initially open counters, whose interior form part of the visible region of the cloud chamber, were used. Later thin-walled counters (30 mg/cm²) were used. The open counters require more care than the thin-walled ones; therefore, most of the data have been taken with the thin-walled counters. The chamber is triggered by coincidence pulses from the two counters (1 microsecond resolving time). The open counters are 10½ in. long. The thin-walled counters consists of a bank of three counters in parallel (each ¾ in. in diameter and 6 in. long). These counters subtend a solid angle between one and two steradians at the source. The single counting rate in each set of thin-walled counters is 80–90 counts/min; in the open counters it is about 500 counts/min.

The cloud chamber is placed in a horizontal position to reduce the number of cosmic rays. Nevertheless, a large percentage of the pictures are horizontal cosmic-ray mesons and showers. Rather than eliminate these events by anticoincidence counters, it was decided to keep these as an interesting sideline.

Helmholtz coils about the chamber give a magnetic field uniform to 1 percent over the chamber volume. The magnetic field is on continuously. Magnetic fields up to 900 gauss were used. However, most pictures were taken with the field in the neighborhood of 200 gauss. A larger magnetic field cannot be profitably used since low energy electrons would then curl up before reaching the counters. The coincidence rate is dependent upon the magnetic field strength. At zero field strength, there is one coincidence per minute; at 185 gauss there is one

[1] M. Goeppert Mayer, Phys. Rev. **48**, 512 (1935).
[2] W. H. Furry, Phys. Rev. **56**, 1184 (1939).
[3] B. Touschek, Z. Physik. **125**, 108 (1948).
[4] A careful analysis of neutrino theories and their effects on the double beta-process is given by Jayme Tiomono in a Princeton thesis (1950).
[5] L. A. Sliv, Zhur. Eksp. Teoret. Fiz. S.S.S.R. **20**, 11, 1039 (1950).
[6] E. L. Fireman, Phys. Rev. **74**, 1238 (1948); **75**, 323 (1949).
[7] M. G. Inghram and J. H. Reynolds, Phys. Rev. **76**, 1265 (1949); **78**, 822 (1950).
[8] Levine, Ghiorso, and Seaborg, Phys. Rev. **77**, 296 (1950).
[9] Marvin I. Kalkstein, University of Chicago thesis (1951).
[10] The apparatus is similar in some respects to one described by E. L. Fireman and G. M. McHaney, Rev. Sci. Instr. **21**, 813 (1950).

[11] The authors wish to thank Y-12 Branch of the Oak Ridge Stable Isotope Division for a four-week loan of this specimen. Presumably, this is the same specimen used by Kalkstein in his experiment.

TABLE I. Tin of normal isotopic constitution (0.003-in. thickness).

Magnetic field (gauss)	Mesons	Electrons	Scattered electrons	Showers	Double electrons	Coincidence pictures taken
350	3	3	6	3	none	26
390	27	18	17	25	none	272
450	24	21	14	23	none	267

coincidence every two and one-half minutes; and at 900 gauss there is one coincidence every three minutes. This dependence is caused mainly by the bending of low energy electrons from the chamber walls.

The sensitive time of the chamber is less than 0.1 second. Therefore at 185-gauss field strength the triggered picture is equivalent to more than 1500 random ones.

For accurate energy measurements, the magnetic curvature should be large compared to the multiple scattering curvature. According to Bethe's formula,[12] the multiple scattering from our chamber gas with our average track length corresponds to a field of $H_s = 31/\beta$ gauss, where β is the ratio of the velocity of the electron to the velocity of light. For 340-kev electrons β is 0.8 and H_s is 39 gauss. It is interesting to note that the ethyl alcohol vapor makes a larger contribution to the multiple scattering than the helium.

A mirror gives a stereoscopic view in addition to the direct view of the chamber. The photographs are reprojected through an optical system identical to the one used in taking the pictures.

RESULTS

Coincidence tracks are classified in the following manner; if they are straight, they are called mesons. If they are bent in the form of a "*C*," they are called electrons. If they are scattered in the source giving the form "3," they are called scattered electrons; these could also be electron-positron pairs arising in the source. If the picture contains more than four tracks with at least one passing through both counters, it is called a shower. And finally, if the track has an "*S*" shape with the sign of curvature correct for electrons leaving the source, it is called a double electron track.

Tracks of the "*S*" type could be due to the double beta-process or to a beta-internal conversion electron

TABLE II. Tin of normal isotopic constitution (0.0008-in. thickness).

Magnetic field (gauss)	Mesons	Electrons	Scattered electrons	Showers	Double electrons	Coincidence pictures taken
0	35	3	28	23	none	424
420	45	43	42	84	none	633

[12] H. A. Bethe, Phys. Rev. **70**, 822 (1946).

TABLE III. Tin enriched with 124 isotope to 95.04 percent abundance (0.0016-in. thickness).

Magnetic field (gauss)	Mesons	Electrons	Scattered electrons	Showers	Double electrons	Coincidence pictures taken
0	1	3	4	none	none	16
80	2	none	1	none	none	6
160	6	7	9	5	none	38
185	156	257	183	171	3	1904
310	39	59	29	58	none	520
400	5	15	4	14	none	100
860	3	2	1	4	none	70

of some contaminant.[13] Multiple scattering from the gas could also give a double electron track by changing the sign of the curvature of an electron passing through the source on the side which it approaches the source.

If sufficient "*S*" type tracks are observed, the double beta-process could be distinguished from a beta-internal conversion process by the energies of the electrons. In the beta-internal conversion process, one of the electrons has a constant energy. This is not true of the double beta-process either with or without neutrinos.

The data are summarized according to the above classification in Tables I, II, and III.

Only three pictures are those of double electrons coming out of the same point in the source and entering the counters. The curvatures and energies of these tracks are given in Table IV.

In addition to these three, there are two photographs of the "*S*" form whose curvatures (18.8 cm, 16.8 cm) and (12.8 cm and 14.2 cm) have the wrong sign for electrons leaving the source. These pictures can only be interpreted as an electron passing through the source and having the sign of its curvature on the side where it leaves the source changed by gas scattering. This leads us to the belief that some of the three double electron pictures are probably multiply scattered electrons with the wrong sign of curvature rather than double beta-electrons from tin 124. It should also be noted that the sum of the energies of the electrons given in Table IV is not constant. All of the coincidence tracks except a few of the meson tracks have close to minimum ionization. In several of the shower pictures there are a number of alpha-tracks.

If the three photographs are interpreted as double

TABLE IV. Curvatures and energies of two electrons out of tin.

Magnetic curvature (cm)	Electron energies (kilovolt)	Sum of energies (kilovolts)
10.2	255	750
15.8	495	
11.0	290	785
15.8	495	
8.8	195	330
7.0	135	

[13] The tin samples were examined spectroscopically for impurities; no impurities of significance were found.

beta-events, a half-life of $2-5\times10^{17}$ years is obtained for the process. A result of three pictures in a field of 175 gauss when the multiple scattering corresponds to a field of 39 gauss is certainly a negative result, and the experiment should be interpreted as giving a half-life greater than 10^{17} years for the double beta-decay process. It was thought worthwhile to report these results, since they differ significantly from those reported in reference 6 and agree with those in reference 9.

The previous result[6] may have been caused by a small trace of an impurity having a coincidence activity in the enriched sample. In fact, some of the three double electron pictures in this experiment may have the same origin.

The authors wish to thank E. Bolze and B. R. Gibbs for aid in designing the apparatus and Anthony Del Duca who designed and constructed the electronics equipment.

PHYSICAL REVIEW VOLUME 86, NUMBER 4 MAY 15, 1952

The Association of Bursts and Penetrating Showers*

DONALD E. HUDSON†
Laboratory of Nuclear Studies, Cornell University, Ithaca, New York
(Received July 19, 1951)

Local cosmic-ray bursts and penetrating showers have been studied together using an arrangement of ionization chambers and shielded counters. The experiment investigated (1) the occurrence of penetrating showers associated with large bursts, and (2) the occurrence of bursts associated with large penetrating showers. Evidence is presented to show that the bursts are mainly locally generated large electronic cascades. Nearly 60 percent of bursts larger than 25 Bev (about 250 electrons) contained observed penetrating component. The transition effect of penetrating and nonpenetrating bursts was in qualitative agreement with a nuclear cascade process. Bursts of a few hundred electrons contained on the average about 1 percent of penetrating particles. Essentially no penetrating showers of multiplicity over 14 were unaccompanied by fairly large electronic cascades. The consistent association of cascade bursts with penetrating showers and vice versa is in qualitative agreement with present neutral meson concepts. The main experimental work was done at Echo Lake, Colorado (elev. 3260 m).

I. INTRODUCTION

THE existence of the electronic component of mixed showers has been of considerable interest in the study of high energy interactions. Recent cloud-chamber experiments[1–8] have established roughly the nature of the phenomenon.

The question of the extent to which the electronic component is associated with the penetrating component, and vice versa, has been incompletely answered. Results obtained with an ionization chamber used in conjunction with a cloud chamber indicate that penetrating particles are frequently produced in those nuclear interactions which give rise to electron showers.[3] British ion-chamber and counter experiments[9] also have found a penetrating component associated with burst production. On the other hand, nuclear interactions have been observed which contained electronic cascades alone, or which have shown a penetrating component associated with no visible electronic cascades.[8]

It was the purpose of the present experiment to study the correlation of electron cascade and penetrating shower production in local nuclear interactions of high energy and multiplicity. We have used the M.I.T. ionization chamber burst method[3,10–12] to detect the cascade radiation produced in the interactions under study. The penetrating component was required to discharge counters under thick lead. A lead shield was disposed above the apparatus to serve as a generator of mixed showers.

The data were obtained at Echo Lake, Colorado, at an elevation of 3260 meters. A light wood building having a roof 2.5 g/cm² thick and walls 1.5 g/cm² thick housed all equipment.

The notation and units used in this paper are those of Rossi and Greisen,[13] while the terminology follows that of the M.I.T. group.[3,14]

* Most of the material presented is from the Cornell University Ph.D. thesis (1950). Preliminary results have been reported in *Proceedings of the Echo Lake Cosmic Ray Symposium* (1949).

† Now at Iowa State College, Ames, Iowa.

[1] (a) W. B. Fretter, Phys. Rev. **73**, 41 (1948) and (b) W. B. Fretter, Phys. Rev. **76**, 511 (1949).

[2] C. Y. Chao, Phys. Rev. **75**, 581 (1949).

[3] H. Bridge and W. Hazen, Phys. Rev. **74**, 579 (1948).

[4] A. E. S. Green, Phys. Rev. **80**, 832 (1950).

[5] B. Gregory and J. Tinlot, Phys. Rev. **81**, 675 (1951).

[6] Butler, Rosser, and Barker, Proc. Phys. Soc. (London) **A63**, 145 (1950).

[7] (a) M. B. Gottlieb, Phys. Rev. **82**, 349 (1951) and (b) A. J. Hartzler, Phys. Rev. **82**, 359 (1951).

[8] W. W. Brown and A. B. McKay, Phys. Rev. **77**, 342 (1950).

[9] E. P. George and P. T. Trent, Nature **161**, 248 (1948) and references found there.

[10] Bridge, Hazen, Rossi, and Williams, Phys. Rev. **74**, 1083 (1948), and bibliography given there. This paper will be referred to as BHRW in the text.

[11] H. Bridge and B. Rossi, Phys. Rev. **75**, 810 (1949).

[12] McMahon, Rossi, and Burditt, Phys. Rev. **80**, 157 (1950).

[13] B. Rossi and K. Greisen, Revs. Modern Phys. **13**, 240 (1941). This reference will be abbreviated in the text by CRT (Cosmic-Ray Theory).

[14] B. Rossi, Revs. Modern Phys. **20**, 537 (1948).

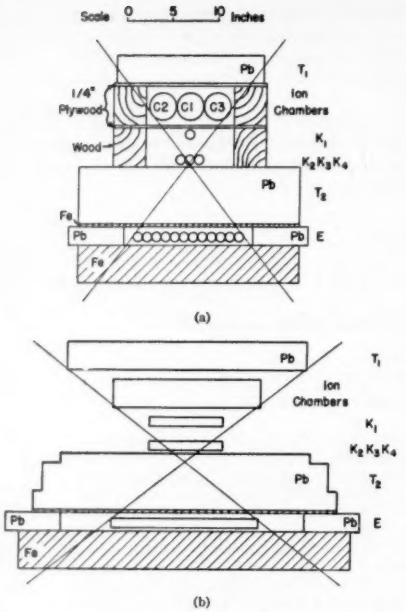

FIG. 1. Experimental geometry. (a) End view; (b) side view.

II. METHOD

A. Apparatus and Triggering

1. Apparatus

The apparatus is shown schematically in Fig. 1. A block diagram of the electronics is shown in Fig. 2. Further details of the instrumentation are found in the Appendices.

Bursts were detected in three cylindrical ion chambers designated $C1$, $C2$, and $C3$. Each had a $\frac{1}{16}$-inch brass wall enclosing an effective volume 16.2 inches long and 2.88 inches in diameter, and the central anodes were 30-mil Kovar wire. The gas filling was 5.0 atmospheres of pure argon at 15°C. Electron-collection pulses were amplified and observed upon individual cathode-ray oscilloscopes. The oscilloscope sweeps were started by a master pulse which was initiated only under certain triggering conditions. The resulting burst pulses were recorded photographically by an automatic camera.

Penetrating particles were detected by the tray E consisting of 12 counters each having a 1×16 in. effective area. This tray was screened on top by the 6-inch absorber T_2, on all sides by at least 6 inches of lead, and on the bottom by 4 inches of iron. Each counter lit a neon bulb in the field of the oscilloscope camera, provided the discharge was in coincidence with the master pulse.

The counters K_1–K_4, each of effective area 1×8 in., were connected in fourfold coincidence and served to help select the events to be studied.

Not shown in Fig. 1 are three air shower trays A_1, A_2, and A_3 each of effective area 200 cm². These were disposed in a horizontal plane 6 feet above the apparatus and arranged in a triangle about 3 meters on a side. Each tray was connected to a neon bulb which would light only in the presence of the master pulse.

A lead radiator-absorber T_1 was placed above the chambers. For most of the experiment this was 3 inches thick; however, for certain parts it was removed, and for other parts used at thicknesses of 0.5 and 8.0 inches.

2. Selection of Events

The experiment was designed to trigger on bursts, in order to observe any coincident penetrating particles in the E tray; and (independently) to trigger on penetrating showers, in order to observe any coincident bursts in the ion chambers.

Triggering on bursts was accomplished as follows: The three amplified burst pulses were fed into pulse-height discriminators operating at identical bias levels. Their mixed output (B) was placed in coincidence with the fourfold $K_1K_2K_3K_4$ coincidence pulse (K) so as to generate a master pulse (M). The result was that if any chamber showed a burst pulse greater than a predetermined bias height, and if the counters K_{1-4} were discharged, then the event was accepted. Discriminator biases were set at a level 1.24 times the height of calibration α-particle pulses to be described.

For the selection of penetrating showers a K coincidence was required, plus the discharge of any three or more E counters. To accomplish this an addition-discriminator was employed which provided an "E pulse" only in the presence of 3 or more coincident responses in the E tray. A coincidence between the K and E pulses generated the M pulse, and the event was recorded.

Triggering on bursts and on penetrating showers was done concurrently so that each recorded event could have been initiated by either one or both of the stated detector combinations. Final selection of data for analysis was always done by visual observation of the photographs, independently of the electronic biases involved.

B. Detection of Bursts

1. Method

The method employed was the pulse-shape method of studying cosmic-ray bursts in electron-collecting ion chambers of cylindrical geometry. This technique has been described by Bridge, Hazen, Rossi, and Williams.[10] Our method differed slightly from theirs, and details will be reported briefly in Appendix II.

An important feature of the method is the utilization

of the shape of the burst pulse to give information about the distribution of ionization in the chamber. Pulses due to cascades, filling a fraction of the chamber length with uniform ionization, exhibit a characteristic linear rise. The pulse due to a heavily ionizing ray crossing the chamber not far from the axis rises slowly at first and later more rapidly. A single track passing radially through the chamber gives a pulse noticeably concave downward. Most often a small number of rays give a pulse concave upward, or a pulse having obvious irregularities due to the successive effects of different rays. As the number of randomly distributed heavy tracks increases, the pulse becomes indistinguishable from that due to a cascade.

We have used the burst pulse shapes to help eliminate bursts due to stars from the data. However, the selection of events was such that bursts due to small numbers of heavily ionizing particles were very rare; hence this procedure was valuable mainly for verification that the pulses were due to showers of numerous particles.

2. Calibration

Calibration of the system was achieved by projecting 3.97-Mev α-particles radially into the chamber from the outer wall. The relation arising from this method, for a cascade burst which produces uniform ionization, is

$$E_B = 1.30 E_\alpha H_B / H_\alpha; \tag{1}$$

where E_B = the energy lost in the production of ions by the burst (in Mev); E_α = the energy lost in the production of ions by an α-particle (in Mev); H_B = the observed height of the burst pulse, measured on the oscilloscope screen; and H_α = the observed height of the α-pulse. The constant 1.30 is calculated from the initial distributions of ionization in the chamber and from the transmission characteristics of the combined chamber and amplifying system. It depends somewhat upon certain electron mobility constants for our chambers which were determined from the shapes of the alpha and burst pulses. The value has an effective probable error of about 2 percent.

The area density of cascade electrons crossing the chamber can be found from E_B by the relation

$$\delta = E_B / [k_\eta(\text{eff}) DV], \tag{2}$$

where δ = the density of all charged particles inside the chamber walls averaged over the chamber (in cm^{-2}), and measured in a plane normal to the direction of motion of the particles; k_η(eff) = the average ionization loss of all the burst particles inside the chamber (in Mev g^{-1} cm^2); η is the upper energy limit for secondary collision electrons set by their range in the ion chamber; D = the density of gas in the chamber (0.00845 g/cm^3); and V = the effective volume of the chamber (1716 cm^3).

Because of electromagnetic cascade transition effects in the brass walls the average density δ inside the chamber differs from the incident density Δ by a factor

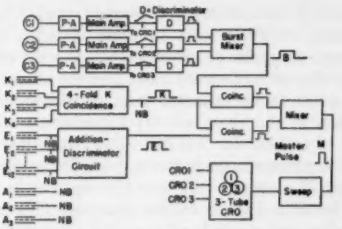

FIG. 2. Block diagram of electronic instrumentation.

Q, so that $\delta = Q\Delta$. Q has been calculated elsewhere[15] for air-brass and lead-brass transitions, considering all particles above zero energy. The result, for the lead-brass transition (local bursts), is $Q = 0.42 \pm 11$ percent. The number S_B of burst particles incident on the chamber can be found, by assuming that they traverse the chamber normal to the axis, from $S_B = \Delta A$, where A is the effective area of the chamber (299 cm^2).

Insertion of the numerical constants (see Appendix III for k_η) gives, for electronic cascades out of lead incident upon the chamber,

$$S_B = 166 H_B / H_\alpha. \tag{3}$$

3. Special Considerations

In most of this experiment we were concerned only with those bursts containing mainly cascade radiation resulting from nuclear interactions in the radiator T_1. Special problems were the elimination of unwanted events and the necessity for proper development of the cascade in the radiator. Unwanted bursts could be due to stars, to the radiation of mesons, and to air showers.

Bursts due to stars were eliminated in three ways: (1) The requirement of the K coincidence discriminated heavily against triggering by stars. Experiments with cloud chambers[10,16] and emulsions[17] show that stars having large numbers of prongs are relatively very infrequent. BHRW find that about 1 percent of the stars causing bursts of $E_B > 6$ Mev in a chamber like ours show more than 6 prongs emerging. Solid angle considerations indicated that less than 0.01 percent of such burst-producing stars in the three chambers were likely to give burst triggers in our geometry. Any true cascade burst large enough to trigger (about 200 particles) was almost certain to discharge the K counters, so their presence exerted little bias against desired events. (2) Observation of the burst pulse shape gave another chance to eliminate an occasional star trigger. This method is not perfect, as BHRW show that a few percent of nuclear disintegrations give pulse shapes simulating those of cascade bursts. Furthermore, the

[15] D. E. Hudson, Cornell University thesis (1950). (The transition calculation will be published soon in a Letter to the Editor.)
[16] W. E. Hazen, Phys. Rev. **65**, 67 (1944).
[17] Bernardini, Cortini, and Manfredini, Phys. Rev. **74**, 845 (1948).

stringent K coincidence requirement tended to limit the (rare) recorded stars to those of many prongs. However, the pulse shape observations were useful to certify that each observed burst had the characteristic pulse shape to be expected from distributed cascade radiation in the chamber. (3) Experiments with adjacent chambers by BHRW show that stars most frequently cause large bursts in a single chamber, and are only 14 percent of the time accompanied by even a small burst in a given nearby chamber. This fact was useful because most local cascades generated in the lead T_1 caused bursts in at least two chambers.

Electromagnetic interactions of μ-mesons caused a fraction of the bursts observed in our experiment at Echo Lake. Their rate was evaluated from auxiliary underground data. (See Part III A.)

Bursts associated with dense air showers were indicated by the shower trays A. These data will be treated in later sections.

Present evidence indicates that most local mixed showers contain slow heavy particles along with the cascade radiation. Few of these should penetrate the remaining lead unless the event occurs very near the bottom of T_1; these particles are thus discriminated against in our geometry. However, some of the ionization in our chambers could have been due to heavy tracks. This ionization was, of necessity, lumped with that due to the soft cascade in our analysis.

In order to study the bursts associated with events triggered on penetrating showers, we were prepared to detect cascade bursts of moderate size initiated at any depth in the lead radiator T_1 (15 radiation lengths thick). Cascade showers far past or far before their maximum are comparatively poor in particles and may give rise to small or undetectable bursts. The worst situation for the absorption of a cascade arises when the initial event is at the top of T_1. In this case a 150-particle shower initiated by a single electron is reduced to the minimum detectable level of about 15 particles after crossing the 15 radiation lengths of T_1.[18] Cascades initiated near the bottom of T_1 can lack development and be undetected. However, a shower of 150 particles at the maximum has 16 after about 1.5 radiation lengths, and larger showers have more. Hence only bursts smaller than this originating in the bottom 1 cm of T_1 are eligible to be missed because they are undeveloped. Auxiliary data were taken (with 0.5 inch of lead as T_1) which provided a correction for this effect. Fortunately, most of the nuclear interactions must occur in the central region of T_1, so that the above considerations will only apply to a portion of the cases. It should be remarked that if the cascade component of mixed showers is produced with some multiplicity, then the resulting showers will be less penetrating for a given total number of particles. This will tend to increase the absorption loss and decrease the development loss of bursts for events triggered on penetrating particles. The experimental results indicate that the loss of bursts was not serious, since few large penetrating showers were unaccompanied by detectable bursts.

C. Detection of Penetrating Showers

1. Detection of Other Phenomena

The penetrating shower trigger was designed to require a shower of at least three particles above T_2 and a penetrating shower of at least three rays under T_2, giving a sevenfold KE coincidence. Such an event was nominally a mixed or penetrating shower initiated in T_1. However, other phenomena may simulate a true penetrating shower starting above T_2.

It can be shown by calculation that electromagnetic interactions of μ-mesons caused practically no such coincidences. A convincing proof is the negligibly small number of such events observed underground with this apparatus (Part IV).

A cogent point is the possible penetration of the absorber T_2 by cascade radiation generated in T_1. The calculation of Greisen[18] leads one to expect that about 0.4 percent of the electrons near the maximum of an air shower shall effectively penetrate another 6 inches of lead. The cascades generated in the lead radiator T_1 should show considerably less penetration than air cascades. This point was verified by the underground experiment which showed that even very large purely cascade bursts under T_1 essentially never were accompanied by counts in the E tray due to the soft component. Hence, a negligible fraction of E counter discharges in the present experiment resulted from the action of the cascade component of mixed showers.

A third possible source of spurious sevenfold coincidences arises from mixed showers occurring near the top of T_2. Such a shower might contain penetrating particles and also some back-projected particles which cause a K coincidence. Such an effect was shown to be small from the observed frequency of penetrating shower triggers with no absorber above the chambers.

The apparent number of penetrating particles was increased slightly because of knock-on secondary electrons. Recent studies[8,19] show that about 7 to 8 percent of penetrating particles emerge from lead accompanied by secondaries with an angular distribution near $\cos^2\theta d\theta$. Taking into account the fact that some large angle secondaries were unable to penetrate a counter wall, we find that about 2 percent of the particles crossing the E tray could discharge additional counters by direct knock-ons. A calculation was made of the effect due to back-scattered secondary electrons[19] out of the absorber on which the E tray rests. The result was that roughly another 1.5 percent of the penetrating rays were accompanied by additional counts in our geometry. The net effect was that only about 3.5 percent of the single penetrating particles emerging from T_2 produced additional counts in the E tray.

[18] K. Greisen, Phys. Rev. **75**, 1071 (1949).
[19] Brown, McKay, and Palmatier, Phys. Rev. **76**, 506 (1949).

Ample evidence exists to show that the secondaries of penetrating and mixed showers can in turn produce further nuclear interactions. These occasionally increase the multiplicity of E counters observed in a burst-triggered event. The experimental evidence is too meagre for an accurate evaluation of this effect. Also, the nuclear cascade can occasionally contribute to the triggering of events by penetrating showers. This effect does no great harm because it indicates the presence of high energy penetrating component as well as a simple hard shower.

2. *Geometrical Efficiency*

It is important to know the approximate efficiency of the E tray for detecting the penetrating component of showers produced in T_1. For the data used, the events were initiated over the central chamber of Fig. 1. The zenith angle distribution of the penetrating particles in local mixed and penetrating showers is about proportional to $\cos^3\theta d\theta$.[8] This means that in our geometry the average efficiency is about 50 percent. The loss of the penetrating particles of burst triggered events will be significant in analyzing later data. Because of the geometrical coherence of the penetrating rays in a given shower, the efficiency must be considered to be averaged over all showers. The value given is only for secondaries penetrating enough to traverse 6 inches of lead. The calculation does not include the effect of simple absorption of less penetrating components.

3. *Triggering Bias for Mixed Showers*

Because of its simplicity, the K–E penetrating shower detector does not select purely penetrating showers in an unbiased fashion. Penetrating showers accompanied by cascade radiation are somewhat favored because of the increased probability of discharging the K counters. For the higher multiplicities of the penetrating component, this bias effect is minimized. The net result will be to record events giving rise to mixed showers with somewhat exaggerated frequency compared with purely penetrating showers. This effect has existed in most penetrating shower experiments previously reported in the literature.

III. RESULTS FOR LOCAL BURSTS

A. The Data

Certain auxiliary experiments were done which contribute to the present interpretation: (1) In addition to the main experimental run (T_1 3 inches thick), three additional runs were made at Echo Lake under the conditions described here except for the thickness of the moderator T_1. One had all absorbers removed from above the chambers.[18,20] Others had T_1 0.5 inch and 8.0 inches thick.[15] (2) An important auxiliary study was done at Ithaca (elev. 200 meters) in a tunnel under 1900 g/cm² air equivalent of sandstone.[15,21,22] This was performed with T_1 three inches thick in a manner identical to the present experiment. The tunnel data showed that essentially all of the events observed there were due to the interactions of μ-mesons. The results of these experiments will be quoted as needed.

Burst pulse heights H_B are specified in units of the height H_α of the calibration α-particle pulses. Heights in the three chambers are designated as H_{B1}, H_{B2}, H_{B3}, and their sum as H. The equivalent number of cascade particles S incident upon all three chambers is given [Eq. (3)] by $S=166H$. This interpretation in terms of numbers of particles rests on the assumption that the burst radiation consists of local cascades out of lead. We believe that this is correct in the majority of cases. However, as we have pointed out, other local phenomena (such as an occasional heavily ionizing particle) may contribute to the burst ionization.

The main experiment ran for a total of 206.4 hours under the combination burst and penetrating shower selection of Part II A, and 1804 photographs were obtained. The data showed bursts, penetrating showers, and mixed showers. Observed pulse shapes were almost universally of the "cascade burst" shape. Queer pulse shapes occurred in only 21 events, indicating the presence of heavily ionizing particles. Only one of these 21 cases was unaccompanied by counts in the E tray and most had more than two; hence they indicate complex showers rather than stars. Almost all of the bursts unaccompanied by air showers showed a large pulse in one chamber with somewhat smaller pulses in one or more of the others. This is to be expected from local cascades generated in lead. Chance events of all kinds were completely negligible.

For this analysis, bursts originating close to the center of the apparatus were chosen by selecting visually those photographs showing the largest pulse in the center chamber. This made maximum use of the geometrical efficiency of the E tray for the detection of penetrating particles, besides including most of the burst radiation within the three chambers. The few events exhibiting "star pulses" were not used. The minimum burst height accepted was set somewhat higher than the electronic bias. The events so selected are called Class 1 and are defined by

$$H_{B1}\geqq 1.5;\quad H_{B2}\leqq 0.75H_{B1};\quad H_{B3}\leqq 0.75H_{B1}.$$

Class 1 is divided into two sub-classes. Class 1U consists of events unaccompanied by counts in any air shower tray. The few accompanied events comprise Class 1A.

Table I shows the penetrating particle content of Class 1 for bursts of more than 250 particles ($H=1.5$). The number of air shower trays discharged is indicated by the "A" column, and N is the number of E counters

[20] D. E. Hudson, to be published. A detail not important to the present work was that T_2 was increased to 8 inches of lead for the runs with T_1 removed.

[21] D. E. Hudson (to be published).

[22] *Proceedings of the Echo Lake Cosmic Ray Symposium*, p. 85 (1949).

TABLE I. Distribution of penetrating particles in bursts of Class 1 (206.4 hours; $T_1=3$ inches lead).

Burst range	A	N=Number of E counters struck: 0	1	2	3	4	5	6	7	8	9	10	11	12	Class 1U totals
$1.5\leqq H<3$	0	57	18	12	9	7	7	4	6	6	2	1	0	1	130
	1	0													
	2	3													
	3	4		1							1				
$3\leqq H<6$	0	56	14	8	11	8	6	3	6	9	0	3	1	1	126
	1	4						1		2				1	
	2	1													
	3	3		1		1		1		1					
$6\leqq H<12$	0	25	4	3	4	1	3	4	0	2	2	0	4	1	53
	1	3	1			1	1		1	1	2				
	2	1	2											1	
	3	2			1		1								
$12\leqq H$	0	7	1	2	4	1	0	1	0	0	1	1	0	3	21
	1	1	1	1					1	1				2	
	2	1													
	3			2	1						1				
Class 1U totals		145	37	25	28	17	16	12	12	17	5	5	5	6	330

struck under the 6-inch absorber T_2. We shall interpret Class 1U as representing events produced locally in T_1 by essentially isolated particles. This conclusion for our particular experiment rests upon a study of the distribution of events among $A=0, 1, 2, 3$; and upon the fact that the rate with $T_1=3$ inches is over 40 times that of Class 1U with T_1 removed. Unless otherwise specified we shall be concerned only with Class 1U, since accompanied events are not necessarily generated locally.

B. Distribution of Penetrating Particles

Table I shows that more than half (56 percent) of all bursts were accompanied by at least one discharge in the penetrating particle (E) tray. This proportion is approximately independent of the burst size. The significance of the events showing $N=0$ will now be studied. Possible contributions due to stars, to μ-mesons, and to geometry will be considered.

It is not hard to show that these events ($N=0$) were not due to stars which slipped through the great adverse bias discussed in Part II B3. The rate of purely star events should not depend greatly on the amount of absorber above the chambers. A study of the data taken with unshielded chambers showed a rate giving only 7 such events in 206 hours; all had $1.5\leqq H<3$. There is no reason to suppose that all of these arise from stars. It follows that essentially none of the $N=0$ events having $H\geqq 3$ were due to stars.

Electromagnetic interactions of μ-mesons caused some of the $N=0$ events. Both bremsstrahlung and knock-on processes can give rise to electronic cascades in T_1, and at least half of the time the original meson can miss the E tray. The underground data can be used to correct for this effect. On the average, only μ-mesons of energy greater than about 30 Bev are eligible to make bursts having $H\geqq 1.5$ (250 particles) in our apparatus.[23] These mesons increase in number by a factor 1.38 between the tunnel station and Echo Lake.[14,24] The number of bursts due to mesons expected in 206.4 hours at Echo Lake has been calculated from the tunnel data and is shown in Table II. About 10 percent of all bursts at Echo Lake were due to μ-mesons, as were about 14 percent of all $N=0$ events. For the larger bursts ($H\geqq 6$), 30 percent of the $N=0$ events were mesonic. In the case of the largest bursts ($H\geqq 12$), about 57 percent (within very poor statistics) appear to be mesonic for $N=0$. Taking into consideration the cases where $N=0$ or 1, the corresponding ratios are 16 percent ($H\geqq 1.5$); 31 percent ($H\geqq 6$); 59 percent ($H\geqq 12$). An important conclusion is that practically none of the bursts having more than one observed penetrating particle were due to μ-mesons. This estimate of the contribution of mesonic bursts at Echo Lake depends upon our burst calibration (in terms of number of particles) and upon the particular cascade theory used. If one neglects the correction for chamber wall thickness and uses the theory in CRT,[13] then the percentages listed are multiplied by 1.7 which should set an upper estimate to the meson-produced burst rate. A similar maximum was determined experimentally by the results with the 8-inch shield (Part IV E).

We found that the average efficiency of the E tray was about 50 percent. A special consideration involves the geometrical coherence of the secondaries in penetrating showers. If the secondaries are all found in a narrow cone, then the efficiency is 50 percent in the sense that in half of the bursts all of the penetrating particles will be missed. If a large number of secondaries are distributed as $\cos^3\theta$, then in each event on the average 50 percent of the particles are missed but seldom all of them. The true situation lies between

[23] S. Z. Belenky, J. Phys. U.S.S.R. **VIII**, 305 (1944).
[24] M. Sands, M.I.T. thesis (1948) and Phys. Rev. **77**, 180 (1950).

these extremes. The net result is a somewhat increased chance of missing all of the E counters in a given event, which exaggerates the number of cases with $N=0$. It is clear that if the expected number of penetrating secondaries per event is low (say 1 or 2), then this effect will be pronounced. An approximate correction for this geometrical inefficiency has been made by a study of the distributions in Table I.

A summary of the distribution of observed penetrating particles is given in Table III. The figures are from Table I minus the contribution of μ-mesons. Statistical errors are indicated, and the geometrical correction is at the bottom. These results on the penetrating component of mixed showers extend the available information to relatively high energies. Our minimum bursts have 25 Bev in the electronic component, while our bursts having $H=12$ possess 200 Bev.[22] The data are in qualitative agreement with those obtained with the cloud chamber. Cloud-chamber experiments often have been limited in this application by triggering bias or by masking of penetrating component by the denser cascades. Bridge and Hazen[3] triggered on bursts (1–5 Bev) and found that half contained penetrating particles under 5 inches of lead. A recent high energy study has been made with a cloud chamber containing many gold plates.[7] Ten showers of over 7-Bev energy showed an average of 11 penetrating particles each. High multiplicity was favored, and considering statistics and geometry, these data do not conflict with ours.

Finally, Table I shows an unusual flatness of the distribution of the penetrating events of high N. This suggests that perhaps the higher multiplicities observed were occasionally due to secondary mixed showers produced in T_2 by the penetrating component of an interaction in T_1.

C. Abundance of Penetrating Particles

A rough estimate of the relative number R of penetrating particles per electron in local bursts can be made from our data. R is calculated from $R=\bar{N}/1.36\bar{S}E$, where $\bar{N}$ is the mean number of E counters struck (corrected for the contribution of mesonic bursts but not for geometry), $\bar{S}$ is the mean burst size, and E is the efficiency of the E tray. The factor 1.36 arises from the fact that in our experiment the lead cascades had more particles at the maximum than were observed.[16] The results of such an estimate are shown in Table IV.

These values of R are subject to uncertainties large compared to the statistical errors. One is the contribution of secondary events to the discharges in the E tray. Another is in the evaluation of the efficiency and in the uncertainty as to the cases having $N=0$. A smaller effect is the failure to observe part of the bursts in our chambers. Fortunately, the first two errors give opposing effects.

The only previous value of R which can be compared to ours is that of George and Trent.[9] A value of $R=(1.7\pm0.7)$ percent was found for local penetrating bursts containing about 350 observed particles (3450 meters altitude). This value agrees within statistics with our value of about 1 percent. However, the uncertainties mentioned in the preceding paragraph apply to both experiments, and the agreement must not be interpreted as profound.

It is interesting to compare this R for local cascade bursts with that found for dense air showers. We found an R close to 0.5 percent for air showers averaging $3500m^{-2}$ in density.[20] In recent counter experiments, Cocconi, Tongiorgi, and Greisen[23] have indicated values of R the order of 1 percent. They also show that R decreases with the shower density. This is similar to our observed decrease of R with $\bar{S}$ (Table IV). A truly meaningful comparison involves considerations of the total energies in the events and the differences in cascade multiplication in air and lead. Such an extended analysis will not be given here. However, the similarity of the results is consistent with the belief that the Auger showers and our local mixed showers are simply different manifestations of the same phenomenon.

D. Burst Frequency Distributions

Integral burst frequency distributions are exhibited in Fig. 3. The data are from Class $1U$ (Table I) minus the contribution of mesonic bursts (Table II). The ordinate shows the number of bursts of size greater than H in 206.4 hours. Three curves are shown, depending on the number N of penetrating particle counters discharged with the burst. The similarity of the lower curves lends weight to the supposition that the events shown have similar origin, independent of the number of penetrating particles observed. It is believed that these are the first distributions published for those local bursts definitely not due to stars, to mesons, or to air showers.

Further analysis of the distributions is beyond the scope of this experiment. The observed shape is partly instrumental in nature. A major cause of the concavity observed is the fact that the smaller bursts must be initiated in a thinner section of T_1 in order to be detected.

TABLE II. μ-mesonic bursts expected at 3260 meters (Class $1U$; 206.4 hours; $T_1=3$ inches lead).

Burst range	N = Number of E counters struck 0	1	2	3	>3	Totals
$1.5\leqq H<3$	4.7	3.6	0.36	0	0	8.7
$3\leqq H<6$	5.8	3.2	0	0	0	9.0
$6\leqq H<12$	5.4	1.5	0.36	0.36	0	7.6
$12\leqq H$	4.0	0.7	0	0	0	4.7
Totals	19.9	9.0	0.7	0.36	0	30.0
Statistical errors[a]	±3.0	±1.8	±0.5			±3.3

[a] Calculated from the percentage errors in the underground rate.

[23] Cocconi, Tongiorgi, and Greisen, Phys. Rev. 75, 1063 (1949) and Phys. Rev. 76, 1020 (1949).

TABLE III. Penetrating particles in nonmesonic bursts (Class $1U$; $H \geqq 1.5$; $T_1 = 3$ inches lead).

	N	Percentage of bursts having N of the E counters struck
	$N=0$	42±3
	$N=1$	9±2
	$N=2$	8±1.5
	$3 \leqq N \leqq 6$	24±2.4
	$7 \leqq N \leqq 12$	17±2
$1 \leqq N \leqq 12$	$(N>0)$	58±3
		Corrected approximately for geometry
	$N=0$	30
	$N>0$	70

E. Absorption of Burst Producers

It is interesting to compare the burst production for thicknesses of 3 inches and 8 inches of the absorber T_1. An extended analysis[15] shows (1) that bursts with a moderate number of observed particles (the order of 10^2) are most likely to be produced in the central region of a three-inch T_1; and (2) that a negligible fraction of cascades with even 10^3 observed particles would be produced more than 3 inches from the bottom of the thick absorber. Hence, the bottom of a thick T_1 acts mainly as a producer of bursts due to radiation emerging from the top five-inch layer.

Table V shows the data obtained with the 8-inch shield. This includes events due to μ-mesons and the totals are directly comparable to Table I. Table VI shows a summary of the distribution after the contribution of μ-mesons to the bursts of Table V has been subtracted. The purely mesonic bursts of this size should have a frequency (Table II) practically independent of the thickness of T_1. The standard statistical errors in the final results are shown.

Comparison of Table VI with Table III shows an outstanding feature of the data: namely, the shift in the distribution of penetrating particles (by a factor two in $\bar{N}$) to higher multiplicities for the thicker shield. This suggests that some of the burst producers of Table V may be secondary to interactions (taking place in the upper layers of T_1) which have already given rise to penetrating particles. Such an interpretation is consistent with our knowledge of the nuclear cascades accompanied by electromagnetic showers.[7]

Table VII shows the burst transition between 3 inches and 8 inches of lead above the chambers. The apparent absorption mean free paths have been computed formally from the observed ratio of rates. The apparent increase of absorption for the cases with small N is a clear indication that the "absorption" is really a complex phenomenon. Again, this effect may be interpreted qualitatively in terms of a cascade process.[16] Our m.f.p. values may be compared with the result of Bridge and Rossi[11] who found an apparent m.f.p. of 430±90 g/cm² of lead. This figure was uncorrected for the effects of air showers and μ-mesons.

TABLE IV. Abundance of penetrating particles in local bursts.

Burst range	$\bar{S}$ (Particles)	$\bar{N}$	E	R (%)
$1.5 \leqq H < 3$	360	2.3	0.5	0.95
$3 \leqq H < 6$	720	2.6	0.5	0.53
$6 \leqq H < 12$	1440	3.4	0.5	0.35

The results with thick lead also provide an experimental upper limit to the rate of bursts caused by μ-mesons for any thickness. This rate should be independent of the thickness of T_1, since only very high energy μ-mesons ($E>30$ Bev) are eligible to make our observed bursts. Furthermore, the total burst rate cannot be less than the rate of μ-meson induced bursts. Hence, the figures of Table V show at least that our meson corrections (Table II) are not unduly low.

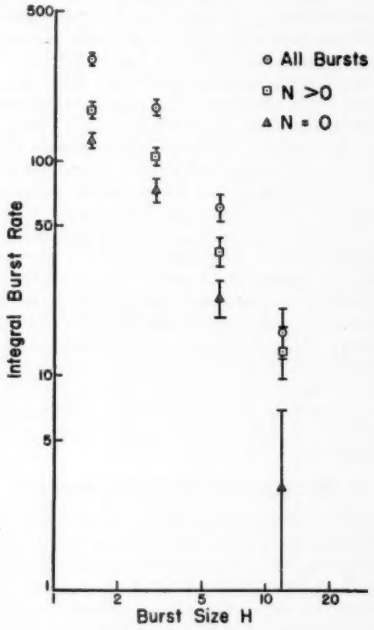

FIG. 3. Integral burst distributions.

F. Summary

In the preceding sections we have studied some properties of local bursts not due to stars, to μ-mesons, or to Auger showers. The actual burst ionization is believed to be mainly due to electronic cascades emerging from the lead T_1. The smallest bursts studied

[16] That is, the occurrence of secondary reactions would increase the number of events with $N \geqq 2$ at the expense of events with $N<2$.

TABLE V. Distribution of penetrating particles in bursts (Class 1U; 128.5 hours; T_1=8 inches lead).

Burst range	N=Number of E counters struck 0	1	2	3	4	5	6	7	8	9	10	11	12	Totals	Expected totals for 206.4 hours
$1.5 \leqq H < 3$	8	4	9	3	0	1	3	2	2	2	2	0	0	36	58
$3 \leqq H < 6$	9	2	2	3	3	3	4	0	8	4	3	1	0	42	68
$6 \leqq H < 12$	1	4	0	0	1	1	2	3	0	1	0	1	1	15	24
$12 \leqq H$	3	1	2	0	0	2	0	3	0	0	0	1	0	12	19
Totals	21	11	13	6	4	7	9	8	10	7	5	3	1	105	
Expected totals for 206.4 hours	34	18	21	9.7	6.4	11	14.5	13	16	11	8	4.8	1.6		169

(Note: Class 1A, bursts accompanied by air showers, consisted of only 5 events in the 128.5-hour period.)

were equivalent to about 250 lead cascade particles incident on the chamber, or to an initial cascade energy of about 25 Bev. Associated penetrating particles were observed. The events studied are interpreted to be the result of nuclear interactions which give rise to both electronic cascades and to a penetrating component.

About 58 percent of nonmesonic bursts were accompanied by observed penetrating particles; a geometrical correction brings this value up to approximately 70 percent, but the value could be much higher if the geometrical coherence effect is pronounced. No information was obtained concerning the presence of heavy particles not sufficiently energetic to traverse 6 inches of lead. The rather consistent association of a hard component with large electronic cascades is in qualitative agreement with present ideas concerning the role of neutral mesons in high energy interactions. However, we have observed a number of large bursts which contained no observed penetrating particles. High energy mixed showers are known to have their penetrating component confined to a relatively narrow cone.[7] Hence, the effects of coherence upon the apparent efficiency of the E tray may account for many of the events having $N=0$.

The ratio of penetrating particles to electrons in bursts of 360 cascade electrons was found to be about 1 percent; this ratio was observed to decrease for larger bursts. These results are comparable to those found for the extensive air cascades.

Integral burst frequency distributions are similar for both penetrating and nonpenetrating bursts. This result is in agreement with the assumption that all of the bursts have a like origin, independent of the penetrating component.

Bursts observed under 8 inches of lead were found to have a higher average multiplicity of penetrating component than those under 3 inches. Nonpenetrating bursts exhibited a much more rapid apparent absorption than the penetrating bursts. These transition effects may be explained qualitatively in terms of a nuclear cascade.

IV. RESULTS FOR LOCAL PENETRATING SHOWERS

A. The Data

The penetrating shower data are part of the 1804 photographs described in Part III A. The auxiliary experiments described there apply also to the present sections; results are presented as required. Burst sizes are specified in units of $1.05H_a$. The equivalent number of cascade particles (S) is given by $S=174H$, where H is the sum of burst pulses in the three ion chambers. Measurement of the pulses was such that the minimum detectable burst had H about 0.1. A conservative lower limit on observable bursts will be taken at $H=0.25$; these certainly contain cosmic-ray ionization. Physical considerations pertinent to the detection of bursts have been described. It is believed that the majority of the bursts arise from electronic cascades; the case of the smaller pulses will be treated later.

For this analysis only events triggered on penetrating showers were considered, in order to investigate the way in which these showers are accompanied by bursts. The events so selected are called Class 2, defined by the condition $N \geqq 3$. The main part, Class 2U, was unaccompanied by discharges in any of the three air shower trays. In these events the burst pulse heights in the three chambers generally differed considerably; however, most events showed visible pulses in more than one chamber. The few events accompanied by air showers comprise Class 2A.

Table VIII shows the distribution of bursts accompanying events of Class 2. The number of air shower trays discharged is indicated by the A column. Because

TABLE VI. Penetrating particles in nonmesonic bursts (Class 1U; $H \geqq 1.5$; T_1=8 inches lead).

N	Percentage of bursts having N of the E counters struck
$N=0$	10±5
$N=1$	6±4
$N=2$	14±4
$3 \leqq N \leqq 6$	30±5
$7 \leqq N \leqq 12$	40±5
$1 \leqq N \leqq 12$ ($N>0$)	90±3

TABLE VII. Transition of bursts according to penetrating component (Class $1U$; 206.4 hours; $H \geqq 1.5$).

Number of E counters discharged under 6-in. Pb	All bursts				Nonmesonic bursts			
	Number of cases		Ratio of rates	Apparent m.f.p. (g/cm²)	Number of cases		Ratio of rates	Apparent m.f.p. (g/cm²)
	$T_1=3$ in.	$T_1=8$ in.			$T_1=3$ in.	$T_1=8$ in.		
$N \geqq 0$ (all cases)	330±18	169±17	0.51±0.06	212± 40	300±19	139 ±17	0.46±0.06	185± 30
$N=0$	145±12	34± 8	0.24±0.05	100± 15	125±13	14 ± 8	0.11±0.06	65± 15
$N=1$	37± 6	18± 6	0.48±0.16	200±100	28± 7	8.7± 6	0.31±0.23	120± 90
$N \geqq 2$	148±12	117±14	0.79±0.11	600+750 −240	147±12	116 ±13	0.79±0.11	600+750 −240

(Note: Only the statistical errors are indicated.)

of the inefficiency of the E tray, the average multiplicity of penetrating particles is greater than N. We interpret Class $2U$ as representing penetrating showers locally produced in the lead above the ion chambers.

B. Distribution of Bursts in Penetrating Showers

About 90 percent of the observed events are accompanied by discernable bursts. Less than 4 percent of the penetrating showers having $N \geqq 7$ are unaccompanied by bursts of $H \geqq 0.25$. It must be recalled that the apparatus exerts considerable triggering bias against the smaller penetrating showers having no cascade radiation. However, the scarcity of pure penetrating showers observed cannot be explained on this basis. Some of the bursts are lost by absorption or lack of cascade development (Part II B3). Hence we can draw the preliminary conclusion that almost every local penetrating shower of more than a few particles is accompanied by some burst-producing radiation. A more complete analysis follows, with particular attention to the cases showing the smallest bursts ($H<0.25$). Points to be considered are (1) apparent penetrating showers caused by μ-mesons and (2) the lack of development of cascades arising from events initiated near the bottom of T_1.

The underground data were used to show that only 11 of the events having $N \geqq 4$ and $H<0.25$ in Table VIII are due to μ-mesons. About 14 of the $N=3$ events having $H<0.25$ are expected to be μ-mesonic processes. The small correction for mesonic events has been applied to Table IX.

It was shown (Part III B3) that cascade bursts originating in the bottom centimeter of T_1 could escape detection through lack of development. This might account for some of those penetrating showers apparently unaccompanied by bursts. An approximate correction for this effect is possible. The events of Class $2U$ originating in the bottom 0.5 inch of T_1 can be subtracted from Table VIII by using the auxiliary data of Table X. However, some correction must be made for the loss of producing radiation in the top 2.5 inches of T_1. This loss takes place mainly through the interaction of the producers in generating further penetrating or mixed showers. The interaction m.f.p. alone cannot be used because the heavy secondaries of the interactions can interact in the bottom 0.5 inch of T_1. The net effect is approximately described by using an absorption m.f.p. of 350 g cm^{-2}. Fortunately, moderate variations of this figure are possible without introducing significant changes in the corrected distributions. We have subtracted 0.81 of the rates indicated in Table X from those in Table VIII in obtaining Table IX.

The final distribution is shown in Table IX, which describes nonmesonic events occurring in the top 2.5 inches of T_1. The correction described also tends to eliminate the effects of the heavily ionizing component of mixed showers, since the slow heavy particles are unlikely to penetrate 0.5 inch of lead. The minimum lead absorber thickness penetrated on the average by the penetrating particles in the events of Table IX is now 6.5 inches.

C. Discussion

The reasons advanced previously lead us to ascribe the larger bursts (say $H \geqq 1$) to electronic cascades generated in the lead T_1. The arguments are stronger here because the events represented by Table IX were generated on the average at least one-half inch up from the bottom of T_1; this practically eliminates heavy tracks from consideration. However, the smaller bursts could be due in part to lightly ionizing heavy particles, some of which penetrate T_2. (About 20 of these would give a burst of $H=0.25$.) Still, it is probable that cascade radiation contributes significantly even to the small bursts, because large hard showers are so rare.

Table IX still shows a very few (15) cases having $H<0.25$. This limit of about 40 particles was chosen conservatively; the true minimum detectable burst was really somewhat smaller than this. We have seen that absorption should occasionally account for failure to observe the electronic component of a mixed shower. It is probable that this effect is small in our apparatus; however, it could easily account for a few of the events having negligible bursts. A possible cause of the burstless events is true failure to produce cascade radiation in the initial event. We can make a rough calculation to see if this is reasonable, using the neutral meson hypothesis. Suppose that on the average about one-third of the mesons produced in an energetic nuclear interaction should give rise to soft component. Then

one might expect about $(2/3)^M$ of events with total multiplicity M to have no electronic radiation. In our case the multiplicity of charged penetrating particles averaged about $2N$ and the total average multiplicity must have been somewhat higher. An estimate of the maximum number of cases with no cascades has been made by taking $M=2N$. The error made in this assumption is compensated by the increase in apparent multiplicity due to secondary nuclear interactions. Calculation shows that we would expect about 30 such failures for the cases having $3 \leqq N < 7$ and about 0.3 for $7 \leqq N < 12$. Slightly fewer (15 and 0) were observed. This could easily be due to the triggering bias against smaller penetrating showers having no cascade component. The penetrating showers of high multiplicity ($N \geqq 7$) were less susceptible to the instrumental bias.

TABLE VIII. Distribution of bursts accompanying penetrating showers (206.4 hours; $T_1=3$ inches lead).

Burst range	A	N = Number of E counters struck: 3	4	5	6	7	8	9	10	11	12	Class $2U$ totals
$H<0.25$	0	36	23	14	8	4	2	0	2	0	1	90
	1	1										
	2											
	3	1						1				
$0.25 \leqq H < 0.5$	0	26	21	15	10	6	4	2	1	2	0	87
	1											
	2						1					
	3		1									
$0.5 \leqq H < 1$	0	51	36	20	18	9	5	9	5	1	0	154
	1	2				1						
	2	0										
	3	1			1	1	1					
$1 \leqq H < 2$	0	54	44	28	20	17	10	11	5	2	3	194
	1		2		2			1				
	2						1					
	3	3			4	1				1		
$2 \leqq H < 4$	0	34	33	29	25	24	25	10	7	5	5	197
	1		1			1	2	2		1	2	
	2	3	1	2	1							
	3	1	1	1	1			4			1	
$4 \leqq H < 8$	0	14	14	14	8	3	7	6	4	7	1	78
	1		1	1	1			2			1	
	2	2		1					2			
	3	2	1	1	2	2	1	1			1	
$8 \leqq H < 16$	0	3	1	5	3	1	7	4	3	3	0	30
	1	1	1	1		3	1	3	1			
	2								1		1	
	3	1	1						1		2	
$16 \leqq H$	0	4	0	3	3	1	3	1	2	2	7	26
	1	1	1		1	1	1				2	
	2											
	3	1		1	1	1	2	2	1		1	
Class $2U$ totals		222	172	128	95	65	63	43	29	22	17	856

The effect of secondary nuclear interactions in increasing the observed multiplicity in the E tray has been discussed. Our knowledge of this does not permit a really quantitative correction to be made. The phenomenon is considered to exert a negligible effect on the general conclusions of Part IV.

The energies E of the cascades accompanying penetrating showers are of considerable interest. For lead[23] E/critical energy$\cong 13.5\times$(number of particles at shower maximum) so that in our experiment the initial energies are always in excess of $90S$ Mev or about $16H$ Bev.

TABLE IX. Corrected distribution of bursts accompanying penetrating showers (Class $2U$; 206.4 hours; $T_1=3$ inches lead).

Burst range	Number of E counters struck: $3 \leqq N < 7$	$7 \leqq N < 12$	Totals
$H<0.25$	15	0	15
$0.25 \leqq H < 0.5$	40	0	40
$0.5 \leqq H < 1$	66	9	75
$1 \leqq H < 2$	111	41	152
$2 \leqq H < 4$	82	67	149
$4 \leqq H < 8$	40	22	62
$8 \leqq H < 16$	12	18	30
$16 \leqq H$	10	16	26
Totals	376	173	549

The bursts of Table IX ranged from about 4 Bev to more than 200 Bev in energy.

D. Summary

Few truly penetrating showers having from 6 to 14 particles are unaccompanied by detectable bursts. Essentially no truly penetrating showers of multiplicity over 14 are unaccompanied by electronic cascades showing energies less than 8 Bev. The neutral meson postulate qualitatively explains the fraction of events unaccompanied by observable bursts.

These results are in agreement with recent cloud-chamber investigations of penetrating showers. Fretter[1] found that about 68 percent of penetrating showers were accompanied by electron cascades in an apparatus selective for relatively low energy events. Hartzler[7] studied penetrating showers of energies larger than 15 Bev and found the corresponding fraction to be 88 percent. Our result of 100 percent was obtained for penetrating showers of even higher multiplicity ($M \geqq 14$, $N \geqq 7$) and energy. This increasing association with increasing energy transferred seems to be real and fits well into the neutral meson picture. The occasional large penetrating shower that has been accompanied by no observable cascade radiation in the cloud chamber[8] is not in essential disagreement with this (statistical) concept of meson production.

The author is sincerely indebted to Professor Kenneth I. Greisen for the suggestion of this problem, for his generous aid in planning the experiment, and for advice and criticism during the analysis of the results.

TABLE X. Distribution of bursts accompanying penetrating showers (Class $2U$; 108.5 hours; $T_1=0.5$ inch lead).

Burst range	N = Number of E counters struck: 3	4	5	6	7	8	9	10	11	12	Totals
$H<0.25$	16	2	3	9	3	1	0	0	1	0	35
$0.25 \leqq H < 0.5$	9	3	4	3	5	1	2	0	0	0	27
$0.5 \leqq H < 1$	5	10	7	6	5	4	2	1	0	1	41
$1 \leqq H < 2$	9	5	3	5	2	0	0	0	0	2	26
$2 \leqq H < 4$	10	6	2	5	0	1	4	1	0	0	29
$4 \leqq H < 8$	1	0	2	1	0	0	3	0	1	0	8
$8 \leqq H$	0	0	0	0	0	0	0	0	0	0	0
Totals	50	26	21	29	15	7	11	2	2	3	166

He also wishes to thank his wife, Hazel, for her aid in examining the many data-photographs.

The stay at Echo Lake was made possible by a grant from the Research Corporation. Some of the facilities at this station were made available through the Inter-University High Altitude Laboratory. Part of the expense of constructing the equipment was covered by a contract with the Office of Naval Research.

APPENDIX I. ELECTRONIC INSTRUMENTATION

Figure 2 shows the block diagram. Our feed-back amplifying system (Los Alamos models 500 and 501) had an effective clipping time of 21 μsec and an over-all gain of about 10^5. The symbol $N\ B$ means that a neon bulb recorded a pulse appearing at that point in coincidence with the master (M). All square gates shown were 25 μsec long except for the 7 μsec M pulse. $N\ B$ circuits had a resolving time of 20 μsec against M delay. Small burst pulses (rising in 10 μsec) gave a delayed M unless $N \geqq 3$, resulting in the loss of some of the beginning of the trace. This effect caused no significant ambiguity in the interpretation. Chance events of all kinds including accidental inefficiencies were negligible for all runs.

Burst pulses were measured to within $\pm 0.05 H_\alpha$ by reprojection of the data photographs, and pulses smaller than $0.05 H_\alpha$ not clearly distinct from noise were called zero. Very large pulses overloaded our system but had a characteristic shape which was calibrated so as to allow deduction of the heights. The errors in pulse measurements were random and had a negligible effect on the final burst distributions.

During the runs, a continual check on the operation of the ion chambers and amplifiers was made by observation of the size and shape of the calibration α-pulses. Rigorous daily and weekly testing schedules insured the proper functioning of all counters and electronic apparatus.

APPENDIX II. ION CHAMBER INSTRUMENTATION

Essential deviations of our method from that of BHRW[10] will be described. The important considerations are those leading to the ionization calibration in terms of pulse heights.

Physically exact formulas were used to calculate numerically the detailed shape of the calibration (α-particle) and burst pulses. The only significant approximation involved was that the electron drift velocity varies as (field/pressure)$^{\frac{1}{2}}$, and the important final pulse heights are essentially independent of this. The transmission characteristics of the combined chamber and amplifiers were taken into account. The distribution of burst ionization was considered to be uniform. The actual distribution of ionization along the tracks of the α-particles was used;[27] these were projected radially into the chamber from the outer wall. The results were that the fractions F of unclipped pulse heights actually observed were $F_\alpha = 0.924$ for an α-pulse and $F_B = 0.785$ for a burst pulse.

An absolute calibration of our chambers was carried out to provide a check on the method, using the 3.97-Mev α-particle pulses. This was based on the fact that the observed voltage pulse heights can be compared to the calculated value of $F_\alpha \times K \times$(amplifier gain)$\times$(total charge liberated)/(effective input capacity). K is a constant which depends on the initial distribution of ions in the chamber. The values of K are 0.985 for an α-pulse and 0.890 for a burst pulse. The pulse height was obtained from an integral bias curve, and precision measurements of all instrumental parameters were made. Each ion pair was assumed to require 27.6 ev in argon.[28] Three independent measurements were made on different ion chambers. An analysis showed that the expected probable errors in the individual calculated and experimental values were 3 and 4 percent exclusive of F and K; the actual differences were only 0.2, 0.3, and 1.7 percent. The much simpler relative calibration [Eq. (1) of text] was obtained from

$$H_B/H_\alpha = (0.890)(0.785)E_B/(0.985)(0.924)E_\alpha.$$

The chambers were operated at a collecting potential of 1800 volts, insuring complete α-particle pulse-height saturation.

APPENDIX III. CASCADE IONIZATION

The burst calibration is partly based on the average ionization $k_\eta(\text{eff})$ of all cascade electrons above zero energy inside of the ion chamber walls. This quantity is the integral of the function $k_\eta(E)$[13] over the electron spectral distribution. We have used the spectra of Richards and Nordheim[29] to find the spectrum under our brass walls.[15] The quantity η (0.5 Mev) was determined by the effective range of electrons in our chamber. The final result was $k_\eta(\text{eff}) = 1.53$ Mev g^{-1} cm^2 for energy lost in argon. This is not far from the usual approximation $k_\eta(\text{eff}) \cong k(\epsilon) = 1.39$ Mev g^{-1} cm^2, where ϵ is the critical energy in lead (6.7 Mev).

[27] M. G. Holloway and M. S. Livingston, Phys. Rev. **54**, 18 (1938).

[28] E. Segrè, *Experimental Nuclear Physics*, Ch. III (John Wiley and Sons, Inc., New York, to be published). We are indebted to Professor H. A. Bethe, author of Ch. III, for making his work available before publication and for valuable advice concerning the energy loss of α-particles in argon.

[29] J. A. Richards and L. W. Nordheim, Phys. Rev. **74**, 1106 (1948).

The Production of Neutrons by μ-Meson Capture in Lead, Magnesium, and Calcium*,†

ANNA MARIA CONFORTO‡ AND R. D. SARD§
Washington University, St. Louis, Missouri
(Received September 24, 1951)

Measurements are reported of the yield of disintegration neutrons from the capture of stopped negative μ-mesons in Pb, Ca, and Mg. A magnetized iron lens is used to separate μ-meson capture from other processes giving rise to neutrons associated with telescope anticoincidences. The functioning of the lens is tested experimentally by observation of decay electrons from stopped mesons; as a byproduct, the competition between capture ($\tau_-=1$ μsec for Mg) and natural decay ($\tau_0=2.15$ μsec) is confirmed. The telescope coincidence and anticoincidence rates are in excellent agreement with recent absolute determinations of the μ-meson spectrum at sea level.

With Pb, there is a striking increase in the coherent neutron rate in switching from focusing positive to focusing negative mesons. This confirms the interpretation of earlier experiments without magnetic field as demonstrating neutron emission resulting from μ-meson capture. The average number of disintegration neutrons per capture appears to be 1.47 ± 0.13 (statistical standard error), as compared with the value 2.16 ± 0.15 (statistical standard error) obtained by Crouch and Sard in an underground experiment. Systematic errors can account for the discrepancy; it is felt that somewhat more weight should be attached to the latter figure. With both Mg and Ca, there is little, if any, neutron production in μ-meson capture. The neutron detecting efficiency is the same as for Pb, but the ratio of neutrons detected to mesons captured is (0.6 ± 0.5) percent for Mg and for Ca, in contrast with (3.1 ± 0.3) percent for Pb. Despite the poor statistics of these preliminary measurements, it is clear that the average neutron multiplicity from Mg and Ca is considerably smaller than from Pb.

1. INTRODUCTION

IN order to study the μ-meson-nucleon interaction, we have begun a series of measurements of the neutron emission resulting from the capture of negative μ-mesons stopped in various elements. In the case of Pb, it has been shown[1,2] that μ-meson capture leads to the emission of neutrons in the range of energies up to about 10 Mev; these neutrons are presumably boiled out of the Tl nucleus as a result of the excitation provided by the neutron recoil in such a reaction as $P+\mu^-\rightarrow N+\nu$. No data for other stopping materials have as yet been published. The present paper reports measurements on Pb, Mg, and Ca. Lead was studied first, in order to confirm the interpretation of the earlier experiments and in order to check our technique. Measurements were then made with Mg and with Ca. The first results with these light absorbers indicated a surprisingly low yield of neutrons in the energy range of our detector, and it was decided to interrupt the measurements in order to improve the detecting efficiency of the system when working with absorbers of low density. As circumstances have since compelled us to suspend work on the experiment, we consider it worthwhile to report at this time the preliminary results obtained before the shut-down.

The earlier work[1,3] had shown that μ-meson capture is only one of various processes by which charged cosmic-ray particles produce disintegration neutrons, and it was necessary to design an experimental arrangement that would permit a clear separation of the neutron production by μ-meson capture. The magnetized-iron lens[4] is ideally suited for this purpose. It gives practically perfect focusing of μ-mesons in a certain momentum band, in our case 490–590 Mev/c on incidence and 0–219 Mev/c on emergence; thus an absorber placed beneath it, of not too great thickness, does not stop any telescope mesons of the wrong polarity. When the sense of the field is such as to focus positive mesons, there is, therefore, no contribution to the neutron coincidence rate from stopped negative mesons. Protons are not focused, because their ranges for the momenta required are too short, even considering only ionization loss. Electrons are not focused because of Coulomb scattering and radiation loss in the iron (30.5 cm Fe is about 17 radiation lengths). π-mesons are scarce at sea level; any that arrived in the telescope would have their focusing spoiled if nuclear energy loss or scattering occurred. In fact, it is likely[5–7] that the cross section for such an interaction is close to the geometrical area of the Fe nucleus; with 30.5 cm Fe there is then only a 10 percent chance of a π-meson getting through the lens without a nuclear collision. Since stopped positive

* The results given here were presented at the New York Meeting of the American Physical Society, February 3, 1951 [Phys. Rev. **82**, 335 (1951)]. The present article, except for the results on Mg and Ca, is a condensation of a thesis presented by Anna Maria Conforto to the Board of Graduate Studies of Washington University in October, 1950 in partial fulfillment of the requirements for the degree of Doctor of Philosophy.

† Supported by the joint program of the ONR and AEC.

‡ Now at the University of Rome, Rome, Italy.

§ Now on leave, as Fulbright Fellow at the University, Manchester, England.

[1] Sard, Ittner, Conforto, and Crouch, Phys. Rev. **74**, 97 (1948).

[2] G. Groetzinger and G. W. McClure, Phys. Rev. **74**, 341 (1948); G. W. McClure and G. Groetzinger, Phys. Rev. **75**, 340 (1949).

[3] Sard, Conforto, and Crouch, Phys. Rev. **76**, 1134 (1949); Sard, Crouch, Jones, Conforto, and Stearns, Nuovo cimento **8**, 326 (1951); Fowler, Sard, Fowler, and Street, Phys. Rev. **78**, 323 (1950).

[4] Bernardini, Conversi, Pancini, Scrocco, and Wick, Phys. Rev. **68**, 109 (1945).

[5] Camerini, Fowler, Lock, and Muirhead, Phil. Mag. **41**, 413 (1950).

[6] K. H. Barker and C. C. Butler, Proc. Phys. Soc. (London) **A64**, 4 (1951).

[7] Bernardini, Booth, Lederman, and Tinlot, Phys. Rev. **82**, 105 (1951); Camac, Corson, Littauer, Shapiro, Silverman, Wilson, and Woodward, Phys. Rev. **82**, 325 (1951).

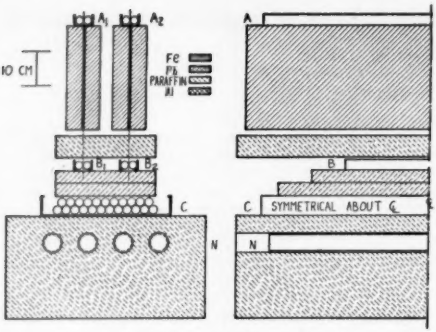

FIG. 1. The geometry of the experiment.

μ-mesons do not interact with nuclei, and since, as just explained, the contribution to the neutron coincidence rate from processes other than μ-meson capture is indifferent to the sense of the magnetic field,[8] the increase in the neutron coincidence rate when the current is reversed so as to focus negative rather than positive mesons must be ascribed exclusively to stopped negative μ-mesons.

2. EXPERIMENTAL APPARATUS

The apparatus was operated at St. Louis (160 meters, or 21 g cm^{-2} air, above sea level) under a thin roof of slate (2.7 g cm^{-2}) and wood (1.4 g cm^{-2}), equivalent to 4.0 g cm^{-2} air. Figure 1 shows the experimental layout. In order to double the counting rates, two lenses are used, mounted side by side; each lens has its own two-fold coincidence telescope, A_1B_1 and A_2B_2, respectively. The prompt coincidences (A_1B_1) and (A_2B_2) are mixed to give one output, designated as (AB). In this way, spurious coincidences due to wrong-sign particles zig-zagging through A_1 and B_2 or through A_2 and B_1 are eliminated. The iron bars constituting the lenses are 239 g cm^{-2} in vertical thickness, sufficient to eliminate completely the atmospheric soft component. Between them and the G-M tubes B is a slab of paraffin 6.3 cm thick. The main function of this barrier is to stop mesons that have just enough energy to get through the iron; these are subject to strong Coulomb scattering in the iron, and could mar the sign discrimination. The barrier also reduces the vulnerability of the telescope to side showers, reduces the efficiency of the neutron detecting system for neutrons from the iron, and increases, by its reflecting action, its efficiency for neutrons originating in the absorber. The absorber, 7.6 cm Pb in the drawing, is placed immediately beneath the B counters. Directly under the absorber is the C tray, containing 23 G-M tubes whose pulse outputs are connected in parallel. This tray fully covers the solid angle of the telescopes with the magnetic field on. The circuit records threefold prompt coincidences, ($AB:C_p$), as well as delayed coincidences ($AB:C_d$) from decay electrons resulting from stopped (AB) mesons. The rate at which stoppings occur in the absorber is clearly given by $(AB)-(AB:C_{pr})$, except for the background due to inefficiency and to stoppings in the counter walls (each 0.41-mm brass) and in the angle-iron supports for the absorber (1.24 g cm^{-2} when averaged over the 30.5×91.5 cm^2 absorber area). This background can be corrected for to a good approximation by subtracting off the value of $(AB)-(AB:C_{pr})$ in the absence of absorber. The block of paraffin under the C tray contains four thermal neutron counters,[9] N. The paraffin serves to thermalize the neutrons incident from above, some of which are then captured by the B^{10} nuclei in the counters to produce pulses, (N). Coincidences are recorded between these pulses (N) and events (AB), ($AB:N$); and between the pulses (N) and events ($AB:C_p$), ($ABC:N$).[10] Again, the difference $(AB:N)-(ABC:N)$ gives the rate of neutron production by stopped particles, while ($ABC:N$) gives the neutron production in penetrating events. The long mean life of a neutron in the detecting system requires the use of long coincidence gate pulses triggered by (AB) and ($AB:C_p$), while the lapse of time (~5 μsec) between emission of a neutron and its reaching thermal speed permits the starting of the gates to be delayed so as to avoid spurious coincidences due to prompt showers.

The circuits, shown in block diagram in Fig. 2, represent a combination of those developed by Sands[11] for recording the distribution in time of decay electrons from stopped mesons and those developed by Crouch[1,12] for recording neutron coincidences in delayed long gates. For obtaining the $(AB-C:N)$ rate from the difference of ($AB:N$) and ($ABC:N$), it is essential that identical gate intervals be involved. Crouch's "master-slave" arrangement of gate generating circuits uses the end of the ($AB:N$) gate to terminate the ($ABC:N$) gate. The ($ABC:N$) gate also starts a little earlier, so that it extends beyond the ($AB:N$) gate at both ends. If this were not the case, some true ($ABC:N$) events would count as $(AB-C:N)$ by occurring when the ($ABC:N$) gate is off but the ($AB:N$) gate on. On the other hand, use of the "operation recorder" chart has made it possible to recognize and reject cases in which the (N) pulse occurs outside the overlap period, as then there is an ($ABC:N$) pip on the chart without an ($AB:N$) pip.

The data reported in this paper were obtained in two periods in 1950, July 4–31, and August 31–October 3.

[8] The observed independence of the sense of the field for the ($ABC:N$) rate (see Tables I and II) supports this assumption.

[9] Proportional counters 5.1 cm×96.6 cm filled with $B^{10}F_3$ to 45 cm Hg pressure. The enriched BF_3 was obtained from the Isotopes Division, Atomic Energy Commission, Oak Ridge, Tennessee. The counters were made and filled by the N. Wood Counter Laboratory, 5646 Harper Avenue, Chicago, Illinois.

[10] Initially provision was also made for recording coincidences between neutron counts (N) and delayed coincidences ($AB:C_d$). As expected, none were observed (see Table I). When the circuit was modified for the second period of data taking, the ($ABC_d:N$) circuit was eliminated.

[11] Rossi, Sands, and Sard, Phys. Rev. **72**, 120 (1947).

[12] M. F. Crouch, thesis, Washington University, September, 1950.

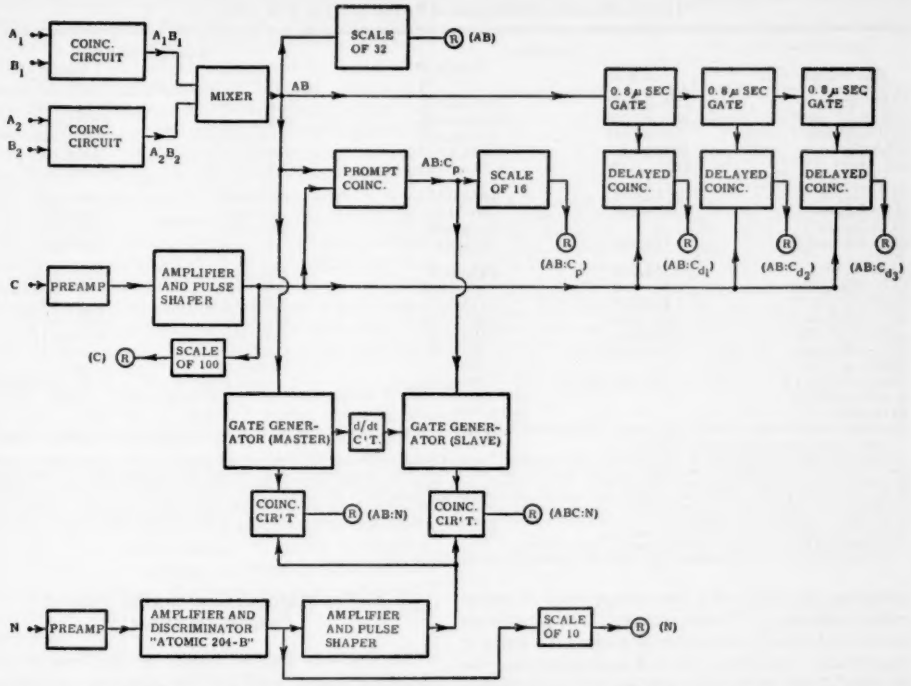

FIG. 2. Block diagram of the circuits. The symbol *R* stands for a "message register" (electromechanical counter) and its associated driving circuit and operation-recorder pen.

The description of the circuit given above refers to the second period of data taking (second Pb series, Mg, Ca) In the earlier period (first Pb series), the delayed coincidence circuit had only two channels, extending from 1.0 to 4.6 μsec and 4.5 to 8.0 μsec, respectively; the $(AB{:}N)$ and $(ABC{:}N)$ gates were each set independently at 188 μsec, with no "master-slave" circuit; and the C tray pre-amplifier did not have as high gain. In addition as has been already remarked,[10] a circuit for detecting events in which neutrons are associated with delayed coincidences, $(ABC_d{:}N)$ was used.

Each magnetic lens consists of two "Armco" iron bars wound with a single layer of enamelled copper wire. The coils (800 turns per bar) are connected in series so as to produce a large flux of induction around the closed iron "circuit." At the operating current of 7.0 amp, the field in the bars measures 15.0×10^3 gauss.

3. THE MEASURED COUNTING RATES

The rates measured in the first and second run are presented in Tables I and II, respectively. The tabulated rates are corrected for accidental coincidences, calculated from measured rates and resolving times. For $(AB{:}C_p)$ an additional correction—for decay electrons appearing in the prompt channel—has been made where necessary. The indicated uncertainties are simply the square root of the uncorrected number of counts divided by the duration. For the events of the first five rows these estimated statistical standard errors are undoubtedly smaller than the systematic errors due to real time-variations of the sea-level cosmic radiation. For the remaining rows, referring to decay electrons and disintegration neutrons, the second line of each entry gives the actual number of counts followed by the expected number of accidentals. For example, in Table I, for $(AB{:}C_{d_2})$, with Pb, focusing μ^+, there are 39 recorded coincidences and 6.4 expected accidentals. The rate, given in the first line of the entry, is $32.6 \pm (39)^{\frac{1}{2}}$, divided by 68.00.

For brevity, details of the corrections are omitted from Table II. The footnotes to Table I should suffice to illustrate the nature and order of magnitude of the corrections.

4. ANALYSIS OF THE FUNCTIONING OF THE APPARATUS

In the remainder of this paper, we consider the physical interpretation of the tabulated rates. We are

TABLE I. Measured counting rates of the first run (July 4–24, 1950).

Type of event	No absorber		Pb absorber (86 g cm^{-2})	
	focusing μ^- (68.50 hr)	focusing μ^+ (53.50 hr)	focusing μ^- (79.00 hr)	focusing μ^+ (68.00 hr)
(AB),[a] min^{-1}	31.30±0.087	33.16±0.102	31.43±0.082	34.21±0.092
$(AB:C_\beta)$,[b] min^{-1}	30.11±0.086	32.05±0.100	28.41±0.077	30.67±0.087
$(AB-C)$,[c] min^{-1}	1.20±0.017	1.11±0.019	3.03±0.025	3.54±0.029
(C),[d] min^{-1}	9678±7.8	9688±8.6	7591±6.9	7532±8.3
(N), min^{-1}	47.88±0.108	46.71±0.120	67.61±0.120	67.44±0.129
$(AB:C_{\beta_1})$, hr^{-1}	0.12±0.05	0.82±0.13	0.17±0.06	2.69±0.20
(1.0–4.6 μsec)	(11–2.9)	(46–2.1)	(20–6.4)	(189–6.4)
$(AB:C_{\beta_2})$, hr^{-1}	0	0.15±0.06	0.01±0.03	0.48±0.09
(4.5–8.0 μsec)	(1–2.9)	(10–2.1)	(7–6.5)	(39–6.4)
$(AB:N)$, hr^{-1}	1.56±0.16	1.45±0.18	6.64±0.30	4.23±0.26
(2.7–190.6 μsec)	(126–19.3)	(93–15.6)	(556–31.6)	(317–29.5)
$(ABC_\beta:N)$, hr^{-1}	1.48±0.16	1.31±0.17	3.56±0.22	3.42±0.24
(2.7–189.6 μsec)	(120–18.4)	(85–15.0)	(311–29.4)	(259–26.3)
$(AB-C:N)$,[e] hr^{-1}	0.08±0.04	0.14±0.05	3.06±0.20	0.81±0.11
(2.7–190.6 μsec)	(6–0.76)	(8–0.54)	(245–3.1)	(58–3.1)
$(ABC_d:N)$, hr^{-1}	0	0	0.01±0.01	0
(delay of (C)+1.1 to delay of (C)+149.0 μsec)	(0–1.4×10^{-3})	(0–6.5×10^{-3})	(1–4.5×10^{-3})	(0–3.8×10^{-3})

[a] The correction for accidentals is −0.0531 min^{-1}.
[b] The correction for accidentals is −0.0072 min^{-1} for μ^- sans Pb, −0.0076 min^{-1} for μ^+ sans Pb, −0.0059 min^{-1} for μ^- with Pb, and −0.0064 min^{-1} for μ^+ with Pb. In calculating it, allowance has been made for the dead-time of the C input circuit, which prevents an accidental $(AB:C_\beta)$ from being detected if the (C) count follows a real $(AB:C_\beta)$ event. When μ^+ are focused, there is an additional correction for decay electron coincidences that appear in the prompt channel. It amounts to −0.0118 min^{-1} sans Pb and −0.0386 min^{-1} with Pb. Both corrections are included in the rates given in the table.
[c] Obtained by subtracting the corrected $(AB:C_\beta)$ rate from the corrected (AB) rate. Any discrepancies of 1 in the last place result from rounding-off in the table. The statistical uncertainty corresponds to the actual number of (AB) events unaccompanied by $(AB:C_\beta)$ events, e.g., for μ^-, sans Pb, 128,864−123,760=5104 and $(5104)^{\frac{1}{2}}/4110=0.0174$.
[d] Determined from brief tests made at intervals during the run.
[e] Obtained by subtracting the number of $(ABC_\beta:N)$ counts from the number of $(AB:N)$ counts.

concerned primarily with the average yield of evaporation neutrons per μ-meson captured, in its dependence on the properties of the capturing nucleus. To arrive at quantitative conclusions, we shall have to first examine in some detail the performance of the magnetic lens (Sec. 4A), the meson stopping rates (Sec. 4B), and the neutron detecting efficiency (Sec. 4C).

A. The Magnetic Lens and the Delayed Coincidence Rates

The lens was designed simply on the basis of the range-momentum relation[13] for μ-mesons, neglecting scattering. A tracing of the meson orbit in magnetized iron (Fig. 3) was laid over a drawing of the apparatus

TABLE II. Measured counting rates of the second run (August 31–October 3, 1950).[a]

Type of event	No absorber		Pb absorber (86 g cm^{-2})		Mg absorber (13.3 g cm^{-2})		Ca absorber (10.5 g cm^{-2})	
	focusing μ^- (123.42 hr)	focusing μ^+ (51.58 hr)	focusing μ^- (51.33 hr)	focusing μ^+ (46.50 hr)	focusing μ^- (182.75 hr)	focusing μ^+ (80.42 hr)	focusing μ^- (109.82 hr)	focusing μ^+ (51.75 hr)
(AB) min^{-1}	31.10±0.091	33.84±0.105	31.33±0.101	34.11±0.111	31.72±0.043	34.56±0.094	30.93±0.074	33.85±0.104
$(AB:C_\beta)$ min^{-1}	31.18[b]±0.090	32.95±0.103	28.62±0.096	31.06±0.105	30.32[a]±0.042	33.04[d]±0.092	29.68±0.073	32.55±0.102
$(AB-C)$ min^{-1}	0.92[b]±0.016	0.90±0.017	2.71±0.030	3.05±0.033	1.40[a]±0.014	1.51[d]±0.020	1.24±0.015	1.31±0.020
(C)[a] min^{-1}	10.08×10^3±4.9	9.72×10^3±12.7	7.55×10^3±13.7	7.57×10^3±14.7	8.91×10^3±6.5	9.33×10^3±6.2	9.68×10^3±9.8	9.70×10^3±10.7
(N) min^{-1}	46.55[f]±0.088	44.60±0.120	66.11±0.146	64.66±0.152	46.61[a]±0.082	47.67[d]±0.110	43.81±0.082	44.60±0.120
$(AB:C_{\beta_1})$ hr^{-1}	0.02[b]±0.02	0.39[g]±0.12	0±0.02	1.16±0.16	0.44[a]±0.06	1.02[d]±0.13	0.12[b]±0.04	0.82±0.13
(1.08–1.95 μsec)	(2–0.528)	(12–0.234)	(1–0.926)	(55–0.935)	(52–1.28)	(67–0.803)	(10–0.813)	(43–0.574)
$(AB:C_{\beta_2})$ hr^{-1}	0.04[b]±0.03	0.33[g]±0.11	0.02±0.03	0.65±0.12	0.16[a]±0.04	0.60[d]±0.10	0.041[b]±0.03	0.61±0.11
(1.91–2.81 μsec)	(3–0.547)	(10–0.242)	(2–0.957)	(31–0.966)	(20–1.32)	(40–0.831)	(4–0.841)	(32–0.594)
$(AB:C_\beta)$ hr^{-1}	0.04[b]±0.03	0.26[g]±0.09	0±0.02	0.41±0.10	0.10[a]±0.03	0.49[d]±0.09	0[b]±0.01	0.45±0.09
(2.69–3.67 μsec)	(3–0.595)	(8–0.264)	(1–1.04)	(20–1.05)	(13–1.44)	(33–0.904)	(1–0.915)	(24–0.647)
$(AB:N)$ hr^{-1}	2.09±0.15	1.86±0.22	8.65±0.43	5.06±0.36	2.37±0.13	1.99±0.18	2.46±0.16	1.91±0.21
(2.5–388.8 μsec)	(327–69.1)	(126–30.1)	(485–41.1)	(275–39.7)	(537–105)	(211–51.3)	(328–57.6)	(129–30.2)
$(ABC:N)$ hr^{-1}	1.91±0.14	1.84±0.22	4.45±0.32	4.36±0.33	1.96±0.12	1.83±0.17	2.13±0.15	1.83±0.21
(2.5–388.8 μsec)	(303–67.0)	(124–29.3)	(266–37.5)	(239–36.1)	(458–99.9)	(196–49.0)	(289–55.2)	(124–29.1)
$(AB-C:N)$ hr^{-1}	0.18±0.04	0.02±0.03	4.20±0.28	0.70±0.13	0.41±0.05	0.16±0.05	0.33±0.06	0.07±0.04
(2.5–388.8 μsec)	(24–2.14)	(2–0.822)	(29–3.61)	(36–3.54)	(79–4.65)	(15–2.25)	(39–2.38)	(5–1.17)

[a] For brevity, details of the corrections for accidentals and decay electrons, as were given with Table I, are omitted.
[b] Determined from only 62.58 hr of data.
[c] Determined from only 116.33 hr of data.
[d] Determined from only 65.08 hr of data.
[e] Determined from brief tests made at intervals during the run.
[f] Determined from only 101.25 hr of data.
[g] Determined from only 29.92 hr of data.
[h] Determined from only 75.48 hr of data.

[13] G. C. Wick, Nuovo cimento **1**, 302 (1943), as plotted by the MIT Cosmic-Ray Group. In these curves allowance is made for the density effect.

(transverse section), and by trial and error a depth for trays B was found such that no wrong-sign mesons emerging from the lens with momentum less than 219 Mev/c could pass through both A_i and B_i. As is evident from the next to last column of Table III, this momentum is barely larger than that needed to penetrate vertically the 5.7 g cm^{-2} paraffin plus the 86 g cm^{-2} Pb absorber, but is well in excess of the greatest momenta involved in stoppings in the Mg or Ca absorbers. For the measurements with our thickness of Pb it would have been wiser to make the calculations with a somewhat higher maximum momentum, but as the experimental results to be described in this section show that the focusing is essentially perfect for mesons stopping in the bottom centimeter of the Pb, we must conclude that the choice of depth for the B counters was made sufficiently conservative to allow for obliquity and scattering in the Pb.

The meson orbits considered are transverse to the magnetic field. For an inclined initial direction, the curve of Fig. 3 represents, however, the projection of the actual orbit, the momentum marked on the curve being its component in the transverse plane. This statement presupposes constancy of the rate of momentum loss along the path, a good approximation down to a total momentum of about 150 Mev/c. In addition, the concentration of mesons near the vertical ($\cos^2$ law) and the rapid falling off of telescope cross section with inclination reduce the contribution of very oblique particles.

The trajectories in magnetized iron were also computed for a rest-mass of 160 Mev/c^2 and 935 Mev/c^2, assuming again energy loss only by nonradiative atomic collisions. These were then used for a graphical study of the focusing. For 160 Mev/c^2, the focusing is almost perfect, indicating that π-mesons (mass 141 Mev/c^2) would be focused if they did not interact strongly with Fe nuclei. For 935 Mev/c^2 (protons), there is practically no focusing, because of the high momentum needed to penetrate the iron.

Multiple Coulomb scattering in the iron perturbs the orbit from the calculated "magnetic" curve. While the paraffin barrier eliminates those mesons for which the scattering effect is greatest, we nevertheless felt it necessary to make an experimental test of the focusing.

TABLE III. Ranges and momenta of the mesons stopped in the absorbers.

	Maximum vertical range beneath the paraffin		Corresponding momentum[a] on emergence from the lens (Mev/c)	Corresponding momentum[a] on entry into the lens (approximate) (Mev/c)
	g cm^{-2}	g cm^{-2} air equivalent		
No absorber	0	0	84	492
Pb absorber	86	49	215	585
Mg absorber	13.3	12.5	130	518
Ca absorber	10.5	9.45	120	511

[a] See reference 13.

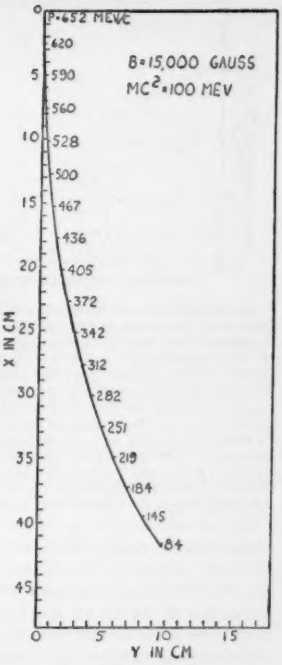

FIG. 3. Trajectory of a singly charged particle of mass 100 Mev/c^2 in iron uniformly magnetized to 15,000 gauss. The plane of the orbit is perpendicular to the magnetic field. The momentum of the particle is marked alongside the curve. As the particle progresses, its momentum decreases and along with it the radius of curvature.

For this test, we made use of the fact that in materials of high Z essentially no stopped negative μ-mesons disintegrate after 1 μsec.[14] Thus, if we detect disintegration electrons while negative mesons are being focused on Pb, we must conclude that some positive mesons are also being stopped. Since the range of the decay electrons rarely exceeds 1 cm Pb, this test only refers to the upper end of the 84–215 Mev/c band of emergent momentum. A similar test in the absence of the Pb, where only stoppings in the brass counter walls and the iron supports (1.8 g cm^{-2} air equivalent altogether) are involved, applies to the lower end of the band. The data with Ca absorber can also be used, covering a somewhat larger part of the bottom of the momentum band.

The delayed coincidence rates are given in Tables I and II and are plotted in Figs. 4 and 5. Their sums are given in Table IV. It is seen that when positive mesons are focused (the situation referred to as "μ^+"), the differential time distribution fits the mean life of 2.15 μsec, for stoppings in Pb, Fe, and brass ("no absorber"), Ca, and Mg. The absolute values of the delayed coincidence rates check reasonably well with crude estimates based on the assumption of an effective

[14] Conversi, Pancini, and Piccioni, Nuovo cimento **3**, No. 6 (1946); references to subsequent work are given in C. F. Powell, Reports on Progress in Physics **13**, 350 (1950).

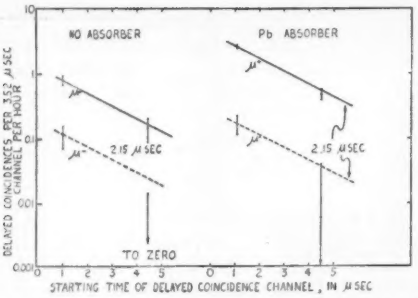
NO ABSORBER
Pb ABSORBER
2.15 μ SEC
2.15 μ SEC
TO ZERO
DELAYED COINCIDENCES PER 3.52 μ SEC CHANNEL PER HOUR
STARTING TIME OF DELAYED COINCIDENCE CHANNEL, IN μ SEC

FIG. 4. Delayed coincidence data of the first run. The rate of delayed coincidences per 3.52-μsec channel width is plotted on a logarithmic scale against the starting time of the channel, to give the differential decay curve of stopped μ-mesons. As the channels do not overlap significantly, the points are statistically independent. All rates are corrected for accidental coincidences. The upper points are for the lenses focusing μ^+ mesons; the lower points for μ^-. On the left side are the rates obtained in the absence of absorber. In this case the mesons are stopped in the iron supports and the brass G-M tube walls (equivalent together to about 1.8 g cm^{-2} air). On the right side are the rates obtained when the 86 g cm^{-2} Pb absorber is inserted. Straight lines of slope corresponding to the natural mean life of 2.15 μsec are drawn in.

range for the decay electrons of 10 g cm^{-2} Pb and 12 g cm^{-2} Mg or Ca. When negative mesons are focused ("μ^-"), the delayed coincidence rates are so low, except in the case of Mg, that it is difficult to draw conclusions about the shape of the time distribution. The data of the first run (Fig. 4) do suggest that counter lags contribute appreciably to the μ^- delayed coincidence rate. The data of the second run (Fig. 5) for Ca give the same impression; they are decidedly incompatible, both in magnitude and slope, with the 0.2 or 0.3 μsec mean life of negative μ-mesons in calcium.[14] For Mg (Fig. 5), the observed μ^- rates fit the reported 1.0 ±0.1 μsec mean life[14,15] very well; and the ratio of the μ^- to μ^+ delayed coincidence rates, 0.33±0.05, is in excellent agreement with the value 0.28±0.06 expected on the assumption of competition between capture and decay, with $\tau_-=1.0\pm0.1$ μsec, $\tau_0=2.15\pm0.07$ μsec, and a positive:negative stopping ratio of 1.23.

An upper limit for the leakage factor, the fraction of wrong-sign mesons that stop, relative to the number of them stopping when they are right-sign, is found by ignoring the contribution of counter lags to the μ^- delayed coincidence rate. It is the ratio of the μ^- delayed coincidence rate to the μ^+ delayed coincidence rate, shown in the last column of Table IV. With the Pb absorber in place, this upper limit is $5.6^{+2.7}_{-2.3}$ percent for the first run, but is decreased to $0.9^{+2.1}_{-0.9}$ percent in the second run, a result, no doubt, of the reduction in lags associated with the increase in sensitivity of the C preamplifier. It appears, then, that the leakage is essentially zero for mesons stopping in the bottom centimeter or so of lead. With no absorber, the upper limit appears to be higher. One would expect the disturbing effect of Coulomb scattering to show itself here if at all, though the observed effect could be entirely statistical. The weighted mean of the upper limits for the Ca and no absorber data of the second run is $(8.8^{+3.3}_{-2.8})$ percent; it applies to the mesons stopped in the top centimeter or so of lead. Since the range distribution of the slow mesons emerging from the lens is essentially flat, the effective upper limit on the leakage factor, as regards stoppings in the whole Pb absorber, is about 5 percent. As regards neutron production by stopped mesons, more weight must be given to the bottom of the Pb, as the efficiency for detecting neutrons decreases with increasing height of the neutron source in the absorber. The measurements with a Ra-α-Be source (described below) show that the efficiencies are in the proportion 2.3:1.7:1 for the bottom, middle, and top of the Pb absorber. Thus, as regards $(AB-C:N)$ events in Pb, the effective leakage factor is less than about 2 percent. For Mg and Ca, the corresponding figure is about 9 percent.

Independent evidence on the quality of the focusing is provided by the very effect with which the present experiment is concerned. The $(AB-C:N)$ rate refers to nuclear disintegrations produced by stopped particles, which are, under the conditions of this experiment, preponderantly μ-mesons. Since positive μ-mesons do not produce nuclear disintegrations, the μ^+ $(AB-C:N)$ rate must be due to leakage μ^- mesons and to other types of particles. Hence an upper limit on the leakage factor is given by the ratio of the μ^+ $(AB-C:N)$ rate to the μ^- one. The rates in question are presented in Tables I and II. The lowest value of the $\mu^+:\mu^-$ ratio is that obtained with Pb in the second run, (16.6±3.3)

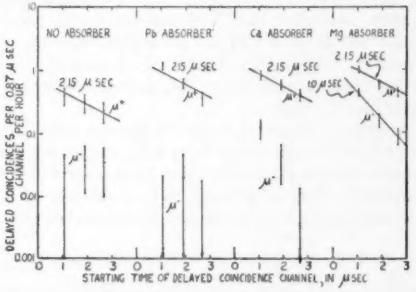

FIG. 5. Delayed coincidence data of the second run. The rate of delayed coincidences per 0.87 μsec channel width is plotted on a logarithmic scale against the starting time of the channel, to give the differential decay curves of stopped μ-mesons. As the channels do not overlap significantly, the points are statistically independent. All rates are corrected for casuals. The upper points are for the lenses focusing μ^+ mesons; the lower points for μ^-. Four sets of data are plotted: from left to right, no absorber (1.8 g cm^{-2} air equivalent Fe and brass), Pb absorber (86 g cm^{-2}), Ca absorber (10.5 g cm^{-2}), and Mg absorber (13.3 g cm^{-2}). Straight lines of slope corresponding to a mean life of 2.15 μsec are fitted to the μ^+ rates. For μ^-, Mg absorber, a line corresponding to a mean life of 1.0 μsec is fitted.

[14] A. H. Benade and R. D. Sard, Phys. Rev. **76**, 489 (1949).

percent. The fact that this upper limit on the leakage factor is well above that given by the delayed coincidence data proves that an appreciable part of the (relatively small) μ^+ $(AB-C:N)$ rate with Pb is not due to stopped mesons.

In comparing the anticoincidence rates with the spectral intensity of mesons at sea level, we shall need to know how the aperture of the lens varies with incident momentum. For right-sign particles, the aperture decreases smoothly toward the limiting value corresponding to no curvature in the iron. For wrong-sign particles the aperture is zero up to a certain momentum, and then increases smoothly toward the same limiting value. In order to calculate these two curves, we have extended the μ-meson trajectory of Fig. 3 back to 2000 Mev/c, and have used it, on a 1:1 scale drawing of the lens, to determine the angular opening in the transverse section as a function of incident momentum. The results are shown in Fig. 6. When these values are weighted in accordance with the momentum spectrum,[16] we find for the effective lens aperture of μ-mesons that produce (AB) events, 10.8° for a right-sign mesons and 4.6° for wrong-sign mesons. Here the assumption has been made that the spectra for positive and negative mesons have the same shape (constant positive excess).[17] For the mesons that stop in the Pb absorber, the effective apertures are 26.2° (right-sign) and 0° (wrong-sign). For Mg and Ca, the opening is slightly larger for right-sign stopped mesons, about 27.0°.

TABLE IV. Data bearing on the leakage factor of the lens.

	Delayed coincidence rate, hr^{-1} (1.0−8.0 μsec in first run, 1.07−3.67 μsec in second run)	$\mu^-:\mu^+$ ratio of the delayed coincidence rates, %
First run:		
No absorber, μ^-	0.09±0.05	+7.7
		9.3
No absorber, μ^+	0.97±0.14	−5.7
Pb absorber, μ^-	0.18±0.07	+2.7
		5.6
Pb absorber, μ^+	3.16±0.22	−2.3
Second run:		
No absorber, μ^-	0.10±0.05	+8.1
		10.3
No absorber, μ^+	0.98±0.18	−5.5
Pb absorber, μ^-	0.02±0.04	+2.1
		0.9
Pb absorber, μ^+	2.22±0.22	−0.9
Ca absorber, μ^-	0.16±0.05	+4.1
		8.8
Ca absorber, μ^+	1.88±0.19	−3.3
Mg absorber, μ^-	0.70±0.08	
Mg absorber, μ^+	2.11±0.18	33±5

[16] J. G. Wilson, Nature **158**, 414 (1946).
[17] J. G. Wilson, Proc. Phys. Soc. (London) **64A**, 417 (1951).

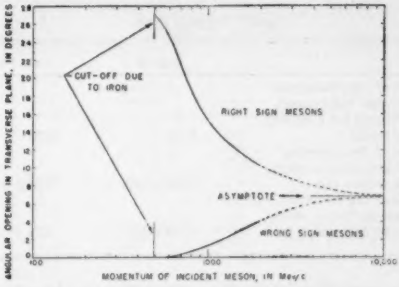

FIG. 6. Aperture of the lens as a function of the momentum of the incident μ-meson. The upper curve refers to "right-sign" mesons, i.e., those of the polarity being focused, the lower one to "wrong-sign" mesons. The curves start at the minimum momentum needed to penetrate the iron and the paraffin barrier. Beyond 2000 Mev/c they are simply an artistic extrapolation. The common asymptote corresponds to zero deviation in the iron.

B. The Meson Stopping Rates

For determining relative values for different elements of the mean number of evaporation neutrons per μ-meson captured, we need only assume that the mean stopping rate is proportional to the corrected anticoincidence rate, $\Delta(AB-C)=(AB-C)$ with absorber minus $(AB-C)$ sans absorber. Strong support for this assumption is provided by the fact that the corrected anticoincidence rates for both μ^- and μ^+ (Table VIB, second column) are indeed in the ratio of the equivalent absorber thicknesses (Table III, third column). The ratios are shown in Table V.

One can go further, and seek to determine the absolute value of the mean neutron multiplicity. This requires knowledge of the actual meson stopping rate, as well as of the absolute neutron detecting efficiency. The former can be determined by comparison of our corrected anticoincidence rates with the known sea-level meson spectrum.[16,18,19] This comparison involves two steps—determination of the total meson flux, and determination of the fraction of it expected to stop in the absorber.

We first calculate the expected (AB) rate in the absence of magnetic field. As all the particles, whether they subsequently stop or not, must penetrate at least 239 g cm^{-2} Fe, we may assume[19] a cosine-squared zenith angle dependence for I, the intensity per unit transverse area per unit solid angle. And as the widths of the counter trays A_i and B_i are small compared to their vertical separation, we may replace them by flat rectangular sensitive areas and assume the intensity and projected area to vary linearly across any transverse slice. When there is no magnetic field, a straightforward double integration along the lines indicated by Greisen[20] gives

$$(A_iB_i)=I_v\frac{bd}{4}[3\varphi\tan\varphi-\cos^3\varphi]_{\varphi=\arctan|(a+c)/2l|}^{\varphi=\arctan|(a-c)/2l|}$$
$$=31.1I_v,$$

[18] B. Rossi, Revs. Modern Phys. **20**, 537 (1948).
[19] W. L. Kraushaar, Phys. Rev. **76**, 1045 (1949).
[20] K. Greisen, Phys. Rev. **61**, 212 (1942).

TABLE V. Comparison of the different absorbers as regards stopping rates.

	Mg:Pb	Ca:Pb
Ratio of air-equivalent absorber thicknesses, corrected for Coulomb scattering	0.24	0.18
Ratio of the corrected anticoincidence rates, μ^-, second run	0.27±0.01	0.18±0.01
Ratio of the corrected anticoincidence rates, μ^+, second run	0.29±0.01	0.19±0.01

where a=sensitive length of top tray=101.6 cm; b=sensitive width of top tray=4.92 cm; c=sensitive length of bottom tray =50.8 cm; d=sensitive width of bottom tray=4.92 cm; and l=vertical distance between counter axes=43.2 cm. This expression reduces to Greisen's when $c=a$, $d=b$. The dimensionless factor in brackets involves only the lengths of the trays and their vertical separation. The transverse dimensions enter only in the factor bd. A measurement of (AB) without magnetic field gave 29.2 min^{-1}, while the value $I_v=7.7\times10^{-3}$ cm^{-2} sec^{-1} sterad^{-1} read from Rossi's curve[18] at a range of 192 g cm^{-2} air[21] leads to (AB) =28.8 min^{-1}. The extreme closeness of the agreement (to within 1.5 percent) must be regarded as fortuitous, as the measurement did not last long enough for meteorological variations to average out. These figures are entered in the first row of Table VIA.

When the magnetic field is on, the geometrical situation is more complicated, the allowed cone for each momentum and each point of the A_1 counter tray being in general multiply connected. But none of the allowed directions in the transverse plane is strongly inclined from the vertical, and it is, therefore, a good approximation simply to use the above formula with b replaced by l times the tangent of the effective net aperture in the transverse plane. Thus, for right-sign particles, $b_{eff}=43.2\times\tan10.8°$ =8.2 cm, while for wrong-sign particles, $b_{eff}=43.2\times\tan4.6°=3.5$ cm. Assuming[17] a positive:negative ratio of 1.23 constant over the incident momentum spectrum, we then compute, for "μ^+," $(AB)=77I_v$, for "μ^-," $(AB)=71I_v$. In the second and third rows of Table VIA the (AB) rates averaged over both runs are compared with those predicted by these expressions with $I_v=7.7\times10^{-3}$ cm^{-2} sec^{-1} sterad^{-1}. There is seen to be agreement to within 5 percent. Furthermore, the ratio of the observed μ^+ to the observed μ^- (AB) agrees perfectly with that predicted by our calculation.

When we consider now the fraction expected to stop, difficulties arise. At the range in question the best determinations of the absolute differential range spectrum are spread over a whole power of 2 (see, e.g., the points plotted in Fig. 6 of reference 18). The elegant G-M tube experiments of Kraushaar[19] do, however, give strong support to the value adopted by Rossi and Sands (curve of Fig. 6 of reference 18). A slightly lower value results from combining the momentum spectrum determined by the cloud chamber technique[18] with the range-momentum relation.[13] We shall compare our apparent stopping rates with both the Rossi-Sands-Kraushaar counter value and the Wick-J. G. Wilson cloud-chamber value for the meson stopping rate. In both cases allowance will be made for the increase in path length in the absorber resulting from Coulomb scattering (10.3 percent in Pb 2 percent in Ca, 1.4 percent in Mg). In the comparison with our rates, an additional uncertainty is introduced by the fact that the lens aperture for right-sign stopped mesons is so large that the approximation we have used, $b_{eff}=l\tan\alpha$, where α is the net aperture in the transverse section, becomes only fair. Some improvement is to be expected from use of the following expression, obtained by integrating the cosine squared distribution across a transverse section:

$$b_{eff}=l\tan\alpha\left[1-\frac{2}{5}\left(1-\frac{\sin\alpha}{\alpha}\right)-\frac{3}{10}\left(1-\frac{\sin2\alpha}{2\alpha}\right)\right].$$

The following sample calculation will illustrate the procedure used in computing the expected values of Table VIB. Consider the case μ^-, Pb. The fraction of the (AB) rate due to negative mesons is 0.66 (this figure follows from a 1.23 positive:negative ratio and the effective apertures 10.8° and 4.6° for right-sign and wrong-sign mesons). These are in an aperture of 10.8°, while the stopped negative mesons are in an aperture of 26.2°. The ratio of the b_{eff} for these two values of α is 2.46, so that the fraction of (AB) that stops is equal to the absorption coefficient for the ranges in question multiplied by $2.46\times0.66=1.62$. The counter value for the absorption coefficient is 3.96 percent (from $i_v=5.7\times10^{-4}$ (g air)$^{-1}$ sec^{-1} sterad^{-1}, $I_v=7.7\times10^{-3}$ cm^{-2} sec^{-1} sterad^{-1}, effective thickness=53.3 g cm^{-2} air), while the cloud-chamber value is 3.38 percent (corresponding to a momentum band from 492 to 595 Mev/c) with a purely statistical error of about 6 percent. Thus the expected meson stopping rate for the second μ^-, Pb run is 31.33 min$^{-1}\times1.62\times3.96\times10^{-2}=2.01$ min^{-1} (counter value) or 31.33 min$^{-1}\times1.62\times3.38\times10^{-2}=1.72$ min^{-1} (cloud-chamber value).

It is seen from the results collected in Table VIB that the observed anticoincidence rates are nicely bracketed by those expected on the basis of the two assumed absorption coefficients, which differ by 16 percent. This agreement, like that in Table VIA, does not involve the use of any adjustable parameter. We conclude that the constant of proportionality relating our apparent stopping rate, $\Delta(AB-C)$, to the actual meson stopping rate is equal to unity to within about 20 percent, perhaps more closely. The loss due to failure of the C tray to intercept all scattered mesons[19] appears to be compensated by the gain due to side showers and knock-on electrons.

Between the first and second run the gain of the C tray amplifier was increased, with the result that the anticoincidence efficiency improved, and the $(AB-C)$ rates decreased (compare Tables I and II). For μ^-, the apparent stopping rate, $\Delta(AB-C)$ is essentially unchanged, 1.79±0.034 min^{-1} as against 1.83±0.031 min^{-1}. For μ^+ there is a discrepancy, the new $\Delta(AB-C)$ being 2.15 ±0.037 min^{-1} as compared with 2.42±0.035 min^{-1} for the old. We know of no objective reason for rejecting any of the data, and are forced to conclude that some unnoticed defect, perhaps in the $(AB:C_p)$ scaler, occurred during one of the two μ^+, Pb runs. The positive:negative ratios, shown in the last column of Table VIB lend some support to the view that the data of the second run are to be preferred, as the ratio 1.32±0.03 is out of line with other determinations.[17] As our main concern is with stopped negative mesons, we do not need to occupy ourselves further with this point.

The positive:negative ratios of the second run (Table VIB) are in excellent agreement with each other and with other observations.[17]

C. The Neutron Detecting Efficiency

As the evaporation neutrons to which our apparatus responds are expected to have energies in the neighborhood of 1–2 Mev, and as our detecting efficiency should be fairly constant up to about 5 Mev, use of a Ra-α-Be source for an efficiency determination seems justified. We used one of 70 μc strength, emitting 1.69×10^8

[21] The average path length through the Fe is 1.09× the vertical thickness, corresponding to 209 g cm^{-2} air. The site is, however, 21−4=17 g cm^{-2} air above sea-level.

neutrons/sec.[22] It was placed at various positions in the absorber, and the efficiency determined for each. We found only a slight dependence on position in the horizontal plane, but a strong dependence on depth in the absorber.[12] With Pb, the efficiencies for the source at the bottom, middle, and top of the absorber are in the ratio 2.3:1.7:1; with Mg, the corresponding figures are 1.8:1.5:1; with Ca, the bottom: top ratio is 1.6:1. Some, but not all, of the effect can be ascribed to solid angle changes. As the range distribution of slow mesons incident on the absorber is essentially flat, the efficiencies for different depths can simply be averaged. We find, then, an effective efficiency of 2.20 percent, *the same, within 1 percent, for all three absorbers.*

In the comparison of the multiplicities from the different absorbers, any systematic errors in the efficiency determination, whether connected with the absolute strength of the test source or the spectrum of evaporation neutrons, cancel out in the first order.

When the neutrons are counted in a gate of finite duration, as is the case for the neutron coincidences, the efficiency is reduced, because of the loss of counts from neutrons captured after the gate has ended. The factor of reduction is $1-\exp(-T/\tau)$, where T is the gate length and τ the neutron mean life. The latter has been determined by comparing the $(AB:N)$ rates, with Pb, of the first and second runs, T being 187.9 and 386.3 μsec, respectively. The result is $\tau=152^{+37}_{-35}$ μsec, in agreement with the values found by other investigators with similar detectors.[23,24] A third set of data, with $T=1042$ μsec, was also taken, and it was verified that the $(AB:N)$ rate at this third value of T fitted very well on the curve of form $1-\exp(-T/152)$ drawn through the first and second points. The coherent efficiency is therefore reduced by the factor $(0.71^{+0.09}_{-0.08})$ for the first run and $(0.92^{+0.04}_{-0.05})$ for the second, giving the efficiency values $(1.56^{+0.20}_{-0.17})$ percent and $(2.03^{+0.09}_{-0.11})$ percent for the first and second runs, respectively.

5. NEUTRON PRODUCTION IN MESON CAPTURE

The neutron production by particles stopped in the absorber is given by the increase in the $(AB-C:N)$ rate when the absorber is inserted. That part of the effect due to stopped negative μ-mesons is the increase in this difference in switching from μ^+ to μ^-. The $(AB-C:N)$ rates (from Tables I and II), the rates resulting from the absorber, and the rates resulting from negative mesons stopped in the absorber are shown in Table VII.

A. Meson Capture in Lead

In both runs the rates with Pb are much larger than the background rates sans Pb, and there is a striking increase in the Pb effect in going from μ^+ to μ^-. This increase constitutes a confirmation[25] of the interpretation of earlier experiments[1] on neutron production by charged cosmic-ray particles as showing neutron production resulting from μ-meson capture.

While the present experiment was not designed primarily for an absolute determination of the mean number of neutrons per capture, the results of the analyses of Sec. 4 show that it is possible to calculate this quantity from our data with fair accuracy. The assumptions made in the calculation are: (a) the μ^- anticoincidence difference $(\Delta(AB-C))$ equals the rate of stopping of negative μ-mesons; (b) the increase in $\Delta(AB-C:N)$ in going from μ^+ to μ^- is the rate of neutron production by stopped negative μ-mesons; (c) the neutron detecting efficiency is sensibly the same for the meson-capture neutrons as for Ra-α-Be neutrons. On the basis of the analyses of the previous paragraphs, we conclude that the systematic error resulting from these assumptions is probably not greater than 25 percent. Thus,

TABLE VI. Comparison of telescope rates with those expected for μ-mesons.

	A. (AB) rate	
	Observed min^{-1}	Expected[a] min^{-1}
$B=0$	29.2	28.8
μ^+	34.0	35.7
μ^-	31.3	32.8

	B. $\Delta(AB-C)$ rate			
	Observed min^{-1}	Expected[b] min^{-1}	Expected[a] min^{-1}	Observed positive:negative ratio
First run:				
Pb, μ^-	1.83±0.031	2.02	1.72	1.32±0.029
Pb, μ^+	2.42±0.035	2.49	2.12	
Second run:				
Pb, μ^-	1.79±0.034	2.01	1.72	1.20±0.031
Pb, μ^+	2.15±0.037	2.48	2.11	
Ca, μ^-	0.32±0.022	0.37	0.31	1.29±0.080
Ca, μ^+	0.41±0.027	0.46	0.39	
Mg, μ^-	0.48±0.021	0.50	0.43	1.28±0.121
Mg, μ^+	0.62±0.026	0.61	0.52	

[a] Assuming $I_0=7.7\times10^{-3}$ cm^{-2} sec^{-1} $sterad^{-1}$, as read from Fig. 5 of reference 18 at $R=192$ g cm^{-2} air.
[b] Assuming an absorption coefficient of 7.4×10^{-4} cm^2 (g air)$^{-1}$, as read from Rossi's curves (Figs. 5 and 6 of reference 18). The vertical thickness of absorber is increased to allow for Coulomb scattering (10.3 percent in Pb, 2 percent in Ca, 1.4 percent in Mg) and is then translated to its air equivalent.
[c] Assuming, on the basis of J. G. Wilson's momentum spectrum (see reference 16), that the ratio of the number of mesons in a 100 Mev/c band centered at 540 Mev/c to the number above 490 Mev/c is 47/1426. The momentum band involved in stoppings in the Pb is taken to be 492–595 Mev/c. The fraction stopping in Ca and Mg is then obtained from that for Pb by applying the ratio of air-equivalent thicknesses after allowance has been made for scattering.

[22] This calibration refers ultimately to the Argonne National Laboratory's "Source No. 38," whose strength is known to only about 10 percent.
[23] M. F. Crouch, Phys. Rev. **81**, 134 (1951); M. F. Crouch and R. D. Sard, Phys. Rev. **85**, 120 (1952).
[24] Cocconi, Tongiorgi, and Widgoff, Phys. Rev. **79**, 768 (1950).
[25] The cloud-chamber pictures of E. J. Althaus (thesis, Washington University, September, 1950) and the underground counter measurements of M. F. Crouch (references 12 and 24) also confirm the production of disintegration neutrons in μ-meson capture in lead. In the meanwhile, Groetzinger, Berger, and McClure (see reference 26) have obtained statistically significant data with a magnetized-iron lens, that also confirm the effect.

TABLE VII. Neutron production by stopped particles.

		Neutrons associated with anti-coincidences ($(AB-C:N)$ hr^{-1})	Neutrons associated with stoppings in the absorber ($\Delta(AB-C:N)$, hr^{-1})	Neutrons associated with negative mesons stopped in the absorber ($\Delta^2(AB-C:N)$, hr^{-1})
First run:				
Pb	μ^- with Pb	3.06±0.20	2.99±0.20	2.32±0.24
	μ^- sans Pb	0.08±0.04		
	μ^+ with Pb	0.81±0.11	0.67±0.12	
	μ^+ sans Pb	0.14±0.05		
Second run:				
Pb	μ^- with Pb	4.20±0.28	4.02±0.29	3.34±0.31
	μ^- sans Pb	0.18±0.04		
	μ^+ with Pb	0.70±0.13	0.68±0.13	
	μ^+ sans Pb	0.02±0.03		
Ca	μ^- with Ca	0.33±0.06	0.16±0.07	0.11±0.09
	μ^- sans Ca	0.18±0.04		
	μ^+ with Ca	0.07±0.04	0.05±0.05	
	μ^+ sans Ca	0.02±0.03		
Mg	μ^- with Mg	0.41±0.05	0.23±0.06	0.09±0.08
	μ^- sans Mg	0.18±0.04		
	μ^+ with Mg	0.16±0.05	0.14±0.06	
	μ^+ sans Mg	0.02±0.03		

first run:

$$\langle m\rangle_{\text{hr}}=\frac{2.32\pm0.24}{(1.83\pm0.03)\times60\times(1.56\pm0.19)\times10^{-2}}$$

$$=1.36\pm0.22.$$

Second run:

$$\langle m\rangle_{\text{hr}}=\frac{3.34\pm0.31}{(1.79\pm0.03)\times60\times(2.03\pm0.10)\times10^{-2}}$$

$$=1.53\pm0.16.$$

The errors indicated are purely statistical. In addition to the systematic errors discussed above, there is an uncertainty in the neutron standard[22] estimated at 10 percent. The results of the two runs are seen to agree; the weighted mean of the two is 1.47±0.13.

This result compares with the value 2.16±0.15 obtained by Crouch[23] in an experiment designed for an absolute determination of $\langle m\rangle_{\text{hr}}$. In the comparison of the two experiments the uncertainty in the primary neutron standard cancels out, as the same Ra-α-Be source was used in the two efficiency measurements. The other systematic errors do, however, remain, and the two results cannot be called definitely inconsistent. Crouch's geometry is superior to ours from the point of view of determining the absolute number of meson stoppings and also as regards "flatness" of neutron response, so we feel that his value is probably nearer the true one.

In this connection we note that even a small leakage of wrong-sign mesons will lower our apparent $\langle m\rangle_{\text{hr}}$. Thus, if the leakage in $\Delta(AB-C)$ is 5 percent and that in $\Delta(AB-C:N)$ is 2 percent, the apparent $\langle m\rangle_{\text{hr}}$ is decreased by 8 percent.

Both values are consistent with the 1.96±0.72 (probable error) found by Groetzinger *et al.*[26] Our value is nearer to the 0.95 predicted[23] on a crude calculation of the neutron evaporation resulting from the nuclear excitation in the reaction $\mu^-+P\rightarrow N+\nu$.

B. Meson Capture in Iron and Brass

The increase in coherent efficiency in the second run, together with better statistics, brought to light neutron production by μ-meson capture in the iron supports for the absorber or the brass G-M tube walls (1.8 g cm^{-2} air altogether). Thus the sans-absorber $(AB-C:N)$ rate goes from 0.02±0.03 hr^{-1} to 0.18±0.04 hr^{-1} when the focusing field is switched from μ^+ to μ^-. The μ^- rate is based on 24 events, with 2.14 expected accidentals.

C. Meson Capture in Magnesium

Magnesium was the first absorber of low Z to be studied. While the $(AB-C:N)$ rate shows a definite increase on switching from μ^+ to μ^-, this increase is not much larger than that in the absence of absorber. The neutron production in the iron supports and brass counter walls (1.8 g cm^{-2} air equivalent) is comparable with that in the magnesium (12.5 g cm^{-2} air equivalent). The net effect ascribable to μ-mesons in Mg is only 0.09±0.08 hr^{-1}. This must be compared with the rate at which mesons are captured, equal to the meson stopping rate times the fraction that escapes decay, $1-(\tau_-/\tau_0)$. With $\tau_-=1.0$ μsec, our data give 0.535 $\times(0.48\pm0.02)$ min$^{-1}=15.4\pm0.6$ hr^{-1}. The ratio of detected neutrons to captured mesons is, therefore, (0.6±0.5) percent. In contrast, the same ratio for Pb (second run) is (3.1±0.3) percent. Thus, the average neutron multiplicity from μ-meson capture in Mg is considerably smaller than that for Pb; in effect, the ratio of the two multiplicites is 0.2±0.2. It appears safe to conclude that the Mg multiplicity is with high probability less than one-half the Pb multiplicity. Evidently further measurements with a geometry giving a higher ratio of Mg effect to background are needed.

D. Meson Capture in Calcium

When it was found that the neutron yield from Mg is small in comparison with Pb, the suspicion arose that the difference might be due to the relatively high excitation energy needed to liberate a neutron from the capturing Mg nucleus (5.5 Mev for $_{11}Na^{24}-{}_{12}Mg^{24}$ mass difference+6.9-Mev neutron binding energy=12.4 Mev, as compared with 8.4 Mev for Pb). At Feenberg's

[26] Groetzinger, Berger, and McClure, Phys. Rev. **81**, 969 (1951).

suggestion we have, therefore, taken data with Ca, a nucleus for which the energy threshold is only 7.3 Mev. If the height of the threshold explains the effect, Ca should be a copious neutron emitter.

The results are seen to be very similar to those for Mg. The neutron production in the Ca (9.45 g cm^{-2} air equivalent) is hardly greater than that in the Fe and brass, and the net effect ascribable to μ-mesons stopped in Ca is only 0.11 ± 0.09 hr^{-1}. With $\tau_-=0.2$ μsec,[14] the fraction of stopped mesons that are captured is 0.91, so the rate of meson capture is $0.91\times(0.32\pm0.02)$ min^{-1} $=17.5\pm1.2$ hr^{-1}. The ratio of detected neutrons to captured mesons is therefore (0.6 ± 0.5) percent, exactly the same as for Mg. For Ca too, the neutron multiplicity is considerably smaller than that for Pb, and is with high probability less than one-half the Pb multiplicity.

E. Discussion

These preliminary results with Mg and Ca indicate a considerably lower neutron yield from these light α-particle nuclei than from Pb. Heidmann (private communication) has remarked that at low Z proton emission will reduce the neutron yield, and his calculation of $\langle m\rangle_{Av}$ for μ-meson capture in Ca gives, on the basis of the excitation energy distribution corresponding to $\mu^-+P\rightarrow N+\nu$ in a Fermi gas, a value somewhat above 0.5. A similar calculation for Pb by Crouch[22] gives 0.95. It is hard to understand why the statistical model should give for Pb too low a value and for Ca one that is probably too high.

Primakoff (private communication) has pointed out that for both Mg and Ca there is a large change in angular momentum between the original nucleus and the ground state of the nucleus formed by capture of the meson. Because of the large momentum and hence angular momentum of the recoiling neutrino, it is possible that transitions to the ground state or to states near the ground state are favored. This would give low average excitation and hence little neutron emission.

6. OTHER RESULTS

Referring to Tables I and II, it is seen that the $(ABC:N)$ rates—neutrons associated with one or more penetrating particles—are sensibly independent of the sense of the magnetic field. This is to be expected, as only slow mesons are focused. One notices also that there is essentially no contribution to the $(ABC:N)$ rate from the Mg or Ca absorbers.

The $(ABC_d:N)$ rates of Table I show that, as expected, there are no neutrons associated with meson decay.[27]

The incoherent (N) rates of Tables I and II are essentially the same for no absorber, Ca (10.5 g cm^{-2}), and Mg (13.3 g cm^{-2}), but are 35 percent higher when the Pb absorber is in place. Most of this increase is probably due to nuclear disintegrations in the Pb produced by cosmic-ray particles, an effect studied thoroughly by Cocconi Tongiorgi[28] with a similar geometry. The capture of μ-mesons cannot account for any appreciable part of the increase, which is probably due mainly to cosmic-ray nucleons. In order to find out how much of it is because of charged particles, the trays A were disconnected and $(B:N)$ events were recorded. The rate observed was 33 ± 1 hr^{-1}, in contrast with the increase in (N) of 1043 hr^{-1}. After allowance is made for the difference in area of the B trays and the Pb absorber and for the loss of efficiency in coherent counting, we find that about 20 percent of the neutron production in the Pb is due to charged particles, in agreement with observations on stars in emulsions.

7. CONCLUSIONS

Our main conclusions are:

1. The production of neutrons by μ-meson capture in Pb is confirmed.

2. The average number of neutrons emitted per capturing Pb nucleus is 1.47 ± 0.13, with an additional systematic error of about 10 percent in the standard of neutron flux and further systematic errors resulting from the geometry that amount to not more than 25 percent. This result is, therefore, not incompatible with the value 2.16 ± 0.15 obtained by Crouch in a measurement underground. We feel that more weight should be given to his result.

3. In both Ca and Mg there is little, if any, neutron production in μ-meson capture. The ratio of neutrons detected to mesons captured is for both absorbers (0.6 ± 0.5) percent, in contrast with the value (3.1 ± 0.3) percent for Pb. The neutron detecting efficiencies are the same in the three cases. Thus, the neutron multiplicity from capture in these α-particle nuclei is with high probability small compared to that from Pb.

8. ACKNOWLEDGMENTS

We are deeply indebted to Mr. J. D. Miller for the construction of almost all of the circuits and for his contributions to their design and maintenance. We are grateful to Mr. A. H. Benade for the construction of the iron lenses, and to Messrs. Benade and Miller for the design and construction of the current supplies. Dr. W. Keller of the Mallinckrodt Chemical Company assisted materially in the procurement of the calcium metal. Finally, we should like to thank Dr. Jean Heidmann for communicating to us before publication the results of his calculations on neutron evaporation from Ca.

[27] V. Tongiorgi-Cocconi and W. L. Kraushaar have previously obtained the same result (private communication).

[28] V. Cocconi Tongiorgi, Phys. Rev. **76**, 517 (1949).

Exchange Current Effects in the Deuteron*

FELIX VILLARS
Department of Physics and Laboratory for Nuclear Science and Engineering, Massachusetts Institute of Technology, Cambridge, Massachusetts
(Received January 2, 1952)

It is well known that the existence of charge carrying nuclear fields, resulting in an exchange of charge between nucleons, also gives rise to additional electromagnetic interaction terms for the nuclear system. It is commonly assumed that these effects are zero for the deuteron ground state, on account of the symmetry properties of the exchange current. The present investigation aims to draw attention to the fact that this conclusion is only true in the adiabatic approximation, which neglects the recoil of the nucleons. In the expression for the electromagnetic interaction of charge exchanging nucleons in motion, nuclear "two-particle currents" appear, in addition to the meson currents encountered in the adiabatic approximation. Whereas the latter are antisymmetric under charge exchange of a nucleon pair, the former are not, and give rise to electromagnetic exchange effects for the deuteron ground state.

I. INTRODUCTION

THE existence of electromagnetic exchange effects, accompanying nuclear charge exchange interaction, has been known for a considerable time.[1] The appearance of additional electromagnetic coupling terms ("exchange" moments) is a straightforward result of a (meson-) field-theoretical treatment of the nuclear interaction problem, since then the total charge-current density automatically satisfies the continuity equation.[2] In a phenomenological treatment of the problem, these extra terms must be added more or less *ad hoc*, guided by the requirement of gauge invariance as an expression for the differential form of the charge conservation relation.[3] Although this latter method lacks uniqueness, it is highly satisfactory inasmuch as it is free from the inherent deficiencies of a meson-field-theoretical model, and also independent of the limitation of the perturbation-calculation approach implied in the former. In the realm of nuclear problems, perturbation methods will always prevent a proper numerical interpretation of the results obtained. Nevertheless, as far as the structure of the obtained expression is concerned, the method provides (or may provide) valuable information, and possibly serve as a basis for the formulation of a more sophisticated phenomenological approach. So far, all field theoretical treatments have been based on the adiabatic approximation (infinitely heavy nucleons); in such an approximation, however, all nucleon *current* effects, resulting from the recoil of the nucleons are dropped, leaving the meson current effects, as exchange corrections of the nuclear *charge*. The well-known result, that the electromagnetic exchange moments (in so far as they are due to the meson currents) have zero diagonal elements for all deuteron states, does not apply to the recoil terms. The former matrix elements are easily seen to be antisymmetric under the substitution $N \rightleftarrows P$, since this implies that the role of a positive meson is taken over by a negative one, and vice versa, and thus reverses the sign of the matrix-element; but of course the same substitution $N \leftrightarrows P$ does not reverse the sign of the electromagnetic interaction of the two nucleons.

In a phenomenological treatment, the limitation of the adiabatic approach may be overcome by extending the discussion to velocity dependent forces.[4] Since such interactions (e.g., the $(\mathbf{L}\cdot\mathbf{S})$ coupling) have been advocated recently,[5] an investigation of its implications on the electromagnetic properties of the deuteron seems desirable, particularly in view of their importance in the problem of fitting the parameters of the static nuclear two-body potential.[6]

A phenomenological approach, however, based on a single time two-particle equation, seems to contain some limitations, of which a field theoretical approach is free; this concerns mainly the introduction of local interaction operators in the former case, and the apparent lack of covariance of the single time formalism.

We present, therefore, in the following pages, an approach to the problem, based on a specific model, introducing pseudoscalar charged mesons (neutral mesons were not included, since they do not contribute to the typical two-particle currents). Pseudoscalar coupling was chosen, but within the approximations of the present calculation the equivalence theorem holds. Pseudovector coupling only provides a different splitting of the electromagnetic exchange terms into such terms resulting from meson currents and nucleon currents.[7] Pseudoscalar coupling, however, was chosen on account of its somewhat greater formal simplicity.

* Assisted in part by the joint program of the ONR and AEC.
[1] A. J. F. Siegert, Phys. Rev. **52**, 787 (1937).
[2] F. Villars, Helv. Phys. Acta **20**, 476 (1947).
[3] R. G. Sachs, Phys. Rev. **74**, 433 (1948); R. G. Sachs and N. Austern, Phys. Rev. **81**, 705 (1951); R. K. Osborn and L. L. Foldy, Phys. Rev. **79**, 795 (1951).
[4] Blanchard, Avery, and Sachs, Phys. Rev. **78**, 292 (1950).
[5] K. M. Case and A. Pais, Phys. Rev. **80**, 203 (1950).
[6] See in this connection Feshbach, Schwinger, and Harr, *Effect of Tensor Range in Nuclear Two-Body Problems* (Computing Laboratory, Harvard University, 1949). This paper includes tables of
$$Q=(\sqrt{2}/10)\int_0^\infty r^2(uw-2^{-\frac{1}{2}}w^2)dr \quad \text{and} \quad p_D=\int_0^\infty dr w^2$$
for various values of the parameters of the two-body interaction.
[7] Ch. Møller and L. Rosenfeld, Kgl. Danske Videnskab. Selskab, Mat.-fys. Medd. **20**, No. 12, 1943; S. T. Ma and F. C. Yu, Phys. Rev. **61**, 138 (1942).

Other types of mesons seem now to be definitely excluded.[8]

This calculation shows that indeed charge symmetric exchange terms exist and give contributions to the magnetic dipole and to the electric quadrupole moment of the deuteron ground state. The former is distinct from the terms calculated by Breit[9] and Sachs,[10] which however might be included, if the appropriate relativistic refinements of the deuteron wave functions were included. But in the present paper only the nonrelativistic deuteron wave function shall be used, since no numerical precision is aimed at. The order of magnitude of the effects discussed may be inferred from the results:

$$Q_{\text{exch}}=\left(\frac{g^2}{4\pi}\right)\left(\frac{\hbar}{mc}\right)\left(\frac{\hbar}{\mu c}\right)I_1\cong\frac{g^2}{4\pi}3\times10^{-27}\ \text{cm}^2 I_1,$$

$$\mu_{\text{exch}}=\left(\frac{g^2}{4\pi}\right)\left(\frac{\mu}{m}\right)\left(\frac{e\hbar}{2mc}\right)I_2=\frac{g^2}{4\pi}\left(\frac{\mu}{m}\right)I_2$$

$\times$nuclear magnetons,

where I_1 and I_2 are dimensionless matrix elements, whose order of magnitude is estimated to $10^{-1}-10^{-2}$. The constant g is the dimensionless coupling constant of the pseudoscalar meson-nucleon coupling. It is obvious that the existence of a exchange quadrupole moment destroys the simple (kinematic) relation, expressing the quadrupole moment in terms of the radial S- and D-state wave functions, $u(r)$ and $w(r)$,

$$Q=(\sqrt{2}/10)\int_0^\infty dr(uw-2^{-\frac{1}{2}}w^2).$$

This brings about an additional uncertainty in the interpretation of the deuteron data in terms of a phenomenological nuclear interaction.

II. THE ELECTROMAGNETIC INTERACTION OF A PROTON-NEUTRON SYSTEM

Let ψ_P and ψ_N be the quantized proton- and neutron-fields, respectively. We assume then, to define our model, a charged pseudoscalar meson field φ responsible for the nuclear interaction. In a time dependent, "free-particle" representation, the nuclear interaction energy is given by

$$H_I(t)=ig\int dv(\bar{\psi}_P\gamma^5\psi_N\varphi+\bar{\psi}_N\gamma^5\psi_P\varphi^*), \qquad (1)$$

g being the dimensionless coupling constant. In the following, we shall use units defined by $c=\hbar=1$. The interaction of the proton and meson fields with an external electromagnetic field A^{ext} is

$$H_{\text{E1}}(t)=ie\int dv[\varphi^*\partial\varphi/\partial x_\mu-\partial\varphi^*/\partial x_\mu\varphi-\bar{\psi}_P\gamma^\mu\psi_P]. \qquad (2)$$

The state vector Ψ of the system will satisfy the Schrödinger equation,

$$i\partial\Psi/\partial t=(H_I+H_{\text{E1}})\Psi. \qquad (3)$$

The solution of the field free problem ($A^{\text{ext}}=0$) will be

$$\Psi(t)=U(t)\Psi_0,$$

and hence, the expectation value of the electromagnetic term,

$$\langle H_{\text{E1}}\rangle=(\Psi_0, U^{-1}H_{\text{E1}}U\Psi_0). \qquad (4)$$

In the g^2-approximation

$$U(t)=\exp[-iS_1(t)]\exp[-iS_2(t)],$$

with

$$S_1(t)=\tfrac{1}{2}\int_{-\infty}^{+\infty}dt'\epsilon(t,t')H_I(t'), \qquad (5a)$$

$$S_2(t)=\frac{i}{8}\int_{-\infty}^{+\infty}\int dt'dt''\epsilon(t,t')\epsilon(t',t'')[H_I(t''),H_I(t')]. \qquad (5b)$$

$U^{-1}H_{\text{E1}}U$ may then be expanded

$$U^{-1}H_{\text{E1}}U=H_{\text{E1}}+H_{\text{E1}}^{(1)}+H_{\text{E1}}^{(2)},$$

but only $H_{\text{E1}}^{(2)}$ will be needed in the present case

$$H_{\text{E1}}^{(2)}=-\frac{1}{4}\int_{-\infty}^{+\infty}\int dt'dt''\epsilon(t,t')\epsilon(t',t'')\times[H_I(t''),[H_I(t'),H_{\text{E1}}(t)]]. \qquad (6)$$

Equation (6) is expressed in terms of free particle operators, and accordingly its two-particle matrix elements will be

$$(p_1',p_2'|H_{\text{E1}}^{(2)}|p_1,p_2).$$

Let then $\Phi_D(p_1,p_2)$ be the deuteron wave function in momentum space. Φ_D is introduced *ad hoc* as that state which satisfies certain requirements imposed by our previous knowledge of the properties of the deuteron. This is a possible inconsistency, inasmuch as the actual model does not provide an adequate solution of the problem of bound proton-neutron states. Nevertheless, the use and interpretation of

$$\langle H_{\text{E1}}^{(2)}\rangle=\int\int\Phi_D^*(p_1',p_2')\times(p_1',p_2'|H_{\text{E1}}^{(2)}|p_1,p_2)\phi_D(p_1,p_2) \qquad (7)$$

[8] K. A. Brueckner, Phys. Rev. **79**, 641 (1950); Marshak, Tamor, and Wightman, Phys. Rev. **80**, 765 (1950); S. Tamor and R. E. Marshak, Phys. Rev. **80**, 766 (1950).

[9] G. Breit, Phys. Rev. **71**, 400 (1947); G. Breit and I. Bloch, Phys. Rev. **72**, 135 (1947).

[10] R. G. Sachs, Phys. Rev. **72**, 91 (1947).

is, in the writer's opinion, the straightforward relativistic formulation of the electromagnetic exchange effects, calculated to the same approximation in g^2.[11] The momenta $p_1 p_2$ involved in (6) will actually be assumed to be small, and no attempt will be made to include in (7) the kinematic relativistic corrections. On the other hand it is important that the actual form of (5a, b) guarantees a proper relativistic treatment of the intermediate states.

$H_{\mathrm{El}}{}^{(2)}$ may be written in the form $-\int dv J_\mu(x) A_\mu{}^{\mathrm{ext}}(x)$. J_μ is the sum of two terms, corresponding to the meson- and nucleon-currents in (2). From (6) it follows at once,

$$J_\mu{}^{\mathrm{Mes}}(x) = +ieg^2 \int\int d^4\xi d^4\eta \bar{\psi}_P(\xi)\gamma^5\psi_N(\xi) \times\left(\bar{D}(\xi-x)\frac{\partial \bar{D}(x-\eta)}{\partial x_\mu} - \frac{\partial \bar{D}(\xi-x)}{\partial x_\mu}\bar{D}(x-\eta)\right) \times\bar{\psi}_N(\eta)\gamma^5\psi_P(\eta), \quad (8a)$$

$$J_\mu{}^{\mathrm{Nucl}}(x) = +ieg^2 \int\int d^4\xi d^4\eta \times(\bar{\psi}_P(x)\gamma^\mu \bar{S}(x-\xi)\gamma^5\psi_N(\xi) \times\bar{D}(\xi-\eta)\bar{\psi}_N(\eta)\gamma^5\psi_P(\eta) +\bar{\psi}_P(\xi)\gamma^5\psi_N(\xi)\bar{D}(\xi-\eta) \times\bar{\psi}_N(\eta)\gamma^5\bar{S}(\eta-x)\gamma^\mu\psi_P(x)). \quad (8b)$$

It is easily verified that $J_\mu(x)$ satisfies the continuity equation

$$\partial J_\mu(x)/\partial x_\mu = 0.$$

An additional property of J_μ is the antisymmetry of the total "exchange charge",

$$Q = -i\int dv J_4(x),$$

under the substitution $P \rightleftarrows N$. Q therefore has zero matrix elements between states of equal charge symmetry. This antisymmetry is obvious for the term arising from $J_\mu{}^{\mathrm{Mes}}$ (8a), since $J_\mu{}^{\mathrm{Mes}}$ itself has this property. But (8b) has no symmetry property, and an explicit calculation is needed. Calling

$$-i\int dv J_4{}^{\mathrm{Nucl}}(x) = (2\pi)^{-1}\int d\omega \exp(-i\omega t)Q(\omega),$$

we get,

$$Q(\omega) = eg^2 \int\int d^4\xi d^4\eta \rho_{PN}(\xi)\bar{D}(\xi-\eta)\rho_{NP}(\eta) \times\{\exp(i\omega_1\xi_0) - \exp(i\omega\eta_0)\}\omega^{-1};$$

the Hermitian operator $\{Q(\omega)+Q(-\omega)\}$ therefore has the desired antisymmetry under the substitution $P \rightleftarrows N$.

Since $J_\mu{}^{\mathrm{Mes}}$ will not affect the properties of the deuteron ground state, we shall give only a very brief discussion of this term: To calculate its matrix elements on the energy shell, we calculate actually

$$\bar{H}'^{(2)} = H'^{(2)}\delta(E_f - E_i) = (2\pi)^{-1}\int_{-\infty}^{+\infty} dt \int dv(-J_\mu{}^{\mathrm{Mes}} A_\mu{}^{\mathrm{ext}}). \quad (8)$$

The evaluation of (8) is straightforward and yields

$$\bar{H}'^{(2)} = \frac{ieg^2}{2\pi}\int_{-1}^{+1} dv \int\int d^4\xi d^4\eta \rho_{PN}(\xi) \times A_\mu\left(\frac{1+v}{2}\xi + \frac{1-v}{2}\eta\right)\frac{\partial F(\xi-\eta)}{\partial \xi_\mu}\rho_{NP}(\eta), \quad (9)$$

where

$$\rho_{PN}(x) = \bar{\psi}_P(x)\gamma^5\psi_N(x),$$

and

$$F(x) = (2\pi)^{-4}\int d^4k \exp(ikx)(k^2+\mu^2)^{-2},$$

provided $A^{\mathrm{ext}}(x)$ satisfies $\Box^2 A^{\mathrm{ext}}(x) = 0$. For a homogeneous magnetic field,

$$A_4 = 0; \quad \mathbf{A}(x) = \tfrac{1}{2}(\mathbf{H}\times\mathbf{x})$$

and a nonrelativistic momentum spectrum of the final and initial states, the matrix elements of $H'^{(2)}$ reduce to the matrix elements of the operator,

$$\frac{1}{8}\left(\frac{e}{2m}\right)\left(\frac{g^2}{4\pi}\right)\frac{\mu}{m}(\boldsymbol{\tau}_1\times\boldsymbol{\tau}_2)_3(\boldsymbol{\sigma}_1\cdot\boldsymbol{\nabla}_1)(\boldsymbol{\sigma}_2\cdot\boldsymbol{\nabla}_2) \times[(\mathbf{H}\cdot\mathbf{x}_1\times\mathbf{x}_2)(e^{-\mu r_{12}}/\mu r_{12})], \quad (10)$$[7]

which is just the result of Møller.[11] In a similar way, we now calculate

$$\bar{H}''^{(2)} = (2\pi)^{-1}\int_{-\infty}^{+\infty} dt \int dv(-J_\mu{}^{\mathrm{Nucl}} A_\mu{}^{\mathrm{ext}}).$$

Carrying out the ξ-integration in the first, the η-integration in the second term of (8b), we get

$$\bar{H}''^{(2)} = (ieg^2/2\pi)\int\int d^4x_1 d^4x_2 \Big\{ \bar{\psi}_P(x_1)\gamma^5\gamma^\mu A_\mu(x_1) \times\int_0^1 dz\{\gamma\partial/\partial x_1 + m(1-z)\}G(x_1-x_2;z) \times\psi_N(zx_1+(1-z)x_2)\cdot\rho_{NP}(x_2) +\rho_{PN}(x_1)\cdot\int_0^1 dz\bar{\psi}_N(zx_2+(1-z)x_1) \times\{\gamma\partial/\partial x_1 + m(1-z)\}G(x_1-x_2;z) \times\gamma^\mu A_\mu(x_2)\gamma^5\psi_P(x_2)\Big\}, \quad (11)$$

[11] Note that Møller's derivation is based on a model using pseudovector coupling of the mesons to the nucleons. His result therefore includes a term (due to the mixed interaction $\propto eg$), which, according to the pseudoscalar coupling scheme, is due to the nucleon currents. This additional term in Møller's result is (in our notation)

$$\tfrac{1}{4}(e/2m)(g^2/4\pi)(\mu/m)(\boldsymbol{\tau}_1\times\boldsymbol{\tau}_2)_3\{(\mathbf{H}\cdot\mathbf{r}_1\times\boldsymbol{\sigma}_1)(\boldsymbol{\sigma}_2\cdot\mathbf{r}_{12}) +(\mathbf{H}\cdot\mathbf{r}_2\times\boldsymbol{\sigma}_2)(\boldsymbol{\sigma}_1\cdot\mathbf{r}_{12})\}\{1+(1/\mu r_{12})\}\exp(-\mu r_{12})/r_{12}{}^2.$$

In the subsequent discussion of the nucleon current effects, we have not singled out this term, but rather focused our attention to the charge symmetric parts.

where G is defined by

$$G(x;z)=(2\pi)^{-4}\int d^4k\,\exp(ikx)\{k^2+\mu^2z+m^2(1-z)^2\}^{-2}. \tag{12}$$

We shall now carry out all time integrations, introducing $G(\mathbf{x},\omega)$ by

$$G(x;z)=(2\pi)^{-1}\int dt\,\exp(-i\omega t)G(\mathbf{x},\omega;z). \tag{13}$$

Let us call p_0', p_0; q_0', q_0 the energies associated with $\bar\psi_P,\psi_N$; $\bar\psi_N,\psi_P$, respectively (i.e., $\bar\psi_P\sim\bar u_P(p')\exp[ip_0't]$), and in addition assume a time-independent potential $A_\mu(x)$. Then time integration gives rise to

$$\delta(p_0'+q_0'-p_0-q_0)\cdot\begin{cases}\delta(p_0'-zp_0-\omega) & \text{for the 1st term in (11)}\\ \delta(q_0'-zq_0-\omega) & \text{for the 2nd term in (11).}\end{cases}$$

The first δ-function expresses just all over energy conservation. To use the second δ-functions, we make the explicit assumption that the wave packet $\Phi_D(p_1,p_2)$(7), used to approximate the deuteron-state, shall contain only nonrelativistic momenta, and only positive frequency parts (no "small" components). Under these conditions, we may use the relations,

$$\begin{aligned}\omega&=p_0'-zp_0\cong m(1-z),\\ \omega&=q_0-zq_0'\cong m(1-z),\end{aligned} \tag{14}$$

(provided the center-of-mass motion is negligible). Corrective terms to (14) will be of order $\mathbf{p}^2$ and neglected. After substituting this into (11), (12), and (13), we get for the operator $H''^{(2)}$ on the energy surface,

$$\begin{aligned}H''^{(2)}=+ieg^2\int\int dv_1dv_2\int_0^1 dz\{&\bar\psi_P(x_1)\gamma^5\gamma^\mu A_\mu(x_1)\\ &\times(\boldsymbol\gamma\cdot\mathbf{x}_1-\mathbf{x}_2)\psi_N(zx_1+(1-z)x_2)\rho_{NP}(x_2)\\ &+\rho_{PN}(x_1)\bar\psi_N(zx_2+(1-z)x_1)(\boldsymbol\gamma\cdot\mathbf{x}_1-\mathbf{x}_2)\gamma^\mu\\ &\times A_\mu(x_2)\gamma^5\psi_P(x_2)\}\\ &\times\exp(-\mu z^{\frac12}|\mathbf{x}_1-\mathbf{x}_2|)/8\pi|\mathbf{x}_1-\mathbf{x}_2|.\end{aligned} \tag{15}$$

III. THE MATRIX ELEMENTS OF $H''^{(2)}$ IN THE NONRELATIVISTIC LIMIT

In this chapter we propose to calculate the matrix element,

$$(p',q'|H''^{(2)}|p,q) \tag{15a}$$

of $H''^{(2)}$ on the energy surface. This matrix element will be expressed in terms of the one particle momentum eigenstates $u_P^*(p')\,u_N(p)$; $u_N^*(q')$, $u_P(q)$ and eventually in terms of the large components χ alone

$$u(p)=(\chi(p);[(\boldsymbol\sigma\cdot\mathbf{p})/2m]\chi(p)).$$

Simultaneously, we shall introduce center of mass and relative coordinates and momenta

$$\begin{aligned}\mathbf{r}&=\mathbf{x}_1-\mathbf{x}_2,\quad \mathbf{R}=\tfrac12(\mathbf{x}_1+\mathbf{x}_2),\\ \boldsymbol\pi&=\tfrac12(\mathbf{p}-\mathbf{q});\quad \mathbf{P}=\mathbf{p}+\mathbf{q};\end{aligned}$$

$\boldsymbol\pi'$ and $\mathbf{P}'$ being defined similarly. The phase factors in the matrix element derived from (15) are then

$$\exp[i(\mathbf{P}-\mathbf{P}')\cdot\mathbf{R}]\times\begin{cases}\exp[i(\boldsymbol\pi^*-\boldsymbol\pi')\cdot\mathbf{r}] & \text{for the 1st term}\\ \exp[i(\boldsymbol\pi-\boldsymbol\pi^{*\prime})\cdot\mathbf{r}] & \text{for the 2nd term,}\end{cases} \tag{16}$$

with

$$\boldsymbol\pi^*=z\boldsymbol\pi-\tfrac12(1-z)\mathbf{P},\quad \boldsymbol\pi^{*\prime}=z\boldsymbol\pi^*+\tfrac12(1-z)\mathbf{P}'. \tag{17}$$

Let us, at this place, list the γ-matrix elements (in their nonrelativistic limit) that will occur in (15). We shall only give the terms arising from the 1st line of (15), but treat separately the cases of a magnetic field: $A_\mu=(\mathbf{A};0)$, and an electrostatic field: $A_\mu=(\mathbf{0};i\phi)$.

Magnetic field

$$u^*(p')\beta\gamma^5u(p)=(1/2m)\chi^*(p')(\boldsymbol\sigma\cdot\mathbf{p}'-\mathbf{p})\chi(p), \tag{18}$$

and

$$\begin{aligned}&u^*(p')\beta\gamma^5(\boldsymbol\gamma\cdot\mathbf{A}(\mathbf{x}_1))(\boldsymbol\gamma\cdot\mathbf{r})u(p)\\ &\quad=(1/2m)\chi^*(p')[(\boldsymbol\sigma\cdot\mathbf{p}'-\mathbf{p})(\mathbf{A}\cdot\mathbf{r})+i(\mathbf{p}'-\mathbf{p}\cdot\mathbf{A}\times\mathbf{r})\\ &\qquad+(\mathbf{p}'+\mathbf{p}\cdot\mathbf{A})(\boldsymbol\sigma\cdot\mathbf{r})-(\mathbf{p}'+\mathbf{p}\cdot\mathbf{r})(\boldsymbol\sigma\cdot\mathbf{A})]\chi(p).\end{aligned} \tag{19a}$$

Electrostatic field

$$u^*(p')\beta\gamma^5i\beta\phi(\mathbf{x}_1)(\boldsymbol\gamma\cdot\mathbf{r})u(p)=-\chi^*(p')\phi(\boldsymbol\sigma\cdot\mathbf{r})\chi(p). \tag{19b}$$

It is obvious from the form of the phase factors (16) that:

$$\mathbf{P}'-\mathbf{P}=-i\boldsymbol\nabla_R,\quad \boldsymbol\pi'-\boldsymbol\pi^*=-i\boldsymbol\nabla_r; \tag{20}$$

these gradients acting on that part of the integrand in (15), which is not included in the phase factors. As a result of (20), we have

$$\mathbf{p}'-\mathbf{p}=-\tfrac12i\boldsymbol\nabla_R+(\boldsymbol\pi'-\boldsymbol\pi),\quad \mathbf{q}'-\mathbf{q}=-\tfrac12i\boldsymbol\nabla_R-(\boldsymbol\pi'-\boldsymbol\pi).$$

A suitable decomposition of $(\boldsymbol\pi'-\boldsymbol\pi)$ is then

$$\begin{aligned}\boldsymbol\pi'-\boldsymbol\pi&=(\boldsymbol\pi'-\boldsymbol\pi^*)+(\boldsymbol\pi^*-\boldsymbol\pi)\\ &=-i\boldsymbol\nabla_r+(\boldsymbol\pi^*+\tfrac12P)(z-1)/z,\end{aligned} \tag{21a}$$

according to the 1st line of (16), and

$$\begin{aligned}(\boldsymbol\pi'-\boldsymbol\pi)&=(\boldsymbol\pi^{*\prime}-\boldsymbol\pi)+(\boldsymbol\pi'-\boldsymbol\pi^{*\prime})\\ &=-i\boldsymbol\nabla_r+(\boldsymbol\pi^{*\prime}-\tfrac12P)(1-z)/z.\end{aligned} \tag{21b}$$

But we are only interested in the matrix elements for

$$P\sim0,\quad P'\sim0.$$

This enables us to use the relations,

$$\begin{aligned}\mathbf{p}'-\mathbf{p}&=-(i/2)\boldsymbol\nabla_R-i\boldsymbol\nabla_r+\boldsymbol\pi^*(z-1)/z\\ &=-i\boldsymbol\nabla_1+\boldsymbol\pi^*(z-1)/z,\end{aligned} \tag{22}$$

$$q'-q=-(i/2)\nabla_R+i\nabla_r-\pi^*(z-1)/z$$
$$=-i\nabla_2-\pi^*(z-1)/z, \quad (23)$$

and similar relations derived from (21b). Note that the factor $\sim z^{-1}$ in (22) will not lead to a divergence, since it will eventually occur in the position

$$[(z-1)/z]\nabla\varphi(zr),$$

and thus cancel out. It may be helpful to write down the matrix element (15a) at this stage of development explicitly:

$$(p', q'|H'^{(2)}|p, q)$$
$$=+(ieg^2)\int d^3R e^{i(P-P')\cdot R}\int_0^1 dz\int d^3r$$
$$\times\{\chi_P^*(p')\chi_N^*(q')e^{-i(\pi'\cdot r)}\Omega\chi_N(p)\chi_P(q)e^{i(\pi^*\cdot r)}$$
$$+\chi_P^*(p')\chi_N^*(q')e^{-i(\pi^{*\prime}\cdot r)}\Omega^*\chi_N(p)\chi_P(q)e^{i(\pi\cdot r)}\}. \quad (24)$$

Ω is the following operator.

(a) Case of an electrostatic field, represented by a potential $\phi(\mathbf{x})$

$$\Omega=-(1/2m)\phi(\mathbf{x}_1)(\boldsymbol{\sigma}_1\cdot\mathbf{r})(\boldsymbol{\sigma}_2\cdot\mathbf{q}'-\mathbf{q})\exp(-\mu z^{\frac{1}{2}}r)/8\pi r,$$
$$\Omega^*=+(1/2m)\phi(\mathbf{x}_2)(\boldsymbol{\sigma}_2\cdot\mathbf{r})(\boldsymbol{\sigma}_1\cdot\mathbf{p}'-\mathbf{p})$$
$$\times\exp(-\mu z^{\frac{1}{2}}r)/8\pi r. \quad (25)$$

(b) Case of a homogeneous magnetic field $\mathbf{H}$ represented by a vector potential

$$\mathbf{A}(\mathbf{x})=\tfrac{1}{2}(\mathbf{H}\times\mathbf{x}).$$

Ω and Ω^* are then of the form $-(\mathbf{M}\cdot\mathbf{H})$ and $-(\mathbf{M}^*\cdot\mathbf{H})$ respectively; and

$$\mathbf{M}=(1/8m^2)(\boldsymbol{\sigma}_2\cdot\mathbf{q}'-\mathbf{q})[(\mathbf{x}_1\times\mathbf{x}_2)(\boldsymbol{\sigma}_1\cdot\mathbf{p}'-\mathbf{p})$$
$$-i\mathbf{r}(\mathbf{p}'-\mathbf{p}\cdot\mathbf{x}_1)+i(\mathbf{p}'-\mathbf{p})(\mathbf{r}\cdot\mathbf{x}_1)$$
$$-(\mathbf{x}_1\times\mathbf{p}'+\mathbf{p})(\boldsymbol{\sigma}_1\cdot\mathbf{r})+(\mathbf{x}_1\times\boldsymbol{\sigma}_1)(\mathbf{p}'+\mathbf{p}\cdot\mathbf{r})]$$
$$\times\exp(-\mu z^{\frac{1}{2}}r)/8\pi r.$$
$$\mathbf{M}^*=(1/8m^2)(\boldsymbol{\sigma}_1\cdot\mathbf{p}'-\mathbf{p})[(\mathbf{x}_1\times\mathbf{x}_2)(\boldsymbol{\sigma}_2\cdot\mathbf{q}'-\mathbf{q}) \quad (26)$$
$$+i\mathbf{r}(\mathbf{q}'-\mathbf{q}\cdot\mathbf{x}_2)-i(\mathbf{q}'-\mathbf{q})(\mathbf{r}\cdot\mathbf{x}_2)$$
$$+(\mathbf{x}_2\times\mathbf{q}'+\mathbf{q})(\boldsymbol{\sigma}_2\cdot\mathbf{r})-(\mathbf{x}_2\times\boldsymbol{\sigma}_2)(\mathbf{q}'+\mathbf{q}\cdot\mathbf{r})]$$
$$\times\exp(-\mu z^{\frac{1}{2}}r)/8\pi r.$$

We shall now evaluate the electric quadrupole moment resulting from (25) and the magnetic moment (26) for the deuteron ground state. Note that in terms of an isotopic spin notation, the two operators (25) and (26) are proportional to $\tau_+^{(1)}\tau_-^{(2)}$, which is equal to

$$\tfrac{1}{4}(\boldsymbol{\tau}^{(1)}\cdot\boldsymbol{\tau}^{(2)}-\tau_3^{(1)}\tau_3^{(2)})-\tfrac{1}{4}i(\boldsymbol{\tau}^{(1)}\times\boldsymbol{\tau}^{(2)})_3;$$

this gives us a factor (-1) for the deuteron ground state. In addition, we have to pick out of Ω the terms even in $(\mathbf{r}, \boldsymbol{\pi})$, and symmetric in $\boldsymbol{\sigma}_1, \boldsymbol{\sigma}_2$.

The Electric Quadrupole Moment

We expand ϕ about the center of mass R, and define a tensor Ω_{ik} as the coefficient of $\partial^2\phi(R)/\partial R_i\partial R_k$, in (25).

If we define, as usual,[12] a quantity q as 3 times the 33-component of the traceless tensor Q_{ik}, appearing in

$$H_{\text{quadr}}=\tfrac{1}{6}e\Sigma(Q_{ik}\partial^2/\partial R_i\partial R_k),$$

we get from (24)

$$q=-2ig^2\int_0^1 dz\int d^3r\{\varphi_D^*(r)(3\Omega_{33}-\mathrm{Tr}\Omega)\varphi_D(zr)$$
$$+\varphi_D^*(zr)(3\Omega_{33}^*-\mathrm{Tr}\Omega^*)\varphi_D(r)\}, \quad (27)$$

where φ_D represents the charge-singlet deuteron ground state, obtained from the momentum eigenstates involved in (24) by a suitable build up of a wave packet. From

$$\Omega_{ik}=\frac{-1}{2m}\left(\frac{r\partial_k}{8}\right)\left\{\left(\frac{1-z}{z}\right)(\boldsymbol{\sigma}_1\cdot\mathbf{r})(\boldsymbol{\sigma}_2\cdot\boldsymbol{\pi}^*)\right.$$
$$\left.+i\left[\boldsymbol{\sigma}_1\cdot\boldsymbol{\sigma}_2-\frac{(\boldsymbol{\sigma}_1\cdot\mathbf{r})(\boldsymbol{\sigma}_2\cdot\mathbf{r})}{r^2}(1+\mu z^{\frac{1}{2}}r)\right]\right\}$$
$$\times\exp(-\mu z^{\frac{1}{2}}r)/8\pi r,$$

we get, by dropping terms $\sim(\boldsymbol{\sigma}_1-\boldsymbol{\sigma}_2)$ and assuming $S=1$:

$$(3\Omega_{33}-\mathrm{Tr}\Omega)=\left(\frac{-1}{2m}\right)\left(\frac{3r_3^2-r^2}{8}\right)\left\{\left(\frac{1-z}{z}\right)\right.$$
$$\times[(\mathbf{S}\cdot\mathbf{r})(\mathbf{S}\cdot\boldsymbol{\pi}^*)+(\mathbf{S}\cdot\boldsymbol{\pi}^*)(\mathbf{S}\cdot\mathbf{r})-(\mathbf{r}\cdot\boldsymbol{\pi}^*)]$$
$$\left.+i[1-(2(\mathbf{S}\cdot\mathbf{r})^2/r^2-1)(1+\mu z^{\frac{1}{2}}r)]\right\}$$
$$\times\exp(-\mu z^{\frac{1}{2}}r)/8\pi r, \quad (28)$$

and a similar expression for $(3\Omega_{33}^*-\mathrm{Tr}\Omega^*)_D$. Remembering that

$$i\boldsymbol{\pi}^*=\nabla_r \text{ on } \varphi_D \text{ alone}, \quad -i\boldsymbol{\pi}^{*\prime}=+\overleftarrow{\nabla}_r \text{ on } \varphi_D^*,$$

and introducing dimensionless integrals by taking $(1/\mu)$ as unit of length, we may write:

$$q=(+\tfrac{1}{5})(g^2/4\pi)(2\mu m)^{-1}\int_0^1 dz\int d^3r(3r_3^2-r^2)$$
$$\times\exp(-z^{\frac{1}{2}}r)/r\times\{\varphi_D^*(r)[\{(\mathbf{S}\cdot\mathbf{r})(\mathbf{S}\cdot\boldsymbol{\nabla})$$
$$+(\mathbf{S}\cdot\boldsymbol{\nabla})(\mathbf{S}\cdot\mathbf{r})-(\mathbf{r}\cdot\boldsymbol{\nabla})\}-(1-[2(\mathbf{S}\cdot\mathbf{r})^2/r^2-1]$$
$$\times(1+z^{\frac{1}{2}}r))]\varphi_D(zr)+\text{c.c.}\}. \quad (29)$$

The Magnetic Dipole Moment

After performing the substitutions (22) and (23), the operator $\mathbf{M}$ will assume the form

$$\mathbf{M}=\mathbf{M}'+\mathbf{RM}'',$$

[12] L. Rosenfeld, *Nuclear Forces* (Interscience Publishers, Inc., New York, 1947), Appendix II.

and it is only $\mathbf{M}'$ that contributes to the internal magnetic moment. Eventually the projection of $\mathbf{M}'$ on $\mathbf{J}$, the total angular momentum, will be taken,

$$\mathbf{M}'_J=\tfrac{1}{2}(\mathbf{M}'\cdot\mathbf{J})\mathbf{J},$$

($J=1$ for deuteron ground state). $(\mathbf{M}'\cdot\mathbf{J})$ will be calculated as $(\mathbf{M}'\cdot\mathbf{L})+(\mathbf{M}'\cdot\mathbf{S})$, and written in the form

$$\tfrac{1}{2}(\mathbf{M}'\cdot\mathbf{J})=(e/2m)\mu_D, \tag{30}$$

μ_D being the value in nuclear magnetons of the "exchange" contribution to the magnetic moment of the deuteron ground state. The evaluation of the two projections $(\mathbf{M}'\cdot\mathbf{L})$ and $(\mathbf{M}'\cdot\mathbf{S})$ is straightforward, but tedious; the result will again be written in terms of a dimensionless matrix element, taking μ^{-1} as unit of length. Then

$$\mu_D=-\tfrac{1}{8}(g^2/4\pi)(\mu/2m)\int_0^1 dz\int dv \times[\varphi_D^*(r)\,\mathfrak{D}_{op}\varphi_D(zr)+\text{c.c.}]. \tag{31}$$

$$\begin{aligned}\mathfrak{D}_{op}=&-4[S^2+(\mathbf{L}\cdot\mathbf{S})]V(r)\\&+[5(T-Y)+2(\mathbf{n}\cdot\mathbf{S})^2\{5(\mathbf{r}\cdot\nabla)-2\}]rdV/dr\\&+[T-Y+2(\mathbf{n}\cdot\mathbf{S})^2(\mathbf{r}\cdot\nabla)]r^3(d/dr)(r^{-1}dV/dr)\\&+[3\{Y-(\mathbf{L}\cdot\mathbf{S})\}(2z-1)/z-4(\mathbf{r}\cdot\nabla)(3z-2)/z\\&-\{Z-Y(\mathbf{r}\cdot\nabla)+(\mathbf{r}\cdot\nabla)^2\}(5z-3)/2z\\&-(\mathbf{L}\cdot\mathbf{S})(\mathbf{r}\cdot\nabla)(z-1)/z-L^2(z+1)/z]V(r)\\&+[\{-2Y+Z+2(\mathbf{r}\cdot\nabla)^2+(\mathbf{L}\cdot\mathbf{S})\\&+((\mathbf{n}\cdot\mathbf{S})^2+2)(\mathbf{r}\cdot\nabla)\}(1-z)/z\\&+\{[1+2(\mathbf{n}\cdot\mathbf{S})^2](\mathbf{L}\cdot\mathbf{S})+T(\mathbf{r}\cdot\nabla)\\&+2(\mathbf{n}\cdot\mathbf{S})^2(\mathbf{r}\cdot\nabla)^2+[1-2(\mathbf{n}\cdot\mathbf{S})^2]L^2\}(1+z)/z\\&-(2/z)Y(\mathbf{r}\cdot\nabla)]rdV/dr\\&+[-Y(\mathbf{r}\cdot\nabla)(2-z-z^2)/z^2+\{[Y-(\mathbf{r}\cdot\nabla)]\\&\times[L^2+(\mathbf{L}\cdot\mathbf{S})-(\mathbf{r}\cdot\nabla)^2]+2(\mathbf{r}\cdot\nabla)^2\\&\quad+r^2(\mathbf{S}\cdot\nabla)^2+Z(\mathbf{r}\cdot\nabla)\}(1-z^2)/z^2]V(r),\end{aligned} \tag{32}$$

where the following abbreviations have been introduced:

$$\begin{aligned}&T=3(\mathbf{S}\cdot\mathbf{n})^2-S^2,\quad Y=\{(\mathbf{S}\cdot\nabla),(\mathbf{S}\cdot\mathbf{r})\}_+,\\&Z=r^2[2(\mathbf{S}\cdot\nabla)^2-\nabla^2],\end{aligned} \tag{32a}$$

and

$$\mathbf{n}=\mathbf{r}/r;\quad V(r)=\exp(-z^{\frac{1}{2}}r)/r.$$

The next step consists in expressing the expectation values (29) and (31) in terms of the radial deuteron S- and D-state wave functions $u(r)$ and $w(r)$:

$$\varphi_D(\mathbf{r})=[u(r)/r]\phi_0+[w(r)/r]\phi_2.$$

The calculation of the matrix elements with respect to L, S, J of the operators appearing in (29) and (31) is most conveniently done following the technique outlined by Rarita and Schwinger.[13] We shall actually restrict the subsequent analysis to (29), the electric quadrupole moment. A fair estimate of (31) seems too involved; the effect is likely to be of the order of magnitude of the uncertain kinematic relativistic corrections,[9,10] and its evaluation would therefore not improve our knowledge of the magnetic moment problem. On the other hand, the discussion of (29) is comparatively simple.

The matrix elements of the operators in (29) are

(a) $\{(\mathbf{S}\cdot\nabla),(\mathbf{S}\cdot\mathbf{r})\}_+-(\mathbf{r}\cdot\nabla)$:

JLS	101	121
101	$\frac{1}{3}(rd/dr-1)$	$\frac{2}{3}\sqrt{2}(rd/dr+2)$
121	$\frac{2}{3}\sqrt{2}(rd/dr-1)$	$-\frac{1}{3}(rd/dr+2)$

(b) $(2(\mathbf{S}\cdot\mathbf{n})^2-1)$:

JLS	101	121
101	1/3	$2\sqrt{2}/3$
121	$2\sqrt{2}/3$	$-1/3$

(c) $(3r_3^2/r^2-1)_{J_3=1}$:

JLS	101	121
101	0	$\sqrt{2}/5$
121	$\sqrt{2}/5$	$-1/5$

Let us now introduce the notations: $s=zr$,

$$u'(s)=du/ds;\ w'(s)=dw/ds;$$

we may then write (29) in terms of u and w as follows:

$$\begin{aligned}q=&\tfrac{1}{4}(g^2/4\pi)(2\mu m)^{-1}\int_0^1 dz/z\int_0^\infty drr\exp(-z^{\frac{1}{2}}r)\\&\times\{(4/15)u(r)[(1+z^{\frac{1}{2}}r)u(s)+\{(1-z)/z\}\\&\times(su'(s)-u(s))]+(\sqrt{2}/15)u(r)[(4+z^{\frac{1}{2}}r)w(s)\\&+\{(1-z)/z\}(sw'(s)+2w(s)]-(\sqrt{2}/15)w(r)\\&\times[(4+z^{\frac{1}{2}}r)u(s)+\{(1-z)/z\}\{su'(s)-u(s)\}]\\&+(1/15)w(r)[(8+5z^{\frac{1}{2}})w(s)\\&\quad+3\{(1-z)/z\}\{sw'(s)+2w(s)\}]].\end{aligned} \tag{33}$$

The value of (33) is estimated by calculating numerically the r-integral for a set of values of z,

$$z=0,\ 0.075,\ 0.10,\ 0.25,\ 0.5,\ 1.0.$$

The functions $u(r)$ and $w(r)$ are those calculated by the Harvard Computation Laboratory,[2] and the values of the interaction parameters adjusted to give the correct triton binding-energy.[14]

According to (33), q is then proportional to

$$I=\int_0^1 (dz/z)F(z), \tag{34}$$

$F(z)$ being the r-integral in question. A plot of $F(z)$ *vs* z (Fig. 1) reveals that the major contributions to I arise

[13] W. Rarita and J. Schwinger, Phys. Rev. **59**, 556 (1941), Appendix I.

[14] R. L. Pease and H. Feshbach, Phys. Rev. **81**, 142 (1951).

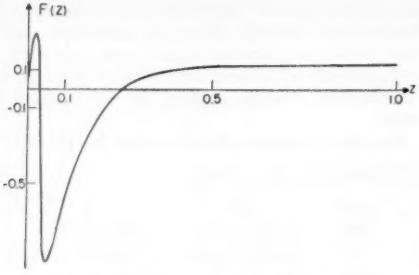

FIG. 1. The r-integral of Eq. (33), $F(z)$, plotted *vs* z.

from values $z<1/5$, and are therefore extremely sensitive to the behavior of the wave function at small values of r. The approximate value of I (34), is -0.1, and leads to a value of

$$q=-(\tfrac{3}{8})(g^2/4\pi)\times 10^{-28}\ \text{cm}^2.$$

Plausible values for $g^2/4\pi$ are as high as 5–6;[15] the electric exchange quadrupole moment q is therefore, on the basis of our model, expected to be approximately -10^{-28} cm^2, corresponding to 7 percent contribution to the actual value[16] of Q:

$$Q=(2.738\pm 0.016)\times 10^{-27}\ \text{cm}^2.$$

IV. DISCUSSION

In this section, we shall rely on the results of a phenomenological description of the deuteron,[6,17] with the interaction

$$V(r)=-V_0\{[1+\tfrac{1}{2}g(\boldsymbol{\sigma}_1\cdot\boldsymbol{\sigma}_2-1)]\exp(-\beta r)/\beta r + \gamma S_{12}\exp(-\tau r)/\tau r\}; \quad (35)$$

S_{12} is the tensor force operator: $S_{12}=2T$ (32a); g, γ, β, τ are dimensionless parameters. The quantity r is measured in units μ^{-1} ($=1.4\times 10^{-13}$ cm for $\mu=276m_{el}$).

In presence of exchange effects, the relation

$$Q^*=Q_{\text{exp}}-q=(\sqrt{2}/10)\int_0^\infty dr r^2(uw-2^{-\frac{1}{2}}w^2), \quad (36)$$

should be used; it appears therefore as indicated to estimate the effect of a variation of Q on the parameter of (35), especially on γ. Keeping these parameters adjusted to reproduce the deuteron data, except Q^*, the following approximate relations hold,

$$\gamma V_0/Q\cong\text{const}, \quad (37a)$$

$$(1+\gamma\beta/\tau)V_0\cong\text{const} \quad (37b)$$

(β and τ being kept constant). According to reference 14, a good choise is $\beta=2.33$, $\tau=1.8$. For $Q=2.74\times 10^{-27}$ cm^2, we derive with the help of (37a, b) and the tables of reference 6 a ratio,

$$\Delta\gamma/\gamma\cong 3\Delta Q/Q.$$

Thus, considering modestly our value of q as the source of an uncertainty in Q^* (36) of the relative order of 5 percent, an uncertainty in γ of about 15 percent. The effect is still much more pronounced, if we assume short-range tensor forces. In both cases, however, the expected D-state admixture is not affected very much by the change in Q of a few percent.

Some general remarks may be added: The actual fact that the behavior of the wave function near the origin (and therefore the high momenta in $\varphi_D(\pi)$) is of critical importance, suggests that our nonrelativistic calculation of the expectation value of q is altogether not on a too firm basis. We should, in this connection, keep in mind that we have, in a way, artificially reduced the effect of high momenta in the deuteron state by the choice of our wave function $\varphi_D(\pi)$, which corresponds to a far less singular interaction than the interaction associated with our actual field theoretical model.[18] It is easily seen that (29) and especially (32) are strongly affected by wave functions more irregular near the origin, and will probably assume values much larger than our actual result. (quite apart from the fact that these formulas themselves become inaccurate, since in deriving (15) we dropped all terms $\mathbf{p}^2/M^2$, assuming $\pi\sim\mu c$ at most). It is hoped to take up this problem again, as soon as a perturbation treatment, which rests upon the covariant wave function for bound states,[19] will be developed. This will also provide a basis for a discussion of the magnetic moment problem. Here, the already known phenomenological relativistic corrections are largely sufficient to "explain" any discrepancy between the observed magnetic moment and the value one expects on the basis of the calculated D-state admixture.

Actually, the astonishingly good internal consistency of the electric and magnetic deuteron data obtainable on the basis of a completely nonrelativistic description, seem to indicate that all additional effects will have to be small. This applies to the kinematic relativistic effects, as well as to the phenomena discussed in the present paper. Their common feature is to depend strongly on the high momentum tail in $\varphi_D(\pi)$, or on the behavior of the wave function near the origin in the configuration space of the relative motion. [See for instance our discussion of Eq. (33)]. The magnitude of the exchange effect discussed in this paper agrees essentially with this condition of smallness. Since we

[15] K. M. Watson and J. V. Lepore, Phys. Rev. **76**, 1151 (1949); R. G. Sachs and M. G. Mayer, Phys. Rev. **53**, 991 (1938).

[16] Kolsky, Phipps, Jr., Ramsey, and Silsbee, Phys. Rev. **81**, 1061 (1951).

[17] Meanwhile some of this material has been published by H. Feshbach and J. Schwinger, Phys. Rev. **84**, 194 (1951).

[18] M. Levy, Phys. Rev. **84**, 441 (1951).

[19] M. Gell-Mann and F. Low, Phys. Rev. **84**, 350 (1951); E. E. Salpeter and H. A. Bethe, Phys. Rev. **84**, 1232 (1951).

have actually calculated the expectation value of a too singular operator, we expect that in a consistent theory the exchange effects will be even smaller than our present results. It remains to be seen, however, whether a completely covariant description of the two nucleon system[19] will corroborate the point of view advocated here.

In concluding this paper, the author wishes to thank Dr. Henry Primakoff, and also Dr. H. Snyder and Dr. M. Newman of the Brookhaven National Laboratory, for interesting discussions. It is also a pleasure to acknowledge the hospitality of the Brookhaven National Laboratory, where most of this manuscript was prepared during a visit in August, 1951.

PHYSICAL REVIEW VOLUME 86, NUMBER 4 MAY 15, 1952

The Total Neutron Cross Section of Nitrogen*

J. J. Hinchey, P. H. Stelson, and W. M. Preston
Laboratory for Nuclear Science and Engineering, Massachusetts Institute of Technology, Cambridge, Massachusetts
(Received January 2, 1952)

The total cross section of nitrogen has been measured for neutrons in the energy range 200 to 1800 kev, using scatterers of liquid nitrogen and of lithium azide. Eleven resonances were found, corresponding to excited states in the compound nucleus N^{15}, with natural widths of from 3 to 54 kev. Nine of these can be identified with resonances previously known in the reactions $N^{14}(n,p)C^{14}$, $N^{14}(n,\alpha)B^{11}$, or $C^{14}(p,n)N^{14}$. From a comparison of the measured and computed elastic scattering cross sections, J-values can be assigned to most of the observed states. In some cases the parity also can be determined and the effective level spacing D_J computed for decay by neutron, proton, or α-particle emission. At least for proton emission, it must be concluded that the quantities D_J, which contain implicitly the matrix elements for the transition, can vary by a factor of at least 100.

I. INTRODUCTION

THE virtual excited states of N^{15} offer an excellent opportunity to study, with present experimental techniques, competitive reactions in a light nucleus. Three different reactions, $n+N^{14}$, $p+C^{14}$ and $\alpha+B^{11}$, lead to virtual levels of N^{15}. Furthermore, the levels of N^{15} become virtual with respect to proton, neutron, and α-particle emission at roughly the same excitation energies: 10.21, 10.83 and 10.99 Mev, respectively.[1] Consequently, with electrostatic generators capable of 3- or 4-million volts, one is able to study the virtual levels in the region above 11 Mev by observing twelve different reactions. Of these, the (p,α), (α,p), (p,p), (α,α), (α,γ), and (p,γ) have thus far not been investigated. The reactions (n,p), (p,n), (n,α), (α,n), (n,γ), and (n,n) have been studied with different degrees of resolution and over various ranges of excitation energy.[2]

In particular, the two inverse reactions, $N^{14}(n,p)C^{14}$ and $C^{14}(p,n)N^{14}$, have been studied with fairly good resolution. Johnson and Barschall[3] measured the absolute cross section for the (n,p) and (n,α) processes and found three strong resonances, with indications of several weaker ones, in the neutron energy range 0.2 to 2.0 Mev. The relative neutron yield from the inverse (p,n) reaction has been measured over this same range of excitation energies by Roseborough *et al.*[4] Using somewhat better resolution, they found nine clearly defined resonances. In general these two investigations are in good agreement, the existing differences being ascribed to the degree of resolution employed.

With these data available, it was thought that a measurement of the total neutron cross section with good resolution would be of considerable interest. From the total neutron cross section and the (n,p) and (n,α) cross sections, one can deduce the elastic neutron scattering cross section, a quantity which is interpreted with some reliability by present nuclear theory. One can then hope to obtain a more detailed picture of the process by assigning total angular momentum and parity values to the virtual states and angular momentum values to the reacting particles.

II. EXPERIMENTAL METHOD

The $Li^7(p,n)Be^7$ reaction was used to produce monoenergetic neutrons of variable energy. Protons of well-defined energy were obtained from the Rockefeller electrostatic generator. After acceleration the protons are analyzed by a ninety-degree deflection in a magnetic field that is both controlled and measured by a proton magnetic moment resonance device. The generator voltage is stabilized by a variable corona load which is driven by an error signal produced by the proton beam

* This work was supported by the Bureau of Ships and the ONR. A portion of it was submitted by J. J. Hinchey (Lieutenant Commander, U.S.N.) in partial fulfillment of the requirements for the degree of Master of Science at the Massachusetts Institute of Technology.

[1] Li, Whaling, Fowler, and Lauritsen, Phys. Rev. **83**, 512 (1951).

[2] For a summary see Hornyak, Lauritsen, Morrison, and Fowler, Revs. Modern Phys. **22**, 291 (1950).

[3] C. H. Johnson and H. H. Barschall, Phys. Rev. **80**, 818 (1950).

[4] Roseborough, McCue, Preston, and Goodman, Phys. Rev. **83**, 1133 (1951).

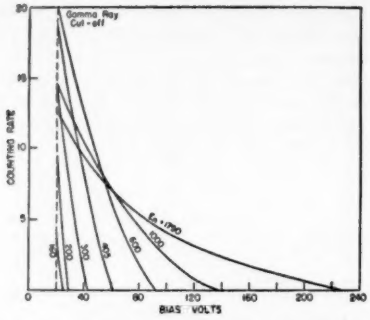

FIG. 1. Relative response of the propane counter to neutrons of energy E_n, as a function of the discriminator bias voltage.

at the exit slits of the magnetic analyzer. Tests have shown that with the entrance and exit slits of the analyzer set at 1.0-mm width, the effective energy spread is approximately 0.075 percent. With this energy definition several microamperes of beam current are available. By narrowing the slits better energy definition is obtained but at the expense of beam current. The voltage scale of the generator is based on the $Li^7(p,n)$ threshold which is taken to be 1.8822 ± 0.0019 Mev as determined by Herb *et al.*[5]

Thin targets of lithium were prepared by evaporation of the metal in vacuum onto 10-mil tantalum disks. Target preparation was carried out in the target assembly of the generator. To prevent deterioration under proton bombardment the targets were rotated eccentrically to the proton beam and cooled by an air jet sprayed on the outside of the tantalum backing. Targets of approximately 10-kev thickness were measured by the previously described "rise" method.[6] The thickness of thinner targets was estimated from the ratio of yields, as measured with a BF_3 long counter, at a proton energy where the $Li^7(p,n)$ cross section is not changing rapidly (3.0 Mev). This method is subject to some uncertainty because of the possibility of target oxidation. Therefore, for the thinnest targets, the overall resolution was established by measuring the width of the sharp resonance at 585 kev in the total neutron cross section of sulfur.

It is now known that the residual nucleus, Be^7, has an excited state at 434 kev which gives rise to a second group of neutrons from the $Li^7(p,n)$ reaction when the energy of the ground-state group is greater than 640 kev. Hence, for the region above 640 kev, the value of the total cross section obtained is a weighted average of the cross section at two different neutron energies which depends both on the relative intensities of the two groups and the efficiency of the detector for the two neutron energies. Fortunately, the intensity of the second group is low; several investigations of the neutron spectrum have shown that for ground-state neutron energies ranging from 900 to 2250 kev the relative intensity of the second group is about 10 percent.[7]

We have endeavored to eliminate the ambiguity resulting from the presence of the two groups by the use of a neutron detector which is made insensitive to the lower energy group. This detector, a proton recoil proportional counter, was constructed by filling a brass cylinder one inch in diameter and four inches effective length with propane gas to a pressure of 55 cm. The counter was operated with 2700 volts on the 4-mil center wire. Pulses were amplified on a four-tube preamplifier and Model 204-B (A.I.C.) amplifier. A typical set of integral bias curves at different neutron energies is shown in Fig. 1. With recourse to these curves, the bias was adjusted to discriminate against the second, lower energy group. The disadvantage of this practice is the reduction in the counter efficiency, especially at higher neutron energies where the relative difference in energy of the two groups decreases. The background counting rate of the counter, which was determined by cutting off the direct neutron flux with a long, thin paraffin cone, varied from $\frac{1}{2}$ to 2 percent of the counting rate with the cone removed.

The first cross-section measurements were carried out with a liquid nitrogen scatterer. The experimental arrangement is shown in Fig. 2. A Dewar flask constructed of glass of 1 mm thickness served as container for the liquid nitrogen. To reduce the rate of evaporation, the flask was silvered except for a sight-line along the axis. The liquid nitrogen used in the experiment is judged by its vendors[8] to have a purity of 99 percent or better. The scatterer thickness, nt, is 0.521×10^{24} nuclei/cm^2, where the density is taken to be 0.808 g/cm^3.

A certain amount of complication results from the fact that neutrons are scattered by the glass of the Dewar flask. The following procedure was used to obtain the cross section. First the counting rate, n_0, with the flask in place but empty was measured. Next, the counting rate, n_b, with the flask full of water was obtained. This thickness of water transmits essentially no neutrons and therefore n_b is interpreted as the counting rate caused by the neutron background plus neutrons scattered into the detector by the glass of the flask. The n_b ranged from 3 to 5 percent of n_0. Finally, the counting rate, n, with liquid nitrogen in the flask was taken. The cross section and its statistical error

[5] Herb, Snowden, and Sala, Phys. Rev. **75**, 246 (1949).
[6] Hanson, Taschek, and Williams, Revs. Modern Phys. **21**, 635 (1949).
[7] Johnson, Laubenstein, and Richards, Phys. Rev. **77**, 413 (1950). Freier, Rosen, and Stratton, Phys. Rev. **79**, 721 (1950). B. Hamermesh and V. Hummel, Phys. Rev. **78**, 73 (1950). P. H. Stelson, Ph.D. thesis, MIT (1950).
[8] Supplied by the Low Temperature Laboratory, MIT.

were calculated as

$$\sigma=\frac{1}{nt}\ln\left(\frac{1}{T}\right),\quad \frac{\Delta\sigma}{\sigma}=\frac{(\Delta T/T)}{\ln(1/T)},$$

where $T=(n-n_b)/(n_0-n_b)$. The neutron flux was monitored with a BF_3 long counter placed 2 meters away from the target at 90° to the proton beam.

A second, independent measurement of the neutron cross section of nitrogen was carried out using as a scatterer the compound lithium azide (LiN_3). This compound, although difficult to prepare and handle, is quite satisfactory from a nuclear viewpoint since the relative percentage of nitrogen nuclei is favorable and the neutron cross section of lithium is particularly simple. The lithium azide was prepared by Dr. T. T. Magel of MIT and his analysis indicated that it had a purity of at least 98.5 percent. Since lithium azide is hydroscopic, the scatterer was made by sealing the compound in a thin-walled (5-mil) steel cylinder one inch in diameter. A scatterer thickness of 0.116×10^{24} molecules/cm^2 was used. The scatterer and the propane counter were placed at mean distances of 12 and 28 cm, respectively, from the target.

A calculation of the correction to the cross section resulting from neutrons scattered into the detector by the scatterer indicates that it is less than 1 percent. This correction was not applied since, in general, the statistical error in the cross section is about 3 percent and since there are uncertainties in its calculation because of the unknown angular distribution of the scattered neutrons and the effect of multiple scattering.

The total neutron cross section of lithium was measured using metallic lithium scatterers. Our values agree well with those of Adair,[9] except that we find the resonance at 256 kev to be somewhat larger. This experiment has been reported.[10]

The total neutron cross section of nitrogen, measured respectively with scatterers of liquid nitrogen and lithium azide, is shown in Figs. 3 and 4. The agreement is in general close. With the azide a very narrow resonance, 5A, was discovered which had been overlooked in the work with liquid nitrogen. Data for each resonance, derived from these curves, have been entered in Table I. In this table, columns 2 and 3 give the resonance energies in the laboratory (E_R) and center of mass (E_R') systems, corrected for target thickness. Wherever the position of the maximum is shifted appreciably by interference with potential scattering, the resonance energy was determined by fitting a theoretical curve.

Column 4 of Table I gives values of the (n,p) and (n,α) cross sections at each resonance based essentially on the absolute measurements of Johnson and Barschall,[3] but with corrections and additional estimates for the weak resonances based on Roseborough *et al.*[4] Column 4 shows also S_t, the total resonant cross section for neutrons measured in the present work. Experimentally, the definition of S_t is somewhat arbitrary. In the energy range under consideration, resonances produced by s-neutrons show a pronounced interference "dip" at energies below resonance, and for these S_t(exp) has been defined as the difference between the maximum and minimum values of the total cross section. For p-neutrons the "dip" is much smaller and it is negligible for higher angular momenta. In these cases, S_t(exp) has been taken as the height of the maximum value of σ_t, above the estimated "background" level. The values given are in some cases averages of the data from both liquid nitrogen and LiN_3 scatterers. Corrections have been applied to the measured values of S_t to take account of the finite value of the resolution employed.

Column 5 of Table I gives $S_{n,n}$(exp), the experimental value of the resonant elastic scattering cross section obtained by subtracting from S_t(exp) the appropriate values of the (n,p) and (n,α) cross sections.

Column 6 gives the natural resonance width, Γ, in the laboratory reference system, calculated from the relation $\Gamma^2=\Gamma_m^2-\Delta^2$, in which Γ_m is the measured width of a resonance and Δ is the resolution width. Including the effects of target thickness, proton energy spread, and variation of neutron energy with angle, the resolution width was 3.8 kev for the measurement of resonance No. 1 and about 5 kev for the remainder of the work with LiN_3; it was 11 kev at resonances Nos. 9 and 10, covered only with the liquid nitrogen scatterer. In cases where it was deemed more accurate, Γ was taken from the work on the $C^{14}(p,n)$ reaction.[4] There is a discrepancy in the data for the narrow resonance No. 1 with the two scatterers. We believe the results with LiN_3 are more reliable, since in this case the experimental resolution was determined directly by an independent measurement of the even sharper resonance at 585 kev in sulfur, for which $\Gamma=1.3$ to 1.5 kev.[11] In the earlier work with liquid nitrogen the resolution width, the result largely of the target thickness, was estimated by the neutron yield method. Oxidation or diffusion, after running for some hours,

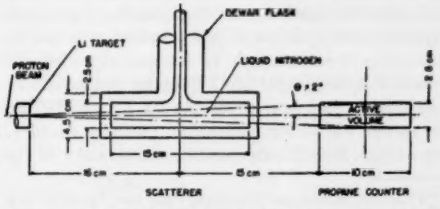

FIG. 2. Experimental arrangement for the measurement of the total neutron cross section of nitrogen. The scatterer is liquid nitrogen in a special Dewar flask.

[9] R. K. Adair, Phys. Rev. **79**, 1018 (1950).
[10] P. H. Stelson and W. M. Preston, Phys. Rev. **84**, 162 (1951).
[11] Peterson, Barschall, and Bockelman, Phys. Rev. **79**, 593 (1950).

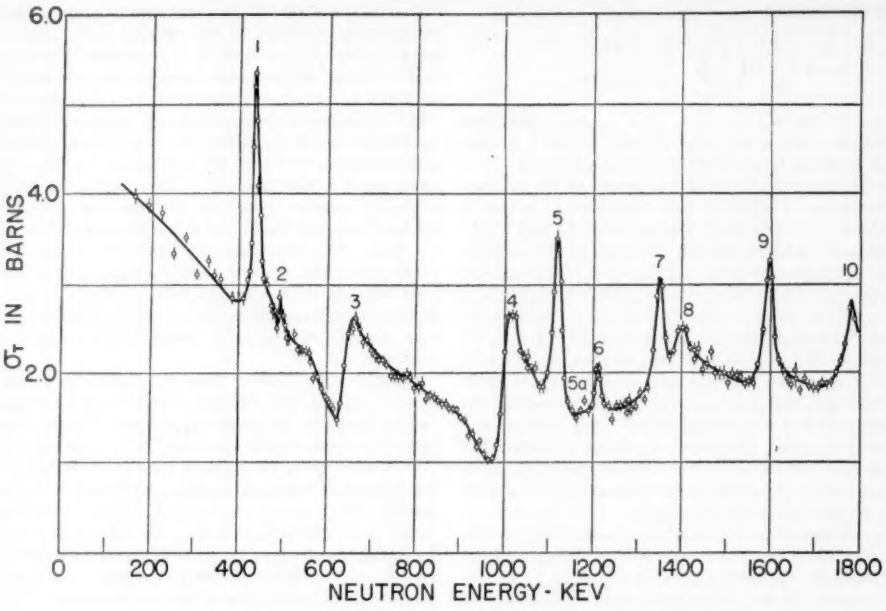

FIG. 3. Total neutron cross section of nitrogen *vs* incident neutron energy in the laboratory coordinate system. Scatterer: liquid nitrogen.

may have significantly increased the effective target thickness.

III. THEORETICAL CROSS SECTION CALCULATIONS

We have used the theory of nuclear reactions as formulated by Feshbach, Peaslee, and Weisskopf,[12] by Blatt and Weisskopf,[13] and by Feld *et al.*[14] The single-level Breit-Wigner formula gives

$$S_J^l(a,b)=4\pi\lambda_a^2(2l+1)g_J{}^l\Gamma_a{}^l\Gamma_b{}^{l'}/\Gamma^2, \qquad (1)$$

where $S_J^l(a,b)$ is the maximum value of the cross section for the reaction: particle a (angular momentum l, spin i, wavelength $2\pi\lambda_a$ in the center-of-mass coordinate system)+nucleus (spin I)→compound nucleus (in a state of spin J)→particle b (angular momentum l')+residual nucleus (state with spin I'). $\Gamma_a{}^l$ and $\Gamma_b{}^{l'}$ are the partial widths for emission of particles a and b, respectively, from the compound nucleus, and Γ is the total width of the resonance J. The statistical weight factor is

$$g_J{}^l=(2J+1)/[(2i+1)(2I+1)(2l+1)]. \qquad (2)$$

It is evident that the important information concerning the nucleus is contained in the partial widths. Theory suggests that these be broken down into two factors,

$$\Gamma_a{}^l=T_a{}^l(D_J{}^a/2\pi), \quad \Gamma_b{}^{l'}=T_b{}^{l'}(D_J{}^b/2\pi), \qquad (3)$$

where $T_a{}^l$ is the probability that an incoming particle will penetrate the centrifugal and Coulomb potential barriers and enter the nucleus. In principle, it is a calculable quantity for neutrons and charged particles. The quantity D_J represents the basic nuclear factor and is related to Wigner's "reduced" width, "γ^2".[15] The statistical theory indicates that D_J should be approximately equal to the average spacing between levels of the compound nucleus, in the neighborhood of the resonance under consideration, and of the same spin J and parity π. However, little is known about the variations in D_J.

[12] Feshbach, Peaslee, and Weisskopf, Phys. Rev. 71, 145 (1947).
[13] J. M. Blatt and V. F. Weisskopf, Laboratory for Nuclear Science and Engineering, MIT, Cambridge, Massachusetts, Technical Report No. 42.
[14] Feld, Feshbach, Goldberger, Goldstein, and Weisskopf, "Final report of the fast neutron data project," USAEC Report No. NYO-636, January 31, 1951.
[15] E. P. Wigner, Am. J. Phys. 17, 99 (1949). Our $D_J=(\pi/\lambda_0)\gamma^2$, where λ_0 is the particle wavelength inside the nucleus.

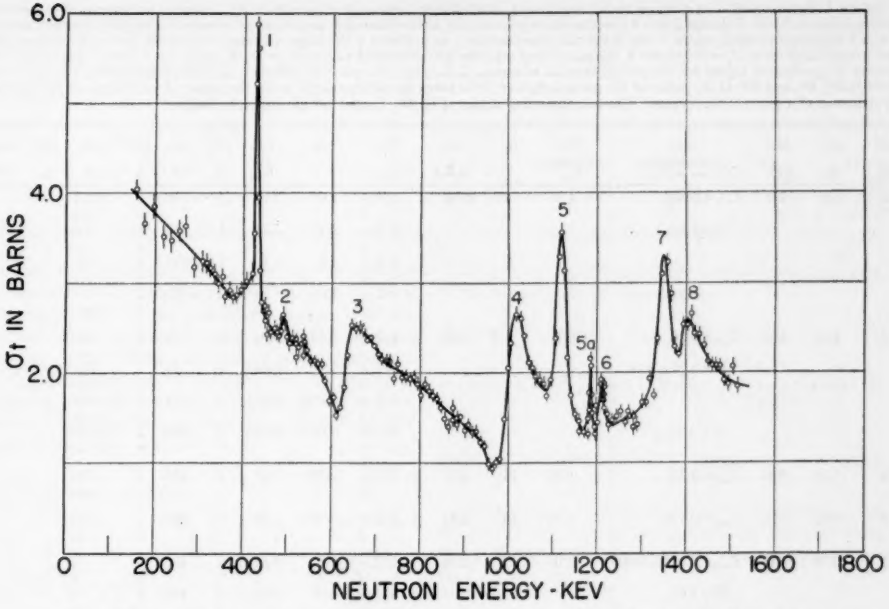

FIG. 4. Total neutron cross section of nitrogen vs incident neutron energy in the laboratory coordinate system. Scatterer: lithium azide.

The quantities T_n^l for neutrons are computed from the formula

$$T_n^l=\frac{4xx_0}{x_0^2|v_l|^2+x^2|v_l'|^2+2xx_0} \tag{4}$$

$$\begin{aligned} &|v_0|^2=1 && |v_0'|^2=1\\ &|v_1|^2=(1+x^2)/x^2 && |v_1'|^2=(1-x^{-2})^2+x^{-2}\\ &|v_2|^2=(9+3x^2+x^4)/x^4 && |v_2'|^2=(1-6x^{-2})^2+(6x^{-3}-3x^{-2})^2\\ &|v_3|^2=(225+45x^2+6x^4+x^6)/x^6 && |v_3'|^2=(1-21x^{-2}+45x^{-4})^2+(45x^{-3}-6x^{-1})^2. \end{aligned} \tag{5}$$

The quantity $x=R/\lambda_n$, and except where noted we have used the simple relation for the radius of nuclear interaction, $R=1.5A^{\frac{1}{3}}\times10^{-13}$ cm, for calculations involving neutrons or protons (A is the atomic weight). $x_0=R(1/\lambda_n^2+1/\lambda_0^2)^{\frac{1}{2}}$ where λ_0 is the wavelength of a neutron in the nucleus. We have used the value $\lambda_0=1\times10^{-13}$ cm, corresponding to a kinetic energy in the nucleus of about 20 Mev.[12] In Fig. 5 we have plotted T_n^0, T_n^1, and T_n^2 as functions of neutron energy in the center-of-mass system, for N^{15}.

The quantities T_p^l for protons have been calculated using a formula identical with Eq. (4). The quantities $|v_l|^2$ and $|v_l'|^2$ are defined for charged particles by

$$|v_l|^2=F_l^2+G_l^2, \quad |v_l'|^2=F_l'^2+G_l'^2. \tag{6}$$

The definitions of the functions F_l, F_l', G_l, and G_l' are given in Bloch *et al.*,[16] and they have been calculated, using tables of Coulomb wave functions,[17] for the case of protons incident on C^{14}, and for values of l up to 3. The corresponding values of T_p^l are plotted in Fig. 5.

The cross section for potential scattering of neutrons is given by

$$\sigma_{\text{pot}}^l=4\pi\lambda_n^2(2l+1)\sin^2\delta_l \tag{7}$$

and the phase constants δ_l are given by

$$\begin{aligned} &\delta_0=x,\\ &\delta_1=x-\tfrac{1}{2}\pi+\cot^{-1}x,\\ &\delta_2=x-\pi+\cot^{-1}[(x^2-3)/3x]. \end{aligned} \tag{8}$$

[16] I. Bloch, *et al.*, Phys. Rev. **80**, 553 (1950).
[17] Bloch, Hull, Broyles, Bouricius, Freeman, and Breit, Revs. Modern Phys. **23**, 147 (1951).

TABLE I. Summary of data relating to N^{15} resonances, derived from neutron reactions with N^{14}. Energies are expressed in kev and cross sections in barns. Columns 2 and 3 give the resonance energies, in the laboratory and center-of-mass systems, respectively. Columns 4 and 5 give experimental values of the maximum cross sections, and column 6 the observed resonance width. For each assumed spin and parity assignment, J, π in column 8, the succeeding columns list: calculated values of $\gamma=\Gamma_n/\Gamma$ and of the resonant scattering cross section $S_{n,n}$; required values for the orbital angular momenta l_n, l_p, and l_α for particle emission; and the corresponding effective levels pacings D^n, D^p, and D^α. If the parity of the ground state of N^{14} is taken as odd, instead of even, the parity of each state in N^{15} (formed by neutrons of a given l_n) is reversed. The corresponding values of l_p, D^p, l_α, and D^α are shown in italics.

(1) No.	(2) E_R	(3) E_R'	(4) Experimental cross sections	(5) Exptal. $S_{n,n}$	(6) Γ	(7) $4\pi\lambda\!\!\!^{-2}$	(8) J,π	(9) γ	(10) Calc. $S_{n,n}$	(11) l_n	(12) D^n	(13) l_p	(14) D^p	(15) l_α	(16) D^α
1	430	401	$S_{n,p}<0.002$	4.8	3.5	6.52	1/2, o	1.0	2.17	1	250	1	<0.4		
							e					*0*	*<0.1*		
			$S_t=4.8\pm?$				3/2, o	1.0	4.34	1	250	1	<0.4		
							e					*2*	*<7*		
							5/2, o	1.0	6.5	1	250	3	<350		
							e					*2*	*<7*		
							5/2, e	1.0	6.5	2	7300	2	<7		
							o					*3*	*<550*		
2	492	459	$S_{n,p}=0.28$	<0.1	7.5	5.69	1/2, o	0.18	0.06	1	76	1	880		
							e					*0*	*$10		
			$S_t=0.26\pm0.10$				3/2, o	0.08	0.024	1	34	1	990		
							e					*2*	*17,000*		
							5/2, o	0.052	0.015	1	22	3	9×10^3		
							e					*2*	*18,000*		
							5/2, e	0.052	0.015	2	600	2	18,000		
							o					*3*	*9×10^3*		
3	639	596	$S_{n,p}=0.20$	1.06	43	4.37	*A* 1/2, e	0.836	1.15	0	440	0	200		
							o					*1*	*780*		
4	998	931	$S_{n,p}=0.020$	1.68	46	2.81	*A* 3/2, e	0.989	1.82	0	480	2	280		
							o					*1*	*85*		
5	1120	1045	$S_{n,p}=0.010\pm0.005$	2.00	19	2.50	1/2, o	1.0	0.81	1	400	1	4		
							e					*0*	*2*		
			$S_t=2.01$				*B* 3/2, o	1.0	1.62	1	400	1	4		
							e					*2*	*50*		
							*A** 5/2, o	1.0	2.43	1	400	3	1600		
							e					*2*	*50*		
							A 5/2, e	1.0	2.48	2	4300	2	50		
							o					*3*	*1600*		
5A	1188	1108	$S_{n,p}<0.01$	$\geqslant1.07$	$\leqslant3.2$	2.36	1/2, o	1.0	0.79	1	65	1	<1		
							e					*0*	*<0.5*		
			$S_t\geqslant1.1$				3/2, o	1.0	1.57	1	65	1	<1		
							e					*2*			
							5/2, o	1.0	2.36	1	65	3	<530		
							e					*2*	*<14*		
							5/2, e	1.0	2.36	2	650	2	<14		
							o					*3*	*<530*		
6	1211	1130	$S_{n,p}=0.010\pm0.005$	0.61	13	2.31	*A* 1/2, o	0.987	0.75	1	260	1	10		
							e					*0*	*4*		
			$S_t=0.62$												
7	1350	1260	$S_{n,p}=0.089$	1.70	22	2.07	1/2, o	0.847	0.48	1	330	1	120		
							e					*0*	*81*		
			$S_t=1.79$				3/2, o	0.931	1.16	1	360	1	53		
							e					*2*	*800*		
							A 5/2, o	0.955	1.83	1	370	3	9300		
							e					*2*	*350*		
							*A** 5/2, e	0.955	1.89	2	3100	2	330		
							o					*3*	*9300*		
8	1401	1308	$S_{n,p}=0.19$	0.81	54	2.00	1/2, o	*i*	—	—	—	—	—		
							e								
			$S_{n,\alpha}=0.03$				*A* 3/2, o	0.792	0.80	1	750	1	330	0	600
							e					*2*	*3000*	*1*	*2500*
			$S_t=1.03$				5/2, o	0.874	1.53	1	820	3	49,000	2	15,000
							e					*2*	*1760*	*1*	*1400*
9	1595	1489	$S_{n,p}=0.020\pm0.010$	1.54	22	1.75	1/2, o	0.964	0.52	1	340	1	22		
							e					*0*	*11*		
			$S_{n,\alpha}\leqslant0.01$				3/2, o	0.976	1.05	1	340	1	15		
							e					*2*	*100*		
			$S_t=1.56$				*A** 5/2, o	0.988	1.64	1	340	3	1500		
							e					*2*	*66*		
							A 5/2, e	0.988	1.72	2	2300	2	65		
							o					*3*	*1500*		

TABLE I.—(*Continued*).

(1) No.	(2) E_R	(3) E_R'	(4) Experimental cross sections	(5) Exptal. $S_{n,a}$	(6) Γ	(7) $4\pi\lambda_n^2$	(8) J, π	(9) γ	(10) Calc. $S_{n,a}$	(11) l_n	(12) D^a	(13) l_p	(14) D^a	(15) l_a	(16) D^a
10	1779	1661	$S_{n,p}=0.010$	0.74	24	1.57	1/2, o	*i*	—	—	—	—	—	—	—
							e								
			$S_{n,\alpha}=0.27\pm0.10$				3/2, o	*i*	—	—	—	—	—	—	—
							e								
			$S_t=1.02$				*A* 5/2, o	0.768	0.85	1	260	3	810	2	13,000
							e					*2*	*80*	*1*	*1700*
							A' 5/2, e	0.768	0.93	2	1500	2	36	1	1700
							o					*3*	*810*	*2*	*13,000*

Near a resonance for neutron scattering, the potential and resonance scattering interfere. In general, it is necessary to add to the (complex) amplitude of the resonance cross section a fraction g_J^l of the potential scattering coming from neutrons of angular momentum l; the remainder of the potential scattering is incoherent with the resonance scattering.[18] The total elastic scattering cross section in the neighborhood of a resonance of a state of spin J is

$$\sigma_J=4\pi\lambda_n^2\left\{\sum_l(2l+1)\sin^2\delta_l + \frac{2J+1}{2(2I+1)}\frac{\gamma}{\epsilon^2+1}\left[\gamma+2\sin\delta_l(\epsilon\cos\delta_l-\sin\delta_l)\right]\right\}, \quad (9)$$

where $\gamma=\Gamma_n^l/\Gamma$ and $\epsilon=(E_n-E_r)/\frac{1}{2}\Gamma$, E_n is the neutron energy, and E_r is the resonance energy. The first term is the potential scattering; it is summed over all values of l. The second term is expressed as a function of ϵ, the distance "off resonance" in units of $\Gamma/2$. In general, it has both positive and negative values and it approaches zero as $\epsilon\to\pm\infty$. It is evaluated for the lowest value of l which can contribute to the state J.[19]

The maximum and minimum values of the second term of Eq. (9) can be found by differentiation with respect to ϵ, assuming δ_l and γ are constant in the region of interest. (This is a good approximation if $E_R\gg\Gamma$.) They occur at the values ϵ_+ and ϵ_- which are the solutions of the equation,

$$\epsilon^2+\epsilon\left[\frac{\gamma+2\sin^2\delta_l}{\sin\delta_l\cos\delta_l}\right]-1=0. \quad (10)$$

By substitution of ϵ_+ and ϵ_- in Eq. (9), the maximum and minimum values of the cross section can be determined.

If only elastic scattering can occur, then $\gamma=1$ and the equations reduce to much simpler forms, equivalent to those given by Adair.[18] The maximum and minimum occur respectively at the energies:

$$E_{max}=E_r+\tfrac{1}{2}\Gamma\tan\delta_l; \quad E_{min}=E_r-\tfrac{1}{2}\Gamma\cot\delta_l \quad (11)$$

$$\sigma_J(\text{min})=4\pi\lambda_n^2\left\{\sum_l(2l+1)\sin^2\delta_l-\frac{(2J+1)}{2(2I+1)}\sin^2\delta_l\right\} \quad (12)$$

$$\sigma_J(\text{max})-\sigma_J(\text{min})=4\pi\lambda_n^2\frac{(2J+1)}{2(2I+1)}. \quad (13)$$

For low neutron energies, potential scattering except for $l=0$ is often negligible. In that case the maximum value of the resonant scattering cross section alone, for $l>0$, is given by

$$S_J^l(n,n)=4\pi\lambda_n^2\frac{(2J+1)}{2(2I+1)}\gamma^2. \quad (14)$$

IV. APPLICATION OF THE THEORY TO NITROGEN

Neutrons incident on N^{14} form virtual excited states of the compound nucleus N^{15}, each of which is characterized by a definite value of total angular momentum, J, and parity, π. The states which can be formed by neutrons with $l_n=0$, 1, 2, and 3 are listed in Table II. At excitation energies of the compound nucleus above

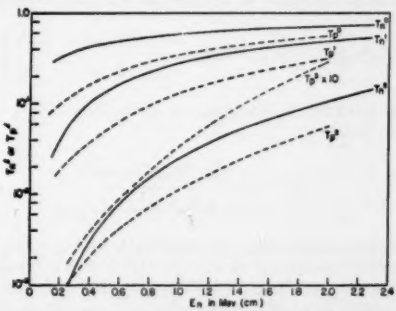

FIG. 5. Calculated barrier penetration factors, T_n^l and T_p^l, for the emission of neutrons and protons of angular momentum l from the nucleus N^{15}. The abscissa gives the neutron energy E_n in the center-of-mass coordinate system and hence the excitation energy of N^{15} above the neutron binding energy. The corresponding proton energy is $E_p'=E_n+Q$, where $Q=626$ kev.

[18] R. K. Adair, Revs. Modern Phys. **22**, 249 (1950). The treatment by Adair assumes that $\Gamma\approx\Gamma_n^l$; we have generalized it to include cases, where $\Gamma=\Gamma_n^l+\Gamma_p^l+\cdots$.

[19] Because of parity restrictions, if l is the lowest value of the angular momentum of neutrons which can form the state J, then only $l+2$, $l+4$, $\cdots$ neutrons can contribute also. At moderate energies, the contribution of $l+2$ neutrons is often negligible relative to that of l neutrons.

TABLE II. Total angular momentum J and parity π (o=odd parity, e=even) of the states of N^{15}. For a given target nucleus in a state of spin I, parity π_I, the table lists the states J, π which can be formed by incident particles of spin i, parity π_i, for various values of the orbital angular momentum l of the incident particle. The parity of N^{15} is assumed to be even.

Target I, π_I	Incident particle i, π_i	$l=0$	$l=1$	$l=2$	$l=3$
N^{14} 1, e	n 1/2, e	1/2, e	1/2, o	1/2, e	3/2, o
		3/2, e	3/2, o	3/2, e	5/2, o
			5/2, o	5/2, e	7/2, o
				7/2, e	9/2, o
C^{14} 0, e	p 1/2, e	1/2, e	1/2, o	3/2, e	5/2, o
			3/2, o	5/2, e	7/2, o
B^{11} 3/2, o	α 0, e	3/2, o	1/2, e	1/2, o	
			3/2, e	3/2, o	
			5/2, e	5/2, o	
				7/2, o	

10.99 Mev, these states are energetically able to decay by emission of a neutron, a proton (leaving C^{14}), an α-particle (leaving B^{11}), or a γ-ray. Analysis is simplified by the fact that N^{14}, C^{14} and B^{11} must be left in their ground states over the energy range considered in the present experiment, since the first excited states of these nuclei lie 2.3, 5.6, and 2.14 Mev, respectively, above the ground states. Also the γ-ray emission probability is small relative to that for particles, and can be neglected.

Table II shows also the states of N^{15} formed by $p+C^{14}$ and by $\alpha+B^{11}$, for various values of l.[20] Since formation and decay are inverse processes, we see from Table II that the state (5/2, o), for example, can be formed by $l=1$ neutrons on N^{14}, and can decay by the emission of $l=3$ protons or $l=2$ α-particles.[21]

Returning now to Table I, column (9) lists, for each observed resonance, values of $\gamma=\Gamma_n/\Gamma$ calculated as follows: we assume that the total level width $\Gamma=\Gamma_n+\Gamma_\alpha+\Gamma_p$. Then from Eq. (1) the sum of the maximum values at resonance of the n,p and n,α cross sections is

$$S_J(n,p)+S_J(n,\alpha)=4\pi\lambda_n^2\frac{(2J+1)}{6}\left[\frac{\Gamma_n\Gamma_p}{\Gamma^2}+\frac{\Gamma_n\Gamma_\alpha}{\Gamma^2}\right].$$

The quantity in brackets can be written as $\gamma(1-\gamma)$, from which

$$\gamma(1-\gamma)=\frac{S_J(n,p)+S_J(n,\alpha)}{4\pi\lambda_n^2\cdot\frac{1}{6}(2J+1)}. \qquad (15)$$

For each resonance, we substitute in Eq. (15) the experimental values of $S_J(n,p)$ and $S_J(n,\alpha)$. For each value assumed for J, in column (8), Eq. (15) yields a quadratic in γ. Of the two solutions, one can be eliminated by comparison with the observed cross sections, the other is entered in column (9). In column (10) of Table I we list the calculated value of the resonance scattering cross section, $S_{n,n}$(calc), for each of the possible assignments (J,π).

Using Table II, we can determine the lowest angular momenta l_n, l_p, and l_α of the neutron, proton, or α-particle which can be emitted from each state J,π. These values are listed in columns (11), (13), and (15) of Table I. In the adjacent columns are the corresponding values of the level spacing, D_J, for each particle and state, calculated from Eq. (3). (The partial widths are obtained from the ratios of the partial cross sections and the relation $\Gamma_p+\Gamma_\alpha+\Gamma_n=\Gamma$, where Γ is the total level width observed experimentally.)

V. DISCUSSION OF RESULTS

A. Assignment of J-Values

As shown in the last section, the assignment of J-values to the resonance levels of N^{15} depends primarily on a comparison of the experimental and computed elastic scattering cross sections at resonance. However, the experimental values for the (n,p) and (n,α) cross sections enter into the calculation of $S_{n,n}$(calc) through the quantity $\gamma=\Gamma_n/\Gamma$. In many cases, $\gamma\approx1$, but it is an important correction for resonances Nos. 3, 8, and 10. As indicated by the symbol "i" in column (9) of Table I, γ is imaginary for $J=1/2$ or 3/2 at No. 10.[22] Resonance No. 2 is exceptional; it is the only one of the eleven resonances for which γ has the lower value of the two solutions of Eq. (15), corresponding to a scattering cross section smaller than the reaction cross section.

Referring to Table I, $S_{n,n}$(exp) is in no case greater than the value computed for $J=5/2$. Thus, there is no direct evidence for states in N^{15} formed by neutrons of $l_n>1$. The most reasonable J-value, based on a comparison of $S_{n,n}$(exp) and $S_{n,n}$(calc), is indicated for each resonance by the letter A. B indicates a less probable assignment, but one judged to be within the range of possible experimental error. No assignment is possible for No. 2, since $S_{n,n}$ was too small to measure. Nos. 1 and 5A are so narrow that the correction for resolution width is uncertain, but $J>1/2$ in both cases. For No. 5, the value of $S_{n,n}$(exp) lies about halfway between those computed for $J=3/2$ and $J=5/2$, an unexpectedly large disagreement. The remainder agree with the A-assignments within 0.2 barn, averaging 0.1 barn lower than the calculated values.

B. Assignment of Parity

The assignment of parity to a state of N^{15} is equivalent to determining the orbital angular momentum l_n

[20] We assume here even parity for N^{14}, although the evidence is conflicting. This is discussed below.

[21] The (5/2, o) state can also be formed by, or can emit, neutrons of $l=3$. The great difference in barrier penetration factors allows us to neglect this process at moderate energies.

[22] The reaction cross section cannot be larger than $\pi\lambda^2(2J+1)/6$; this sets a lower limit on J. The large correction which we have applied to Johnson and Barschall's value of $S_{n,\alpha}$ for resonance No. 10, because of poor resolution, makes the conclusion that $J>3/2$ very tentative. We have assumed a resolution width of 45 kev. (C. H. Johnson, private communication.)

of the neutron by which it is formed from N^{14}. In the present energy range the S-wave potential scattering is considerably larger than that resulting from neutrons of $l_n>0$. The resulting large "interference dip" at $(1/2, e)$ and $(3/2, e)$ resonances ($l_n=0$) distinguishes them at once from the $(1/2, o)$ and $(3/2, o)$ states ($l_n=1$). A state $J=5/2$, however, can be formed by neutrons of $l_n=1$ or 2. At resonance No. 9, the interference dip is at most 0.08 barn for $J=5/2$, $l_n=1$, while it is negligible for $l_n=2$. The difference is experimentally indistinguishable, so that the parity cannot be determined in this manner.

C. The Level Spaicng D

We may call the quantities $D_{J,\pi}{}^n$, $D_{J,\pi}{}^p$, and $D_{J,\pi}{}^\alpha$ the effective level spacings, for a particular resonance, for neutrons, protons, and α-particles. Whatever their connection with the actual separation in energy of resonance levels of the same type, the D's contain implicitly the unknown matrix elements associated with each transition. They are subject to the upper limit imposed on Wigner's reduced width[15]

$$D\leqslant 3\pi\hbar^2/2MR\lambda_0,$$

where M is the particle mass and λ_0 its wavelength in the nucleus. For N^{15}, this requires that D^n and $D^p\leqslant 53$ Mev, $D^\alpha<13$ Mev, if we set $\lambda_0=1\times10^{13}$ cm for all three particles. These upper limits are not of much help, in the present case, in assigning parities. For resonance No. 10, D^α has its limiting value for $J=5/2$ and parity odd, but the uncertainty both in the (n,α) cross section and in the barrier penetration calculations makes this indecisive.

We have observed 11 resonances altogether in a range of 1600 kev, or an average level spacing $\bar{D}=145$ kev. Most of these resonances can be reasonably assigned to 5, or, at most, 6 states. We may therefore suppose that an order of magnitude estimate of the average value of $D_{J,\pi}$ will be given by $\bar{D}_{J,\pi}=5\times145=725$ kev.

In Table I, in the four cases for which the most reasonable assignment is $J=5/2$, let us choose the parity which makes the values of $D_{J,\pi}$ nearer to 700 kev, as indicated by A^*. Omitting the data for resonances Nos. 1, 2, and 5A, the remaining eight then give as an estimate of the minimum range of variation of the D's:

D^n	260–3100 kev, average	900 kev	(8 resonances)
D^p	9–1600 kev, average	540 kev	(8 resonances)
D^α	600–1700 kev, average	1150 kev	(2 resonances).

Of the three resonances omitted, Nos. 1 and 5A either have very low values of D^p, or $S_{n,n}(\text{exp})$ has been considerably underestimated; nothing definite can be said of No. 2.

D. The Parity of N^{14}

The shell model predicts that the ground states of N^{14} and C^{14} both have even parity, but this has been questioned by Gerjuoy[23] and others. In Table I, we have indicated in italics the parity assignments which apply if the ground state of N^{14} is assumed to have odd parity, and the corresponding values of l_p, D^p, l_α, and D^α. Because of the large variation of D^p in either case, there seems to be little reason to favor one parity or the other. However, it may be pointed out that the small (n,p) cross section of resonance No. 4, relative to No. 3, is perhaps more naturally explained by the difference in barrier penetration factors, which follows if C^{14} and N^{14} have the same parity, rather than by attributing it to a large difference in the D-values, as in the case of opposite parity.

E. The Interaction Radius R

There is considerable uncertainty about the magnitude of the interaction radius R. For neutrons and protons, we have used the relation $R=1.5A^{\frac{1}{3}}\times10^{-13}$ cm, which gives $R=3.7\times10^{-13}$ cm for $A=15$. We have taken $R=5.35\times10^{-13}$ cm for calculations involving α-particles. To illustrate the dependence of the barrier penetration factors, T, on the interaction radius, we have recalculated them for neutrons and protons using $R=4.9\times10^{-13}$ cm.[24] The ratios of the penetration factors for the two radii are plotted in Fig. 6 as a function of neutron energy; they are large for higher angular momenta. Use of the larger radius would lower the computed D-values and their minimum range of variation.

Figure 7 shows the result of subtracting off from the total cross section of nitrogen the contributions of the known resonances. The calculated potential scattering is shown for comparison. The large residual cross section below 1 Mev presumably comes in part from an S-

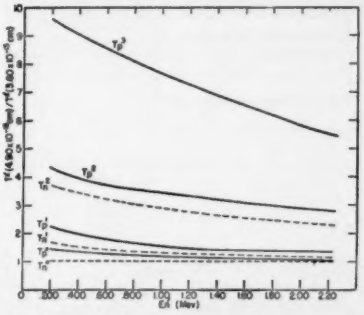

FIG. 6. The ratio of the calculated values of the barrier penetration factor, T, for N^{15}, for two assumed values of the interaction radius R (4.90×10^{-13} cm and 3.60×10^{-13} cm) plotted as a function of the incident neutron energy in the center of mass coordinate system. The subscripts p and n refer to protons and neutrons, respectively, the superscripts give the angular momentum l.

[23] E. Gerjuoy, Phys. Rev. **81**, 62 (1951).

[24] This value is given by $R=1.4(A^{\frac{1}{3}}+1)\times10^{-13}$ cm, $A=14$, as used by R. F. Christy and R. Latter, Revs. Modern Phys. **20**, 185 (1948).

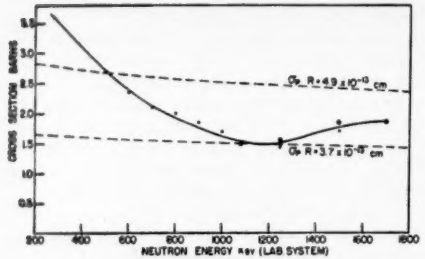

FIG. 7. The solid line is the residual cross section of nitrogen, after subtracting from the total cross section the contributions of the observed resonances. Circled points were computed from data taken with the liquid nitrogen scatterer, the remainder from LiN_3 data. The dashed curves show the computed potential scattering cross section for two values of the interaction radius R.

resonance below 0.2 Mev, since both its magnitude and slope are too great to be accounted for by potential scattering alone. The rise beyond 1.2 Mev seems real, but may be caused by some unknown systematic error. A radius $R=3.7\times10^{-13}$ cm gives a potential scattering cross section in good agreement with the observed value near $E_n=1200$ kev.

F. Comparison with Other Work

After this article was written, a paper on the total cross section of nitrogen by Johnson, Petree, and Adair[25] was published. Their measurements agree with ours very closely within the range covered by both experiments, 0.2 to 1.4 Mev, but with somewhat poorer resolution they did not observe the resonances which we have numbered 2, 5A, and 6. The agreement at both of the S-resonances (our Nos. 3 and 4) is within 0.1 barn for the measured cross sections and 1 kev for the resonance energies.

In conclusion, we wish to express our appreciation to Dr. Victor F. Weisskopf for many helpful discussions, to Dr. Herman Feshbach and Miss Mida Karakashian for aid in the computation of barrier penetration factors, and to Mr. Donald Thompson and Mr. I. E. Slawson for their invaluable help with the Rockefeller generator.

[25] Johnson, Petree, and Adair, Phys. Rev. **84**, 775 (1951).

The Electron Spectra Produced by a Co^{60} Source in Water*

EVANS HAYWARD
National Bureau of Standards, Washington, D. C.
(Received January 24, 1952)

The spectra of secondary electrons produced by a Co^{60} gamma-ray source have been measured at distances of 10, 20, 41.6, 81.6, 121.6, and 161.6 cm in a large tank of water. The pulse-height distribution representing the energy lost in an anthracene crystal was determined for each separation of detector and source. The shape of the spectrum was found to change appreciably with distance. The results agree remarkably well with theoretical predictions.

INTRODUCTION

As gamma-radiation penetrates matter, it interacts with it through the photoelectric effect, Compton scattering, and pair production, the predominance of one effect over the others depending on the energy of the quanta and the atomic number of the material. Various calculations[1] have been made that give the general characteristics of the radiation such as intensity, energy, and angular distribution as a function of distance from the source, energy of incident radiation, and atomic number of the medium. Experimental determination of these quantities is difficult, since they should be measured in an infinite medium using detectors that do not appreciably disturb any of the quantities being observed. A measurement of radiation intensity as a function of distance from the source has recently been determined by White[2] for the Co^{60} radiation in water. It is now possible, since the development of scintillation spectroscopy, to measure with low resolution, the energy spectrum of the secondary electrons produced in an infinite medium as a function of distance from the source.

Since anthracene has an atomic number and density close to those of water, its absorption coefficient is practically the same as that of water and an anthracene crystal may be used to represent an equal mass of water. Thus, the distribution of pulse heights observed with an anthracene crystal would correspond to the energy distribution of the electrons produced in an equal mass of water occupying the same position, provided that none of the auxiliary measuring equipment distorts the spectrum.

EXPERIMENTAL DETAILS

The experimental arrangement is shown in Fig. 1. The experiment was performed in a large (12 ft×12 ft ×25 ft) tank of water so that there would be no boundary effects. The counter consisted of an anthracene crystal, Lucite light pipe, RCA 5819 photomultiplier tube, and cathode follower all enclosed in an aluminum and Lucite can; the cables came out of the water through a piece of copper pipe. The counter was designed to have its active volume surrounded by water-equivalent material, so that it would be separated from discontinuities such as the vacuum within the photomultiplier tube. A Lucite light pipe one inch in length separated the crystal from the photomultiplier tube and a Lucite cap fitted over the crystal, light pipe, and the top of the 5819 to protect them from the water. A thin piece of aluminum foil served as a reflector, and was introduced between the crystal and the Lucite cap. Both the source and the counter were suspended near the center of the water tank from a wooden rack.

The counter was designed to measure the energy of any electron that was produced in and totally absorbed by the anthracene crystal. Electrons created outside of, but scattered into the crystal, and those created inside, but ending outside of the crystal, produce a heightening at the low energy end and a lowering of the high energy end of the spectrum. A study of the shape of the

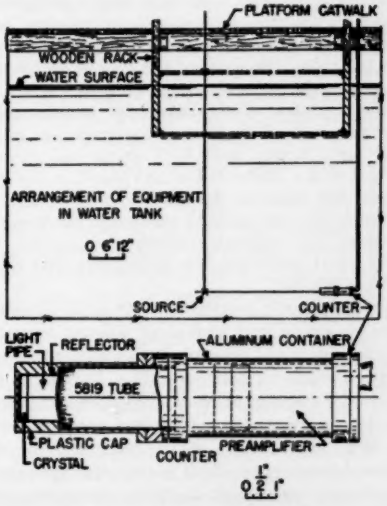

FIG. 1. The experimental arrangement.

* This work was supported by the ONR and AEC.
[1] L. V. Spencer and U. Fano, J. Research Natl. Bur. Standards 46, 446 (1951); Phys. Rev. 81, 464 (1951); L. V. Spencer and F. Stinson, Phys. Rev. 85, 662 (1952).
[2] Gladys R. White, Phys. Rev. 80, 154 (1950).

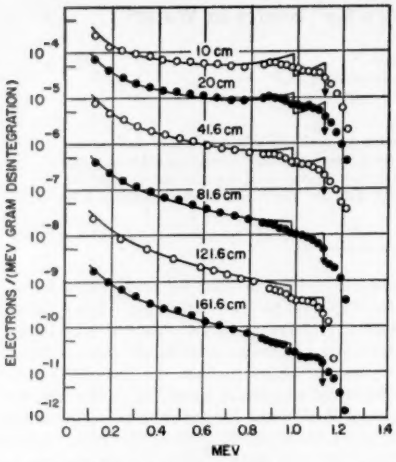

FIG. 2. The differential spectra of the electrons produced by a Co^{60} source as a function of the distance in water. The solid curves were calculated according to the method of Spencer and Fano (see reference 1).

spectrum as a function of crystal thickness showed the magnitude of this effect to be negligible. Checks were also made to be sure that the shape of the spectrum was sensitive neither to light pipe length, nor to the presence of a second photomultiplier tube close to the crystal.

The pulse from the preamplifier was fed into a linear amplifier, and then into a single channel differential pulse-height analyzer. The pulse-height analyzer observed the spectrum through a $1\frac{1}{2}$ volt window (corresponding to $\sim$18 kev) which was moved between 10 and 100 volts. The linearity and zero of the discriminator were checked with a pulse generator.

The resolution of the instrument was determined from the width of the internal conversion line of Cs^{137} (632 kev). A very weak Cs^{137} source was prepared, covered with a Formvar film and placed on top of the crystal and inside of the reflector, so that the beta-spectrum and the internal conversion electrons were observed. The pulse-height distribution resulting from the internal conversion line is Gaussian with a half-width of 110 kev.

Six Co^{60} sources ranging from 10^6 to 10^{11} disintegrations per second were used at six different separations between source and detector. It was necessary to use a different source for each separation, in order to have low enough counting rates to avoid "pile-up" from the very large number of low energy electrons characteristic of these spectra. The relative intensities of these sources have been measured in pairs and compared to a standard; their specific activities are known within $\pm$6 percent.

When a slowly and smoothly varying spectrum such as this, is measured with a low resolution device, the shape of the spectrum is changed very little except at points where discontinuities exist. For example, the Compton spectrum that is generated by a monochromatic gamma-ray falls sharply to zero after a pronounced peak at the maximum possible energy. This peak, when measured with a scintillation spectrometer, is smeared out, but the energy corresponding to the maximum electron energy may be taken with fair accuracy as the point of maximum slope.[3] In the early stages of the experiment Cs^{137}, as well as Co^{60} gamma-ray sources, were used to calibrate the instrument. Later it was found that the spectrum measured under actual operating conditions in the water tank fell off sharply at the point corresponding to the end of the Co^{60} spectrum and thus a separate calibration was eliminated.

RESULTS

The electron spectrum produced by the 1.17- and 1.33-Mev Co^{60} gamma-rays has been measured at 10, 20, 41.6, 81.6, 121.6, and 161.6 cm from the source. Figure 2 shows the six spectra plotted on semi-logarithmic paper.

The ordinates are given as the number of electrons per Mev interval, per disintegration of the source, and per gram of anthracene. In order to express the data in these units, it is necessary to know not only the counting rate but also the disintegration rate of the source and the window width of the discriminator. The standard error for the absolute intensities is $\pm$10 percent, due mostly to uncertainties in the determination of the latter two quantities. The energy scale of the abscissa was obtained by making a linear plot of the data and taking the two points of inflection at the end of the spectrum as corresponding to 0.96 and 1.12 Mev, the maximum energy Compton electrons that can result from the 1.17- and 1.33-Mev gamma-rays. This calibration is good to about $\pm$1.5 percent. The standard deviations based on the number of counts are all less than $\pm$5 percent and almost all less than $\pm$3 percent. The background was negligible, since the large mass of water provides an excellent shield to stray radiation.

The solid curves in Fig. 2 were calculated according to the methods outlined in reference 1 and were very kindly supplied by Dr. L. V. Spencer. It is clear that the experimental data have the same general characteristics as the theory predicts; the measured spectrum changes with penetration in the same way as the theoretical one and the absolute intensities agree very well.

At 10 cm the high energy end of the spectrum is quite intense, and the two peaks corresponding to the two gamma-rays are obvious. At greater distances, the energy loss becomes more and more concentrated in

[3] P. R. Bell and J. M. Cassidy, Phys. Rev. **77**, 409 (1950).

the lower energy electrons and the rate at which the spectrum changes becomes less and less. In fact, at distances of a meter or more, the changes in the shape of the spectrum are too small to be measured with this low resolution spectrometer.

White[2] has already made some measurements in a similar experiment, using shielded ionization chambers, and found that the spectrum is still changing as far out from the source as 135 cm. These data do not, however, contradict the results of the present experiment since the ionization chambers are sensitive mostly to very soft radiation, so soft in fact as to have had no effect in this experiment. Furthermore, the spectra of photons calculated by Spencer and Fano[1] show the features of both experiments. The calculated spectra show a peak below 100 kev the height of which, relative to the high energy portion of the spectrum, is still changing at large distances; this component is primarily the one measured by White.[2] On the other hand, the shape of the calculated spectra at high energies change very slowly with distance, too slowly for any variation to be observed with the spectrometer used in the present experiment.

The author wishes to thank Mr. Eaton and the staff of the Hydraulics Laboratory for their hospitality and for their many courtesies. It is a pleasure to thank both Dr. U. Fano and Dr. L. V. Spencer for their many illuminating discussions.

PHYSICAL REVIEW VOLUME 86, NUMBER 4 MAY 15, 1952

The Radial Distribution Function in Liquid Helium*

P. J. PRICE
Department of Chemistry, Duke University, Durham, North Carolina
(Received January 10, 1952)

It is pointed out that the Ornstein-Zernike-Gibbs formula, which is commonly used to connect the intensity of coherent scattering of radiation in a liquid with the thermodynamic functions, is not valid for liquid helium. Alternative formulas involving the radial distribution function are discussed.

IN the coherent scattering of radiation by a monatomic liquid, the scattered intensity is proportional to[1]

$$1+n\int[g(r)-1]e^{i(\mathbf{k}_1-\mathbf{k}_2)\cdot\mathbf{r}}d^3\mathbf{r}, \tag{1}$$

where n is the number density, $g(r)$ the radial distribution function, and $\mathbf{k}_1$ and $\mathbf{k}_2$ the incident and scattered wave vectors. Consequently, for large wavelengths the scattering cross section is multiplied by the factor

$$S(T)\equiv 1+n\int_a^\infty (g-1)4\pi r^2 dr, \tag{2}$$

and the scattered intensity can be related to the thermodynamic magnitudes of the liquid by the formula

$$S=nkT\chi_T, \tag{3}$$

where χ_T is the isothermal compressibility. This formula (3) is valid for "classical" conditions, but has recently been applied to the analysis of scattering in liquid helium.[2]

It is the present purpose to point out that this application to a *quantum* liquid is incorrect. To see this, we break down (3) into the two equations from which it derives. Consider a small fixed cell of volume v in the liquid, which is supposed homogeneous, and define the function $f(\mathbf{r})$ such that f is unity when $\mathbf{r}$ ends in the cell and zero otherwise; and hence the function $F=\sum_i f(\mathbf{r}_i)$, summed over the position-vectors $\mathbf{r}_i$ of the atoms, whose expectation is the average of the number of atoms in the cell, $\langle F\rangle=\overline{F}_{ii}=nv$. Then the fluctuation of the expectation of F, over the probability distribution of the $\mathbf{r}_i$, can be shown to be given by (2):

$$[\langle F^2\rangle-\langle F\rangle^2]/\langle F\rangle=S. \tag{4}$$

This result (4) is true equally for "classical" and "quantum" conditions [as is (1)], and depends on the assumptions that (i) there is a radius a beyond which $g(r)$ tends to its (normalized) limit of unity, and such that $\int_a^\infty(g-1)4\pi r^2dr$ is negligible; and (ii) v is large compared with $4\pi a^3/3$ and small compared with the volume of the whole liquid. For a quantum liquid the left-hand side of (4) must remain finite even at absolute zero, owing to the zero-point motion of the atoms, since the probability distribution of the atoms is essentially positive. This shows that (3) cannot then be true, since for a quantum liquid $n\chi_T$ remains finite, and hence $nkT\chi_T$ becomes zero, when $T\to 0$. Another case to which the same argument applies is that of the ideal Fermi gas. To arrive at (3) we would have to combine (4) with

* This work was begun at the Royal Society Mond Laboratory, Cambridge, England, where it was supported by the Department of Scientific and Industrial Research, and it was completed under contract between the ONR and Duke University. I would like to express my thanks to Professor F. London for the hospitality of his department.

[1] A general reference on the results (1)–(5) is: J. de Boer, Reports on Progress in Physics **12**, 305 (1949), §10.

[2] Goldstein, Sommers, King, and Hoffman, Proceedings of the International Conference on Low Temperature Physics, Oxford, 1951, p. 88; see L. Goldstein, Phys. Rev. **84**, 466 (1951), Fig. 1.

the Gibbs formula for the fluctuation of the number of atoms N_v in the cell,

$$[\overline{N_v^2}-(\overline{N_v})^2]/\overline{N_v}=nkT\chi_T, \tag{5}$$

by equating their left-hand sides. It is this step which is clearly not permissible in general, because (5) refers to a thermal fluctuation *between* different quantum states (what is meant by "fluctuation" in statistical thermodynamics); while the average $\langle\ \rangle$ in (4) is given by a trace of the von Neumann density matrix, and at absolute zero becomes an expectation of the ground state. There is no difference when the variable in question is the energy, or another constant of the motion, but for the local density these two fluctuations are the same only in the classical (high temperature) limit.

In the absence of an adequate understanding of the excitations of a quantum liquid, an at least plausible formula to replace (3) in the low temperature range may be constructed as follows. We suppose that only "phonon" excitations are involved in the density fluctuation, and attribute $S(T)-S(0)$ to their effect. A phonon causes a fluctuation of the mass density ρ, for which we suppose the macroscopic formula

$$\text{energy density}=c^2\overline{(\delta\rho)^2}/\rho, \tag{6}$$

where c is the velocity of sound, to hold.[3] Accordingly, putting $U\equiv E(T)-E(0)$, where E is the total energy density, we would expect

$$S(T)-S(0)=U_{\text{phon}}/\rho c^2 \tag{7}$$

to give the variation of (2) at low temperatures. Using the specific heat data of Kramers[4] for liquid helium, (7) gives

$$S(T)-S(0)=1.05\times10^{-4}\ \text{deg}^{-4}T^4. \tag{7'}$$

The tentative formula (7) may be compared with an exact one, valid for both classical and quantum conditions. If K is the kinetic-energy density and $\phi(r)$ the potential of the interaction between two atoms, then the energy equation gives

$$E=K+\tfrac{1}{2}n^2\int g(r)\phi(r)d^3\mathbf{r},$$

and the virial theorem[5] gives

$$3p=2K-\tfrac{1}{2}n^2\int g(r)r\phi'(r)d^3\mathbf{r}.$$

Eliminating K between these two equations,

$$2E-3p=\tfrac{1}{2}n^2\int g(r)[2\phi+r\phi']d^3\mathbf{r}. \tag{8}$$

From Kramers' results, the change in $g(r)$ below 0.6° implied by (8) is consistent with that given by (7'), in dependence on T^4, and also in order of magnitude. The implications of (8) at higher temperatures are also of interest. For liquid helium at saturated vapor pressure the left-hand side of (8) is -43.7 atmos at absolute zero, and increases by 0.3 atmos up to 1.4° and by a further 7.8 atmos between 1.4° and the lambda-point. This large increase of (8), and hence appreciable change in $g(r)$, in the high temperature range of helium II suggests (if (7) is correct at lower temperatures) that either the other kinds of excitation of the liquid also induce density fluctuations or they are strongly coupled to the "phonons" so that the energy contribution of the latter increases faster than the Debye expression. The increase of (8) seems to demand a large change in $g(r)$ between 3 and 6A. On the other hand the absence of a latent heat at the lambda-transition implies, by (8), that $g(r)$ is continuous through it, as expected.

Applied to a gas, (3) leads to an expression for the second virial coefficient,

$$B(T)=\lim_{n\to0}\left\{\tfrac{1}{2}N\int[1-g(r)]d^3\mathbf{r}\right\}, \tag{9}$$

which has been used[6] to obtain a formula for $B(T)$ under quantum conditions. It appears from the discussion above that this application of (9) is not permissible.

Note added in proof:—It is conceivable that a (the range beyond which $g=1$) is, for liquid helium, some orders of magnitude greater than the range of ϕ, corresponding to a long-range order of quantal origin. This would lead to unusual effects in the scattering of radiation, in the soft x-ray to visible range; and would make possible anomalies in the scattering of light, as a function of temperature, not reflected in the left-hand side of Eq. (8).

[3] This step was made, long ago, for solids: A. Einstein, Ann. Physik **33**, 1275 (1910). It is curious how close this paper came to anticipating the Debye theory.

[4] H. C. Kramers, Proceedings of the International Conference on Low Temperature Physics, Oxford, 1951, page 93; and private communication.

[5] There has been some controversy over the applicability of the virial theorem in quantum conditions. See H. S. Green, Proc. Roy. Soc. (London) **A194**, 244 (1948); P. J. Price, Phil. Mag. **41**, 948 (1950).

[6] B. Beth and G. E. Uhlenbeck, Physica **4**, 915 (1937).

Second-Order Acoustic Fields: Streaming with Viscosity and Relaxation*

JORDAN J. MARKHAM†
Applied Physics Laboratory, Johns Hopkins University, Silver Spring, Maryland
(Received June 11, 1951)

The streaming caused by an acoustic field, which has been previously considered by Eckart, is re-examined. The concept of mass flow is introduced, and a relaxational relation, between the excess pressure and the excess density, is employed. Further, various proofs of Eckart are modified. The results are essentially the same as those given by Eckart except that they apply to the mass flow instead of the particle velocity. Also, an explicit frequency dependence of the flow is obtained which explains Liebermann's result in ethyl formate. In general to have an average mass flow, viscosity is needed, and the time average of the product of the density and the particle velocity, to second order, is solenoidal. The proof regarding mass flow is not sufficiently general to preclude the possibility of flow under every acoustic field.

I. INTRODUCTION

THE first basic approach to the problem of the second-order effects of acoustics was presented by Rayleigh.[1] More recently interest has been stimulated in this field by experiments of Liebermann[2] and by theoretical work of Eckart.[3] The latter has given a more general formulation of the problem and a clearer meaning to the various terms of the acoustic field equations than was done earlier.

A study of Eckart's theory has raised some questions concerning the meaning of some of his derivations.[4] For example, it can be shown that if Eckart's proof is applied to the mass flow (the mass crossing unit area per second) instead of to the particle velocity, one reaches the incorrect conclusion that there is no streaming even in a viscous fluid. Further, Eckart's theory does not explain the frequency dependence of the bulk viscosity coefficient found in ethyl formate.[5] In the present paper it will be shown that the basic physical conclusions of Eckart can be obtained in an alternative way.

The first point of difference between Eckart's theory and the one to be given here is that we shall focus attention on the mass flow of the fluid instead of on the particle velocity. It will be recalled that in the Eulerian system of coordinates, the frame of reference is fixed and so the particle velocity is associated with a point in the field and not with any single particle. Thus, the time average of the particle velocity need not be the same as the time average of the velocity of a single particle.

The second major modification is in the equation which relates the excess pressure to the excess density. We shall employ here the relaxational acoustical equation of state.[6] This leads to a natural explanation of the results on ethyl formate.[2]

Let us now derive some general relations for a sound field. First, we shall consider the case where there is no dissipation; later, we shall consider the effects of viscosity and relaxation. In many ways the development given here is similar to methods used in electromagnetic theory. The major difference is that here we have first- and second-order equations.

II. SOUND FIELD RELATIONS WITH NO DISSIPATION

We will now derive the basic equations governing the acoustic field for a medium with no dissipation in terms of the density, the pressure, and the mass flow. It will be shown that the radiation pressure of the field does not influence the mass flow, but governs the second order density distribution.

Basic Equation for an Acoustic Field

In a dissipationless fluid the three basic equations are:

(1) the equation of continuity of Euler,[7]

$$\partial\rho/\partial t+\nabla\cdot(\rho\mathbf{u})=0; \tag{1}$$

(2) with the help of (1), Euler's equation of motion,[7]

$$\partial(\rho\mathbf{u})/\partial t+\rho(\mathbf{u}\cdot\nabla)\mathbf{u}+\mathbf{u}[\nabla\cdot(\rho\mathbf{u})]=-\nabla p; \tag{2}$$

and (3) the nonabsorptive equation of state, obtained by assuming that $p=f(\rho)$ and using the first two terms of a Taylor expansion about the equilibrium values, namely,[8]

$$p_e=c_0^2\rho_e+\tfrac{1}{2}[\partial C^2/\partial\rho]_{\rho_0}\rho_e^2. \tag{3}$$

* This paper was supported by the Bureau of Ordnance, U. S. Navy.
† This paper was started when the author was at Brown University, Providence, Rhode Island.
[1] Lord Rayleigh, *The Theory of Sound* (MacMillan and Company, Ltd., London, 1940), Sec. 352.
[2] L. N. Liebermann, Phys. Rev. **75**, 1415 (1949).
[3] C. Eckart, Phys. Rev. **73**, 68 (1948).
[4] The author would like to thank Dr. P. J. Westervelt for pointing out some of the difficulties.
[5] Liebermann has artificially modified Eckart's theory to include the observed facts. The modifications seem hard to justify and indicate the necessity of a new approach.
[6] See for example Markham, Beyer, and Lindsay, Revs. Modern Phys. **23**, 353 (1951), particularly Secs. 13, 14, and 15.
[7] H. Lamb, *Hydrodynamics* (Dover Publications, New York, 1945), Chap. 1.
[8] The assumptions leading to (3) are not very general. First, it has no terms which allow for the streaming, i.e., one should follow a particle which is moving in the medium. The streaming does not seem to be important. (See a forthcoming paper in the Physical Review by the author.) Second, it assumes that the thermodynamic path is known. For the first-order terms the path is approximately isentropic but probably this assumption breaks down beyond the first order. We shall see shortly that a time-

The meaning of the symbols is:

ρ	the total density
$\rho_e=\rho-\rho_0$	the excess density
p	the total pressure
$p_e=p-p_0$	the excess pressure
$\mathbf{u}$	the velocity of a particle
$c_0^2=\partial p/\partial\rho$	evaluated at $\rho=\rho_0$.

In acoustics we are interested in situations where $\mathbf{u}$, p_e, and ρ_e are small, and therefore, following Eckart[3] we assume that one can find solutions by successive approximations—namely:

$$p=p_0+p_1+p_2\cdots,\quad \rho=\rho_0+\rho_1+\rho_2\cdots,$$
and
$$\mathbf{u}=0+\mathbf{u}_1+\mathbf{u}_2\cdots. \tag{4}$$

Here we shall consider the subscript zero to be of zeroth order, the subscript one of first order, and the subscript two of second order. A product of two first-order terms is assumed to give a second-order term, while a product of a zeroth-order term with a first- or second-order term does not affect the order.

The first-order equations, on which acoustics is usually based, are:

$$\partial\rho_1/\partial t+\rho_0\nabla\cdot\mathbf{u}_1=0; \tag{1.1}$$

$$\rho_0\partial\mathbf{u}_1/\partial t=-\nabla p_1; \tag{2.1}$$

and

$$p_1=c_0^2\rho_1. \tag{3.1}$$

The second-order equations are:

$$\partial\rho_2/\partial t+\rho_0(\nabla\cdot\mathbf{u}_2)+\nabla\cdot(\rho_1\mathbf{u}_1)=0; \tag{1.2}$$

$$\rho_0\partial\mathbf{u}_2/\partial t+\partial(\rho_1\mathbf{u}_1)/\partial t+\rho_0[(\mathbf{u}_1\cdot\nabla)\mathbf{u}_1+\mathbf{u}_1(\nabla\cdot\mathbf{u}_1)]=-\nabla p_2; \tag{2.2}$$

and

$$p_2=c_0^2\rho_2+[c\partial c/\partial\rho]_{\rho_0}\rho_1^2. \tag{3.2}$$

Acoustic Field Equations—Second-Order Terms

Equation (1.1) is a relation between a mass flow, $m_1=\rho_0\mathbf{u}_1$, and a rate of change of density while Eq. (2.1) is a relation between mass flow and the gradient of a pressure. The same kind of relations might be expected between the second-order terms. We, therefore, define

$$\mathbf{m}_2=\rho_0\mathbf{u}_2+\rho_1\mathbf{u}_1. \tag{5}$$

The two terms should be roughly of the same order of magnitude, although at times one term may be considerably larger than the other. Equation (1.2) now reads

$$\partial\rho_2/\partial t+\nabla\cdot\mathbf{m}_2=0, \tag{6}$$

and Eq. (2.2) with the help of Eq. (3.2) reads

$$\partial\mathbf{m}_2/\partial t=-c_0^2\nabla\rho_2-\mathbf{F}, \tag{7}$$

where

$$\mathbf{F}=c_0(\partial c/\partial\rho)_{\rho_0}\nabla\rho_1^2+\rho_0[(\mathbf{u}_1\cdot\nabla)\mathbf{u}_1+\mathbf{u}_1(\nabla\cdot\mathbf{u}_1)]. \tag{7a}$$

The additional $\mathbf{F}$ term may at first be a surprise. It is due, however, to the radiation tensor of the wave.[9] The first term in F occurs because we are not using a simple linear relation between p_e and ρ_e. The second term can be thought of as arising from the momentum of the wave; this term depends on the direction of the particle velocity as well as the changes in this velocity.

Equation (7) combined with (6) yields the following equation for $\mathbf{m}_2$:

$$\partial^2\mathbf{m}_2/\partial t^2-c_0^2\nabla(\nabla\cdot\mathbf{m}_2)=-\partial\mathbf{F}/\partial t. \tag{8}$$

while for ρ_2,

$$\partial^2\rho_2/\partial t^2-c_0^2\nabla^2\rho_2=\nabla\cdot\mathbf{F}. \tag{9}$$

These are the basic second-order field equations in terms of mass flow. As far as the author knows, these equations have not been solved, yet several general conclusions regarding the time average of the mass flow are possible.

The Time-Independent Mass Flow

We restrict our consideration to the case where the first-order solution depends harmonically on time. Products of ρ_1 and p_1, p_1^2, or ρ_1^2 give a time independent term and a term which depends on twice the frequency of ρ_1. As a consequence one would expect that the second-order terms have a time-dependent part (ac) and a time independent part.[10] We shall attempt to solve the equations by separating the two parts and treating them independently.

From (7) we see that the equation for the time-independent part of ρ_2, ρ_2'' is

$$\nabla\rho_2''=-(1/c_0^2)\mathbf{F}''. \tag{10}$$

The ac part of ρ_2 is a solution of Eq. (9), where $\nabla\cdot\mathbf{F}'$ is

independent excess pressure and density may exist and there is no reason to believe that these portions of the excess pressure and density should be related isentropically. If anything, one would suspect that they are related isothermally. We shall, however, develop the theory using (3) for simplicity and assume that $p=f(\rho)$ is along an isentropic path. We shall also assume that p_0 and ρ_0 are constants independent of any of the variables.

[9] To convince ourselves that $\mathbf{F}$ gives the usual expression for the radiation pressure, let us consider the simplest case of a plane wave where $u_x=v(x)$; $u_y=u_z=0$. Here the usual radiation pressure matrix is

$$\begin{bmatrix} W\left[1+\frac{\rho_0}{c_0}\left(\frac{\partial c}{\partial\rho}\right)\right] & 0 & 0 \\ 0 & W\frac{\rho_0}{c_0}\left(\frac{\partial c}{\partial\rho}\right) & 0 \\ 0 & 0 & W\frac{\rho_0}{c_0}\left(\frac{\partial c}{\partial\rho}\right) \end{bmatrix}.$$

W is the accepted energy density term for a wave, i.e.,

$$W=\tfrac{1}{2}\rho_0 u_1^2+\tfrac{1}{2}(1/c_0^2\rho_0)p_1^2=\rho_0 v^2=(c_0^2/\rho_0)\rho_1^2.$$

The matrix combined with the operation $-\partial p_{xx}/\partial x-\partial p_{yx}/\partial y-\partial p_{zx}/\partial z$, gives $\mathbf{F}$. For more details, see L. Brillouin, Revue d'acoustique **5**, 99 (1936) and *Les Tenseurs en Mécanique et en Elasticite* (Dover Publications, New York, 1946), Chapter 11.

[10] Single primes on quantities will indicate that they depend on the time; double primes will indicate that they are time-independent.

a driving force with a frequency of 2ω. We would also expect that $\mathbf{m}_2$ has two parts. $\mathbf{m}_2''$, the solution of the time-independent terms, would produce mass flow.

It is possible to show that Eqs. (7) and (9) indicate that $\mathbf{m}_2''$ is determined from the initial and boundary condition. For this purpose we shall use Helmholtz's vector theorem[11] and write

$$\mathbf{m}_2''=-\nabla g+\nabla\times\mathbf{G}. \tag{11}$$

From (6) it follows that $\nabla\cdot\mathbf{m}_2''=0$ and that g is determined from the boundary conditions, but not from the field forces. Since $\nabla\times\mathbf{u}_2$ does not appear explicitly in (1.2), (2.2), and (3.2), we may conclude that $\nabla\times\mathbf{u}_2''$ is not governed by the field forces. $\mathbf{u}_1$ and ϱ_1 are known from the first-order equation, so that $\nabla\times\langle\rho_1\mathbf{u}_1\rangle$ of $\nabla\times\mathbf{m}_2''$ can be evaluated independently.[12] In general $\nabla\times\langle\rho_1\mathbf{u}_1\rangle$ need not be zero and there may be some mass flow. In a special case, however, $\nabla\times\mathbf{m}_2=0$. This occurs when $\mathbf{u}_1$ is of the form $\mathbf{A}(\mathbf{r})\cos(\omega t-\varphi(\mathbf{r}))$, where $\mathbf{A}$ and φ are functions of the coordinates and ω is the angular frequency. Under the above conditions by the use of a vector relation[13]

$$\nabla\times\rho_1\mathbf{u}_1=-\mathbf{u}_1\times\nabla\rho_1=-(\rho_0/c_0^2)\mathbf{u}_1\times\partial\mathbf{u}_1/\partial t=0.$$

For a plane wave the following solutions may be assumed:

$$u_1=V\cos(\omega t-kx),\quad \rho_1=(\rho_0/c_0)V\cos(\omega t-kx).$$

Substituting in (7a) we see that $F''=0$ and that ρ_2'' should be a constant. This is in agreement with the calculations of Westervelt,[14] from which one may show that there is an average space-independent pressure for a plane wave. These solutions assume that $\mathbf{m}_2$ is determined from the boundary conditions so that we may assume for a medium at rest $\mathbf{m}_2''=0$. From Eq. (5) it follows that

$$\mathbf{u}_2''=(1/\rho_0)\langle\rho_1\mathbf{u}_1\rangle,$$

or for a plane wave, the value of $\mathbf{u}_2''$ is $(1/2c_0)V^2$. This should be contrasted with Eckart's results which imply that $\mathbf{u}_2''=0$.

[11] This theorem states that any vector $\mathbf{V}$ which is known in a region τ bounded by a surface S and has a finite discontinuity $\Delta\mathbf{V}$ on the surface S_1 can be represented

$$\mathbf{V}=-\nabla\varphi+\nabla\times\mathbf{G}$$

$$\varphi(r)=\frac{1}{4\pi}\int_\tau\frac{\nabla\cdot\mathbf{V}(\mathbf{r}')}{|\mathbf{r}'-\mathbf{r}|}d\tau'+\frac{1}{4\pi}\int_{S_1}\frac{\mathbf{n}\cdot\Delta\mathbf{V}(\mathbf{r}')}{|\mathbf{r}'-\mathbf{r}|}d\sigma'-\frac{1}{4\pi}\int_S\frac{\mathbf{n}\cdot\mathbf{V}(\mathbf{r}')}{|\mathbf{r}'-\mathbf{r}'|}d\sigma'$$

$$\mathbf{G}(\mathbf{r})=\frac{1}{4\pi}\int_\tau\frac{\nabla\times\mathbf{V}(\mathbf{r}')}{|\mathbf{r}'-\mathbf{r}'|}d\tau'+\frac{1}{4\pi}\int_{S_1}\frac{\mathbf{n}\times\Delta\mathbf{V}(\mathbf{r}')}{|\mathbf{r}'-\mathbf{r}'|}d\sigma'-\frac{1}{4\pi}\int_S\frac{\mathbf{n}\times\mathbf{V}(\mathbf{r}')}{|\mathbf{r}'-\mathbf{r}'|}d\sigma'.$$

$d\tau'$ is a volume element at $\mathbf{r}'$ where $\nabla\cdot\mathbf{V}$ and $\nabla\times\mathbf{V}$ are evaluated and $\mathbf{n}$ is a unit vector normal to the surface. The theorem is explicitly stated to recall that φ and $\mathbf{G}$ depend on the boundary conditions as well as $\nabla\cdot\mathbf{V}$ and $\nabla\times\mathbf{V}$. See H. B. Phillips, *Vector Analysis* (John Wiley and Sons, New York, 1933), Chapters 5 and 8.

[12] We shall use angular brackets throughout to denote time averages.

[13] From (2.1) we see that $\nabla\times\mathbf{u}_1=0$.

[14] P. J. Westervelt, J. Acoust. Soc. Am. **22**, 319 (1950).

III. SOUND FIELD RELATIONS WITH VISCOSITY AND RELAXATION

In this section we shall derive the general field equations when the effects of viscosity and relaxation are included. Then the vector form of the mass flow will be considered. Finally, we shall obtain the differential equation for the second-order particle velocity when relaxation effects are included.

Basic Field Equations

Stokes has defined the stress tensor arising because of a flow in a viscous fluid in terms of two coefficients μ and λ. The coefficient μ is the shear viscosity and $\lambda+2/3\mu$ is the bulk viscosity. The assumption will be made here that λ and μ are, to a good approximation, independent of the density and the pressure.

This assumption leads to the conventional equation of motion, i.e.,[15]

$$\partial(\rho\mathbf{u})/\partial t+\mathbf{u}[\nabla\cdot(\rho\mathbf{u})]+\rho(\mathbf{u}\cdot\nabla)\mathbf{u}$$
$$=-\nabla p+(2\mu+\lambda)\nabla(\nabla\cdot\mathbf{u})-\mu\nabla\times(\nabla\times\mathbf{u}). \tag{12}$$

This equation is a combination of the equation of motion and part of an equation of state (because it states how some of the stresses are obtained). We cannot calculate the forces directly from the p in (12) since p is not actually the pressure for the medium in motion.

To find a relation between p_s and ρ_s is not easy. The viscous approximation uses Eq. (12) as the equation of motion and relates $\nabla\rho$ linearly to ∇p of this equation. A purely relaxational process is described by omitting the last two terms in Eq. (12) and relating the excess pressure to the excess density by the relation,

$$\frac{1}{\rho_0}\frac{d\rho_s}{dt}-\frac{1}{\kappa_s^\infty}\frac{dp_s}{dt}+\omega_0\left(\frac{\rho_s}{\rho_0}-\frac{1}{\kappa_s{}^0}p_s\right)=0, \tag{13}$$

where κ is the bulk modulus and ω_0 is the relaxation frequency. The superscripts 0 and ∞ mean that at low frequency κ has one value κ_s^0, while at high frequency it has a slightly larger value, κ_s^∞. The subscript s reminds us that we usually use the adiabatic coefficient.

Although Eq. (13) rarely appears in the literature it has been used implicitly since Stokes considered the effects of heat radiation. One may develop acoustics in such a manner that it appears explicitly.[6] It is to be stressed that Eq. (13) represents a basic absorption mechanism (thermal or structural relaxation) in fluids. The inclusion of this mechanism is just as important as the viscous terms which appear in (12).

A viscous relaxational medium can be described by combining (12) and (13). This step allows us to study the effects of relaxation on streaming. This is the point on which the present discussion differs most from that of Eckart.

[15] See reference 7, Chapter 11.

It is important to know the accuracy of Eqs. (12) and (13). Equation (13) cannot be used beyond the first-order term, for in its derivation higher order terms are omitted. Stokes's derivation of Eq. (12) assumes, of course, that no higher order terms exist. For a gas, Enskog (see Jeans[16]) has considered terms beyond Eq. (12) and they do exist. A relaxational "shift" of μ and λ may very well occur in liquids and this would mean that Eq. (12) is incomplete in another respect. Further, the assumption of the density independence of μ and λ is an approximation. In the following analysis we shall assume, however, that (12) is true to second order, while (13) holds only to first order. The importance of the terms omitted in Eqs. (12) and (13) has not been explored.

Since Eq. (13) holds only to first approximations, we apply it only to harmonic functions. We, therefore, transform it by writing

$$p_1 = P(\mathbf{r})\exp i\{\omega t - \varphi(\mathbf{r})\},$$

and

$$\rho_1 = R_1(\mathbf{r})\exp i\{\omega t - \varphi(\mathbf{r}) + \theta(\omega)\},$$

where P, R, and φ are functions of $\mathbf{r}$ and θ is the phase angle between ρ_1 and p_1. Substituting in (13) and solving for p, one may show that

$$p_1 = c^2(\omega)\rho_1 + \Delta\partial\rho_1/\partial t, \tag{14}$$

where

$$c^2(\omega) = \frac{1}{\rho_0}\frac{\kappa_s{}^0\omega_r{}^2 + \kappa_s{}^\infty\omega^2}{\omega_r{}^2+\omega^2}, \quad \Delta(\omega) = \frac{\omega_r}{\rho_0(\omega_r{}^2+\omega^2)}(\kappa_s{}^\infty - \kappa_s{}^0),$$

$$\omega_r = \omega_0\kappa_s{}^\infty/\kappa_s{}^0,$$

where $c^2(\omega)$ is a good approximation to the square of the sound velocity.

In the following we shall assume that the terms with Δ, μ, and λ are of the first order.[17] The first-order equations are

$$\rho_0\partial\mathbf{u}_1/\partial t = -\nabla p_1 + (2\mu+\lambda)\nabla(\nabla\cdot\mathbf{u}_1) - \mu\nabla\times(\nabla\times\mathbf{u}_1) \tag{15.1}$$

$$\partial\rho_1/\partial t + \rho_0\nabla\cdot\mathbf{u}_1 = 0 \tag{16.1}$$

and

$$p_1 = c^2(\omega)\rho_1 + \Delta\partial\rho_1/\partial t. \tag{17.1}$$

The second-order equations are

$$\rho_0\partial\mathbf{u}_2/\partial t + \partial(\rho_1\mathbf{u}_1)/\partial t + \rho_0[\mathbf{u}_1(\nabla\cdot\mathbf{u}_1) + (\mathbf{u}_1\cdot\nabla)\mathbf{u}_1] = -\nabla p_2 + (2\mu+\lambda)\nabla(\nabla\cdot\mathbf{u}_2) - \mu\nabla\times(\nabla\times\mathbf{u}_2) \tag{15.2}$$

$$\partial\rho_2/\partial t + \rho_0(\nabla\cdot\mathbf{u}_2) + \nabla\cdot(\rho_1\mathbf{u}_1) = 0. \tag{16.2}$$

Acoustic Field Equations—First-Order Terms with Viscosity and Relaxation

Let us examine the wave equation obtained from the first approximation. We substitute Eq. (17.1) into (15.1) and then eliminate ρ_1 from Eq. (15.1) by means of Eq. (16.1). Making the usual assumption of the interchangeability of space and time derivatives, we get,

$$\partial^2\mathbf{u}_1/\partial t^2 = c^2\nabla(\nabla\cdot\mathbf{u}_1) + (1/\rho_0)(2\mu+\lambda+\rho_0\Delta)\nabla(\nabla\cdot\partial\mathbf{u}_1/\partial t) - (\mu/\rho_0)\nabla\times(\nabla\times\partial\mathbf{u}_1/\partial t). \tag{18}$$

The simple way to solve this equation is to use Helmholtz's theorem for a continuous region. $\mathbf{u}_1$ splits up into an irrotational and a solenoidal part, namely,

$$\mathbf{u}_1 = \mathbf{v}_1 + \mathbf{w}_1,$$

where

$$\nabla\times\mathbf{v}_1 = 0 \text{ (irrotational)}, \quad \nabla\cdot\mathbf{w}_1 = 0 \text{ (solenoidal)};$$

each part is assumed to be a solution of (18).

Equation (18) gives the $\mathbf{v}_1$

$$\partial^2\mathbf{v}_1/\partial t^2 = c^2\nabla^2\mathbf{v}_1 + (1/\rho_0)(2\mu+\lambda+\rho_0\Delta)\nabla^2\partial\mathbf{v}_1/\partial t, \tag{19}$$

where we have used a standard vector equation. The wave represented by Eq. (19) will be absorbed. The absorption per unit length can be obtained in the usual way by assuming that $\mathbf{v}_1$ is proportional to $\exp i(\omega t - kx)$ where k is a complex constant.[6] The absorption per unit length, α, is given by

$$\alpha = \tfrac{1}{2}(\omega^2/\rho_0 c^3)\mu b, \tag{20}$$

where

$$b = (1/\mu)(2\mu+\lambda+\rho_0\Delta). \tag{20a}$$

μb can be obtained from absorption measurements while μ is obtained from nonacoustical measurements. Thus b can be assumed known if sufficient data has been taken on a liquid.

The solution for the solenoidal part gives nothing new. The relaxational equation in the form (13) does not affect the transverse viscous wave.

Combining Eqs. (16.1) and (17.1),

$$p_1 = c^2\rho_1 - \rho_0\Delta(\nabla\cdot\mathbf{u}_1). \tag{21}$$

We can now use Eqs. (15.1) and (21) to obtain the first-order equations,

$$\rho_0\partial\mathbf{u}_1/\partial t = -c^2\nabla\rho_1 + b\mu\nabla(\nabla\cdot\mathbf{u}_1) - \mu\nabla\times(\nabla\times\mathbf{u}_1). \tag{22}$$

Equations (22) and (16.1) are almost the same as Eckart's Eq. (17.1) and (18.1). The difference is in the parameter b which here has an explicit frequency dependence. Following Eckart, by simple addition of the various equations we may show the following

[16] J. Jeans, *An Introduction to the Kinetic Theory of Gases* (University Press, Cambridge, 1940), Chap. 9.

[17] To see how the higher order terms compare with the viscous term, we select $\rho_0\mathbf{u}_1(\nabla\cdot\mathbf{u}_1)$ to represent the second order term and $\mu\nabla(\nabla\cdot\mathbf{u}_1)$ to give the viscous term. If we assume that the pressure amplitude in air is 10^{-1} dynes/cm^2, then the terms are equal at 100 cycles, the viscous term being larger above. For water at cavitation (0.03 watts/cm^2) the frequency where the terms are equal is 5 Mc. Since one usually works below cavitation pressures, we may assume that the transition point is at a lower frequency. We therefore assume that the viscous terms are larger than the second-order terms and include terms like $(2\mu+\lambda)\nabla(\nabla\cdot\mathbf{u}_1)$ in the first-order equations.

equation to hold

$$\partial(\rho_1\mathbf{u}_1)/\partial t+\rho_0[(\mathbf{u}_1\cdot\nabla)\mathbf{u}_1+\mathbf{u}_1(\nabla\cdot\mathbf{u}_1)] -\nabla(\tfrac{1}{2}\rho_0 u_1^2-\tfrac{1}{2}(c^2/\rho_0)\rho_1^2)+\rho_0\mathbf{u}_1\times(\nabla\times\mathbf{u}_1) =(\rho_1/\rho_0)b\mu\nabla(\nabla\cdot\mathbf{u}_1)-\mu(\rho_1/\rho_0)\nabla\times(\nabla\times\mathbf{u}_1). \quad (23)$$

Acoustic Field-Equations—Second-Order Terms with Viscosity and Relaxation

We may now develop the second-order term. Introduction of $\mathbf{m}_2$ in Eqs. (15.2) and (16.2) gives

$$\partial\rho_2/\partial t+\nabla\cdot\mathbf{m}_2=0, \quad (24)$$

and

$$\partial\mathbf{m}_2/\partial t=-\nabla p_2-\rho_0[\mathbf{u}_1(\nabla\cdot\mathbf{u}_1)+(\mathbf{u}_1\cdot\nabla)\mathbf{u}_1] +(2\mu+\lambda)\nabla(\nabla\cdot\mathbf{u}_2)-\mu\nabla\times(\nabla\times\mathbf{u}_2). \quad (25)$$

The first two terms on the right of Eq. (25) appear in Eq. (7a); the last two terms are the result of viscosity.

We shall explore first the behavior of $\mathbf{m}_2$ by neglecting relaxation, and assuming that Eq. (3.2) holds in this case, Eq. (25) takes the form

$$\partial\mathbf{m}_2/\partial t=-c_0^2\nabla\rho_2-\mathbf{F}+(2\mu+\lambda)\nabla(\nabla\cdot\mathbf{u}_2) -\mu\nabla\times(\nabla\times\mathbf{u}_2), \quad (26)$$

and Eq. (24) still applies. Since the equation of continuity has not changed by the introduction of viscosity, the field does not contribute to g of Eq. (11). It is influenced by the boundary condition but not by the field. Using the condition $\nabla\cdot\mathbf{m}_2''=0$ we know that

$$\nabla\cdot\mathbf{u}_2''=(1/\rho_0)\nabla\cdot\langle\rho_1\mathbf{u}_1\rangle,$$

or from (26)

$$c_0^2\nabla\rho_2''+\mathbf{F}''=(2\mu+\lambda)\nabla(\nabla\cdot\langle\rho_1\mathbf{u}_1\rangle)-\mu\nabla\times\nabla\times\mathbf{u}_2''. \quad (27)$$

Eq. (27) shows the essential difference between the viscous and the nonviscous case. Here an explicit requirement is imposed on $\mathbf{u}_2''$.[18]

We have neglected relaxation in this argument. For the general case, where we have viscosity and relaxation, we must use a more exact equation than (3). As far as the author knows, no such relation has been proposed. One cannot write down the explicit equation for $\partial\mathbf{m}_2/\partial t$; however, it would have the form

$$\partial\mathbf{m}_2/\partial t=-c^2\nabla\rho_2-\mathbf{F}_1+(2\mu+\lambda)\nabla(\nabla\cdot\mathbf{u}_2) -\mu\nabla\times(\nabla\times\mathbf{u}_2), \quad (28)$$

where $\mathbf{F}_1$ is similar to $\mathbf{F}$, except that it includes additional terms arising from the more complete equation of state. The argument concerning Eq. (28) would be the same as with Eq. (26) with the same conclusions being reached.

The proof that $\mathbf{m}_2''$ is solenoidal rests not only on the form of Eq. (28) but also on the equation of continuity. Indeed, it is Eq. (26) which is important. This result is implied in a comment by Fox and Herzfeld.[19]

Method of Solving for N_2''

Since the equations for $\mathbf{m}_2''$ contain $\mathbf{u}_2''$, it is convenient to solve for $\mathbf{u}_2''$ directly and then find $\mathbf{m}_2''$ by using Eq. (5). Using Eq. (15.2) and (23), and the assumption $\nabla\times\mathbf{u}_1=0$, we get

$$\rho_0\partial\mathbf{u}_2/\partial t=-\nabla p_2-\nabla(\tfrac{1}{2}\rho_0 u_1^2-\tfrac{1}{2}(c^2/\rho_0)\rho_1^2) +(2\mu+\lambda)\nabla(\nabla\cdot\mathbf{u}_2) -\mu\nabla\times(\nabla\times\mathbf{u}_2)-(b/\rho_0)\mu\rho_1\nabla(\nabla\cdot\mathbf{u}_1). \quad (29)$$

To find the solenoidal part of $\mathbf{u}_2$, we define $\mathbf{R}_2=\nabla\times\mathbf{u}_2$ and obtain

$$\rho_0\partial\mathbf{R}_2'/\partial t+\mu\nabla\times(\nabla\times R_2)=-(b/\rho_0)\mu\nabla\times[\rho_1\nabla(\nabla\cdot\mathbf{u}_1)],$$

or

$$\rho_0\partial\mathbf{R}_2/\partial t-\mu\nabla^2\mathbf{R}_2=(b/\rho_0^2)\mu(\nabla\rho_1)\times(\nabla\partial\rho_1/\partial t), \quad (30)$$

where we have used Eq. (16.1) and two common vector relations. The dc part of $\mathbf{R}_2$ satisfies the equation.

$$\nabla^2\mathbf{R}_2''=-\frac{b}{\rho_0^2}\left\langle(\nabla\rho_1)\times\left(\nabla\frac{\partial}{\partial t}\rho_1\right)\right\rangle. \quad (31)$$

μ does not appear, which implies that $\mathbf{R}_2''$ is independent of the shear viscosity. This apparent paradox occurs because Eq. (31) is a steady state equation; consequently as μ approaches zero, the time to reach a steady state must increase, becoming presumably infinite at $\mu=0$.

According to the present theory, the experimenter on streaming measures the ratio of b to μ, much the same as in Eckart's, but our b includes a frequency dependent term ∇ and explains Liebermann's results on ethyl formate in a natural way.

Eckart assumes in his paper that $\mathbf{m}_2''=\rho_0\mathbf{u}_2''$. This is a good approximation if $\omega^2>c$, which is true for Liebermann's work on liquids.[20] Eckart has also applied this expression to air at 256 cycles. In this case his results are incorrect for in this case the mass flow is governed by $\langle\rho_1\mathbf{u}_1\rangle+\rho_0\mathbf{u}_2''$, and the first term cannot be omitted.

IV. DISCUSSION

One serious limitation to the above development is that we have assumed the viscosity coefficients to be constant. We know, however, that during the passage of the sound wave the medium is alternately heated and cooled. This means that μ and λ are continually changing so that one should assume that

$$\mu=\mu_0+(\partial\mu/\partial\rho)\rho_1, \quad (32)$$

[18] Using Eckart's Eq. (11) and Eq. (21) one may show that $\nabla\cdot\mathbf{F}=0$ for the nonviscous case but not for the viscous case. The usual assumption $\nabla\times\mathbf{u}_1=0$ is made.

[19] F. E. Fox and K. F. Herzfeld, Phys. Rev. **78**, 156 (1950).

[20] This follows from Eckart's Eq. (41) and (33); (in his Eq. (33) k should appear squared).

where $\partial\mu/\partial\rho$ is taken along an adiabatic path. One is tempted first of all, to substitute this expansion into Eq. (12). If this is done, the results are interesting. For example, it shows that the b which is measured from absorption differs from the b that is measured by the Eckart and Liebermann method. Since this correction does not affect Δ but only $2\mu+\lambda$, it implies the existence of a method to distinguish between the viscosity effects and the relaxational effects. The correction is small for water and mercury but in general is not small unless $2\mu+\lambda \ll \Delta$.

In other words, one would conclude that there is a fundamental difference between evaluating b by absorption and by means of streaming. This conclusion disagrees with Fox and Herzfeld. Unfortunately, the data of Liebermann are inconclusive on this point.

Actually this approach to the problem which starts with Eq. (12) seems incorrect to the author. One should return to the definition of the revised stress tensor and there assume Eq. (32). The problem seems quite complicated and therefore will not be attempted at present.

The author would like to thank Dr. C. Eckart, Dr. P. Westervelt, and Dr. G. Heller for some very helpful discussions. He is indebted to Dr. R. C. Morse for help in writing the manuscript and to Miss Agnes Fogelgren for the typing. Finally, the author would like to thank his wife for her encouragement.

PHYSICAL REVIEW VOLUME 86, NUMBER 4 MAY 15, 1952

Excited States of P^{32} from the $P^{31}(d,p)P^{32}$ Reaction*

D. M. VAN PATTER, P. M. ENDT,† A. SPERDUTO, AND W. W. BUECHNER
Physics Department and Laboratory for Nuclear Science and Engineering, Massachusetts Institute of Technology, Cambridge 39, Massachusetts

(Received January 14, 1952)

The $P^{31}(d,p)P^{32}$ reaction has been investigated by means of magnetic analysis of the protons emitted from thin targets containing phosphorus bombarded by 1.8- and 2.0-Mev deuterons. Sixteen of the proton groups observed have been assigned to the $P^{31}(d,p)P^{32}$ reaction, corresponding to the ground state and fifteen excited states of P^{32}, in a region of excitation from zero to 4.3 Mev.

The position of the first excited state of P^{32} has been measured as 77.0 ± 1.7 kev. Three other pairs of closely spaced levels were observed. These occurred at 2.2-, 2.7-, and 3.3-Mev excitation with spacings of 50 ± 2, 92 ± 7, and 59 ± 3 kev, respectively. Because of the presence of contaminant groups, it is possible that some $P^{31}(d,p)P^{32}$ groups were missed, corresponding to states in a region of excitation from 3.3 to 4.3 Mev. The nucleus P^{32} appears to have a large number of low-lying states, with the first level very near to the ground state.

I. INTRODUCTION

UNTIL recently, very little was known about the excited states of the nucleus P^{32}, although transitions to the ground state had been found with several reactions. The ground-state $P^{31}(d,p)P^{32}$ proton group was observed by Pollard[1] using 3.3-Mev deuterons, with a Q-value of 5.9 ± 0.3 Mev measured by range methods. The ground-state transition of the $S^{32}(n,p)P^{32}$ reaction was found by Huber[2] to have a Q-value of -0.93 ± 0.10 Mev, in agreement with the value of -0.929 ± 0.005 Mev, which can be calculated from the beta-decay of P^{32}. The characteristic 14.5-day period of P^{32} was found by King *et al.*[3] after bombarding quartz with 16-Mev alpha-particles. This was attributed to the $Si^{29}(\alpha,p)P^{32}$ reaction, for which a reaction energy of -2.45 ± 0.01 Mev may be calculated.

Prior to 1950, the only evidence for an excited state of P^{32} was the measurement by Metzger *et al.*,[4] who found an alpha-particle group with Q-value of 0.44 ±0.20 Mev from the neutron bombardment of chlorine, which they attributed to the $Cl^{35}(n,\alpha)P^{32}$ reaction. Since the ground-state Q-value of this reaction can be calculated to be 1.11 ± 0.07 Mev from masses,[5] this group evidently corresponds to an excited state in P^{32} at 0.67 ± 0.21 Mev.

At present, no levels in the compound nucleus P^{32} have been reported. Fields and his co-workers[6] measured the total neutron cross section for P^{31} in an energy region from 0.2 to 0.8 Mev and found no resonances. However, since they measured at only a few selected neutron energies, it is possible that some resonances were missed. Additional measurements of the total neutron cross section for P^{31} have been compiled by Adair.[7]

* This work has been assisted by the joint program of the ONR and AEC.

† On leave of absence from the University of Utrecht, Utrecht, Holland.

[1] E. Pollard, Phys. Rev. **57**, 1086 (1940).

[2] P. Huber, Helv. Phys. Acta **14**, 163 (1941).

[3] King, Henderson, and Risser, Phys. Rev. **55**, 1118 (1939).

[4] Metzger, Alder, and Huber, Helv. Phys. Acta **20**, 236 (1947).

[5] The authors are indebted to A. H. Wapstra for the communication of his mass table prior to publication.

[6] Fields, Russell, Sachs, and Wattenberg, Phys. Rev. **71**, 508 (1947).

[7] R. K. Adair, Revs. Modern Phys. **22**, 249 (1950).

Recently, Allen and Rall[8] studied the proton groups emitted at zero and 90 degrees from phosphorus targets bombarded by 3.76-Mev deuterons. Using range measurements, they observed eight groups which they attributed to transitions to the ground state and seven excited states of P^{32} in a region of excitation from 0 to 3.3 Mev. They measured the Q-value of the ground-state $P^{31}(d,p)P^{32}$ group as 5.52 ± 0.10 Mev.

At the same time, an independent investigation of the $P^{31}(d,p)P^{32}$ reaction was made at this laboratory, using magnetic analysis.[9] Several proton groups were found that were identified with the $P^{31}(d,p)P^{32}$ reaction. The highest energy group had a measured Q-value of 5.704 ± 0.009 Mev, as reported in a later publication.[10] This result was communicated to Kinsey and his collaborators, who were in the process of measuring the gamma-rays from the capture of thermal neutrons by phosphorus, using a pair spectrometer. Upon further investigation, they found a high energy gamma-ray[11] of energy 7.94 ± 0.03 Mev, corresponding to a direct transition to the ground state of P^{32}. After subtraction of the deuteron binding energy of 2.23 Mev, a value of 5.71 ± 0.03 Mev may be calculated for the $P^{31}(d,p)P^{32}$ reaction, in excellent agreement with the measured value of 5.704. Kinsey *et al.* have detected a total of twenty gamma-rays from the $P^{31}(n,\gamma)$ reaction, many of which can be correlated with the known levels of P^{32}.

The results of the first preliminary survey of the $P^{31}(d,p)P^{32}$ reaction,[9] made at 1.8-Mev bombarding energy, indicated that several contaminants were present, which made the identification of the observed proton groups subject to uncertainty. In addition, the yield of the proton groups from phosphorus was considerably lower than that observed from lighter nuclei, which also contributed to the uncertainty of the assignment. It was decided to repeat the experiment using different targets and also to make surveys at both 1.8- and 2.0-Mev bombarding energy in order to obtain a more positive identification of the proton groups.

II. EXPERIMENTAL PROCEDURE

The essential details of the experimental equipment and methods of analysis have been described previously.[10,12] The protons from the phosphorus targets were analyzed at 90 degrees to the incident deuteron beam by means of a 180-degree focusing magnet and registered on nuclear-track plates. The use of nuclear-track plates permitted the observation of extremely low counting rates for charged particles. For example, it was possible to detect a high energy proton group containing only ten tracks, after exposing the plate for a period of one hour or longer and to measure the Q-value of the group to better than 15 kev. The background between proton groups with energies greater than that for the $C^{13}(d,p)C^{13}$ ground-state group was nearly zero for such an exposure.

The targets used for the present investigation consisted of thin layers of copper phosphate and zinc phosphide evaporated in vacuum onto platinum backings. The targets varied in thickness from 2 kev to 12 kev for the $P^{31}(d,p)P^{32}$ ground-state group. Deuteron bombarding energies of 1.81 and 2.00 Mev were used. It was necessary to run the electrostatic generator at the highest voltage that could be reliably maintained, since the yield of the $P^{31}(d,p)P^{32}$ groups was observed to increase rapidly with bombarding energy. In addition, it was desirable to observe the $P^{31}(d,p)$ groups at more than one bombarding energy in order to observe the resulting change in proton energy. A change in bombarding energy of 200 kev was found to be sufficient to distinguish between the proton groups caused by phosphorus and those which were due to the usual contaminants of carbon, nitrogen, and oxygen.

The spectra of protons observed were obtained by exposing a series of nuclear-track plates successively over a wide range of analyzing-magnet field strengths. These field strengths were chosen so as to give considerable overlapping of the data obtained from successive plates. A total of fifteen exposures was necessary to obtain a spectrum of proton energies from 3.0 to 7.5 Mev. For each exposure, the deuteron bombarding energy was determined to an accuracy of ±4 kev. For a deuteron bombarding energy of 2.0 Mev, proton groups with energies less than 4.0 Mev were recorded in the presence of deuterons elastically scattered from the target backing by covering the nuclear-track plates with aluminum foils sufficiently thick to stop the scattered deuterons.

III. RESULTS

The proton groups with energies of 2.9 to 7.6 Mev observed from a 12-kev target of copper phosphate are shown in Fig. 1. In the upper curve are shown the results for a bombarding energy of 1.81 Mev; in the lower curve, the results for 2.0-Mev bombarding energy are presented. In these curves, a total of thirty-two proton groups can be distinguished. Sixteen of these groups are assigned to contaminants of D^2, C^{12}, C^{13}, N^{14}, O^{16}, and Si^{28}. The contaminant Si^{28} contributes eight groups, for which the Q-values are accurately known.[13] In all cases the measured Q-values of the contaminant groups agreed within ±5 kev with the previously measured values. The remaining sixteen groups, numbered (0) through (15), are assigned to the $P^{31}(d,p)P^{32}$ reaction.

Some reservation must be made concerning the assignment of group (11). The yield of this group was

[8] R. C. Allen and W. Rall, Phys. Rev. **81**, 60 (1951).
[9] Endt, Van Patter, and Buechner, Phys. Rev. **81**, 317 (1950).
[10] Strait, Van Patter, Buechner, and Sperduto, Phys. Rev. **81**, 747 (1951).
[11] B. B. Kinsey (private communication).
[12] Buechner, Strait, Stergiopoulos, and Sperduto, Phys. Rev. **74**, 1569 (1948).
[13] Endt, Van Patter, Buechner, and Sperduto, Phys. Rev. **83**, 491 (1951).

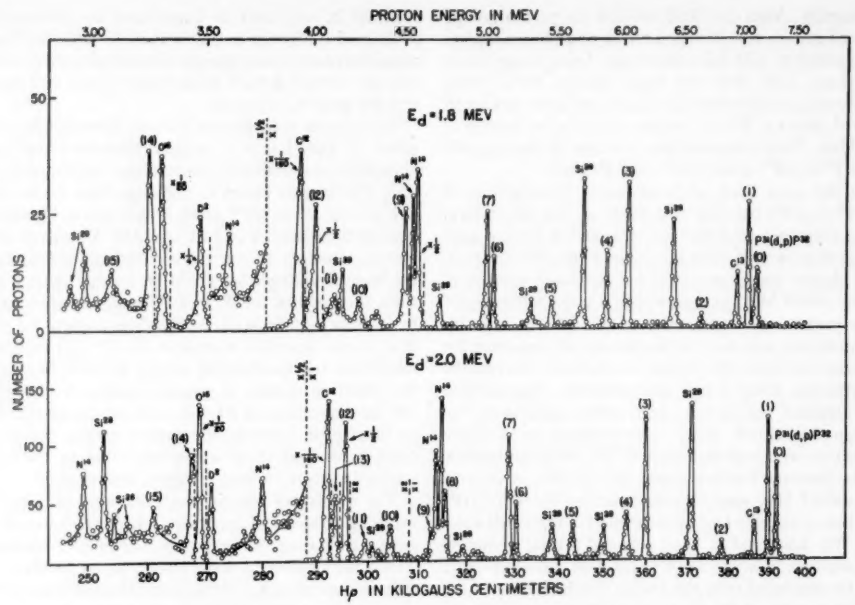

FIG. 1. Spectra of proton groups observed from a copper-phosphate target bombarded by 1.81- and 2.00-Mev deuterons.

so low that it could barely be detected. Although this group has been observed from two different targets containing phosphorus, its yield was not sufficient for positive identification.

The presence of the intense $N^{14}(d,p)N^{15*}$ doublet indicated that there was considerable nitrogen contamination on the copper-phosphate target. At 1.8-Mev bombarding energy, these groups obscured the $P^{31}(d,p)P^{32}$ group (8). However, at 2.0-Mev bombarding energy, the energy of proton group (8) was sufficiently greater than that of the nitrogen groups to permit the resolution of group (8).

Group (13) has been observed only at 2.0-Mev bombarding energy, because at 1.8-Mev bombarding energy, it is obscured by the $C^{12}(d,p)C^{13}$ ground-state group. However, it has been observed from targets of both copper phosphate and zinc phosphide with the same intensity relative to group (12).

The region of proton energies below the $C^{12}(d,p)C^{13}$ ground-state group was largely obscured by various contaminant groups. It is quite possible that some $P^{31}(d,p)P^{32}$ groups were missed, particularly between groups (13) and (14). However, two groups (14) and (15), which evidently could be attributed to a target mass in the region of P^{31}, were observed in this region, as indicated by their shift in energy from 1.8- to 2.0-Mev bombarding energy relative to the contaminant groups. A further check was provided by the observation of these groups from a 2-kev zinc-phosphide target, where the groups were more clearly resolved, with approximately the same intensities relative to group (12). In addition, groups (14) and (15) can be closely correlated to $P^{31}(n,\gamma)$ gamma-rays observed by Kinsey *et al.*, indicating that the assignment of these two groups is correct.

The measured Q-values of the proton groups assigned to the $P^{31}(d,p)P^{32}$ reaction are listed in Table I, together with the resulting energy levels for the P^{32} nucleus. The relative intensities of the groups observed at 90 degrees at 1.8- and 2.0-Mev bombarding energies are also given. In the case of groups (8), (9), and (15), which were not completely resolved from contaminant groups, these relative intensities cannot be relied upon to better than a factor of 2. It is interesting to note that the intensity of nearly all the groups increased a factor of 2 when the bombarding energy was increased from 1.8 to 2.0 Mev.

In Table I and in Fig. 2, the P^{32} levels observed by Allen and Rall[8] are compared with the present results. For the range of excitation covered in their experiment, the agreement between the two sets of results is within the stated errors. However, additional structure has been found in the present experiment because of the higher resolution provided by magnetic analysis. It is noted that levels at 3.00 and 3.14 Mev were not found by Allen and Rall.

TABLE I. Q-values for $P^{31}(d,p)P^{32}$ groups and energy levels in P^{32}.

Group	The $P^{31}(d,p)P^{32}$ reaction Present results Relative intensity 1.8 Mev	2.0 Mev	Q-value (Mev)	Calculated Q-value Kinsey *et al.*	Levels in P^{32} $P^{31}(d,p)P^{32}$ reaction Present results	Allen+Rall	Reaction Kinsey *et al.*
(0)	1.0	2.2	5.704±0.008	5.71±0.03	0	0	0
(1)	1.7	2.7	5.627±0.008	5.62±0.05	0.077±0.002	—	0.08±0.05
(2)	0.3	0.5	5.189±0.010	5.19±0.03	0.515±0.005	0.50±0.05	0.51±0.03
(3)	1.8	4.7	4.550±0.007	4.53±0.03	1.154±0.007	1.10±0.03	1.17±0.03
(4)	0.7	2.0	4.388±0.007	—	1.316±0.008	1.36±0.05	—
(5)	0.4	1.4	3.954±0.007	3.91±0.03	1.750±0.009	1.71±0.04	1.79±0.03
(6)	0.6	1.0	3.527±0.008	—	2.177±0.009	2.22±0.04	—
(7)	1.2	4.	3.477±0.008	3.48±0.03	2.227±0.009		2.22±0.03
(8)	~0.5	1.6	3.054±0.006	3.04±0.03	2.650±0.008	2.72±0.03	2.66±0.03
(9)	~0.8	—	2.962±0.006	—	2.742±0.008		—
(10)	0.4	0.5	2.705±0.008	2.69±0.03	2.999±0.010	—	3.01±0.03
(11)	0.2	0.2	(2.563±0.010)	—	(3.141±0.012)	—	—
(12)	4.8	8.	2.445±0.006	2.45±0.03	3.259±0.009	3.27±0.04	3.25±0.03
(13)	—	1.8	2.386±0.006	—	3.318±0.009	—	—
(14)	4.2	—	1.672±0.005	1.69±0.03	4.032±0.009	—	4.01±0.03
(15)	~0.7	~1.3	1.497±0.008	—	4.207±0.010	—	4.20±0.03

It is possible to fit at least twelve of the twenty $P^{31}(n,\gamma)$ gamma-rays observed by Kinsey *et al.*, to the level scheme of P^{32} established by the present experiment, as indicated in Table I and in Fig. 2. In the case of nine of these gamma-rays, very good agreement is obtained by assuming that they represent transitions from the capturing state at 7.93 Mev to various excited states. In this case, the gamma-ray energies can be compared with the Q-values of the $P^{31}(d,p)$ groups corresponding to the same excited states by subtraction of the deuteron binding energy of 2.23 Mev. As can be seen in Table I, the calculated values agree with the measured $P^{31}(d,p)P^{32}$ Q-values within 40 kev in all cases.

In addition, the energies of three $P^{31}(n,\gamma)$ gamma-rays agree within 40 kev with the established positions of three P^{32} levels, indicating that these gamma-rays may well represent direct transitions to the ground state. It is noted that the 3.00-Mev level of P^{32} can be associated with two gamma-rays in cascade. However, no verification has been found for the doubtful level at 3.14 Mev, which makes the assignment of proton group (11) more uncertain.

The present experiment has revealed the existence of four pairs of closely spaced levels in P^{32} at approximate excitations of 0.1, 2.2, 2.7, and 3.3 Mev. In the case of three of these "doublets," it was possible to make a rather precise estimate of the level spacing, since both members could be recorded on the same nuclear-track plate. The measured level spacings were 77.0±1.7, 50±2, 92±7, and 59±3 kev, respectively. The spacing of the proton groups (8) and (9), corresponding to levels at 2.7-Mev excitation, could not be determined so accurately because of the presence of the $N^{14}(d,p)N^{15*}$ doublet.

IV. CONCLUSIONS

An investigation of the $P^{31}(d,p)P^{32}$ reaction using magnetic analysis has revealed the presence of fourteen and possibly fifteen excited states of the nucleus P^{32}, of which seven have not been previously reported. The range of excitation covered was 0 to 4.3 Mev. A level diagram for P^{32} incorporating these results is shown in Fig. 3.

The positions of the P^{32} levels found from these measurements are in agreement with the recent results of Allen and Rall[8] for the $P^{31}(d,p)P^{32}$ reaction using range measurements. However, because of the increased resolution provided by magnetic analysis, considerably more structure has been found in the present experiments. The average spacing for levels in P^{32} up to 3.3-Mev excitation is approximately 260 kev. As can be seen in Fig. 3, the level density appears to be increasing up to 3.3-Mev excitation. Between 3.3- and 4.3-Mev excitation, it is probable that some levels were missed because of the presence of contaminant groups in the observed $P^{31}(d,p)P^{32}$ spectrum.

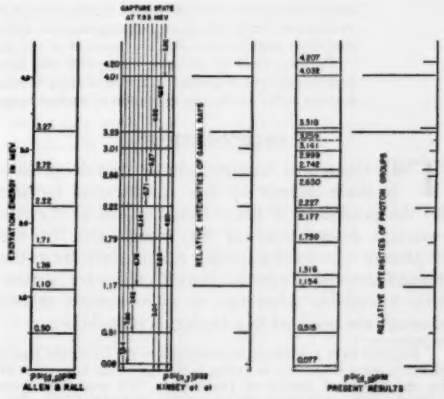

FIG. 2. Comparison of the results of various experimenters concerning the energy levels of P^{32}.

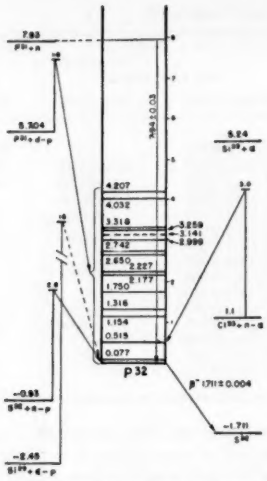

FIG. 3. Energy-level diagram for P^{32}.

The pattern of the established P^{32} levels is quite distinctive. Of particular interest is the discovery of the first excited state at 77.0±1.7 kev. This state has been verified by Kinsey *et al.*,[11] who found two high energy $P^{31}(n,\gamma)P^{32}$ gamma-rays, evidently corresponding to the ground state and an excited state at 80±50 kev. In this region of the periodic table, the only other known case for such a low-lying level is Al^{28}, where the first excited state occurs at 31 kev.[14]

In addition to this ground-state doubtlet, there are three other pairs of closely spaced levels at excitations of 2.2, 2.7, and 3.3 Mev, with spacings of 50±2, 92±7, and 59±3 kev, respectively. At present, none of these doublets has been verified by other workers.

The present results for the $P^{31}(d,p)P^{32}$ reaction can be closely correlated with the results of Kinsey and co-workers for the $P^{31}(n,\gamma)P^{32}$ reaction, as indicated in Table I. The measured energies of twelve of the $P^{31}(n,\gamma)$ gamma-rays agree to 40 kev or less with the established P^{32} levels, when assigned to the transitions indicated in Fig. 2. Except for the case of the ground-state doublet, the relative intensities of the observed gamma-rays have generally the same pattern as the relative intensities of the $P^{31}(d,p)P^{32}$ proton groups.

[14] Enge, Buechner, Sperduto, and Van Patter, Phys. Rev. **83**, 31 (1951).

PHYSICAL REVIEW VOLUME 86, NUMBER 4 MAY 15, 1952

The Interpretation of Image Transitions in Beta-Decay Theory*†

GEORGE L. TRIGG‡
Washington University, St. Louis, Missouri
(Received January 14, 1952)

The allowed favored beta-transitions are studied in relation to problems of nuclear structure and beta-decay theory. These problems include (1) the influence of deviations from *L-S* coupling on the beta-decay matrix elements of the light nuclei, (2) the relation between the observed magnetic moments, simple nuclear models and deviations from *L-S* coupling, (3) determination of the ratio of Fermi to Gamow-Teller type coupling constants, and (4) determination of the absolute magnitudes of the coupling constants.

The analysis of all available data yields two mutually supporting conclusions: (a) a substantial Fermi-type component is present in the beta-decay interaction and (b) deviations from *L-S* coupling are an important factor in the interpretation of nuclear magnetic moments.

I. INTRODUCTION

THE theoretical interpretation of beta-decay data is made difficult by two complicating factors: (a) the possibility of linear combinations of the five covariant formulations of the theory and (b) the occurrence of unknown nuclear matrix elements in the derived formulas. Under (b) the difficulties are particularly formidable when two or more nuclear matrix elements are involved in a transition probability.

Because of these general complications the testing of the theory outside of the allowed range has been largely dependent on the occurrence of transitions subject to special selection rules for which only one nuclear matrix element appears in the theoretical transition probability.[1,2] The study of such transitions (especially $\Delta I=\pm 2$, yes) proves the need for a tensor or axial vector component in the general linear combination, but does not exclude the presence of other components (scalar, polar vector, and pseudoscalar).

In allowed transitions the tensor and axial vector components are responsible for the Gamow-Teller

* Adapted from a dissertation presented to the Graduate Board of Washington University in partial fulfilment of the requirements for the degree of Doctor of Philosophy. This work was done while the author was the holder of an AEC predoctoral fellowship.
† Assisted by the joint program of the ONR and AEC.
‡ Present address: Knox College, Galesburg, Illinois.

[1] C. S. Wu, Revs. Modern Phys. **22**, 386 (1950).
[2] J. P. Davidson, Phys. Rev. **82**, 48 (1951).

selection rules:

$$\Delta I=0, \pm 1 \text{ (no)}, \quad 0\rightarrow 0 \text{ excluded} \tag{1}$$

while the Fermi selection rules

$$\Delta I=0 \text{ (no)} \tag{2}$$

derive from scalar and polar vector components.

An additional important distinction within the allowed group is that between transitions within a supermultiplet (allowed favored or superallowed $-ft \sim 10^3$) and those between states belonging predominantly to different supermultiplets (allowed unfavored or just plain allowed $\rightarrow ft \sim 10^{5-6}$).[3] The occurrence of these distinct types in widely separated ranges of ft values proves both the approximate nature of the supermultiplet formalism and the general excellence of the approximation—approximate because the allowed unfavored transitions would not occur at all if the supermultiplet formalism were exact and an excellent approximation because the nuclear matrix elements for allowed unfavored transitions are actually quite small.

In this paper the allowed favored group (including the image transitions) is studied in relation to problems of nuclear structure and beta-decay theory, developing further earlier studies by Wigner[3,4] and Grönblom.[5] These problems include:

1. The influence of deviations from L-S coupling on the beta-decay matrix elements of the light nuclei.

2. The relation between the observed magnetic moments, simple nuclear models and deviations from L-S coupling.

3. Determination of the ratio of Fermi to Gamow-Teller type coupling constants.

4. Determination of the absolute magnitudes of the coupling constants.

II. THE METHOD OF CALCULATION

In the general formulation of the theory the half-life t for an allowed transition is given by

$$\frac{1}{t}=\frac{1}{2\pi^3 \ln 2}\frac{mc^2}{\hbar}\left[(G_S^2+G_V^2)\left|\int 1\right|^2 + (G_T^2+G_A^2)\left|\int \boldsymbol{\sigma}\right|^2\right] f(Z, W_0), \tag{3}$$

where

$$f(Z, W_0)=\int_1^{W_0}(W_0-W)^2 pW \frac{2(1+S_0)}{\Gamma^2(2S_0+1)}(2pR)^{2S_0-2} \times e^{\pi\gamma W/p}\cdot|\Gamma(S_0+i\gamma W/p)|^2 dW, \tag{4}$$

$$\gamma=Ze^2/\hbar c, \quad S_0=(1-\gamma^2)^{\frac{1}{2}}$$

and G_S, G_V, G_T, and G_A are the coupling constants for scalar, vector, tensor, and axial vector couplings, respectively. These constants are real numbers in consequence of the postulated invariance of the interaction Hamiltonian under the operation of time reversal[6] or of charge conjugation.[7] Fierz's conditions[8]

$$G_S G_V=G_T G_A=0 \tag{5}$$

insure that the theoretical Kurie plots for allowed transitions are straight lines. They are also necessary conditions for complete symmetry between positron and negatron emission when the effect of the Coulomb field of the product nucleus on the wavefunctions of the emitted particle is neglected.[8] The experimental evidence[1,9] cannot establish Eq. (5), but does require strong inequalities

$$2G_S G_V \ll G_S^2+G_V^2, \quad 2G_T G_A \ll G_T^2+G_A^2. \tag{6}$$

The notation

$$G_S^2+G_V^2=G_F^2, \quad G_T^2+G_A^2=G_{GT}^2, \quad G_F^2=rG_{GT}^2 \tag{7}$$

is useful in indicating, respectively, the Fermi and Gamow-Teller coupling types and permits rewriting Eq. (3) as

$$ft\left(r\left|\int 1\right|^2+\left|\int \boldsymbol{\sigma}\right|^2\right)=\frac{\hbar}{mc}\frac{2\pi^3 \ln 2}{G_{GT}^2}. \tag{8}$$

The right side of Eq. (8) contains only constant factors; so the left side must also be constant for all allowed transitions.

In evaluating r and G_{GT}^2 the matrix elements are first computed; then the left side is a known linear function of r, the coefficients varying with the transition as prescribed by the assumed nuclear model. The left side is made as nearly constant as possible in the sense of minimizing the mean square deviation from the average. This fixes the value of r; setting the right side of Eq. (4) equal to the average value of the left side gives a value for G_{GT}^2 and, hence, through Eq. (7), for G_F^2. The mean square deviation from the average provides a figure of merit for the nuclear model used in the calculation. The resulting theory is applied to a number of transitions not included in the least squares evaluation of r and the coupling constants. Three models are tested and compared in this manner. Finally a compromise solution is developed in an attempt to achieve a satisfactory fit with all the data while maintaining a close correspondence with the more plausible of the three nuclear models.

The transitions used in the least squares calculation are those between ground states of mirror nuclei. In evaluating the nuclear matrix elements, these states are assumed to be pure spin doublets. The calculation is sketched below for $|\int \boldsymbol{\sigma}|^2$; that for $|\int 1|^2$ is similar, but simpler.

[3] E. P. Wigner, Phys. Rev. **56**, 519 (1939).
[4] E. P. Wigner and A. M. Feingold, privately circulated notes (1949).
[5] B. O. Grönblom, Phys. Rev. **56**, 508 (1939).
[6] L. C. Biedenharn and M. E. Rose, Phys. Rev. **82**, 982 (1951).
[7] H. A. Tolhoek and S. R. de Groot, Phys. Rev. **84**, 150 (1951).
[8] H. A. Tolhoek and S. R. de Groot, Physica **16**, 456 (1950).
[9] C. S. Cook and G. E. Owen, Am. J. Physics **18**, 453 (1950).

The explicit form of the matrix element, with the charge operator included, is

$$\left|\int\sigma\right|^2=\sum_{m'}|(T_\xi',I,m'|\mathbf{Y}_\xi\pm i\mathbf{Y}_\eta|T_\xi,I,m)|^2, \quad (9)$$

where

$$\mathbf{Y}_\xi=\tfrac{1}{2}\sum_1^A\tau_{\xi k}\boldsymbol{\sigma}_k,$$
$$\mathbf{Y}_\eta=\tfrac{1}{2}\sum_1^A\tau_{\eta k}\boldsymbol{\sigma}_k, \quad (10)$$

with τ_ξ and τ_η the components of the isotopic spin operator, the subscript k referring to the kth nucleon.[10] T_ξ and T_ξ' are eigenvalues of the operator $\frac{1}{2}\sum\tau_{\xi k}$, equal to the initial and final values of $\frac{1}{2}(A-2Z)$. The plus sign in Eq. (9) refers to positron emission and K-capture, the minus sign to negatron emission.

Under the assumption of pure doublet states[11] the wave function can be expressed in the form

$$\psi=\alpha\psi_{L=I-\frac{1}{2}}+(1-\alpha^2)^{\frac{1}{2}}\psi_{L'=I+\frac{1}{2}}, \quad (11)$$

the individual components being assumed normalized. This represents a linear combination of the two L-S coupling states possible for a given value of I. Since parity is a good quantum number, both components in Eq. (11) have the same parity.

Since $\mathbf{Y}_\xi\pm i\mathbf{Y}_\eta$ does not operate on the space coordinates and hence has no matrix elements between states of different L, Eq. (9) becomes

$$\left|\int\sigma\right|^2=\sum_{m'}|\alpha^2(T_\xi',I,L,S,m'|\mathbf{Y}_\xi\pm i\mathbf{Y}_\eta|T_\xi,I,L,S,m)$$
$$+(1-\alpha^2)(T_\xi',I,L',S,m'|\mathbf{Y}_\xi$$
$$\pm i\mathbf{Y}_\eta|T_\xi,I,L',S,m)|^2. \quad (12)$$

These matrix elements can now be evaluated directly by the use of the theory of angular momentum operators and supermultiplet formalism. The result is (see Appendix)

$$\left|\int\sigma\right|^2=|\alpha^2(I+1)-(1-\alpha^2)I|^2/[I(I+1)]. \quad (13)$$

In a similar manner

$$\left|\int 1\right|^2=1. \quad (14)$$

Equation (8) becomes

$$ft\left[\tau+\frac{1}{I(I+1)}\{\alpha^2(I+1)-(1-\alpha^2)I\}^2\right]$$
$$=\frac{\hbar}{mc}\frac{2\pi^3\ln 2}{G_{GT}^2}=C. \quad (15)$$

The mixing coefficients α^2 must now be determined from a theoretical interpretation of the nuclear magnetic moments. Plots of moments against spin in conjunction with the theoretical single particle (Schmidt) and uniform model (Margenau-Wigner) limits[12] are helpful in devising a reasonable interpolation procedure for α^2. As a rule the observed moments are close enough to one or the other of the Schmidt limits to permit an unambiguous assignment of parity and a predominant orbital angular momentum L. These assignments are strongly supported by the success of shell model considerations in interpreting a wide range of nuclear properties.

In the single particle model the odd particle is assumed to move in the spherically symmetric field produced by a core containing all the other particles; this core is assumed to have zero angular momentum, so that if the odd particle is a proton $g_L=1$, while if it is a neutron $g_L=0$. A difficulty arises when an attempt is made to explain deviations from the moments predicted in this way since states with $L=I-\frac{1}{2}$ and $L'=I+\frac{1}{2}$ have opposite parities in a single particle model and cannot be put into the same linear combination. Direct interpolation between the Schmidt limits is therefore meaningless and some other procedure must be used.

If it is assumed that one pure L-S coupling component can be described more or less accurately as representing a single particle interacting with a symmetrical core of even parity, the other component necessarily has a many particle character in order to maintain the same parity in both components. A reasonable estimate of the extent to which both components are present can be derived from a simple interpolation procedure on the moment diagrams. One component is referred to the nearest Schmidt limit (μ_S) and the other to the opposite Margenau-Wigner limit (μ_{MW}); then one computes the quantity

$$\Delta_{S\text{-}MW}=(\mu_S-\mu)/(\mu_S-\mu_{MW}). \quad (16)$$

This interpolation coefficient is interpreted as α^2 or $1-\alpha^2$ depending on the location of μ relative to the Schmidt limits.[13]

For comparison purposes another coefficient $\Delta_{MW\text{-}MW}$ is defined by linear interpolation between the MW

[10] L. Rosenfeld, *Nuclear Forces* (Interscience Publishers, New York, 1949), Chapter IV and Appendix I.

[11] A consequence of the assumed validity of the supermultiplet analysis.

[12] E. Feenberg, Phys. Rev. **77**, 771 (1950).

[13] Interesting and perhaps significant regularities appear in the application of Eqs. (11) and (16) to the available data on moments and spins (private communication from J. P. Davidson).

TABLE I. $C=ft[r|\int 1|^2+|\int \sigma|^2]$ for L-S coupling.

Transition	I	α^2	$\|\int\sigma\|^2$	ft	C	$\Delta=C-\bar{C}$	$C(r=0)$
$n^1\to H^1$	1/2	1	3	1400	$1400r+4200$	$-1777r-48$	4200
$H^3\to He^3$	1/2	1	3	1100	$1100r+3300$	$-2077r-948$	3300
$Be^7\to Li^7$	3/2	1	5/3	2300	$2300r+3830$	$-877r-418$	3830
$C^{11}\to B^{11}$	3/2	1	5/3	3900	$3900r+6500$	$723r+2252$	6500
$N^{13}\to C^{13}$	1/2	0	1/3	4800	$4800r+1600$	$1623r-2648$	1600
$O^{15}\to N^{15}$	1/2	0	1/3	3700	$3700r+1230$	$523r-3018$	1230
$F^{17}\to O^{17}$	5/2	1	7/5	2250	$2250r+3150$	$-927r-1098$	3150
$Ne^{19}\to F^{19}$	1/2	1	3	2000	$2000r+6000$	$-1177r+1752$	6000
$Mg^{23}\to Na^{23}$	3/2	1	5/3	4600	$4600r+7670$	$1423r+3422$	7670
$Si^{27}\to Al^{27}$	5/2	1	7/5	3700	$3700r+5180$	$523r+932$	5180
$S^{31}\to P^{31}$	1/2	1	3	4300	$4300r+12900$	$1123r+8652$	12900
$Cl^{33}\to S^{33}$	3/2	0	3/5	3500	$3500r+2100$	$323r-2148$	2100
$A^{35}\to Cl^{35}$	3/2	0	3/5	3400	$3400r+2040$	$223r-2208$	2040
$K^{37}\to Cl^{37}$	3/2	0	3/5	2700	$2700r+1620$	$-477r-2628$	1620
$Ca^{39}\to K^{39}$	3/2	0	3/5	4000	$4000r+2400$	$823r-1848$	2400
$Na^{21}\to Ne^{21}$	(3/2)	1	5/3	3600	$3600r+6000$		6000
$Na^{21}\to Ne^{21}$	(5/2)	1	7/3	3600	$3600r+8400$	not used in	8400
$Al^{25}\to Mg^{25}$	5/2	1	7/5	(3000)[a]	$3000r+4200$	calculating	4200
$P^{29}\to Si^{29}$	(1/2)	1	3	3800	$3800r+11400$	r and $\bar{C}$	11400
$Sc^{41}\to Ca^{41}$	(7/2)	1	9/7	2550	$2550r+3280$		3280
$Be^7\to Li^{7*}$	3/2→1/2		4/3	3600	$^2P_{\frac{3}{2}}\to{}^2P_{\frac{1}{2}}$; $\int 1\,]^2=0$		4800
$He^6\to Li^6$	0→1		6	550	$^1S_0\to{}^3S_1$; $\int 1\,]^2=0$		3300
$C^{10}\to B^{10*}$	(0→1)		6	2000	$^1S_0\to{}^3S_1$; $\int 1\,]^2=0$		12000
$C^{10}\to B^{10**}$	(0→0)		0	—	$^1S_0\to{}^1S_0$; $\int 1\,]^2=2$		0
$O^{14}\to N^{14*}$	(0→0)		0	3300	$^1S_0\to{}^1S_0$; $\int 1\,]^2=2$		0
$F^{18}\to O^{18}$	(1→0)		2	3700	$^3S_1\to{}^1S_0$; $\int 1\,]^2=0$		7400

( ) assumed value; ( )[a] estimated, $W_0=7.08mc^2$.

$\bar{C}=3177r+4248$; $\langle\Delta^2\rangle_{Av}=(122r^2+143r+892)\times10^6$.

r (for minimum $\langle\Delta^2\rangle_{Av}$) $=0$; minimum $\langle\Delta^2\rangle_{Av}=8.92\times10^6$.

C (for minimum $\langle\Delta^2\rangle_{Av}$) $=4250$; probable error $=2000$.

All ft values were taken from A. M. Feingold, Revs. Modern Phys. **23**, 10 (1951), except for the neutron in which case ft was computed from data given in reference 14, and the mass numbers $A=23$, 27, 31, 33, 37 and 39 for which the ft values were taken from F. I. Boley and D. J. Zaffarano, Phys. Rev. **84**, 1059 (1951).

All spins and moments were taken from J. E. Mack, Revs. Modern Phys. **22**, 64 (1950) except O^{15}—F. Alder and F. C. Yu, Phys. Rev. **81**, 1067 (1951); and S^{33}—moment from Eshbach, Hillger, and Jen, Phys. Rev. **80**, 1106 (1950).

limits and interpreted as α^2 or $1-\alpha^2$ depending on the location of μ. In the uniform model it is assumed that a large number of nucleons contribute in a more or less random fashion to the total orbital angular momentum which is still a constant of motion. As in the single particle model, all spins but one are paired off resulting in a doublet state with a definite value of L (L-S coupling). The orbital gyromagnetic ratio is just the fraction of the orbital angular momentum carried by the protons, or $g_L\sim Z/A$, which has very nearly the value 0.5 for most mirror nuclei. Since this is a many-particle model, states with $L=I+\frac{1}{2}$ and $L=I-\frac{1}{2}$ can have the same parity and hence can enter into a linear combination.

In a few cases (including Li^7 and Na^{23}) $\Delta_{MW\text{-}MW}$ is probably a better measure of the deviations from pure L-S coupling than $\Delta_{S\text{-}MW}$. For Li^7, g_L between 1/3 and 17/42 appears reasonable on theoretical grounds. For Na^{23} the shell model interpretation of the ground state is predominantly $^2P_{\frac{1}{2}}$ of even parity compounded from configurations containing 3, 5, and 7 nucleons in $1d$ orbits. The moment diagram indicates a substantial amount of $^2D_{\frac{1}{2}}$ component.

III. RESULTS

The numerical analysis and results are shown in Tables II and III for the S-MW and MW-MW interpolation procedures. Table I gives the results of the same computation made on the basis of pure L-S coupling, for comparison purposes. In the three tables, $\sigma=(\langle\Delta^2\rangle_{Av})^{\frac{1}{2}}$ is the standard (root-mean-square) deviation, while $e=0.6745\sigma$ is the probable error. Table IV summarizes the calculations. No experimental uncertainties are listed for the ft products, but it is likely that few of the given values are in error by as much as 20 percent.

Let us first dispose of L-S coupling (Table I). Here the addition of a Fermi-type term makes matters worse in 9 transitions out of 15 and the best value of r is clearly 0. The square of the standard deviation is 8.9×10^6 and $\bar{C}$ is 4250 with a probable error of 2000. About $\frac{3}{4}$ of $\langle\Delta^2\rangle_{Av}$ is contributed by the $S^{31}\to P^{31}$ transition. Actually $\langle\Delta^2\rangle_{Av}$ depends only slightly on r and $r=0.5$ is only slightly inferior to $r=0$. The good agreement between the H^3 and He^6 transitions for $r=0$ is balanced by the difficulty with the 0→0 interpretation of the $O^{14}\to N^{14*}$ transition.

In Table II (S-MW interpolation procedure) the need for a Fermi-type term is clearly indicated by 12 out of 15 transitions. However, even with $r=0$ the square of the standard deviation is only 2.0×10^6 (compare with 8.9×10^6 for L-S coupling). Much of this reduction comes from the greatly reduced value of

TABLE II. $C=ft[r|\int 1|^2+|\int \boldsymbol{\sigma}|^2]$ from *S-MW* interpolation procedure.

Transition	I	α^2	$\lvert\int\boldsymbol{\sigma}\rvert^2$	ft	C	$\Delta=C-\bar{C}$	C
$n^1\to H^1$	1/2	1	3	1400	$1400r+4200$	$-1777r+2152$	5360
$He^5\to H^3$	1/2	1	3	1100	$1100r+3300$	$-2077r+1252$	4210
$Be^7\to Li^7$	3/2	0.88	1.09	2300	$2300r+2510$	$-877r+462$	4420
$C^{11}\to B^{11}$	3/2	0.76	0.61	3900	$3900r+2380$	$723r+332$	5620
$N^{13}\to C^{13}$	1/2	0	1/3	4800	$4800r+1600$	$1623r-448$	5580
$O^{15}\to N^{15}$	1/2	0	1/3	3700	$3700r+1230$	$523r-818$	4300
$F^{17}\to O^{17}$	5/2	0.99	1.37	2250	$2250r+3080$	$-927r+1032$	4950
$Ne^{19}\to F^{19}$	1/2	0.95	2.65	2000	$2000r+5300$	$-1177r+3252$	6960
$Mg^{23}\to Na^{23}$	3/2	0.65	0.33	4600	$4600r+1520$	$1423r-528$	5340
$Si^{27}\to Al^{27}$	5/2	0.78	0.57	3700	$3700r+2110$	$523r+62$	5180
$S^{31}\to P^{31}$	1/2	0.45	0.22	4300	$4300r+950$	$1123r-1098$	4520
$Cl^{35}\to S^{35}$	3/2	0.20	0.13	3500	$3500r+450$	$323r-1598$	3350
$A^{39}\to Cl^{39}$	3/2	0.22	0.10	3400	$3400r+340$	$223r-1708$	3160
$K^{37}\to Cl^{37}$	3/2	0.18	0.16	2700	$2700r+430$	$-477r-1618$	2670
$Ca^{39}\to K^{39}$	3/2	0.08	0.33	4000	$4000r+1320$	$823r-728$	4640
$Al^{29}\to Mg^{29}$	5/2	0.80	0.59	(3000)	$3000r+1770$	not used in calculating $\bar{C}$ and r	4260
$Be^7\to Li^{7*}$	3/2→1/2		$4/3\times 0.88$	3600	$0.88(^3P_2\to{}^3P_1)$		4220
$C^{10}\to B^{10*}$[a]	(0→0)		0	—	$^1S_0\to{}^1S_0;\ \lvert\int 1\rvert^2=2$		—
$O^{14}\to N^{14*}$	(0→0)		0	3300	$^1S_0\to{}^1S_0;\ \lvert\int 1\rvert^2=2$		5470

( ) assumed value from Table I; He^6, $C^{10}(0\to1)$, F^{18} as in Table I.
$\bar{C}=3177r+2048$; $\langle\Delta^2\rangle_{Av}=(122r^2-203+194)\times10^4$.
r (for minimum $\langle\Delta^2\rangle_{Av}=0.83$; minimum $\langle\Delta^2\rangle_{Av}=1.1\times10^6$.
$\bar{C}$ (for minimum $\langle\Delta^2\rangle_{Av}=4700$; probable error $=710$.
[a] A weak branch with energy and intensity about right for the 0→0 interpretation has been observed recently (private communication from Professor R. Sherr).

$|\int\boldsymbol{\sigma}|^2$ for the $Si^{31}\to P^{31}$ transition. The optimum value of r (0.83) cuts $\langle\Delta^2\rangle_{Av}$ nearly in half and gives $\bar{C}=4700$ with a probable error of 700. A more impressive measure of the improvement resulting from the *S-MW* interpolation procedure is shown in the bottom line of Table IV; the square of the relative standard deviation $\langle\Delta^2\rangle_{Av}/\bar{C}^2$ is reduced by a large factor when the optimum amount of Fermi-type coupling is put into the calculation.

Table III shows that the *MW-MW* interpolation procedure results in a substantially better fit to beta-decay theory than pure *L-S* coupling, but is definitely less satisfactory than the generally more plausible *S-MW* procedure. It is perhaps significant that both interpolation procedures yield substantially the same value of $\bar{C}$, slightly smaller than 5000 and nearly the same value for r.

The still sizeable dispersion found in the two mixed

TABLE III. $C=ft[r|\int 1|^2+|\int \boldsymbol{\sigma}|^2]$ from *MW-MW* interpolation procedure.

Transition	I	α^2	$\lvert\int\boldsymbol{\sigma}\rvert^2$	ft	C	$\Delta=C-\bar{C}$	C
$n^1\to H^1$	1/2	1	3	1400	$1400r+4200$	$-1777r+1980$	5350
$H^3\to He^3$	1/2	1	3	1100	$1100r+3300$	$-2077r+1080$	4200
$Be^7\to Li^7$	3/2	0.99	1.61	2300	$2300r+3700$	$-877r+1480$	5580
$C^{11}\to B^{11}$	3/2	0.85	0.96	3900	$3900r+3740$	$723r+1520$	6940
$N^{13}\to C^{13}$	1/2	0.10	0.13	4800	$4800r+620$	$1623r-1600$	4550
$O^{15}\to N^{15}$	1/2	0.09	0.13	3700	$3700r+480$	$523r-1740$	3510
$F^{17}\to O^{17}$	5/2	1	7/5	2250	$2250r+3150$	$-927r+930$	4990
$Ne^{19}\to F^{19}$	1/2	0.95	2.65	2000	$2000r+5300$	$-1177r+3080$	6940
$Mg^{23}\to Na^{23}$	3/2	0.74	0.55	4600	$4600r+2530$	$1423r+310$	6300
$Si^{27}\to Al^{27}$	5/2	0.96	1.24	3700	$3700r+4590$	$523r+2370$	7620
$S^{31}\to P^{31}$	1/2	0.51	0.36	4300	$4300r+1550$	$1123r-670$	5070
$Cl^{35}\to S^{35}$	3/2	0.41	0.01	3500	$3500r+50$	$323r-2170$	2920
$A^{39}\to Cl^{39}$	3/2	0.39	0.00	3400	$3400r+0$	$223r-2220$	2780
$K^{37}\to Cl^{37}$	3/2	0.40	0.00	2700	$2700r+0$	$-477r-2220$	2210
$Ca^{39}\to K^{39}$	3/2	0.29	0.03	4000	$4000r+120$	$823r-2100$	3400
$Al^{29}\to Mg^{29}$	5/2	1	7/5	(3000)	$3000r+4200$	not used in calculating $\bar{C}$ and r	6660
$Be^7\to Li^{7*}$	3/2→1/2		$0.99\times4/3$	3600	$0.99(^3P_2\to{}^3P_1)$		4750

( ) assumed value from Table I; He^6, $C^{10}(0\to1)$, F^{18} as in Table I; $C^{10}(0\to0)$, O^{14} as in Table II.
$\bar{C}=3177r+2220$; $\langle\Delta^2\rangle_{Av}=(122r^2-199r+338)\times10^4$.
r (for minimum $\langle\Delta^2\rangle_{Av}=0.82$; minimum $\langle\Delta^2\rangle_{Av}=2.6\times10^6$.
$\bar{C}$ (for minimum $\langle\Delta^2\rangle_{Av}=4800$; probable error $=1100$.

TABLE IV. Summary of results from Tables I–III.

	L–S coupling		S-MW for α^2		MW–MW for α^2	
r	0	1	0	1	0	1
$\langle\Delta^2\rangle_{Av}$	8.9×10^6	11.6×10^6	1.9×10^6	1.1×10^6	3.4×10^6	2.6×10^6
$\bar{C}$	4250	7420	2050	5220	2220	5400
$\langle\Delta^2\rangle_{Av}/\bar{C}^2$	0.49	0.21	0.45	0.041	0.70	0.089

state models can be assigned to three causes in addition to experimental errors involved in the ft values. One is the fact that in making the calculations, the same mixing of states was tacitly assumed in parent and daughter nuclei. This is the expected relation from the symmetry principle on which the supermultiplet analysis is founded; but it may not be exactly correct. The second, and probably more important, factor is that the wave functions are in any case not exact. The true wave functions probably contain quartet and even higher spin multiplet terms, which may make fairly strong contributions to $|\int\sigma|^2$. Such additional terms may possibly not produce serious alteration in the values of either $\bar{C}$ or r in virtue of the averaging process by which these values are computed.

Actually there is evidence,[14] based on calculations with tensor forces, that the ground states of H^3 and He^3 contain an admixture of a $^4D_{\frac{1}{2}}$ component with a statistical weight of 4 percent. The beta-decay matrix element for the $^4D_{\frac{1}{2}}$ component is identical with that of $^2P_{\frac{1}{2}}$, so that Eq. (13) can be used without change if $1-\alpha^2$ is identified with the statistical weight of the $^4D_{\frac{1}{2}}$ component.[15]

A third and perhaps most important source of error is the probable inaccuracy of the interpolation procedures used to determine the amount of mixing. Recognition of this possibility is helpful in restoring some freedom of action. To discover in which direction to go consider $ft|M|^2$ for $He^6\rightarrow Li^6$ from Table I. This value,[16] 3300, may be compared with $\bar{C}$ computed from Table II:

$$\bar{C}=2050,\quad r=0$$
$$=5220,\quad r=1.$$

To bring $\bar{C}$ into agreement with the He^6 transition requires $r^2\sim0.5$ (or $\bar{C}\sim3600$). Similarly $ft|M|^2$ for $O^{14}\rightarrow N^{14*}$ is reduced to 3300 for $r=0.5$ in line with $\bar{C}$ and the He^6 transition. These considerations suggest seeking a compromise solution with $r=0.5$ and α^2 adjusted slightly from the S-MW values to improve the over-all constancy of $ft|M|^2$. Actually the adjustments, shown in Table V, are generally rather small.

One may conclude that a variety of errors, both theoretical and experimental, tend to an overestimate of r in the analysis of Tables II and III. A compromise solution with $r=0.5$ fits all the data fairly well except for $n^1\rightarrow H^1$, $C^{10}(0)\rightarrow B^{10*}(1)$, $F^{18}(1)\rightarrow O^{18}(0)$ and $Ne^{19}\rightarrow F^{19}$. The first exception may be improved by a substantial reduction in the measured half-life of the neutron just outside the present reported limits of error.[17] The second can be interpreted in terms of a linear combination $^3S_1+{}^3D_1+{}^1P_1$ for the excited state of B^{10} with $^3S_1$ having a statistical weight of 30 percent. This makes the lowest $I=1$ state of B^{10} intermediate in mixing properties between the ground states of Li^6 (almost pure $^3S_1$) and N^{14} (relatively little $^3S_1$). A similar explanation fits the F^{18} transition. The fourth exception may perhaps indicate a small error in the measurement of the transition energy.

The end results are values for Gf^2 and G_{GT}^2. Computed from Table II on the basis of the S-MW interpolation procedure they are

$$G_{GT}^2=(1.16\pm0.15)\pm10^{-23},$$
$$Gf^2=(0.96\pm0.13)\pm10^{-23}. \tag{17}$$

The error is simply the statistical error in the evaluation of $\bar{C}$. The compromise solution yields what are thought to be more reliable values

$$G_{GT}^2=1.65\times10^{-23},\quad Gf^2=0.82\times10^{-23}. \tag{18}$$

The compromise ratio, $r=0.5$, is just outside the upper limit derived by Moszkowski from an analysis

TABLE V. Compromise solution: $r=0.5$ and α^2 adjusted for best fit.

Transition	I	α^2 (S-MW)	α^2 (adjusted)	$\lvert\int\sigma\rvert^2$	$\lvert M\rvert^2$	$ft\lvert M\rvert^2$
$n^1\rightarrow H^1$	1/2	1	1	3	3.51	4900
$H^3\rightarrow He^3$	1/2	1	0.95	2.61	3.11	3400
$Be^7\rightarrow Li^7$	3/2	0.85	0.85	0.96	1.46	3350
$C^{11}\rightarrow B^{11}$	3/2	0.76	0.68	0.40	0.90	3500
$N^{13}\rightarrow C^{13}$	1/2	0	0.05	0.21	0.71	3400
$O^{15}\rightarrow N^{15}$	1/2	0	0	0.33	0.83	3100
$F^{17}\rightarrow O^{17}$	5/2	0.99	0.95	1.17	1.67	3800
$Ne^{19}\rightarrow F^{19}$	1/2	0.95	0.90[a]	2.35	2.85	5700
$Na^{21}\rightarrow Ne^{21}$	(3/2)	—	0.70	0.45	0.95	3400
$Na^{21}\rightarrow Ne^{21}$	(5/2)	—	0.75	0.46	0.96	3400
$Mg^{23}\rightarrow Na^{23}$	3/2	0.65	0.60	0.22	0.72	3300
$Al^{25}\rightarrow Mg^{25}$	5/2	0.80	0.80	0.59	1.09	3300
$Si^{27}\rightarrow Al^{27}$	5/2	0.78	0.73	0.40	0.90	3300
$P^{29}\rightarrow Si^{29}$	(1/2)	—	0.52	0.39	0.89	3400
$P^{29}\rightarrow Si^{29}$	(3/2)	—	0.07	0.40	0.90	3400
$Si^{31}\rightarrow P^{31}$	1/2	0.45	0.48	0.28	0.78	3400
$Cl^{35}\rightarrow S^{35}$	3/2	0.20	0.10	0.32	0.82	2900
$A^{35}\rightarrow Cl^{35}$	3/2	0.22	0.12[b]	0.28	0.78	2700
$K^{37}\rightarrow A^{37}$	(3/2)	—	0.00	0.60	1.10	3000
$Ca^{39}\rightarrow K^{39}$	3/2	0.08	0.08	0.33	0.83	3300
$Sc^{41}\rightarrow Ca^{41}$	(7/2)	—	0.88	0.79	1.29	3300
$Be^7\rightarrow Li^{7*}$	3/2→1/2	$x(^3P_{\frac{1}{2}}\rightarrow{}^3P_{\frac{1}{2}})$		$4/3x$	$4/3x$	4800x[c]
$He^6\rightarrow Li^6$	0→1	$^1S_0\rightarrow{}^3S_1$		6	6	3300
$C^{10}\rightarrow B^{10*}$	(0→1)	$y(^1S_0\rightarrow{}^3S_1)$		$6y$	$6y$	12000y[d]
$C^{10}\rightarrow B^{10**}$	(0→0)	$^1S_0\rightarrow{}^1S_0$		0	1	—
$O^{14}\rightarrow N^{14*}$	(0→0)	$^1S_0\rightarrow{}^1S_0$		0	1	3300
$F^{18}\rightarrow O^{18}$	(1→0)	$z(^3S_1\rightarrow{}^1S_0)$		$2z$	$2z$	7400z[e]

( ) assumed value.
a,b—a good fit would require excessively large adjustment.
c—$x\sim0.7$ consistent with 85 percent $^3P_{3/2}$ and 85 percent $^3P_{1/2}$.
d—$y\sim0.3$ consistent with 30 percent $^3S_1$ in the linear combination $^3S_1+{}^3D_1+{}^1P_1$.
e—$z\sim0.45$ consistent with 45 percent $^3S_1$ in the linear combination $^3S_1+{}^3D_1+{}^1P_1$.

[14] H. Feshbach and R. L. Pease, private communication.
[15] Private communication from Dr. E. Feenberg.
[16] Based on data reported by V. Perez-Mendez and H. Brown, Phys. Rev. 77, 404 (1950).
[17] J. M. Robson, Phys. Rev. 83, 349 (1951).

using only a small part of the available data.[18] Equation (17) is roughly consistent with the Wigner-Critchfield interaction containing equal weights of the scalar, axial vector, and pseudoscalar combinations. However, recent analyses[19,20] seem to favor the tensor over the axial vector. In any event tentative conclusions that the correct interaction is a pure Gamow-Teller type should be carefully re-examined.

The author wishes to express his appreciation to Dr. Eugene Feenberg for suggesting this problem and for much valuable advice and criticism. Thanks are due Dr. D. C. Peaslee and Dr. C. S. Cook for helpful and stimulating discussion. He also derived much of value from unpublished notes on the image transitions by E. P. Wigner and A. M. Feingold.

APPENDIX. DERIVATION OF EQUATION (13)

If a vector operator $\mathbf{Q}$ satisfies the commutation relations

$$[I_x, Q_x]=0, \quad [I_x, Q_y]=iQ_z, \quad [I_x, Q_z]=iQ_y,$$

and others obtained from these by cyclic permutation of subscripts, then the general theory of angular momentum gives[21]

$$(\gamma' Im'|\mathbf{Q}|\gamma Im) = (Im'|\mathbf{I}|Im)(\gamma' Im|\mathbf{I}\cdot\mathbf{Q}|\gamma Im)/[I(I+1)], \quad \text{(A1)}$$

where the first factor on the right is independent of γ and the last independent of m; γ and γ' represent all the additional quantum numbers necessary to specify the state completely. Since the operators $\mathbf{Y}_\xi \pm i\mathbf{Y}_\eta$ are of this type, the rule (A1) can be applied to the matrix elements in Eq. (6), giving

$$\left|\int\sigma\right|^2=\frac{1}{I^2(I+1)^2}\sum_{m'}|(Im'|\mathbf{I}|Im)|^2|\alpha^2(T_t'LSI|\mathbf{I}\cdot(\mathbf{Y}_\xi\pm i\mathbf{Y}_\eta)|T_tLSI)+(1-\alpha^2)(T_t'L'SI|\mathbf{I}\cdot(\mathbf{Y}_\xi\pm i\mathbf{Y}_\eta)|T_tL'SI)|^2, \quad \text{(A2)}$$

where only the parameters on which a matrix element depends have been retained. But

$$\sum_{m'}|(Im'|\mathbf{I}|Im)|^2=(Im|\mathbf{I}^2|Im)=I(I+1),$$

so Eq. (A2) becomes

$$\left|\int\sigma\right|^2=\frac{1}{I(I+1)}|\alpha^2(T_t'LSI|\mathbf{I}\cdot(\mathbf{Y}_\xi\pm i\mathbf{Y}_\eta)|T_tLSI) +(1-\alpha^2)(T_t'L'SI|\mathbf{I}\cdot(\mathbf{Y}_\xi\pm i\mathbf{Y}_\eta)|T_tL'SI)|^2. \quad \text{(A3)}$$

It is now possible to make use of an important feature of the supermultiplet formalism, namely, that the values of the matrix elements of any operator connecting only states within a supermultiplet depend only on the quantum numbers of the states involved and the character of the supermultiplet. It is thus possible to calculate these matrix elements using functions and operators appropriate to the simplest configuration capable of generating the supermultiplet. For the nuclei involved in the image transitions, these are either one- or three-particle functions. In the one-particle case, the calculation can be carried out without recourse to explicit functions, as shown below; the final results are the same for the three-particle case, as has been verified by direct calculation.

For one particle, the operator $\mathbf{I}\cdot(\mathbf{Y}_\xi\pm i\mathbf{Y}_\eta)$ takes the form

$$\mathbf{I}\cdot(\mathbf{Y}_\xi\pm i\mathbf{Y}_\eta)=(\mathbf{L}+\mathbf{S})\cdot\mathbf{S}(\tau_\xi\pm i\tau_\eta) =(\mathbf{L}\cdot\mathbf{S}+\mathbf{S}^2)(\tau_\xi\pm i\tau_\eta). \quad \text{(A4)}$$

But

$$\mathbf{L}\cdot\mathbf{S}=1/2(\mathbf{I}^2-\mathbf{L}^2+\mathbf{S}^2),$$

so Eq. (A4) becomes

$$\mathbf{I}\cdot(\mathbf{Y}_\xi\pm i\mathbf{Y}_\eta)=(T_\xi\pm iT_\eta)(\mathbf{I}^2-\mathbf{L}^2+\mathbf{S}^2).$$

Insertion of this into Eq. (A3) gives

$$\left|\int\sigma\right|^2=\frac{1}{I(I+1)}|(T_t'|T_\xi \pm iT_\eta|T_t)|^2|\alpha^2(LSI|\mathbf{I}^2-\mathbf{L}^2+\mathbf{S}^2|LSI) +(1-\alpha^2)(L'SI|\mathbf{I}^2-\mathbf{L}^2+\mathbf{S}^2|L'SI)|^2. \quad \text{(A5)}$$

Now for the mirror transitions,

$$|(T_t'|T_\xi\pm iT_\eta|T_t)|^2=1;$$

moreover, the partial wave functions are chosen to be eigenfunctions of $\mathbf{I}^2$, $\mathbf{L}^2$, and $\mathbf{S}^2$. Thus Eq. (A5) becomes

$$\left|\int\sigma\right|^2=\frac{1}{I(I+1)}|\alpha^2(I(I+1)-L(L+1)+S(S+1)) +(1-\alpha^2)(I(I+1)-L'(L'+1)+S(S+1))|^2.$$

Insertion into this of the assumed values $S=\frac{1}{2}$, $L=I-S$, $L'=I+S$ gives just Eq. (13).

[18] S. A. Moszkowski, Phys. Rev. **82**, 118 (1951).
[19] H. W. Fulbright and J. C. D. Milton, Phys. Rev. **82**, 274 (1951).
[20] L. M. Langer and R. J. D. Moffat, Phys. Rev. **82**, 635 (1951).
[21] E. U. Condon and G. H. Shortley, *The Theory of Atomic Spectra* (Cambridge University Press, London, 1935), p. 61.

Mean Life of the Positive π-Meson*

WILLIAM L. KRAUSHAAR
Department of Physics and Laboratory for Nuclear Science and Engineering, Massachusetts Institute of Technology, Cambridge, Massachusetts

Received January 25, 1952)

Photoproduced π^+ mesons stopped and decayed in a xylene-terphenyl liquid scintillation counter. The pulses from the counter were amplified and displayed on two oscilloscopes. The entire sequence $\pi^+ \rightarrow \mu^+ \rightarrow e^+$ could be observed, and from the measurement of 670 π-μ decay times, a value of $(2.53 \pm 0.10) \times 10^{-8}$ sec was obtained for the π^+ mean life.

I. INTRODUCTION

IN a previous communication[1] the writer, Thomas, and Henri have described some preliminary results of an experiment designed to measure the mean life, τ_{π^+}, of π^+ mesons. Photoproduced π^+ mesons were allowed to decay in a stilbene crystal, and on the basis of 57 observed decays a value for τ_{π^+} of $(1.65 \pm 0.33) \times 10^{-8}$ sec was obtained. Subsequently, Chamberlain, Mozley, Steinberger, and Weigand[2] and Weigand[3] using similar techniques found a value of $(2.58 \pm 0.14) \times 10^{-8}$ sec, and Jakobson, Schulz, and Steinberger[4] using an electronic counting method found $(2.54 \pm 0.11) \times 10^{-8}$ sec. An improved version of our preliminary experiment has now been completed and a value of $(2.53 \pm 0.10) \times 10^{-8}$ sec has been found.

The most recent determination of the π^- mean life,[5] $(2.92 \pm 0.32) \times 10^{-8}$ sec, was based upon observations of the decay of π^- mesons in flight. This value is seen to be in reasonable agreement with the later π^+ mean life determinations.

II. EXPERIMENTAL ARRANGEMENT

The experimental arrangement used in the present measurement is shown in Fig. 1. γ-rays from the MIT synchrotron struck the polyethylene target, producing π^+ mesons. Some of these mesons traversed the two absorbers, S_1 and S_2, passed through counter A and stopped in counter B. Counters A, B, and C consisted of aluminum cans cemented to photomultiplier tubes and filled with a terphenyl-xylene solution. The pulses originating in counter B were amplified, delayed, and displayed on two oscilloscopes, one having sufficient over-all resolution to show the π-μ decay when the decay time was not too short, and the other arranged to show the μ-e decay. Hence the complete decay, $\pi \rightarrow \mu \rightarrow e$, could be observed when the decay times were favorable. The sweep circuits associated with the two oscilloscopes were triggered by AB–C anticoincidences. That is, the sweeps were triggered whenever simultaneous pulses were received from counters A and B unaccompanied by a pulse from counter C. The oscilloscope traces were photographed on a continuously moving film.

The apparatus was located 16 feet from the synchrotron target, and the beam at this location was 2 inches in diameter after collimation. The synchrotron was pulsed twice a second, and the γ-rays were emitted more or less uniformly over a period of about 1600 microseconds. Each burst of γ-rays produced an ionization of about $0.4r$ in a Victoreen r meter placed 1 meter from the synchrotron target and surrounded by $\frac{1}{8}$ in. of lead. The polyethylene target was 2 g cm^{-2} thick and essentially covered the beam in its transverse dimensions.

The experimental data were obtained in about 40 hours of synchrotron running time. During this time, there were approximately 12,000AB–C anticoincidences, and hence about 12,000 oscilloscope sweeps. Of these events, about 1500 corresponded to the stopping of π^+ mesons in counter B.

The background rate of pulses with heights corresponding to an energy loss greater than 1 Mev in counter B, was about 2 per synchrotron pulse. The AB coincidence rate was about three times as large as the AB–C anticoincidence rate.

III. SELECTION OF EVENTS

For purposes of discussion the various pulses will be given phenomenological descriptions. The times referred

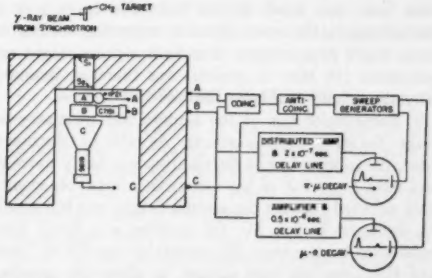

FIG. 1. Schematic representation of experimental arrangement.

* Assisted by the joint program of the ONR and AEC.

[1] Kraushaar, Thomas, and Henri, Phys. Rev. **78**, 486 (1950).

[2] Chamberlain, Mozley, Steinberger, and Wiegand, Phys. Rev. **79**, 394 (1950).

[3] C. Weigand, Phys. Rev. **83**, 1085 (1951).

[4] Jakobson, Schulz, and Steinberger, Phys. Rev. **81**, 894 (1951).

[5] Lederman, Booth, Byfield, and Kessler, Phys. Rev. **83**, 685 (1951).

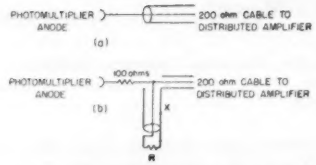

FIG. 2. Photomultiplier connections. Part *a* shows the arrangement as used in the experiment proper. Part *b* shows the arrangement for producing simulated π-μ decays. The cable x determined the decay time, and the resistor R determined the relative height of the μ-pulse. The 100-ohm resistor served to keep the photomultiplier clipping time the same for arrangements *a* and *b*.

to are measures of the interval from the start of the trace to the peak of the pulse in question.

π, the pulse responsible for the AB–C anticoincidence.
μ, a pulse following the π if $t_\mu - t_\pi < 30\times10^{-8}$ sec.
e, a pulse with a delay between 30×10^{-8} sec and 10.8×10^{-10} sec relative to the μ, or if no μ was resolved, relative to the π.

There follows a summary of the various criteria used in selecting those events suitable for inclusion in the mean life evaluation.

1. No π-μ-like event was included that was not accompanied by an electron or e pulse as defined above. The number of accidental e pulses was small, and this criterion made possible the very small number of accidental π-μ-like events.

2. It was required that the height of the e pulse correspond to an energy loss of at least 1 Mev.

3. π-μ-e decays having μ-e decay times less than 30×10^{-8} sec were excluded, because there was a fair probability that the electron would go through the anticoincidence counter, and so be instrumental in rejecting selectively those events with a total π-μ-e decay time as short or shorter than the anticoincidence resolving time (15×10^{-8} sec). The π^+ mean life value would have been effected by about 1 percent if this point had been neglected.

4. The discriminator on the counter C coincidence amplifier was set at 8 Mev, and the resolving time was about 8×10^{-8} sec. This relatively long resolving time resulted in successful triggering of the apparatus on some short π-μ decays where the π-pulse alone would have been too small. Hence for pulse heights in a limited region, there was selective triggering tending to favor short decay times. The final π-pulse-height requirement (10 Mev or greater) was therefore imposed after the heights had been measured *on the film*.

5. Some finite size of the μ-pulse was necessary to make the time measurements. As will be discussed later, the μ-pulse-height distribution was fairly narrow, and only 3 percent of the otherwise acceptable events were rejected because the μ-pulse height was too small. As discussed in Sec. IV, the smallest π-μ decay time considered for the mean life evaluation was 2×10^{-8} sec, and this time was long enough to allow the μ-pulse-height measurements to be made in all cases.

IV. FILM READING TECHNIQUE

It was felt desirable to examine the relative merits of various proposed methods of measuring the π-μ pulse separation, and to determine rationally the smallest π-μ decay time to be included in the mean life evaluation. Artificial π-μ decays with known time separation were produced, using the arrangement shown in Fig. 2. The electrical length of the cable x (as measured by resonating it as a half-wave line) determined the time difference of the pulses simulating π-μ decay, and the resistor R determined the relative height of the "μ"-pulse. A large number of these pulses were photographed and examined. Included were relative π- and μ-heights that covered the spread known to exist in the actual data, and delays from 10^{-8} to 17×10^{-8} sec. The method of measurement adopted involved measuring the distance from the start of the trace to the projection of the peak of the π- and μ-pulses on the baseline. The times corresponding to these distances were read from a graph of the sweep time *versus* distance, and the π-μ time separation was obtained by subtraction. Many measurements of the same time difference gave a distribution with a rms deviation about the average of 5×10^{-10} sec, provided this difference was at least 1.7×10^{-8} sec. Seven time differences were measured, and in no case did the average differ from the true value by more than 6×10^{-10} sec. The nature of the deviations of the averages from the true values were such, that we believe there to be no systematic error larger than 2 percent in the mean life arising from the measuring technique alone. Although the time measurements were accurate at 1.7×10^{-8} sec, they became very inaccurate at smaller times. It was felt, therefore, that 2×10^{-8} sec was a safe lower limit for the π-μ decay time measurements.

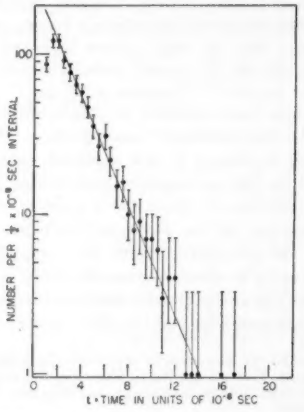

FIG. 3. Differential plot of the number of π-μ decay times per $\frac{1}{2}\times10^{-8}$ sec interval *versus* time. The slope of the line corresponds to a mean life of 2.53×10^{-8} sec. Only those decay times $>2\times10^{-8}$ sec were included in the mean life evaluation.

The sweep was recalibrated at approximately one hour intervals throughout the experiment. For this purpose, a 50.00 mc sine wave was fed directly into the amplifier and these sweeps were photographed exactly as was done for the data. The largest deviation from the original calibration was 1.5 percent. The small corrections for these deviations were applied directly to the π-μ time differences.

V. RESULTS

As mentioned before, there were about 12,000 AB–C anticoincidences. Examination of the film revealed that 1831 of these were accompanied by an e pulse. About 900 of those having an e pulse had also a pulse interpretable as a μ, and the μ was delayed relative to the π by at least 2×10^{-8} sec in 670 cases out of the 900.

A differential plot of the number of acceptable π-μ decays per 5×10^{-9} sec interval *versus* time is shown in Fig. 3, and the corresponding integral plot of the number of decays observed after time t *versus* t is shown in Fig. 4. As has been shown by Peierls,[6] the best approximation to the mean life is just the mean of all the time observed. In the present case only decay times longer than 2×10^{-8} sec have been considered, so we have evaluated the mean life from the equation

$$\tau_m=\left(\frac{1}{N}\sum_{i=1}^{N}\tau_i-2\times10^{-8}\right)\text{ sec.}$$

This gave $\tau_m=2.54\times10^{-8}$ sec. The procedure described is valid only when there is no sensible upper limit to the time being measured. In the present case, no delay longer than 30×10^{-8} sec would have been counted. The correction for the possible neglect of these decays is entirely negligible.

There were no acceptable π-μ decays with time differences greater than 17.5×10^{-8} sec, so if any accidental events have contributed to our result, they must

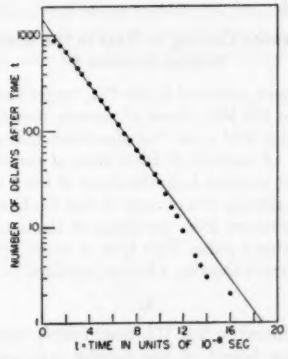

FIG. 4. Integral plot of the number of π-μ decay times larger than t *versus* time, t.

[6] R. E. Peierls, Proc. Roy. Soc. (London) **149**, 467 (1935).

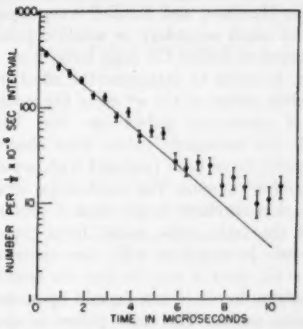

FIG. 5. Differential plot of the number of μ-e decay times per $\frac{1}{2}\times10^{-8}$ sec interval *versus* time. The slope of the line corresponds to a mean life of 2.15×10^{-6} sec.

have occurred in the interval 2 to 17.5×10^{-8} sec. The most likely source of accidental events involved real but unresolved π-μ decays having the μ-e decay time in the interval 2 to 17.5×10^{-8} sec. An accidental but acceptable e pulse would then cast the event among those included in the mean life evaluation. The total number of events of this type is calculated to be 0.5. A second possible source of accidental events involved cases such as the $1831-900=931$ events in which there was an acceptable e pulse and no resolved μ. An accidental μ-pulse in the interval 2 to 17.5×10^{-8} sec would then cast an event such as this among those included in the mean life evaluation also. The total number of events of this type is calculated to be 0.2. The calculated number of accepted but accidental events for the entire experiment is then 0.7, and the best value for the mean life is changed to 2.53×10^{-8} sec. The lines on the differential and integral plots, Figs. 3 and 4, have been drawn with slopes corresponding to this mean life, and with a normalization such that the number of decays after 2×10^{-8} sec is 670.

Figure 5 shows a differential plot of the number of e pulses per 0.5×10^{-6} sec interval *versus* time. The line has been drawn with a slope corresponding to the known mean life of the μ-meson, 2.15×10^{-6} sec. The calculated number of accidental events included here is 7 per 0.5×10^{-6} sec interval. A background of this number of accidentals is evident from an inspection of Fig. 5.

VI. DISCUSSION OF ERRORS

The largest uncertainty in the result is due to the finite number of observations, N, and Peierls has shown that the fractional standard error is just $1/\sqrt{N}$. As discussed above, systematic errors in the measuring technique have been investigated, and have been shown to be not larger than 2 percent. This should be lowered to about 1.5 percent for consistent inclusion with the statistical uncertainty, which is given as a standard error.

Godfrey, Harrison, and Keuffel[7] have reported the existence of small secondary or satellite pulses which were observed to follow the main pulse from a photomultiplier. In order to determine the effect, if any, of these satellite pulses on the π^+ mean life result, a large number of cosmic-ray pulses (see Sec. VIII) were examined. No secondary pulses were observed that could possibly have been confused with μ-pulses from the decay of π^+ mesons. The oscilloscope arrangement was such that satellites larger than 5 percent of the height of the main pulse would have been noticed. This is not inconsistent with the observations of Godfrey *et al.*, since it may be that the satellite pulse-height distribution does not depend upon the heights of the main pulses. The main pulses in the present experiment probably arose from many more photoelectrons than did the main pulses discussed by Godfrey *et al.*

It is important to note that the test measurements using artificially produced π-μ decays, as discussed in Sec. IV, reflect only on the accuracy of the film-ready technique and do not imply the existence of similar accuracy in the determination of any individual real π-μ decay time. This is because both the π- and μ-pulses in these tests were derived from the same photomultiplier current pulse. The time from the creation of the ionization and excitation in the scintillator to the appearance of the peak of the pulse is subject to fluctuations, arising for the most part, from the finite number of photoelectrons ejected from the cathode of the photomultiplier tube and from fluctuations in the photomultiplier response time. Examination of the rise times of many pulses has shown that these fluctuations are certainly much less than 10^{-8} sec. Anyway, such fluctuations as did exist were randomly distributed among all of the π-μ decays observed. It can be shown that the effect on the π^+ mean life is just to increase the standard error by a factor of $[1+(\alpha/\tau)^2]^{\frac{1}{2}}$ over what it would be from statistics alone. Here τ is the mean life and α is the rms deviation of the distribution of fluctuations in the π-μ time difference measurements. Since α is appreciably less than τ, the above factor does not differ sensibly from one.

The statistical error has been combined with the estimated systematic error, and the result for the π^+ mean life is

$$\tau_m=(2.53\pm0.10)\times10^{-8}\text{ sec.}$$

This value for τ_m is not in good agreement with the preliminary value $(1.65\pm0.33)\times10^{-8}$ sec reported previously. We are not aware of any systematic error in the earlier measurement as large as would apparently be necessary to account for this discrepancy. On the other hand, systematic errors were more carefully investigated in the present experiment, and the final result for τ_m given above has been evaluated using only the 670 π-μ decays from this experiment.

[7] Godfrey, Harrison, and Keuffel, Phys. Rev. **84**, 1248 (1951).

VII. UNRESOLVED π-μ DECAYS

There were a total of 1831 traces with acceptable e pulses, and 670 of these had μ-pulses with delays of 2×10^{-8} sec or greater. The calculated number of π-μ decays that occurred in the interval 0 to 2×10^{-8} sec is 800 ± 40, the uncertainty arising from the uncertainty in the π^+ mean life. The total number of π-μ decays is therefore 1470 ± 40, and it is interesting to inquire as to the origin of the remaining 360 ± 40 traces which had e pulses but no μ's. There were several contributing effects as discussed below.

1. Accidentals

There were $12{,}200AB$–C coincidences and 1831 of the resulting traces had at least an acceptable e pulse. Since the background rate of single pulses in counter B was about 1 per 750 microseconds, the calculated number of traces showing an accidental e pulse is 145.

2. Decay of $\pi^{\pm}$ Mesons in Flight

Some of the π-mesons produced in the CH_2 target decayed in flight, producing μ-mesons which could stop in counter B. Negative as well as positive mesons contribute here, since there is essentially no nuclear capture of negative μ-mesons in carbon. The probability that a π-meson produced in the CH_2 target (with energy and angle favorable for detection) would decay before stopping was 4.2 percent. This probability was almost independent of the meson energy at production. The contribution of $\pi^{\pm}$ mesons that decayed in flight is then $0.042\times1470\times(1+\gamma)$, where 1470 is the total number of π^+ mesons stopped in counter B and γ is the ratio of negative to positive mesons produced at the appropriate energy and angle in CH_2. Since the protons in a carbon nucleus are only $\frac{1}{3}$ as effective as free protons in producing π^+ photomesons,[8] and the ratio of π^- to π^+ production in carbon is about 1.4,[9,10] γ is about 0.7. The contribution of $\pi^{\pm}$ mesons that decayed in flight is then 102.

3. Mesons Coming to Rest in the Material Behind Counter B

The mesons produced in the CH_2 target had energies up to about 150 Mev. Some π^+ mesons, therefore, came to rest in the 0.37 g cm^{-2} of aluminum that separated the liquid of counter B from that of counter C. In general, the μ-meson from the decay of the π would not succeed in getting into counter B, but in about half the cases the electron from the decay of the μ would give an acceptable e pulse. This type of event contributed about 90 traces showing e but no μ-pulses.

4.

As mentioned in Sec. III, some events were rejected because the height of the μ-pulse was less than a

[8] J. Steinberger and H. A. Bishop, Phys. Rev. **78**, 494 (1950).
[9] Peterson, Gilbert, and White, Phys. Rev. **81**, 1003 (1950).
[10] I. Lebow, M.I.T. thesis (1951).

preassigned value. Those rejected for this reason alone comprised 3 percent of the total. Although only 670 π-μ decay times were 2×10^{-8} sec or longer, 900 were actually resolved, leaving 570 completely unresolved. Included then, among the 360 traces which had e pulses but no μ's, were 3 percent of 570 or 17 events that would have been rejected had it been possible to measure the μ-heights.

Also, π-heights corresponding to energy losses less than 10 Mev were rejected. Since it was not possible to measure the π-heights alone for the 570 unresolved π-μ decays, π-heights between 6 and 10 Mev were presumably accepted, whereas they would have been rejected had it been possible to measure the π-heights alone. The calculated number of these is 76.

Combining 1, 2, 3, and 4, we have $145+102+90+(17+76)=430\pm25$, the uncertainty arising mostly from uncertainty in the background rate of single pulses in counter B. This is seen to be in satisfactory agreement with the observed 360 ± 40 traces showing e pulses but no μ's. It would have been possible to reverse the above argument and to use the calculated number of unresolved π-μ decays as a part of the π^+ mean life evaluation. However, the mean life evaluation as it stands, does not, it is believed, contain systematic errors beyond those discussed. No such confidence could be placed in the above estimates, and it is felt that some contributing factors of importance could have been overlooked.

VIII. PULSE-HEIGHT DISTRIBUTION

Shortly after the experimental data were obtained, small scintillation counters connected in twofold coincidence were placed above and below counter B. Coincidences, caused by fast cosmic-ray μ-mesons that succeeded in penetrating the 10 cm of lead piled above the apparatus, triggered the oscilloscope associated with the counter B. The pulses resulting from the traversal of the counter by these mesons were photographed and the pulse-height distribution is shown in Fig. 6. The width of the distribution arose from photomultiplier statistics and the only fair geometry for light collection, and from fluctuations in the energy loss of

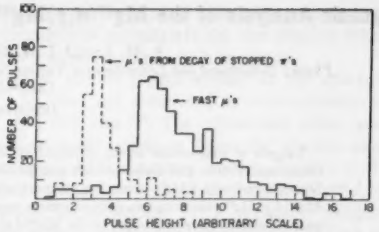

FIG. 6. Pulse-height distributions of μ-mesons from the decay of stopped π-mesons and of fast cosmic-ray μ-mesons.

the μ-mesons.[11,12] Also plotted in Fig. 6, is the distribution of μ-pulse heights as taken from a portion of the π^+ mean life data. Here the entire kinetic energy, 4.15 Mev, was expended in the liquid so the width of the distribution must be attributed to instrumental effects, such as photomultiplier statistics and light collection geometry, alone. If an energy scale is established by relating the average height of the cosmic-ray pulses to their calculated average energy loss (8.1 Mev), the average height of the pulses from the π^+ mean life data corresponds to an energy of 4.0 Mev. This is in good agreement with the known kinetic energy, 4.15 Mev, that a μ-meson receives from the decay of a π-meson at rest, and can be taken as an indication that the light output from a xylene-terphenyl solution per unit of energy lost is not a sensitive function of the specific energy loss over the range involved. For the cosmic-ray μ-mesons, $dE/dx=2.5$ Mev/g cm^{-2}, and 75 percent of the energy of a 4-Mev μ-meson is lost while $50>dE/dx>15$ Mev/g cm^{-2}.

It is a pleasure to acknowledge helpful discussions with Professor Bruno Rossi. Mr. W. B. Smith ably assisted with many of the electronic problems. A. Odian and L. Sartori spent many tedious hours examining film. The cooperation of the M.I.T. synchrotron staff is greatly appreciated.

[11] L. Landau, J. Phys. (U.S.S.R.) 8, 201 (1944).
[12] K. R. Symon, Harvard thesis (1948).

Magnetic Analysis of the $Mg^{25}(d,p)Mg^{26}$, $Mg^{26}(d,p)Mg^{27}$, and $Mg^{25}(d,\alpha)Na^{23}$ Reactions*

P. M. Endt,† J. W. Haffner, and D. M. Van Patter
Physics Department and Laboratory for Nuclear Science and Engineering, Massachusetts Institute of Technology, Cambridge 39, Massachusetts

(Received January 24, 1952)

Targets of magnesium oxide, enriched in Mg^{25} and Mg^{26} content, have been bombarded by 1.8-Mev deuterons. Proton and alpha-particle groups observed at an angle of 90 degrees to the incident beam have been studied with a high-resolution magnetic spectrograph. Eleven proton groups have been assigned to the $Mg^{25}(d,p)Mg^{26}$ reaction; two proton groups were assigned to the $Mg^{26}(d,p)Mg^{27}$ reaction; and three alpha-particle groups were attributed to the $Mg^{25}(d,\alpha)Na^{23}$ reaction. The Q-values for the ground-state transitions are 8.880 ± 0.010, 4.207 ± 0.006, and 7.019 ± 0.013 Mev, respectively.

The following level excitations have been measured:

Mg^{26}: 1.825, 2.972, 3.969, 4.353, 4.863, 4.924, 5.270, 5.322, 5.502, and 6.147 Mev;
Mg^{27}: 0.987 Mev;
Na^{23}: 0.43 and 2.07 Mev.

I. INTRODUCTION

THE element magnesium in its natural form has three isotopes with the following abundances: Mg^{24}, 78.6 percent; Mg^{25}, 10.1 percent; and Mg^{26}, 11.3 percent. If natural magnesium is bombarded with 1.8-Mev deuterons, four reactions can produce charged particles with energies greater than 4 Mev. These are the $Mg^{24}(d,p)Mg^{25}$, $Mg^{25}(d,p)Mg^{26}$, $Mg^{26}(d,p)Mg^{27}$, and $Mg^{25}(d,\alpha)Na^{23}$ reactions. An investigation of the $Mg^{24}(d,p)Mg^{25}$ reaction, using magnetic analysis, has been described in a separate publication.[1] The present paper is concerned with the remaining three reactions.

The reaction energy for the $Mg^{25}(d,p)Mg^{26}$ ground-state transition has not been previously published. A value of 9.06 ± 0.15 Mev may be calculated from the masses listed by Mattauch and Flammersfeld.[2] Pollard and Humphreys[3] reported levels of Mg^{26} at 1.85 and 3.00 Mev from an investigation of the proton groups from natural magnesium bombarded by deuterons. States of Mg^{26} can also be excited by means of the $Na^{23}(\alpha,p)Mg^{26}$ reaction. The results of several measurements of this reaction have been summarized by Alburger and Hafner,[4] who list values of 0.44, 1.91, 2.85, 4.0, and 5.0 Mev for the level positions.

Allan *et al.*[5] have reported a value of 4.21 ± 0.10 Mev for the $Mg^{26}(d,p)Mg^{27}$ ground-state transition from a study of the proton groups from an enriched Mg^{26} target bombarded by 0.93-Mev deuterons. No excited states have been reported by Mg^{27}.

The $Mg^{25}(d,\alpha)Na^{23}$ ground-state Q-value has been reported as 7.2 Mev[6] from a rough estimate of the range of the alpha-particles.[7] An excited state of Na^{23} at 3.03 Mev[8] is observed from the beta-decay of Ne^{23}. A preliminary study of the inelastic scattering of 14-Mev deuterons from sodium by the MIT Cyclotron Group[9] indicated seven excited states of Na^{23}, of which the two lowest were 1.9 and 2.6 Mev.

In view of the large ground-state Q-values of the $Mg^{25}(d,p)Mg^{26}$ and $Mg^{25}(d,\alpha)Na^{23}$ reactions and the paucity of precise data concerning the level schemes of Mg^{26}, Mg^{27}, and Na^{23}, it was decided to investigate the charged-particle reaction products from the deuteron bombardment of magnesium enriched in Mg^{25} and Mg^{26}. Bombardment of thin targets of natural magnesium has shown[1] the presence of many charged-particle groups of low intensity, which could not be assigned to the Mg^{24} isotope. It was necessary to use enriched targets in order to identify correctly these groups either with the Mg^{25} or the Mg^{26} isotope.

II. EXPERIMENTAL PROCEDURE

A beam of 1.8-Mev deuterons accelerated by the air-insulated electrostatic generator at MIT was analyzed by means of a 90-degree deflecting magnet. The deuteron beam was then used to bombard a thin target of magnesium or magnesium oxide. A small fraction of the charged particles emitted at an angle of 90 degrees to the incident beam was deflected by the magnetic field of a 180-degree focusing spectrograph and detected by means of nuclear-track emulsions. Details of the experimental arrangement have been published previously.[10–12]

* This work has been assisted by the joint program of the ONR and AEC.

† On leave from the University of Utrecht, Utrecht, Netherlands.

[1] Endt, Enge, Haffner, and Buechner (to be published).

[2] J. Mattauch and A. Flammersfeld, Z. Naturforsch. (1949) (special edition).

[3] E. Pollard and R. F. Humphreys, Phys. Rev. **59**, 466 (1941).

[4] D. E. Alburger and E. M. Hafner, Revs. Modern Phys. **22**, 373 (1950).

[5] Allan, Wilkinson, Burcham, and Curling, Nature **163**, 210 (1949).

[6] M. S. Livingston and H. A. Bethe, Revs. Modern Phys. **9**, 245 (1937).

[7] Lewis, Livingston, and Lawrence, Phys. Rev. **44**, 55 (1933).

[8] H. Brown and V. Perez-Mendez, Phys. Rev. **78**, 812 (1950).

[9] MIT, Lab. for Nuclear Sci. and Eng., Progress Report, July 1, 1950.

[10] Buechner, Strait, Stergiopoulos, and Sperduto, Phys. Rev. **74**, 1569 (1948).

[11] Buechner, Strait, Sperduto, and Malm, Phys. Rev. **76**, 1543 (1949).

[12] Strait, Van Patter, Buechner, and Sperduto, Phys. Rev. **81**, 747 (1951).

On each nuclear-track plate, a small spectrum of charged particles was recorded, covering a range of 10 percent in energy. By successively exposing a series of such plates over a wide range of field strengths of the spectrograph, a continuous spectrum of groups with energies from 4.0 to 10.5 Mev was obtained from the overlapping of several small spectra. The observed track-density distributions were normalized to the same beam exposure and area of plate counted so that the observed relative intensities of the groups could be correctly represented in the final plot.

A thin target of natural magnesium was prepared by evaporating magnesium ribbon in vaccum onto a platinum backing. The thickness of this target was 15 kev for the ground-state $Mg^{24}(d,p)Mg^{25}$ proton group at 1.8-Mev deuteron bombarding energy.

The enriched material was obtained from the Stable Isotopes Division of the AEC, Oak Ridge in the form of magnesium oxide, in which the Mg^{25} and Mg^{26} concentrations were considerably higher than in natural magnesium. Attempts to evaporate this compound in vacuum were unsuccessful because of its high boiling point. It was therefore not possible to prepare thin targets of the enriched material in the usual way. The method finally adopted did not give very thin targets but was satisfactory for the present purposes. First, the enriched material was finely ground in a procelain crucible. A suspension of fine powder in acetone was then prepared. In a few minutes, when the coarser crystals had sunk to the bottom of the crucible, a platinum backing was placed in the suspension a few millimeters below the surface. After several hours, the acetone evaporated, and a thin layer of magnesium oxide had settled onto the target backing.

The $Mg^{25}O$ target prepared in this fashion had a thickness of 130 kev for the ground-state $Mg^{25}(d,p)Mg^{26}$ proton group at 1.8-Mev bombarding energy. The $Mg^{26}O$ target was 100-kev thick for the $Mg^{26}(d,p)Mg^{27}$ reaction ground-state group. Precise determinations of the Q-values of reaction groups observed from these targets were not possible. However, these enriched targets could be used to identify the proton and alpha-particle groups observed from the thin target of natural magnesium, for which Q-values could be calculated with probable errors of 6 to 15 kev.

III. RESULTS

The $Mg^{25}(d,p)Mg^{26}$ Reaction

The spectrum of proton groups with energies from 4.0 to 10.5 Mev observed from the bombardment of the natural magnesium target by 1.8-Mev deuterons is shown in Fig. 1A. This spectrum consists of two parts, which are divided by a change in scale of a factor of five. The proton groups with energies greater than 6.9 Mev were recorded using beam exposures five times that used for the lower energy region. The two parts of the spectrum were recorded on different occasions, resulting in considerable uncertainty for the relative intensities of the groups over the whole spectrum.

Several proton groups appear in the spectrum of Fig. 1A that are attributed to contaminants of C^{12}, C^{13}, N^{14}, Si^{28}, and S^{32}. The silicon and sulfur contaminants probably originate from the silicone stopcock grease used in the vacuum system. Several of the remaining groups were attributed to the $Mg^{24}(d,p)Mg^{25}$ reaction, as described in a separate publication.[1] There remain several low intensity groups that can be attributed to either the Mg^{25} or Mg^{26} isotope.

The proton spectrum in the same energy range observed from the $Mg^{25}O$ target is shown in Fig. 1B. This spectrum was obtained from a series of plates exposed consecutively using the same beam bombardment. The relative intensities of the groups in Fig. 1B are considered to be more reliable than in Fig. 1A. However, since many of the groups overlap considerably, it is difficult to estimate their relative intensities.

The $Mg^{25}O$ target contained an isotopic abundance of 86.8 percent Mg^{25} compared with the 10.1 percent of Mg^{25} in natural magnesium. Comparing Figs. 1A and 1B, it can be seen that eleven proton groups from the $Mg^{25}O$ target have increased considerably in intensity, indicating they can be assigned to the $Mg^{25}(d,p)Mg^{26}$ reaction. These groups are numbered (0) through (10) and correspond to the ground state and ten excited states of Mg^{26}. It is possible that additional low-intensity $Mg^{25}(d,p)Mg^{26}$ groups were present which were not detected in the spectrum of Fig. 1A because of lack of intensity or in the spectrum in Fig. 1B because of the poor resolution provided by the thick $Mg^{25}O$ target. The $Mg^{25}(d,p)$ group (4) does not stand out clearly in Fig. 1A because it is situated on the high energy slope of the intense $Mg^{24}(d,p)$ group (1). However, the intensity of this group from the $Mg^{25}O$ target was sufficient so as to leave no doubt concerning its existence. It is also noted that the proton groups attributed to the Mg^{24} and Mg^{26} isotopes are relatively less intense from the $Mg^{25}O$ target, as expected from their isotopic abundances in the $Mg^{25}O$ target.

In Table I are listed the Q-values calculated for the eleven proton groups assigned to the $Mg^{25}(d,p)Mg^{26}$ reaction, together with the resulting level positions for Mg^{26}. A level diagram for Mg^{26} incorporating these results is shown in Fig. 3. No estimates have been given for the relative intensities of the groups because of the uncertainties already noted. Comparison has been made with the levels in Mg^{26} listed in Alburger and Hafner[4] from the $Na^{23}(\alpha,p)Mg^{26}$ reaction. The agreement is quite good except for the level given at 0.44 Mev, which has been reported only once[13] while the remaining levels have been observed by several groups of experimenters. A $Mg^{25}(d,p)Mg^{26}$ proton group corresponding to this level would occur at $H\rho = 452$ kilo-

[13] H. T. Motz and R. F. Humphreys, Phys. Rev. 74, 1232 (1948).

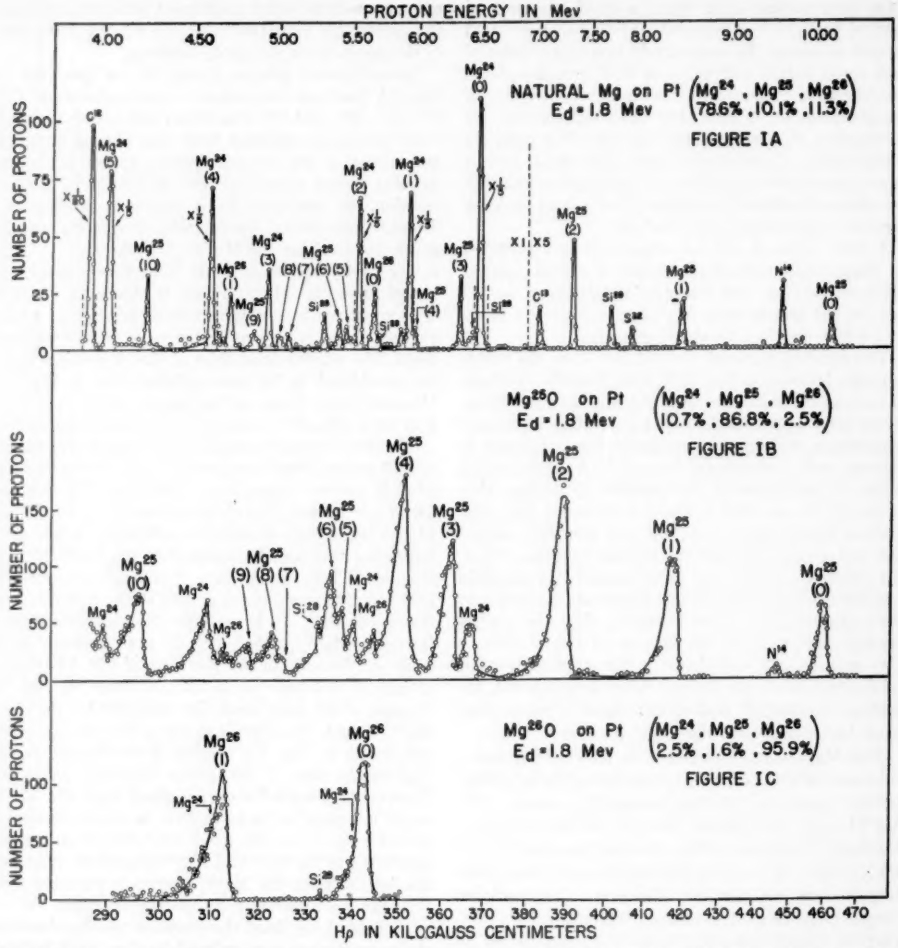

FIG. 1. Proton groups from targets of natural magnesium and magnesium oxide enriched in Mg^{25} and Mg^{26} content bombarded by 1.8-Mev deuterons.

gauss-centimeters in Fig. 1B, where no trace of a group was observed.

It is possible to estimate the ground-state Q-value for the $Mg^{25}(d,p)Mg^{26}$ reaction from a combination of other nuclear disintegration energies. By using the Q-values for the $Mg^{26}(d,p)Mg^{27}$ reaction (4.207±0.006 Mev, as measured in the present experiment), the $Mg^{27}(\beta^-)Al^{27}$ disintegration (2.62±0.06 Mev[14,15]), and the $Al^{27}(d,\alpha)Mg^{25}$ reaction (6.694±0.010 Mev[15]), together with the mass differences $2D^2-He^4$(23.834±0.007 Mev[16]) and $2H^1-D^2$(1.443±0.002 Mev[16]), a value of 8.87±0.06 Mev may be calculated for the $Mg^{25}(d,p)Mg^{26}$ reaction. Since the highest energy $Mg^{25}(d,p)Mg^{26}$ group observed in the present experiment had a measured Q-value of 8.880±0.012 Mev, it is concluded that this group represents the ground-state transition.

The $Mg^{26}(d,p)Mg^{27}$ Reaction

In Fig. 1C are shown the proton groups with energies from 4.1 to 5.9 Mev observed from an enriched

[14] Benes, Hedgran, and Hole, Arkiv Mat. Astron. Fysik **35A**, No. 12 (1948).
[15] A. Hedgran (private communication).
[16] Li, Whaling, Fowler, and Lauritsen, Phys. Rev. **83**, 512 (1951).

$Mg^{26}O$ target bombarded by 1.8-Mev deuterons. This target contained an isotopic abundance of 95.9 percent of Mg^{26} compared with the 11.3 percent of Mg^{26} in natural magnesium. Two proton groups (0) and (1) are clearly indicated, which are both assigned to the $Mg^{26}(d,p)Mg^{27}$ reaction. These groups were also observed with considerably lower intensities from the natural magnesium target. The measured Q-values of these groups were 4.207 ± 0.006 and 3.320 ± 0.005 Mev, corresponding to the ground state of Mg^{26} and an excited state at 0.987 ± 0.006 Mev. The Q-value for the ground-state transition is in agreement with the previously reported value[5] of 4.21 ± 0.1 Mev obtained from range measurements. The level at 0.987 Mev has not been previously reported.

The $Mg^{25}(d,\alpha)Na^{23}$ Reaction

In the upper curve of Fig. 2 is shown the spectrum of alpha-particles with energies from 5.4 to 7.7 Mev observed from the natural magnesium target bombarded by 1.8-Mev deuterons. The energies of these alpha-groups are sufficiently high so that they cannot be attributed to either the Mg^{24} or the Mg^{26} isotope. In order to verify the assignment of these groups to the Mg^{25} isotope, a similar spectrum was observed from the enriched $Mg^{25}O$ target, which is shown in the lower curve of Fig. 2. It can be seen that, in each case, the intensity of the group is considerably greater from the $Mg^{25}O$ target, indicating that the groups may be attributed to the $Mg^{25}(d,\alpha)Na^{23}$ reaction. The spectrum of alpha-particles with energies from 4.0 to 5.4 Mev is not shown, because the yield of $Mg^{25}(d,\alpha)Na^{23}$ groups in this energy region was not sufficient to permit detection in the present experiment.

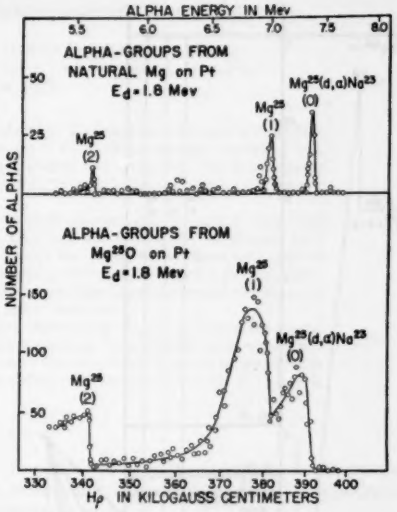

FIG. 2. Alpha-particles from targets of natural magnesium and magnesium oxide enriched in Mg^{25} bombarded by 1.8-Mev deuterons.

The measured Q-values for the three $Mg^{25}(d,\alpha)Na^{23}$ groups were 7.019 ± 0.013, 6.592 ± 0.015, and 4.946 ± 0.012 Mev, corresponding to the ground state and excited states of Na^{23} at 0.427 ± 0.018 and 2.073 ± 0.015 Mev, respectively. The level at 2.07 Mev probably corresponds to the 1.9-Mev level reported from inelastic scattering of deuterons from sodium.[9] The level at 0.43 Mev has not been reported before. An attempt was made to confirm the existence of this level by investigating the $Na^{23}(p,p')$ and $Na^{23}(d,d')$ inelastic scattering for bombarding energies of 1.8 and 2.0 Mev. The target used for this investigation consisted of a thin layer of sodium iodide evaporated in vacuum onto a 0.1-micron nickel backing. No group of particles inelastically scattered from the sodium-iodide target at 90 degrees was observed with an intensity greater than 1 percent of the elastically scattered group.

The Q-value of 7.019 ± 0.013 Mev measured for the $Mg^{25}(d,\alpha)Na^{23}$ ground-state transition is in agreement with the early value of 7.2 Mev from range measurements.[6,7] It is also possible to estimate this value from a combination of the ground-state Q-values of the $Na^{23}(d,p)Na^{24}$ reaction (4.731 ± 0.009 Mev),[12] the $Na^{24}(\beta^-)Mg^{24}$ disintegration (5.512 ± 0.006 Mev),[15,17] and the $Mg^{24}(d,p)Mg^{25}$ reaction,[1] together with the mass differences $2D^2-He^4$ and $2H^1-D^2$. The Q-value resulting from this calculation is 7.051 ± 0.016 Mev, which is 32

TABLE I. Q-values for the observed proton and α-particle groups.

Group	Q-value (Mev)	$Mg^{25}(d,p)Mg^{26}$ reaction: Mg^{26} levels ($Mg^{25}(d,p)Mg^{26}$)	Mg^{26} levels ($Na^{23}(\alpha,p)Mg^{26}$)
(0)	8.880 ± 0.012	0	0
...	...	...	0.44
(1)	7.055 ± 0.015	1.825 ± 0.005	1.91
(2)	5.908 ± 0.008	2.972 ± 0.010	2.85
(3)	4.911 ± 0.007	3.969 ± 0.010	4.0
(4)	4.527 ± 0.008	4.353 ± 0.011	...
(5)	4.017 ± 0.009	4.863 ± 0.011	...
(6)	3.956 ± 0.007	4.924 ± 0.011	5.0
(7)	3.610 ± 0.007	5.270 ± 0.011	...
(8)	3.558 ± 0.007	5.322 ± 0.011	...
(9)	3.378 ± 0.007	5.502 ± 0.011	...
(10)	2.733 ± 0.005	6.147 ± 0.011	...

Group	$Mg^{25}(d,p)Mg^{27}$ reaction: Q-value (Mev)	Mg^{27} levels
(0)	4.207 ± 0.006	0
(1)	3.320 ± 0.005	0.987 ± 0.006

Group	$Mg^{25}(d,\alpha)Na^{23}$ reaction: Q-value (Mev)	Na^{23} levels ($Mg^{25}(d,\alpha)Na^{23}$)	Na^{23} levels ($Na^{23}(d,d')Na^{23}$)
(0)	7.019 ± 0.013	0	0
(1)	6.592 ± 0.015	0.427 ± 0.018	...
(2)	4.946 ± 0.012	2.073 ± 0.015	1.9

[17] K. Siegbahn, Phys. Rev. **70**, 127 (1946).

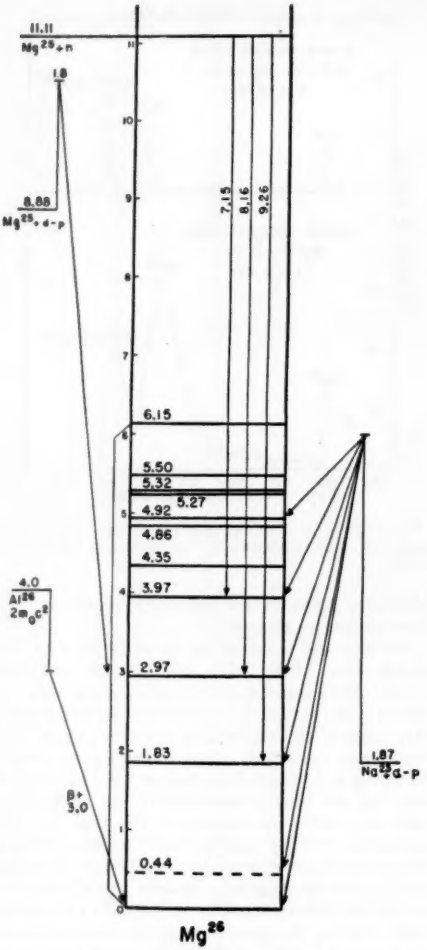

FIG. 3. Energy-level diagram for Mg^{26}.

kev lower than the measured value, indicating that there is some inconsistency between the nuclear reaction data and the $Na^{24}(\beta^-)Mg^{24}$ disintegration energy. However, the agreement is good enough to establish that the $Mg^{25}(d,\alpha)Na^{23}$ ground-state group has been correctly identified.

IV. CONCLUSIONS

Investigation of the $Mg^{25}(d,p)Mg^{26}$, $Mg^{26}(d,p)Mg^{27}$, and $Mg^{25}(d,\alpha)Na^{23}$ reactions using magnetic analysis has indicated the presence of several reaction groups not previously reported. In the case of each reaction, the measured Q-values for the ground-state transitions were in reasonable agreement with the Q-values of other reactions linking the same nuclei.

The results for the $Mg^{25}(d,p)Mg^{26}$ reaction indicated ten excited states of Mg^{26} in a region of excitation from 0 to 6.2 Mev, of which six have not been previously reported. A previously reported level[12] at 0.44 Mev from the $Na^{23}(\alpha,p)Mg^{26}$ reaction has not been verified.

Included in the level diagram for Mg^{26} (Fig. 3) are three of the gamma-rays observed by Kinsey *et al.*,[18] from the capture of thermal neutrons by magnesium. If these gamma-rays represent transitions from the capturing state of Mg^{26} at 11.11 Mev to excited states as indicated, then it is possible to compare their measured energies with the corresponding $Mg^{25}(d,p)Mg^{26}$ transitions to the same excited states. After subtracting 2.23 Mev for the deuteron binding energy, the corresponding $Mg^{25}(d,p)Mg^{26}$ Q-values are calculated to be 7.03 ± 0.04, 5.93 ± 0.03, and 4.92 ± 0.04 Mev, in excellent agreement with our measured Q-values of 7.055 ± 0.015, 5.908 ± 0.005, and 4.911 ± 0.007 Mev.

A hitherto unreported level at 0.987 ± 0.006 Mev in Mg^{27} was found by investigating the $Mg^{26}(d,p)Mg^{27}$ reaction. Excited states at 0.427 ± 0.018 and 2.073 ± 0.015 Mev were found for the nucleus Na^{23} from the $Mg^{25}(d,\alpha)Na^{23}$ reaction. The level at 0.43 Mev has not been reported previously.[19]

We wish to acknowledge the generous cooperation of our colleagues at the High Voltage Laboratory. We are particularly indebted to Miss Jane Pann, Mrs. Helene Harris, and Mr. W. A. Tripp for their care in counting the nuclear-track plates.

[18] Kinsey, Bartholomew, and Walker, Phys. Rev. **83**, 519 (1951).

[19] The results of Stelson, Preston, and Goodman [Bull. Am. Phys. Soc. **27**, No. 1, 54, (1952)] for the gamma-rays from sodium bombarded by protons have recently been reported. They find a gamma-ray of energy 0.45 ± 0.01 Mev which they attribute to the Na^{23} level at 0.43 ± 0.02 Mev found in the present experiment.

Cloud-Chamber Identification of Photodeuterons from Copper*

WARREN H. SMITH† AND L. JACKSON LASLETT
Institute for Atomic Research and Department of Physics, Iowa State College, Ames, Iowa
(Received January 28, 1952)

The presence of a prominent group of photodeuterons, produced by the irradiation of copper with 65-Mev bremsstrahlung, was demonstrated by experiments employing a 12-in. cloud chamber traversed by a magnetic field. The mean curvature of each acceptable track studied was determined over a fixed range interval; the distribution of the curvatures so obtained provided a clear indication of proton and deuteron groups.

Helium was used as the noncondensible component of the cloud-chamber gas, in order to reduce the effect of scattering. The spread in curvature produced by scattering was determined, for protons, by a control experiment in which essentially only protons were present and the spread expected for deuterons under similar conditions was then readily estimated. The stopping power of the chamber gas was determined from the measured range of polonium alpha-particles and permitted computation of the expected mean curvatures for the unscattered trajectories of protons and of deuterons.

Analysis of the experimental composite distribution curve, representing the particles obtained in the photodisintegration of copper, into proton and deuteron components of the prescribed mean values and widths, was then uniquely possible. The deuteron to proton ratio was thus found to be 0.7$_6$ for equal range and solid angle intervals. It is estimated that the corresponding ratio for equal intervals of energy is approximately 0.5.

INTRODUCTION

EVIDENCE has been reported for the production of deuterons in the disintegration of copper[1] and sulfur[2] by bremsstrahlung below 24-Mev energy. In the more direct of these investigations,[1] the presence of a deuteron group was inferred on the basis of range and grain-density measurements in nuclear emulsions, and led to a ratio of photodeuterons to photoprotons cited as 0.32 for copper. Because of the bearing which such an abundant deuteron group must have on the theory of photonuclear processes, an independent investigation of the photodeuteron yield from copper was undertaken. The present experiment affords an estimate of the relative yield, in equal range and solid angle intervals, of photodeuterons and photoprotons produced by the irradiation of a thick copper target with 65-Mev bremsstrahlung.

METHOD

A 12-in. cloud chamber traversed by a magnetic field was employed, in conjunction with the Iowa State College Synchrotron, to permit the observation of tracks formed by heavy photoparticles from copper. A determination was made of the mean curvature of each track studied, in a fixed range interval extending between 4 and 14 cm from the end. Thus all protons had, except for straggling, a fixed energy interval and, similarly, the deuterons had another fixed energy interval. The distribution of the curvatures so obtained for such tracks afforded, as will be seen, a clear indication of a deuteron group.

The cloud-chamber arrangement used by Stokes[3] in the measurement of electron pairs was adapted to the measurement of heavy particles. To reduce scattering by the chamber gas, helium was used as the major, noncondensible component, together with ethanol, acetone, and water. A magnetic field of 3440 $\pm$100 gauss was attained, for a short period coincident with the synchrotron beam, by ignitron switching of the currents used to excite the chamber coils (1057 turns). The photon beam, admitted to the chamber through a coated beryllium window 0.005 in. thick, was approximately $\frac{1}{4}$ in. in diameter and traversed a target of commercial copper, 0.018 in. thick, at an angle of about 10 deg.

The tracks were stereoscopically photographed and reprojected to full size. All tracks ending in the illuminated portion of the chamber at least 1 cm from the wall, longer than 7 cm, and directed away from the copper target, were studied. Portions of track containing observable[4] point scattering were not used; if no section at least 3 cm long and more than 4 cm from the end of a given track could be found free from noticeable point scattering, that track was completely rejected. The average length of track over which the curvature was measured was 7.0 cm. Tracks attributable to alpha-particles or to electrons could be recognized by their appearance and were excluded from measurement. The mean curvature of the projected image was determined for each usable track by choice of the closest fitting circular arc and corrected[3] for the inclination of the track to the magnetic field. The stopping power of the

* Contribution No. 182 from the Institute for Atomic Research and Department of Physics. Work performed in the Ames Laboratory of the AEC. A preliminary account of this work was reported by one of us (W.H.S.) at the Chicago meeting of the American Physical Society in October, 1951.

† Present address: General Electric Company, ANP Project, Oak Ridge, Tennessee.

[1] P. R. Byerly, Jr., and W. E. Stephens, Phys. Rev. **81**, 473 (1951); **83**, 54 (1951).

[2] Harrington, Katz, Haslam, and Johns, Phys. Rev. **81**, 660 (1951); L. Katz and A. S. Penfold, Phys. Rev. **81**, 815 (1951).

[3] R. H. Stokes, Phys. Rev. **84**, 991 (1951).

[4] Point scattering by 0.01 radian may be observed.

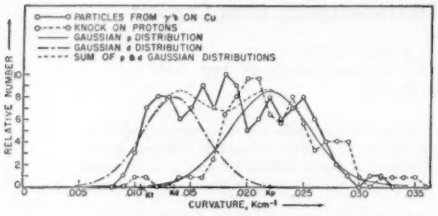

FIG. 1. Experimental curvature distribution obtained for tracks of particles produced by the photodisintegration of copper with 65-Mev bremsstrahlung. The curvature distribution obtained in a control experiment with recoil protons is also shown with the ordinate scale chosen to facilitate comparison of the two curves. The separation of the former curve into deuteron and proton components is indicated. The abscissas designated K_p, K_d, and K_t represent, respectively, the curvatures expected for tracks of unscattered protons, deuterons, and tritons.

cloud-chamber gas was determined from the measured range of polonium alpha-particles. From the stopping power, the energy and momentum were calculated as a function of range for protons and for deuterons, using published range-energy data.[5] The momentum and the magnetic field strength determine the radius of magnetic curvature, which was averaged over the standard interval to give the expected mean curvature for an unscattered path; the values so obtained for a proton and deuteron were 0.022 and 0.014 cm^{-1}, respectively. For those tracks for which the average curvature was not measured directly over the standard range interval, a suitable correction was applied to the curvature. This correction was made without prior identification of the particles and was estimated from the range-energy relation for protons. The correction was less than 12 percent except for 4 tracks; it is fair approximation for deuterons and, as applied, would not give a spurious contribution to the deuteron group.

Because of small-angle multiple scattering in the chamber gas, the measured tracks exhibited a distribution in curvature which, for each type of particle, may be shown to be Gaussian in form. This is deduced from the Gaussian character of the distribution expected for the angle of scattering, which is given by the theory of multiple scattering.[6–10] The width of the distribution in curvature, to be expected for protons under the conditions of the present investigation, was determined by a control experiment. Recoil protons were used for this purpose, and were obtained from irradiation, with polonium-beryllium neutrons, of a plastic enclosure situated within the cloud chamber. Application of scattering theory[6–9] permits a simple evaluation to be made of the width expected for the curvature distribution of deuterons, in terms of that found for protons. In this way 0.005 and 0.004 cm^{-1} were estimated as the $1/e$ half-widths for the proton and deuteron distributions, respectively, as they would occur in the present investigation.

RESULTS

The corrected curvatures of the 67 measurable tracks obtained from photonuclear reactions in the copper target were plotted in the form of a distribution curve to represent the number of tracks in a curvature interval, 0.002 cm^{-1} wide, as a function of curvature. To facilitate the interpretation, points were so plotted at increments of 0.001 cm^{-1} in curvature. This distribution, and that obtained from the control experiment, in which essentially only protons were present, may be compared in Fig. 1 and clearly indicate the presence of a strong deuteron group. By use of the known width and location of the maximum for a pure proton distribution, and the corresponding values expected for a deuteron group, a separation of the composite distribution into proton and deuteron components, also shown in Fig. 1, was performed without ambiguity. Since both the mean curvatures and widths of the separate distributions were known, this analysis involved solely the adjustment of the magnitudes of the proton and deuteron abundances.

The analysis of the distribution curve permitted an estimate to be made of the relative abundance of photodeuterons and photoprotons. The deuteron to proton ratio was thus found to be 0.7$_6$ for equal range and solid angle intervals. It is estimated that protons originating principally normal to the x-ray beam with energies in the range 1 to 15 Mev and deuterons in the range 1 to 20 Mev are included in this investigation. The sampling favors particles at the high-energy end of the range accepted because the section of target from which they arise is proportional to dR/dE, which increases considerably with particle energy. The deuterons lose energy more rapidly along their range, and the energy interval associated with a given range interval is larger than for protons. It is estimated, accordingly, that the deuteron to proton abundance ratio for equal intervals of energy is approximately 0.5 The large photodeuteron abundance indicated by this ratio is in agreement with the findings of Byerly and Stephens[1] from nuclear emulsion studies of the particles produced by 24-Mev bremsstrahlung.

It is a pleasure to express our thanks to Dr. J. M. Keller for many helpful discussions concerning this work and to Dr. R. H. Stokes for valuable suggestions concerning operation of the cloud chamber. We are also indebted to Mr. L. S. Ring for his very significant help in measuring the tracks.

[5] Aron, Hoffman, and Williams, *Range-Energy Curves* (Technical Information Division, ORE, Oak Ridge, Tennessee, 1949), AECU 663 (1949); UCRL-121 (1949), 2nd revision.

[6] E. J. Williams, Proc. Roy. Soc. (London) **A169**, 531 (1939).

[7] E. J. Williams, Phys. Rev. **58**, 292 (1940).

[8] B. Rossi and K. Greisen, Revs. Modern Phys. **13**, 240 (1941).

[9] H. A. Bethe, Phys. Rev. **70**, 821 (1946).

[10] For the variance of radius of curvature to be expected to arise from scattering under various conditions of curve fitting, see W. Bothe, Sitzber. Heidelberg. Akad. Wiss., Math.-naturw. Klasse **5**, 105 (1948).

Multiple Scattering of Protons in Gases*

EUGENE H. GERBER
University of Buffalo, Buffalo, New York
(Received January 17, 1952)

The tracks left in a cloud chamber by low energy protons were observed in the absence of a magnetic field. Measurements of the curvature of the tracks due to multiple scattering verified quantitatively the results predicted by H. A. Bethe and W. T. Scott. For 1.08-Mev protons in air under a pressure of one atmosphere, the mean square curvature $\langle C^2\rangle_{Av}$ of the measured tracks was found to be $\langle C^2\rangle_{Av}=0.323\times10^{-3}$ cm^{-2}, for 1.05-Mev protons in argon $\langle C^2\rangle_{Av}=0.935\times10^{-3}$ cm^{-2}. For helium only qualitative results were obtained; they indicated smaller curvatures than for the other gases.

BETHE[1] showed that widely varying experimental results for the rest mass of the meson were compatible with a single rest mass, if multiple scattering of the particles was taken into account. Following this theoretical development, Luebke, Klaiber, and Baldwin[2] obtained qualitative results for the scattering of low energy protons in air. Their observations confirmed Bethe's calculations, which have since been extended by Scott.[3] The purpose of the investigation reported here was to extend the work of Luebke *et al.* and obtain quantitative results, and compare them with the results of Bethe and those of Scott.

The experiments were performed in a six-inch cloud chamber filled with each of the following gases: air, argon, and helium. The protons were obtained by bombarding a 0.001-inch aluminum foil with alpha-particles from a 10-millicurie polonium source. 6085 pictures were taken and 1134 measurable tracks were obtained. Stereoscopic pictures were not taken, as the experimental data were compared with calculations that hold for two-dimensional projections.

Measurements were made on the last five centimeters of all measurable tracks ending in the cloud chamber. The proton energy E at the half range (2.5 cm) was determined from the range-energy curves, giving for air $E=1.08$ Mev and for argon $E=1.05$ Mev. The radii of curvature ρ were obtained by matching circles to the tracks. For a C-type track, ρ was measured if it was less than 150 cm; if ρ was greater than 150 cm, the track was called an O-(zero curvature) track and recorded as such. S-tracks also were only tabulated. Histograms of the observed number of tracks in a given interval of radius of curvature are shown for tracks in air in Fig. 1A and in argon in Fig. 1B.

In order to compare the experimental data with the theory a mean square curvature was calculated. As no measurements were made on S-tracks they were not included in this calculation. This is in keeping with Scott's result that the distribution of curvature is not narrowed by considering only symmetrical tracks. In this calculation, if the total number of tracks was taken as all the C- and O-type tracks, a large error could occur, as it is difficult to determine in many cases whether a track is of the O- or S-type. This difficulty can be avoided by assuming, as predicted by the theory, that the distribution of curvatures should be Gaussian. It is then only necessary to know the mean square curvature $\langle C'^2\rangle_{Av}$ of all tracks with a radius of curvature less than some arbitrary ρ'. The mean curvature $\langle C^2\rangle_{Av}$ for all C-tracks can then be calculated from $\langle C'^2\rangle_{Av}$. ρ' was taken as 100 cm rather than 150 cm, as there are only a few tracks between 100 and 150 cm and this might cause an error due to poor statistics. For the N' C-tracks having a curvature between 0 and 100 cm, a $\langle C'^2\rangle_{Av}$ was obtained; a $\langle C^2\rangle_{Av}$ for all C-tracks was then calculated and can be found in Table I. The total number N of C-tracks, calculated from N' under the

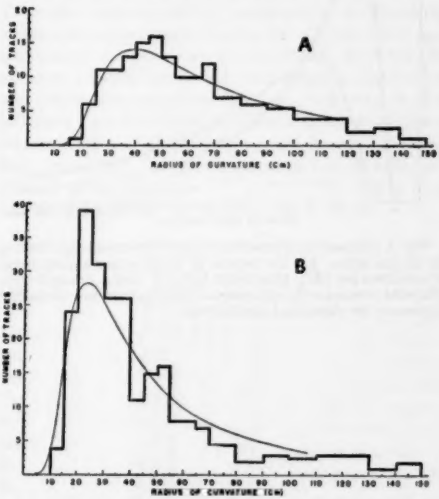

FIG. 1. Histograms of the number of tracks having a given range of radius of curvature. The smooth curves are theoretical distributions normalized to have the experimental N' (number of tracks with radius of curvature less than 100 cm) and $\langle C'^2\rangle_{Av}$ (mean square curvature of the N' tracks). A, scattering gas, air; B, scattering gas, argon.

* Part of a dissertation submitted in partial fulfillment of the requirements for the degree of Doctor of Philosophy at the University of Buffalo.

[1] H. A. Bethe, Phys. Rev. **70**, 821 (1946).
[2] Luebke, Klaiber, and Baldwin, Phys. Rev. **71**, 657 (1947).
[3] W. T. Scott, Phys. Rev. **76**, 212 (1949).

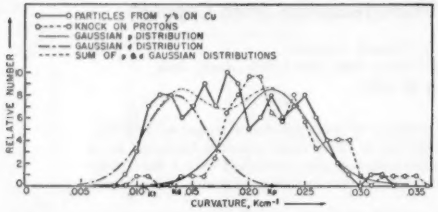

FIG. 1. Experimental curvature distribution obtained for tracks of particles produced by the photodisintegration of copper with 65-Mev bremsstrahlung. The curvature distribution obtained in a control experiment with recoil protons is also shown with the ordinate scale chosen to facilitate comparison of the two curves. The separation of the former curve into deuteron and proton components is indicated. The abscissas designated K_p, K_d, and K_t represent, respectively, the curvatures expected for tracks of unscattered protons, deuterons, and tritons.

cloud-chamber gas was determined from the measured range of polonium alpha-particles. From the stopping power, the energy and momentum were calculated as a function of range for protons and for deuterons, using published range-energy data.[5] The momentum and the magnetic field strength determine the radius of magnetic curvature, which was averaged over the standard interval to give the expected mean curvature for an unscattered path; the values so obtained for a proton and deuteron were 0.022 and 0.014 cm^{-1}, respectively. For those tracks for which the average curvature was not measured directly over the standard range interval, a suitable correction was applied to the curvature. This correction was made without prior identification of the particles and was estimated from the range-energy relation for protons. The correction was less than 12 percent except for 4 tracks; it is fair approximation for deuterons and, as applied, would not give a spurious contribution to the deuteron group.

Because of small-angle multiple scattering in the chamber gas, the measured tracks exhibited a distribution in curvature which, for each type of particle, may be shown to be Gaussian in form. This is deduced from the Gaussian character of the distribution expected for the angle of scattering, which is given by the theory of multiple scattering.[6–10] The width of the distribution in curvature, to be expected for protons under the conditions of the present investigation, was determined by a control experiment. Recoil protons were used for this purpose, and were obtained from irradiation, with polonium-beryllium neutrons, of a plastic enclosure situated within the cloud chamber. Application of scattering theory[6–9] permits a simple evaluation to be made of the width expected for the curvature distribution of deuterons, in terms of that found for protons. In this way 0.005 and 0.004 cm^{-1} were estimated as the $1/e$ half-widths for the proton and deuteron distributions, respectively, as they would occur in the present investigation.

RESULTS

The corrected curvatures of the 67 measurable tracks obtained from photonuclear reactions in the copper target were plotted in the form of a distribution curve to represent the number of tracks in a curvature interval, 0.002 cm^{-1} wide, as a function of curvature. To facilitate the interpretation, points were so plotted at increments of 0.001 cm^{-1} in curvature. This distribution, and that obtained from the control experiment, in which essentially only protons were present, may be compared in Fig. 1 and clearly indicate the presence of a strong deuteron group. By use of the known width and location of the maximum for a pure proton distribution, and the corresponding values expected for a deuteron group, a separation of the composite distribution into proton and deuteron components, also shown in Fig. 1, was performed without ambiguity. Since both the mean curvatures and widths of the separate distributions were known, this analysis involved solely the adjustment of the magnitudes of the proton and deuteron abundances.

The analysis of the distribution curve permitted an estimate to be made of the relative abundance of photodeuterons and photoprotons. The deuteron to proton ratio was thus found to be 0.7$_6$ for equal range and solid angle intervals. It is estimated that protons originating principally normal to the x-ray beam with energies in the range 1 to 15 Mev and deuterons in the range 1 to 20 Mev are included in this investigation. The sampling favors particles at the high-energy end of the range accepted because the section of target from which they arise is proportional to dR/dE, which increases considerably with particle energy. The deuterons lose energy more rapidly along their range, and the energy interval associated with a given range interval is larger than for protons. It is estimated, accordingly, that the deuteron to proton abundance ratio for equal intervals of energy is approximately 0.5 The large photodeuteron abundance indicated by this ratio is in agreement with the findings of Byerly and Stephens[1] from nuclear emulsion studies of the particles produced by 24-Mev bremsstrahlung.

It is a pleasure to express our thanks to Dr. J. M. Keller for many helpful discussions concerning this work and to Dr. R. H. Stokes for valuable suggestions concerning operation of the cloud chamber. We are also indebted to Mr. L. S. Ring for his very significant help in measuring the tracks.

[5] Aron, Hoffman, and Williams, *Range-Energy Curves* (Technical Information Division, ORE, Oak Ridge, Tennessee, 1949), AECU 663 (1949); UCRL-121 (1949), 2nd revision.
[6] E. J. Williams, Proc. Roy. Soc. (London) **A169**, 531 (1939).
[7] E. J. Williams, Phys. Rev. **58**, 292 (1940).
[8] B. Rossi and K. Greisen, Revs. Modern Phys. **13**, 240 (1941).
[9] H. A. Bethe, Phys. Rev. **70**, 821 (1946).
[10] For the variance of radius of curvature to be expected to arise from scattering under various conditions of curve fitting, see W. Bothe, Sitzber. Heidelberg. Akad. Wiss., Math.-naturw. Klasse **5**, 105 (1948).

Multiple Scattering of Protons in Gases*

EUGENE H. GERBER
University of Buffalo, Buaffalo, New York
(Received January 17, 1952)

The tracks left in a cloud chamber by low energy protons were observed in the absence of a magnetic field. Measurements of the curvature of the tracks due to multiple scattering verified quantitatively the results predicted by H. A. Bethe and W. T. Scott. For 1.08-Mev protons in air under a pressure of one atmosphere, the mean square curvature $\langle C^2\rangle_{Av}$ of the measured tracks was found to be $\langle C^2\rangle_{Av}=0.323\times10^{-3}$ cm^{-2}, for 1.05-Mev protons in argon $\langle C^2\rangle_{Av}=0.935\times10^{-3}$ cm^{-2}. For helium only qualitative results were obtained; they indicated smaller curvatures than for the other gases.

BETHE[1] showed that widely varying experimental results for the rest mass of the meson were compatible with a single rest mass, if multiple scattering of the particles was taken into account. Following this theoretical development, Luebke, Klaiber, and Baldwin[2] obtained qualitative results for the scattering of low energy protons in air. Their observations confirmed Bethe's calculations, which have since been extended by Scott.[3] The purpose of the investigation reported here was to extend the work of Luebke *et al.* and obtain quantitative results, and compare them with the results of Bethe and those of Scott.

The experiments were performed in a six-inch cloud chamber filled with each of the following gases: air, argon, and helium. The protons were obtained by bombarding a 0.001-inch aluminum foil with alpha-particles from a 10-millicurie polonium source. 6085 pictures were taken and 1134 measurable tracks were obtained. Stereoscopic pictures were not taken, as the experimental data were compared with calculations that hold for two-dimensional projections.

Measurements were made on the last five centimeters of all measurable tracks ending in the cloud chamber. The proton energy E at the half range (2.5 cm) was determined from the range-energy curves, giving for air $E=1.08$ Mev and for argon $E=1.05$ Mev. The radii of curvature ρ were obtained by matching circles to the tracks. For a C-type track, ρ was measured if it was less than 150 cm; if ρ was greater than 150 cm, the track was called an O-(zero curvature) track and recorded as such. S-tracks also were only tabulated. Histograms of the observed number of tracks in a given interval of radius of curvature are shown for tracks in air in Fig. 1A and in argon in Fig. 1B.

In order to compare the experimental data with the theory a mean square curvature was calculated. As no measurements were made on S-tracks they were not included in this calculation. This is in keeping with Scott's result that the distribution of curvature is not narrowed by considering only symmetrical tracks. In this calculation, if the total number of tracks was taken as all the C- and O-type tracks, a large error could occur, as it is difficult to determine in many cases whether a track is of the O- or S-type. This difficulty can be avoided by assuming, as predicted by the theory, that the distribution of curvatures should be Gaussian. It is then only necessary to know the mean square curvature $\langle C'^2\rangle_{Av}$ of all tracks with a radius of curvature less than some arbitrary ρ'. The mean curvature $\langle C^2\rangle_{Av}$ for all C-tracks can then be calculated from $\langle C'^2\rangle_{Av}$. ρ' was taken as 100 cm rather than 150 cm, as there are only a few tracks between 100 and 150 cm and this might cause an error due to poor statistics. For the N' C-tracks having a curvature between 0 and 100 cm, a $\langle C'^2\rangle_{Av}$ was obtained; a $\langle C^2\rangle_{Av}$ for all C-tracks was then calculated and can be found in Table I. The total number N of C-tracks, calculated from N' under the

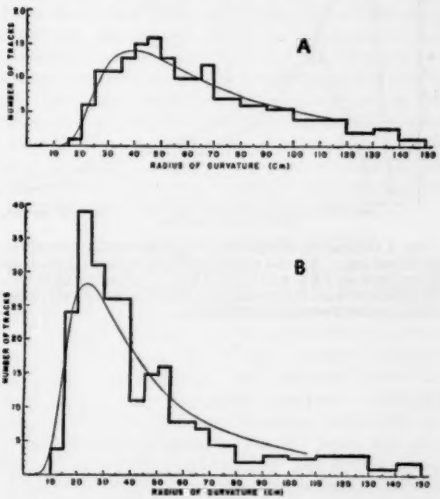

FIG. 1. Histograms of the number of tracks having a given range of radius of curvature. The smooth curves are theoretical distributions normalized to have the experimental N' (number of tracks with radius of curvature less than 100 cm) and $\langle C'^2\rangle_{Av}$ (mean square curvature of the N' tracks). A, scattering gas, air; B, scattering gas, argon.

* Part of a dissertation submitted in partial fulfillment of the requirements for the degree of Doctor of Philosophy at the University of Buffalo.

[1] H. A. Bethe, Phys. Rev. **70**, 821 (1946).

[2] Luebke, Klaiber, and Baldwin, Phys. Rev. **71**, 657 (1947).

[3] W. T. Scott, Phys. Rev. **76**, 212 (1949).

TABLE I. Experimental and theoretical results for the multiple scattering of low energy protons in gases.

	Air	Argon	Helium
Number of pictures	1570	2521	1994
Number of measurable tracks N_T	477	582	75
C-type $0<\rho<150$ cm	182	257	22
Curvature to left	95	135	13
Curvature to right	87	122	9
O-type 150 cm$<\rho$	159	104	30
S-type	136	221	23
N', number of C-type $0<\rho<100$ cm	155	234	
Corresponding N $0<\rho<\infty$ / 58% N_T	268 / 277	315 / 338	
Exp. $\langle C'^2\rangle_{Av}$	0.536×10^{-3} cm^{-2}	1.25×10^{-3} cm^{-2}	
Theor. $\langle C'^2\rangle_{Av}$ for the N' tracks	0.470×10^{-3} cm^{-2}	1.15×10^{-3} cm^{-2}	
Exp. ρ_0'	43.2 cm	28.3 cm	
Theor. ρ_0'	46.1 cm	29.5 cm	
Exp. $\langle C^2\rangle_{Av}$	0.323×10^{-3} cm^{-2}	0.935×10^{-3} cm^{-2}	
Theor. $\langle C^2\rangle_{Av}$ for the N tracks	0.269×10^{-3} cm^{-2}	0.847×10^{-3} cm^{-2}	
Exp. ρ_0	55.6 cm	32.7 cm	
Theor. ρ_0	61.0 cm	34.4 cm	

assumption of a Gaussian distribution, can also be found in Table I.

The theoretical results contained in Table I were obtained from the following relations:

$$\langle C^2\rangle_{Av}^{-1}=\rho_0=416(E/Z)(x/BP)^{\frac{1}{2}},$$

where

$$B=1+0.468\log_{10}(p/mc)\theta_{\max}Z^{-\frac{1}{2}},$$

E is the proton energy in Mev, m the electron mass, p the momentum of the proton, Z the atomic number of the scattering gas, and x the half range of the protons (2.5 cm here). $\theta_{\max}$ was taken as 0.1 radian. $P=2$ for air and 1 for argon. It can be shown that the above relations are equivalent to Scott's results and they are identical with Eqs. (9) and (10) of Bethe's paper,[1] except that, following Rossi and Greisen,[4] $\theta_{\min}$ was taken as

$$\theta_{\min}=(mc/p)(Z^{\frac{1}{2}}/137).$$

The agreement between experiment and theory is good, if it is remembered that the experimental results have attached to them two errors, one due to statistics, of approximately the square root of the number of tracks, and one due to the matching of circles, which in each individual measurement can be of the order of 5 cm for the small radii and 10 cm for the larger ones.

In order to compare the histograms with the theoretical distributions in ρ, such distributions normalized to give the experimental $\langle C'^2\rangle_{Av}$ and N' are drawn on Figs. 1A and 1B. These same curves were compared with distributions using the theoretical $\langle C^2\rangle_{Av}$; these are the dotted lines of Fig. 2. All 4 curves shown are normalized to $N=100$ tracks. Scott's result that 58 percent of the tracks would be of the C-type was also compared with the experimental result. It is seen that N is equal, within the experimental error, to 58 percent of the total number of tracks photographed.

The above results apply only to air and argon. For helium, only 75 tracks were measurable out of 1994 pictures, therefore all that can be said for helium is of a qualitative nature, and that is that the scattering curvatures were smaller than those for air and argon.

The author wishes to thank Professor G. S. Klaiber for suggesting this problem and for his advice during the course of the experiment. He is also indebted to Professor H. A. Nye for many helpful discussions of the theory.

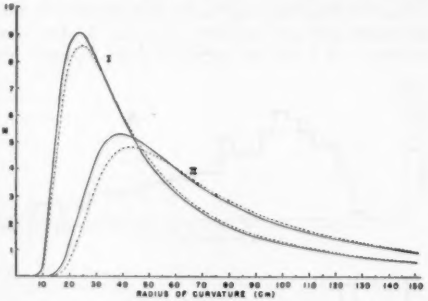

FIG. 2. Comparison of experimental and theoretical distributions for air and argon. N is the number of tracks having a given range of curvature per 100 C-type tracks. Group I—argon; group II—air. The solid curves are the experimental distributions, and the dashed curves are the theoretical distributions.

[4] B. Rossi and K. Greisen, Revs. Modern Phys. **13**, 240 (1941).

The Disintegration of N^{15} by Protons*

ALOIS SCHARDT, WILLIAM A. FOWLER, AND CHARLES C. LAURITSEN
Kellogg Radiation Laboratory, California Institute of Technology, Pasadena 4, California
(Received February 8, 1951)

The absolute cross sections of the reactions (1) $N^{15}(p,\alpha)C^{12}$, (2) $N^{15}(p,\alpha\gamma)C^{12}$, and (3) $N^{15}(p,\gamma)O^{16}$ have been measured from 0.2 to 1.6 Mev. The thick target yield of reaction (1) was also measured at 0.100 Mev. Resonances were found at 0.338, 1.05, and 1.210 Mev for reaction (1); at 0.429, 0.898, 1.210, and possibly 1.05 Mev for reaction (2); and at 1.05 Mev for reaction (3). Most of the resonances follow closely the shape of the single level dispersion formula. The 1.05-Mev resonance is asymmetric and cannot be explained as easily. The cross section of reaction (1) has been extrapolated to stellar energies and is given by $\sigma=(110/E)\times\exp(-6.95E^{-\frac{1}{2}})$ barns for E in Mev in the energy region near 0.030 Mev.

I. INTRODUCTION

ON bombardment of N^{15} with protons of energy below 2 Mev the following reactions are energetically possible:

$$N^{15}+H^1\rightarrow(O^{16})\rightarrow C^{12}+He^4 \quad Q=5.0 \text{ Mev} \quad (1)$$
$$\rightarrow C^{12*}+He^4 \quad Q=0.5 \text{ Mev} \quad (2)$$
$$\rightarrow O^{16}+\gamma \quad Q=12.1 \text{ Mev}. \quad (3)$$

The first to observe reaction (1) were Burcham and Smith.[1] They bombarded a mixture of oxygen and nitrogen with 0.5-Mev protons. The alpha-particle group found varied in intensity with the nitrogen content and had approximately the correct energy. Fowler, Lauritsen, and Lauritsen[2,3] observed reaction (2) for proton energies between 0.6 and 1.4 Mev. They measured the quantum energy to be 4.5 Mev and found resonances at 0.88, 1.03, and 1.20 Mev. Tangen[4] observed a gamma-ray resonance at 0.428 Mev which he attributed to reaction (3).[5]

Measurement of the absolute cross sections of these reactions became of interest when Bethe[6] investigated the carbon-nitrogen cycle as a source of stellar energy. For his calculations it was necessary to know the cross sections at stellar energies, near 30 kev. Holloway and Bethe[7] measured the cross sections of reaction (1) near 360 kev, but did not measure the bombarding energy with great accuracy. Cochrane and Hester[8] measured the excitation of reaction (1) from 0.2 to 0.5 Mev and found a resonance near 0.4 Mev.

In order to extrapolate the cross sections from the energy at which they are measured to stellar energies it is desirable to know the excitation curves of the reactions in some detail. We have measured the yield of alpha-particles and quanta from the disintegration of N^{15} by protons from 0.2 to 1.6 Mev. Two groups of alpha-particles corresponding to reactions (1) and (2) were found. At most of the resonances only 4.5-Mev radiation was present. However, at 1.05-Mev coincidence absorption measurements showed the presence of 13-Mev radiation. As reaction (1) is of primary interest in connection with stellar energy production, its yield was also measured at 0.10 Mev to check the extrapolation.

The excitation curves give information about the nature and frequency of levels in the compound nucleus, O^{16}. The levels formed are at an excitation energy between 12.1 and 13.6 Mev in O^{16}. The presence of only one short range alpha-particle group indicates that no level in C^{12} below 4.5 Mev is produced in these reactions. From the cross sections and experimental widths at the resonances approximate widths for alpha-particle and gamma-ray emission can be calculated. However, an accurate analysis has to wait until angular distribution and correlation measurements now underway in this laboratory are concluded. As these angular distribution measurements of the reaction products have not yet been completed, the results are most conveniently expressed as 4π times the differential cross sections per unit solid angle in the direction of observation.

II. EXPERIMENTAL ARRANGEMENT

A solid nitrogen compound enriched with N^{15} was bombarded with mono-energetic protons and the yield of alpha-particles and quanta was measured as a function of proton energy. For most of the work the protons were accelerated by the 1.6-Mev pressure insulated electrostatic accelerator of the California Institute of Technology.[9] An electrostatic analyzer,[9] calibrated with the 873.5-kev $F^{19}(p,\alpha\gamma)$ resonance, held the proton energy within 0.02 percent. The H^+ beam was used from 0.4 to 1.6 Mev and the HH^+ and HHH^+ beams from 0.2 to 0.4 Mev. The target arrangement described by Snyder *et al.*[10] was used. Above bombarding energies

* This work was assisted by the joint program of the ONR and AEC.
[1] W. E. Burcham and C. L. Smith, Nature **143**, 795 (1939).
[2] W. A. Fowler and C. C. Lauritsen, Phys. Rev. **58**, 192 (1940).
[3] Lauritsen, Lauritsen, and Fowler, Phys. Rev. **59**, 241 (1941).
[4] R. Tangen, Kgl. Norske. Videnskabs Selskabs Skr. No. 1 (1946).
[5] Our results indicate that this resonance is due to reaction (2).
[6] H. A. Bethe, Phys. Rev. **55**, 103, 434 (1939); and Astrophys. J. **94**, 37 (1940).
[7] M. G. Holloway and H. A. Bethe, Phys. Rev. **57**, 747 (1940).
[8] W. Cochrane and A. G. Hester, Proc. Roy. Soc. (London) **199**, 458 (1949).
[9] Fowler, Lauritsen, and Lauritsen, Rev. Sci. Instr. **18**, 818 (1947).
[10] Snyder, Rubin, Fowler, and Lauritsen, Rev. Sci. Instr. **21**, 852 (1950).

of 0.85 Mev a magnetic spectrograph,[10] capable of focussing 2-Mev alpha-particles, was used to separate the long-range alpha-particles from the elastically scattered protons. It detected particles emitted at 138° with the incident beam. A thin mica foil mounted in the foil holder of the target chamber slowed the alpha-particles down from about 5 to below 2 Mev. Below 0.85 Mev, a proportional counter at 90° with the beam was substituted for the spectrograph because a larger solid angle was needed to compensate for the decrease in yield. The counter window, 0.317 inches in diameter, was 0.800 inches from the center of the target spot and thus subtended 0.12 steradians.

The quanta were detected using a Geiger-Müller counter coincidence arrangement[11,12] at 90° with the beam. The counters made by Radiation Counter Laboratories of Chicago, have an effective length of $3\frac{1}{8}$ inches and a diameter of 23/32 inch. The wall thickness is 30 mg/cm² of glass plus a thin silver deposit. The two rear counters were 0.75 inches from the front counter, which in turn was 1.50 inches from the target. This corresponds to poor geometry and the solid angle has to be found empirically. At a strong resonance the yield was measured in this position and also with the counter 4.0 inches from the target. In the latter position the solid angle can be calculated using standard formulas.[11] The ratio of the readings then was used to determine the solid angle in the near position.

For the 0.10-Mev measurement the low voltage accelerator and high current ion source described by Hall *et al.*[13,14] were used. A horizontal section through the target arrangement is shown in Fig. 1. The long range alpha-particles were detected with a proportional counter. Its aperture was 0.700 inches from the center of the target. Apertures 0.532 and 0.750 inches in diameter were used, giving solid angles of 0.40 and 0.75 steradians. Air cooling of the target support was necessary as 10 watts had to be dissipated. To reduce the deposition of carbon by the beam, a liquid air trap was provided as shown.

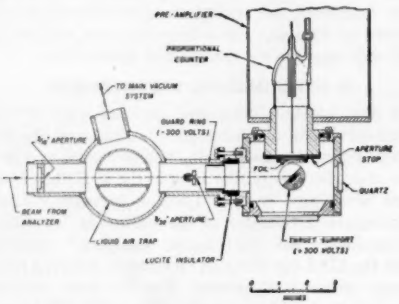

FIG. 1. Experimental arrangement used in the 0.100-Mev measurement of long-range alpha-particles.

III. TARGETS

The choice of target material was primarily dictated by the availability of compounds enriched with N^{15}. The most suitable compound we could find was KNO_3, which is available from the Eastman Kodak Company enriched to 61 percent N^{15}. The proton disintegration cross sections of potassium, N^{14}, and oxygen are sufficiently small as not to interfere with the N^{15} measurements. KNO_3 decomposes at 400°C but will evaporate in vacuum at a slightly lower temperature. To show that it does not decompose in the evaporation, a thin target deposited on a silver leaf was analyzed with elastically scattered protons[10] and the results compared with those using a thick target of the material before evaporation.

It was possible to evaporate targets of any desired thickness onto a copper target holder. It was found that the target decomposed under prolonged bombardment by the proton beam ($\sim 0.2\mu a$). The loss of nitrogen was assumed to be proportional to the total charge collected. The rate of loss was checked frequently by comparing yields at selected bombarding energies. The current density of the proton beam was not constant over the target area; therefore, the central part lost nitrogen more quickly. Since the beam wandered slightly, the yield showed appreciable fluctuations and the target had to be replaced frequently.

The energy-equivalent target thickness in kev was always measured at the 0.898-Mev resonance, either by width at half maximum or by the area under the curve. The accuracy of this measurement was about ± 10 percent. The result was converted into a number of N^{15} atoms by dividing the width by the stopping cross section per N^{15} nucleus. For KNO_3 enriched to 61 percent N^{15} this cross section is equal to 5.57×10^{-17} kev cm at 0.90 Mev. On all graphs in this report the target thickness is given at 0.90 Mev.

For the measurement at 0.10 Mev a more stable nitrogen compound was needed. Titanium nitride was prepared by heating a pellet of sintered titanium metal in an atmosphere of enriched ammonia.[15] The surface layer was analyzed with elastically scattered protons.[10] Light scattering nuclei were indicated by steps or peaks superimposed on the thick target scattering curve of titanium. The measurements indicated that there was some oxygen in the surface; probably a layer a fraction of a kev thick. The concentration of nitrogen was smaller than corresponds to TiN. A comparison of the quantum yield at the 0.898-Mev resonance between KNO_3 and this target showed that the surface layer had only $\frac{2}{3}$ as much nitrogen as expected in the compound TiN.

[11] Fowler, Lauritsen, and Lauritsen, Revs. Modern Phys. **20**, 236 (1948).
[12] Fowler, Lauritsen, and Tollestrup, Phys. Rev. **76**, 1767 (1949).
[13] R. N. Hall, Rev. Sci. Instr. **18**, 703 (1947).
[14] R. N. Hall and W. A. Fowler, Phys. Rev. **77**, 197 (1950).

[15] The authors are greatly indebted to Professor Don Yost, Dr. David L. Douglas, and Mr. Sidney Gibbons for suggesting this compound and preparing the targets.

Another difficulty encountered with this target was the presence of a slight boron contamination. The $B^{11}(p,\alpha)2He^4$ reaction produces alpha-particles in the same energy range as $N^{15}(p,\alpha)C^{12}$. At 0.10 Mev a compressed amorphous boron target gave more than 10^4 times the yield of TiN[15]. To measure the effect of this contamination, a titanium pellet was nitrided with ordinary nitrogen. The two targets were prepared under identical circumstances and were washed together in the same solutions. Thus, it may be assumed that the same amount of boron was on or in both targets. Different spots on the same target gave consistent results. About twice as many counts were observed with the enriched target as with the normal TiN target.

IV. OBSERVATIONS OF THE LONG-RANGE ALPHA-PARTICLES

At 100 kev the energy variation of the cross sections is primarily determined by the Gamow penetration factor. Neglecting the effects of resonance factors, Hall and Fowler[14] have derived an expression for the cross section using the thick target yield:

$$\sigma=\frac{0.993\epsilon Z_0 Y}{2E^{\frac{1}{2}}}\left(1+\frac{E^{\frac{1}{2}}}{Z_0}+\cdots\right)\text{cm}^2, \qquad (1)$$

where E is the proton energy in Mev, Y the thick target yield in disintegrations per proton, ϵ the stopping cross sections per active nucleus in Mev cm^2, and Z_0 the atomic number of the target nucleus. At 100 kev the stopping cross section of TiN is 3.8×10^{-20} Mev cm^2 per nitrogen atom and is thus 5.7×10^{-20} Mev cm^2 for the targets we employed, since only $\frac{2}{3}$ titanium in the surface layer had been converted into TiN. The target was enriched to 31.5 percent with N^{15} so that $\epsilon=1.8\times10^{-19}$ Mev cm^2 per N^{15} atom. From the observed yield, we calculated that $\sigma=5\times10^{-7}$ barns at 101.5 kev. The actual bombarding energy was slightly lower ($\sim$2 kev) because of the thin oxide layer on the target. The uncertainty in determining the effect of the boron contamination limits the accuracy to about 50 percent. Statistical and geometric errors are negligible compared to this.

Up to bombarding energies of 0.85 Mev the alpha-particles were counted at 90° to the beam with a proportional counter. The effective cross section was determined using a thin target (2-kev equivalent thickness at 0.9-Mev proton energy or 7 kev at 0.2 Mev). However, below 0.25 Mev a target 60-kev thick at 0.90 Mev was used to increase the yield. The slope of the yield curve was used to compute the effective cross section. A small correction of at most 10 percent was made in converting the semi-thick target slope into the thick target slope used in computing the cross section.

Above 0.85 Mev, the bombarding energy at which proton and alpha-particle ranges became equal, separation of scattered protons and alpha-particles was accomplished with the magnetic spectrograph. Since its maximum field cannot deflect alpha-particles of greater than 2 Mev into the counter, mica foils of 1.69 and 2.00 cm air equivalent were mounted on a foil holder and could be turned in front of the spectrograph as needed. The foils were calibrated using protons scattered by a thin silver foil. The proton energy (1.190 Mev) was chosen to give the same velocity as the velocity of the long-range alpha-particles. The number of protons scattered into the spectrograph with and without the mica foils was the same with 5 percent. The displacement of the proton peak gave the energy loss in the mica foil. The width of the peak gave the straggling.

The alpha-particle yield was measured by the method described by Brown *et al.*[16] At intervals of 0.12 Mev an alpha-profile curve[17] was taken. The number of doubly charged alpha-particles entering the spectrograph is then given by

$$n(\text{He}^{++})=1.602\times10^{-12}\frac{R}{q}\int\frac{N(I)}{I}dI. \qquad (2)$$

In this equation $R=P/\delta\rho$ is the momentum resolution of the spectrograph and $N(I)$ is the number of alpha-particle counts at a given magnetometer[18] current I, for a charge of q microcoulombs of protons. As long as the shape of the profile curve is determined primarily by the straggling in the mica foil one would expect that the quantity, η, defined by

$$\eta=\frac{1}{N_{\max}}\int\frac{N(I)}{I}dI \qquad (3)$$

would be a constant. This proved to be the case within the experimental error of 5 percent. For a 25-kev target $\eta=0.0605$ with foil No. 1 (1.69 cm of air) and $\eta=0.106$ with foil No. 2 (2.00 cm of air). Thus, at intermediate points only, the maximum value, $N_{\max}$, on the profile curve had to be measured.

The formula used in computing the cross section was as follows:[16]

$$\sigma_{\text{eff}}=\frac{1.602\times10^{-13}}{qnt}\frac{4\pi R}{\Omega_L}\left(\frac{d\Omega_C}{d\Omega_L}\right)^{-1}\left(1+\frac{n(\text{He}^{+})}{n(\text{He}^{++})}\right)\eta N_{\max},$$

where nt is the number of N^{15} atoms per cm^2 of target, Ω_L and Ω_C are the acceptance solid angles of the spectrograph in laboratory and center-of-mass systems, respectively, while $n(\text{He}^{+})/n(\text{He}^{++})$ is the ratio of singly to doubly charged alpha-particles entering the magnet. The ratio was determined as described in reference 16.

The effective cross section computed in this way is not greatly distorted by the target thickness, since the

[16] Brown, Snyder, Fowler, and Lauritsen, Phys. Rev. **82**, 159 (1951).

[17] At a fixed bombarding energy the alpha-particles are counted as a function of magnetic field to yield a "profile" curve.

[18] C. C. Lauritsen and T. Lauritsen, Rev. Sci. Instr. **19**, 916 (1948).

target used was 25 kev thick. Only at the 1.21-Mev resonance is a correction for target thickness necessary. Here the resonance cross section was calculated by assuming that the half width is the same for both long- and short-range alpha-particles.

The accuracy is limited primarily by target deterioration. With the exception of the region 1.3 to 1.6 Mev at least 100 and generally over 500 counts were taken at each point; thus statistical errors are small. The data taken with the proportional counter are more consistent because less bombardment was needed for the desired number of counts. In the region where proportional counter and spectrograph data overlap, the agreement (see Fig. 6 which is discussed in Part VII) is better than might be expected, especially since the data correspond to two different angles of observation. The stopping cross section enters into all computations. It has not been measured for potassium and interpolation between measured elements is probably only good to 10 percent. Thus the over-all accuracy is approximately 15 percent.

Cochrane and Hester[8] have measured the long-range alpha-cross section from 0.2 to 0.5 Mev. Within experimental errors the shape of their excitation curve agrees with our results. However, their cross section at the low resonance is only 0.013, compared to 0.09 barn obtained in this investigation. This discrepancy is not too surprising if one considers the difficulties associated with nitrogen targets, especially since only small quantities of separated isotopes are available. Cochrane and Hester started with $N^{15}H_4N^{14}O_3$ and transformed it by Kjeldahl's method into NH_4Cl. From this they evolved NH_3 for use in a gas target. The amount of $N^{15}H_4NO_3$ available to them was sufficient for only one target and no check could be made on the efficiency of the chemical process. On the other hand, we were able to use $KN^{15}O_3$ which had been analyzed by the Eastman Kodak Company. Three different KNO_3 targets gave consistent results and agree with preliminary data taken with the TiN target.

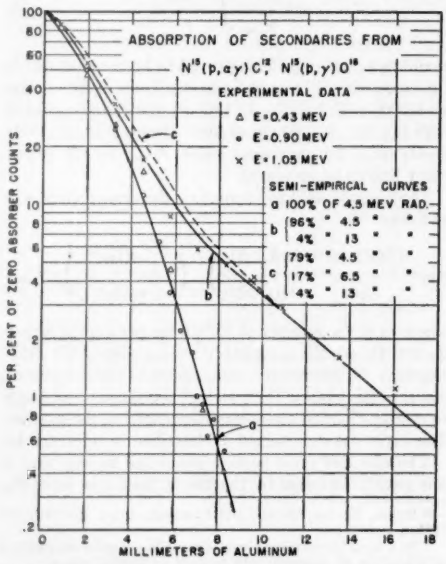
ABSORPTION OF SECONDARIES FROM
N15(p,αγ)C12, N15(p,γ)O16
EXPERIMENTAL DATA
△ E=0.43 MEV
• E=0.90 MEV
× E=1.05 MEV
SEMI-EMPIRICAL CURVES
a 100% OF 4.5 MEV RAD.
b 96% " 4.5 " "
4% " 13 " "
c 79% " 4.5 " "
17% " 6.5 " "
4% " 13 " "
PER CENT OF ZERO ABSORBER COUNTS
MILLIMETERS OF ALUMINUM

FIG. 2. Absorption of the secondaries produced in a thick aluminum converter by the $N^{15}(p,\gamma)$ radiations.

V. OBSERVATIONS OF THE GAMMA-RADIATION

The singles counts from the front counter of the coincidence arrangement together with the efficiency curves similar to those given by Fowler, Lauritsen, and Lauritsen[11] were used in computing quantum yields. A revised efficiency curve for counters and electroscopes with aluminum walls will be published in the near future. The counter efficiency is 3.0 percent for 4.5-Mev quanta and 9.7 percent for 13-Mev radiation. The absorption of the gamma-radiation in the converter and target chamber was calculated using the absorption coefficients of Streib.[19] This correction amounted to 10 percent and 7 percent for the 4.5- and 13-Mev quanta.

Absorption of secondaries was measured by the coincidence counts using different absorber thickness between the counters (Fig. 2). To interpret these data, curves similar to Fig. 10 in Fowler *et al.*[11] were prepared for the geometric arrangement used. From these curves it was possible to fit semi-empirical curves to the $N^{15}+H^1$ data. The curves taken at the 0.43- and 0.90-Mev resonances are consistent with simple 4.5-Mev radiation. The points taken at 1.05 Mev can be fitted best by assuming that 4 percent of the radiation has an energy of 13 Mev. The slope of curve (b) or (c) of Fig. 2 in the 9- to 16-mm region is typical of 13-Mev gamma-rays. Unfortunately the standard curves are not very accurate and thus the quantum energy may fall anywhere between 11 and 15 Mev. From mass differences the energy of the capture radiation leading to the ground state in O^{16} is 13 Mev. Furthermore curve (c) of Fig. 2 shows that cascade radiation cannot be ruled out entirely.

To measure the excitation curve of the hard component, coincidence counts were measured with 8.9 mm of aluminum absorber. On a typical run the background amounted to 4 counts out of 25. To check this excitation curve, a coincidence absorption curve was also taken at 1.12-Mev bombarding energy. It showed the expected decrease in hard quanta.

The accuracy of gamma-ray cross sections cannot be as high as that for alpha-particles. There is always an uncertainty in the Geiger counter efficiency and its sensitive volume. Measurements on the thick target yield at the 0.898-Mev resonance varied as much as 15 percent. The solid angle measurement at the 1½-inch position is only accurate to 10 percent. Thus the over-all

[19] Streib, Fowler, and Lauritsen, Phys. Rev. **59**, 253 (1941).

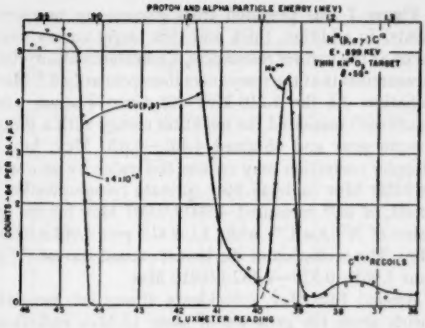

FIG. 3. Profile curve of alpha-particles from $N^{15}(p,\alpha\gamma)C^{12}$ and fluxmeter calibration using protons elastically scattered from a clean copper surface.

accuracy is about 20 percent for the 4.5-Mev quanta and somewhat poorer for the hard component. At the 0.898-Mev resonance the short range alpha-particles were measured at 58° simultaneously with the gamma-rays at 90°. The ratio turned out to be 0.85 alphas per quantum. The deviation from one alpha per quantum is not unexpected in view of the possibility that the angular distribution of the alpha-particles is not isotropic. The position of the two sharp resonances 0.429 and 0.898 Mev is accurate to 1 kev, since they were compared directly with the 0.8735-Mev F^{19} resonance.

VI. OBSERVATIONS OF THE SHORT-RANGE ALPHA-PARTICLES

The yield of alpha-particles from $N^{15}(p,\alpha\gamma)C^{12}$ was large enough at the 0.898- and 1.210-Mev resonances for observation with the spectrograph. In the backward direction the alpha-particles are focused by approximately the same magnetic field as the elastically scattered protons. However, by observing at 58°, it was possible to separate the two groups. Figure 3 shows the profile curve for a thin KNO_3 target bombarded with 0.899-Mev protons. For positive identification of the alpha-particles, their excitation curve was measured simultaneously with that of the gamma-rays at the 0.898-Mev resonance [Fig. 4(a)] and the curves were found to be identical. Also as noted above, the alpha-particle and quantum yields agree within experimental error.

In computing the alpha-particle energy, the midpoint of the front slope of the profile curve is generally taken to correspond to alpha-particles produced at the surface of the target. But the 0.898-Mev resonance is only 2.25-kev wide in terms of the bombarding proton energy, thus the alpha-particle spread ($\sim$10 kev) even with a thick target is not enough to fill the spectrograph window. A detailed analysis was made by folding the spectrograph window into the known yield of alpha-particles as a function of energy and fitting the observed and calculated curves. This fitting furnished the energy of the alpha-particles produced by the protons at resonance. The Q-value of the reaction was then computed using the standard nonrelativistic formula. From the three independent measurements at the 0.898-Mev resonance the following values were obtained: 0.5281, 0.5361, and 0.5302 Mev. At the 1.210-Mev resonance, 0.5226 Mev was measured. This is probably not as accurate as the results at the lower resonance because the scattered protons interfered slightly with the alpha-particle measurements. The average is 0.529 Mev. The angle of observation was measured to within $\pm\frac{1}{2}°$. This together with other systematic errors gives an uncertainty of ± 8 kev so that $Q^*=0.529\pm0.008$ Mev.

VII. RESULTS AND DISCUSSION

The over-all picture of the cross sections is given in Fig. 5. For graphical purposes the width of the two narrow resonances (at 0.429 and 0.898 Mev) has not been drawn to scale. Details of the curves with experimental points are given in Figs. 4, 6, and 7. The curves give 4π times the cross section per unit solid angle in the direction of observation. All gamma-ray measurements were made at 90°, as were the long-range alpha-particles up to 0.85 Mev. Between 0.7 and 1.6 Mev the long-range alpha-particles were observed at 137.8° with the incident proton beam.

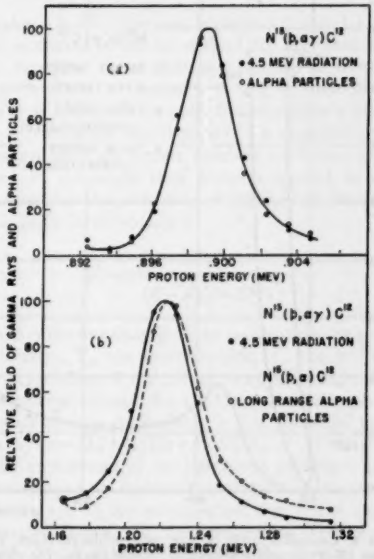

FIG. 4. (a) Excitation curve of alpha-particles and gamma-rays of $N^{15}(p,\alpha\gamma)C^{12}$ at the 0.898-Mev resonance. (b) Displacement of the excitation of gamma-radiation and long-range alpha-particles at the 1.210-Mev resonance. A 30 kev (at 0.90 Mev) target was used.

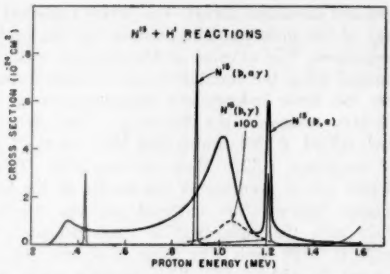

FIG. 5. Schematic excitation curves for the $N^{15}+H^1$ reactions. (The width of the narrow resonances are not shown to scale.)

Figure 6 shows the excitation curve for long-range alpha-particles. The measurements with the spectrograph showed that their energy agrees within 0.1 Mev with the energy to be expected for reaction (1) using masses given by Li *et al.*[20] The alpha-particles observed with the proportional counter had an energy greater than 3 Mev. No increase in counts was observed if all alpha-particles with energy greater than 2.2 Mev were counted. The yield was also linear in the N^{15} content of the target.

Figure 7 was prepared from gamma-ray measurements. In addition, thick and thin target curves were taken at the various resonances. Coincidence absorption measurements at the resonances show primarily 4.5-Mev radiation. At the 1.210-Mev resonance Thomas and Lauritsen[21] measured the quantum energy with a β-ray spectrometer and obtained 4.465 ± 0.020 Mev, but a Doppler correction may reduce this value by as much as 0.020 Mev to 4.445 Mev (private communication). Strait, *et al.*[22] measured 4.960 ± 0.007 Mev for the Q-value of $N^{14}(p,\alpha)C^{12}$, while Li *et al.*[20] give 4.961 ± 0.006 Mev. The excitation of the lowest excited stateof C^{12} is thus $4.961-0.529=4.432\pm0.010$ Mev.

Around 1.05 Mev, coincidence absorption measurements show the presence of some 13-Mev radiation. Capture radiation to the ground state in O^{16} is the only process which is sufficiently energetic. The other part of the radiation is probably mostly 4.5 Mev. Unfortunately the measurements are not very energy sensitive, and a large fraction of 6- or 7-Mev quanta cannot be ruled out. One would expect radiation in this energy range if cascading occurs in some of the capture radiation. Thus the 4.5-Mev component may be smaller in the 0.95- to 1.2-Mev region than has been shown on the graph.

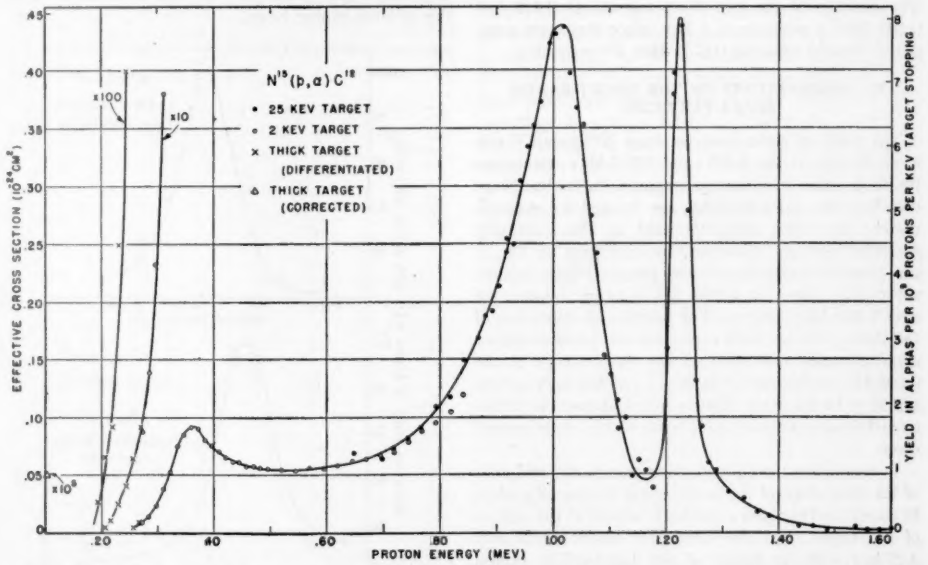

FIG. 6. Excitation curve of long range alpha-particles. The angle of observation is 90° for points designated by open circles and crosses, 137.8° for points designated by solid circles. The yield is given for a KNO_3 target enriched to 61 percent with N^{15}. Target thickness distorts the curve only at the 1.21-Mev resonance.

[20] Li, Whaling, Fowler, and Lauritsen, Phys. Rev. **83**, 512 (1951).
[21] R. G. Thomas and T. Lauritsen (to be published).
[22] Strait, Van Patter, Buechner, and Sperduto, Phys. Rev. **81**, 747 (1951).

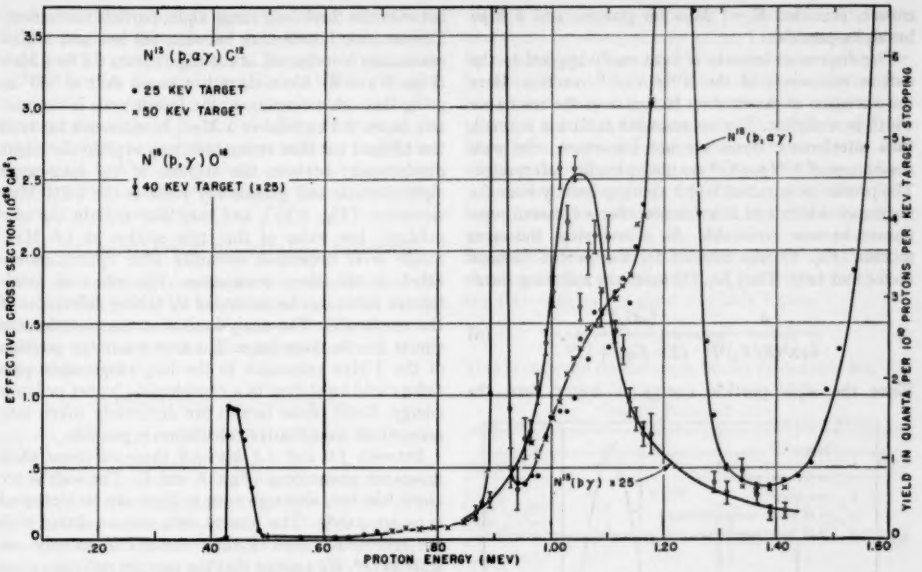

FIG. 7. Excitation curve of gamma-radiation. All measurements were made at 90°. The yield is given for a KNO_3 target enriched to 61 percent with N^{15}.

Since the target contained other nuclei besides N^{15}, one has to check whether any of them influence the measurements. Both KNO_3 and TiN targets were used above 0.4 Mev. The results agree if the variation of nitrogen concentration with depth in the TiN target is taken into account. At the bombarding energies used, the Coulomb barrier of both titanium and potassium is large; therefore, their transmutation cross sections are small. The $N^{14}+H^1$ cross sections have been investigated by Duncan and Perry[23] and were found to be much smaller than the N^{15} cross sections. For $N^{15}(p,\gamma)O^{16}$ the largest resonance is at 1.065 Mev, with a cross section of 3.5×10^{-28} cm^2 and $\Gamma=5$ kev. Thus, it is about ½ of the $N^{15}(p,\gamma)O^{16}$ cross section, but because of its small width the yield was negligible compared to the N^{15} reaction. Blank runs with normal KNO_3 showed no detectable gamma-radiation. For the measurements below 0.4 Mev, special care was taken to eliminate B^{11} contaminations. All measurements were reproducible in both yield and position of resonances.

As can be seen from Fig. 5 most of the resonances of the short- and long-range alpha-particles are not common. The 1.210-Mev resonance, however, is common to both reactions. Figure 4(b) shows the yields of the two reactions plotted on a relative scale. Since both yields were measured together, the displacement of a few kev is real and will be discussed below. The cross section curve (Fig. 7) for the short-range alpha-particles indicates a small resonance between 1.0 and 1.1 Mev which is masked by the tail of the 1.210-Mev resonance.

To interpret these excitation curves in terms of energy levels it is necessary to use a Breit-Wigner multi-level dispersion formula. Unfortunately a knowledge of the angular distribution of the cross sections is necessary. With the results obtained until now, one is limited to the single level formula applied at each resonance plus the possibility of interference terms.

The single level formula is

$$\sigma=\pi\lambda^2\frac{\omega\Gamma_p\Gamma_s}{(E-E_R)^2+\Gamma^2/4}, \tag{5}$$

where λ is the wavelength of the incident proton in the c.m. system, Γ_p the proton width, Γ_s the width of emitted radiation, Γ the full width at half maximum of the resonance, E and E_R are the proton energy and resonance energy, respectively, ω is a statistical factor given by $\omega=(2J+1)/(2s+1)(2i+1)$, J is the total angular momentum of the compound nucleus, s and i are the spins of the incident and target nucleus, respectively. Γ_p and Γ_s are not constant due to the barrier penetration factors. In the notation of Christy and Latter[24] $\Gamma=(E/E_1)^{\frac{1}{2}}PG$. Here P is the Gamow penetration factor. $(E/E_1)^{\frac{1}{2}}$ gives the velocity normalization. G is the width without barrier at a velocity of 1.4×10^9

[23] D. B. Duncan and J. E. Perry, Phys. Rev. **80**, 136 (1950).

[24] R. F. Christy and R. Latter, Revs. Modern Phys. **20**, 185 (1948).

cm-sec, provided $E_1=1$ Mev for protons and 4 Mev for alpha-particles.

The dispersion formula is most easily applied to the narrow resonances of the $N^{15}(p,\alpha\gamma)C^{12}$ reaction. Here the variation of penetration factors over the resonance width is negligible. The nonresonant radiation is small, thus interference terms are not important; the wide resonances of $N^{15}(p,\alpha)C^{12}$ are not as readily interpreted. The proton penetration factor changes greatly over the resonance width and interference effects between resonances become noticeable. As a first step, the cross section (Fig. 6) was divided by the proton Gamow factor and $4\pi\lambda^2$. Then Eq. (5) takes the following form:

$$\frac{\sigma}{4\pi\lambda^2(E/E_1)^{\frac{1}{2}}P}=\frac{\frac{1}{4}\omega G_p\Gamma_\alpha}{(E-E_R)^2+\frac{1}{4}\Gamma^2}. \tag{6}$$

Since the alpha-particle energy is larger than the potential barrier, Γ_α may be considered constant. In Fig. 8 we plot experimental points representing the quantity given on the left-hand side of Eq. (6). The values for P were taken from the curves of Christy and Latter for s-wave protons incident on nitrogen.[25] As shown in the figure the experimental points below 0.4 Mev can be fitted by a resonance curve (right-hand side of Eq. (6) with the maximum at 0.338 Mev and a width of 94 kev. The agreement is rather remarkable considering the change in cross section from 0.09 barn at 0.360 Mev to 5×10^{-7} barn at 0.100 Mev.

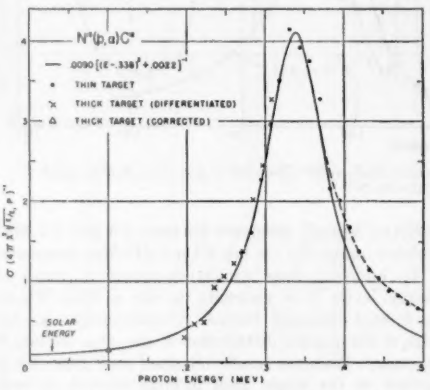

FIG. 8. Excitation curve of long-range alpha-particles after barrier factors have been divided out (s-wave protons were assumed).

Above 0.4 Mev, however, the experimental points start to deviate markedly from the resonance curve. The asymmetry of the next resonance, at about 1 Mev, is even more marked after a penetration factor is taken out. This behavior can be explained by interference between the three long-range alpha-particle resonances. Constructive interference between the low and 1-Mev resonances is indicated in the region from 0.4 to 1 Mev (Figs. 6 and 8). Since there is a phase shift of 180° in going through a resonance, the interference is destructive below 0.3 and above 1 Mev. Interference between the 1.0 and 1.2 Mev resonances may explain the slight displacement between the maxima of the long-range alpha-particle and gamma-ray yield at the 1.210-Mev resonance [Fig. 4(b)], and may also explain the surprisingly low value of the cross section at 1.6 Mev. Single level dispersion formulas were approximately fitted at the three resonances. The effect of interference terms can be estimated by taking differences of the amplitudes. The analysis showed that interference effects can be quite large. The true resonance position of the 1-Mev resonance in the long-range alpha-particles could be shifted to a considerably higher or lower energy. Until phase factors are accurately taken into account no quantitative calculation is possible.

Between 1.0 and 1.1 Mev all three reactions show resonance phenomena (Figs. 6 and 7). The widths are about 150 kev, although none of them can be measured very accurately. The present data are consistent with the assumption that all three correspond to only one state in O^{16}. We assume that the capture radiation gives the true position of the resonance, 1.05 Mev, and we quote this value for all three reactions. The maximum of the long-range alpha-yield is displaced toward lower energies by the interference with the 1.210-Mev resonance. The maximum of the short-range alpha-particles is displaced toward higher energies by the penetration factor of the alphas. The exact position and width of this resonance is masked by the tail of the 1.210-Mev resonances.

The pertinent experimental information about the resonances has been summarized in Table I. The thick target yield is given only for the narrow resonances. The $N^{15}(p,\alpha\gamma)$ resonance above 1.6 Mev has not been included. The gamma-ray yield was rising rapidly at the highest energy available. The long-range alpha-particles do not participate in this rise.

The data from Table I can be used to calculate the nuclear width without barrier, Γ, provided the statistical weight of the levels involved is known. Then by the usual intensity arguments, it is possible to limit the angular momentum and parity assignments of the states involved. This was done by one of the authors.[26] It was possible to find selection rules which determined whether the resonances were common between reactions (1), (2), and (3) or not.[27]

The Γ_γ involved for the capture radiation at the 1.05-Mev resonance indicates that it is an electric

[25] In the low energy region it makes very little difference which partial wave is used.

[26] A. W. Schardt, Ph.D. thesis, California Institute of Technology (1951).

[27] *Note added in proof:*—For example, states in O^{16} with angular momentum and parity given by 0^-, 1^+, 2^- ... cannot decay by long-range alpha-particle emission.

dipole transition. In that case one would expect very little cascading through the 6.13-Mev levels in O^{16}, but about 10 percent cascading through the pair state at 6.05 Mev. On the other hand, if the 13-Mev radiation is electric quadrupole, then considerable cascading through the 6.13-, 6.9-, and 7.1-Mev level is to be expected. Unfortunately the pairs could not be detected since a thick Al converter was used and the experimental results are not sufficiently accurate to determine the amount of cascading.

VIII. EXTRAPOLATION TO STELLAR ENERGIES

For stellar energy production only the value of the cross sections around 30 kev is important. This can be estimated by extrapolating as shown in Fig. 8. At low energies the tail of the cross section curve is given approximately by

$$\sigma_\alpha(E)=(110/E)\exp(-6.95E^{-\frac{1}{2}}), \qquad (7)$$

where σ_α is in barns provided E is in Mev. This yields $\sigma_\alpha=1.5\times10^{-14}$ barns at 30 kev.

The above expression would be quite accurate except for two facts. The amplitudes at 30 kev contributed by the 1.05-Mev resonance and the 0.338-Mev resonance are comparable. The interference of the two amplitudes is probably destructive and the value given in Eq. (7) may be high by a factor of 2. Furthermore, from the present experiments no information can be gained regarding resonances below 0.1 Mev and Eq. (7) assumes that none exist. Thus $\sigma_\alpha=1.5\times10^{-14}$ barns at 30 kev is consistent with the present observations but may be considerably in error if a low-lying resonance exists.

Compared to $N^{15}(p,\alpha)C^{12}$, the $N^{15}(p,\alpha\gamma)C^{12}$ reaction gives no appreciable contribution to stellar energy production. Its main resonances are very narrow (Table I) and no nonresonant radiation was found. An extrapolation of the $N^{15}(p,\gamma)O^{16}$ cross section to stellar energies is of interest, because this process removes nitrogen permanently from the carbon cycle. The reaction could be observed only at the 1.05-Mev resonance, because its yield is small. There is no reason to suppose, however, that it does not have other resonances. For instance, it may compete with the long-range alpha-particles at the 0.338-Mev resonance. This could not have been detected in laboratory measurements, but might make a significant contribution at 30 kev in stars.

In extrapolating from 1.05 Mev to 0.03 Mev it is important to use the correct incident proton wave. This resonance is probably also due to s-wave protons.[28] Equation (5) was used in the extrapolation. In order to obtain a minimum estimate $\Gamma=135$ kev was used. This together with values given in Table I gives

$$\sigma_\gamma(E)=(0.009/E)\exp(-6.95E^{-\frac{1}{2}}). \qquad (8)$$

This is only the contribution of one resonance, and the actual value of σ_γ is probably larger. Combining Eqs. (7) and (8), one gets $\sigma_\gamma/\sigma_\alpha\geq0.8\times10^{-4}$. This value is larger than assumed by Bethe[6] but is still small enough not to interfere with the carbon cycle during the age of the sun.

TABLE I. Resonance data.

Resonance energy (Mev)	Γ kev	$\sigma(p,\alpha)$ barns	$\sigma(p,\alpha\gamma)$ barns	$Y(p,\alpha\gamma)$ quanta/proton[a]	$\sigma(p,\gamma)$ barns
0.338[b]	94	0.075	...	...	...
0.429±0.001	0.9	...	0.3	4×10^{-9}	...
0.898±0.001	2.2	...	0.8	5×10^{-8}	...
1.05[c]	~150	0.5	0.015	...	0.001
1.210±0.003[d]	22.5[d]	0.6	0.3	1.8×10^{-7}	...

[a] Yield is for thick KNO_3 target containing 61 atom percent of N^{15}.
[b] Experimental data has been corrected for s-wave penetration factor. $E_{max}=0.36$ Mev. $\sigma_{max}=0.09$ barn.
[c] This value taken from the $N^{15}(p,\gamma)$ resonance.
[d] These values were measured from the $\sigma(p,\alpha\gamma)$ curve and may be different for $\sigma(p,\alpha)$.

The authors want to express their gratitude to Professors R. F. Christy and T. Lauritsen for many discussions during the course of this research.

The Primary Cosmic Radiation at High Latitudes*

MARTIN A. POMERANTZ AND GORDON W. MCCLURE
Bartol Research Foundation of the Franklin Institute, Swarthmore, Pennsylvania
(Received December 14, 1951)

Various properties of the new group of low energy primary cosmic-ray particles ($E<1.6$ Bev for protons) which enter the top of the atmosphere at geomagnetic latitudes north of 52° were investigated during the summer of 1950. Measurements at both 52°N (Swarthmore, Pennsylvania) and 69°N (Fort Churchill, Manitoba) were obtained with the same quadruple-coincidence counter trains used previously, oriented either horizontally or vertically, and with pulsed ionization chambers biased to detect bursts exceeding 1.0 Po-α.

No diurnal or temporal variations in the cosmic-ray intensity were detected, and no change between 1949 and 1950 was indicated.

Flights were conducted with counter trains containing various thicknesses of interposed Pb absorber.

In contrast with the 46 percent increase in the vertical intensity between the two stations, no latitude effect was revealed either in the flux of cosmic rays traveling in the horizontal direction or in the frequency of bursts detected by the ionization chambers, at the highest altitudes attained (~9 mm of Hg).

The data permit conclusions to be drawn regarding the horizontal component, the solar dipole-moment, the nature of the low energy spectrum, as well as nuclear disintegrations and primary heavy nuclei.

I. INTRODUCTION

EXPERIMENTS which have revealed the presence in the primary cosmic radiation of particles having momenta below that required for entrance at geomagnetic latitude 50°N have been described previously.[1] The original conclusions were based upon a direct comparison, by identical instruments, of the vertical cosmic-ray intensity near the "top of the atmosphere" at Fort Churchill, Manitoba (geomagnetic latitude 69°N), during the summer of 1949 with that at Swarthmore, Pa. (geomagnetic latitude 52°N).

After it had thus been established that a new group of particles was reaching the earth north of the previously-assumed knee of the latitude effect which had heretofore been attributed to a cut off imposed by the magnetic field of the sun, it was of interest further to investigate certain other features of these particles. In particular, it was considered desirable:

(a) to determine whether any change of conditions such as might be produced by a variable solar magnetic dipole-moment had occurred subsequent to the initial observations;

(b) to conduct additional attempts to detect either diurnal variations or short-time temporal variations (over a period of weeks);

(c) to obtain measurements of the intensity *vs* altitude curves with an interposed absorber of thickness intermediate between those utilized previously (4 cm of Pb);

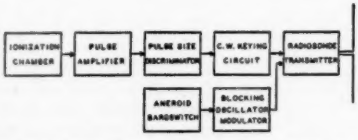

FIG. 1. Block diagram of circuits associated with ionization chamber.

(d) to compare the intensity in the horizontal direction at 69°N with that at 52°N in order to secure additional information regarding the nature of the new group of primary particles entering at the higher latitude;

(e) to observe the effect of the new low energy group of primaries upon the rate of bursts produced within the walls of an ionization chamber at high altitudes.

Under the sponsorship of the National Geographic Society, a second expedition to Fort Churchill, Manitoba, was therefore conducted during the summer of 1950. Two types of instruments, a burst-detecting ionization chamber and a quadruple coincidence counter train, were utilized to accomplish the aforementioned objectives.

II. EXPERIMENTAL PROCEDURE

A. Ionization Chamber Apparatus

A block diagram of the ionization chamber and associated circuitry is shown in Fig. 1. The instrument functions as follows: Voltage pulses produced in the ionization chamber (mainly by primary heavy nuclei and by nuclear disintegrations occurring in the chamber walls) are amplified by a linear pulse-amplifier and fed into a pulse-height discriminator. The latter permits the passage only of those pulses having amplitudes exceeding a predetermined size. Each discriminator output pulse triggers a keying univibrator, thereby causing the transmitter to emit a 75 megacycle C. W. signal for a period of 0.06 sec.

The telemetering system as well as the method for the determination of atmospheric pressure and temperature within the gondola during the balloon flights have already been described in detail elsewhere.[2]

The ionization chamber (Fig. 2) is composed essentially of an outer cylindrical pressure vessel, a concentric cylindrical cathode, and a central electron-collecting wire. The cathode, which operates at a potential of

* Assisted by the joint program of the ONR and AEC.
[1] M. A. Pomerantz, Phys. Rev. **77**, 830 (1950).
[2] M. A. Pomerantz, Electronics **24**, 88 (1951).

−300 v relative to the wire, is closed at the ends by copper guard disks having ½-inch center holes to pass the collector wire. The collector connects directly to the first grid of the linear amplifier and is maintained at dc ground potential by means of a 10^8-ohm grid-leak resistance. To eliminate the possibility of leakage from the high voltage cathode to the collector wire, the insulators supporting the wire are mounted on the grounded outer case.

In all measurements made to date, the chambers have been filled with 5 atmospheres of tank argon rated 99.9 percent pure. Before assembly, the internal parts are cleaned with an acid rinse, and immediately after the soldering operation, the chambers are evacuated for 24 hours while being maintained by an oven at a temperature of 125°C. The outgassing and filling procedures are accomplished on a special pressure-vacuum system, which permits both operations to be performed without the intervening admission of air into the chamber. A pressure gauge mounted permanently on each ion chamber permits the detection of leaks which might develop subsequent to sealing-off the unit.

For the purpose of calibration, each chamber contains a Po-α source plated onto an insulated silver electrode. The source protrudes slightly through a hole in the cathode and is "turned on or off" by connecting the probe to the cathode supply (−300 v) or to ground, respectively. In the "off" state, the α-particle ionization electrons are collected on the grounded source probe and are thus not permitted to reach the central wire.

The Po-α pulses reach voltage saturation at a cathode potential of −200 v immediately after a chamber is filled. However, the saturation voltage drops to an equilibrium value some 50 volts lower in the course of a few days. This tendency, which is probably caused by the "getter" action of the clean copper walls, insures that the normal operating potential of −300 v is adequate for saturation even long after the chambers are filled. The calibration source is used only for setting the discriminator and checking the over-all stability of the instrument in preflight tests. During flight the source is turned off so as not to interfere with the detection of cosmic-ray bursts. In the case of every instrument which has been recovered immediately after landing, postflight checks have revealed no detectable change in calibration.

The linear amplifier comprises three stages of amplification with 0.015 percent inverse feedback and has an over-all gain of 5×10^3. This amount of feedback, although not large, is sufficient to reduce to 2 percent the change in amplifier gain resulting from battery voltage drops during the normal (five hour) flight duration. The interstage coupling components of the amplifier are chosen to give a rise time (5 μsec) comparable to the electron collection time of the ionization chamber, and a decay time (100 μsec) sufficiently small that the inductive effect of positive ion motion is not amplified. Through careful selection of vacuum

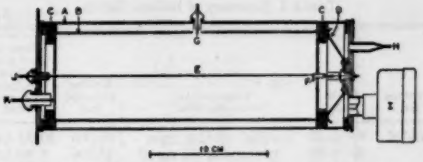

FIG. 2. Constructional details of ionization chamber. **A**, pressure vessel (0.032-in. Cu); **B**, cathode (0.032-in. Cu); **C**, cathode insulating rings (Mykroy); **D**, retaining spring; **E**, electron collector (0.010-in. Kovar); **F**, glass insulator; **G**, Po-α source electrode; **H**, pinch seal; **I**, 0–100 lb/in.[2] pressure gauge; **J**, connection to amplifier; **K**, −300 v cathode connection.

tubes, the amplifier output noise level is approximately 0.2 v, which is 5 percent of the amplitude of the smallest pulses allowed past the discriminator in the measurements reported here.

The discriminator stage is a triode biased beyond cut off by a variable potentiometer adjustment. The (positive) amplifier output pulses reach the discriminator plate circuit (and thence trigger the subsequent keying univibrator) only when their amplitudes exceed the difference between the negative bias potential and the triode cut off potential. For all of the flights reported in the present paper, the discriminator was adjusted so that only bursts >1.0 Po-α were relayed to the ground station.

B. Quadrupole Coincidence Counter Train

The counter trains utilized in measurements of the intensity both in the vertical and horizontal directions were identical with those used in 1949[1] and previously.[3] The complete balloon-borne apparatus, as well as the ground receiving station, have also been described in detail.[2]

III. RESULTS

A. Search for Diurnal and Temporal Variations

The detection of a small diurnal variation had not been specifically attempted in 1949, although the data obtained in flights conducted at different times of the day revealed no indication of any marked differences which could be attributed to a diurnal effect. If the sun possesses a permanent dipole-moment of the magnitude which had previously been assumed, a diurnal variation of the intensity of the primary cosmic radiation must necessarily occur, for reasons which have already been discussed.[1] Observations conducted at a high northern latitude are optimum from the point of view of the magnitude of the change expected during the course of a day, since the variation is maximum at locations appreciably north of the previously-assumed knee of the latitude effect. Furthermore, the extreme change expected at high latitudes occurs during daylight hours,

[3] For details regarding geometry, see M. A. Pomerantz, Phys. Rev. 75, 1721 (1949).

TABLE I. Summary of balloon flights.

Geomag. lat.	Flight date	Instrumental arrangement	Ceiling altitude, feet	Time of arrival at ceiling altitude, local solar time
69°N	8- 6-49	Vertical counter train	96,000	10:32 A.M.
	8- 9-49	containing 7.5 cm of	85,500	8:40 A.M.
	8-11-49	interposed Pb	74,000	4:24 P.M.
	8-16-49	absorber.	81,000	10:17 A.M.
	8-21-49		73,500	10:13 A.M.
	7-24-50		67,000	8:31 A.M.
	7-25-50		100,500	9:07 A.M.
	7-26-50		76,000	10:18 A.M.
	7-31-50		74,800	9:04 A.M.
	8- 5-50		84,500	1:37 P.M.
	8-12-50		97,000	12:43 P.M.
52°N	7-26-47		89,000	6:39 A.M.
	7-20-49		83,000	8:33 A.M.
	9-27-49		112,000	10:52 A.M.
	5-25-50		94,000	8:52 A.M.
69°N	8- 2-50	Vertical counter train	91,000	8:17 A.M.
	8- 5-50	containing 4.0 cm of	81,800	8:15 A.M.
	8-29-50	interposed Pb	74,500	4:16 P.M.
	8-30-50	absorber.	100,000	9:44 A.M.
52°N	6-24-48		95,000	8:24 A.M.
	10- 6-49		68,000	10:26 A.M.
	10-14-49		81,500	10:33 A.M.
69°N	8-18-50	Horizontal counter	80,000	6:14 P.M.
	8-19-50	train containing no	97,000	2:28 P.M.
	8-24-50	interposed Pb absorber.	83,000	10:00 A.M.
52°N	7- 7-50		105,000	9:37 A.M.
	10-17-50		102,200	10:43 A.M.
	10-27-50		104,200	11:13 A.M.
	11- 7-50		108,000	3:22 P.M.
52°N	7- 9-48	Horizontal counter	109,500	9:51 A.M.
	10- 7-48	train containing 1.0	109,000	11:18 A.M.
	10-28-49	cm of interposed Pb absorber.	117,500	11:02 A.M.
69°N	8- 9-50	Horizontal counter	83,000	9:26 A.M.
	8-16-50	train containing 7.5	72,500	10:25 A.M.
	8-18-50	cm of interposed Pb	87,500	9:14 A.M.
	8-29-50	absorber.	85,400	9:29 A.M.
52°N	7- 7-48		104,000	8:24 A.M.
	10-29-48		102,000	11:03 A.M.
	11-23-48		115,000	10:59 A.M.
69°N	9- 2-50	Ionization chamber bi-	78,500	6:01 P.M.
	9- 3-50	ased to record events	91,500	4:59 P.M.
	9- 4-50	exceeding 1 Po-α.	110,500	10:46 A.M.
52°N	4-30-50		83,000	9:50 A.M.
	6- 2-50		103,500	9:00 A.M.
	6- 9-50		94,000	8:25 A.M.
	3- 7-51		80,000	12:35 P.M.

to which the present flights were necessarily confined owing to technical limitations imposed by the absence of heating by solar radiation at night. Finally, and most important of all, the intensity at the higher latitude should actually be lower than that at Swarthmore in the early morning, and equal in the late afternoon, according to Dwight's calculations.[4]

Therefore, the flights in 1950 were released over a wider range of times to broaden the scope of this important phase of the investigation. For reasons cited earlier,[1] measurements were obtained principally with counter trains containing 7.5 cm of interposed lead absorber. Table I contains a summary of the 1950 series at Fort Churchill, and as may be seen in Figs. 3 and 4, there is no detectable dependence of the results upon the time of day.

Furthermore, it is apparent in Fig. 3 that the present measurements have quantitatively confirmed the earlier data, thus indicating no observable difference in the conditions existing during the summers of 1949 and 1950. Finally, it is to be noted that, during the course of continuous observations extending over a period of more than a month, no changes sufficient to be detected by the instruments utilized in these investigations are manifested.

B. Intensity *vs* Altitude Curve with 4 cm Pb

The nature of the dependence of the intensity upon altitude at 69°N in the case of particles capable of penetrating 4 cm of Pb is of particular interest. The fact that a definite maximum in the curve is observed at 52°N for 4 cm but not 6 cm provided a basis for the prediction that the maximum with 4 cm would disappear at the higher latitude. Low energy primaries, such as were presumably entering at Fort Churchill, were expected, through their progeny, to contribute appreciably to the intensity only near the top of the atmosphere.

This hypothesis is supported by the results plotted in Fig. 4. It is observed that, at Fort Churchill, the intensity of particles having a residual range of 4 cm of Pb is essentially constant throughout the upper seven percent of the atmosphere.

This latitude dependence of the critical thickness of interposed absorber for which the maximum in the intensity *vs* altitude curve disappears, arising from the change in the minimum allowed primary energy, would result in the appearance of a maximum at low latitudes even for thick absorbers. Thus, Rao *et al.*,[4a] at 3°N, have observed a distinct peak in the vertical intensity of cosmic radiation penetrating 10 cm of Pb, at a pressure of 90 mm of Hg. This is entirely in accord with expectations on the basis of the present considerations. Furthermore, as a consequence of this effect, the atmospheric pressure at which the maximum occurs for any particular amount of absorber would increase as the latitude is decreased.

C. Intensity in the Horizontal Direction

Investigations[5-7] of the cosmic-ray intensity at various zenith angles have revealed an appreciable

[4] K. Dwight, Phys. Rev. **78**, 40 (1950).

[4a] Rao, Balasubrahmanyam, Gokhale, and Pereira, Phys. Rev. **83**, 173 (1951).

[5] Swann, Locher, and Danforth, Natl. Geographic Soc. Contributed Tech. Papers, Stratosphere Series **2**, 13 (1936).

[6] M. A. Pomerantz, Phys. Rev. **75**, 1335 (1948).

[7] Winckler, Stroud, and Shanley, Phys. Rev. **76**, 1012 (1949).

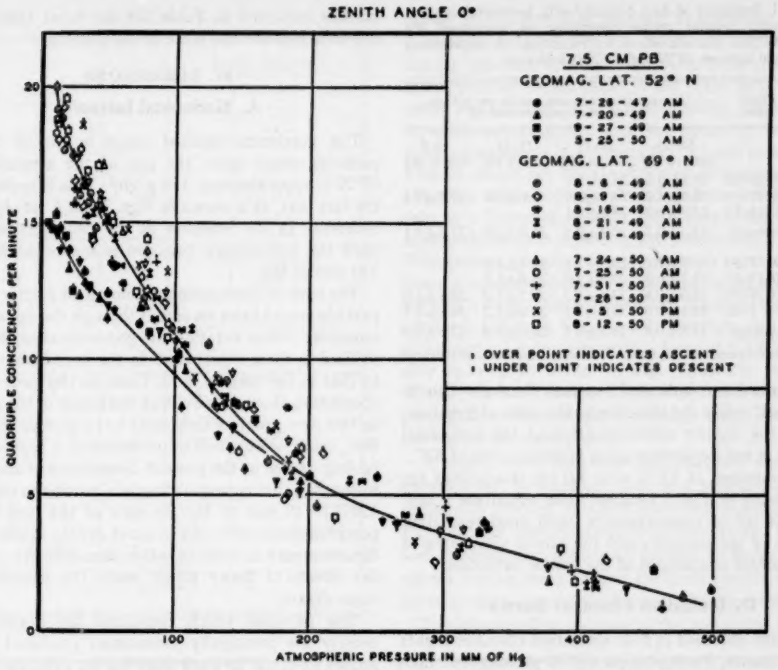
ZENITH ANGLE 0°
7.5 CM PB
GEOMAG. LAT. 52° N
7 - 28 - 47 AM
7 - 20 - 49 AM
9 - 27 - 49 AM
5 - 25 - 50 AM
GEOMAG. LAT. 69° N
8 - 8 - 49 AM
8 - 9 - 49 AM
8 - 18 - 49 AM
8 - 21 - 49 AM
8 - 11 - 49 PM
7 - 24 - 50 AM
7 - 25 - 50 AM
7 - 31 - 50 AM
7 - 26 - 50 PM
8 - 5 - 50 PM
8 - 12 - 50 PM
OVER POINT INDICATES ASCENT
UNDER POINT INDICATES DESCENT
QUADRUPLE COINCIDENCES PER MINUTE
ATMOSPHERIC PRESSURE IN MM OF Hg
0
5
10
15
20
100
200
300
400
500

FIG. 3. Intensity *vs* altitude curves for cosmic rays arriving vertically, and penetrating 7.5 cm of Pb at $\lambda = 52°$N (Swarthmore, Pennsylvania) and $\lambda = 69°$N (Fort Churchill, Manitoba). Note the absence of detectable diurnal or temporal variations.

component at large angles. The observed horizontal intensity at very high altitudes appreciably exceeds that at the terminus of a corresponding effective atmospheric path in the vertical direction, and must consist predominantly of secondary particles emitted in acts in which the initial direction is not propagated. It was of interest to ascertain whether the new group of low energy primary particles entering at Fort Churchill would enhance the horizontal intensity at that station. Therefore, a direct comparison of the horizontal intensities at the two latitudes was conducted.

The measurements were obtained with the same counter trains used in the other phases of these experiments. When the instruments are oriented horizontally, the maximum aperture between the extreme ray and the horizontal plane is 4.5°. Telescopic observations of the swinging of the instruments during flight revealed that the maximum excursion was usually less than 2° from the vertical even during the more turbulent initial portions of the ascent.

In some of the flights, a 7.5 cm Pb absorber was interposed in the counter train. In others, no absorber was present other than the counter walls. In this case all particles capable of penetrating 4.4 g/cm² were detected. This corresponds to a minimum energy for mesons of approximately 20 Mev.

A detailed statistical analysis of flights under the latter condition is summarized in Table II. These

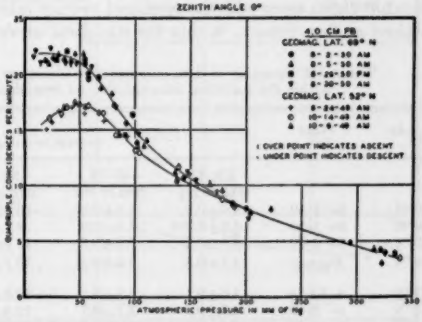
ZENITH ANGLE 0°
4.0 CM PB
GEOMAG. LAT. 69° N
8 - 2 - 50 AM
8 - 5 - 50 AM
8 - 25 - 50 PM
8 - 30 - 50 AM
GEOMAG. LAT. 52° N
8 - 24 - 49 AM
10 - 14 - 49 AM
10 - 6 - 49 AM
OVER POINT INDICATES ASCENT
UNDER POINT INDICATES DESCENT
QUADRUPLE COINCIDENCES PER MINUTE
ATMOSPHERIC PRESSURE IN MM OF Hg

FIG. 4. Intensity *vs* altitude curves, obtained with concidence-counter trains containing 4 cm of Pb, for cosmic rays arriving vertically at $\lambda = 52°$N and $\lambda = 69°$N. The maximum disappears at the more northern station.

TABLE II. Summary of data obtained with horizontal quadruple-coincidence counter trains containing no interposed Pb absorber. Within the statistical uncertainties, no dependence upon latitude between 52°N and 69°N is indicated.

Geomag. lat.	Flight date	Average counting rates, counts per minute, in indicated pressure interval			
		54–33 mm of Hg	33–21 mm of Hg	21–13 mm of Hg	13–8 mm of Hg
69°N	8–18–50	19.3±0.8	25.4±1.1		
69°N	8–19–50	18.1±1.0	25.0±1.0	31.0±0.9	33.3±1.1
69°N	8–24–50	17.9±0.9	28.1±1.1		
69°N	Average	18.5±0.5	26.3±0.6	31.0±0.9	33.3±1.1
52°N	7– 7–50	17.7±1.1	25.8±1.1	29.5±1.0	
52°N	10–17–50	17.2±0.9	27.1±1.9	28.8±1.1	
52°N	10–27–50	18.0±0.8	23.1±1.2	29.7±1.2	32.1±1.0
52°N	11– 7–50	18.1±0.9	29.0±2.1	33.6±1.2	34.5±1.1
52°N	Average	17.8±0.5	25.7±0.7	30.9±0.6	32.5±0.6

experiments have indicated, as may be seen also in Fig. 5, that, unlike the situation in the vertical direction, even at the highest altitudes attained the horizontal intensity is not dependent upon latitude north of 52°.

Data obtained at 52°N with 1.0 cm of absorber are also included in Fig. 5 because these constitute a self-consistent set of measurements, with good resolution in zenith, of the intensity and the rate of absorption of the horizontal component of the cosmic radiation.

D. Ionization Chamber Bursts

The data obtained in four ionization chamber flights at Swarthmore, Pennsylvania (52°N geomagnetic latitude) and in three flights at Fort Churchill (69°N geomagnetic latitude) are plotted in Fig. 6. Statistical errors (not shown in the figure) are approximately ±10 percent for points near the top of the atmosphere and ±20 percent for the lower points. A statistical analysis of the data from the seven separate flights at the two locations (Table III) shows that all individual flights agree within statistical expectation. Similarly, the combined average counting rates of the Fort Churchill flights agree with the combined average rates obtained at Swarthmore. Within the statistical uncertainties indicated in Table III the burst rates at the two locations are the same at all altitudes.

IV. DISCUSSIONS

A. Horizontal Intensity

The maximum residual range in air of the new particles which enter the top of the atmosphere at 69°N is approximately 150 g/cm². This is indicated by the fact that, as is shown in Figs. 3 and 4, no observable difference in the intensity at the two locations arises until the atmospheric pressure is somewhat less than 120 mm of Hg.

The ratio of the minimum amount of matter which a particle would have traversed through the spherical atmosphere before entering the geometrical arrangement utilized in these experiments in the horizontal direction to that in the vertical is 12. Thus, on the basis of mass-absorption alone, it is evident that none of the particles in this new group, which must have energies below 1.6 Bev, could be expected to penetrate to a horizontal detecting device of the present dimensions at an altitude lower than that corresponding to a maximum pressure of 120/12=10 mm of Hg. In view of the fact that the particles observed at the greatest depths in the vertical direction may be mesons rather than primary nucleons, the effects of decay would make the situation even more drastic.

The particles which constitute the horizontal intensity are principally secondaries produced at wide angles from the forward direction by primaries moving essentially downward through the atmosphere. This is immediately evident from the comparison of the counting rates recorded at high altitudes in the horizontal direction with those predicted on the basis of measurements obtained with an identical instrument oriented vertically. The expected counting rate $I_H(p_0)$ of a horizontal train at pressure p_0 can be computed on the basis of the assumption that the contribution at angle ζ is $I_\zeta(p_0)=I_0(p_0 f_\zeta)$, where f_ζ would be $\sec\zeta$ for a flat atmosphere of infinite extent. $I_0(p_0 f_\zeta)$ is obtained from the corresponding vertical intensity *vs* altitude

TABLE III. Summary of data obtained with ionization chambers biased to record pulse of height exceeding 1 Po-α. Within the statistical uncertainties, no dependence upon latitude between 52°N and 69°N is indicated.

Geomag. lat.	Flight date	Average counting rates, counts per minute, in indicated pressure interval						
		200–87 mm of Hg	87–54 mm of Hg	54–33 mm of Hg	33–21 mm of Hg	21–13 mm of Hg	13–8 mm of Hg	8–5 mm of Hg
69°N	9– 2–50	4.9±0.5	6.5±0.5	10.0±0.7	12.8±0.5			
69°N	9– 3–50	4.0±0.7	7.3±0.9	8.1±0.8	12.6±0.8	17.1±0.8		
69°N	9– 4–50	3.5±0.4	7.3±0.5	11.2±0.6		15.6±0.6	19.1±0.6	21.2±0.8
69°N	Average	4.1±0.3	7.0±0.3	10.2±0.4	12.7±0.4	16.3±0.5	19.1±0.6	21.2±0.8
52°N	4–30–50	5.0±0.3	6.8±0.6	10.0±0.6		17.0±1.0		
52°N	6– 2–50	4.5±0.3	8.5±0.7	10.4±0.7	13.1±1.0	15.6±0.8	19.0±0.8	20.8±1.4
52°N	6– 9–50	5.2±0.3	7.2±0.5	10.7±0.7	13.8±0.9	15.8±0.8	19.5±1.3	
52°N	3– 7–51	5.6±0.4	9.1±0.6	12.4±0.8	13.2±1.2			
52°N	Average	5.0±0.2	8.0±0.3	10.8±0.4	13.4±0.6	16.0±0.5	19.2±0.7	20.8±1.4

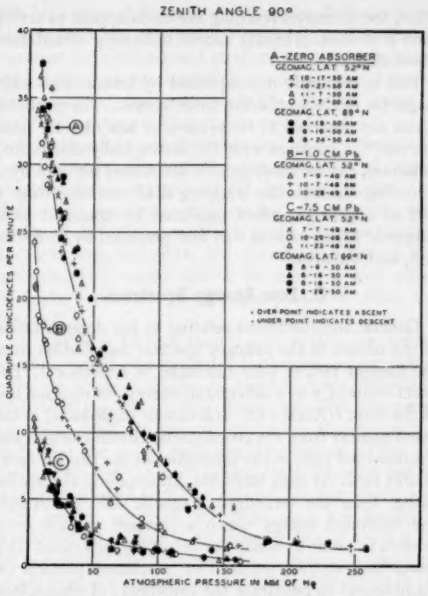

FIG. 5. Data obtained with counter trains oriented horizontally. No dependence upon latitude north of $\lambda = 52°$ is indicated.

curve. In the case of a spherical atmosphere, although f_T remains finite at 90°, the calculated counting rates are far less than the observed even if the attenuation introduced by meson decay is not taken into consideration. For example, at $p_0 = 30$ mm of Hg, the maximum expected counting rate with the geometry utilized in these experiments is 2 counts per minute as compared with 24 counts per minute observed with no interposed absorber. Meson decay should reduce this expected rate by a factor of at least 1000, depending upon the assumptions made regarding the production of mesons. This general situation (becoming even more drastic at lower altitudes), prevails for all thicknesses of absorber for which data are available up to the highest altitudes attained, although the disparity between the expected and observed intensities with 7.5 cm of Pb is considerably reduced at 5 mm of Hg. Thus, the horizontal intensity is far in excess of that expected for rectilinear propagation of an isotropic primary beam incident at the top of the atmosphere.

It might have been expected that low energy primaries would be most productive of wide-angle events, principally through the formation of low energy mesons. Furthermore, the spectrum is richest at the low end, and intensity considerations seemed to favor the primaries having energies near the geomagnetic cutoff at 52°N as the source of the horizontal component.

The absence of an increase in the horizontal intensity

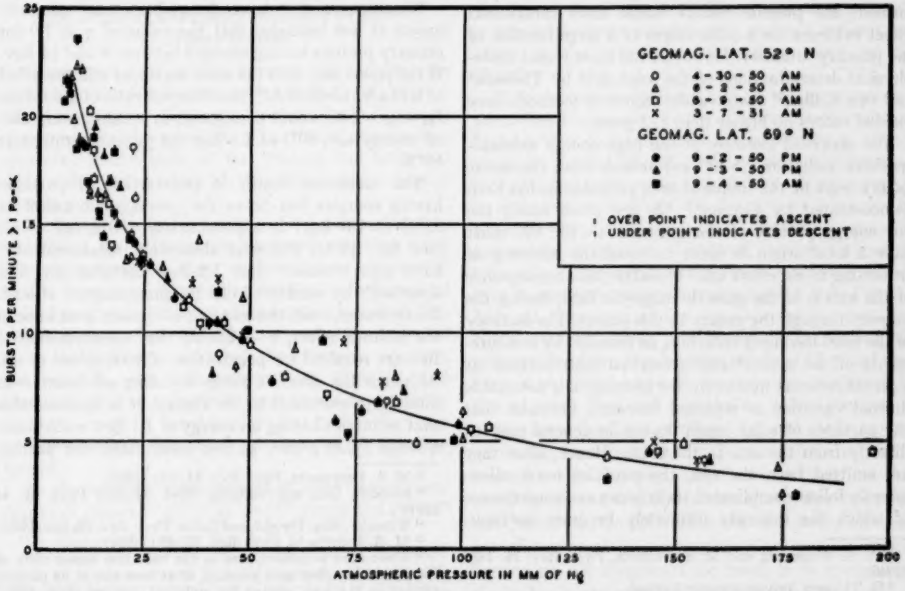
GEOMAG. LAT. 52° N
GEOMAG. LAT. 69° N
▼ OVER POINT INDICATES ASCENT
▲ UNDER POINT INDICATES DESCENT
BURSTS PER MINUTE > 1 Po-α
ATMOSPHERIC PRESSURE IN MM OF Hg

FIG. 6. Dependence of burst-rate upon altitude, as measured by ionization chambers biased to record events >1.0 Po-α. No variation with latitude north of $\lambda = 52°$ is revealed.

at the highest altitude attained, corresponding to about 9 mm of Hg, is not consistent with this hypothesis. On the contrary, the results indicate that the secondary particles which constitute the horizontal component do not arise from primaries having energies near the minimum permitted at 52°N. Hence, they must be the progeny of the less numerous high energy primaries. The latter are particularly effective in contributing to the counting rate of a counter train inclined at a zenith angle of 90° because the total flux of vertically-directed particles which can produce wide-angle secondaries capable of actuating the horizontal instrument is, of course, much larger than the total flux through the same counter train oriented vertically.

B. Solar Dipole-Moment

The original conclusion[8] that the maximum value of the solar dipole-moment does not exceed 6×10^{32} gauss-cm^3 remains unchanged. It must be emphasized that this deduction from the present experimental results presupposes an infinitely distant source for most of the cosmic radiation reaching the earth. The concept of a solar allowed-cone created at the earth by a permanent magnetic field of the sun certainly does not apply to particles produced at that body and proceeding more or less directly to the earth. Hence, if it had been independently demonstrated that the sun did possess a dipole-moment of the previously assigned magnitude during the period when these experiments were performed, the present results would have constituted direct evidence for a solar origin of a large fraction of the primary intensity. However, the most recent astrophysical determinations of the solar field by Thiessen[9] and von Klüber[10] using vastly improved methods have yielded values no higher than 1–2 gauss.

The observed isotropy of the high energy nonfield-sensitive radiation ($>10^{13}$ ev) reveals that the entire galaxy must be the source of such particles, as has been demonstrated by Cocconi.[11] On the other hand, the low energy portion of the spectrum ($<10^{10}$ ev) must have a local origin in order to avoid the necessity of traversing an excessive mass of matter, as a consequence of the action of the galactic magnetic field, during the journey through the galaxy to this planet. The isotropy of the total incoming radiation, as revealed by measurements of the zenith[6] and azimuthal distributions[7] at high altitudes as well as by the absence of a detectable diurnal variation as reported herewith, indicates that the particles of solar origin do not in general proceed directly from the sun to the earth Hence, after they are emitted from the sun, the particles must subsequently follow complicated trajectories as a consequence of which the intensity ultimately becomes isotropic. Thus, the primaries reaching the earth appear to arrive from a distant (virtual) source uniformly distributed about the earth.

This is evidently accomplished by interactions with magnetic fields within the solar system. The particles which are observed to come more or less directly from the sun,[12] in contrast with the isotropically-distributed radiation, can be consequently accounted for only by a tunneling through the trapping field resulting from a sort of degaussing effect produced by transient local magnetic fields, such as was first proposed by Forbush, Gill, and Vallarta.[13]

C. Low Energy Spectrum

General considerations relating to the determination of the nature of the primary spectral distribution from the present results were discussed in reference 1. The exact value of γ in a differential energy distribution law of the form $i(E)dE=kE^{-\gamma}dE$ cannot be deduced in the usual manner from the geomagnetic cut-off energies and the observed ratio of the intensities at the two latitudes in this case. At high latitudes, atmospheric absorption rather than the terrestrial magnetic field determines the minimum energy which a primary particle must possess in order to reach the detecting apparatus. This lower limit $\epsilon_n(l, \lambda)$, required by a primary particle (or its progeny) to penetrate the thickness l of atmosphere above the detecting apparatus plus the counter walls, cannot be assigned a precise value.

Winckler, *et al.*,[14] have determined from measurements at low latitudes that the value of γ is 1.9 for primary protons having energies between 4 and 14 Bev. If the power law with the same exponent still prevailed at latitudes north of 52°, the observed ratio of intensities $I_{69°}/I_{52°}=1.46$ would correspond to an absorption cut-off energy $\epsilon_n(l, 69°)$ of 1.1 Bev for primary protons at 69°N.

The maximum depth of penetration of particles having energies just below the geomagnetic cutoff at 52°N ($\approx$1.6 Bev) is approximately 150 g/cm^2 of air (see Sec. IVA). Previous absorption measurements[15] have also revealed that 1.6-Bev particles are first absorbed[16] by something like the same amount of lead. Furthermore, from the location of the sea-level knee of the latitude effect, it is known that approximately 3 Bev are required for penetration of 1000 g/cm^2 of air. Although the effective range is falling off faster than directly proportional to the energy, it is inconceivable that primaries having an energy of 1.1 Bev would have a range $l\leq20$ g/cm^2. In any event, after the particle

[8] M. A. Pomerantz and M. S. Vallarta, Phys. Rev. **76**, 1889 (1949).
[9] G. Thiessen (private communication).
[10] H. von Klüber, Proc. Roy. Ast. Soc. **111**, 8 (1951).
[11] G. Cocconi, Phys. Rev. **83**, 1193 (1951).
[12] M. A. Pomerantz, Phys. Rev. **81**, 731 (1951).
[13] Forbush, Gill, and Vallarta, Revs. Modern Phys. **21**, 44 (1949).
[14] Winckler, Stix, Dwight, and Sabin, Phys. Rev. **79**, 656 (1950).
[15] M. A. Pomerantz, Phys. Rev. **83**, 459 (1951).
[16] Absorption is defined here as the reduction below unity of the probability that each primary, or at least one of its progeny created in the lead, always has sufficient residual range and is propagated in the proper direction to actuate the coincidence train.

has been slowed down to a velocity such that nuclear interactions are relatively improbable and ionization becomes the predominant mode of energy degradation, the residual range appreciably exceeds this amount. For example, the experimentally observed range of 340-Mev protons is 70 g/cm² in carbon.[17]

It is, therefore, necessary to conclude that the power-law spectrum observed for the primaries of higher energies does not apply at the low end. In fact, the differential spectrum may exhibit a maximum even south of 52°, followed by a rapid decrease toward the low energies which are permitted north of this latitude. This would not be inconsistent with either Winckler's results[14] or with those of Van Allen and Singer.[18]

A spectrum of this shape, poor in the low energy portion, would be expected if the regions where cosmic rays are being produced on the sun were distributed statistically uniformly over the surface. The low energy particles could, in general, move off toward infinity only near the poles, owing to the presence of the one gauss field, and the contribution from the polar regions would be a small part of the total. On the other hand, high energy particles, if indeed any are produced, would not be subject to trapping fields and could move off to infinity. The observed spectrum would, therefore, result from a combination of effects involving both the production and acceleration processes and the solar geomagnetic effects.

D. Nuclear Disintegrations and Primary Heavy Nuclei

When biased as in the present experiments, the ionization chamber instrument responds to: (1) relativistic heavy nuclei of atomic number $Z>8$; (2) single slow protons and α-particles; (3) nuclear disintegrations produced in the walls by fast protons and neutrons; (4) air showers in which at least 60 electrons traverse the chamber.

Of the above-listed events, air showers probably contribute the least to the observed counting rates. Chambers similar to those used in the present investigation have been operated in twofold coincidence as detectors of dense showers at mountain altitudes.[19] The results indicate that only a few percent of the bursts at these heights are produced by electron showers. Furthermore, the measurements of Kraybill and Ovrebo[20] show an altitude increase in the frequency of showers which is considerably less rapid than the observed altitude increase in the rate of ion chamber bursts.

In photographic emulsions exposed at atmospheric depths of 10 and 16 g/cm² at $\lambda=55°$, Bradt and Peters[21] have measured the collision mean free paths of heavy nuclei as a function of atomic number Z, and have calculated that the primary intensity of nuclei of $Z\geq 6$ is 1.4×10^{-3}/cm²/sec/sterad. The computation takes into account the absorption by nuclear collisions, but neglects a small fraction of the primary flux which is stopped as a consequence of ionization loss before reaching the depth at which the plates were exposed. On the basis of the above primary intensity value, and the Z-spectrum obtained by the same authors, the ionization chamber used in the present experiments should record 30 heavy nucleus counts per minute at the top of the atmosphere. In arriving at this result, isotropic incidence was assumed, and full account was taken of the rather complicated geometry of the chamber.

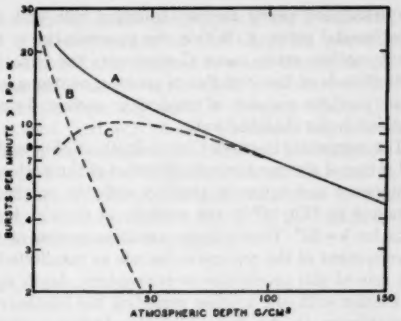

FIG. 7. Resolution of observed burst-rate, A, into the contributions by heavy primaries, B, and nuclear disintegrations, C.

If the emulsion observations[21] of the spectrum and the collision mean free paths of heavy nuclei are combined with a computation of the sensitivity of the ion chamber as a function of Z, the average collision mean free path in air for nuclei recorded by the chamber can be estimated as 30 g/cm². On the basis of this value for the absorption mean free path of the heavy primaries, and on the assumption of isotropic incidence above the atmosphere, the approximate heavy nucleus counting rate *vs* atmospheric depth curve labeled B in Fig. 7 is deduced. Inasmuch as the same absorption mean free paths used by Bradt and Peters in calculating the primary flux from observations at about 15 g/cm² were used in obtaining curve B, the counting rate given by the latter at 15 g/cm² is probably quite accurate. At atmospheric depths exceeding 15 g/cm² the computed curve may be somewhat high because of the neglect of ionization loss. However, this effect is partially compensated by the assumption of an absorption mean free path equal to the collision mean free path, although actually some of the heavy nuclei are not completely broken up into fragments too small to be counted by the ionization chamber in their first collision.

Curve C in Fig. 7 represents the difference between

[17] R. Mather and E. Segrè, Phys. Rev. **84**, 191 (1951).
[18] J. A. Van Allen and S. F. Singer, Phys. Rev. **78**, 818 (1950).
[19] C. G. Montgomery and D. D. Montgomery, Phys. Rev. **76**, 1482 (1949).
[20] H. L. Kraybill and P. J. Ovrebo, Phys. Rev. **72**, 351 (1947).
[21] H. L. Bradt and B. Peters, Phys. Rev. **77**, 54 (1949).

the calculated heavy nucleus counting rate and the experimental curve A. Within the uncertainties in the heavy nucleus rates, curve C represents the variation with altitude of the total flux of protons, neutrons, and other particles capable of producing nuclear disintegrations in the chamber walls.

The maximum in curve C at a depth of 35 g/cm² is indicative of the cascade multiplication of the nucleonic component and agrees in position with the maximum obtained by Whyte[22] in the analysis of Coor's[23] burst data for $\lambda=52°$. Photographic emulsion studies of the development of the nucleonic cascade as manifested in the rate of star production *vs* atmospheric depth seem to conflict with one another regarding the existence of a maximum in the flux of star-producing particles. Freier *et al.*[24] report evidence of strong maxima below 45 g/cm² in the production rates of stars of all sizes up to and including those with more than 10 prongs. On the other hand, Lord[25] finds that the frequencies of stars of all sizes from 3 to more than 16 prongs decrease monotonically at atmospheric depths greater than 15 g/cm². The present results are qualitatively in accord with the former, whereas there appears to be a definite inconsistency with the latter which is not as yet understood.

The absorption mean free path of the burst-producing radiation as determined by the best exponential representation of the counting rate *vs* altitude curve between 60 and 200 mm of Hg is $L=165$ g/cm². This is in reasonable agreement with the value $L=160$ g/cm² derived from Coor's ionization chamber data in the same altitude range. In a similar manner, the star production *vs* altitude curves of Lord between 60 and 200 mm of Hg yield absorption mean free paths $L=165$, 120 and 110 g/cm² for the radiations producing stars with 3, 4, 5 prongs, 6, 7, 8, 9 prongs and more than 9 prongs, respectively. It seems reasonable to expect that the L value obtained from the ionization chamber results should lie somewhere within the above limits. However an exact comparison between ion chamber and emulsion data is precluded by inadequate knowledge of (1) the relative cross sections in Cu and emulsion for the production of stars of given size and (2) the burst-producing efficiency of stars as a function of size for the particular ion chamber geometry involved.

According to the emulsion work of Camerini, *et al.*[26] the integral cross section for production by neutrons and protons of stars with more than 2 prongs closely approximates the geometrical nuclear cross section. Assuming this to hold for primary cosmic rays incident upon copper, and using the value 0.17 particle/cm²/sec/sterad as the primary intensity[3] at $\lambda=52°$, we find that stars with more than 2 prongs should occur in the ion chamber walls at the rate of 240 per minute at the top of the atmosphere. Comparison of this rate with any reasonable extrapolation of curve C, Fig. 7, to zero g/cm² shows that at most 3 percent of the stars produced in the wall by primaries give rise to bursts >1.0 Po-α. Some knowledge of the extent to which this surprisingly small efficiency can be attributed to the absorption of low energy star fragments before their entry into the gas could be obtained by employing chambers with various wall thicknesses in future flights.

According to the curves B and C in Fig. 7, the heavy nuclei and nuclear disintegrations contribute 13 counts per minute and 8 counts per minute, respectively, at a depth of 10 g/cm² at geomagnetic latitude 52°N. The latitude effect between 52°N and 69°N at 10 g/cm² is 0 ± 5 percent. Considering the extreme case of a possible 5 percent increase (1.0 std. dev.) assignable solely to heavy nuclei, the increase in the latter at 10 g/cm² would be 8 percent. On the other hand, if the heavy nucleus flux were assumed to be unchanged, the corresponding increase in the nuclear disintegration rate would be 13 percent.

Extrapolation of the curves of Figs. 3 and 4 to the top of the atmosphere yields a lower limit of 45 percent for the increase in the vertical primary intensity between $\lambda=52°$ and $\lambda=69°$. Comparison of this result with the aforementioned 0 ± 13 percent latitude effect shows that primaries of energy below the geomagnetic cutoff at $\lambda=52°$ yield at a depth of 10 g/cm² less than one-third as many nuclear bursts per primary particle as the primaries entering at $\lambda=52°$.

It should be noted that the nuclear disintegration latitude effect deduced from the present measurements at 10 g/cm² does not necessarily apply at higher altitudes, for a considerable portion of the nuclear bursts at 10 g/cm² is produced by secondaries. (Note the shape of curve C, Fig. 7.) In addition, the primaries undergo some energy loss by ionization and nuclear collisions in the residual atmosphere. The magnitudes of these effects are undoubtedly quite different for the primary protons of energy $E>1.6$ Bev entering at $\lambda=52°$ and for those of energy $E<1.6$ Bev which comprise the additional proton intensity at $\lambda=69°$.

If the multiplicity of secondary nucleon production increases with the energy of the primary, and the probability of burst production in the chamber wall increases with the energy of the incident particles, a latitude effect should become apparent above 10 g/cm². In this case the low energy primaries at $\lambda=69°$ as they exist above the atmosphere could have a considerably higher burst-producing efficiency relative to the primaries at $\lambda=52°$ than the data at 10 g/cm² indicate.

It is not possible to deduce from the present measurements any quantitative information regarding the low energy portion of the heavy primary spectrum because a substantial fraction of the particles of atomic number $Z>8$ in the band of energies admitted between $\lambda=52°$

[22] G. N. Whyte, Phys. Rev. **82**, 204 (1951).
[23] T. Coor, Phys. Rev. **82**, 478 (1951).
[24] Freier, Ney, and Oppenheimer, Phys. Rev. **75**, 1451 (1949).
[25] J. J. Lord, Phys. Rev. **81**, 901 (1951).
[26] Camerini, Fowler, Lock, and Muirhead, Phil. Mag. **41**, 413 (1950).

and $\lambda = 69°$ (where the vertical cut-off energies are 0.57 Bev per nucleon and 0.025 Bev per nucleon, respectively) are absorbed as a result of energy loss by ionization in the 10 g/cm² residual atmosphere above the apparatus.

V. ACKNOWLEDGMENTS

The continued support of the National Geographic Society, sponsor of the Expeditions to Hudson Bay, and the constant encouragement of Dr. Lyman J. Briggs, Chairman of the Committee on Research, are gratefully acknowledged. Appreciation is expressed for the kind cooperation of the Canadian government, particularly to the Defence Research Board for making its facilities at Fort Churchill available; individual thanks are especially due Dr. Kenneth Fisher, Superintendent, and Mr. A. V. Hannam, Administrative Officer of Defence Research Northern Laboratories; and Mr. G. W. Rowley of D. R. B. Arctic Division. E. R. Swoffer provided valuable technical assistance. Finally, the authors are grateful to Dr. W. F. G. Swann for his constant interest in this work.

PHYSICAL REVIEW VOLUME 86, NUMBER 4 MAY 15, 1952

The Emission of L X-Rays of Lead in Po^{210} Decay*

WILLIAM RUBINSON† AND WILLIAM BERNSTEIN‡
Brookhaven National Laboratory, Upton, New York
(Received January 7, 1952)

By use of a proportional counter x-ray spectrometer, it is established that Po^{210} sources emit characteristic L photons of Pb, in yield $2.93\times10^{-4}(\pm15$ percent) per alpha-particle. The excitation of these photons is ascribed to the ejection of L electrons from the electronic cortege of the nucleus in the act of alpha-decay, in a manner treated by Migdal's theory. The probability of L electron ejection is about 8.8×10^{-4} per alpha-particle, as computed from the observed photon yield and Kinsey's fluorescence yields. The theory in its present state accounts for only 13 percent of the photons observed.

I. INTRODUCTION

THE emission of low energy photons of low intensity from Po^{210} sources was observed and studied experimentally by Curie and Joliot[1] and has been noticed by others.[2,3] Curie and Joliot detected the photons by means of an ionization chamber connected to an electroscope, and identified photon energies by absorption coefficients. They found, within the limitations of this technique, that the photon energies were those expected for the L and M x-radiations of Po. Further, they thought that the intensities of the radiations increased with the thickness of the Po^{210} source (they used sources of roughly constant area and of strengths up to about 50 mC), and hence, were inclined to believe that the radiations were Po x-rays excited by alpha-particle bombardment of the undecayed Po atoms in the source.

We study these radiations by means of a proportional counter x-ray spectrometer, and establish that the L x-rays, at least, are the characteristic L radiations of Pb. We ascribe their production to the ejection of L electrons from the electronic cortege of the nucleus in the act of alpha-decay, a process which has been the subject of a theoretical study by Migdal.[4]

II. THE APPARATUS

The proportional counter x-ray spectrometer is an improved version of the one which has been described elsewhere.[5] The counter tube is a cylinder of brass, or brass with an inner cylindrical liner of aluminum (to eliminate fluorescence radiations from the brass wall), about four inches in diameter and twelve inches long, with an axial center-wire of stainless steel 0.004 inch in diameter. The window is a hole, one inch in diameter, drilled through a flat surface built up at the center of the cylindrical counter wall, and covered with a beryllium disk 0.005 inch thick. The counter gas is a 9:1 mixture of noble gas (A or Kr) and methane or ethane, at a total pressure of one atmosphere. With the argon-methane filling, pulses of convenient height are obtained with the center wire at about +2600 volts. The counter wall is grounded.

The stability requirements on the high voltage supply are quite stringent; if one demands that the pulse height be stable to better than 0.5 percent during the course of a run, the high voltage supply must be stable to

* Research carried out under the auspices of the AEC.
† Chemistry Department.
‡ Electronics and Instrumentation Division.
[1] I. Curie and F. Joliot, J. phys. et radium **VII**, 20 (1931).
[2] S. DeBenedetti and E. H. Kerner, Phys. Rev. **71**, 122 (1947).
[3] Zajac, Broda, and Feather, Proc. Phys. Soc. (London) **60**, 501 (1948).
[4] A. Migdal, J. Phys. (U.S.S.R.) **IV**, 449 (1941). This paper also contains the theory of the corresponding process for beta-decay. The theory of ejection of K electrons in beta-decay has been worked out very elaborately by E. L. Feinberg, J. Phys. (U.S.S.R.) **IV**, 424 (1941).
[5] Bernstein, Brewer, and Rubinson, Nucleonics **6**, 39 (1950).

better than 0.01 percent. It must also be completely free of noise or ripple. Our present supply, designed by Higinbotham,[6] meets these requirements admirably.

The preamplifier and the non-overloading linear amplifier are described in reference 5. The essential feature of the amplifier is that it registers pulses of a given height in the presence of pulses several thousand times higher without distortion of the pulses of interest, displacement of the base line, or the introduction of spurious pulses. This permits the study of the K, L, and M radiations from Po^{210} sources without interference from each other or from the 0.77-Mev gamma emitted in a small fraction of the Po^{210} decays. The maximum output of the amplifier is 60 volts.

The amplifier output goes to a single sliding-channel pulse-height analyzer of Oak Ridge design.[7] The channel width, which we ordinarily set at 1.7 volts, shows excellent stability and independence of channel position. The analyzer output is fed to a commercial scale of 64.

Provision is also made for automatic operation, which is very convenient for exploratory experiments. A motor moves the channel at constant speed across the pulse-height range of interest, and the analyzer output is fed to a counting-rate meter,[8] whose output, in turn, is fed to a 0–25 mv Brown recorder. The chart drive of the Brown recorder is synchronized with the channel drive so that the chart scale reads directly in volts.

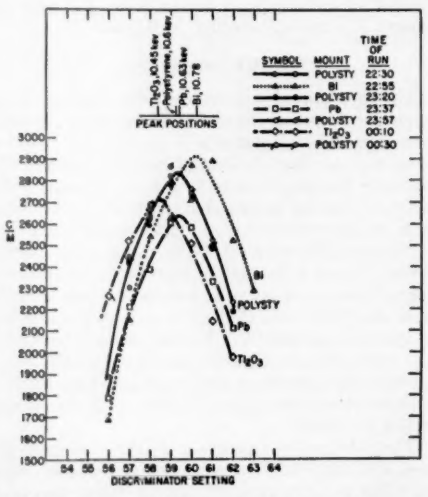

FIG. 1. Comparison of the 10.6-kev radiations from Po^{210} mounted on polystyrene, Bi, Pb, and Tl_2O_3.

The line voltage to the amplifier and the analyzer is stabilized by means of a Sorenson voltage regulator.

As an example of what the instrument can do at its best, we have obtained a curve of the 10.6-kev arsenic K line (from Se^{75} K capture) with a width at half-height of 12.5 percent, and drifts have been negligible over a period of six hours.

III. THE Po^{210} SOURCES

The Po^{210} sources were prepared from a stock solution that consisted of Oak Ridge Po^{210} made up to 10 ml with 0.5 N HNO_3. The stock solution was assayed with an accuracy of ± 3 percent by the method of dilution and alpha-counting. Its specific activity was about 10 mC/ml.

To prepare a source, an aliquot of the stock solution was placed in a depression 1 mm deep and 15 mm in diameter in a polystyrene disk, evaporated under a heat lamp, and covered with Cellophane 2.7 mg/cm² thick. Polystyrene was chosen as a source backing because of the softness of the radiations excited in it by the alpha-particles. The strengths of the different sources were between 0.5 and 4 mC, as computed from the assay of stock solution. The sources prepared from small aliquots showed practically no visible deposit. With large aliquots, there was some chemical reaction between the polystyrene and the nitric acid of the solvent.

The stock solution was not tested for radiochemical purity beyond insuring that the half-life was correct. That the x-radiations we study are associated in some way with Po^{210} decay is adequately established by the fact that their intensity decreases in time with the Po^{210} half-life.

IV. PROOF THAT THE OBSERVED PHOTONS ARE CHARACTERISTIC L X-RAYS OF Pb

A critical absorption experiment (experiment 4, below) establishes that the radiations we study are characteristic L x-rays of Pb. We describe a few other experiments for their value as confirmatory evidence, and as illustrations of technique that may be useful to others.

Experiment 1

The observed pulse height (and, therefore, energy) of the most prominent x-ray line from a Po^{210} source is experimentally identical with that of the 10.56-kev arsenic K line from a Se^{75} (K capture) source. The listed L_α line of Pb has energy 10.57 kev.[9] This establishes that the radiations from Po^{210} have approximately the correct energy to be L x-rays of Pb.

Experiment 2

The intensity of the radiations from a Po^{210} source containing 1 mg of added Bi was only slightly greater

[6] W. A. Higinbotham, Rev. Sci. Instr. **22**, 429 (1951).
[7] Francis, Bell, and Gundlach, Rev. Sci. Instr. **22**, 133 (1951).
[8] W. C. Elmore and M. Sands, *Electronics, Experimental Techniques* (McGraw-Hill Book Company, Inc., New York, 1949), National Nuclear Energy Series, Plutonium Project Record, Vol. 1, Div. IV, p. 254.
[9] A. H. Compton and S. K. Allison, *X-Rays in Theory and Experiment* (D. Van Nostrand Company, Inc., New York, 1935), p. 787. We use the factor 12.393 to convert from angstroms to kev.

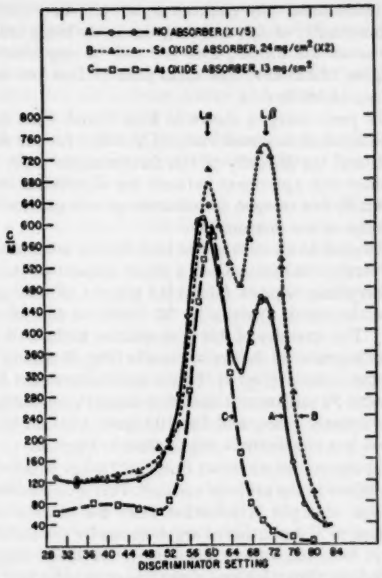

FIG. 2. L-radiations from Po^{210}; absorption in Se and As.

than that from a source of identical strength containing no added Bi, although the former source contained 40,000 times as much Bi as Po. Therefore, the observed radiations cannot be Po L lines excited by alpha-particle bombardment of Po atoms in the source.

Experiment 3

Four identical aliquots, ~1 mC each, of the Po^{210} stock solution were evaporated on thick plates of polystyrene, Pb, Bi, and Tl_2O_3, respectively. Alpha-particle bombardment of the plate material excites its characteristic x-rays, which we observe superimposed on the radiations from Po^{210}. (This is not inconsistent with experiment 2; in the present case, a much greater number of heavy element atoms is available for excitation by alpha-particles.) The observed intensities from the four sources were adjusted to approximate equality by means of beryllium absorbers, and then the different ~10.6-kev peaks were run in rapid succession, each run with a source on Pb, Bi, or Tl_2O_3 being sandwiched between two runs with the source on polystyrene. The results are shown in Fig. 1. The four runs with the source on polystyrene are essentially identical, showing that the instrument did not drift during the two hours required to take the data. It is clearly seen in Fig. 1 that the source on polystyrene gives a peak position experimentally identical with that of the source on Pb, and different from the peak positions given by the sources on Tl_2O_3 and Bi. Therefore, the ~10.6-kev radiation from Po^{210} is the characteristic $L\alpha$ x-radiation of Pb.

Experiment 4

There is no critical absorber that distinguishes between the $L\alpha$ lines of Pb and Bi, but Se, which has its K edge at 12.675 kev, can distinguish between the $L\beta$ lines: Pb $L\beta_1 = 12.635$ kev, $L\beta_2 = 12.635$ kev; Bi $L\beta_1 = 13.045$ kev, $L\beta_2 = 13.001$ kev. Curves A and B in Fig. 2 show the radiations from a Po^{210} source before and after passage through 24 mg/cm² of selenium oxide absorber. The $L\beta$ energy is obviously less than the energy of the Se K edge. (The clean effect that would have been obtained had Se absorbed $L\beta$ critically can be seen in curve C, Fig. 2, where the absorber was 13 mg/cm² of As_2O_3. The arsenic K edge is at 11.886 kev.) Therefore the $L\beta$ line cannot be that of an element higher in atomic number than Pb. The source certainly contained no quantities of elements below Pb that could give rise to the observed intensity of radiation. Therefore the radiations are Pb radiations.

V. THE MEASUREMENT OF THE L PHOTON YIELD

The L photon yield, i.e., the probability of L photon emission per alpha-particle emitted, was determined as the ratio of the rates of photon and alpha emission. The measurement of the rate of alpha emission from the source is discussed in Sec. III above. The rate of photon emission was obtained from the observed photon

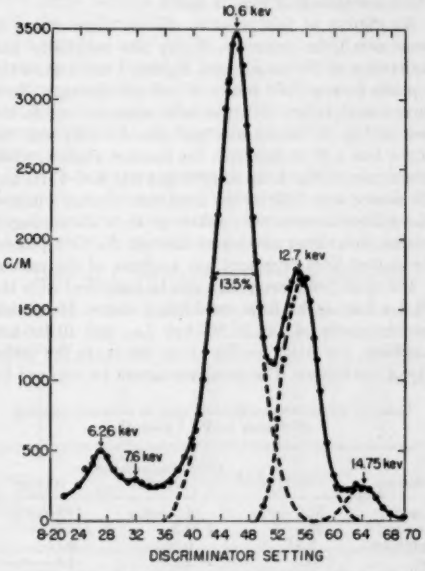

FIG. 3. Pb L-lines from Po^{210}. Counter gas: 650 mm A+70 mm CH_4.

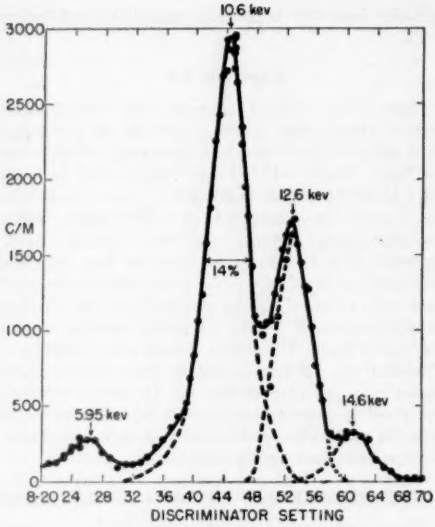

FIG. 4. Pb L-lines from Po^{210}. Counter gas: 670 mm Kr+70 mm C_3H_8.

counting rate and a computed counting efficiency. The photon counting rate was obtained by graphical integration of the experimental curves, two examples of which are shown as Figs. 3 and 4.

We digress at this point to discuss these curves in some detail, in order to display the reliability and limitations of the instrument. Figures 3 and 4 show the L peaks from a Po^{210} source of ~3 mC strength. Both curves were taken with the same counter, but in the case of Fig. 3 the counter gas was A+CH_4 and the source was 1.69 inches from the counter window, while in the case of Fig. 4 the counter gas was Kr+C_3H_8 and the source was 2.19 inches from the counter window. One-minute counts were taken at each discriminator setting. Solid lines are drawn through the data points; the dotted lines represent our analyses of the curves.

The most prominent peak can be identified with the Pb $L\alpha$ line, as we have established above. It consists predominantly of the 10.569-kev $L\alpha_1$ and 10.466-kev $L\alpha_2$ lines, the latter having about one-tenth the intensity of the former. The two lines cannot be resolved by the instrument. The peak at about 12.6 kev consists predominantly of $L\beta_1$ and $L\beta_2$, the latter being half as intense as the former, and the two having identical energies, 12.635 kev. The small peak at 14.6 kev must be $L\gamma_1$, 14.789 kev.

TABLE I. Absorption coefficients used to compute counting efficiencies for Pb L photons.

Substance	Absorption coefficients 10.57 kev	12.64 kev	14.79 kev
Argon	52.0 cm²/g	31.5 cm²/g	19.8 cm²/g
Krypton	47.0	29.2	138.0
Beryllium	0.83	0.56	0.37
Air	4.2	2.5	1.5
Cellophane	0.0134(=μl)	0.008(=μl)	0.006(=μl)

The peak energies shown in Figs. 3 and 4 are computed from an assumed value of 10.6 kev for the main peak, and the linearity of the discriminator scale. We consider such agreement between the observed and the known Pb line energies as indication of very satisfactory behavior of the instrument.

The peak at about 6 kev in both figures is 6.4-kev Fe fluorescence radiation from a small amount of iron in the beryllium window (about 0.5 percent, according to a spectrographic analysis by M. Slavin of this laboratory). The intensity of this peak relative to the 10.6-kev peaks is greater in the argon counter (Fig. 3) than in the krypton counter (Fig. 4). This is ascribable to the facts that the Fe radiation is absorbed almost completely in both counter gases, and the 10.6-kev radiation is absorbed less efficiently in argon than in krypton.

The argon counter shows a peak at 7.6 kev which does not appear in the krypton counter. This is ascribable to the loss of argon K radiation from the counter subsequent to K ionization of argon atoms by the 10.6-kev x-rays from the source. Since the K ionization edge of argon is at about 3.2 kev, a peak is expected to appear at about 7.4 kev, and to be of low intensity because of the low K fluorescence yield in argon.

In analyzing the experimental curves into their components, the peak shapes were modeled after the shape of the clean arsenic K peak from a Se^{75} (K capture) source. There is, however, considerable arbitrariness in the drawing of the wings, which may lead to an error of several percent in the intensity.

With the original curves drawn to a fairly large scale, the areas under each of the peaks were measured (in units of "counts/min×discriminator unit") by planimeter or by counting squares, and divided by the channel width (calibrated in discriminator units) to give the "observed intensities" (counts/min) listed in Table II.

To calculate the counting efficiency ϵ, suppose that the source is a point source at the origin of a coordinate system. Let the counter axis be parallel to the y axis, with the window centered on, and perpendicular to, the z axis. Let θ be the angle between a photon path and the z axis, and let ϕ be the angle between the x axis and the plane of the z axis and the photon path. Then

$$\epsilon=\frac{1}{4\pi}\int_0^{2\pi}d\phi\int_0^{\theta_{\max}}\sin\theta e^{-\sec\theta\sum\mu_i t_i}(1-e^{-\mu_2\sec\theta(z-h)})d\theta,$$

with

$$z=\{p+[p^2-(p^2-a^2)(\tan^2\theta\cos^2\phi+1)]^{\frac{1}{2}}\}/(\tan^2\theta\cos^2\phi+1),$$

where a is the counter radius, h is the distance from the

source to the window, p is the distance from the source to the counter axis, μ_g is the absorption coefficient of the counter gas, μt denotes absorption coefficient times thickness, and $\Sigma\mu t$ is the sum of the μt's of the beryllium window, the air between source and window, and the cellophane cover of the source.

The various absorption coefficients were obtained by graphical interpolation of tabulated data,[10,11] and are listed in Table I.

The integral was evaluated by numerical integration. For a point source 2.19 inches from the counter window, the counting efficiencies computed in this fairly elaborate fashion differ by only a few percent from those computed by simply taking an average photon path length equal to the geometric mean of the minimum and maximum path lengths in the counter.

The assumption of a point source (our sources were ~15 mm in diameter) introduces a negligible error in the geometry,[12] but it may underestimate the counting efficiency by a few percent because it underestimates the average path length in the counter.

Table II is a synopsis of our data on six curves obtained with the use of two different counters, two different counting gases, three different distances between source and window, and three different Po^{210} sources of independently determined source strength.

Table III lists the photon yields computed from the data in Table II. Note that the results obtained with different sources under different counting conditions agree almost as well as do the two results, curves 5 and 6, obtained with the same source under identical counting conditions.

The total L photon yield,[13] 2.93×10^{-4}, is probably reliable to better than ±15 percent. Most of the sources of systematic error that can be imagined would tend to make this yield an underestimate. The L photon yield found by Curie and Joliot was 4×10^{-4}, about 35 percent greater than our result.

It is interesting to compare the relative intensities of the Pb L lines from Po^{210} with those obtained from targets in x-ray tubes. We find for Po^{210}

$$L\alpha:L\beta:L\gamma=1:0.635:0.12.$$

The corresponding ratios for heavy element targets in x-ray tubes are

$$L\alpha:L\beta:L\gamma=1:0.786:0.09,$$

as computed from Jönsson's[14] values for Pt by assuming that the sum of the l, α_1, and α_2 intensities correspond to our 10.6-kev peak, the sum of the η, β_1, β_2, β_3, β_4, and β_6 intensities to our 12.6-kev peak, and the γ_1 intensity to our 14.6-kev peak.

TABLE II. Data for computing L photon yields in Po^{210} decay.

Experiment	Line	Observed intensity (counts/min)	Counting efficiency	Po^{210} source strength (disintegs/min)
1. June 12, 1950	$L\alpha$	2970	0.0140	1.24×10^{3}
A+CH_4 counter	$L\beta$	1437	0.00978	
1.41 in. from window	$L\gamma$	140	0.00670	
2. April 13, 1951	$L\alpha$	13,912	0.00972	7.95×10^{3}
A+CH_4 counter	$L\beta$	5957	0.00688	
1.69 in. from window	$L\gamma$	810	0.00463	
3. April 20, 1951	$L\alpha$	11,586	0.0088	7.68×10^{3}
Kr+C_3H_8 counter	$L\beta$	5312	0.0068	
2.19 in. from window	$L\gamma$	1215	0.0120	
4. May 4, 1951	$L\alpha$	7283	0.0059	7.56×10^{3}
A+CH_4 counter	$L\beta$	3106	0.00414	
2.19 in. from window	$L\gamma$	461	0.00284	
5. May 8, 1951	$L\alpha$	5110	0.00458	7.48×10^{3}
A+CH_4 counter	$L\beta$	2742	0.00348	
0.3071 g/cm² Be	$L\gamma$	443	0.00253	
2.19 in. from window				
6. May 10, 1951	$L\alpha$	5615	0.00458	7.40×10^{3}
A+CH_4 counter	$L\beta$	2664	0.00348	
0.3071 g/cm² Be	$L\gamma$	421	0.00253	
2.19 in. from window				

VI. THE ORIGIN OF THE Pb L PHOTONS

The Pb L photons are in some way associated with Po^{210} decay because their intensity decreases in time with the Po^{210} half-life. They cannot be attributed to alpha-bombardment of Pb impurity in the source, as shown by Experiment 2, Sec. III, and by the fact that sources prepared from both fresh and aged stock solution gave the same photon yield although the aged source contained forty times the impurities of the fresh source.

The Pb L photons cannot be attributed to L conversion of the well-known 0.77-Mev gamma-ray of Po^{210}, whose intensity has recently been measured[15] to be $1.8\pm0.14\times10^{-5}$ per alpha, because even complete L

TABLE III. L photon yields in Po^{210} decay (computed from the data in Table II).

Experiment	Photon yield $L\alpha$	$L\beta$	$L\gamma$	Total
1	1.71×10^{-4}	1.18×10^{-4}	0.17×10^{-4}	3.06×10^{-4}
2	1.80	1.09	0.22	3.11
3	1.71	1.02	0.13	2.86
4	1.63	0.99	0.21	2.83
5	1.49	1.05	0.23	2.77
6	1.66	1.04	0.23	2.92
Mean	1.67×10^{-4}	1.06×10^{-4}	0.20×10^{-4}	2.93×10^{-4}
% spread	18.5	17.0	50	11.4
% standard deviation	6.9	6.3	20	4.6

[10] A. H. Compton and S. K. Allison, reference 9, Chapter VII and Appendix IX.

[11] C. S. Barret, *Structure of Metals* (McGraw-Hill Book Company, Inc., New York, 1943), Appendix III.

[12] See Blachman's equation for the geometry of an extended source in the Appendix to a paper by B. P. Burtt, Nucleonics 5, 28 (1949).

[13] In Phys. Rev. 82, 334 (1951) and Brookhaven National Laboratory Quarterly Progress Report, Oct. 1–Dec. 31, 1950, p. 98, we reported a total L photon yield of 7.2×10^{-4}, which is incorrect because of an arithmetic error. We reported the correct result at the September 1951 New York Meeting of the XIIth International Congress of Pure and Applied Chemistry.

[14] See reference 9, p. 645.

[15] Grace, Allen, West, and Halban, Proc. Phys. Soc. (London), 64, 493 (1951).

conversion of this gamma could account for only a few percent of the L photon intensity we observe.[16]

It is highly unlikely that some hitherto unobserved gamma is being completely converted in the L shell, and this mode of excitation of Pb L lines becomes even less likely in view of the fact that we have also observed what are presumably Pb K photons with considerably smaller intensity, and Pb M photons with considerably greater intensity,[17] than the L photon intensity, in qualitative agreement with Migdal's theory.

We conclude that the Pb L radiations are excited by ejection of L electrons from the electronic cortege of the nucleus in the act of alpha-decay in a manner described by Migdal's theory.[4]

VII. THE THEORETICAL L PHOTON YIELD

Migdal[4] deduces the probability of ejection of an extra-nuclear electron in the alpha-decay process by a perturbation calculation in which the potential change due to the change of nuclear charge, and the potential due to the moving alpha-particle, are treated as small perturbations on the nuclear potential. The probability of transition of an electron from a given initial state to an allowed continuum state is derived, and integration is then made over the continuum states. The approximations of the theory are:

(1) $\Delta Z^*/Z^* \ll 1$, where Z^* is the effective nuclear charge of the daughter nucleus. In the present case, $\Delta Z^*/Z^* = 0.025$.

(2) $v_\alpha/v_e \ll 1$, where v_α is the speed of the alpha-particle, and v_e is the speed of the electron in the bound state. For Po^{210} alphas and Pb L electrons, this ratio is ~ 0.2.

(3) The use of nonrelativistic hydrogenic wave functions. The hydrogenic wave function approximation is reasonably good for Pb L electrons. As concerns the nonrelativistic approximation, the speed of the electron in the bound state is about $0.3c$, and is about the same in the continuum state, according to Migdal's theory. At these speeds, relativity effects should not be prominent.[18]

With these approximations, the probability W_{nl} for ejection of an nl electron is

$$W_{nl} = (v_\alpha/v_e)^2 (C_{nl}/Z^{*2}), \tag{1}$$

where, for the L shell, the sum of the two C_{2l}'s is equal to 7.2, and the sum of the six C_{21}'s is equal to 13.3.

In applying this equation to the ejection of L electrons in Po^{210} decay, we have $v_\alpha = 1.6\times 10^9$ cm/sec (the speed of a 5.3-Mev alpha-particle), and v_e, the speed of an electron in the second hydrogenic orbit about a nucleus of effective charge Z^*, is $\frac{1}{2}Z^*$ times the average electron speed in the first hydrogen orbit, or $v_e = 1.09 \times 10^8 Z^*$ cm/sec. With these numbers, and changing the notation so that W_i (i=I, II, III) denotes the probability of electron ejection from the L_i shell, Eq. (1) becomes

$$W_i = 215 C_i/Z^{*4}, \quad (C_{\rm I} = 7.2;\ C_{\rm II,III} = 13.3). \tag{2}$$

The choice of Z^* in this equation offers some trouble. Imagine the L shells to lie entirely between the K and the M, N, $\cdots$ shells. Then the L shell eigenfunctions are relatively unaffected by the presence of the outer shells, so that the correct Z^* is the nuclear Z decreased by only the inner screening constant. But the presence of electrons in the outer shells has some effect on the amplitude of the continuum state eigenfunctions at the position of the L shell, and, therefore, on the magnitude of the transition probability. And, in fact, the magnitude of the transition probability may be quite sensitive to the existence of external screening, because the overlap of the bound state and continuum state eigenfunctions is small (as shown by our measured photon yields), so that a small absolute change in the amplitude of the continuum state eigenfunctions may result in a large relative change in the overlap. There is further discussion of this point below.

However, a literal interpretation of Migdal's theory seems to require that only the inner screening be used. We can expect this to result in an electron ejection probability that is too low.

Using the semi-empirical inner screening constants deduced by Sommerfeld and Wentzel,[19] we get $Z^* = 80$ for the Pb $L_{\rm I}$ shell, and $Z^* = 78.5$ for the $L_{\rm II,III}$ shell. With these Z^*'s, Eq. (2) gives the following theoretical electron ejection probabilities:

$$\begin{aligned} W_{\rm I}(L_{\rm I}\ \text{shell}) &: 0.38\times 10^{-4} \\ W_{\rm II,III}(L_{\rm II,III}\ \text{shell}) &: 0.75\times 10^{-4} \\ \text{Total} &: 1.13\times 10^{-4}. \end{aligned} \tag{3}$$

These numbers must be multiplied by the appropriate fluorescence yields in order to get the theoretical photon yields for comparison with our experiments. With the L fluorescence yields deduced by Kinsey,[20] who has

[16] D. E. Alburger and G. Friedlander, Phys. Rev. **81**, 523 (1951), report that the 0.77-Mev Po^{210} gamma is about 10 percent K converted and about 2 percent L converted.

[17] Curie and Joliot, reference 1, report an M photon yield of 15×10^{-4}. They were not able to detect the K photons.

[18] In a theoretical study of the Auger effect in Au, where an L electron is ejected with a speed of $\sim 0.5c$, H. S. W. Massey and E. H. S. Burhop, Proc. Roy. Soc. (London) **A153**, 661 (1936), find that a relativistic calculation gives a result twice as large as that of the nonrelativistic calculation, and in good agreement with experiment. In a similar calculation for Ag, where the electron is ejected with speed $\sim 0.27c$, the difference between the relativistic and nonrelativistic calculations is much less.

[19] See H. E. White, *Introduction to Atomic Spectra* (McGraw-Hill Book Company, Inc., New York, 1934), p. 318.

[20] B. B. Kinsey, Can. J. Research **26A**, 404 (1948). In his analysis, Kinsey takes account of the "Coster-Kronig transitions," which are radiationless transitions whereby a hole in the $L_{\rm I}$ shell is filled by an electron from $L_{\rm II}$ or $L_{\rm III}$ with simultaneous emission of an electron from an M or higher shell. This effect, which accounts for the very low intensity of $L_{\rm I}$ lines and the high intensity of $L_{\rm II}$ and $L_{\rm III}$ satellite lines in Pb and its neighboring elements, was first recognized by D. Coster and R. Kronig, Physica **2**, 13 (1935). See the review article by F. R. Hirsch, Jr., Revs. Modern Phys. **14**, 45 (1942).

made a careful analysis of the available empirical and theoretical information on the fluorescence yields of heavy elements, the theoretical photon yields, q_i, are

$$\begin{aligned} q_{\mathrm{I}} &= 0.095 W_{\mathrm{I}} = 0.036 \times 10^{-4} \\ q_{\mathrm{II}} &= 0.495 W_{\mathrm{II}} = 0.124 \times 10^{-4} \\ q_{\mathrm{III}} &= 0.285 (W_{\mathrm{III}} + 0.685 W_{\mathrm{I}}) = 0.217 \times 10^{-4} \\ \text{Total} &= 0.377 \times 10^{-4}. \end{aligned} \tag{4}$$

In this computation, we have assigned one-third of $W_{\mathrm{II,III}}$ to the L_{II} shell and the other two-thirds to the L_{III} shell.

This theoretical total photon yield is about 13 percent of the experimental value, 2.93×10^{-4}, which we believe to be reliable to 15 percent.

Two sources of this large discrepancy suggest themselves—the use of nonrelativistic eigenfunctions, and the neglect of the influence of the outer screening on the shape of the continuum eigenfunctions at the position of the L shell.

The effect of relativistic eigenfunctions has been discussed above, where we concluded tentatively that these would not make any large change in the theoretical result.

The major portion of the discrepancy is probably ascribable to neglect of the outer screening. In a theoretical study of the K ionization of heavy atoms by collision with relatively slow electrons, Soden[21] found that the continuum eigenfunctions deep within a Fermi-Thomas potential were considerably contracted toward the nucleus, as compared with the corresponding eigenfunctions in the absence of external screening. Such an inward contraction of the continuum eigenfunctions would increase the theoretical transition probabilities, but whether it would do so sufficiently to give satisfactory agreement with our measurements cannot be seen without an accurate calculation.

VIII. THE PROBABILITY OF L ELECTRON EJECTION IN Po^{210} DECAY

From our data on the L photon yield, we can compute the probability of L electron ejection if we can assume that Migdal's theory gives the correct ratios for the ejection of electrons from the different L shells. For, from Eqs. (3) and (4), the average L fluorescence yield is $\frac{1}{3}$. Then, since the observed total L photon yield is 2.93×10^{-4}, the total L electron yield is 8.8×10^{-4}, and the electron yields from the different L shells are

$$L_{\mathrm{I}}: 3.0 \times 10^{-4}; \quad L_{\mathrm{II}}: 1.9 \times 10^{-4}; \quad L_{\mathrm{III}}: 3.9 \times 10^{-4}.$$

Thus, the ejection probability per electron in L_{I} is 1.5 the corresponding probability of ejection from L_{II} or L_{III}.

IX. CONCLUDING REMARKS

In the course of these experiments, we have observed that Po^{210} sources also emit what are presumably K and M radiations of Pb, but we have not as yet established their identities or measured their intensities. Using a scintillation counter, we were not able to find a radiation reported to be at 105 kev with an intensity about 25 percent that of the K radiation,[9] although we would have been able to detect one-fifth the reported intensity.

In their investigations on the radiations from Po^{210}, Grace *et al.*[18] established by critical absorption experiments that at least part of the ~80-kev radiations from the source are characteristic K lines of Pb, with a yield of $\sim 1.5 \times 10^{-6}$ K photons per alpha-particle. They ascribe these to internal conversion of the 0.77-Mev Po^{210} gamma-ray. This implies a K conversion coefficient of about 7 percent, from which Grace *et al.* drew certain conclusions concerning the multipole nature and parity change of the 0.77-Mev gamma-ray. However, Migdal's theory predicts that a K photon intensity of the order of 10^{-6} per alpha is excited by ejection of K electrons by alpha-particles, so that considerable doubt attaches to their conclusions. The fact that they also observed the internal conversion electrons (which can be easily distinguished from electrons ejected by alphas) in numbers equal to their observed number of K photons cannot be reconciled with our own results on L photons, unless the theory overestimates electron ejections from the K shell as badly as it underestimates those from the L shell.

We wish to thank Dr. R. Sternheimer of this Laboratory for illumination on some points of the theory.

[21] D. G. Soden, Ann. Physik. **19**, 409 (1934).

Electronic Energy Bands in Crystals*

R. H. PARMENTER
Massachusetts Institute of Technology, Cambridge, Massachusetts
(Received February 6, 1952)

A study is made of the feasibility of calculating valence and excited electronic energy bands in crystals by making use of one-electron Bloch wave functions. The elements of the secular determinant for this method consist of Bloch sums of overlap and energy integrals. Although often used in evaluating these sums, the approximation of tight binding, which consists of neglecting integrals between non-neighboring atoms of the crystal, is very poor for metals, semiconductors, and valence crystals. By partially expanding each Bloch wave function in a three-dimensional Fourier series, these slowly convergent sums over ordinary space can be transformed into extremely rapidly convergent sums over momentum space. It can then be shown that, to an excellent approximation, the secular determinant vanishes identically. This peculiar behavior results from the poorness of the atomic correspondence for valence electrons. By a suitable transformation, a new secular determinant can be formed which does not vanish identically and which is suitable for numerical calculations. It is found that this secular determinant is identical with that obtained in the method of orthogonalized plane waves (plane waves made orthogonal to the inner-core Bloch wave functions).

Calculations are made on the lithium crystal in order to test how rapidly the energy converges to its limiting value as the order of the secular determinant is increased. For the valence band, this convergence is rapid. The effective mass of the electron at the bottom of the valence band is found to be closer to that of the free electron than are those of previous calculations on lithium. This is probably because of the use of a crystal potential here rather than an atomic potential. The former varies less rapidly than the latter over most of the unit cell of the crystal, and thus should result in a value of effective mass more nearly free-electron-like. Unlike previous calculations on lithium, the computed value of the width of the filled portion of the valence band agrees excellently with experiment. By making use of calculated transition probabilities between the valence band and the 1s level, a theoretical curve is drawn of the shape of the soft x-ray K emission band of lithium. The comparison with the shape of the experimental curve is only fair.

I. INTRODUCTION

IN this paper we will study the properties of electrons in unbounded, crystalline solids. We will assume that any given electron of the crystal can be considered to move in the electric field resulting from fixed nuclei plus the time-averaged charge distribution of all the other electrons of the crystal. It is well known that such an assumption neglects correlation and exchange between the electrons of the crystal. No attempt will be made to correct for correlation directly, but an approximate method of correcting for exchange will be included (see Appendix A).

Within the framework of the above assumption there are great difficulties involved in solving Schrödinger's equation for an electron in a crystal. A number of approximate methods have been introduced.[1] Here we will be concerned with two such methods, the method of Bloch waves[2,3] and the method of orthogonalized plane waves.[4] In connection with these two methods, it might be appropriate to indicate how the work here reported actually developed. It was originally planned to make a study of the Bloch method. As a test of the method's practicability for numerical calculation, it was planned to calculate electronic energy bands in the lithium crystal. Such a procedure was in fact carried out, but only after mathematical manipulation had been made in the Bloch method for the purposes of convenience in the numerical computations. It was later realized by the writer that the secular equation obtained from the Bloch method by means of this mathematical manipulation was identical with the secular equation which could be obtained from the orthogonalized plane wave method in a more straightforward fashion. For this reason, after having shown that the Bloch method is equivalent to the orthogonalized plane wave method, we will consider only the latter method in obtaining explicit results for the lithium crystal.

II. METHOD OF BLOCH WAVES

Let us consider an unbounded crystalline solid, which can be divided into a set of identical unit cells. We may define an enumerable, infinite set of displacement vectors, $\mathbf{r}_n$, where the nth vector is drawn from an origin of coordinates to the center of the nth unit cell. For convenience, the origin will be taken at the center of one of the unit cells. It is now possible to form an unbounded reciprocal lattice which can be divided into a set of identical unit cells. (We will pick each cell such that it is equivalent to the first Brillouin zone.) This reciprocal lattice is defined such that the quantity $\mathbf{K}_i \cdot \mathbf{r}_n/2\pi$ is some integer for all values of i and n, where the $\mathbf{K}_i$'s form an enumerable, infinite set of reciprocal vectors drawn from an origin of coordinates (centered on one of the unit cells) to the center of the ith unit cell in reciprocal space. The factor $1/2\pi$ appears since atomic units are being used; e.g., energy is expressed in units of the Rydberg energy, distance in units of the Bohr radius, etc.

* Part of a thesis submitted in partial fulfillment of the requirements for the degree of Doctor of Philosophy in Physics in the Graduate School of the Massachusetts Institute of Technology. This work was supported by the ONR.

[1] For a survey of such methods, see F. Seitz, *The Modern Theory of Solids* (McGraw-Hill Book Company, Inc., New York, 1940), Chapter IX.

[2] F. Bloch, Z. Physik **52**, 555 (1928).

[3] Jones, Mott, and Skinner, Phys. Rev. **45**, 379 (1934).

[4] C. Herring, Phys. Rev. **57**, 1169 (1940); C. Herring and A. G. Hill, Phys. Rev. **58**, 132 (1940).

It can be shown that the wave functions in a crystal must satisfy Bloch's theorem; namely, that any such wave function $\Psi(\mathbf{r})$ must be of the form[5]

$$\Psi_{\mathbf{k}}(\mathbf{r}+\mathbf{r}_n)=e^{i\mathbf{k}\cdot\mathbf{r}_n}\Psi_{\mathbf{k}}(\mathbf{r}). \tag{1}$$

Let us define

$$\mathbf{k}_i=\mathbf{k}+\mathbf{K}_i. \tag{2}$$

Then (1) can be written in the form

$$\Psi_{\mathbf{k}_i}(\mathbf{r}+\mathbf{r}_n)=e^{i\mathbf{k}\cdot\mathbf{r}_n}\Psi_{\mathbf{k}_i}(\mathbf{r}),$$

so that, as far as the translational properties of the Ψ's are concerned, all the different $\mathbf{k}_i$'s corresponding to a given $\mathbf{k}$ are equivalent, and we need consider only values of $\mathbf{k}$ lying in the first Brillouin zone. It was first pointed out by Bloch[2] that such a wave function can be formed by a spacial Bloch sum of atomic or molecular wave functions, $\psi(\mathbf{r})$,

$$\Psi_{\mathbf{k}}(\mathbf{r})=\sum_n e^{i\mathbf{k}\cdot\mathbf{r}_n}\psi(\mathbf{r}-\mathbf{r}_n). \tag{3}$$

In the discussion to follow, it will be assumed that there is only one atom in the unit cell of the crystal. The discussion can be generalized to the case of many atoms per unit cell, however, simply by everywhere replacing the word atomic by the word molecular, the molecule in question being that formed by the atoms of the unit cell.

If the crystal potential, $\mathbf{V}(\mathbf{r})$ is essentially the same as the potential, $V(\mathbf{r})$, of the isolated atom in the vicinity of each nucleus, then $\Psi(\mathbf{r})$ will be an approximate solution for the crystal potential if $\psi(\mathbf{r})$ is a solution for the atomic potential. This approximation will be good for the ion-core electrons but poor for the valence electrons. Thus, if $u_s(\mathbf{r})$ is the set of isolated-atom wave functions for the ion-core electrons, then

$$\Phi_s(\mathbf{r})=\sum_n e^{i\mathbf{k}\cdot\mathbf{r}_n}u_s(\mathbf{r}-\mathbf{r}_n) \tag{4}$$

is the set of ion-core Bloch wave functions for the crystal. If $v_s(\mathbf{r})$ is the set of isolated-atom valence and excited wave functions, then the two sets $u_s(\mathbf{r})$ and $v_s(\mathbf{r})$ combine to form $\psi_s(\mathbf{r})$, the complete set of solutions to the Schrödinger equation for the isolated atom potential. For reasons that will be discussed in Sec. III, it is convenient to work with valence and excited Bloch wave functions that are orthogonal to the ion-core Bloch wave functions, Φ_s. In order to obtain these, we define

$$w_s=v_s-\sum_t \sigma_{st}u_t, \tag{5}$$

where

$$\sigma_{st}=\frac{\sum_n e^{-i\mathbf{k}\cdot\mathbf{r}_n}\int_\infty u_t^*(\mathbf{r}-\mathbf{r}_n)v_s(\mathbf{r})d\tau}{\int_\infty u_t^*(\mathbf{r})u_t(\mathbf{r})d\tau}. \tag{6}$$

[5] Actually this theorem holds only for wave functions satisfying periodic boundary conditions. Other types of wave functions may be used when phenomena at the surface of the crystal are being studied. For an excellent proof of Bloch's theorem, see W. Shockley, *Electrons and Holes in Semiconductors* (D. Van Nostrand Company, Inc., New York, 1950).

(Here $\int_\infty d\tau$ represents an integral over the entire crystal.) We now define

$$\Psi_s(\mathbf{r})=\sum_n e^{i\mathbf{k}\cdot\mathbf{r}_n}w_s(\mathbf{r}-\mathbf{r}_n) \tag{7}$$

as the set of valence and excited Bloch wave functions. Assume that

$$\int_\infty u_s^*(\mathbf{r}-\mathbf{r}_n)u_t(\mathbf{r})d\tau=\delta_{st}\delta_{n0}\int_\infty u_s^*(\mathbf{r})u_s(\mathbf{r})d\tau; \tag{8}$$

i.e., the ion-core atomic wave functions are mutually orthogonal and the overlap integrals between ion-core wave functions on different atoms are negligible. It now follows immediately that

$$\int_\infty \Psi_s^*\Phi_t d\tau=0, \tag{9}$$

for all the values of s and t.

Assume that the exact Bloch wave function, Ψ_s for a valence or an excited electron can be expanded in terms of the Ψ_t's,

$$\Psi=\sum_t \alpha_t\Psi_t. \tag{10}$$

Let us define as energy and overlap integrals, respectively,

$$H_{stn}=\int_\infty w_t^*(\mathbf{r})Hw_s(\mathbf{r}-\mathbf{r}_n)d\tau,$$
$$I_{stn}=\int_\infty w_t^*(\mathbf{r})w_s(\mathbf{r}-\mathbf{r}_n)d\tau, \tag{11}$$

where H is the one-electron Hamiltonian for the crystal. If we require that (10) satisfies Schrödinger's equation, then by making use of the usual variation method we get the set of equations,

$$\sum_s \alpha_s\sum_n e^{i\mathbf{k}\cdot\mathbf{r}_n}(H_{stn}-EI_{stn})=0. \tag{12}$$

The corresponding secular equation is

$$\det[\textstyle\sum_n e^{i\mathbf{k}\cdot\mathbf{r}_n}(H_{stn}-EI_{stn})]=0. \tag{13}$$

The elements of the secular determinant are thus Bloch sums of overlap and energy integrals.

A major problem of the method of Bloch waves is the accurate evaluation of these Bloch sums. The approximation of "tight binding" has been used extensively in the past in obtaining these sums.[3] This approximation consists of neglecting all integrals between non-neighboring atoms of the crystal. This approximation is usually excellent for ion-core wave functions ([Eq. (8)] is a strengthened version of this approximation), but the approximation may be very bad for valence and excited wave functions, whence the corresponding Bloch sums converge very slowly. An accurate method of calculating such Bloch sums will be discussed in Sec. IV.

III. METHOD OF ORTHOGONALIZED PLANE WAVES

One of the earliest methods of treating valence electrons in a crystal involved expanding the wave function in plane waves.[6] This method is not accurate, however, for the following reason. When using a small number of plane waves, the lowest root of the secular equation gives an energy in the region of the valence band, but, of necessity, if a complete set of plane waves were used, the lowest root should give the energy of the lowest ion-core band. This indicates that a very large number of plane waves is necessary to represent accurately the wave function, a fact which results from the rapid variation with position of the wave function close to each nucleus.

Herring[4] has shown that this difficulty can be removed by expanding the valence wave function in terms of orthogonalized plane waves. An orthogonalized plane wave, by definition, is a plane wave which has been made orthogonal to the ion-core Bloch wave functions by the Schmidt orthogonalization procedure. It is well known that the complete set of plane waves for an unbounded crystal is $e^{i\mathbf{k}_i\cdot\mathbf{r}}$. (The symbols used here have the same meaning as in Sec. II.) The corresponding set of orthogonalized plane waves is

$$\mathrm{X}_i(\mathbf{r})=e^{i\mathbf{k}_i\cdot\mathbf{r}}-\sum_j \mu_{ij}\Phi_j(\mathbf{r}), \tag{14}$$

$$\mu_{ij}=\int_\infty e^{i\mathbf{k}_i\cdot\mathbf{r}}u_j^*(\mathbf{r})d\tau \Big/ \int_\infty u_j^*(\mathbf{r})u_j(\mathbf{r})d\tau. \tag{15}$$

It is easily shown that

$$\int_\infty \mathrm{X}_i^*\Phi_j d\tau=0 \tag{16}$$

for all the values of i and j.

Assume that the exact Bloch wave function, Ψ, for a valence or an excited electron can be expanded in terms of the X_i's,

$$\Psi=\sum_i \beta_i \mathrm{X}_i. \tag{17}$$

Define

$$D_{ij}=(1/\Omega N)\int_\infty \mathrm{X}_j^*(H-E)\mathrm{X}_i d\tau, \tag{18}$$

where Ω is the volume of the unit cell and N is the number of unit cells in the crystal, so that ΩN is the volume of the crystal. Making use of the variation method, we get the set of equations

$$\sum_i \beta_i D_{ij}=0. \tag{19}$$

The corresponding secular equation is

$$\det D_{ij}=0. \tag{20}$$

Let us assume that the Hamiltonian is of the form

$$H=-\nabla^2+\mathbf{V}(\mathbf{r}), \tag{21}$$

where the crystal potential $\mathbf{V}$ is a spacial sum of atomic-like potentials, V, i.e.,

$$\mathbf{V}(\mathbf{r})=\sum_n V(\mathbf{r}-\mathbf{r}_n). \tag{22}$$

(See Appendix A for the determination of V.) D_{ij} can now be put in a form more convenient for numerical computation, namely,

$$\begin{aligned} D_{ij}=(k_i^2-E)\delta_{ij}-\Omega^{-1}\sum_s\Big[&(k_i^2+k_j^2-E)\mu_{is}\mu_{js}^* \\ &\times\int_\infty u_s^*(\mathbf{r})u_s(\mathbf{r})d\tau-\mu_{is}\mu_{js}^*\int_\infty \nabla u_s^*(\mathbf{r}) \\ &\cdot\nabla u_s(\mathbf{r})d\tau\Big]+\Omega^{-1}\int_\infty V(\mathbf{r})e^{i\mathbf{K}_{ij}\cdot\mathbf{r}}d\tau \\ &-\Omega^{-1}\sum_{s,n}\Big[\mu_{is}\int_\infty e^{-i\mathbf{k}_j\cdot\mathbf{r}}u_s(\mathbf{r})V(\mathbf{r}-\mathbf{r}_n)d\tau \\ &+\mu_{js}^*\int_\infty e^{i\mathbf{k}_i\cdot\mathbf{r}}u_s^*(\mathbf{r})V(\mathbf{r}-\mathbf{r}_n)d\tau \\ &-\mu_{is}\mu_{js}^*\int_\infty u_s^*(\mathbf{r})u_s(\mathbf{r})V(\mathbf{r}-\mathbf{r}_n)d\tau\Big]. \end{aligned} \tag{23}$$

Here we have used the shortened notation $\mathbf{K}_i-\mathbf{K}_j\equiv\mathbf{K}_{ij}$.

As Herring has pointed out, by using a set of orthogonalized plane waves, X_i, rather than a set of ordinary plane wave, $e^{i\mathbf{k}_i\cdot\mathbf{r}}$, the energy of the lowest root of the secular equation converges to the energy of the lowest valence band (rather than to the energy of the lowest ion-core level) as the order of the secular determinant is increased (in the approximation that the Φ_i's are the exact solutions for the ion-core levels). Therefore it might be expected that the series in Eq. (17) would be much more rapidly convergent than a similar series using ordinary plane waves. This expectation will be shown to be justified in the case of the lithium crystal. It was for essentially the same reason that we went to the trouble of insuring orthogonality between the ion-core and the valence Bloch functions in Sec. II.

An alternative, but equivalent, method of explaining the rapid convergence of the series in Eq. (17) is the following. The reason that an ordinary Fourier expansion of the valence Bloch wave function does not converge rapidly lies in the fact that the wave function varies rapidly with position in the vicinity of each atomic nucleus—this rapid variation requiring plane waves of short wavelength for the accurate representation of the wave function. The mathematical necessity for this rapid variation with position arises from the requirement that the valence Bloch wave function be orthogonal to the ion-core Bloch wave functions combined with the fact that the latter vary rapidly with position near each nucleus. If we use orthogonalized plane waves in place of simple plane

[6] A. Sommerfeld and H. Bethe, *Handbuch der Physik* (Verlag J. Springer, Berlin, Germany, 1933), Vol. 24, No. 2, p. 385.

waves for expanding the wave function, however, the Schmidt orthogonalization procedure insures that the rapidly varying portion of the wave function is *not* expanded in plane waves but is kept in its unexpanded form. Thus we break up Ψ into two parts, Ψ' and Ψ'', where

$$\Psi'=\sum_i \beta_i e^{i\mathbf{k}_i\cdot\mathbf{r}}$$

is that portion which *is* expanded in plane waves, while

$$\Psi''=\sum_{i,j} \beta_i \mu_{ij} \Phi_j(\mathbf{r})$$

is that portion which is not expanded in plane waves. There is no reason why the expansion of Ψ' should not converge rapidly.

IV. TRANSFORMATION FROM THE METHOD OF BLOCH WAVES TO THE METHOD OF ORTHOGONALIZED PLANE WAVES

It was pointed out in Sec. II that a major problem in the method of Bloch waves is the accurate evaluation of the Bloch sums of energy and overlap integrals. For ionic and molecular crystals, where the approximation of "tight binding" is valid, these sums can be evaluated in a straightforward manner. For metals, semiconductors, and valence crystals, however, any attempt at evaluation in a straightforward manner is discouraging, since the sums converge very slowly. Henceforth, we shall consider only crystals where such a situation holds.

The following device is effective under such a situation. Expand in three-dimensional Fourier series that portion of each Bloch wave function which contains an isolated-atom valence or excited wave function, $v_s(\mathbf{r})$. A corresponding portion of each Bloch sum over crystal space can thereby be transformed into a Bloch sum over reciprocal space. Recalling the uncertainty principle, we would expect that a slow convergence over crystal space would correspond to a rapid convergence over reciprocal space. Such is the case. This is equivalent to the fact that a valence electron in a crystal will have a very sharply defined momentum when it has a very poorly defined position.

In obtaining the Fourier series, the correct set of expansion functions to use is the set of ordinary plane waves, $e^{i\mathbf{k}_i\cdot\mathbf{r}}$, already discussed in Sec. III. If we define the coefficients, A_{si}, by the equation

$$\sum_i A_{si} e^{i\mathbf{k}_i\cdot\mathbf{r}} \equiv \sum_n e^{i\mathbf{k}\cdot\mathbf{r}_n} v_s(\mathbf{r}-\mathbf{r}_n), \tag{24}$$

then it immediately follows that

$$A_{si}=\Omega^{-1}\int_\infty e^{-i\mathbf{k}_i\cdot\mathbf{r}} v_s(\mathbf{r})\,d\tau. \tag{25}$$

The coefficients σ_{si} and μ_{ij}, used in the Schmidt orthogonalization procedures for the Bloch waves and the orthogonalized plane waves, respectively, can be related through the equation,

$$\sigma_{si}=\sum_i A_{si}\mu_{ij}. \tag{26}$$

Combining Eqs. (4), (5), (7), (14), (24), and (26), we get

$$\Psi_s(\mathbf{r})=\sum_i A_{si}X_i(\mathbf{r}). \tag{27}$$

Thus our device of expanding only a portion of the Bloch wave function in a Fourier series is equivalent to expanding the entire Bloch wave function in orthogonalized plane waves. It is interesting that the Eq. (27) is exact despite the fact that the set X_i is not a complete set. (27) holds since the set X_i may be considered a complete set for the purpose of expanding any function which is orthogonal to the set of ion-core Bloch wave functions, Φ_s.

It is possible to write the Bloch sums of overlap and energy integrals in the form

$$\sum_n e^{i\mathbf{k}\cdot\mathbf{r}_n}(H_{stn}-EI_{stn})=N^{-1}\int_\infty \Psi_t^*(H-E)\Psi_s\,d\tau. \tag{28}$$

Substituting (18) and (27) into (28), we get

$$\sum_n e^{i\mathbf{k}\cdot\mathbf{r}_n}(H_{stn}-EI_{stn})=\Omega\sum_{ij} A_{si}A_{tj}^*D_{ij}. \tag{29}$$

Thus the secular equation in the Bloch method can be written

$$\det[\Omega\textstyle\sum_{ij} A_{si}A_{tj}^*D_{ij}]=0. \tag{30}$$

Applying the law of determinant multiplication, we get

$$\det[\textstyle\sum_{ij} A_{si}A_{tj}^*D_{ij}] = (\det A_{si})(\det A_{tj}^*)(\det D_{ij}), \tag{31}$$

so that (30) is equivalent to

$$\det D_{ij}=0. \tag{32}$$

Since Eqs. (32) and (20) are identical, we have shown that the Bloch method is equivalent to the orthogonalized plane wave method.

Let us now study the practicability of the Bloch method for numerical calculation. We will show that while Eq. (29) is a very useful way of evaluating Bloch sums of overlap and energy integrals, Eq. (30) is absolutely useless for calculating energy bands. To do this we must determine A_{si}, which depends upon $v_s(\mathbf{r})$. In the types of crystals under consideration, the atomic correspondence is very poor for valence electrons, so that it is not necessary to use accurate analytic approximations to the true set, $v_s(\mathbf{r})$, of isolated-atom valence and excited wave functions when making numerical calculations. Indeed, it is not even necessary that the analytic approximations to $v_s(\mathbf{r})$ have radial nodes. When we form $w_s(\mathbf{r})$ from $v_s(\mathbf{r})$ by the Schmidt orthogonalization procedure [Eq. (5)], we automatically insure that $w_s(\mathbf{r})$ has the proper number of nodes. We will approximate $v_s(\mathbf{r})$ by a set of Gaussian functions,[7]

$$v_{lm}(\mathbf{r})=i^l P_l^{|m|}(\cos\theta)e^{im\varphi}r^l\exp(-b_l r^2). \tag{33}$$

[7] The use of Gaussians in place of the more conventional exponential wave functions in problems involving many atoms was first suggested by S. F. Boys, Proc. Roy. Soc. (London) **200**, 542 (1950). Boys pointed out that energy and overlap integrals could be obtained much more easily by using Gaussians rather than exponentials.

Substituting (33) into (25), we get

$$A_{lm_i}=\Omega^{-1}(\pi/b_i)^{\frac{1}{2}}(k_i/2b_i)^l P_l^{|m|}(\cos\theta_i)e^{im\varphi_i} \times\exp[-(k_i^2/4b_i)], \quad (34)$$

where θ_i and φ_i give the orientation of $\mathbf{k}_i$. We can see the relative magnitudes of the various A's by considering the example of lithium. For a $2p$ Gaussian wave function in an isolated lithium atom, the values of b_l obtained by minimizing the one-electron energy can be shown to be $b_1=0.0557$. (The atomic potential, $V(r)$, used in such a calculation is that obtained in Appendix A.) In the crystal b_1 is probably still smaller, since the wave function is probably more spread out in the crystal than it is in an isolated atom. For the lithium crystal $\mathbf{K}_i$ is the form

$$\mathbf{K}_{n_1n_2n_3}=K(\mathbf{i}_1n_1+\mathbf{i}_2n_2+\mathbf{i}_3n_3),$$

where $\mathbf{i}_1$, $\mathbf{i}_2$, and $\mathbf{i}_3$ are fixed, mutually orthogonal unit vectors, $(n_1+n_2+n_3)$ is an arbitrary even integer (face-centered-cubic reciprocal lattice), and $K=0.957$. Since k_i usually increases with i (by convention), we can see that, because of the factor $\exp[-(k_i^2/4b_i)]$ in A_i, the ration A_{i+1}/A_i will usually be a very small number, often smaller than one millionth. Because of this fact, the double series on the right-hand side of Eq. (29) will converge extremely rapidly. This situation will hold in general provided that the Bloch sums on the left-hand side are slowly convergent. It is thus usually a very good approximation to replace Eq. (29) by

$$\sum_n e^{i\mathbf{k}\cdot\tau_n}(H_{stn}-EI_{stn})\cong\Omega A_{s0}A_{t0}^*D_{00} \quad (35)$$

when the Bloch sums converge slowly. (Here we have replaced the double series over reciprocal space by its leading term.) If we attempt to use this approximation in Eq. (30), however, we find that the secular determinant vanishes identically (since the rows and columns are mutually proportional), so that it is impossible to solve for the energy eigenvalues. This is a convincing demonstration of the fact that it is necessary to determine the Bloch sums extremely accurately, since the solution to the secular equation depends upon the minute deviations from proportionality of the rows and columns of the secular determinant.

It is now apparent that Eq. (30) is not practical for numerical calculations. The key to this lack of usefullness of the Bloch method lines in Eq. (27). Just as we approximated Eq. (29) by Eq. (35), we may approximate Eq. (27) by

$$\Psi_s(\mathbf{r})\cong A_{s0}\mathbf{X}_0(\mathbf{r}). \quad (36)$$

We thus see that in Eq. (10) we are attempting to expand the exact crystal wave function, Ψ, in terms of a set of wave functions, Ψ_s, the members of this set all being, to an excellent approximation, numerical multiples of a single function, $\mathbf{X}_0$. In other words, Ψ_s is an extremely poor set to use in expanding Ψ. Disregarding numerical factors, we see that Ψ_s depends almost entirely on $\mathbf{X}_0$ and almost not at all on v_s. Because of the large amount of overlapping of valence atomic wave functions centered on different nuclei of the crystal, the valence atomic correspondence of Ψ_s is almost completely lost.

It is possible to reformulate the Bloch method in order to remove the difficulty of a secular determinant which vanishes identically (for practical purposes). This reformulation is rather unwieldy for numerical computations, however. From the set of valence Bloch wave functions, $\Psi_s(\mathbf{r})$, let us form the set of doubly orthogonal valence Bloch wave functions, $\mathbf{\Psi}_s(\mathbf{r})$, where

$$\mathbf{\Psi}_s(\mathbf{r})=\Psi_s(\mathbf{r})-\sum_{r<s}\xi_{sr}\mathbf{\Psi}_r(\mathbf{r}) \quad (37)$$

and

$$\xi_{sr}=\int_\infty \mathbf{\Psi}_r^*\Psi_s d\tau \Big/ \int_\infty \mathbf{\Psi}_r^*\mathbf{\Psi}_r d\tau. \quad (38)$$

As well as being orthogonal to the ion-core Bloch waves, the $\mathbf{\Psi}_s(\mathbf{r})$ are mutually orthogonal. Similarly, let us form the set of doubly orthogonalized plane waves, $\mathbf{X}_i(\mathbf{r})$, where

$$\mathbf{X}_i(\mathbf{r})=\mathrm{X}_i(\mathbf{r})-\sum_{j<i}\eta_{ij}\mathbf{X}_j(\mathbf{r}) \quad (39)$$

and

$$\eta_{ij}=\int_\infty \mathbf{X}_j\mathrm{X}_i d\tau \Big/ \int_\infty \mathbf{X}_j\mathbf{X}_j d\tau. \quad (40)$$

As well as being orthogonal to the ion-core Bloch waves, the $\mathbf{X}_i(\mathbf{r})$ are mutually orthogonal. As might be expected, it is possible to expand $\mathbf{\Psi}_s(\mathbf{r})$ in terms of the $\mathbf{X}_i$'s.

$$\mathbf{\Psi}_s(\mathbf{r})=\sum_i B_{si}\mathbf{X}_i(\mathbf{r}). \quad (41)$$

It can be shown that

$$B_{si}=\sum_{\mu,\nu}\gamma_{s\mu}A_{\mu\nu}\eta_{\nu i}, \quad (42)$$

where

$$\sum_\nu \gamma_{s\nu}\xi_{\nu t}=\delta_{st}. \quad (43)$$

Using the fact that $A_{\mu\nu}\gg A_{\mu,\nu+1}$, we can show that $B_{ss}\gg B_{s,s\pm1}\gg B_{s,s\pm2}\cdots$, so that, to a very good approximation, we have

$$\mathbf{\Psi}_s(\mathbf{r})\cong B_{ss}\mathbf{X}_s(\mathbf{r}). \quad (44)$$

Equation (44) should be contrasted with Eq. (36). Associated with each doubly orthogonal valence Bloch function there is a particular doubly orthogonalized plane wave—the two being very nearly proportional—so that there are no difficulties with vanishing secular determinants. Just as with $\Psi_s(\mathbf{r})$, the valence atomic correspondence of $\mathbf{\Psi}_s(\mathbf{r})$ is almost completely lost.

V. APPLICATION TO LITHIUM

We shall now apply the method of orthogonalized plane waves to the case of the lithium crystal. The calculations are simplified by the fact that there is only one type of ion-core atomic wave function, namely, a $1s$ wave function, u_{1s}. We approximate this by the

exponential

$$u_{1s}=e^{-ar}. \tag{45}$$

a is determined by minimizing the expectation value of the 1s energy in the isolated lithium atom; i.e., we solve the equation

$$\partial E_{1s}'/\partial a=0,$$

where

$$E_{1s}'=\int_\infty u_{1s}H'u_{1s}d\tau \Big/ \int_\infty u_{1s}u_{1s}d\tau, \tag{46}$$

$$H'=-\nabla^2+V(r), \tag{47}$$

$V(r)$ being the atomic potential determined in Appendix A; i.e.,

$$V(r)=-\frac{2}{r}\sum_{\nu=1}^{4}C_\nu \exp(-c_\nu r^2) \tag{48}$$

(the C's and c's being suitably chosen constants). The results obtained are $a=2.788$ and $E_{1s}'=-4.572$ (to be compared with the experimental value of $E_{1s}'=-4.799$).

By substituting Eqs. (45) and (48) into Eq. (23), we can explicitly evaluate the integrals occurring in the expression for D_{ij}. After considerable mathematical manipulation it is possible to obtain an approximate but numerically accurate expression from which D_{ij} may easily be calculated as a function of $\mathbf{k}_i$ and $\mathbf{k}_j$.

When we approximate Ψ by the first n terms of the series in Eq. (17), then we obtain in Eq. (20) an nth order secular determinant. For example, if we use only the leading term of the series in (17), then (20) becomes

$$D_{00}=0, \tag{49}$$

and we get a single solution for E *versus* $\mathbf{k}$, this solution being independent of the direction of $\mathbf{k}$. For higher approximations, involving a secular determinant of order greater than the first, the energy will not be completely independent of the direction of $\mathbf{k}$. If the crystal wave function in the lowest valence band can be closely approximated by a single orthogonalized plane wave, however, then the energy will be nearly independent of direction. That such is the case for lithium can be seen from an examination of the results given in Table I, where it is apparent that as the order of the secular determinant is increased, E converges rapidly to its limiting value. It is this behavior which makes the orthogonalized plane wave method useful for numerical calculation.

Knowing E as a function of $\mathbf{k}$, we can find the ratio of free to effective electronic mass in the valence band. For $\mathbf{k}$ along a symmetry axis of the reciprocal lattice, the ratio is given by

$$m/m^*=\tfrac{1}{2}d^2E/dk^2.$$

We obtain as values along the 110, 111, and 100 directions at the bottom of the band

$$(m/m^*)_{110}=0.8190,$$
$$(m/m^*)_{111}=0.7936,$$
$$(m/m^*)_{100}=0.8030,$$
$$\langle m/m^*\rangle_{Av}=0.8075.$$

(The directional average is obtained in an approximate fashion by averaging the values for the three symmetry directions—weighting these values according to the fact that there are six 110 axes, four 111 axes, and three 100 axes.) Silverman and Kohn[8] computed $(m/m^*)=0.727$ at the bottom of the band. The difference is probably because of their use of an atomic rather than a crystal potential. The latter varies less rapidly than the former over most of the unit cell, and thus should result in a value of m^* more nearly "free-electron-like" (see Appendix A).

Knowing E as a function of $\mathbf{k}$, we can compute the energy-width of the filled portion of the valence band, obtaining a value of 4.06 electron volts. By means of the soft x-ray K emission band of lithium, Skinner[9] measured this to be 4.1 ± 0.3 volts. This excellent comparison is in contrast with the results of previous calculations on lithium.[5,10] For example, the results of Silverman and Kohn, who use the Wigner-Seitz ap-

TABLE I. E *versus* $\mathbf{k}$ for the valence band of lithium. For convenience, $E+(4\pi C_1/\Omega c_1)$ has been denoted simply by E. The number in the parentheses after E refers to the order of the secular determinant used in solving for E.

110 direction		
k	$E(1)$	$E(2)$
0.0	0.188567	0.188527
0.2	0.222039	0.221287
0.4	0.330156	0.326336
0.6	0.509509	0.487387
0.67675	0.598254	0.527035

111 direction			
k	$E(1)$	$E(2)$	$E(4)$
0.0	0.188567	0.188527	0.188437
0.2	0.222039	0.221456	0.220183
0.4	0.330156	0.328368	0.324709
0.6	0.509509	0.504317	0.495564
0.67675	0.598254	0.589861	0.578193
0.75	0.693473	0.677700	0.663656
0.82885	0.807631	0.756032	0.756032

100 direction			
k	$E(1)$	$E(2)$	$E(5)$
0.0	0.188567	0.188527	0.188394
0.2	0.222039	0.221674	0.220513
0.4	0.330156	0.329050	0.325783
0.6	0.509509	0.507119	0.501071
0.67675	0.598254	0.595096	0.587910
0.75	0.693473	0.689234	0.681002
0.82885	0.807631	0.801213	0.792210
0.9	0.921154	0.909060	0.901722
0.95707	1.019513	0.985029	0.994526

[8] R. A. Silverman and W. Kohn, Phys. Rev. **80**, 912 (1950).
[9] H. W. B. Skinner, Reports on Progress in Physics, **V** (1938).
[10] J. Millman, Phys. Rev. **47**, 286 (1935); F. Seitz, Phys. Rev. **47**, 400 (1935); J. Bardeen, J. Chem. Phys. **6**, 367 (1938).

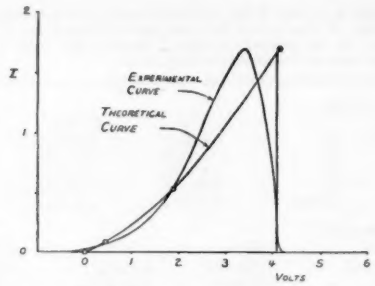

FIG. 1. Soft x-ray K emission band of lithium.

proximation, would predict the filled portion of the band to have a width of only 3.51 volts.

It is instructive to compute the $1s$ energy level in the lithium crystal; i.e.,

$$E_{1s}=\int_{\infty}\Phi_{1s}^{*}H\Phi_{1s}d\tau\Big/\int_{\infty}\Phi_{1s}^{*}\Phi_{1s}d\tau, \qquad (50)$$

where

$$\Phi_{1s}(\mathbf{r})=\sum_{n}e^{i\mathbf{k}\cdot\mathbf{r}_{n}}u_{1s}(\mathbf{r}-\mathbf{r}_{n}), \qquad (51)$$

and H is given by Eq. (21). (Note the distinction between Eqs. (50) and (46)—the former holding for the crystal and the latter for the isolated atom.) Having done this, we can compute the energy-difference between the Fermi level and the $1s$ level in the crystal to be 57.8 volts. This should be compared with the experimental value of 54.8 ± 0.6 volts.[11]

Let us now compute the shape of the soft x-ray K emission band of lithium. The experimental shape of the emission band will be proportional to the optical transition probability between the valence band and the $1s$ level and proportional to the density of filled states per unit energy range in the valence band. In the approximation of E being independent of the direction of $\mathbf{k}$ in the valence band, then $k^{2}dk/dE$ is proportional to the density of states per unit energy range. The optical transition probability between a $1s$ wave function Φ_{1s} and a valence wave function Ψ is proportional to the quantity P, defined as

$$P=\left|\int_{\infty}\Phi_{1s}^{*}\nabla\Psi d\tau\right|^{2}\Big/\left(\int_{\infty}\Phi_{1s}^{*}\Phi_{1s}d\tau\int_{\infty}\Psi^{*}\Psi d\tau\right). \qquad (52)$$

If we define the quantity

$$I=Pk^{2}dk/dE, \qquad (53)$$

then, for energies below the Fermi level, I should be proportional to the experimental shape of the emission band. As can be seen from Fig. 1, the comparison between theory and experiment[9] is only fair. The computed values of I are roughly proportional to $E^{\frac{1}{2}}$. The reason for the drop in the experimental curve at high energies is not known.

[11] H. M. O'Bryan and H. W. B. Skinner, Phys. Rev. **45**, 370 (1934).

VI. CONCLUSION

Let us briefly recapitulate the basic results of this paper. For ion-core electrons (i.e., electrons associated with a given nucleus), the crystal wave functions can be conveniently expressed as Bloch wave functions formed from the appropriate atomic wave functions. As is shown in Appendix B, it is permissible to use simple analytic approximations for these atomic wave functions if our primary interest lies in the valence and excited bands.

For valence and excited electrons (i.e., electrons which cannot be associated with any given nucleus), the ordinary Bloch method leads to computational difficulties. The elements of the secular determinant involve slowly convergent spacial sums of overlap and energy integrals between the various atoms of the crystal. An approximation often used, that of tight binding, which consists of neglecting integrals between non-neighboring atoms of the crystal, is quite unjustified because of the slow convergence of these sums. By expanding each valence Bloch wave function in terms of orthogonalized plane waves, however, these slowly convergent sums over ordinary space are transformed into extremely rapidly convergent sums over reciprocal space. It thereupon becomes apparent that, for the purpose of numerical computation, the secular determinant occurring in the Bloch method will vanish identically. This difficulty is caused by the fact that, to a good approximation, all the valence Bloch wave functions (in terms of which we attempt to expand the true wave function) differ among themselves only by a multiplicative constant. By a simple process, however, the secular equation of the Bloch method can be transformed into the secular equation of the method of orthogonalized plane waves. The latter equation is quite suitable for numerical computations. Thus we see that the valence and excited wave functions are most conveniently expressed in terms of orthogonalized plane waves. The latter have most of the advantages and none of the overwhelming disadvantages of ordinary plane waves.

There are, of course, electrons which fall into neither of the two general classes considered in the last two paragraphs (e.g., the $3d$ electrons in the transition elements). About such electrons nothing can be said here.

Concerning the crystal potential, two important facts stand out, as is shown in Appendix A. In the first place, within a given unit cell of the crystal, the crystal potential is not approximately the same as the corresponding potential for the isolated atom. As we have seen for the case of lithium, the two give significantly different answers to the same problem, so that one should not be used in place of the other. Secondly,

Slater's method of including exchange in a one-electron approximation (by using an effective potential) seems to be well-suited for the calculation of energy bands in crystals.

The writer is indebted to the members of the Solid-State and Molecular Theory Group at MIT for their helpful discussion and criticism during the course of the investigation reported herein. In particular, the writer is indebted to the director of the group, Professor John C. Slater, for much-needed advice and encouragement.

APPENDIX A

Determination of the Crystal Potential

First we shall justify Eq. (22),

$$\mathbf{V}(\mathbf{r})=\sum_n V(\mathbf{r}-\mathbf{r}_n), \tag{1a}$$

which states that the crystal potential, $\mathbf{V}(\mathbf{r})$, can be taken as a spacial sum of atomic-like potentials. This is certainly true for that part of the crystal potential resulting from the ion-cores of the various atoms of the crystal, since the charge distributions of different ion-cores do not overlap. We now show that the same is true for that portion of the crystal potential resulting from valence electrons. The exact (one-electron) wave function $\Psi(\mathbf{r})$ for the valence electrons can be written in the form

$$\Psi(\mathbf{r})=\sum_n e^{i\mathbf{k}\cdot\mathbf{r}_n}a(\mathbf{r}-\mathbf{r}_n), \tag{2a}$$

where (2a) may be taken as an implicit definition of the Wannier function, $a(\mathbf{r})$.[12] This function is similar to an atomic wave function, a fact which might be suspected by comparing Eqs. (2a) and (3). If we define

$$\rho(\mathbf{r})=\sum_n e^{i\mathbf{k}\cdot\mathbf{r}_n}a^*(\mathbf{r})a(\mathbf{r}-\mathbf{r}_n), \tag{3a}$$

then it follows that

$$\Psi^*\Psi=\sum_n \rho(\mathbf{r}-\mathbf{r}_n). \tag{4a}$$

We have now fully justified (1a), since (4a) shows that that portion of the crystal potential arising from the valence electrons can be taken as a spacial sum of atomic potentials, the atomic potential being that arising from the atomic-like charge distribution, $\rho(\mathbf{r})$.

We shall use the spherical average of $\rho(\mathbf{r})$, rather than $\rho(\mathbf{r})$ itself, in computing $V(\mathbf{r})$—this approximation being used universally in atomic problems. We will make the further approximation of replacing the series in (3a) by its leading term; i.e.,

$$\rho(\mathbf{r})=a^*(\mathbf{r})a(\mathbf{r}). \tag{5a}$$

These two approximations tremendously simplify the calculations. Incidentally, it can be shown that (5a) follows from the spherical averaging unless $a(\mathbf{r})$ has the character of an s wave function.

In order to include electron exchange in our one-electron Hamiltonian, we will form our potential by a method introduced by Slater.[13] If we define $\mathcal{U}(\mathbf{r})$ as the conventional potential of an electron in the field of the neutral crystal, then $\mathbf{V}(\mathbf{r})$, the potential including exchange, is given by

$$\mathbf{V}=\mathcal{U}+(3/2)(3/\pi^2)^{\frac{1}{3}}(\nabla^2\mathcal{U})^{\frac{1}{2}}. \tag{6a}$$

It follows from the previous discussion that we may decompose $\mathcal{U}(\mathbf{r})$ into a spacial sum of atomic potentials; i.e.,

$$\mathcal{U}(\mathbf{r})=\sum_n \mathcal{W}(\mathbf{r}-\mathbf{r}_n), \tag{7a}$$

where[14]

$$\mathcal{W}(r)=-(2/r)Z_p(r) \tag{8a}$$

serves to define the effective atomic number $Z_p(r)$. Instead of properly applying the exchange correction to the crystal potential as is done in Eq. (6a), we will adopt the approximate procedure of applying it to the atomic potential $\mathcal{W}(r)$. Thus we take

$$\begin{aligned} V(r)&=-(2/r)Z_{p1}(r),\\ Z_{p1}(r)&=Z_p+3(3/32\pi^2)^{\frac{1}{3}}(r^3d^2Z_p/dr^2)^{\frac{1}{2}}, \end{aligned} \tag{9a}$$

where $V(r)$ and $\mathbf{V}(\mathbf{r})$ are related by Eq. (22). The second term in Z_{p1} results from a free-electron approximation to the exchange hole correction.

In computing Z_p for lithium, isolated-atom wave functions (with exchange) for lithium were taken from Fock and Petrashen.[15] It was assumed that the appropriate configuration to use for the neutral lithium atom in computing Z_p is $(1s)^2(2s)^{\frac{1}{3}}(2p)^{\frac{2}{3}}$. This assumption is based on the following approximate calculation. Let the valence atomic wave function for lithium be of the form,

$$\psi=a_s(\mathbf{k})\psi_{2s}+a_p(\mathbf{k})\psi_{2p}.$$

Following Jones, Mott, and Skinner,[3] we assume that $|a_p|=k/K_1$, where $\mathbf{k}=\mathbf{K}_1$, at the edge of the first Brillouin zone. Denote by Ω_K the volume of the first Brillouin zone, so that approximately $\Omega_K=(4/3)\pi K_1^3$. Two valence electrons would fill the valence band. Since for lithium there is only one valence electron per atom, the band is exactly half full, and $\frac{1}{2}\Omega_K=(4/3)\pi k_1^3$, k_1 being defined as the maximum value of k associated with an occupied state. We now find that

$$\langle a_p^2\rangle_{\text{Av}}=\int_0^{k_1}4\pi k^2a_p^2dk\Big/\int_0^{k_1}4\pi k^2dk$$

$$=\tfrac{3}{5}(\tfrac{1}{2})^{\frac{1}{3}}=0.3780\cong\tfrac{3}{8}$$

is the fraction of $2p$ electrons in the valence band of the lithium crystal.

It was found that Z_{p1} could be very closely approximated by a sum of Gaussians,

$$Z_{p1}(r)=\sum_{\nu=1}^{4}C_\nu\exp(-c_\nu r^2), \tag{10a}$$

[12] G. H. Wannier, Phys. Rev. **52**, 191 (1937).
[13] J. C. Slater, Phys. Rev. **81**, 385 (1951).
[14] It should be emphasized that $\mathcal{W}(r)$ is the conventional potential energy of an electron in the field of the neutral, isolated atom.
[15] V. Fock and M. J. Petrashen, Physik. Z. Sowjetunion **8**, 547 (1935).

where

$C_1=0.9256$, $C_2=1.2278$, $C_3=0.5901$, $C_4=0.2369$,
$c_1=0.014408$, $c_2=1.0642$, $c_3=11.939$, $c_4=107.37$.

If we define

$$V_\nu(r)=-(2/r)C_\nu \exp(-c_\nu r^2), \tag{11a}$$

then

$$V(r)=\sum_{\nu=1}^{4} V_\nu(r). \tag{12a}$$

It is convenient to speak of V_1, as the long-range part of the atomic potential and $(V_2+V_3+V_4)$ as the short-range portion. Similarly, we call $\sum_n V_1(\mathbf{r}-\mathbf{r}_n)$ the long-range portion of the crystal potential and

$$\sum_n \sum_{\nu=2}^{4} V_\nu(\mathbf{r}-\mathbf{r}_n)$$

the short-range portion. Because of the values of c_2, c_3, and c_4, it can be seen that the short-range portion of the crystal potential near a given nucleus is the same as the short-range portion of the atomic potential centered on the given nucleus. Because of the smallness of c_1, this is not true of the long-range portion. By expanding the long-range crystal potential in a Fourier series, it can be shown that near a given nucleus the long-range crystal potential acts like the long-range atomic potential (centered on the given nucleus) multiplied by a screening factor, $S(r)$, of the form

$$S(r)=\left[1-(2/\pi)\int_0^{K_1 r} x^{-1}\sin x dx\right], \tag{13a}$$

K_1 having already been defined such that $\Omega_K=(4/3)\pi K_1^3$. This screening factor has the important effect of making a crystal potential more "free-electron-like" than is the corresponding atomic potential.

The long-range crystal potential further contains a small term not strongly dependent on position and a very large term independent of position. This latter is called the divergence term and has the value $-(4\pi C_1/\Omega c_1)$ (-77.6 volts for lithium). (Ω is the volume of the polyhedral cell of the crystal.) Apart from this divergence term, $\mathbf{V}(\mathbf{r})$ is rather insensitive to changes in c_1. This means that the variation with position of the crystal potential is insensitive to the value of the corresponding atomic potential at large distances (large r) since the latter is largely dependent on c_1. Such a situation is fortunate, since the atomic potential we are using is clearly incorrect at large distances; i.e., Z_{p1} approaches zero whereas it should approach unity as $r\to\infty$. This incorrect behavior is a result of the free-electron approximation to the exchange hole correction in (9a), and is the cause of the excessively large value of the divergence term. Since our primary interest lies in energy bands, then an error in the divergence term is unimportant, for the shape and relative separation of the bands are independent of any constant terms in the potential.

APPENDIX B

The Use of Approximate Ion-Core Wave Functions

Let us investigate the error in the lithium valence band resulting from the approximation of the $1s$ atomic wave function by a single exponential. We do this in the following way. Consider the approximation of a first-order secular determinant, so that the secular equation is given by Eq. (49). In this approximation we can expand E in powers of k^2,

$$E=E_0+E_2k^2+E_4k^4+\cdots. \tag{1b}$$

Solving for the coefficients, we get

$$E_0+(4\pi C_1/\Omega c_1)=0.1886,\ E_2=0.8792,\ E_4=0.0199. \tag{2b}$$

If we approximate our $1s$ wave function by a Gaussian, $\exp(-a'r^2)$, rather than by an exponential, e^{-ar}, and then repeat the above calculation, we get

$$E_0+(4\pi C_1/\Omega c_1)=0.1905,\ E_2=0.8751,\ E_4=0.0224. \tag{3b}$$

There is some work involved in getting (3b). First we must obtain the best value of a' from the equation

$$\partial E_{1s}'/\partial a'=0,$$

where E_{1s}' is given by Eq. (46), where now

$$u_{1s}=\exp(-a'r^2). \tag{4b}$$

The results obtained are $a'=2.076$ and $E_{1s}'=-3.248$. Comparing this energy with those given in the discussion following Eq. (46), we can see that a Gaussian is a decidedly poorer approximation to the $1s$ wave function than is an exponential. Substituting (4b) into Eq. (23) we can evaluate D_{00} and thus obtain (3b). The point that should be made is that (3b) is remarkably similar to (2b), despite the fact that a much poorer $1s$ wave function was used in obtaining (3b). This leads us to hope that the error resulting from approximating the $1s$ wave function by a single exponential will be negligible.

Letters to the Editor

PUBLICATION of brief reports of important discoveries in physics may be secured by addressing them to this department. The closing date for this department is five weeks prior to the date of issue. No proof will be sent to the authors. The Board of Editors does not hold itself responsible for the opinions expressed by the correspondents. Communications should not exceed 600 words in length.

Third-Order Elastic Coefficients in Trigonal and Hexagonal Crystals

FAUSTO G. FUMI
Institute of Theoretical Physics, University of Milan, Milan, Italy
(Received March 28, 1952)

THE independent third-order elastic coefficients $pqr=prq=qpr$ $(p, q, r=1$ to $6)$ have been reported previously for twenty-five of the thirty-two crystal classes.[1] Table I completes these results. The numbers of coefficients obtained agree, of course, with those predicted by group theory.[2] Symmetries C_3, S_6, C_{3v}, D_3, and D_{3d} are treated again but with reference to the usual frames having $z\|C_3$.[3]

TABLE I. Third-order elastic coefficients: sixth-order polar tensor $pqr=qpr=prq$.[a, b]

Symmetry group	C_1, S_2	C_2, S_4	D_2, D_{2d}	C_{2v}	C_{2h}, C_4	D_4, D_{4h}	C_{4v}
Reference frame	Any	$z\|C_2$	$z\|C_2'$ $z\|C_2$	$z\|C_2$ $yz\|\sigma_v$	$z\|C_2, C_4$	$x\|C_2'$ $z\|C_2, C_4$	$z\|C_4$ $yz\|\sigma_v$
111	111	111	111	111	111	111	
112	112	112	112	112	112	112	
113	113	113	113	113	113	113	
114	114	114	0	0	0	0	
115	115	0	0	0	0	0	
116	116	0	116	0	0	0	
122	111−222+112	111−222+112	111−222+112	111−222+112	111−222+112	111−222+112	
123	123	123	123	123	123	123	
124	124	124	0	0	0	0	
125	125	0	0	0	0	0	
126	−116	0	−116	0	0	0	
133	133	133	133	133	133	133	
134	134	134	0	0	0	0	
135	135	0	0	0	0	0	
136	0	0	0	0	0	0	
144	144	144	144	144	144	144	
145	145	0	145	0	0	0	
146	$-\frac{1}{2}\cdot115-\frac{1}{2}\cdot125$	0	0	0	0	0	
155	155	155	155	155	155	155	
156	$\frac{1}{2}\cdot114+\frac{1}{2}\cdot124$	$\frac{1}{2}\cdot114+\frac{1}{2}\cdot124$	0	0	0	0	
166	$(\frac{1}{2}\cdot222-\frac{1}{2}\cdot111$ $-\frac{1}{2}\cdot112)$	$(\frac{1}{2}\cdot222-\frac{1}{2}\cdot111$ $-\frac{1}{2}\cdot112)$	$(\frac{1}{2}\cdot222-\frac{1}{2}\cdot111$ $-\frac{1}{2}\cdot112)$	$(\frac{1}{2}\cdot222-\frac{1}{2}\cdot111$ $-\frac{1}{2}\cdot112)$	$(\frac{1}{2}\cdot222-\frac{1}{2}\cdot111$ $-\frac{1}{2}\cdot112)$		
222	222	222	222	222	222		
223	113	113	113	113	113		
224	−114−2·124	−114−2·124	0	0	0		
225	−115−2·125	0	0	0	0		
226	116	0	116	0	0		
233	133	133	133	133	133		
234	−134	−134	0	0	0		
235	−135	0	0	0	0		
236	0	0	0	0	0		
244	155	155	155	155	155		
245	−145	0	−145	0	0		
246	$\frac{1}{2}(125-115)$	0	0	0	0		
255	144	144	144	144	144		
256	$\frac{1}{2}(114-124)$	$\frac{1}{2}(114-124)$	0	0	0		
266	$(\frac{1}{2}\cdot111-\frac{1}{2}\cdot222$ $-\frac{1}{2}\cdot112)$	$(\frac{1}{2}\cdot111-\frac{1}{2}\cdot222$ $-\frac{1}{2}\cdot112)$	$(\frac{1}{2}\cdot111-\frac{1}{2}\cdot222$ $-\frac{1}{2}\cdot112)$	$(\frac{1}{2}\cdot111-\frac{1}{2}\cdot222$ $-\frac{1}{2}\cdot112)$			
333	333	333	333	333			
334	0	0	0	0			
335	0	0	0	0			
336	0	0	0	0			
344	344	344	344	344			
345	0	0	0	0			
346	−135	0	0	0			
355	344	344	344	344			
356	134	134	0	0			
366	$\frac{1}{2}(113-123)$	$\frac{1}{2}(113-123)$	$\frac{1}{2}(113-123)$	$\frac{1}{2}(113-123)$			
444	444	444	0	0			
445	445	0	0	0			
446	145	0	145	0			
455	−444	−444	0	0			
456	$\frac{1}{2}(155-144)$	$\frac{1}{2}(155-144)$	$\frac{1}{2}(155-144)$	$\frac{1}{2}(155-144)$			
466	124	124	0	0			
555	−445	0	0	0			
556	−145	0	−145	0			
566	125	0	0	0			
666	−116	0	−116	0			

[a] $p, q, r=1, 2, 3, 4, 5, 6$.
[b] The symmetries listed at the top of each column are equivalent for the third-order elastic coefficients (and generally for polar properties of even order).

The last three columns of Table I have been derived from column C_3 by the "direct inspection" method.[4] Indeed, the Cartesian orthogonal coordinates chosen (which are of the usual type) do not transform into linear combinations of themselves under the generating elements to be added to the group C_3 to obtain the groups D_3 and C_{3h} or to be added to the group C_3 to obtain the group D_6. Column C_3 has been obtained by imposing invariance directly on each tensor component.[5]

The results of Table I have been obtained also by group theory. The method used can be applied to any tensor property of a material system of finite symmetry; it consists essentially in constructing the totally symmetrical linear combinations of tensor components in each group of interest, and in equating to zero the nontotally symmetrical linear combinations of the components contained in them. The equations of invariance that the method yields are very simple, since the vanishing components are eliminated from the start. Important simplifications are provided by the correlation tables of irreducible representations of groups and subgroups and by the replacement of Cartesian orthogonal components by coordinate products; the results for all subgroups can be obtained from the results for a group treated with proper completeness and the results for higher order tensors can be obtained from those for lower order tensors. Details of this method will be given in a paper to be published in *Nuovo Cimento*.

[1] F. G. Fumi, Phys. Rev. **83**, 1274 (1951).
[2] S. Bhagavantam and D. Suryanarayana, Acta Cryst. **2**(1), 21 (1949); H. A. Jahn, Acta Cryst. **2**(1), 30 (1949).
[3] The reference frames which are not distinguishable in relation to the symmetry elements of a given group are equivalent for it.
[4] F. G. Fumi, Acta Cryst. **5**, 44 (1942).
[5] C. Hermann, Z. Kryst. **89**, 32 (1934).

The Decay Energy of Si^{31}

A. H. WAPSTRA
Nobel Institute of Physics, Stockholm, Sweden *
(Received March 27, 1952)

THE difference in binding energies of P^{31} and Si^{28}, computed from Ewald's[1] mass spectrographical measurements, is 26.314 ± 0.036 Mev. This is in disagreement with the Q-values of some nuclear reactions studied at M.I.T.;[2] from $P^{31}(p, \alpha)Si^{28}$ Mev it follows that $P^{31}-Si^{28}=26.374\pm0.011$ Mev; from $P^{31}(d, \alpha)Si^{29}$ and $Si^{28}(d, p)Si^{29}$ it follows that $P^{31}-Si^{32}=26.373\pm0.015$ Mev. A check on these values can be made with the Q-values for the d, p reactions on the three Si isotopes in combination with the disintegration energy of Si^{31}. However, existing values[3-5] for this decay energy were not very precise.

We first tried to compare the Si^{31} and P^{32} absorption curves by the Feather method. We hoped that the similar end points and shapes of the β-spectrum (Si^{31} was expected to have an allowed form) would result in an accurate Feather plot. This hope was not substantiated in agreement with the later results of Wennerblom *et al.*[6] We found a range of 690 ± 20 mg/cm^2 in Al; with Glendenin's[7] range-energy relation this yields a β-energy of 1.53 ± 0.04 Mev. This part of the work was done in the Instituut voor Kernphysisch Onderzoek, Amsterdam, Netherlands.

We have now measured the β-spectrum of Si^{31} in an intermediate image β-spectrometer,[8] calibrated for this purpose with the internal conversion lines of Cs^{137} [9,10] and Co^{60} [11,12] The Si^{31} samples were prepared in the way described by Wennerblom *et al.*[6] The best sample used had a mean thickness of 0.5 mg/cm^2 and a backing of 0.15 mg/cm^2 Al; with this sample the Fermi plot was linear above 700 kev (lower energies were not measured for lack of suffi-

cient activity). This is in agreement with the fact that in the absorption experiments mentioned above no trace was found of any γ-rays.

The mean end point of two good agreeing runs was 1.486 ± 0.012 Mev, in agreement with the value 1.471 ± 0.008 Mev of Motz[15] that came to our attention after these measurements were completed.

With our value of this disintegration energy and the Q-values[2] of the (d, p) reactions on the three Si isotopes we find $P^{31}-Si^{28}=26.380\pm0.020$ Mev, in complete agreement with the results derived from Q-values above. So we must conclude that there is an error in Ewald's mass-spectrographic values.

The author wants to thank Professor M. Siegbahn for the opportunity to work in the Nobel Institute and the Instituut voor Kernphysisch Onderzoek for grants which made his stay in Sweden possible.

* On leave from the Instituut voor Kernphysisch Onderzoek, Amsterdam, Netherlands.

[1] H. Ewald, Z. Naturforsch. **6a**, 293 (1951).
[2] Endt, van Patter, Sperduto, and Buechner, Phys. Rev. **83**, 491 (1951); private communication of P. M. Endt.
[3] Kurie, Richardson, and Paxton, Phys. Rev. **49**, 203 (1936).
[4] H. W. Newson, Phys. Rev. **51**, 624 (1937).
[5] E. E. Widdowson and F. C. Champion, Proc. Phys. Soc. (London) **50**, 185 (1938).
[6] Wennerblom, Zimen, and Ehn, Svenskakemisk Tidskrift **63**, 207 (1951).
[7] L. E. Glendenin, Nucleonics **2**, No. 1, 12 (1948).
[8] H. Slätis and K. Siegbahn, Ark. Fys. **1**, 339 (1949).
[9] L. M. Langer and R. D. Moffat, Phys. Rev. **78**, 74 (1950).
[10] Lindström, Wapstra, and Siegbahn (to be published).
[11] Lind, Brown, and Dumond, Phys. Rev. **76**, 1838 (1949).
[12] D. A. Lind and A. Hedgran, Ark. Fys. (to be published).
[13] H. T. Motz, Phys. Rev. **85**, 501 (1952).

The Decay Energy of Pb^{209}

A. H. Wapstra *
Nobel Institute of Physics, Stockholm, Sweden
(Received March 27, 1952)

If we compute the decay energy of Pb^{209} from a closed cycle of decay energies and reaction energies,[1-4] we find a value ~0.4 Mev larger than the maximum energy of its β-spectrum. No γ-rays were found in the decay of this isotope. This may be explained in two ways: It is possible that the missing 0.4 Mev is emitted in the form of some successive, rather highly converted low energy γ-rays, as supposed by Harvey;[5] it is also not excluded that the decay of Pb^{209} yields a long-lived isomeric state in Bi^{209}.

We first investigated the second possibility. A very strong source of Pb^{209} was made by bombarding metallic lead with 26-Mev deuterons in the Philips' synchrocyclotron and purified. After 24 hours' decay the formed Bi was extracted. This Bi sample first decayed with a 6-day period due to some Bi^{206}, which had survived the purification, but after some months there was still a small activity that did not show any sign of decay. If interpreted as Bi^{209m} its half-life should be about 3×10^4 years. However, it is rather sure that this activity is due to the 60-year Bi^{207}, which was not known when we made these experiments. Thus Bi^{209m} should have a half-life much longer than expected for an isomer with such a rather high excitation energy (0.4 Mev).

In the same experiments we investigated the absorption curve of Pb^{209}. No sign was found of γ- or x-rays. The range, obtained by a Feather comparison with P^{32} and Au^{198}, was 220 ± 15 mg/cm^2 Al; with Glendenin's range-energy relation[6] this corresponds to 0.64 ± 0.03 Mev. This value is somewhat lower than the values reported before.[7-10] This part of the work was done in the Instituut voor Kernphysisch Onderzoek, Amsterdam, Netherlands.

We have now studied Pb^{209} in an intermediate image β-spectrometer.[11] The samples were prepared in the small Stockholm cyclotron. The best sample used had a mean thickness of 0.9 mg/cm^2 and a backing of 0.15 mg/cm^2 Al. With it the Fermi plot was linear above 200 kev; below this value some scattered electrons appeared. The mean end point of several runs was 635 ± 10 kev. This value is lower than the values reported before but in agreement with our absorption value above. The calibration of the β-spectrometer was checked with the F-line of the Th active deposit[12] and the internal conversion lines of Kr^{85}.[13]

A special search was made for conversion lines in the low energy region. No lines with an energy >30 kev and an intensity of more than 2 percent of the β-spectrum were found. In addition, we studied a strong sample in a NaI(Tl) scintillation spectrometer.[14] No γ-lines nor the K-radiations reported by Shure[6] were found. Lines with an intensity of 1 percent of the number of decays would be detected quite easily. So we must conclude that all evidence points to this β-transition being a ground-state transition.

We thank Professor M. Siegbahn for permission to work in the Nobel Institute the Nobel Institut för Fysik and the Instituut voor Kernphysisch Onderzoek for grants.

* On leave from the Instituut voor Kernphysisch Onderzoek, Amsterdam Netherlands.

[1] Kinsey, Bartholomew, and Walker, Phys. Rev. **82**, 380 (1951).
[2] J. A. Harvey, Phys. Rev. **81**, 353 (1951).
[3] Huizenga, Magnusson, Simpson, and Winslow, Phys. Rev. 79, 908 (1950).
[4] A. H. Wapstra, Physica **17**, 628 (1951).
[5] J. A. Harvey, private communication.
[6] L. E. Glendenin, Nucleonics **2**, No. 1, 12 (1948).
[7] W. Maurer and W. Ramm, Z. Physik **119**, 602 (1942).
[8] K. Fajans and A. F. Voigt, Phys. Rev. **60**, 619 (1941).
[9] W. Rall and R. G. Wilkinson, Phys. Rev. **71**, 321 (1947).
[10] J. S. Levinger and M. B. Sampson, reported in *Nuclear Data*, National Bureau of Standards Circular No. 499 (1950).
[11] H. Slätis and K. Siegbahn, Ark. Fys. **1**, 339 (1950).
[12] G. Lindström, Ark. Fys. **4**, 1 (1951).
[13] I. Bergström, Ark Fys. (to be published).
[14] B. Aström, Ark. Fys. (to be published).

Stopping Power of Polystyrene and Acetylene for Alpha-Particles*

R. H. Ellis, Jr., H. H. Rossi, and G. Failla
Radiological Research Laboratory, Columbia University, New York, New York
(Received April 4, 1952)

Uncertainty has existed for some time as to whether the same matter in different phases—solid, liquid, and gas—may exhibit different stopping powers. The question is of particular interest to radiological physicists who wish to determine the energy imparted to tissue by measuring the ionization in gases.

Theory has suggested that molecular binding should have little effect on stopping powers. Fermi[1,2] and Halpern and Hall[3,4] concluded that denser media should stop slightly less than their gaseous counterparts (on a mass basis) because of polarization of the stopping substance and a resulting distortion of the field of a particle.

Three experiments, on the other hand, have shown that water has a higher stopping power for alpha-particles than its vapor. Michl,[5] Philipp,[6] and Appleyard[7] have agreed that there is a difference of this sort of about 15 percent. De Carvalho,[8] however, found that the range of alpha-particles in water agreed with that in water vapor.

An apparatus has been developed for comparing directly the stopping of thin films with that of an equivalent thickness of gas. It is intended for use with water, but as an initial study polystyrene films have been compared with acetylene.

In an enclosure containing purified acetylene, a well-collimated beam of polonium alpha-particles reaches a windowless ionization chamber. A thin polystyrene film is interposed, and the change of ionization can be correlated with the stopping thickness of the film in terms of the number of milligrams per square centimeter of gas to which it is equivalent.

The thickness of the film is measured by optical means, using the interference fringes in light reflected from the film. This determination depends upon the assumption that the film has the density and index of refraction measured by using a prism of bulk polystyrene. The assumption concerning the index has been checked by photographing the interference spectrum from the films at various angles. The resulting shift of fringes yields the same index within a fraction of a percent.

A further check of the thickness measurement has been accomplished by weighing circles punched from the films. The accuracy of this method is restricted to ±5 percent, but within these limits there is agreement with the optical measurements and the assumption concerning density.

There is indication that polystyrene has a stopping power slightly less than that of acetylene. The difference is less than one percent, and this is probably smaller than the present limits of accuracy of the measurements. Since this condition was found to exist throughout the alpha-range, it is concluded that the relative stopping power of gas and solid is independent of alpha-energy.

* This document is based on work performed for the AEC.
[1] E. Fermi, Phys. Rev. **56**, 1242 (1939).
[2] E. Fermi, Phys. Rev. **57**, 485 (1940).
[3] O. Halpern and H. Hall, Phys. Rev. **57**, 459 (1940).
[4] O. Halpern and H. Hall, Phys. Rev. **73**, 477 (1948).
[5] W. Michl, Sitz. Kl. Akad. Wiss, Wien, **123**, 1965 (1914).
[6] K. Philipp, Z. Physik **17**, 23 (1923).
[7] R. K. Appleyard, Proc. Cambridge Phil. Soc. **47**, 443 (1950).
[8] H. G. De Carvalho, Phys. Rev. **78**, 330 (1950).

Scattering of Protons by the Loosely Bound Neutron in Beryllium

K. Strauch* and J. A. Hofmann†
Harvard University, Cambridge, Massachusetts
(Received March 24, 1952)

A STUDY is being made of the energy distribution of neutrons emitted by various targets when bombarded with a nominally 112-Mev internal proton beam (38-in. radius) of the Harvard cyclotron. This letter reports results observed with Be and C. Bodansky and Ramsey[1] have previously reported such data obtained in the forward direction at a slightly higher energy.

The ejected neutrons, after passing through the tank wall, were collimated by slits cut into a lead shield (28-in. thick) at angles of 0°, 5°, 10°, 16°, and 28° with respect to the proton beam. The neutrons were observed using a scintillation counter telescope to measure the energy distribution of recoil protons from a CH_2-C subtraction. Three points of the differential range spectrum were obtained simultaneously. The observed proton spectrum was converted into the original neutron spectrum by interpolating the results of Hadley *et al.*[2] for the angular dependence of the $n-p$ cross section and the more recent measurements[3] of total scattering cross section.

To obtain absolute cross sections, the proton beam was monitored by the activity induced in thin polystyrene foils placed against the targets.

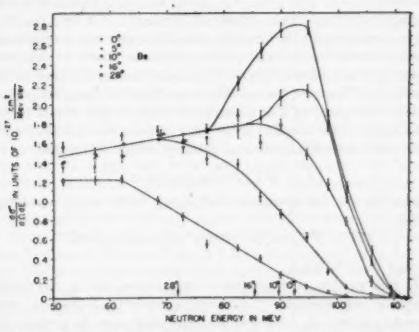

FIG. 1. Energy distribution of neutrons emitted from a 0.125-inch Beryllium target at several angles. The angles are measured with respect to the direction of the incoming proton beam. Arrows indicate the energy corresponding to 92.5 $\cos^2\theta_n$ Mev.

Figure 1 shows the results observed with a Be target. The standard deviations shown are due to counting statistics only. The high energy peak observed at 0° decreases rapidly with increasing angle. No such peak is observed in the neutrons emitted from C as shown in Fig. 2.[4] The angular dependence is not very pronounced at the smaller angles. These results suggest that the loosely bound neutron in Be^9 is responsible for the observed peak,[5]

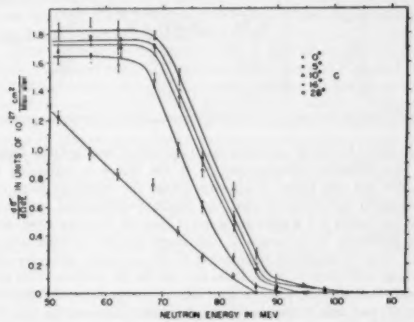

FIG. 2. Energy distribution of neutrons emitted from a 0.196-inch C target at several angles.

while the inner core corresponding to Be^8 might behave very much like the carbon nucleus.[6] A good estimate of the contribution of Be^8 to the observed spectrum from Be^9 might be the C^{12} spectrum multiplied by $(8/12)^1$. This factor follows from the observed A-dependence of high energy neutron yield measurements[7] and is also suggested by the theoretical considerations of Mandl and Skyrme.[8]

The results of this subtraction are shown in Fig. 3. It is believed that the shape of the peak obtained at 0° reflects primarily the energy distribution of the incident protons.[1] This depends on the position of the target (i.e., the effective thickness presented to the beam); to insure consistency in this respect the target was not moved during the course of a complete set of measurements. Other variables such as the ion source position could also affect the energy spread and it was not possible to keep these constant; this is estimated to introduce an additional 5 percent uncertainty into the measurements. The width of the peaks increases with the angle of observation.

If our interpretation is correct, then the area under the peaks in Fig. 3 represents the differential scattering cross section for the

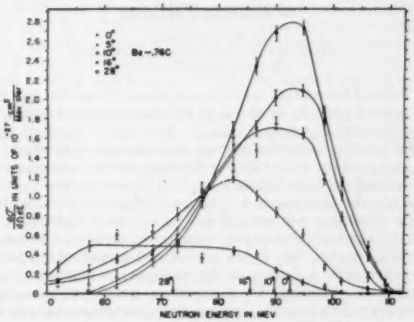

FIG. 3. Energy distribution of neutrons emitted by Be^9 after contributions from the "inner core" have been subtracted.

proton interaction with the loosely bound neutron in Be. The results given in Table I represent the average of two measurements (except for 16° where only one measurement was taken) and errors are estimated with respect to the 0° result only. The cross section

TABLE I. Differential cross section in units of 10^{-27} cm²/sterad for n-p scattering in the laboratory system.

		Free n-p (90 Mev)	
θ_n	n-p in Be	Hadley *et al.*	Fox
0°	55.9	67.8	~50
5°	49.7±2.6	51.3	49.2
10°	41.5±2.1	44.7	39.9
16°	30.4±2.2	35.2	
28°	17.7±0.9	21.8	

scale could be off by as much as 20 percent. Cross sections based on two different measurements[2,3] of the free n-p scattering at 90 Mev are also given. It appears within the relatively large experimental uncertainties that the absolute differential cross section for bound n-p scattering is lower than in the free case, and this tendency is increased at the larger angles of observation. This is to be expected since some of the outgoing neutrons will undergo collisions with the inner core of the Be nucleus. This secondary interaction becomes more important the lower the neutron energy, and thus accounts for the decreased cross section and the broadening of the neutron energy spectrum at the larger angles. In addition, since the bound n-p scattering takes place in a potential well, it should be compared with free n-p scattering at about 120 Mev.

* Society of Fellows.
† Central Scientific Company Fellow.
[1] D. Bodansky and N. F. Ramsey, Phys. Rev. **82**, 831 (1951).
[2] Hadley, Kelly, Leith, Segrè, and York, Phys. Rev. **75**, 351 (1949).
[3] J. DeJuren and N. Knable, Phys. Rev. **77**, 606 (1951); R. H. Hildebrand and E. C. Leith, Phys. Rev. **80**, 842 (1951); Taylor, Pickavance, Cassels, and Randals, Phil. Mag. **42**, 328 (1951).
[4] Cassels, Randle, Pickavance, and Taylor, Phil. Mag. **12**, 215 (1951), have observed a neutron peak using a C target with 171-Mev protons. The large difference in the shape of the neutron spectra obtained with 112-Mev and 171-Mev protons might be related to the rapid decrease of the total neutron cross section (reference 10) in the same energy interval.
[5] C. J. Mullin and E. Guth, Phys. Rev. **76**, 682 (1949), have shown that the low energy photodisintegration of Be^9 can be explained by assuming that the loosely bound neutron moves in the "effective field" of Be^8.
[6] This is supported by the similarity in neutron binding energies in C^{13} (18.7 Mev) and Be^8 (18.8 Mev).
[7] W. J. Knox, Phys. Rev. **81**, 687 (1951); K. Strauch and J. A. Hofmann (to be published).
[8] F. Mandl and T. H. R. Skyrme, A.E.R.E. (Harwell) Report No. TR745.
[9] R. H. Fox, University of California Radiation Laboratory Report No. 867 (1950).
[10] J. DeJuren and B. J. Noyer, Phys. Rev. **91**, 919 (1951).

An Argument Against the Majorana Theory of Neutral Particles

E. R. CAIANIELLO
Instituto di Fisica dell'Università, Turin, Italy
(Received March 27, 1952)

IT is well known that the Majorana theory[1,2] describes spin 1/2 neutral particles by means of self charge-conjugate fields, so that particles and antiparticles are described by identical half-fields[3] and the distinction between them ceases to be significant—or, as is more currently stated, a Majorana particle coincides with its antiparticle. In particular, it has been till now an open question whether the neutrino is a Dirac or a Majorana particle; the latter alternative has been invoked as a possible explanation of double beta-decay phenomena (whose actual occurrence, however, is still far from certain. For an exhaustive discussion of this point, see reference 3.) A decision on this matter is also of interest when investigating the possibility of a universal Fermi-type interaction among any four fermions, because such interaction would be incompatible with Majorana neutrinos.[4–6]

We prove here that the condition of self charge-conjugation is incompatible with the usual invariance requirements; identity of a field with its charge-conjugate is impossible, because they transform differently under space reversal. Clearly, this suffices to rule out the Majorana theory. What follows is merely an alternative and perhaps more rigorous proof of a statement already contained in reference 6, to which the reader is referred for further details, references, and discussion.

Let ψ and ψ^c represent a spin 1/2 field and its charge conjugate, I_S the operator which reverses the sign of all space coordinates. When $\mathbf{x}\rightarrow-\mathbf{x}$, it is known that $\psi\rightarrow\rho_S\gamma^4\psi$, $\psi^c\rightarrow\bar{\rho}_S\gamma^4\psi^c$.[2,6,7] The phase factor (type) ρ_S can have one of the values ±1, $\pm i$ with, eventually, different determinations for different particles. It is then clear that, as is well known, a Majorana theory is compatible only with the choices $\rho_S=\pm i$, or, which amounts to the same, $I_S^2=-1$. Our proof consists in showing that the only allowed possibilities are $\rho_S=\pm1$, i.e., $I_S^2=+1$. (See reference 6 for a simple proof of the fact that the square of any inversion operator, $+1$ or -1, must have always the same value regardless of the nature of the fermion field on which it acts, contrary to what was thought before[6,7] to be the case.)

The operator I_S is the product, in a given fixed order, of the operators I_λ corresponding to reversal of only one of the spatial coordinates x^λ, say $I_S=I_1I_2I_3$. We use the standard form of the Dirac equation, with imaginary time coordinate and Hermitean γ^μs. One finds immediately, in a purely algebraic manner, the explicit expressions for the I_λ's and their commutation properties: $I_\lambda=\rho_\lambda\gamma^\lambda\gamma^5$; $I_\lambda I_k+I_kI_\lambda=2\delta_{\lambda k}I_\lambda^2$; so that $I_S^2=(\rho_S\gamma^4)^2=(I_1I_2I_3)^2=-I_1^2I_2^2I_3^2$. It will suffice, therefore, to prove that $I_\lambda^2=-1$ (any λ), i.e., that the phase factors ρ_λ, which can again be restricted to have only the values ±1, $\pm i$, must all be real.

The reason for introducing four types as *a priori* possible under space reversals lies in the discontinuous nature of these operations, as well as in the singularity at the origin peculiar of spinorial functions and transformations, which shows up in their characteristic double-valuedness. One cannot thus decide *a priori* whether the square of an inversion must be $+1$ or -1. It is possible, however, to analyze the singularity and to eliminate the discontinuity in a quite simple manner by considering—as is certainly allowed and is standard procedure in algebraic geometry—the physical four-dimensional world as a manifold imbedded in a five-dimensional space, with an added space-like coordinate x^4 (to which is associated γ^5, which duly anticommutes with the γ^μs). In this enlarged world, I_λ becomes a rotation of $\pm\pi$ in the $(x^\lambda x^5)$-plane. We are, therefore, reduced to the study of rotations (that is, of continuous operations) in the five-dimensional space. The infinitesimal rotation in the plane $(x^\lambda x^\nu)$, as determined from the condition

$$\gamma^\mu T^{\lambda\nu}-T^{\lambda\nu}\gamma^\mu=\delta_{\lambda\mu}\gamma^\nu-\delta_{\nu\mu}\gamma^\lambda, \tag{8}$$

must be of the form $T^{\lambda\nu}=\frac{1}{4}\gamma^\lambda\gamma^\nu+\Delta_{\lambda\nu}\cdot1$, with $\Delta_{\lambda\nu}=-\Delta_{\nu\lambda}$ pure numbers ($\lambda\neq\nu$). The terms $\Delta_{\lambda\nu}$ are in reference 8 put=0 by imposing Sp $T^{\lambda\nu}=0$. This we are not allowed to do here because, when passing to finite rotations, the $\Delta_{\lambda\nu}$'s give rise to arbitrary phase factors; this is exactly the problem at hand, so that care must be taken of not introducing unjustified restrictions in the proof. It is, however, just as easy to see directly that all $\Delta_{\lambda\nu}$ must be=0. The proof of this statement—which is not trivial in our case, since a new coordinate has been introduced—follows simply from Lie's second fundamental theorem, which states that

$$[T^{\lambda\nu},\,T^{\rho\sigma}]_-=\Sigma_{\alpha\beta}\,c_{\lambda\nu,\,\rho\sigma,\,\alpha\beta}T^{\alpha\beta},$$

where the c's are constant coefficients. With $\lambda=\rho$, $\nu\neq\sigma$ this yields

$$[T^{\lambda\nu},\,T^{\lambda\sigma}]_-=[\tfrac{1}{4}\gamma^\lambda\gamma^\nu,\,\tfrac{1}{4}\gamma^\lambda\gamma^\sigma]_-=\tfrac{1}{4}\gamma^\sigma\gamma^\nu=T^{\sigma\nu},$$

so that $\Delta_{\sigma\nu}=0$, q.e.d.

It follows then, clearly, that a rotation of $\pm\pi$ in the $(x^\lambda x^5)$-plane is represented by $I_\lambda=\exp(\pm\frac{1}{2}\pi\gamma^\lambda\gamma^5)=\pm\gamma^\lambda\gamma^5$, so that $\rho_\lambda=\pm1$, $I_\lambda^2=-1$, $I_S^2=+1$, and our statement is proved. Although the case of time inversion requires quite different considerations,[6] we remark here that one finds, for both the Wigner and the Pauli type of time inversion, $I_4^2=-1$, as here with I_λ^2.

It is a by-product of the considerations reported above that spaces with an odd number of dimensions would behave in a quite different manner from spaces with an even number of dimensions when subjected to inversions (the relations $\gamma^\mu\gamma^5+\gamma^5\gamma^\mu=2\delta_{\mu 5}$, with $\gamma^5=\gamma^1\gamma^2\gamma^3\gamma^4$, can be extended only to the latter). This supports the view expressed by several authors that, should our world become too limited with only four dimensions, the natural generalization of it would be a six-dimensional, rather than a five-dimensional world.

Coming back to physics, we wish to point out, finally, that the rejection of the Majorana theory for the neutrino would not forbid the interpretation of double beta-decay phenomena, should they be definitely proved to occur. Some suggestions have already been made in this direction;[8,9] others may be advanced, in our opinion, but a discussion of this matter is, perhaps, premature.

[1] E. Majorana, Nuovo cimento **14**, 171 (1937).
[2] W. Pauli, Revs. Modern Phys. **13**, 203 (1941).
[3] J. Tiomno, thesis, Princeton University, 1950.
[4] E. R. Caianiello, Nuovo cimento **8**, 534 (1951).
[5] E. R. Caianiello, Nuovo cimento **8**, 749 (1951).
[6] E. R. Caianiello, Nuovo cimento (to be published).
[7] C. N. Yang and J. Tiomno, Phys. Rev. **79**, 495 (1950).
[8] W. Pauli, *Handbuch der Physik* (Verlag J. Springer, Berlin, 1933), Vol. 24, pp. 222–224.
[9] B. Touschek, Z. Physik **125**, 108 (1948).

An Experimental Search for Self-Trapped Electrons in the Alkali Halides*

WILLIAM H. DUERIG
University of Maryland, College Park, Maryland, and Applied Physics Laboratory, The Johns Hopkins University, Silver Spring, Maryland
(Received March 28, 1952)

TWO detailed calculations have been made on the self-trapped electron problem in ionic crystals originally proposed by Landau. Frohlich, Pelzer, and Zienau[1] treated the dielectric as a continuous medium with a single vibrational frequency for long longitudinal polarization waves. They concluded that the energy levels of these electrons do not exist below the conduction band and, in fact, differ little from the free electron. Thus, electrons would never be self-trapped but would move through the lattice almost as the free electron. Markham and Seitz[2] considered the dielectric as a discontinuous medium and utilized a self-consistent field method. Their calculations for NaCl gave thermal and optical activation energies of -0.13 ev and -0.68 ev, respectively. Therefore the self-trapping centers should be stable at 4.2°K, provided that the smearing out of the electron over several lattice sites does not permit it to diffuse rapidly through the crystal until it forms a more stable, e.g., F_2 center.

Since there is a fundamental difference in these approaches to the problem, it seemed advisable to perform an experimental observation on NaCl and KCl at 5°K. Crystals[3] produced by the Harshaw Chemical Company were mounted in a low temperature optical cell[4] and then x-rayed at 5°K[5] using a Machlett C-524A, molybdenum target x-ray tube operated at 50 kv and 48 ma. That this released large numbers of electrons into the conduction band was evidenced by the rapid growth of the F-band. The crystals were x-rayed in the dark for periods up to two hours and their absorption spectrum then measured at 5°K on three instruments to cover the spectrum from the F-band to about 15μ. This was necessary since the calculated optical activation energy of -0.68 ev (about 1.8μ in the absorption spectrum) is only an approximation. The spectral region 0.4μ to 1.2μ was measured on a Beckman Model DU Spectrophotometer taking care not to expose the crystal to any radiation except during the actual measurements. For the region from 1.0μ to 3.5μ a rapid scanning spectrometer[6] was used. A shutter arrangement permitted a complete spectrum to be obtained within 0.01 second after the light from a Nernst glower source first struck the crystal, thus preventing the possibility of optically bleaching the centers before a spectrum was obtained. The spectrum beyond 3.5μ was obtained with a Perkin-Elmer infrared spectrophotometer using a Golay detector. Here it was necessary to expose the crystal to the globar source continuously.

This experiment was repeated three times for NaCl and once for KCl. With the exception of a possible small F'-band in NaCl no bands were found to the infrared side of the F-band. KBr was also x-rayed at 5°K (1 hour at 50 kv and 20 ma) and its spectrum run only on the Beckman and Perkin-Elmer. Again no bands were found to the infrared of the F-band.

These measurements suggests that if the self-trapped electron exists, it diffuses easily through the lattice, even at 5°K, and thus that the binding energy is not greatly affected by the mean location of the electron, i.e., it can jump from a position of minimum binding energy to another even at these low temperatures, as suggested by Markham and Seitz. Perhaps at lower temperatures one might be able to freeze the electron at a lattice point long enough to be observed. In any event, the results appear to provide a strong justification for disregarding the lattice structure of the crystal above 5°K as was done by Frohlich, Pelzer, and Zienau.

The author would like to thank Dr. J. J. Markham for suggesting the problem and for his continued interest, and Mr. B. W. Bullock and Dr. S. Silverman for the use of their scanning spectrometer.

* This research was supported by the Bureau of Ordnance, U. S. Navy.
[1] Frohlich, Pelzer, and Zienau, Phil. Mag. **41**, 221 (1952).
[2] J. J. Markham and F. Seitz, Phys. Rev. **74**, 1014 (1948).
[3] The purity of these crystals is discussed in a paper on color centers at 5°K by the author and J. J. Markham (to be published).
[4] This cell is described in a paper by the author and I. Mador (to be published).
[5] This is the measured temperature the crystals attained when liquid helium was used as the coolant in the cell.
[6] B. W. Bullock and S. Silverman, J. Opt. Soc. Am. **40**, 608 (1950).

Energy Dependence of $(n, 2n)$ Reactions in Ni^{58}, Cu^{63}, and Tl^{203} from 11 to 19 Mev*

H. C. MARTIN AND B. C. DIVEN
University of California, Los Alamos Scientific Laboratory, Los Alamos, New Mexico
(Received March 31, 1952)

THE energy dependence of the $Ni^{58}(n, 2n)Ni^{57}$, $Cu^{63}(n, 2n)Cu^{62}$, and $Tl^{203}(n, 2n)Tl^{202}$ reactions has been investigated, using neutrons from the $D(T, n)He^4$ reaction[1] produced by the Los Alamos 2.5-Mev electrostatic accelerator.

A 1-cm long gas target[2] filled to 23-cm Hg pressure of deuterium was bombarded with a monatomic triton beam of approximately 1 microampere having an energy of 1.80 Mev in the center of the target gas volume. This gave a yield of about 1.4×10^7 neutrons/sec. Energies of the neutrons from the reaction varied from 18.5 Mev at 0° to 11.3 Mev at 180°. In the measurements presented here, it has been assumed that the neutron flux is symmetric in the laboratory coordinate system, which is true within experimental error of ±10 percent for triton bombarding energies near 1.2 Mev.

Samples were positioned accurately as to angle and distance from the center of the target gas volume by means of a light aluminum ring clamped near the end of the target tube. The nickel samples were folded strips 0.002-in. thick and weighing about 2 grams, while the copper samples were rolled strips 0.020-in. thick and weighing 20 grams. Four blocks of thallium, about 0.4 cm×1 cm×1 cm and weighing 5 grams each, were stacked at the angular positions corresponding to the neutron energies indicated in Fig. 3. The nickel and thallium samples were irradiated for 26 hours, the copper samples for 20 minutes.

After irradiation each nickel strip was wound in a helix around the outside of a thin-wall Geiger counter, and the activity was followed for 80 hours. In each case the 36-hour Ni^{57} decay was clearly observed as well as an activity of about 2 hours half-life, apparently due to the $Ni^{61}(n, p)Co^{61}$ reaction. Figure 1 shows the

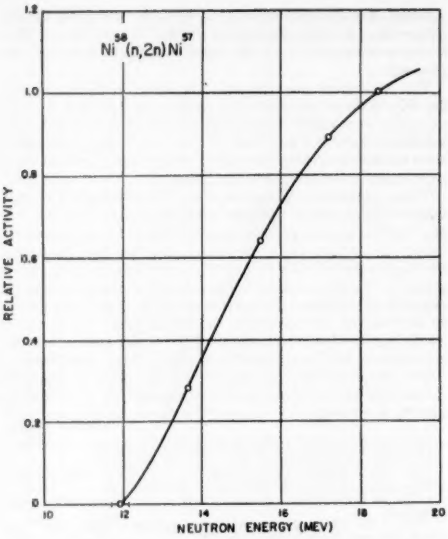

FIG. 1. Energy dependence of the $Ni^{58}(n, 2n)Ni^{57}$ reaction. Error in the relative activities is approximately ±5 percent.

relative 36-hour activities of the samples corrected for counter efficiencies and small sample weight differences. Relative efficiencies of the four Geiger tubes were determined by counting a uranium-glass source. Target length and sample size give a maximum spread in neutron energy of approximately ±1 Mev for each data point; the threshold indicated is that reported for the (γ, n) reaction,[3] corrected for the small center-of-mass effect. Counting rates were too low to permit a satisfactory measurement of the 72-day activity from the $Ni^{58}(n, p)Co^{58}$ reaction. A few percent of this activity could be present without noticeably distorting the 36-hour decay.

Two sets of copper samples were irradiated and counted in the same manner as the nickel. The activities yielded 9.8-minute decay curves in each case and were followed for several half-lives with no longer lived activities becoming apparent. The relative induced activities due to the $Cu^{63}(n, 2n)$ reaction are shown in Fig. 2, with a maximum neutron energy spread of about ±0.2 Mev at each point. Data from the two sets of samples are normalized at the highest neutron energy; the threshold indicated is again taken from the reported (γ, n) threshold.[4] The absolute value of the $Cu^{63}(n, 2n)Cu^{62}$ cross section near the threshold has been investigated by Fowler and Slye,[5] who report a cross section increasing somewhat more sharply with energy than the present data indicate.

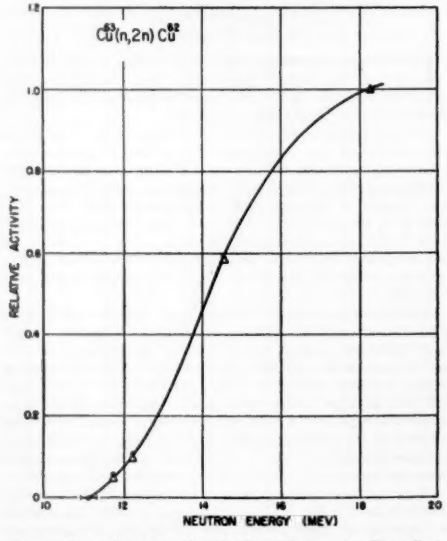

FIG. 2. Energy dependence of the $Cu^{63}(n, 2n)Cu^{62}$ reaction. The ordinate error at high energies is approximately ±3 percent, and for the points near threshold, ±10 percent.

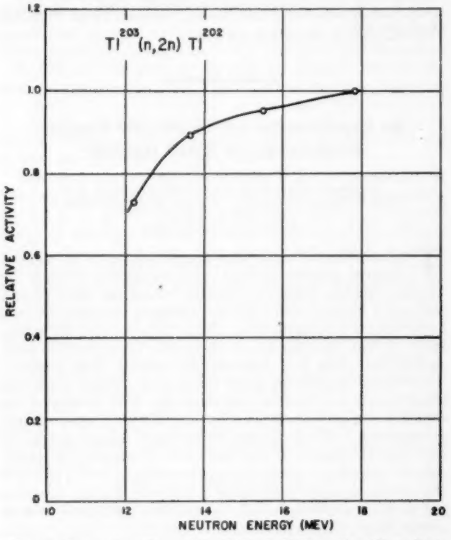

FIG. 3. Energy dependence of the $Tl^{203}(n, 2n)Tl^{202}$ reaction. The ordinate error is approximately ±6 percent. The threshold for this reaction is approximately 7.5 Mev.

For counting, the thallium samples were mounted about 1 mm from the surface of a 1½-in. diameter ×2-in. long crystal of a NaI(Tl) scintillation detector. A single channel analyzer was used to count pulses in the photopeak for the 431-kev thallium gamma-ray. The counting rate due to the Tl^{203} activity was initially about five times background. Each day the gain of the detector system was adjusted by observing the photopeak from the Cr^{51} gamma-ray and then the single channel analyzer was set to count on the photopeak of the Tl^{202} gamma. The decay of the thallium gamma-ray was followed for three half-lives and best fitted a 300±15 hour half-life in agreement with the measurement of 296±4 hours made by Prestwood[6] but not in good agreement with the 276 hours observed by Wilkinson.[7] The energy of the thallium gamma-ray was measured by comparison with the gammas of Cr^{51} (323 kev) and Cs^{137} (663 kev) and was found to be 431±10 kev, which is in agreement with the value 435±5 kev found by Wilkinson.[7]

The relative induced activities due to the $Tl^{203}(n, 2n)Tl^{202}$ reaction are shown in Fig. 3. The maximum neutron energy spread

is about ±1 Mev at each point. The statistical errors in counting, as well as variations in relative activities as observed from day to day are small compared to effects of uncertainties in positions of samples during the irradiation.

The authors are indebted to Miss Violet Kissee for counting the thallium samples, and to the electrostatic accelerator group for the irradiation.

* Work done under the auspices of the AEC.

[1] Hanson, Taschek, and Williams, Revs. Modern Phys. **21**, 635 (1949).
[2] Jarvis, Hemmendinger, Argo, and Taschek, Phys. Rev. **79**, 929 (1950).
[3] Ogle, Brown, and Carson, Phys. Rev. **78**, 63 (1950).
[4] J. McElhinney and W. E. Ogle, Phys. Rev. **78**, 63 (1950).
[5] J. L. Fowler and J. M. Slye, Phys. Rev. **77**, 787 (1950).
[6] Private communication from R. J. Prestwood of this Laboratory.
[7] G. Wilkinson, Phys. Rev. **79**, 1014 (1950).

The Neutron-Electron Interactions

SIDNEY BOROWITZ
Physics Department, New York University, University Heights, New York 53, New York
(Received April 1, 1952)

FOLDY[1] has recently shown that the magnetic moment of the neutron can interact with the electrostatic field of an electron. This interaction is usually expressed as a uniform potential extending over a distance equal to the classical electron radius. If one chooses the neutron moment as -1.91 nuclear magnetons, the interaction is attractive, and its strength is 3900 ev. This surprisingly large value has its origin in the "zitterbewegung" of the magnetic moment of the neutron, which is assumed to be a Dirac particle. This effect does not constitute, however, the total neutron-electron interaction. There is another attractive potential whose physical origin stems from the fact that the neutron is sometimes a proton with a negative meson charge cloud surrounding it.

The two effects differ as follows: They arise from the interaction of the field of the electron with the neutron polarization current in the first case, and with the neutron convection current in the second. Each of these effects can be calculated from meson theory. Although they depend separately on the coupling constant, their ratio is independent of it.

This ratio has been calculated, assuming an interaction of the neutron with symmetric pseudoscalar mesons. Equations (5.10) and (6.11) of Borowitz and Kohn[2] have been used in conjunction with a meson mass of $282m_e$. The result is that $\delta j_{\mu p}\cdot A_\mu/\delta j_{\mu c}\cdot A_\mu$ is equal to 3.23; here $\delta j_{\mu p}$ and $\delta j_{\mu c}$ are the corrections to the neutron polarization and convection currents, respectively. If one fixes the coupling constant in order that the theory yield the phenomenological value for the neutron moment, the convection current contribution to the neutron-electron interaction is 1208 ev. The total interaction would thus be equal to 5108 ev. The Slotnick and Heitler[3] formulas give 5073 ev if one uses the same meson mass and fixes their coupling constant to give the correct value of the neutron moment. These results are in good agreement with previously reported values,[4,5] and with the one recently measured by Hughes,[6] 4200 ± 700 ev.

This agreement, while interesting, is probably fortuitous for the following reasons: (1) The anomalous proton moment using the same coupling constant in the same theory would be about eight times too small. (2) It is unreasonable to suppose that a second-order perturbation calculation is correct, when the expansion parameter is so large.

Foldy's[1] conjecture that Slotnick and Heitler,[3] and Dancoff and Drell[7] have included both parts of the neutron-electron interaction in their results is thus supported. The discrepancy between their results and those of Case[8] and of Borowitz and Kohn[2] is largely resolved.[9]

[1] L. L. Foldy, Phys. Rev. **83**, 688 (1951).
[2] S. Borowitz and W. Kohn, Phys. Rev. **76**, 818 (1949).
[3] M. Slotnick and W. Heitler, Phys. Rev. **75**, 1645 (1949).
[4] E. Fermi and L. Marshall, Phys. Rev. **72**, 1139 (1947).
[5] Rainwater, Rabi, and Havens, Phys. Rev. **72**, 634 (1947); **75**, 1295 (1949).
[6] D. J. Hughes, Bull. Am. Phys. Soc. **27**, No. 1, 31 (1952).
[7] S. M. Dancoff and S. D. Drell, Phys. Rev. **76**, 205 (1949).
[8] K. M. Case, Phys. Rev. **76**, 1 (1949).
[9] Since this letter was completed, similar work by B. D. Fried has appeared [Phys. Rev. **86**, 464 (1952)]. The conclusions reached by him are essentially the same as those reported here.

Energy Available for Double Beta-Decay of Sn^{124}†

BENJAMIN G. HOGG AND HENRY E. DUCKWORTH
McMaster University, Hamilton, Ontario, Canada
(Received March 28, 1952)

THERE has been considerable interest in the possibility that double beta-decay may occur with a measurable half-life. This interest has been heightened by Fireman's observation[1] of a half-life of $0.4\text{–}0.9\times10^{16}$ years for the $Sn^{124}\text{–}Te^{124}$ transition. However, this observation has not been confirmed,[2–4] and studies of other potential double beta-emitters have yielded[5–7] negative results. Since the energy available for the decay is an essential datum for estimating the half-life, we have undertaken to measure this quantity with a mass spectrograph.

The $Sn^{124}-Ni^{62}$ and $Te^{124}-Ni^{62}$ doublets, photographed at mass number 62, yield the following mass differences: $\frac{1}{2}Sn^{124}-Ni^{62}=0.02378\pm12$ amu and $\frac{1}{2}Te^{124}-Ni^{62}=0.02297\pm19$ amu. The $Sn^{124}-Te^{124}$ mass difference is, therefore, 0.00162 ± 44 amu, or 1.5 ± 0.4 Mev. This value, according to the experiments[2] of Kalkstein and Libby, gives a lower limit for the lifetime of the Sn^{124} double beta-decay of $2.1\pm0.3\times10^{17}$ years.

This measurement was in part undertaken at the suggestion of K. G. Standing. The authors wish to acknowledge a most helpful conversation on this general subject with W. F. Libby.

† This research was supported by the National Research Council of Canada.
[1] E. L. Fireman, Phys. Rev. **75**, 323 (1949).
[2] M. I. Kalkstein and W. F. Libby, Phys. Rev. **85**, 368 (1952).
[3] John McCarthy, private communication, March 4, 1952.
[4] J. S. Lawson, Jr., Phys. Rev. **81**, 299 (1951).
[5] M. G. Inghram and J. H. Reynolds, Phys. Rev. **76**, 1265 (1949).
[6] Levine, Ghiorso, and Seaborg, Phys. Rev. **77**, 296 (1950).
[7] W. F. Libby, private communication, March 19, 1952.

Theory of Antiferromagnetic Resonance in a Crystal of Rhombic Symmetry at the Absolute Zero

J. UBBINK
Kamerlingh, Onnes Laboratory, Leiden, Netherlands
(Received March 24, 2952)

THE observed antiferromagnetic resonance phenomena in copper chloride, $CuCl_2\cdot2H_2O$, are only slightly dependent upon temperature at temperatures below about 3°K.[1] It appears to be possible to account for them on the basis of the analysis of antiferromagnetism in a crystal of rhombic symmetry at the absolute zero proposed by Gorter and Haantjes.[2]

We divide the lattice of magnetic ions into two sublattices i and j. An ion i is supposed to have a moment of momentum $(\hbar/2)\sigma^i$ and a magnetic moment $(\mu_1\sigma_1{}^i,\ \mu_2\sigma_2{}^i,\ \mu_3\sigma_3{}^i)$. Let the exhange energy between two neighboring ions i and j be $\Sigma_k(\gamma_k/z)\sigma_k{}^i\sigma_k{}^j$ (z is the number of nearest neighbors).

Introducing $h_k=\mu_kH_k$ (**H** is the external field), Gorter and Haantjes, who follow the phenomenological treatment of Néel[3] and Van Vleck,[4] find at each value and direction of **h** three solutions for the magnetic moments which are mathematically permissible. They show which of these solutions will be realized physically. On this basis the resonance problem has been treated following the method used by Kittel[5] and Nagamiya.[6]

The equation of motion for the sublattice averages of the moments is

$$\alpha\bar{\sigma}_1{}^i/dt=(2/\hbar)[\bar{\sigma}_3{}^i(h_2-\gamma_2\bar{\sigma}^j)-\bar{\sigma}_2{}^i(h_3-\gamma_3\bar{\sigma}^j)]$$

(cyclic, and the same for i and j interchanged). Taking the variation of this equation and assuming the dependence upon time of the variations of the variables to be $\exp(i\omega t)$, one finds the resonance condition by putting equal to zero the determinant of the coefficients of the variations of $\bar{\sigma}_1{}^i$, $\bar{\sigma}_2{}^i$, $\bar{\sigma}_3{}^i$, $\bar{\sigma}_1{}^j$, $\bar{\sigma}_2{}^j$, $\bar{\sigma}_3{}^j$. To find the resonance condition in the form of a direct relation between **h** and ω one has to substitute the physically realized solution of Goerter and Haantjes into the equation which is obtained.

Supposing $\gamma_1>\gamma_2>\gamma_3$, we confine ourselves to two cases corresponding to those which have been investigated experimentally.

1. $h_2=0$. According to Gorter and Haantjes there is a threshold hyperbola $(h_1^2/c^2)-(h_3^2/a^2)-1=0$, where $a^2=\gamma_3^2-\gamma_2^2$, $c^2=\gamma_1^2-\gamma_2^2$ are supposed to be small with respect to γ^2. When $\mathbf{h}$ passes this curve, the moments jump from the X–Z-plane (solution I) to directions near the Y-axis (solution II). The resonance condition applied to solution II yields $h_1^2/(c^2+\nu^2)-h_3^2/(a^2-\nu^2)-1=0$ (where $\nu=k\omega/2$), which is a hyperbola outside the threshold hyperbola (i.e., in the area which does not contain the center). The resonance condition applied to solution I yields a complicated equation, which for $\nu\to 0$ reduces to the threshold hyperbola and the points $h_1=\pm b=\pm(a^2+c^2)^{\frac{1}{2}}$, $h_3=0$. An approximation for small ν shows that the part which for $\nu\to 0$ coincides with the threshold hyperbola has moved inwards; the parts which for $\nu\to 0$ coincide with the points $h_1=\pm b$, $h_3=0$ have become closed curves in the neighborhood of these points. The latter curves, however, are irrelevant, since they lie in the region where solution *I* is not realized.

2. $h_2=0$. In this case the moments of the realized solution always have directions in the X–Y-plane. Applying the resonance condition yields again a complicated expression, which for $\nu\to 0$ reduces to the points $h_1=\pm c$, $h_3=0$. The approximation for small ν yields closed curves around these points, which, of course, intersect the h_1 axis in the same points as do the two curves found under 1.

All these results as well as the sign of the expected dispersion are in qualitative agreement with the observed phenomena. A fuller account and a quantitative comparison with the experiments will be published in *Physica*.

[1] Poulis, van den Handel, Ubbink, Poulis, and Gorter, Phys. Rev. **82**, 552 (1951); J. Ubbink, Proc. of the Internat. Conf. on Low Temp. Phys., Oxford, 163 (1951); Ubbink, Poulis, Gerritsen, and Gorter, Leiden Communications 288b (to be published in *Physica*).
[2] C. J. Gorter and J. Haantjes, Leiden Communicatoins, Supplement 104b (to be published in *Physica*).
[3] L. Néel, Ann. Phys. **11**, 232 (1936); **12**, 137 (1948).
[4] J. H. Van Vleck, J. Chem. Phys. **9**, 85 (1941).
[5] C. Kittel, Phys. Rev. **82**, 565 (1951).
[6] T. Nagamiya, Prog. Theoret. Phys. **6**, 350 (1951).

Scintillation Response of Organic Crystals to Low Energy α-Particles

J. W. KING AND J. B. BIRKS
Department of Physics, Rhodes University, Grahamstown, South Africa
(Received April 2, 1952)

THE scintillation responses of single flat crystals of anthracene, stilbene, and terphenyl to low energy α-particles have been studied, using a collimated Po^{210} source, and a 14-stage photomultiplier tube E.M.I. type 6262. The mean pulse size S, derived from the integral pulse distribution, was measured as a function of the mean residual air range r (at 15°C and standard pressure) of the α-particles incident on the crystal. Range corrections, which were small, were applied for the source thickness and for the slight divergence of the α-particle beam. The experimental response curve S *versus* r for stilbene is plotted in Fig. 1. Similar results were obtained for anthracene and terphenyl. It is found that for $r>$about 8 mm, S increases linearly with r, as observed previously by Birks,[1] but for $r<$about 8 mm the response S varies nonlinearly with r.

Birks[2,3] has formulated an exciton theory to account for the variation of the specific fluorescence dS/dr with the specific energy loss dE/dr of the exciting particle, leading to an expression

$$dS/dr=\frac{AdE/dr}{1+kBdE/dr}. \qquad (1)$$

The values for anthracene of $A=82.5$, $kB=7.15$ have been obtained experimentally. This theory accounts satisfactorily for the fluorescent response of organic crystals to electrons of energies >about 20 kev, to protons and deuterons>1 Mev (the minimum energy as yet investigated), and α-particles>about 1.6 Mev.[4]

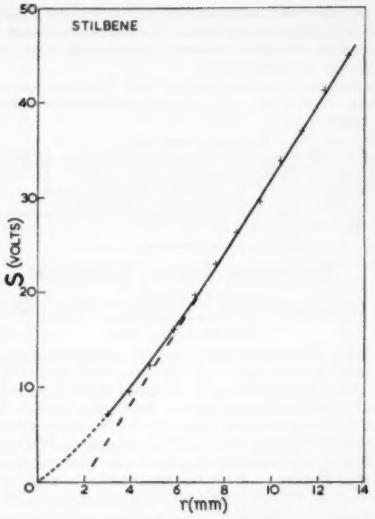

FIG. 1. Response of stilbene to α-particles of air-range r.

In particular, the theory indicates that for α-particles originating from Po^{210}, dS/dr is practically constant and independent of dE/dr. The experimental results in Fig. 1, and the similar curves for anthracene and terphenyl, show, however, that for $r<$about 8 mm, the value of dS/dr is less than that given theoretically by (1). The ratio ϕ of the experimental value of dS/dr from Fig. 1, to the theoretical value from (1), is plotted against r in Fig. 2. As r decreases from about 8 mm to zero, ϕ decreases from unity to 0.5. The value of r at which ϕ starts to decrease is approximately 8 mm for stilbene and terphenyl and 6 mm for anthracene. An extension of the exciton theory to account for this general effect has been formulated by Birks.[5]

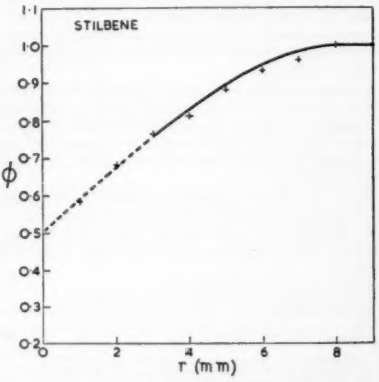

FIG. 2. ϕ [$=(dS/dr)$ experimental/(dS/dr) theoretical] *vs* α-particle air-range r.

A fuller account of this work will be published elsewhere. We are indebted to the South African Council for Scientific and Industrial Research for a grant, to Dr. M. E. Szendrei for the design of the amplifier used, and to Dr. S. W. Watson for the preparation of the Po^{210} source.

[1] J. B. Birks, Proc. Phys. Soc. (London) **A63**, 1294 (1950).
[2] J. B. Birks, Phys. Rev. **84**, 364 (1951).
[3] J. B. Birks, Proc. Phys. Soc. (London) **A64**, 874 (1951).
[4] Taylor, Jentschke, Remley, Eby, and Kruger, Phys. Rev. **84**, 1034 (1951)
[5] J. B. Birks, Phys. Rev. **86**, 569 (1952).

Theory of the Response of Organic Scintillation Crystals to Short-Range Particles

J. B. Birks
Department of Physics, Rhodes University, Grahamstown, South Africa
(Received April 2, 1952)

A GENERAL exciton theory has been previously formulated[1,2] to account for the dependence of the specific fluorescence dS/dr of an organic crystal on the specific energy loss dE/dr of the exciting particle. If AdE/dr is the number of excitons produced per unit path length, BdE/dr is the local concentration of molecules damaged by the incident particle, and k is the relative exciton capture probability of a damaged molecule, then

$$dS/dr=\frac{AdE/dr}{1+kBdE/dr}. \tag{1}$$

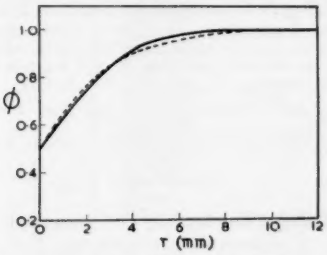

FIG. 1. ϕ *versus* r for electrons in anthracene. ——— Experimental (Taylor *et al.*); – – – Theoretical (a_0=1.6 mm air).

This theory accounts satisfactorily for the scintillation response of organic crystals to all types and energies of incident ionizing particles, except those of short range.

Taylor *et al.*[3] have observed that the specific fluorescence of anthracene excited by electrons of energy <20 kev (i.e., of residual air range r<about 7 mm) falls below the general smooth curve of dS/dr *versus* dE/dr, that is below the value given by (1). The specific fluorescence $(dS/dr)_{expt}$ for electrons in anthracene has been calculated from these observations, using the range-energy data of Curie,[4] and it has been compared with the value $(dS/dr)_{theor}$ given by (1). The ratio $\phi=(dS/dr)_{expt}/(dS/dr)_{theor}$ is plotted as a function of r in Fig. 1. ϕ decreases from unity at r>about 7 mm to 0.5 at $r=0$. Very similar behavior has been observed by King and Birks,[5] when anthracene and other organic crystals are excited by short-range α-particles. The experimental curve of ϕ *versus* r for α-particle excitation is similar to Fig. 1 for electron excitation.

This effect may be accounted for by an extension of the exciton theory. Equation (1) is valid for exciton production and capture within the bulk of an organic crystal, but an additional multiplying factor ϕ, which is a function of r, must be introduced into (1) to account for the behavior of excitons produced near the crystal surface. If the exciton originates at a point O, then its probability of travelling a distance a from O is $\exp(-a/a_0)$, where a_0 is the mean free path of the exciton. If O is at a distance r from the crystal surface (Fig. 2), and it is assumed that an exciton reaching the surface without capture escapes from the crystal, then the probability of exciton capture within the crystal is given by

$$\phi=\int_{-\infty}^{r}dz\int_{0}^{\infty}\exp(-a/a_0)2\pi x\,dx\Big/\int_{-\infty}^{\infty}dz\int_{0}^{\infty}\exp(-a/a_0)2\pi x\,dx$$
$$=1-\tfrac{1}{2}(r/a_0+2)\exp(-r/a_0). \tag{2}$$

The complete theoretical expression for dS/dr is now given by the R.H.S. of (1), multiplied by ϕ. ϕ decreases from unity to 0.5,

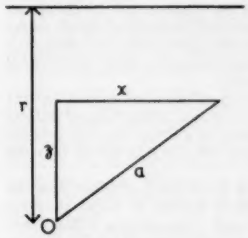

FIG. 2. Coordinates for Eq. (2).

as r decreases from ∞ to zero. The curve of ϕ *versus* r from (2), taking a value of a_0=1.6 mm air equivalent, is plotted in Fig. 1. It is in fair agreement with the experimental curve, considering that no allowance has been made for electron scattering. The probable existence of preferred directions of exciton propagation has also been neglected in the derivation of (2).

A similar comparison with the α-particle observations[5] gives a_0 about 3–4-mm air equivalent for anthracene, terphenyl, and stilbene. The relative stopping power of each material for slow α-particles[6] is about 1200, so that the exciton mean free path within the crystal is the order of 3 microns, corresponding to about 5000 molecular lengths.

The results of Taylor *et al.*[3] on the scintillation response to protons and deuterons of energies>1 Mev, indicate that at lower energies ϕ decreases in a similar manner, but no direct measurements are yet available for these particles at low energies. Experiments are now in progress on the response to low energy electrons produced *within* the crystal by x-rays. According to the theory outlined above, ϕ should be equal to unity for such internal electrons, and the response should differ from that excited by external electrons of the same energy. An investigation is also being made of the properties of very thin crystals.

I am indebted to the South African Council for Scientific and Industrial Research for a grant in support of this work.

[1] J. B. Birks, Phys. Rev. **84**, 364 (1951).
[2] J. B. Birks, Proc Phys. Soc. (London) **A64**, 874 (1951).
[3] Taylor, Jentschke, Remley, Eby, and Kruger, Phys. Rev. **84**, 1034 (1951).
[4] Mme. P. Curie, *Radioactivité* (Hermann & Cie, Paris, 1935).
[5] J. W. King and J. B. Birks, Phys. Rev. **86**, 568 (1952).
[6] M. S. Livingston and H. A. Bethe, Revs. Modern Phys. **9**, 245 (1937).

Composition and Time Variation of Primary Cosmic Radiation

D. Lal, Yash Pal, M. F. Kaplon, and B. Peters
Tata Institute of Fundamental Research, Bombay, India, and University of Rochester, Rochester, New York
(Received March 24, 1952)

THE flux of heavy primary nuclei at geomagnetic latitude $\lambda=3°$ has been measured in nuclear emulsions exposed during balloon flights in the stratosphere.[1] This experiment com-

pletes essentially the investigations begun in 1948 for the purpose of studying the latitude effect of primary nuclei of charge $Z>1$. The flux values obtained in two separate flights near the magnetic equator agree well within statistical accuracy and are given by $I(\lambda=3^{\circ})=1.30\pm0.25$ particles/m² sec steradian for $6\lesssim Z\lesssim 10$, and $I(\lambda=3^{\circ})=0.30\pm0.07$ particles/m² sec steradian for $Z>10$.

Previously[2] it has been shown that all primaries arrive from outer space completely stripped of orbital electrons and that, therefore, the flux values at different latitudes permit the construction of an integral energy spectrum for the various components. The flux values obtained at the equator are in good agreement with the energy spectrum given in reference 2.

Our knowledge of the spectrum in the energy region above geomagnetic cut-off energies is less complete both for the proton and the heavy components. However, the results of various recent investigations permit us to describe quite reliably the charge and energy dependence of primary particles up to about one hundred times the equatorial cut-off energy.

On the basis of Fermi's theory of meson production and the range spectrum of mesons below ground, Haber-Schaim[3] deduces an integral spectrum proportional to $\epsilon^{-1.66}$ for the total primary radiation in the energy interval $10^{11}<\epsilon<1.2\times10^{13}$ ev (ϵ is the energy per nucleon).

Independent support for this power law is obtained from the photographic emulsion technique applied to Auger showers.[4] Preliminary results[5] obtained with this technique indicate that the flux, not only of protons but also of primary helium nuclei, is in the energy interval $10^{10}<\epsilon<4\times10^{12}$ ev consistent with the power law exponent derived from observations on mesons.

Also heavy nuclei of charge $Z>10$ seem to follow the same power spectrum. This was verified up to energies of 5×10^{10} ev/per nucleon with the help of nuclear collisions.[3] Occasional observations on nuclei of still larger energies, however, make it certain that no drastic change in the exponent occurs up to about 5×10^{11} ev/nucleon.

Thus we are led to the conclusion that the chemical composition of the primary beam is essentially constant not only in the latitude sensitive region but even at much higher energies. The uniformity of composition holds at least over a factor 1000 in the energy per nucleon, a range of energies which comprises all but one part in ten thousand of the incoming primaries and at least 95 percent of the incident energy.

The incident cosmic-ray energy carried by various primary components is approximately distributed as follows:

66 percent due to protons;
26 percent due to helium nuclei;
5 percent due to carbon, nitrogen, and oxygen;
3 percent due to nuclei of atomic number $Z\geq10$.

It is important to note that this distribution, which has previously been obtained[6] for a much more restricted range of energies, has now been shown to be valid for the primaries which produce the bulk of cosmic radiation at sea level ($5\times10^{9}<\epsilon<5\times10^{11}$ ev/nucleon) and therefore represents also the relative contribution of different components to the sea level intensity. Thus, since the sea level intensity if corrected for barometric and temperature effects shows a variation with solar time of only about 0.3 percent and a variation with sidereal time of less than 0.02 percent,[7] it follows that even for the heaviest primary nuclei in this energy range the variation with solar time must be less than 10 percent and with sidereal time less than 1 percent.

[1] A full description of these experiments, which were carried out jointly by the Tata Institute of Fundamental Research and the University of Rochester will be published elsewhere.
[2] Kaplon, Peters, Reynolds, and Ritson, Phys. Rev. **85**, 295 (1952).
[3] U. Haber-Schaim, Phys. Rev. **84**, 1199 (1951).
[4] Kaplon, Peters, and Ritson, Phys. Rev. **85**, 900 (1952).
[5] Kaplon, Ritson, and Woodruff, Phys. Rev. **85**, 933 (1952).
[6] B. Peters, *The Nature of Primary Cosmic Radiation* (North-Holland Publishing Company, 1952), Chapter IV, "Progress in Cosmic Ray Physics."
[7] H. Elliot, see reference 6, Chapter VIII.

Internal Conversion of the 0.411-Mev Gamma-Ray of Hg^{198}

LENNART SIMONS
Institute of Physics, University of Helsingfors, Helsingfors, Finland
(Received March 25, 1952)

ON the basis of the measured spectra of the beta- and gamma-rays of Au^{198} [1] the K, L, and M conversion coefficients of the 0.441-Mev gamma-ray were found with an accuracy better than one percent to be $\alpha_K=0.0318$; $\alpha_L=0.0103$; $\alpha_M=0.0031$. The values were obtained on the supposition of a one-to-one occurrence of a 0.965-Mev electron and a 0.411-Mev gamma-quantum. On the other hand, if one assumes according to Cavanagh[2] that in addition to the 0.965-Mev beta-ray the 0.29-Mev beta-ray (branching ratio 1.76 percent) is followed in part by the 0.411-Mev gamma-ray after a 0.67-Mev gamma-emission (branching ratio 1.43 percent), one obtains for the 0.411-Mev gamma-ray $\alpha_K=0.0307$. The vanishing intensity of the 1.37-Mev beta-ray has been neglected and the branching ratio of the K-capture transition to Pt^{198} has been estimated to be approximately five percent. Considering the accuracy of the measurements, this latter value of the K conversion coefficient for the 0.411-Mev gamma-ray of Hg^{198} agrees exceptionally well with the theoretical value, $\alpha_K=0.031$, obtained by interpolation of the coefficients calculated by Rose *et al.*[3] for electric quadrupole radiation. An agreement between theory and experiment has thus been established and one may unambiguously conclude that the 0.411 gamma-ray of Hg^{198} is a pure electric quadrupole radiation.

[1] L. Simons and E. P. Tomlinson, Soc. Sci. Fenn. Comm. Phys. Math. XVI, 6 (1952).
[2] P. E. Cavanagh, Phys. Rev. **82**, 791 (1951).
[3] Rose, Goertzel, Spinrad, Harr, and Strong, Phys. Rev. **83**, 79 (1951).

Thermal Conductivity of Germanium

A. GRIECO AND H. C. MONTGOMERY
Bell Telephone Laboratories, Murray Hill, New Jersey
(Received March 21, 1952)

A MEASUREMENT has been made of the thermal conductivity of high purity, single-crystal germanium, made by the method of Teal and Little.[1] Conductivity was determined from the relative temperature drops along rods of germanium and some material of known conductivity, placed thermally in series. Nickel and cast zinc of high purity were used for the comparison materials. With precautions taken to minimize errors from heat losses, it is believed the measurements are accurate to better than ±10 percent.

The germanium specimen was cut from a single crystal of n-type material of resistivity about ten ohm-cm. Its dimensions were 5/16 inch square cross section by 3/4 inch long, with the long dimension oriented along a 100 crystal axis. The thermal conductivity was found to be 0.14 cal/sec cm °C at 25°C, and roughly 20 percent less at 100°C.

[1] G. K. Teal and J. B. Little, Phys. Rev. **78**, 647 (1950).

Short Duration Afterglow of Nitrogen in the Photographic Infrared

R. HERMAN, L. HERMAN, AND G. HEPNER
Observatoire de Meudon, Meudon (Seine et Oise), France and Laboratoire des Recherches Physiques, Sorbonne, Paris, France
(Received March 31, 1952)

KAPLAN[1] was the first to study the afterglow of long duration (0.1 to 1 sec) which produces the first negative band system, $B^2\Sigma-X^2\Sigma$, of N_2^+. A short duration afterglow (10^{-4} to 10^{-2} sec) emitting the same band system has been described by us elsewhere.[2] The present note is concerned with an extension of

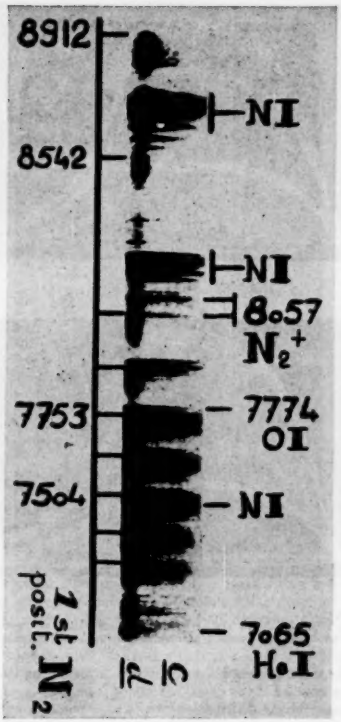

FIG. 1. Emission spectrum of a helium-nitrogen gas mixture. *d*-discharge spectrum. *c*-afterglow spectrum. In *d*, the 7065 He I line and the first positive system $B^3\Pi - A^3\Sigma$ of N_2 are very strong. In *c*, the 8057 band of N_2^+ is clearly visible.

our short duration afterglow studies into the photographic infrared.

A pulse discharge was used to excite a mixture of helium, at a pressure of 5 mm, and a small amount of nitrogen. The spectra of the discharge and the afterglow were separated by a rotating disk.

An example of the spectrum obtained is shown in Fig. 1. Part *d* of this spectrum is emitted during the discharge and part *c* during about 10^{-4} second immediately after the discharge is stopped. It is seen that relative intensities of the several spectral features are quite different in the afterglow from those in the discharge proper. The apparent electronic excitation during the discharge is much lower than during the afterglow. For example, the first positive band system, $B^3\Pi - A^3\Sigma$ ($T_e = 7.4$ ev), is strong in *d* and weak in *c*. In the violet and ultraviolet region, the second positive band system, $C^3\Pi - B^3\Pi$ ($T_e = 11.0$ ev) of N_2, is also very weak in the afterglow spectrum. On the other hand, high level emissions, such as the Meinel system of N_2^+, $A^2\Pi - X^2\Sigma$, ($T_e = 16.8$ ev) and the N I (I.P. = 14.54 ev), N II (I.P. = 44.14 ev), and O I (I.P. = 13.61 ev) lines show a much smaller contrast between the discharge and the afterglow intensities. In the negative system of N_2^+ emitted during the afterglow the intensity of the 8057 (3, 1) band is higher than the 7828 (2, 0). On the other hand, in the auroral spectrum the (2, 0) band is the more intense.

The present results indicate that the process of excitation of the positive bands is different from that of the negative bands and atomic lines. These latter may be emitted by ion electron recombination, a process which becomes relatively more important during the afterglow.

[1] J. Kaplan, Phys. Rev. **42**, 807 (1932); **54**, 176 (1938).
[2] R. Herman and L. Herman, J. phys. et radium (VIII) **10**, 132 (1949).

498-kev Gamma-Ray of Ru^{103}

ARTHUR W. KNUDSEN
Nucleonics Division, Naval Research Laboratory, Washington, D. C.
(Received March 26, 1952)

AN accurate value for the energy of the 498-kev gamma-ray from Ru^{103} has been obtained with a double-focusing beta-spectrometer of the type described by Kurie, Osaba, and Slack.[1] The gamma-ray source was double, consisting of pile-irradiated ruthenium powder sealed in a glass tube and a metal enclosure (beryllium) providing annihilation quanta from the positron-emitting sodium-22 contained inside. Gammas from the two sources simultaneously irradiated a 0.7-mil thick uranium foil radiator, and the *K*-level photoelectric lines were recorded in the spectrometer. The difference in energy between the two lines (that of the annihilation gamma being the greater) was found to 13.1 ± 0.8 kev.

When the value 510.969 ± 0.010 kev given by DuMond and Cohen[2] for the energy of annihilation quanta is used, we obtain the value

$$497.9 \pm 0.8 \text{ kev}$$

for the energy of the ruthenium gamma-ray. A value of 494 kev (presumably for this same gamma-ray) has been given by Mei, Huddleston, and Mitchell.[3]

[1] Kurie, Osaba, and Slack, Rev. Sci. Instr. **19**, 771 (1948).
[2] J. W. N. DuMond and E. R. Cohen, Phys. Rev. **82**, 555 (1951).
[3] Mei, Huddleston, and Mitchell, Phys. Rev. **79**, 237 (1950).

Pion Production and Charge Independence*

J. M. LUTTINGER
Department of Physics, University of Wisconsin, Madison, Wisconsin
(Received March 26, 1952)

THE purpose of this letter is to point out that the observation of pion production in nucleon-nucleon and in nucleon-deuteron collisions provides a very severe test of the assumption that the interaction between pions and nucleons is charge independent. Just as we think of the proton-neutron field as having an intrinsic isotopic spin of $\frac{1}{2}$ ($+\frac{1}{2}$ for proton, $-\frac{1}{2}$ for neutron), we may also think of the meson field as having an intrinsic isotopic spin of 1 ($+1$ for π^+, 0 for π^0, -1 for π^-).[1] The assumption of charge independence will then mean that we assume the interaction to be such that the total isotopic spin is not changed as a result of it.

For simplicity let us consider first the case of meson production by proton (or neutron) collisions with deuterium. Since the deuteron is in a $^3S + {}^3D$ state, it is symmetric in space and spin and, therefore, antisymmetric in isotopic spin. The total isotopic spin of the deuteron is therefore zero. Thus, the system proton plus deuteron has total isotopic spin $T = \frac{1}{2}$, three component of total isotopic spin $T_3 = \frac{1}{2}$. After the pion has been produced, the final state will consist of three nucleons and one pion. For the three nucleons, each with isotopic spin $\frac{1}{2}$, we get as possible states $T^N = \frac{3}{2}$ or $\frac{1}{2}$. This gives us two cases to consider:

1. Final nucleon state $T^N = \frac{3}{2}$. Using the well-known transformation properties of angular momenta,[2] we may write for the final state (t denoting the isotopic spin of the meson)

$$\phi(T = \tfrac{1}{2}, T_3 = \tfrac{1}{2}) = (1/\sqrt{2})\Psi(T_3{}^N = \tfrac{3}{2}, t_3 = -1) - (1/\sqrt{3})\Psi(T_3{}^N = \tfrac{1}{2}, t_3 = 0) + (1/\sqrt{6})\Psi(T_3{}^N = -\tfrac{1}{2}, t_3 = 1).$$

This is the same as saying

$$p+d\rightarrow\tfrac{1}{3}(p+p+p+\pi^-)+\tfrac{1}{3}(p+p+n+\pi^0)+\tfrac{1}{3}(p+n+n+\pi^+),$$

where the coefficients give the relative probabilities of the different processes.

2. Final nucleon state $T^N=\frac{1}{2}$. As before,

$$\phi(T=\tfrac{1}{2},\ T_3=\tfrac{1}{2})=(1/\sqrt{3})\Psi(T_3{}^N=\tfrac{1}{2},\ t_3=0)+(\sqrt{2}/\sqrt{3})\Psi(T_3{}^N=-\tfrac{1}{2},\ t_3=1),$$

from Condon and Shortley. This is the same as writing

$$p+d\rightarrow\tfrac{1}{3}(p+p+n+\pi^0)+\tfrac{2}{3}(p+n+n+\pi^+),$$

the coefficients giving the relative probabilities once again.

Now suppose the probability of going into $T^N=\frac{3}{2}$ is x, $T^N=\frac{1}{2}$ is $1-x$ (x is of course a function of angle and energy in general). Then, apart from a common factor, we have

$$\sigma_+=\tfrac{1}{3}(x)+\tfrac{2}{3}(1-x)=\tfrac{2}{3}-\tfrac{1}{3}x,$$
$$\sigma_-=\tfrac{1}{3}(x),$$
$$\sigma_0=\tfrac{1}{3}(x)+\tfrac{1}{3}(1-x)=\tfrac{1}{3},$$

where σ_+ is the cross section for producing π^+ mesons at any angle and energy, and σ_-, σ_0 are the corresponding cross sections for π^- and π^0 mesons, respectively. Adding the first two equations, we obtain $\sigma_++\sigma_-=\frac{2}{3}$ and thus

$$\sigma_++\sigma_-=2\sigma_0 \quad (p+d \text{ or } n+d \text{ collisions}). \qquad (1)$$

This relationship between the production cross sections for pions must hold independent of energy and angle, and it should be subject to direct experimental check as soon as our knowledge of these cross sections improves.

Proceeding in an exactly similar manner, we can obtain the following relationship among the cross sections for pion production in nucleon-nucleon collisions:

$$\sigma(p+p\rightarrow p+n+\pi^+)=2[\sigma(n+p\rightarrow n+p+\pi^0)+\sigma(p+p\rightarrow p+p+\pi^0)-\sigma(n+p\rightarrow n+n+\pi^+)], \qquad (2)$$

which is also independent of energy or angle. This result may also be derived at once from Watson and Brueckner's[1] Eq. (17). In the special cases they considered, it reduces to their results. It is important to stress, however, that (1) and (2) assume only charge independence of the pion-nucleon interaction and make no assumptions whatever as to the details of this interaction.

* Since completing this work, I have been informed by Mr. A. M. L. Messiah that he has submitted identical results in the Letters to the Editor Section [Phys. Rev. **86**, 430 (1952)].

[1] W. Heitler, Proc. Roy. Irish Acad. **51**, 33 (1946); K. M. Watson and K. A. Brueckner, Phys. Rev. **83**, 1 (1951).

[2] E. V. Condon and G. Shortley, *The Theory of Atomic Spectra* (Cambridge University Press, London, 1951), p. 76.

Angular Distributions of Inelastically Scattered Protons from C^{12} and Mg^{24} †

H. E. Gove and H. F. Stoddart

Department of Physics and Radioactivity Center of the Laboratory for Nuclear Science and Engineering, Massachusetts Institute of Technology, Cambridge, Massachusetts

(Received March 27, 1952)

A NaI scintillation counter for detecting heavy charged particles has been built and used for measuring the angular distributions of inelastically scattered protons from targets bombarded with 7.3-Mev protons from the M.I.T. cyclotron. A complete description of this detector will be published at a future date but, briefly, it consists of a thin flat NaI crystal cleaved on all six sides and mounted in an aluminum reflector arrangement on the end of an RCA 5819 photomultiplier. Sodium iodide was chosen because of the linear relation between the output pulse height and the proton energy.[1]

The counter, which has no window and can detect protons of all energies, is mounted on one of the movable arms in the M.I.T. scattering chamber.[2] Its angular position relative to the incident proton beam can be varied continuously from 20° to 160° to an accuracy of ±0.5°.

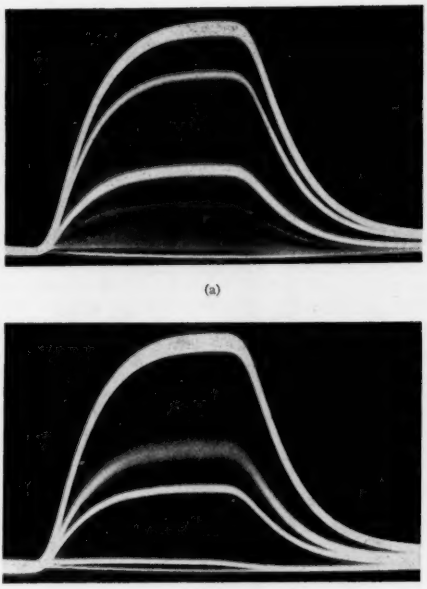

(a)

(b)

FIG. 1. Photographs of the pulse-height distribution of protons from magnesium (a) and carbon (b) bombarded by 7.26-Mev protons.

The pulse-height distribution can be obtained by photographing the oscilloscope face with a time exposure. In the photographs presented here there are a total of about 10^5 counts. Figure 1(a) shows the proton groups emitted at about 45° from a thin isotopic magnesium target. The two strongest inelastic groups correspond to the well-known levels in Mg^{24} at 1.38 and 4.14 Mev.[3] From the position of these two groups and the elastic group it is possible to calculate the incident proton energy (7.26±0.04 Mev) and to conclude that NaI has a linear response to proton energy to within 4 percent. Figure 1(b) shows the proton groups from a 0.4 mg/cm² aquadag target. The two sharp groups correspond to the ground state and first excited level in C^{12} at 4.45 Mev.[4] The broad group is due to elastically scattered protons from hydrogen contamination.

The angular distributions of the inelastic proton groups corresponding to the 1.38-Mev level in Mg^{24} and the 4.45-Mev level in C^{12} have been measured with a very stable single-channel analyzer.[5] The results are shown in Fig. 2. The broken curves through the data points represent the best fit obtained with a Legendre polynomial expansion whose coefficients are given in Table I. The average standard deviation of the data from the expansion is 3 percent for C^{12} and 4.5 percent for Mg^{24}, which can be accounted for on the basis of statistical fluctuations in the counts and, in the case of Mg, inaccuracies in subtracting out a small satellite peak,

TABLE I. Legendre polynomial coefficients for center-of-mass angular distributions.

Reaction	A_0	A_1	A_2	A_3	A_4	A_5	A_6	A_7
$C^{12}(p,p')$	1.00	0.24	0.77	0.17	0.06	−0.04	−0.08	0
$Mg^{24}(p,p')$	1.00	0	0.65	0.40	−0.45	0.10	0	−0.10

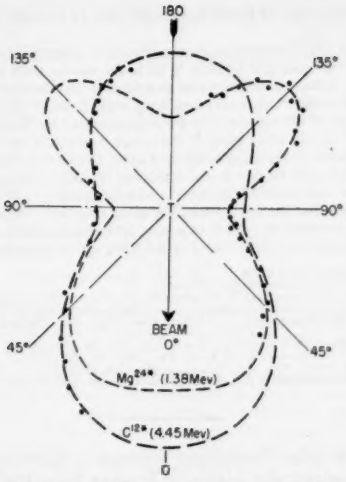

FIG. 2. The angular distributions of the $C^{13}(p,p')C^{13*}$ $Q=-4.45$ Mev and the $Mg^{24}(p,p')Mg^{24*}$ $Q=-1.38$ Mev-reactions in the center-of-mass system.

present to about 10 percent on the low energy side of the 1.38-Mev level.

In both cases the spin of the target nucleus is zero, even parity, and that of the residual Mg^{24} nucleus in the first excited state is two, even parity,[6] while that of the first excited state of C^{12} is also predicted to be two, even parity.[7] Both angular distributions are asymmetric about 90°, indicating that at least two levels of different parity are involved in the compound nuclei (Al^{25} and N^{13}), but nothing is known about the levels of these nuclei in this region. It is not too surprising that such a striking difference exists in the lobe pattern of the two distributions in view of the possible complexities in the compound nucleus.

† This work was supported in part by the joint program of the ONR and AEC.

[1] Taylor, Jentschke, Remley, Eby, and Kruger, Phys. Rev. **84**, 1034 (1951).
[2] Boyer, Gove, Harvey, Deutsch, and Livingston, Rev. Sci. Instr. **22**, 310 (1951).
[3] *Nuclear Data*, National Bureau of Standards Circular No. 499 (1950).
[4] Hornyak, Lauritsen, Morrison, and Fowler, Revs. Modern Phys. **22**, 291 (1950).
[5] Designed by C. W. Johnstone, Los Alamos Scientific Laboratory.
[6] E. L. Brady and M. Deutsch, Phys. Rev. **78**, 558 (1950).
[7] R. R. Haefner, Revs. Modern Phys. **23**, 228 (1951).

Nuclear Resonance and the Electronic Structure of Transition Metals*

W. D. KNIGHT AND C. KITTEL
Department of Physics, University of California, Berkeley, California
(Received March 31, 1952)

ZENER[1] has suggested that the occurrence of body-centered cubic (b.c.c.) crystal structures in the transition metals V, Cr, Nb, Mo, Ta, and W may be attributed to antiferromagnetic coupling between the 3*d* shells on adjacent atoms, because a b.c.c. lattice has a lower ground state with respect to nearest-neighbor antiferromagnetic interactions than a closest-packed lattice. The usefulness of this model has been emphasized in a series of papers by Zener[2] and his collaborators.

It is fair to ask to what extent the ground states of the b.c.c. transition metals actually exhibit characteristic antiferromagnetic properties in the ordinary antiferromagnetic salts. States with alternating spin arrangements in solids may be described by diverse types of wave functions.[3] We may represent antiferromagnetism at one extreme by an ionic model using Heitler-London wave functions. This gives a fairly good account of the properties of MnO, MnF_2, and similar antiferromagnetics. At the other extreme we have a free electron or running wave model, with a kind of antiferromagnetism implied in the correlation energy[4] which keeps electrons of parallel spin farther apart than electrons of antiparallel spin, as in metallic Na. Therefore, it may not be necessary to accept all the literature consequences of the Zener theory in order to retain some of the insight it brings to cohesive energy problems.

The experimental evidence is rather against the possibility that all of these metals have "ordinary" antiferromagnetism:

(1) Susceptibility and heat capacity data do not show the susceptibility peaks and thermal anomalies commonly associated with the Curie point of antiferromagnetics, but of course it may be that the Curie points are too high to be observed.

(2) Shull[5] has been unable to detect the presence of an ordered spin state at room temperature in V, Nb, and W, using the neutron diffraction technique successfully employed on the antiferromagnetic salts. Weak antiferromagnetism is observed in Cr and Mn.

(3) Nuclear resonance results[6] for V and Nb are incompatible with a static antiferromagnetic array, as discussed below.

If vanadium had an antiferromagnetic array of the spins of the 3*d* electrons, then the nuclear resonance spectrum would have a zero-field splitting of the order of 2×10^8 oersteds, caused by electron spin-nuclear spin interaction. The experimental results[6] for V (and Nb) do not show any splitting within the experimental limits of about five oersteds. From these facts we may conclude either (a) the 3*d* bonding is completely covalent in V or (b) if the 3*d* shell is in a magnetic configuration, the direction of the total spin of each ion must change with a correlation time much less than 10^{-4} sec, corresponding to the observed nuclear resonance line width. That is, if an antiferromagnetic array exists, it must move about rapidly.[7]

The coupling of the nuclear spin with the $3d^x$ shell in a solid occurs principally (for $x\leq5$) through the excited configuration $3s3p^63d^{x}4s$, as shown by Abragam.[8] In ionic crystals containing Mn^{++} or V^{++} ions it is known from paramagnetic resonance studies[9] that the hyperfine interaction term $A\mathbf{S}\cdot\mathbf{I}$ has $A\approx0.01$ cm^{-1}. In terms of an effective field acting on the nuclei, we have $H_{max}=ASI/\mu_{nuc}$, which for Mn^{++} is $\approx3\times10^8$ oersteds, and for V^{++} is $\approx2\times10^8$ oersteds. Experimental work is planned on the direct observation of the predicted zero-field nuclear splitting in paramagnetic salts.

It is interesting to speculate on the basis of the first transition group whether the presence of a static antiferromagnetic (or ferromagnetic) array is not incompatible with superconductivity, either because the dipolar magnetic fields exceed the critical field or for other reasons.

We are indebted to Dr. C. G. Shull for several helpful letters.

* This work has been assisted in part by the ONR.
[1] C. Zener, Phys. Rev. **81**, 440 (1951).
[2] C. Zener, Phys. Rev. **83**, 299 (1951); **85**, 324 (1952); I. Isenberg, Phys. Rev. **83**, 637 (1951); Yee-Chuang Hsu, Phys. Rev. **83**, 975 (1951).
[3] Preliminary work on this question is reported by J. C. Slater, Phys. Rev. **82**, 538 (1951).
[4] C. Herring, Phys. Rev. **82**, 282 (1951), has suggested that the correlation energy may be higher as the effective mass of the electrons increases. H. Jones and N. F. Mott, Proc. Roy. Soc. (London) **A162**, 49 (1937), account on the band model for the high heat capacity and magnetic susceptibility of the transition metals using a high effective mass.
[5] C. G. Shull and M. K. Wilkinson, Phys. Rev. (to be published).
[6] W. D. Knight, Phys. Rev. **85** 762 (1952).
[7] Shull's negative result by neutron diffraction suggests that the correlation time is less than 10^{-12} sec. Similar correlation time considerations apply to ferromagnetic elements for which Shull and collaborators find good agreement with the calculated form factors; it is not then possible to postulate a model with two different types of magnetic ions present unless these exchange positions in a time $<10^{-12}$ sec. This objection may be raised against Zener's latest models and also that of K. H. Stevens, Proc. Phys. Soc. (London) **A65**, 149 (1952).
[8] A. Abragam, Phys. Rev. **79**, 534 (1950).
[9] B. Bleaney, Physica **17**, 175 (1951); A. Abragam and M. H. L. Pryce, Proc. Roy. Soc. (London) **A205**, 135 (1951); Tinkham, Weinstein, and Kip, Phys. Rev. **84**, 848 (1951).

Thermal Conductivity in the Intermediate State of Pure Superconductors*

D. P. DETWILER†‡ AND HENRY A. FAIRBANK
Sloane Physics Laboratory, Yale University, New Haven, Connecticut
(Received April 3, 1952)

IN 1950 Mendelssohn and Olsen[1,2] measured the thermal conductivity of niobium and a lead-bismuth alloy (0.1 percent Bi). Their measurements showed a thermal conductivity minimum and marked hysteresis effects in the intermediate state. Webber and Spohr[3] have found similar effects in pure lead below about 4° Kelvin.

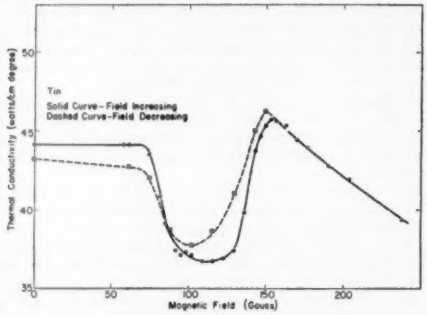

FIG. 1. The thermal conductivity of tin in a transverse magnetic field at 2.5°K.

Measurements carried out in this laboratory of the thermal conductivity of Johnson-Matthey spectroscopically pure tin and indium as a function of transverse magnetic field strength suggest that this phenomenon may be characteristic of all pure superconductors. (See Figs. 1 and 2.) The specimens used were 3 to 4 mm in diameter and approximately 10 cm long, and consisted of a few large crystals. The temperature gradient was determined with carbon composition resistors. A total temperature difference between the thermometers of approximately 0.05°K was used, so that the critical field was practically identical throughout the specimen.

In both these materials a very distinct minimum occurs in the thermal conductivity in the intermediate state, along with strong magneto-resistance for fields greater than critical, as shown by the figures. This characteristic behavior was observed at several temperatures below the zero-field transition temperature. The fact that our indium specimen exhibits a very much higher conductivity than that of Hulm[4] is probably due to its much greater purity.

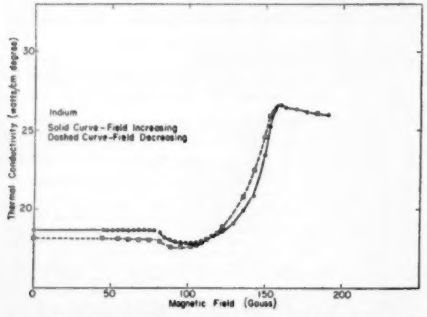

FIG. 2. The thermal conductivity of indium in a transverse magnetic field at 2.1°K.

If the heat transport in the superconducting state is primarily due to electrons as it appears to be in the normal state for both tin and indium, it is reasonable to attribute the minimum in the thermal conductivity to the scattering of electrons by the laminar structure of the intermediate state as suggested by Webber and Spohr.[3] On the other hand, if the lattice conduction has become appreciable in the superconducting state the intermediate state minimum may be due to the scattering of lattice waves by the laminar boundaries.[5] Whichever mechanism proves to be correct, it is likely that further investigation along these lines will lead to a fuller understanding of the structure of the intermediate state.

A detailed account of these experiments will be published later.

* Assisted by the ONR.
† AEC Predoctoral Fellow, 1950–1952.
‡ This material is part of a dissertation presented to the faculty of Yale University in partial fulfillment of the requirements for the Ph.D. degree.
[1] K. Mendelssohn and J. L. Olsen, Proc. Phys. Soc. (London) **A63**, 2 (1950).
[2] K. Mendelssohn and J. L. Olsen, Phys. Rev. **80**, 859 (1950).
[3] R. T. Webber and D. A. Spohr, Phys. Rev. **84**, 384 (1951).
[4] J. K. Hulm, Proc. Roy. Soc. (London) **A204**, 98 (1950).
[5] We are indebted to J. K. Hulm and R. T. Webber for a discussion of this point.

Angular Correlation between γ-Rays and Inelastically Scattered Protons from Mg^{24} †

H. E. GOVE AND A. HEDGRAN‡
Department of Physics and Radioactivity Center of the Laboratory for Nuclear Science and Engineering, Massachusetts Institute of Technology, Cambridge, Massachusetts
(Received March 27, 1952)

THE 7.3-Mev proton beam from the M.I.T. cyclotron has been used to bombard a magnesium target in a scattering chamber which has been described previously.[1] The correlation between the inelastically scattered protons from Mg^{24} (78 percent abundance) leaving the nucleus in the 1.4-Mev state[2] and the subsequent gamma-ray has been investigated in a preliminary way.

The protons were detected in the first section of a triple proportional counter[1] using range absorption and the method of peaking. The counter could be rotated from 30° to 145° with respect to the proton beam. The gamma-counter, which consisted of a cylindrical NaI crystal two inches in diameter and one inch thick mounted on a 5819 photomultiplier, was coplanar with the beam and the scattered protons. Only the two positions of −30° and −90° to the beam were available for the gamma-counter. The NaI crystal subtended a solid angle of about 2 percent of a sphere at the target. It was shielded around the sides with about two inches of lead to reduce background. No energy selection was attempted except for low level discrimination to eliminate noise and

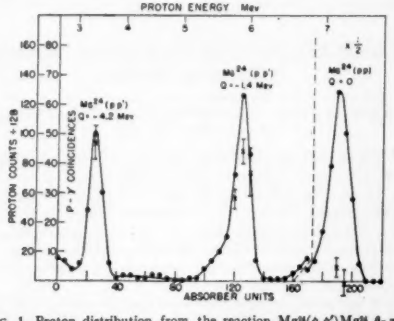

FIG. 1. Proton distribution from the reaction $Mg^{24}(p,p')Mg^{24}$ $\theta_p = 90°$ shown by solid circles and lines. The $p-\gamma$ coincidences under each peak taken with the gamma-counter at $\theta_\gamma = -90°$ are indicated with crosses.

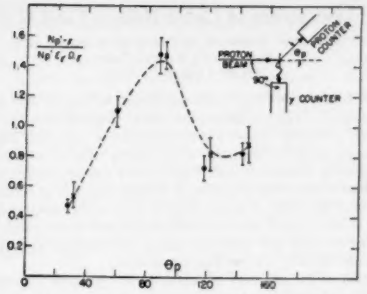

FIG. 2. Proton-gamma angular correlation from the reaction $Mg^{24}(p,p')Mg^{24*}\rightarrow\gamma+Mg^{24}+1.4$ Mev for $\theta_\gamma=-90°$. Two sets of data, one from a 0.7-mil and the other from a 1.4-mil magnesium target are shown.

a ½-inch lead shield in front to eliminate low energy gamma-rays. The product of efficiency and solid angle for 1.2-Mev gamma-rays was determined by placing a calibrated Co^{60} source in the target position. It was found that this factor could be made as high as 0.5 percent corresponding to a 25 percent efficiency without background affecting the measurements seriously.

The chance coincidence rate was measured with a second gamma-counter similar to the first, installed adjacent to the beam catcher and shielded in such a way that no gammas from the target were counted. Its counting rate could be made approximately equal to that of the first, and both gamma-counter outputs were placed in coincidence with the proton counter. The coincidence resolving time was 0.4 microsecond.

Figure 1 shows the proton spectrum from magnesium with the proportional counter at 90° to the beam. The two low energy peaks correspond to inelastically scattered protons from the known 4.2 and 1.4-Mev levels in Mg^{24}. The observed $p-\gamma$ coincidences under each peak are also indicated, taken with the gamma-counter at $-90°$.

Before and after each coincidence point was measured, the proton peak was recorded to insure that it was well resolved and the scintillation counter efficiency and circuit resolving times were checked.

In the correlation measurements each coincidence point was taken with an absorber thickness corresponding to the proton peak inserted in front of the proportional counter. The proton beam intensity was kept low enough to reduce the chance coincidences to a value well below that of the true.

Figure 2 shows the $p-\gamma$ correlation with the gamma-counter at $-90°$ as a function of proton angle. Two sets of data, one from a 0.7-mil and the other from a 1.4-mil magnesium target are indicated to show the consistency of the results. The ordinate scale is chosen in such a way that unity is the value of $(p-\gamma)/p$ that would occur if the gamma-ray following the proton has the same probability of emission in any direction. This normalization was based on the calibrated Co^{60} source. It can be seen that the maximum correlation occurs when the proton and gamma-ray are emitted back to back at 90° to the beam.

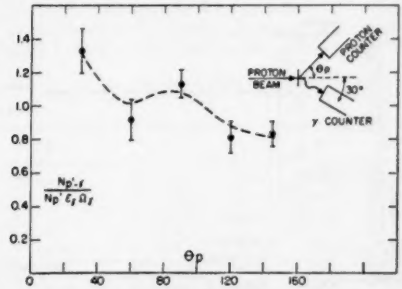

FIG. 3. Proton-gamma angular correlation from the reaction $Mg^{24}(p,p')Mg^{24*}\rightarrow\gamma+Mg^{24}+1.4$ Mev for $\theta_\gamma=-30°$.

Figure 3 shows the correlation for a gamma-ray angle of $-30°$ indicating much less pronounced variations.

It is planned to extend these measurements using improved counters and faster circuits.

† This work has been supported in part by the joint program of the AEC and ONR.

‡ Present address: Nobel Institute for Physics, Stockholm, Sweden. Participation in this work was made possible through the support of the American-Scandinavian Foundation and the Swedish Atomic Energy Committee.

[1] Boyer, Gove, Harvey, Deutsch, and Livingston, Rev. Sci. Instr. **22**, 310 (1951).

[2] K. Way *et al.*, *Nuclear Data*, National Bureau of Standards Circular No. 499 (1950).

The Radioactive Decay of Ruthenium 103†

J. M. CORK, J. M. LEBLANC, F. B. STUMPF, AND W. H. NESTER
Department of Physics, University of Michigan, Ann Arbor, Michigan

(Received April 4, 1952)

SINCE the early discovery[1] of a 46-day radioactivity in ruthenium and its subsequent assignment to the isotope of mass 103, many investigations have been made of the energies of its radiations. There has come to be a general agreement, to the extent shown in Table I, that two beta-rays and two gamma-rays are associated with the radioactive decay. Coincidence measurements indicate[2] that the higher energy gamma is associated with the lower energy beta-ray. The 40-kev gamma-ray showed no coincidence with either beta-ray or the other gamma and is believed to result from the well-known, 57-minute, isomeric transition in rhodium 103.

Using photographic spectrometers with sources of both Ru^{103} and Ru^{106}, obtained from Oak Ridge, several previously unreported gamma-rays are found to be present. The energies of the conversion electrons and their interpretations are shown in Table II. Some lines resulting from the long-lived Ru^{106} are always present and are identified by their relative increase intensity in aged specimens. Two of these have energies of 510.0 and 621.7 kev. By the use of a recording microphotometer and emulsion sensitivity data, the relative line intensities for several of the gamma-rays are evaluated as shown in column 5. From the empirical relationships noted[3] by Goldhaber and Sunyar and from "shell" theory it is possible to propose the type of transition for certain of the gamma-rays.

The 39.6-kev isomeric transition in Rh^{103} appears to be $E3$ as previously assigned;[4] however, the logarithm of the radiation lifetime $\tau\gamma$ seems to be more nearly 6 than 7, as noted. From its K/L value of 8.5, the 499-kev transition might be $M3$, $E2$, or $E3$, but

TABLE I. Reported energies in ruthenium 103.

Item	BH[a]	H[b]	SSG[c]	MS[d]	MHM[e]	K[f]
Half-life, days	41		42		43	39.8
Energy in kev						
Beta 1		350	200	150	204	217
2	750	665	200	680	684	698
Gamma 1					40.4	40
2	400	312	530	520	494	498

[a] E. Bohr and N. Hole, Arkiv. Mat. Astr.-fys. **32A**, 15 (1945).
[b] N. Hole, Arkiv. Mat. Astr.-fys. **36A**, 2 (1948).
[c] Sullivan, Sleight, and Gladrow, *Radiochemical Studies: The Fission Products* (McGraw-Hill Book Company, Inc., New York, 1950), Paper No. 111, National Nuclear Energy Series, Plutonium Project Record, Vol. 9, Div. IV.
[d] C. Mandeville and E. Shapiro, Phys. Rev. **77**, 439 (1950).
[e] Mei, Huddleston, and Mitchell, Phys. Rev. **79**, 429 (1950).
[f] See reference 2.

TABLE II. Energy of conversion electrons from ruthenium 103.

Electron energy, kev	Interpretation	Energy sum, kev	Gamma-energy, kev	K/L ratio
16.2	K(Rh)	39.4		
19.1	Auger			
29.8	K	53.0		
36.7	L_3	39.6		
39.0	M	39.6		
39.5	N	39.6	39.6	0.10±0.04
49.7	$L_{1,2}$	52.9	52.9	1.0±0.3
272.0	K	295.2	295.2	
475.5	K	498.7		
488.8	K	512.0		
495.1	L	498.4		
497.8	M	498.4	498.5	8.5±1.5
509.0	L	512.0		
587.2	K	610.7	610.6	4.0±1.5
598.5	K	621.7	510.0(106)	
607.2	L	610.6	621.7(106)	

from the very short lifetime the $E2$ process appears most probable. Similarly the 53-kev gamma-ray with a K/L ratio of unity must result from an $E2$ transition. The 610-kev gamma-ray, whose Z^2/W is 3.33, has a K/L ratio of approximately 4. This value is somewhat too small for an $M4$ transition and would best suit an $E4$ or $E5$ process. The very short radiation lifetime would be more in agreement with $E4$.

The proposed energy level scheme shown in Fig. 1 includes all of the gamma-rays except the 295-kev radiation for which only a

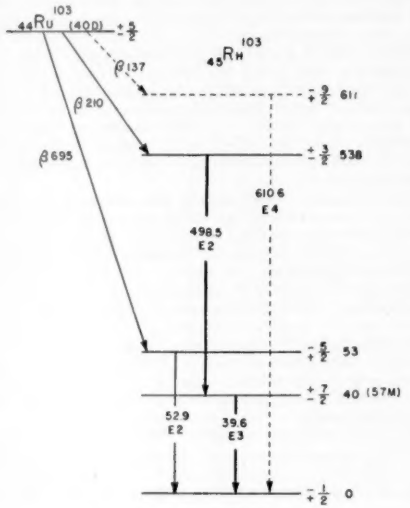

FIG. 1. Proposed decay scheme for Ru^{103}.

single electron line was observed. The 610-kev level suggests the existence of an additional beta-ray of lower energy. In view of the wide variation both in the energies and in the relative decay probabilities reported for the 210- and the 695-kev beta-rays, the existence of a 137-kev beta might have been overlooked. The 499-kev transition is now a better fit between the observed beta-energies than in the older, simpler level schemes, and the spin changes are compatible with the observed intensities, in that the 210-kev beta is allowed and the 499-kev is a first forbidden transition. The spin values of the states are not in disagreement with shell theory predictions.

† This project received the joint support of the AEC and ONR.

[1] J. Livingood, Phys. Rev. **50**, 425 (1939).
[2] E. Kondaiah, Phys. Rev. **79**, 891 (1950).
[3] M. Goldhaber and A. Sunyar, Phys. Rev. **83**, 906 (1951).

Coexistence of Liquid Helium I and II

PHILIP CLOSMANN AND RICHARD T. SWIM
Rice Institute, Houston, Texas
(Received March 31, 1952)

SINCE the transition between liquid helium I and liquid helium II is one of the second order, showing no latent heat, no phase boundary between the liquids can be expected. The two liquids can never be coexistent at any given value of temperature and pressure. However, both liquid forms can be present at the same time if one of the variables of state has a gradient within the space of observation. It seems that in none of the experiments on liquid helium carried out so far did a gradient of temperature or pressure covering the transition region exist, and it is, therefore, of interest to carry out such an experiment.

In view of the difficulty of establishing a pressure gradient, an arrangement involving a temperature gradient was chosen. This arrangement consisted of a thermally isolated column of helium. In this way the radial heat flow is zero, and one end could be at temperatures below the lambda-point, while the other end could be above the critical point. It is to be expected that in such an arrangement the main contribution to the heat transport will be provided by the liquid helium II. In view of the complex nature of this heat flow and also because of the inversion of the thermal expansion at the lambda-point, the question of the temperature distribution cannot, however, be solved through mathematically rigorous procedures.

The apparatus (see Fig. 1) consisted of a vertical glass tube 55 cm long and 0.86-cm diameter which was enclosed in a vacuum jacket. The tube was thermally connected by means of copper-glass seals to a container with liquid nitrogen at the upper end and a bath of liquid helium II at the lower end. The whole arrangement was placed into a Dewar vessel which contained liquid helium II at the bottom and a metal reservoir with liquid nitrogen at the top. In this way the influence of radiation can be neglected. The tube could be filled with helium at more than the critical pressure, and the temperature at any place in it determined by a small resistance thermometer which could travel through the length of the tube. This temperature probe consisted of a hollow Lucite cylinder carrying on its outside a coiled resistance wire of leaded brass. Care was taken to make the heat resistance of the metal partition between the helium in the tube and that in the outer bath small enough to allow for a temperature below the lambda-point inside the lower end of the tube.

The results show that at pressures above 2.2 atmospheres and under equilibrium conditions, practically the whole of the tube was full of liquid helium II, leaving only about 4 cm at the top of the tube for the temperature gradient between 2.16°K and 80°K. The exact point where the liquid helium II ended was indeterminate to the extent of 1.5 cm, this being the length of the thermometer. As expected, the transition region between liquid helium II and liquid helium I as well as between liquid helium I and the gas

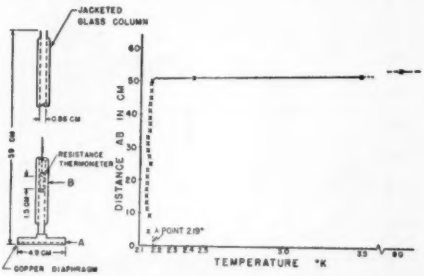

FIG. 1. Diagram of the apparatus and experimental results on liquid helium I and II.

showed no phase boundary or any other anomalous optical properties. However, on releasing the pressure slightly below the critical value, critical opalescence and subsequently the appearance of a meniscus was observed in this region. Prior to these observations when helium was being introduced into the tube, it was noted that the evaporation of liquid from the pumped helium II bath increased rapidly because the tube containing liquid helium II and reaching up into the Dewar vessel constituted a very good heat conductor. This fact is of importance for the design of cryogenic apparatus, showing that tubes reaching from higher temperatures into a bath of liquid helium II and containing helium of more than critical pressure will constitute a very serious heat leak.

The authors wish to thank Professor Kurt Mendelssohn, F.R.S., for suggesting the problem and directing the research during his visit at The Rice Institute. The advice and assistance of Professor C. F. Squire is also acknowledged.

The High Latitude North-South Asymmetry of Cosmic-Rays

D. W. P. BURBURY
Department of Physics, University of Tasmania, Hobart, Tasmania, Australia
(Received March 27, 1952)

THE east-west asymmetry of cosmic rays in latitudes above the knee of the latitude-intensity curve has been explained as a secondary radiation effect by Johnson[1] and Burbury and Fenton,[2] who showed that the deflection of secondary mesons by the earth's magnetic field during their passage through the atmosphere can produce an asymmetry of the value observed. A sea-level north-south asymmetry has recently been observed at Hobart, Tasmania (geomagnetic latitude 51.7 degrees south) for zenith angle 30 degrees under 12 centimeters of lead, the excess being in the north. The value obtained is 0.0056 ± 0.0013 (probable error), clearly different from zero. The east-west asymmetry observed at the same zenith angle and lead thickness is 0.0113 ± 0.0043. If the north-south asymmetry can also be explained as a secondary radiation effect, it is still not necessary to invoke any asymmetry in the primary radiation giving rise to the sea-level radiation in high latitudes. The following explaination is suggested:

The magnetic field in the latitude of Hobart is inclined at 18° to the vertical. Particles traveling in the N–S vertical plane will experience a deflecting force normal to this plane, and since the total deflection of secondary mesons is only a few degrees, the path of a particle arriving at sea level at a zenith angle θ may be said to lie in an inclined plane whose line of greatest slope coincides with the final direction of the path. The initial direction of such a particle will be at a greater zenith angle than θ, and if this be denoted by θ', it can be shown simply that

$$\cos\theta' = \cos\theta\cos\delta, \tag{1}$$

where δ is the total deflection of the particle.

In the theory of the east-west asymmetry[2] the deflection of particles arriving at various zenith angles in the east-west vertical plane was obtained by integrating the curvature along a straight line having the final direction of the particle. For the small deflections considered, this approximation is sufficiently good. Since the curvature at any point is proportional to the component of the magnetic field normal to the plane of the trajectory, so is the deflection. Also, since the distribution of air mass along a straight path at a zenith angle θ is independent of azimuth, we may write

$$\delta_N(\theta) = \delta(\theta)H\sin(\theta-18°)/H\sin 18°, \tag{2a}$$

and

$$\delta_S(\theta) = \delta(\theta)H\sin(\theta+18°)/H\sin 18°, \tag{2b}$$

where $\delta_N(\theta)$ and $\delta_S(\theta)$ are the deflections of particles arriving from the north and south at zenith angle θ, and $\delta(\theta)$ is the deflection of corresponding particles traveling in the east-west vertical plane. The mean deflection taken over the energy spectrum with lower limits corresponding to 12 and 24 centimeters of lead absorber in the measuring apparatus was computed for the east-west direction at several zenith angles and is denoted by $\bar{\delta}$. Table I gives the values of $\bar{\delta}$ (Burbury and Fenton[2]) and values of $\bar{\delta}_N$ and $\bar{\delta}_S$ calculated from Eqs. (2a) and (2b).

The rate of energy loss by ionization in the atmosphere increases rapidly with decreasing altitude, and consequently the bending of the path of a particle is greater near sea level. Thus the radiation arriving at zenith angle θ north or south of the vertical is made up of particles which have traveled through most of the atmosphere at an average zenith angle given approximately by

$$\cos\bar{\theta}_N = \cos\theta\cos\bar{\delta}_N, \tag{3a}$$

or

$$\cos\bar{\theta}_S = \cos\theta\cos\bar{\delta}_S. \tag{3b}$$

The attenuation of these particle intensities due to decay and energy loss will be approximately the same as that sustained by particles traveling at zenith angles $\bar{\theta}_N$ and $\bar{\theta}_S$ if the magnetic field were absent. Since the zenith distribution of such undisturbed radiation is given by

$$j(\theta) = j_0\cos^{2.2}\theta, \tag{4}$$

the north and south intensities are given by

$$j_N = j_0\cos^{2.2}\bar{\theta}_N, \tag{5a}$$

and

$$j_S = j_0\cos^{2.2}\bar{\theta}_S. \tag{5b}$$

The north-south asymmetry is now

$$\frac{2(j_N-j_S)}{(j_N-j_S)} = \frac{2(\cos^{2.2}\bar{\delta}_N-\cos^{2.2}\bar{\delta}_S)}{\cos^{2.2}\bar{\delta}_N+\cos^{2.2}\bar{\delta}_S}, \tag{6}$$

by Eqs. (3a) and (3b).

TABLE I. The mean deflection of particles in radians in the east-west, north and south directions as a function of zenith angle and lead absorber thickness.

$\theta=$		15°	30°	45°	60°
12 cm lead	$\bar{\delta}=$	0.031	0.034	0.037	0.043
	$\bar{\delta}_N=$	0.005	0.023	0.054	0.093
	$\bar{\delta}_S=$	0.055	0.082	0.107	0.136
24 cm lead	$\bar{\delta}=$	0.028	0.031	0.034	0.040
	$\bar{\delta}_N=$	0.005	0.021	0.050	0.087
	$\bar{\delta}_S=$	0.049	0.075	0.098	0.127

TABLE II. North-south asymmetry as a function of zenith angle and lead absorber thickness.

θ	15°	30°	45°	60°
12 cm lead	0.0030	0.0070	0.0095	0.0107
24 cm lead	0.0025	0.0055	0.0078	0.0091

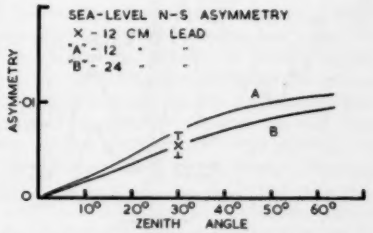

FIG. 1. Sea-level north-south asymmetry as a function of zenith angle and lead thickness.

The computed values are given in Table II, and Fig. 1 shows the asymmetry as a function of zenith angle and lead thickness compared with the result for 30 degrees and 12 centimeters of lead. In view of the approximate nature of the theory the agreement can be regarded as satisfactory.

The author acknowledges gratefully the assistance of the Commonwealth Scientific and Industrial Research Organization whose financial aid made this work possible.

[1] T. H. Johnson, Phys. Rev. **59**, 11 (1941).
[2] D. W. P. Burbury and K. B. Fenton, Australian J. Sci. Research (to be published).

Gamma-Radiations from 36.5-hr Rh^{105g}

G. E. Boyd
Chemistry Division, Oak Ridge National Laboratory, Oak Ridge, Tennessee
(Received April 3, 1952)

INCIDENTAL to our continuing investigations on the radioactivities in technetium there was an occasion to examine the radiations from 36.5-hr Rh^{105}. There has been some question recently as to whether gamma-radiations are emitted in the decay of this radionuclide. Duffield and Langer[1] have reported a magnetic lens spectrometer study in which only one beta-group of 570-kev maximum energy was found. Neither conversion electrons in the neighborhood of 300 kev nor any gamma-radiations were observed. Mandeville and Shapiro,[2] on the other hand, have obtained absorption and beta-gamma coincidence rate data which indicate a 0.3-Mev gamma-ray in approximately 8 percent of the disintegrations.

Purified RuO_2 was irradiated with slow neutrons for 11 hours in the Oak Ridge pile. One mg of rhodium carrier was added, and the ruthenium was separated by distillation with perchloric acid. Two additional distillations were made after adding inactive ruthenium; then the residue was taken up in HCl and the rhodium isolated by reduction to its metal with magnesium. Gamma-ray spectra (Fig. 1) from this source at various times showed photolines at 322±5, 157±5 (very weak), and possibly at 80±5 kev

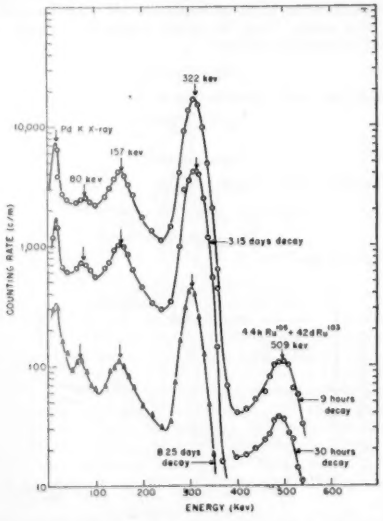

FIG. 1. Gamma-ray spectrum of 36-hr Rh^{105g} taken at varying times with a Tl+NaI scintillation counter spectrometer.

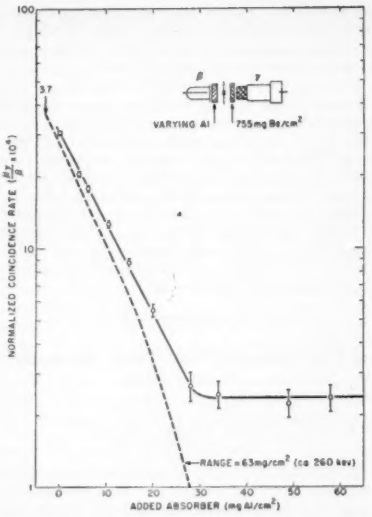

FIG. 2. Coincidence rate absorption measurements taken on 36-hr Rh^{105g} after 57-hours decay.

which decayed with a 36-hr half-life. Measurements were conducted with a scintillation counter spectrometer consisting of a 1×2-inch cylindrical, thallium-activated sodium iodide crystal (hermetically packed in powdered MgO) together with a selected RCA-5819 photomultiplier, $A-1$ linear pulse amplifier, and sliding channel differential discriminator.[3] The resolution at 661 kev was about 10 percent with a peak to valley ratio exceeding 30:1.

Energy-dependent beta-gamma coincidences were also observed, (Fig. 2) suggesting that the beta-spectrum was complex. A mica end-window beta-proportional counter and a 1×1-inch Tl+NaI crystal for gamma-rays together with a coincidence detector[4] set at a resolving time of 1.6 μsec were employed for these measurements. Absorption of the coincidences in aluminum gave a range of 63-mg Al/cm² corresponding to a maximum beta-energy of about 260 kev. This energy added to that of the coincident gamma-ray (320 kev) gives 580 kev in satisfactory agreement with the energy of the main beta-transition. A comparison of the normalized coincidence rate extrapolated to zero total absorber with the rate for 2.69-day Au^{198} counted in the same geometry indicated that 10±2 percent of the 36.5-hr Rh^{105g} disintegrations go through the 320-kev gamma-ray, assuming the latter is not appreciably delayed nor converted.

Log*ft* values for the 570- and 250-kev beta-groups are 5.7 and 5.6, respectively, so that both transitions are empirically allowed. Spin values of 5/2 ("most probable") and 3/2 ("possible") for Pd^{105g} have been reported recently.[5] If, therefore, Pd^{105g} is $d_{5/2}{}^{+}$, then Rh^{105g} should be $(7/2)^{+}$ and the 320-kev level may be $g_{7/2}{}^{+}$. It is of interest to note that other levels in Pd^{105} have been observed[6] in the decay of 45-day Ag^{105}.

The interest of our colleague, Dr. A. R. Brosi, is gratefully acknowledged.

[1] R. B. Duffield and L. M. Langer, Phys. Rev. **81**, 203 (1951).
[2] C. E. Mandeville and E. Shapiro, J. Franklin Inst. **253**, 145 (1952). References to earlier work may be found in this paper.
[3] E. Fairstein, Rev. Sci. Instr. **22**, 761 (1951).
[4] R. A. Dandl and C. J. Borkowski, Chemistry Division Quarterly Progress Report, Oak Ridge National Laboratory Report No. 286, p. 206 (September, 1949).
[5] P. Brix and A. Steudel, Naturwiss. **38**, 431 (1951).
[6] R. W. Hayward, Phys. Rev. **85**, 760 (1952).

Proceedings of the American Physical Society

Minutes of the 1951 Autumn Meeting of the New England Section at Trinity College, Hartford, Connecticut, November 3, 1951

THE thirty-seventh meeting of the New England Section of the American Physcial Society was held at Trinity College, Hartford, Connecticut on Saturday, November 3, 1951. Approximately eighty members of the section were in attendance. Luncheon was held in the Hamlin Dining Hall, and the Department of Physics of Trinity College offered tea to the members and guests of the Society after the meeting.

There were two contributed papers, of which the abstracts follow. There were five invited papers, of which this is the list:

Recent Advances in Radiofrequency Astronomy. E. G. Bowen, *Radiophysics Division, Australia.*

Radiation of the hfs Levels from Galactic Hydrogen. H. I. Ewen, *Harvard University.*

Positronium. Martin Deutsch, *M.I.T.*

Physics of the Transistor. W. H. Brattain, *Bell Telephone Laboratories.*

Propagation of Second Sound in Liquid Helium II. M. A. Herlin, *M.I.T.*

The following officers were elected for 1952: Chairman—Nora Mohler, Smith College; Vice-Chairman—F. W. Constant, Trinity College; Secretary-Treasurer—A. G. Hill, M.I.T.; Executive Committee—W. M. Fairbank, Amherst College; D. H. Frisch, M.I.T.

A. G. Hill, *Secretary-Treasurer*
M.I.T., Cambridge 39, Massachusetts

1. The Energy and Volume Changes Attending the Mixing of Nonpolar Liquids. Robert D. Dunlap and Harold F. Crandall, *University of Maine.*—Recent articles have dealt with the irregular solvent power of hydrocarbon liquids for fluorocarbon liquids. A large increase in volume attending the mixing of these liquids places the molecules in the mixture at a higher potential energy than in the pure components. The resulting energy change is much larger than would be expected from the existing theory of regular solutions. When the volume of n_1+n_2 moles of mixture is represented by $V=n_1v_1+n_2v_2$, the Hildebrand equation for the partial molal energy of mixing becomes

$$\bar{E}_1-E_0=\left(\frac{n_2v_2}{n_1v_1+n_2v_2}\right)^2v_1\left[\left(\frac{v_1}{v_1^2}\Delta E_1\right)^{\frac{1}{2}}-\left(\frac{v_2}{v_2^2}\Delta E_2\right)^{\frac{1}{2}}\right]^2-\left(\frac{v_1-v_1}{v_1}\right)\Delta E_1,$$

in which v_1, v_2, ΔE_1, and ΔE_2 are the molal volumes and energies of vaporization of the pure components and v_1 and v_2 are the partial molal volumes. It is possible to represent the volume of n_1+n_2 moles of mixture by the equation $V=(v_1-v_2+b)\times n_1-bn_1^2+v_2$. The parameter b may be obtained for various fluorocarbon-hydrocarbon systems by assuming random mixing, coiled molecules and taking the distance between the centers of hydrogen-fluorine atoms on adjacent molecules to be the same in the different systems. The systems considered are: $n-C_6F_{12}-n-C_6H_{12}$, $n-C_7F_{14}-n-C_7H_{16}$, and $n-C_7F_{14}$ $-\text{iso}-C_8H_{18}$. The apparent anomalous solubility of these systems may be explained by considering the volume changes attending their mixing.

2. Rotated Piezoelectric, Elastic, and Dielectric Constants of Quartz. Karl S. Van Dyke and Elva Sterns Creeger, *Wesleyan University.**—Based on accepted values of the elastic, dielectric, and piezoelectric constants of quartz, matrices of these constants have been computed for a complete cycle of rotations of the X'- and Z'-reference axes within the planes of both AT- and BT-cut plates. The matrices will appear in the Sixth Quarterly Report of this laboratory on Piezoelectric Crystal Studies to the Signal Corps dated November 30, 1951. They will also be incorporated in a new edition of *A Manual of Piezoelectric Data* by the senior author to appear as a supplementary volume to the Seventh report, February 29, 1952.

* This work was supported by contract with the U. S. Signal Corps.

Proceedings of the American Physical Society

Minutes of the 1952 Annual Meeting Held at New York City, January 31, February 1–2, 1952

(*Bulletin of the American Physical Society*, Volume 27, no. 1)

THE 1952 Annual Meeting of the American Physical Society, being the 311th meeting altogether, was held on January 31st and February 1st and 2nd in the buildings of Columbia University in New York City. In respect of attendance this was apparently the largest meeting ever, the registration reaching the unprecedented figure of 2215. In respect of the number of contributed papers it was close to the ceiling of recent years, a little short of 300. One might suspect that this is a permanent ceiling for the Annual Meeting; but any such inference is rendered very dubious by the fact that the number of ten-minute papers in electron-physics and solid-state physics has been and is declining while the number of nuclear papers is mounting, and the decline of the former cannot go much farther because the number cannot become negative. (Among the invited papers, nuclear physics did not predominate.) This drifting of non-nuclear physics away from our Annual Meeting has its deplorable aspects, but had it not occurred one may well doubt whether even Columbia University and our extremely able and self-sacrificing Local Committee—headed as usual by W. W. Havens, Jr.,

with A. M. Sachs and L. Lederman—could have continued to bear the burden.

The features which make this meeting "Annual" by definition are two prescribed by our Constitution and one which is based on tradition. The traditional feature is a joint session with the American Association of Physics Teachers, composed of their Richtmyer Lecture (this year delivered by Enrico Fermi), of their presentation of the Oersted Medal (this year received by A. A. Knowlton), and of our constitutionally required Retiring Presidential Address (this made by C. C. Lauritsen). This annual three-headed feature provides an afternoon of good talk for which our largest theater is none too roomy and the time is none too ample. The other distinctive feature of the Annual Meeting is furnished by the Business Meeting of the Society, the reports which are brought before it, and the actions which it takes. Before going on to these, I chronicle that the diners at the banquet in the Hotel New Yorker on Friday evening—also a joint function of our Society and of the Association—were addressed by O. E. Buckley speaking under the title "Observations and Experiences of a Neophyte in Washington" and R. E. Peierls speaking of physicists in Great Britain. As always, the number of people at the banquet was mute but puissant evidence of the power of the counter-attractions of New York City on a winter evening.

Now we turn to the Business Meeting of the Society, held on Friday morning and slimly attended.

Its first business was to hearken to the report of the Tellers of Election (S. K. Allison, A. W. Lawson, J. R. Platt, and H. R. Voorhees). This confirmed that the following Fellows had been elected to office in the Society for terms commencing at the end of this Annual Meeting: J. H. Van Vleck as President, Enrico Fermi as Vice-President, K. K. Darrow as Secretary, G. B. Pegram as Treasurer (all these for one-year terms); R. B. Brode and W. V. Houston as Councilors for four-year terms; W. P. Allis, F. G. Brickwedde, W. B. Fretter, Conyers Herring, H. W. Leverenz, and Arnold Nordsieck for three-year terms as Members of the Board of Editors with special allocation to *The Physical Review;* S. K. Allison and N. F. Ramsey for three-year terms as members of that Board with special allocation to *Reviews of Modern Physics.*

The main business laid before the meeting was that of taking heed of the financial situation and providing for the financial future of the Society. The financial status as of that date of February 1, 1952, was indeed cheerless and the outlook sinister; the Treasurer reported that the surplus of the Society had wasted away to such an extent that within a few months the Society might be literally unable to pay its bills. This was the result of the almost explosive expansion of *The Physical Review;* our surplus was accumulated during the war years when there was little to publish, was depleted during the subsequent years when there was much to publish, and practically vanished at the end of 1951 after the *Review* had suddenly swollen from 4000 pages annually to nearly 5000!

Two problems faced the Council at its meeting of January 30, the long-range problem of forestalling the recurrence of such a situation and the short-range problem of bridging the gap until the inflow of 1953 dues. The Council attacked the long-range problem by voting to recommend to the Society at its Business Meeting the adoption of an Amendment to Article I Section 1 of the By-Laws. Hitherto this section has prescribed the rates of annual dues; in its latest form it prescribed $14 as the annual dues of Members and $20 as those of Fellows. The new version reads: "The Council shall be empowered to fix the annual dues of Members at any figure not to exceed twenty dollars, and the annual dues of Fellows at any figure not to exceed thirty dollars, these dues to be payable on January first." The Society at its Business Meeting adopted this alteration as an Amendment to the By-Laws. It will be for the Council at its Washington meeting to decide where the new level of dues shall be set for 1953.

Other contributions toward the solving of the long-range problem were made by the Council in raising the (nonmandatory) page charge for articles in *The Physical Review* from $8 to $15 per page in raising the corresponding charge for a "Letter to the Editor" from $10 to $15, in raising from $25 to $30 the subscription rate which nonmembers of the Society must pay for *The Physical Review;* and in imposing a nonmandatory registration fee of one dollar at the impending Washington meeting and at subsequent meetings. The effect of these upon the short-range problem is very slight; but since the meeting ended, this problem has been alleviated by a generous grant from the National Science Foundation, which is available to assist in defraying the deficits which *Physical Review* will have incurred and will yet incur in 1952 and 1953. A fuller description of this grant may be given in a later issue of these Minutes.

The Council set up the 1952 Nominating Committee to provide nominations for terms of office beginning in 1953: its members are C. C. Lauritsen (*Chairman*), S. A. Goudsmit, P. Kusch, R. S. Mulliken, E. M. Piore, C. G. Shull, J. A. Van Allen, V. F. Weisskopf, and J. H. Williams.

The Metropolitan Section of the Society was dissolved at the request of its officers, the sad experience of some twenty years having shown that most of the members of our Society who reside in

the Metropolitan area do not attend its meetings however skilfully and attractively these are organized.

The Council elected one candidate to Fellowship and 213 to Membership; their names are appended.

Elected to Fellowship: Carl Wagner.

Elected to Membership: Lawrence K. Akers, James W. Albrecht, William A. Allen, Charles G. Amato, Weston A. Anderson, Charles M. Apt, William F. Arendale, William H. Arnold, Jr., Philip M. Aronson, Kenneth R. Atkins, Walter W. Atkins, Delbert S. Barth, Eugen Baumgartner, John E. Bigelow, Douglas S. Billington, Charles A. Bittmann, Gerhard A. Blass, Thomas H. Blewitt, Eugene I. Blount, Fritz E. Borgnis, Bennett Bovarnick, Mark M. Bowman, Jr., Bob M. Brown, Fred P. Burus, Kenneth J. Button, Cleo C. Byers, Addison D. Campbell, Robert F. Carpenter, Paul E. Carroll, Chang Cheng-Hsiu, Hung-Chi Chang, Syama D. Chatterjee, Francis F. Chen, Walter G. Chesnut, Curtis G. Chezem, Marion E. Cieslicki, Solomon I. Ciolkowski, Ezio Clementel, John V. Crable, Horace D. Crockford, George T. Croft, Thomas L. Cullen, Jackie W. Culvahouse, David W. Curtis, Basil D. Darwent, Alfons J. Daverio, Handel Davies, Marguerite I. Davis, William R. Davis, Michel A. Degallier, Donald W. Denniston, Jr., Bernard G. d'Espagnat, Richard N. Dexter, Donald G. Doran, Rene C. Dugas, Arthur W. Ehler, Andrew H. Eschenfelder, David C. Evans, Marjorie W. Evans, Heinz Ewald, William W. Farley, 3rd, Amiel Feinstein, Paul J. Flory, Robert S. Flum, Anthony H. Foderaro, Alan B. Fowler, Elbert M. Fox, Raymond Friedman, Lawrence W. Friedrich, S.J., Fritz E. Froehlich, Yoshio Fukioka, Thomas E. Gilmer, Jr., Thomas N. K. Godfrey, Philip Goldstein, Lionel Goodman, Edwin K. Gora, Alvin S. Gordon, Selma W. Greenwald, Joseph W. Griffith, Samuel B. Gunst, Paul J. Haigh, Neil E. Handel, Francis B. Harrison, John A. Harvey, Shigoaki Hatano, Albert R. Hibbs, Peter Hofmann, Harry D. Holmgren, Richard B. Holtzman, John H. Hubbell, Isao Imai, Akira Isihara, John Jagger, David Jaffe, G. Sargent Janes, Russell D. Johnson, Jr., Robert W. Johnston, Willard C. Jordan, Marvin I. Kalkstein, Osamu Kawaguchi, Jerome P. Keuper, Joseph A. Kies, William E. Kinney, Jean I. King, Ralph Klein, Jere D. Knight, Yoriko Komiya, Cecilia M. Kotin, Eugene H. Koziana, Paul Kruger, Behram Kursunoglu, John E. Lancaster, Robert D. Laughlin, Harlan W. Lefevre, Howard B. Levine, Harry Letaw, Jr., Wei-chuwan Lin, Stephen J. Lukasik, Jr., Marvin L. Luther, Irving L. Mador, Joseph A. Mangiapane, Louis Marick, Hans M. Mark, Clyde L. McClelland, Bruce R. McGarvey, Austin D. McGuire, Carman C. McMullen, Lawrence R. Megill, Donald A. Melnick, Ralph I. Mendenhall, James W. Meyer, George H. Minton, Robert C. Mitchell, Ralph Monaghan, Fulvio R. Monticelli, Richard T. Mooney, Jimmy J. Moore, Donald R. Morey, Stanley R. Morrison, Steven A. Moszkowski, Georges Mourier, John E. Mulhern, Jr., Seitaro Nakamura, V. Alexander Nedzel, Mark S. Nelkin, William A. Newcomb, Gerard J. Nijgh, John B. Nims, Jr., Lee C. Northcliffe, Jr., Richard M. Noyes, Syuzo Ogawa, Carl C. Old, Howard R. Padgitt, Cornelius A. Papp, Eugene N. Parker, William W. Parkinson, Jr., Alfred T. Peaslee, Jr., Frank M. Pelton, Marguerite Perey, Edward L. Peterson, Jr., Russell E. Peterson, Selmer W. Peterson, Elzie Louis Powell, Abbott Pozefsky, Louis A. Rayburn, Theo T. Reboul, John F. Reed, Renato Ricamo, Michael S. Ridout, William A. Robba, Glen P. Robinson, Lawrence G. Rubin, Rudolf Ruetschi, Samuel M. Sanders, Jr., Edward R. Sanford, Donald L. Schaefer, John P. Schiffer, Mark Schindler, Alvin G. Schulz, Jr., William D. Schulz, Felix Schweizer, Louis Segal, Sidney M. Selis, David W. Seymour, Robert C. Shutt, Leonard S. Singer, Charles C. Snow, John Spanos, John A. Spiers, Marilyn J. Stafne, Robert V. Steele, Neil R. Steenberg, Charles C. Sterett, James E. Stewart, Melbourne G. Stewart, Charles H. Sutcliffe, Benjamin E. Tabler, Warren E. Taylor, John H. Tolan, William J. Veigele, Seymour H. Vosko, Rayjor W. H. Webeler, Frederic E. Wells, George R. White, Harrison C. White, Homer C. Wilkins, Michael K. Wilkinson, John C. Williams, Marvin A. Williamson, Jr., Arthur W. Winston, Gordon K. Woodgate, Truman O. Woodruff, and Michael Yamin.

KARL K. DARROW, *Secretary*
American Physical Society
Columbia University
New York 27, N. Y.

Errata Pertaining to Papers F2, F10, G13, H5, J14, M6, O2, P11, and ZC7

F2, by W. F. G. Swann and D. W. Seymour. In line 3, begin should read being. In line 8, observer should read absorber.

F10, by Martin Annis, Herbert S. Bridge, and Stanislaw Olbert. In line 8, $p\beta aR^{\alpha}$ should read $p\beta=f(M)R^{\alpha}$.

G13, by D. W. Seymour and W. F. G. Swann. A footnote should be added reading: Assisted by the joint program of the ONR and AEC.

H5, by W. E. Kreger, R. O. Kerman, and W. K. Jentschke. In the next to the last line, a $P_{\frac{1}{2}}$-wave phase-shift of 180° 47′ should read a $P_{\frac{1}{2}}$-wave phase-shift of 108° 47′.

J14, by T. R. McGuire, Louis N. Howard, and J. Samuel Smart. In the by-line, the same of W. G. Schindler should be omitted.

M6, by Walter F. Dudziak. In lines 16 and 17, the sentence, The σ^- peak occurs at $T_\pi<25$ Mev while the σ^+ peak occurs at $T_\pi>70$ Mev, should read, The σ^- peak occurs at $T_\pi(52<T_\pi<88$ Mev), while the σ^+ peak occurs at $T_\pi'(70<T_\pi'<113$ Mev).

O2, by Ruth F. Schwarz. In line 9, since for $\rho'>\rho$, the···, should read, since for $\rho'+\rho$, the···.

P11, by Edwin A. Crosbie. The first sentence should read: Christian and Noyes[1] have shown that the 32- and 340-Mev P-P scattering data are consistent with the scattering to be expected from the usual singlet square well and a triplet tensor interaction of the form ± 18 Mev $\exp(-r/R)\times(r/R)^{-3}$, $R=1.6\times10^{-13}$ cm.

ZC7, by M. W. Johns, C. D. Cox, and C. C. McMullen. In line 8, the word uniquely should be deleted. In line 10, (86 percent) and (14 percent) should read (96.5 percent) and (3.5 percent). In line 11, 66° should read 0°.

PROGRAMME

THURSDAY MORNING AT 10:00

McMillin

(C. C. LAURITSEN presiding)

Invited Papers

A1. Effects of Chemical Combination and of Pressure on the Lifetime of a Nucleus. K. T. BAINBRIDGE, *Brookhaven National Laboratory* (on leave from Harvard University). (40 min.)

A2. Problems of Nuclear Shell Structure. V. F. WEISSKOPF, *M.I.T.* (45 min.)

A3. The Scattering of Fast Electrons by Nuclei. H. FESHBACH, *M.I.T.* (45 min.)

THURSDAY MORNING AT 10:00

Pupin 301

(L. J. RAINWATER presiding)

Apparatus of Nuclear Physics

B1. Radial Oscillations in the Cyclotron.* P. V. C. HOUGH, *University of Michigan.*—The excitation and evolution of the radial oscillations of ions in the cyclotron have been studied theoretically and experimentally. If the median plane magnetic field is expanded about $r=r_0$ as $B(r,\theta)=Bo(r_0/r)^n[1+\Sigma_1^\infty h_p(r_0)\cos p\theta]$, it is known[1] that near $n=0$ only the $p=1$ term induces important radial motion and that this motion corresponds simply to a secular shift of the orbit center. The path of the instantaneous orbit center is calculated under the assumptions $(\Delta n/n)$ and $(\Delta h_1/h_1)$ per revolution $\ll 1$. The center moves initially in a direction perpendicular to the axis of h_1 (i.e., the line of excess magnetic field) and then spirals into a circle which corresponds to a precession of the node of the radial oscillation without further change in amplitude. Values of h_1 and n for the Michigan 42″ cyclotron yield a radius for this circle of $\sim 2\frac{1}{2}$ cm, as a result of accidental azimuthal variations of the order 0.1 percent. Asymmetric settling under vacuum of the gasketed iron lid (by a few mils) had previously altered the axis of excess field at each evacuation making a reliable external beam impossible. A systematic shimming procedure is indicated by the theory and discussed in the accompanying abstract.

* Supported in part by the AEC.

[1] Henrich *et al*, Rev. Sci. Instr. **20**, 887 (1949); or Hamilton and Lipkin, Rev. Sci. Instr. **22**, 783 (1951).

B2. Radial Oscillations in the Cyclotron—Experimental.* W. H. BEACH, W. J. CHILDS, P. V. C. HOUGH, J. S. KING, AND W. C. PARKINSON, *University of Michigan.*—With the aid of the calculations indicated in the preceding abstract we have found it possible to follow a systematic procedure in shimming to obtain an external beam from a cyclotron. The order of the steps is: (1) central shimming to obtain proper magnetic focusing, (2) adjustment of the median plane, (3) removal of the first harmonic of any azimuthal asymmetries, (4) measurement and elimination of residual radial oscillations, and (5) controlled excitation of an oscillation desirable for extraction of the beam. The adjustment of the median plane is extremely important if the fall-off in the central field region is small. Shims placed around the edge of one of the poles (with care that no first harmonic is introduced) are used for this adjustment. Since azimuthal asymmetries of the order of 0.1 percent introduce serious oscillations, high accuracy in the measurement of the field is required. This may be obtained with the magnetic resonance absorption method. The magnitude of the oscillation, and the center of the orbit may be determined by the use of three internal probes, or by two probes, one of which carries a specially constructed head for determining the angle of the beam at a given radius. A small shim suitably placed may be introduced to excite oscillations in a preferred direction in order that the beam approach the septum at the optimum extraction angle.

* Supported in part by the AEC.

B3. A New Method for Focusing Ion Beams.* F. C. SHOEMAKER, R. J. BRITTEN,† AND B. C. CARLSON, *Princeton University.*—An arrangement of small magnetic lenses has been developed for obtaining double focusing of high energy ion beams without the expense of a magnet sufficiently powerful to produce large-angle deflections. The individual lenses have triangular plane-parallel poles and, although the deflection angle is small ($\sim 4°$), have short focal lengths $[f=\rho/(2\tan\frac{1}{2}\theta)]$ where θ ($\sim 90°$) is the angle between the field boundaries. Under these conditions, because of the curvature of the fringing field, their focal lengths in the plane of the field are very nearly equal but opposite in sign to their focal lengths in the plane of the pole faces. However, if two of these astigmats are spaced a distance comparable with their focal lengths with their field directions orthogonal, a point image of a point source may be obtained. If the source distance, the separation of the astigmats, and the desired image distance are specified, the focal lengths required for double focusing can be reliably calculated from the thin lens equation. This arrangement has been applied to the focusing of the 18.5-Mev external proton beam from the Princeton cyclotron. Two 400-pound magnetic lenses, with 400 watts each, focus 25 percent of the internal deflected beam on a $\frac{1}{4}$″ spot 15 feet from the cyclotron.

* Supported by the AEC.
† Now at the Carnegie Institution of Washington.

B4. Monoenergetic Gamma-Rays from the Synchrotron.* J. W. WEIL† AND B. D. MCDANIEL, *Cornell University.*—A method of selecting gamma-rays of specific energy from the bremsstrahlung spectrum of the synchrotron has been devised. The magnetic field of the synchrotron analyzes electrons which

have undergone thin-target bremsstrahlung emission. Electrons of specified energy are detected by a crystal, the signals from which are then used to gate an external detector so that the detector is only allowed to respond to events which occur in time coincidence with the pulse from the crystal. As an initial test of this method, the internal crystal was counted in coincidence with the Cornell pair spectrometer. The resolution of this arrangement was twenty percent at 170 Mev, the pair spectrometer having a minimum width of ten percent. A fast coincidence apparatus has been constructed to allow the use of moderate intensity beams. A measurement of the velocity of 170-Mev gamma-rays was made as a test of this new apparatus.[1] With this technique, a study of photoproduction of protons from various materials at high energies is now being attempted.

* Supported in part by the ONR.
† AEC Predoctoral Fellow.
[1] D. Luckey and J. W. Weil (to be published).

B5. Čerenkov Radiation Counting.* JOHN MARSHALL, *University of Chicago.*—Scintillation counting is being done in this laboratory with the Čerenkov radiation as a source of light. Since the radiation is dependent in intensity and angle of emission on particle velocity, it is possible with Čerenkov counters to discriminate in various ways among different charged particles of varying velocities. High resolution coincidence work can be done conveniently with these counters because of the extremely short pulses of light. Intensities are rather low so that only quite penetrating particles can be counted conveniently. The design and performance of some of the counters, together with their application to various problems in connection with the Chicago 170-inch synchrocyclotron, will be discussed.

* This work was supported by the joint program of ONR and AEC.

B6. SiO Films.* G. A. SAWYER, W. R. ARNOLD, J. A. PHILLIPS, E. J. STOVALL, JR., AND J. L. TUCK, *Los Alamos Scientific Laboratory.*—Thin self-supporting films of silicon monoxide have been prepared by evaporation into organic (Zapon) film backings which are subsequently removed by ion bombardment or solvents. The films are approximately 100 atoms ($8\ \mu g/cm^3$) thick and will withstand 3-mm gas pressure differential while transmitting several μa of 30-kev deuterons at 5-kev energy loss. The measured rms multiple scattering angle in such films at this energy is 7°. Thus beams of low energy charged particles can be introduced into a gas from vacuum with good geometry, small energy loss, and accurately measured intensity. The films are uniform, but at these small thicknesses, the statistics of the energy loss process gives appreciable straggling. We observe a Gaussian distribution of half-width 500 ev about the mean 5-kev energy loss. Al films seem to be equally strong, but have proved unsuitable for precise measurements on account of a growth in stopping power under bombardment, by about 10 percent per hour, presumably by chemical reaction with residual gas.

* Work performed under the auspices of the AEC.

B7. A Diffusion Cloud-Ion Chamber for Detection of Nuclear Interactions.* M. M. BLOCK, W. W. BROWN, AND G. G. SLAUGHTER, *Duke University.*—An ionization chamber has been placed into the sensitive volume of a diffusion cloud chamber consisting of a glass cylinder 16 in. diameter × 9 in. high (filled with argon and amyl alcohol vapor at 1.4 atmospheres), having a sensitive height of ~4 in. The ion chamber outer electrode, consisting of six $\frac{1}{8}$ in. stainless steel rods arranged in a hexagonal cylindrical array, 3 in. in diameter and 9 in. long, is maintained at a potential of −1200 volts; the central wire, $\frac{1}{8}$ in. stainless steel, is grounded. The amplified ionization pulse can be recorded and fed into delay circuits which cut off the high voltage after electron collection and trigger the flash lamps after track formation. The pulse height can be used to select nuclear events. To date, the chamber has been tested with a polonium alpha source. Successful cloud-ion chambers have been reported[1] using Wilson expansion chambers. However, simplicity and reliability of operation, continuous sensitivity, low cost of fabrication, and large volumes possible in diffusion cloud chambers are distinct advantages.

* This work was supported by the joint program of the ONR and AEC.
[1] Lewis, Brown, Seevers, and Hones, Rev. Sci. Instr. 22, 259 (1951); Brown, Rau, and Reynolds, Paper E6, Bull. Am. Phys. Soc. 26, No. 6 (1951) (Chicago meeting).

B8. Gamma-Energy Resolution with Sodium Iodide Scintillation Spectrometer.* C. J. BORKOWSKI AND R. L. CLARK, *Oak Ridge National Laboratory.*—With selected 5819 photomultipliers and 1″×1½″ cylindrical sodium iodide crystals activated with thallium iodide, an 8.0 percent full width at half maximum is obtained for the photoelectric peak from a 670-kilovolt gamma-ray. The peak to valley ratio is 52 to 1. At 42 kilovolts the width is 26 percent. An electron energy loss of 200 electron volts in the crystal releases a single photoelectron from a photocathode whose efficiency is 60 microamperes per lumen. MgO diffuse reflectors were found superior to aluminum foil, especially for the larger crystals; 30 percent more light was obtained. Energy distribution of recoil electrons, photoelectrons, and electron pairs from various energy gamma-rays and for different size crystals up to 3″×3″ cylinders will be shown. Methods for mounting the crystal directly on the photocathode and hermetically sealing the assembly in order to obtain long time surface stability will be given. Variations in sodium iodide crystals and photomultipliers will be discussed.

* This document is based on work performed under contract for the AEC at Oak Ridge National Laboratory.

B9. Mixed NaI−LiI Crystal for a Neutron Spectrometer.* A. W. SCHARDT AND W. BERNSTEIN, *Brookhaven National Laboratory.*—Hofstadter[1] showed that thallium-activated LiI crystals give scintillation pulses with neutrons. This process may be used for rough neutron energy measurements, provided the pulse height is proportional to energy and the resolution is good. The best resolution we obtained with thermal neutrons for a small (2 g) Tl-activated crystal is 14 percent (full width at half maximum). This is to be expected since the pulse height is at most 10 percent of that obtained with NaI − Tl at the same energy. Unfortunately, large crystals give a spread in pulse height caused apparently by nonuniform activation. Clear crystals have been grown from a mixture of 92 percent NaI, 7 percent LiI, and 1 percent TlI by weight. If separated Li^6 were used, this mixture would have the same neutron detection efficiency as natural LiI. The lithium concentration increased by a factor of two from the tip, where the crystal started to grow, to the top part of the melt. A 0.1-g crystal from the tip gave ½ the pulse height of pure NaI and 6.5 percent resolution. Unfortunately, the pulse height is inversely proportional to the lithium concentration and as yet no uniform crystal has been grown. Linearity between gamma-ray and neutron pulses was established. The fluorescent band of the mixed crystal falls between the 4200A and 5400A bands of NaI−Tl and LiI−Tl, respectively.

* This work was performed under the auspices of the AEC.
[1] Hofstadter, McIntyre, Roderick, and West, Jr., Phys. Rev. 82, 749 (1951).

B10. An Automatic Recording Scintillation Spectrometer for Gamma-Rays. THOMAS D. STRICKLER AND W. G. WADEY, *Yale University.*—The spectrometer to be described makes use of a large NaI/TlI crystal mounted on an RCA 5819 photomultiplier tube and was designed for the high efficiency requirements connected with a study of elastic scattering of gamma-rays. It has proved to have reasonably good resolution and has the added advantage of being completely automatic. This enables it to be used over a considerable period

of time for measurement of weak spectra without the constant attention normally required by the single channel pulse height analyzer.

B11. Magnetic Compton Spectrometer. J. W. MOTZ, WILLIAM MILLER, AND H. O. WYCKOFF, *National Bureau of Standards.*—A magnetic spectrometer has been constructed to determine absolute photon intensities and energies over the energy range from approximately 0.5 to 10 Mev with an accuracy of about 5 percent. The instrument measures the momentum distribution of Compton electrons ejected by a photon beam from a thin beryllium foil into a *small* solid angle in the forward direction.[1] The energies of these selected Compton electrons are directly related to the energies of the incident photons. The conversion to absolute photon intensities is based on the integration of the Klein-Nishina differential cross section over the spectrometer acceptance angle. The finite size of the foil requires that the energy and intensity determinations account for (a) the energy loss by the Compton electrons in traversal of the foil and (b) scattering of these electrons in the foil. These effects are evaluated from studies of line shapes obtained with a 10 curie Cs^{137} source for foils of various sizes. The contribution of pair production electrons accepted by the spectrometer at a given energy is found by reversing the field and measuring the corresponding number of positrons.

[1] Similar measurements with radioactive sources have been made by G. D. Latyschev *et al*, J. Phys. (U.S.S.R.) **3**, 251 (1940).

B12. Deterioration of Boron Trifluoride Counters Due to Rapid Counting Rates.* R. K. SOBERMAN AND S. A. KORFF, *New York University.*—Twenty-two boron trifluoride counters were run at counting rates ranging from 2,300,000 to 330,000 counts per minute in the proportional region from a radium gamma-source until they all had lost their plateaus. This occurred in from 10^8 to 10^9 counts. The pulse heights decreased to the point where maximum sensitivity of the circuitry failed to record more than a few hundred counts per minute. Although a grass background could be detected on the oscilloscope, raising the voltage will not restore the pulse heights and the counters do not recover after resting up to three months. Samples of the gas and several counters were analyzed on a mass spectrometer. From the appearance potential curves for the BF_3, the analysis of the counters, and from the behavior of the counters, a theory was formulated which would explain the deterioration on the basis of the formation of a negative ion sheath formed when the BF_3 dissociates.

* This work was supported by the ONR.

B13. Photographic Gray Wedge Pulse Height Analysis.* W. BERNSTEIN, R. L. CHASE, M. SLAVIN, J. GARFIELD, AND A. W. SCHARDT, *Brookhaven National Laboratory.*—The gray wedge-oscilloscope method of pulse height analysis described by Maeder[1] has been refined. The pulses from a pulse spectrometer are stretched to give constant vertical deflection across the oscilloscope screen. Photographs of the screen are taken on Kodak 35 mm type IV-F spectroscopic film through a wedge mounted on the oscilloscope face. This film was selected for its good reciprocity, speed, grain size, and color response. The gray wedge is neutral filter glass ground into a wedge which may be stepped or continuous. We have used wedges covering either one or two decades of intensity. Photographic wedges are unsatisfactory because of excessive scattering in the dense portion. The pictures are enlarged on Kodalith paper. The distance along the wedge to the transition is proportional to the logarithm of the counting rate; the distance from the base line gives the energy. The requirements on the oscilloscope are linear deflection amplifier, uniform sweep intensity, no change in focus and intensity with counting rate, blanking of the sweep outside the wedge dimensions, and no shift in the baseline with counting rate. Most commercial oscilloscopes have to be modified. Spectra obtained by this method will be compared to single sliding channel analyzer results.

* This work was performed under the auspices of the AEC.
[1] D. Maeder, Helv. Phys. Acta **20**, 139 (1947).

THURSDAY MORNING AT 10:00

Schermerhorn 501

(W. BLEAKNEY presiding)

Invited Papers of the Division of Fluid Dynamics

C1. A Mixing Theory for Dissipative Flows with Increasing Pressure in the Flow Direction. L. CROCCO AND L. LEES, *Princeton University.* (40 min.)

C2. Application of Linearized Characteristic Systems to Supersonic Non-Linear Problems. A. FERRI, *Polytechnic Institute of Brooklyn.* (40 min.)

C3. Flows in the Vicinity of Mach-Number One. G. GUDERLEY, OAR, *Wright-Patterson Air-Force Base.* (40 min.)

Business Meeting of the Division of Fluid Dynamics

THURSDAY MORNING AT 10:00

Havemeyer 309

(J. B. JOHNSON presiding)

Electron Physics: Liquid State

D1. A New Dispenser Type Cathode. JACK MARTIN, *Signal Corps Engineering Laboratories.*—A cathode utilizing the dispenser principle of filtering barium to the outer surface is discussed. Comparisons as regards cathode activation, current density, life and cathode characteristics are indicated in relation to the Philips cathode, and standard nickel sleeved

triple carbonate cathodes. It is found that a cathode utilizing a molybdenum sleeve with a triple carbonate coating sprayed under a magnesium oxide surface is simple to activate, gives current densities of 1 to 2 amp per square centimeter under dc conditions at 1000–1050°C brightness, and has a life in the order of several hundred hours, the main limitation being filament burnouts.

D2. Field Dependent Secondary Emission. HAROLD JACOBS AND JOHN FREELY, *Signal Corps Engineering Laboratories.*—Experiments were conducted with magnesium oxide in which high dc fields were applied to the surface at the same time that secondary emission ratios were being observed. It was found under static conditions that the secondary emission ratios increased exponentially with increasing fields. Yields of several hundred to one were observed for two hundred hours and longer. Square wave measurements were also made modulating both the applied field and the bombarding current. The mechanism of this field dependent secondary emission was found to be related to an avalanche effect triggered by bombarding electrons. Several analogies were found between this type of electron emission and phenomenon in a glow discharge.

D3. Basic Principles of an Electron Interferometer. L. MARTON, *National Bureau of Standards.*—The feasibility of an interferometer operated with electrons instead of light is discussed. Such an interferometer preferably should be a wide-beam interferometer, closer to the Mach-Zehnder type than the narrow-beam interferometers of the double-slit type. A wide-beam interferometer requires an efficient beam splitter. The most efficient method of splitting found up to now consists of utilizing Bragg reflection on thin lamellar crystals. The making of such crystals by means of epitaxy is briefly discussed. It is shown that of several possible designs of an interferometer, the one using three parallel crystals seems to have advantages. The usefulness of an electron beam interferometer for various physical measurements such as the determination of very weak field gradients, investigation of the coherence limit of the deBroglie wave, interference spectroscopy and the measurement of band structure of solids, measurement of internal potentials, etc., shall be briefly mentioned.

D4. Limitations of the Electron Interferometer. J. AROL SIMPSON, *National Bureau of Standards.*—Calculations have been carried out to determine the useful design parameters of the electron beam interferometer conceived by L. Marton. It is found that the initial conception of the instrument will need at least eleven degrees of adjustments for the three crystals and two beam-limiting apertures. The main adjustments are: alignment of the crystals to parallel positions, their adjustments with respect to the optical axis of the instrument, and rotation of the crystals to align their crystalline axes. It is found that for all these adjustments the tolerances are well within the limits of present-day experimental techniques and no undue difficulties are expected on this account. The distance of separation of the crystals is prescribed by the fringe spacing, and for reasonable values of the latter the separating distances have been found to be realizable very conveniently in experiment. Further details are added to those contained in the previous abstract on the making of thin lamellar crystals by means of epitaxy.

D5. Electron Mobilities in Liquid and Solid Argon and Liquid Helium.* M. S. MALKIN,† *Yale University.*—The electron mobilities in liquid and solid argon and in liquid helium are measured using a synchroscope technique. The electron mobilities in liquid and solid argon are proportional to the inverse half power of the electric field strength. From comparison of the liquid argon data with data published for gaseous argon, it is shown that liquid argon may be treated as a gas at high pressure. The electron mobility in liquid helium is measured but does not show the same dependence on electric field strength. Attempts were made to observe pulses due to electron collection in solid helium and in liquid helium below the λ-point, but were unsuccessful. A new unexplained effect is noted in the liquid helium work which must be attributed to liquid helium and not to an apparatus defect.

* This work was supported by the ONR.
† Now at Schlumberger Well Surveying Corporation, Ridgefield, Connecticut.

D6. The Diffraction of X-Rays by Liquid Sodium-Potassium Alloys.* R. E. HENDERSON AND N. S. GINGRICH, *University of Missouri.*—Crystal-monochromated x-rays (0.710A) were directed upon samples of sodium-potassium alloys of several different compositions at 105°C, and the diffraction patterns were recorded photographically. Cleaned samples of liquid sodium and potassium were mixed in an evacuated system, sealed off in thin-walled glass tubes, and later analyzed by spectroscopic analysis for composition. The intensity patterns were corrected for absorption, polarization, and incoherent radiation as usual. Five of these patterns were analyzed to determine the electron density distribution, using approximations that are similar to those used for molecular liquids having more than one kind of atom. These distribution curves show the existence of maxima which are generally suggestive of analogous curves for pure sodium or pure potassium but with the positions of the maxima shifting gradually from that for sodium to that for potassium, and with the first peak never tending towards being a discrete peak as in other molecular liquids. Contrary to the conclusion from earlier x-ray diffraction studies,[1] the present work indicates that in liquid sodium-potassium alloys, there are no permanent molecules.

* This work supported by the Research Corporation.
[1] Banerjee, Ind. J. Phys. 3, 399 (1929).

D7. The Self-Diffusion of Liquid Mercury.* R. E. HOFFMAN, *General Electric Research Laboratory.*—Haissinsky and Cottin[1] have recently reported data on the self-diffusion of liquid mercury from measurements on the rate of exchange between radioactive mercury and aqueous solutions of mercurous nitrate. Their results were expressed by the equation $D=1.4(10)^{-4}\exp(-3100/RT)$. These results are abnormal in that the absolute values of the diffusion coefficient are much lower, and the activation energy much higher, than is to be expected from viscosity data. We have used the conventional capillary technique[2] to measure self-diffusion coefficients of liquid mercury, and in the temperature range 0–90°C, our data fit the equation $D=1.26(10)^{-4}\exp(-1150/RT)$. These results are much more compatible with viscosity data. It is concluded, therefore, that diffusion in the mercury is not the rate-controlling step of the exchange process used by Haissinsky and Cottin. Complete details are to be published elsewhere in the near future.

* Work supported by AEC Contract.
[1] M. Haissinsky and M. Cottin, J. phys. radium 11, 611 (1950).
[2] J. S. Anderson and K. Saddington, J. Chem. Soc., S381 (1949).

D8. Production of Electric Turbulences in a Fluid Medium. OLEG YADOFF, *Columbia University.*—The phenomenon of the influence of electric field on electric current in metallic or carbon conductors, described by the author at the last Washington meeting, leads to the observation, under the same experimental conditions, of a new peculiar phenomenon: the production of electric turbulences of a singular nature; they are certainly due to the effect of interaction between the electric field (acting in a closed system concentrically towards the conductor of electric current) and the electro-magnetic field (being part of the electric current). Such turbulences are visible to the eye if colored fumes are introduced into the experimental apparatus. They have the very marked property

of decomposing fumes and aerosols. The decomposition is rapid and forceful, but is effected progressively, which facilitates the observation of the formation of the turbulences and their rotation. The change in the direction of the direct current causes the change in the direction of the rotation of the turbulences, which shows their dependence on the electromagnetic field of the direct current. The observations made from the experiments provide evidence that the lines of force forming these turbulences carry through a fluid medium free electrons under atmospheric pressure. These free electrons penetrate into the conductor carrying the electric current. Their existence explains the effect of the chemical decomposition of the fumes and aerosols of every type.

D9. Angular Points in Liquids Versus Temperature. G. ANTONOFF, A. YAKIMAC, A. URMANCZY, AND R. MADRAZO, JR.—Vapor pressures, densities, latent heats, etc. follow a discontinuous path, contrary to classical views. This appears clearly, if density of liquid d_l less density of vapor d_v, which we call d $(d=d_l-d_v)$, is elevated into power $\frac{1}{4}$. Plotted against temperature $d^{\frac{1}{4}}$ gives a broken line. The angles of intersection correspond accurately to simple integer values of $X=4$, 8, 16, 32, etc., where $X=d_l/d_v$, which according to Antonoff is the association factor.[1] The recent figures for water by N.B.S.[2] show it clearly. Although these values have been "smoothed," the third significant figure has not been affected. One of the authors, H. F. Stimson, wrote: "I have looked over the original papers . . . and failed to find the discrepancies in formulations from our observed values by as much as 1 part in 1000." The effects described are exhibited by the third figure. Therefore our results are beyond all doubts. They are a manifestation of a definite law of nature: Aggregation takes place in stages, according to the law of multiple proportions.

[1] Jerome Alexander, Colloid Chem. **7** (1950).
[2] Natl. Bur. Standards, RP 1229, Washington, D. C.

Post-Deadline Papers, if any

THURSDAY MORNING AT 10:00

Pupin 428

(A. G. SHENSTONE presiding)

Optical Spectroscopy and X-Rays

E1. Spectroscopy from the Point of View of Communication Theory. Part III. Line Shapes. GILBERT W. KING AND A. G. EMSLIE, *Arthur D. Little, Inc.*—The finite aperture of a spectroscope cuts off the Fourier transform of the output signal. Shannon has shown that the amount of information in such a signal, $\Psi(x)$, is limited to amplitudes at intervals $\pi/2$ diffraction widths apart. Intermediate values are given by the interpolation formula $\Sigma\Psi(n\pi/2)\sin(2x+n\pi)/(2x+n\pi)$. Diffraction actually multiplies the transform by a *triangular* filter. This, equivalent to the Fejèr summation process, leads to the more rapidly convergent expression $\Sigma\Phi(n\pi/2)\times[\sin(x+n\pi/2)/(x+n\pi/2)]^2$. The $\Phi(n\pi/2)$ are particular values of the signal without diffraction, seen through a square filter. They can be obtained as correlation sums of Fourier coefficients of the truncated transforms of the separate functions, representing the slits, natural line shape and electrical filter. For a function, such as Beer's law, whose transform is not known, the coefficients can be obtained by correlating with $\sin x/x$. The complicated expression for the contour of a single line at the output should not be fitted by a one-parameter (triangle, Gaussian or Cauchy) formula; nevertheless, it is completely characterized by amplitudes at points $x=n\pi/2$ only. This is borne out experimentally. When there is no distortion by Beer's law or filtering, the shape can be expressed in closed form, involving exponential integrals.

E2. Diffraction by Finite and Infinite Gratings.* SAMUEL N. KARP, *New York University*.—Diffraction of an obliquely incident plane wave by a grating of arbitrary cylinders is investigated mathematically, under the restriction that the spacing is large compared to wavelength and to the dimensions of the obstacle; no restriction is imposed upon the relation of the latter to the wavelength. It is found that the current density induced in each cylinder in the grating can be expressed as a linear combination of the current densities induced upon an *isolated* cylinder by (a) the obliquely incident plane wave, (b) a plane wave progressing to right and to left along the grating. Specialization to the case of circular cylinders small compared to wavelength is also undertaken, and certain resonances are discussed. The excitation of finite or semi-infinite gratings of isotropic scatters [e.g., thin wires] is investigated. In both cases the variation of the amplitude of the cylindrical wave contributed by each scatterer, and also the far field can be obtained simply and without neglect of end effects, when the interaction of scatterers is restricted to that between N nearest neighbors. The validity of this assumption is discussed in terms of the solution for an infinite grating. In the semi-infinite case the restriction may be removed at the expense, however, of extreme complication of the form of the result.

* Research supported in part by the Geophysical Research Division of the Air Force Cambridge Research Center.

E3. Multiple Scattered Reflection from a Striated Surface.* VIC TWERSKY, *New York University*.—The general solution for the multiple scattering of a plane electromagnetic wave by parallel cylinders derived previously is applied to nonspecular reflection from a random configuration of semicylindrical bosses on a perfectly conducting plane; correlations higher than the second are ignored. For spacing between neighbors large compared to wavelength and radii, the far field form of the multiply scattered waves are summed explicitly to obtain a solution in closed form for normal incidence, $\alpha=0$, and for $\alpha>60°$. It is found that the effects of multiple scattering are negligible for the component polarized parallel to the bosses for all α, and are significant for the perpendicular component only for large α. The most pronounced departures from single scattering theory occur for the immediate vicinity of grazing incidence. For an infinite distribution and $\alpha\to\pi/2$, each polarization component of the total reflected wave reduces simply to a plane wave differing from the corresponding incident component only by a phase factor of π. This is in agreement with observations for an approximately plane surface of arbitrary surface texture or physical constants.

* Research supported in part by the Geophysical Research Division of the Air Force Cambridge Research Center.

E4. The $3\nu_3$ Bands of CO_2 and CS_2. NORMAN M. GAILAR AND EARLE K. PLYLER, *National Bureau of Standards*.—The $3\nu_3$ band of CO_2 has been studied,[1,2] but in the present invest-

gation the molecular constants and band origin, previously unreported, are determined. A 15,000 line/in. grating spectrometer was employed. A multiple reflection absorption cell with a path length of 6 meters was used. The cell will be described. The presence of atmospheric H_2O displaced some of the rotational lines of this band, and the molecular constants could not be determined with the highest accuracy. The constants determined are in good agreement with the latest values reported.[1] The band origin is 6972.4 cm^{-1}. The spectrum of CS_2 in the region of 2.2μ was examined. Five overlapping bands were observed. The rotational structure of the transition 000→003 was resolved, and band heads of transitions from excited lower states were present. Two band heads involving the S^{34} isotope were observed. Some of the molecular constants for CS_2 have been determined and will be reported.

[1] E. F. Barker and T. Y. Wu, Phys. Rev. **45**, 1 (1934).
[2] L. Goldberg, O. Mohler, A. Pierce, and R. McMath, Phys. Rev. **78**, 74 (1950).
[3] W. S. Benedict, Robert C. Herman, and Shirleigh Silverman, J. Chem. Phys. **19**, 1325 (1951).

E5. Absorption Spectrum of Free NH_2 Radicals. G. HERZBERG AND D. A. RAMSAY, *National Research Council of Canada.*—It is well known that oxy-ammonia flames and discharges through streaming ammonia emit an extremely complicated many-line spectrum in the region 4200–8300A called the α-bands. These bands have been tentatively assigned to the NH_2 radical although other possibilities have also been considered. Since photochemical investigations suggest that NH_2 is formed as the primary step in the photolysis of NH_3, an attempt was made to observe the absorption spectrum of NH_2 in a flash photolysis apparatus. The spectra of the photodecomposition products of NH_3 were photographed within 1 millisecond of the photolysis flash using a 21 ft grating. In the region 5700–6900A many absorption lines were indeed observed which coincide exactly with emission lines from an oxy-ammonia flame. The fact that these α-bands occur in absorption and that they have a structure characteristic of an asymmetric top molecule of small moment of inertia leaves no doubt that they are due to the free NH_2 radical. This conclusion was confirmed by the observation of the α-bands in absorption in the flash photolysis of N_2H_4. In this case the NH band at 3360A also appears strongly in absorption while it does not appear in the NH_3 photolysis.

E6. Emission of the Atmospheric Bands in Discharges and Afterglows in Pure O_2. LEWIS M. BRANSCOMB,* *Harvard University.*—The atmospheric bands of O_2 result from a forbidden $^1\Sigma_g^+ - {}^3\Sigma_g^-$ magnetic dipole transition with a probability of only 0.14 sec. Conditions are described which permit the strong excitation of these bands in emission in both a direct discharge and the subsequent afterglow in spectroscopically pure oxygen. The spectrum of the afterglow at 1-cm pressure contains only the (0, 0) and (0, 1) atmospheric bands and a weak continuum. Bands up to (4, 4) appear in the direct discharge, along with very strong OI lines. The Schumann-Runge and Herzberg bands are absent, as are bands of O_2^+. Rotational and vibrational "temperatures" measured in both discharge and afterglow show that thermal equilibrium is attained before radiation occurs. This result further justifies the reliance of Meinel[1] and Dufay[2] on the rotational temperature of the (0, 1) band in the night afterglow spectrum.

* Now at the National Bureau of Standards.
[1] A. B. Meinel, Astrophys. J. **112**, 464 (1950).
[2] J. Dufay, Compt. rend. **231**, 1531 (1950) and **232**, 426 (1951).

E7. Forbidden Lines in Spectra of Sb I and As I. M. HULTS AND S. MROZOWSKI, *University of Buffalo.*—The excitation of multipole transitions and their hyperfine structure has been already investigated in bismuth vapor.[1] The purpose of this work was to extend the observations to lighter elements. The spectra were excited by high frequency oscillations. The vapor pressure of the metal was varied and several millimeters of helium were added to bring the lines to maximum intensity. Under the optimum conditions the intensity of corresponding line decreases in order Bi I, Sb I, and As I. For antimony two lines $^3P_{\frac{1}{2},\frac{3}{2}} \rightarrow {}^4S_{\frac{3}{2}}$ were observed and their structure studied with Fabry-Perot etalons up to 18-mm separation. The line λ5415 shows a partly resolved structure mainly because of the splitting of the upper level $^3P_{\frac{1}{2}}$; the line λ6098 is a wide doublet ($\sim$0.5 cm^{-1}), the components of which split further into two unresolved groups each (isotopes 121 and 123). The splitting of the doublet compared with results of Badami[2] (0.475 cm^{-1}) indicates a total splitting of $\sim$0.05 cm^{-1} for the level $^4S_{\frac{3}{2}}$. For corresponding transitions in arsenic λ5362 was found to be single, and λ5498 was found to be a doublet with a separation of 0.155 cm^{-1}.

[1] S. Mrozowski, Phys. Rev. **69**, 169 (1946).
[2] J. S. Badami, Z. Physik **79**, 224 (1932).

E8. Term Values in Mn III. HOWARD D. GOLDGRABER, *University of Pennsylvania.*—The analysis of the spectrum of Mn III by Catalan and Riguelme[1] gives the sextet and the four quartets of the $3d^3$ configuration. These terms were used to calculate the radial integral parameters, which lead to a mean deviation between the observed and calculated terms of 461 cm^{-1}, neglecting configuration interaction. With the correction proportional to $L(L+1)$, first noted by Trees, added as an extra parameter, the mean deviation is reduced to 90 cm^{-1}. Many has estimated the effect of additional parameters on the agreement between theory and experiment by computing the mean error. For the case of three parameters the mean error is 729 cm^{-1}. With the $L(L+1)$ correction added, the mean error is 201 cm^{-1}. The positions of the unknown terms are predicted. The intervals of the terms were calculated from the d^3 spin-orbit matrix which was computed using Racah's methods.

[1] Private communication, courtesy of Dr. Charlotte M. Sitterly.

E9. The Detection of Water-Alcohol Azeotropes through Ultraviolet Spectra.* GLADYS A. ANSLOW AND IRENE S. WHITE, *Smith College.*—In the spectra of numerous alcohols in isooctane recently reported,[1] appear several absorptions in the longer wavelength region, the strongest of which originate in OH...O and OH^+...O hydrogen bridges, and certain weaker absorptions less certainly in CH...O associations[2] possibly between the solvents and the alcohols. To examine the effect of water-alcohol azeotropes the normal alcohols have been redistilled over silica-gel in a Podbielniak column with helical-glass packing, and successive samples of the first and second distillates examined with the Beckman ultraviolet spectrophotometer. The presence of these azeotropes in the earlier samples of the first distillate shifted the OH^+...O absorptions to lower frequencies than those of the final dry samples, the latter being identical with the onsets reported.[1] In the first samples of methyl and ethyl alcohols a variety of weak onsets appear. Calculations indicate their origins in azeotropes with various numbers of water molecules. In the later samples fewer onsets appear, the strongest from two or four H_2O's per unit; even these are absent in the spectra of the final samples.

* Supported by the ONR.
[1] Gladys A. Anslow, Faraday Society Discussion, No. **9**, 299 (1950).
[2] Gladys A. Anslow and Helen H. Fife, Phys. Rev. **83**, 192 (1951).

E10. Absorption by Beryllium in the Neighborhood of the *K* Edge. R. W. JOHNSTON* AND D. H. TOMBOULIAN, *Cornell University.*—Following the experimental procedure described in a previous report,[1] measurements have been carried out on

the absorption by metallic Be in the spectral range 70 to 250A. The absorbers consisted of metallic foils or layers of Be deposited on Zapon-wire mesh substrates by evaporation. The absorption curve reveals a sharp K edge located at approximately 110A, an intense absorption band centered at about 100A and the existence of secondary structure on the short wavelength side of the K edge. The present data have yielded consistent results for the mass absorption coefficient, where values range from approximately 1.0×10^4 to 1.6×10^5 cm²/g in the above spectral range. In an effort to determine whether the dip at 100A was caused by the oxide, the absorption by BeO was investigated in this spectral range. It was found that the absorption by BeO was essentially uniform from 70A to 250A.

* Now at the Electronics Research Laboratory, Electronics Park, Syracuse, New York.
[1] E. M. Pell and D. H. Tomboulian, Phys. Rev. **76**, 172 (1949).

E11. Scattering of X-Rays by Atoms. G. PLACZEK, *Institute for Advanced Study.*—The incoherent scattering cross section of an atom for x-rays depends on the distance correlation of electron pairs which is caused by the Pauli principle[1] and by interaction between the electrons. The influence of the latter effect, which has so far been neglected, on the angular variation of the cross section will be discussed. It is also shown that the usual procedure of applying the Breit relativistic correction to the incoherent cross section has to be modified. This correction does not refer to the incoherent cross section, but to the part of the cross section which corresponds to scattering by free electrons.

[1] W. Heisenberg, Physik Z. **33**, 737, 1931.

E12. Scintillation Spectrometer for Measuring Total Energy of X-Ray Photons. M. R. CLELAND AND H. W. KOCH, *National Bureau of Standards.*—A large, liquid-scintillator, x-ray spectrometer has been successfully tested with bremsstrahlung from a 50-Mev betatron. The scintillator tank is so constructed that individual high energy x-ray photons will dissipate a major portion of their energy in the tank if initially directed along the major axis in the cylinder of liquid. The tank is 48 inches long and 7½ inches in diameter and contains xylene with two grams per liter of terphenyl. Sixteen selected 5819 photomultiplier tubes are placed in a line parallel to the cylinder axis and on the surface of the cylinder. The combined photomultiplier output pulse is proportional to the total light produced by an x-ray photon expending its energy in the liquid. Monte Carlo calculations have been made to test the expected loss of x-ray energy by radiation escaping through the side or end of the xylene cylinder. The energy resolution is limited by the variation of light collection efficiency throughout the liquid. The variation was computed and measured to be of the order of plus or minus 10 percent. Bremsstrahlung spectra determined with the betatron operating between 25 and 44 Mev are in agreement with a corrected theoretical[1] energy distribution modified by the expected energy resolution.

[1] L. I. Schiff, Phys. Rev. **83**, 252 (1951).

THURSDAY MORNING AT 10:00

Horace Mann Auditorium

(E. O. SALANT presiding)

Cosmic Rays, I

F1. Altitude Effects on Cosmic-Ray Fine Structure. DANA T. WARREN, *Colorado A. and M. College.*—Measurements have been made on the detailed zenith-angle dependence of cosmic-ray intensity in the east and west azimuths in Fort Collins. The latitude is the same as that of Missouri, where previous fine structure observations have been carried out, but the altitude is about 4000 feet higher. Fluctuations have been observed similar to those in Missouri, amounting to two or three standard deviations in several instances. Comparison with the Missouri results in the same azimuths indicates that the relations are similar, though detailed identification is not yet possible. The agreement seems to be best if the comparison is made on the basis of the atmospheric path length, as would be expected if the effects are the result of atmospheric absorption. Evidence has also been obtained of the importance of side showers and other spurious effects in measuring the value of the exponent in the zenith-angle variation law.

F2. Latitude Variation of the Vertical Cosmic-Ray Intensity at High Altitudes.[1] W. F. G. SWANN AND D. W. SEYMOUR,[2] *Bartol Research Foundation.*—The results, uncorrected for meteorological effects, are shown in Table I, R begin the ratio of the maximum to minimum intensity at the altitudes expressed, in thousands of feet, by the subscripts.

Our 1946 results agree with those of Schein and Gill where, in both cases, the lead observer was placed above the apparatus. Our 1951 data with lead between the counter trays give much larger values of R. Our observations also show that the change in the hard component ratio for increasing depth of atmosphere is equal to the change for a mass equivalent increase of lead absorber.

TABLE I.

	Bartol (Telescopes)				Neher (Ion Chamber)		Neher	Schein and Gill
Date	1946	1951			1948–49		1948–49	1947
Lead	16 cm[a]	0 cm	9 cm[b]	18 cm[b]	0 cm	11 cm[c]	0 cm	20 cm[a]
R_{12}	1.33	1.80	2.09	1.87				1.4
R_{30}		1.66	1.89	1.68	1.56	1.89	1.58	1.4
R_{50}	1.50	1.53	1.67	1.64				1.4

[a] Lead above telescope.
[b] Lead between counter trays.
[c] Lead around chamber.

[1] Assisted by the Joint Program of the ONR and the AEC and Brookhaven National Laboratory.
[2] Introduced by W. F. G. Swann.

F3. The Primary Cosmic Radiation at High Latitudes.* MARTIN A. POMERANTZ AND GORDON W. MCCLURE, *Bartol Research Foundation.*—Various properties of the new group of low energy primary cosmic-ray particles ($E<1.6$ Bev for protons) which enter the top of the atmosphere at geomagnetic latitudes north of 52° were investigated during the summer of 1950. Measurements were obtained with the same quadruple-coincidence counter trains used previously,[1] oriented either horizontally or vertically, and with pulsed ionization chambers biased to detect bursts exceeding 1 Po-α. No diurnal or temporal variations in the cosmic-ray intensity were detected, and no change between 1949 and 1950 was indicated. Flights were conducted with counter trains con-

taining various thicknesses of interposed Pb absorber. No latitude effect was revealed for cosmic rays traveling in the horizontal direction at the highest altitudes attained (~9 mm of Hg). A similar result was obtained in the case of bursts detected by the ionization chambers. The data permit conclusions to be drawn regarding the horizontal component, the solar dipole-moment, the nature of the low energy spectrum, as well as nuclear disintegrations and primary heavy nuclei.

* Supported by the joint program of the ONR and AEC. Field Expedition sponsored by the National Geographic Society.
[1] M. A. Pomerantz, Phys. Rev. 77, 830 (1950).

F4. Scintillation Counter Measurements of the Cosmic Radiation.* R. V. ADAMS, DOROTHY MONTGOMERY HIRSHFELDER, J. A. NORTHROP, AND N. R. WHETTEN, *Yale University.*—Scintillation crystals, operated in coincidence with Geiger counters, have been used to detect cosmic radiation at New Haven† and at Climax, Colorado. Four cubical anthracene crystals were cemented together to form a phosphor with a 3×3-cm² horizontal surface and a 1.5-cm depth. Pulses from two 1P28 photomultiplier tubes, placed on either side of the phosphor, were added and amplified to obtain pulse-height distribution curves. Above and below the phosphor were placed Geiger-counter trays, each having a sensitive area of 400 cm². Pulse-height distributions, obtained for several thicknesses of lead absorber which were placed above the apparatus, indicate that the particles detected at sea level consist principally of the meson component. Between sea level and 3500 meters elevation there is a factor of 2 increase in the number of small pulses, while the largest pulses increase by a factor of about 20. Preliminary experiments have also been carried out at Climax with NaI crystals in coincidence with Geiger counters. Measurements of counting rates for three sizes of crystal have been made to determine whether the particles detected are principally (1) single minimum ionizing particles, (2) showers, or (3) stars.

* Supported in part by the joint program of the ONR and AEC.
† The sea level experiments were carried out by Dorothy Montgomery Hirshfelder, who is now at Madison, Wisconsin.

F5. An Analysis of the Hard Component of Cosmic Rays in the Upper Atmosphere.* M. A. CLARK, *Massachusetts Institute of Technology.*—An experiment has been carried out to study the hard component of cosmic rays in the upper atmosphere. The balloon-borne apparatus consisted of a lead absorber, three trays of Geiger-Mueller tubes, a coincidence circuit, and radio telemetering equipment. The arrangement yielded a separation of the hard component into two groups, depending on whether or not the particles suffered nuclear interactions on traversing 20 cm of lead. The rate of occurrence of particles in these two groups has been determined as a function of atmospheric depth from 16 gm-cm^{-2} to 400 gm-cm^{-2}. An analysis of the results provides information about the numbers of mu-mesons and nucleons in the upper atmosphere.

* This work has been supported in part by the joint program of the ONR and AEC.

F6. Diurnal Effect on Cosmic-Ray Neutrons at High Altitudes.* M. J. SWETNICK, H. A. C. NEUBURG, AND S. A. KORFF, *New York University.*—A neutron counting arrangement was flown at high altitudes from day into night by means of a plastic balloon[1] in order to investigate whether there existed a diurnal effect on cosmic-ray neutrons. The flight was launched at 4:30 P.M. from Minneapolis, Minnesota. At 6:00 P.M. the balloon leveled off at 87,000 feet and floated until sunset (approximately 8:00 P.M.) Just after sunset the balloon descended to 84,000 feet where it remained for three hours. The experiment consisted of an enriched and a regular BF_3 counter, associated circuitry, and a pressure recording device. To prevent corona discharge, the counters and high voltage were pressurized. The apparatus was placed in a styrofoam box along with containers of warm water to prevent it from freezing. Data were radioed to a ground station. The average counting rate at 87,000 feet obtained before sundown was determined, as was the average counting rate at 84,000 feet after sundown. Because of the difference in floating levels during day and night the average day counting rate at 87,000 feet was corrected to 84,000 feet. The correction was made by an interpolation process using the slope calculated from the daytime counting rate *versus* pressure curve. On comparing the day and night counting rates at 84,000 feet an average diurnal effect of 17±7 percent was found. Such an effect could be produced by neutrons coming directly from the sun or by a diurnal effect in the neutron producing component at high elevations.

* This work was assisted by the joint program of the ONR and AEC.
[1] Flight service carried out by Project Skyhook.

F7. Cosmic Ray Neutron Production.* ARTHUR BEISER, *New York University.*—Much information on the production of neutrons by the cosmic radiation in air and in other absorbers can be obtained from a consideration of information determined from nuclear emulsion experiments. These neutrons are produced in nuclear disintegrations ("stars"), and their rates of production under various circumstances may be calculated by properly interpreting: (1) the alpha-particle-proton and deuteron-proton ratios in stars and their variation with atomic weight and star size; (2) the dependence of prong multiplicity upon various parameters, including absorption depth; (3) the cross sections for star production in different materials; and (4) the extrapolation of such rates of production to include prong multiplicities smaller than three. Calculations of this nature have been performed previously but were inaccurate because of certain omissions and misconceptions which will be discussed. The present method has been employed in the determination of neutron production rates under several experimental conditions, and these values will be compared with values obtained under similar conditions by the use of counter techniques.

* This work was supported by the joint program of ONR and AEC.

F8. Collision Mean-Free-Path of Secondary Particles from Nuclear Interactions.* M. ANNIS AND H. S. BRIDGE, *Massachusetts Institute of Technology.*—A cloud-chamber experiment has been performed at Echo Lake, Colorado (10,600 feet) to measure the collision mean free path of the secondary particles from nuclear interactions. An estimate has been made that 75 percent of these secondary particles are mesons, and that 25 percent are protons. Several events have been interpreted as either "nuclear stoppings" or $\pi^+ \rightarrow \pi^0$ charge exchange. Use has been made of the Olbert calculations (see following abstract) on multiple scattering to differentiate clearly between multiple Coulomb scattering and nuclear scattering. The average kinetic energy of the secondary protons and mesons was estimated to be 800 Mev. The collision mean-free-path in Pb and Al has been found to be geometrical within the statistical errors of about 25 percent.

* Supported in part by ONR.

F9. Application of the Multiple Scattering Theory to Cloud-Chamber Measurements, I. STANISLAW OLBERT, *Massachusetts Institute of Technology.*—We discuss in this paper some theoretical questions concerning the application of the multiple scattering theory to the analysis of cloud-chamber pictures: (a) We modify Molière's theory taking into consideration the finite nuclear dimensions. For this purpose, we assume that the probability of single scattering goes abruptly to zero for angles greater than $\phi_0 = a\phi_m/r_n$, where a is the Thomas-Fermi radius of the atom, r_n the radius of the nucleus, and ϕ_m is the screening angle as derived by Molière. The cut off

affects especially the "tail" behavior of the distribution function for the multiple scattering. While Molière's function decreases as ϕ^{-3} for projected angles of scattering, ϕ, large compared with rms angle, our distribution function decreases approximately as a Gaussian function of $(\phi-\phi_0)$. (b) We derive the distribution function for the mean value of the square angle of scattering in the plates of a multiple-plate cloud-chamber. (c) We estimate quantitatively the effect of observational errors on the distribution functions considered in (a) and (b).

F10. Application of the Multiple Scattering Theory to Cloud-Chamber Measurements, II. MARTIN ANNIS, HERBERT S. BRIDGE AND STANISLAW OLBERT, *Massachusetts Institute of Technology.*—When a particle comes to rest in a multiple-plate cloud-chamber, for each plate traversed, one can define a scattering variable, $\zeta=\phi R^{\alpha}$, where ϕ is the projected angle of scattering in the plate, R is the residual range, and α is the coefficient in the empirical relation, $p\beta\alpha R^{\alpha}$ (p and β are momentum and velocity of the particle). The variable ζ obeys a distribution function analogous to that for the scattering angle of mono-energetic particles (*cf.* preceding paper). The parameters entering in this function depend only on the mass of the particle. We have applied the method outlined above to an analysis of the secondary particles resulting from high energy nuclear interaction of cosmic rays. We have separated mesons (π or μ) from protons on the basis of the mean value of ζ^2 for the various plates traversed by each particle. We have then plotted two distribution curves, including the measured values of the scattering variable, ζ, for all particles of each group. We have thus obtained a value of $1860_{-130}{}^{+170}$ electron masses for protons, and $230_{-20}{}^{+30}$ electron masses for mesons.

Invited Paper

F11. Cosmic Rays Underground. E. P. GEORGE, *Birkbeck College, University of London.* (30 min.)

THURSDAY AFTERNOON AT 2:15

Horace Mann Auditorium

(S. A. KORFF presiding)

Cosmic Rays, II

G1. High Energy Nuclear Interactions in Lead.* E. M. HARTH,† F. E. FROEHLICH, AND K. SITTE, *Syracuse University.*—A large cloud chamber containing 8¼-in. lead plates was run in conjunction with a 134-counter hodoscope placed directly underneath the chamber. Thus it was possible to study details of the interactions produced in the chamber from the photographs and to follow the further development of the "nuclear cascade" through about 600 g/cm² of lead in the hodoscope. In particular, the "integral path length" of the nuclear cascade is a measure of the energy of the primary particle. The analysis of some 400 events shows over a primary energy interval from about 1–2 Bev to about 10 Bev a variation of the primary mean free path from 220 g/cm² to 160 g/cm², while the ratio of the numbers of charged mesons and of protons increases from about 0.4 to 1.5, and the ratio of charged to neutral mesons remains constant (~2). The statistics are not good enough to decide whether the mean free path of the secondaries also varies with the primary energy; a mean value of 270 g/cm² was observed. A distribution function of the energy transfer as a function of the energy can be derived: It shows a low probability for small transfers, followed by a rather flat section slowly decreasing for large fractional transfers.

* Supported in part by the AEC.
† Now at the NRL, Washington, D. C.

G2. The Ratio of Soft to Hard Particles in Air Showers.* K. SITTE, *Syracuse University.*—Some doubt has recently been cast upon the validity of the customary procedure of identifying the energy spectrum of air showers with the primary spectrum. These two distributions would differ if the mechanism of energy transfer to the electron component itself varied with energy. As a result, one would then expect a variation in the amount and composition of the penetrating component of extensive showers. An experiment was therefore carried out to compare the penetrating component of 10^{13} ev showers at Mt. Evans, altitude 4300 m, with that of 10^{13} ev showers at Echo Lake, altitude 3260 m. The results are: (number of penetrating particles)/(number of electrons) $=(2.0\pm0.11)\times10^{-3}$ at Mt. Evans, and $=(1.30\pm0.12)$ at Echo Lake; (number of N-particles)/(number of μ-mesons) ≈ 2.0 at Mt. Evans, and ≈ 0.7 at Echo Lake. If the change in the composition due to nuclear interactions and decay is accounted for, one finds that the ratio of μ-mesons to electrons is about equal for the two energies, while the ratio of N-particles to μ-mesons is slightly larger for the lower energy. The results are therefore consistent with a uniform picture for the processes involved, demanding only a slightly increased multiplicity of meson production for the higher primary energy.

* Supported in part by the AEC.

G3. Large Air Showers at Airplane Altitudes.* HENRY L. KRAYBILL, *Yale University.*—The change of extensive shower rate with variation of counter area of a threefold coincidence detector has been measured at pressure altitudes of 25,000 ft, 30,000 ft, and 33,000 ft between Lima, Peru, and Rome, New York, in a B-29 airplane flown by the U. S. Air Force. Coincident discharges of individual counters in a fourth tray, located centrally with respect to the other three trays, were recorded for each shower. The area of the counter trays was varied from 80 cm² to 560 cm². In this range, measured mean values of γ ($\gamma=\ln C/d\ln A$, where C is the shower rate and A is the counter area) are 1.45 at 25,000 ft, 1.5 at 30,000 ft, and 1.56 at 33,000 ft.

* Supported by the joint program of the ONR and AEC.

G4. Monte Carlo Study of Shower Production. ROBERT R. WILSON, *Cornell University.*—Monte Carlo calculations of cascades produced by photons and electrons incident on lead have been completed for initial energies in the range from 20 to 1000 Mev. The results will be exhibited and are quite different from those by conventional cascade theory, as would

be expected for lead. The number of electrons near the shower maximum is considerably less and the shower penetrates farther into the lead. The Monte Carlo results have also been corrected for the effects of multiple scattering on the motion of the electrons.[1] The effects are quite different depending on the measurement considered. Thus, ionization current measurements are only slightly changed (the transition curves are foreshortened by a nearly constant amount), but the number of electrons counted behind successive lead plates in a cloud chamber can be reduced by as much as 50 percent by multiple scattering.[2] The comparison of the calculated curves with the ionization measurements of Blocker *et al.*[3] and the cloud-chamber measurements of Shapiro[2] is satisfactory.

[1] R. R. Wilson, Phys. Rev. **84**, 100 (1951).
[2] A. M. Shapiro, Phys. Rev. **82**, 307 (1951).
[3] Blocker, Kenney, and Panofsky, Phys. Rev. **79**, 419 (1950).

G5. Characteristic Functionals in Cascade Theory.* W. T. SCOTT, *Smith College*.—The enormous complexity of cascade shower theory has been somewhat unraveled by the introduction of master functions[1] giving the probability of finding N particles of specified energies at depth t, and by the use of certain generating functions.[2] Further progress seems possible through the use of characteristic functionals.[3] We define $C[\sigma(E);\ E_0,\ t]=\Sigma_N(1/N!)\int_0^\infty dE;\ldots\int_0^\infty dE_N\sigma(E_1)\ldots\sigma(E_N)\times P_N(E_1,\ E_2,\ \ldots E_N;\ E_0,t)$ as a functional of an arbitrary function $\sigma(E)$. P_N is the master function, E_0 the initial energy. From C we may obtain by functional differentiation and suitable choice of σ all subsidiary functions of interest. The fact that a shower propagates itself from any depth t' as a new starting point leads to a functional iteration: $C[\sigma;\ E_0,t+t']=C[C[\sigma;\ E,\ t];\ E_0,t']$. Two equations for $\partial C/\partial t$ may be derived from this and from the elementary multiplication and energy loss laws. One is a linear functional equation and the other ("adjoint") is a nonlinear differential-integral equation. Two examples will be given for which C can be found explicitly, and various theorems stated.

* Research performed at Brookhaven National Laboratory, under AEC auspices.
[1] W. T. Scott, Phys. Rev. **82**, 893 (1951); H. J. Bhabha, Proc. Roy. Soc. (London) **A202**, 301 (1950).
[2] L. Jánossy, Proc. Phys. Soc. (London) **A363**, 241 (1950).
[3] M. S. Bartlett and D. G. Kendall, Proc. Cambridge Phil. Soc. **47**, 65 (1951). These authors define the characteristic functional differently.

G6. Cosmic-Ray Stars Produced in the Gas of a Cloud-Ion Chamber. FIELDING BROWN, R. RONALD RAU, GEORGE T. REYNOLDS, *Princeton University*.*—Using a cloud-ion chamber, which has been described previously,[1] several hundred stars have been observed in the cloud-chamber gas during 40 days of operation at Echo Lake, Colorado. The chamber was filled successively with neon, argon, and krypton, and operation was found to be feasible with each gas. Statistical analysis of the resulting data is in progress and preliminary results on prong angles and numbers distributions will be given.

* Supported by the joint program of the ONR and AEC.
[1] Brown, Rau, and Reynolds, Bull. Am. Phys. Soc. **26**, No. 6, 16 (1951).

G7. Z-Dependence of Cross Section and Energy in Cosmic-Ray Stars.* IAN BARBOUR, *Kalamazoo College*.—Cosmic-ray induced disintegrations of nuclei of metal foils "sandwiched" between face-to-face Ilford G5 emulsions exposed at balloon altitudes have been studied using Au, Pt, Sn, Cu, Ni, and Al. After removal of the foil and development, each pair of plates is reconstructed in its original orientation and scanned for stars originating in the metal,[1] and then separated again for re-examination under high magnification. Previous results[1] have been extended and integral cross sections for stars of various sizes as they vary with the atomic number of the target nucleus will be presented. Measurements on the location and dip angle of each star track allow comparison with the expected angular distribution and calculation of the path length in the foil for each particle. Grain density measurements enable approximate energy distributions and excitation temperatures to be obtained.

* This work has been aided by a Cottrell Grant from the Research Corporation.
[1] I. Barbour and L. Greene, Phys. Rev. **79**, 406 (1950).
[2] I. Barbour, Phys. Rev. **82**, 280 (1951).

G8. Absorption in Carbon of Protons in the Cosmic Radiation at Sea Level.* J. BALLAM,† *University of California*.—The absorption mean free path of protons of energies between 150 and 570 Mev was measured by placing carbon absorber above two counter-controlled cloud chambers, one in a magnetic field of 4800 gauss and the other containing copper plates. The protons were identified by a measurement of their curvature and range. A counter tray, connected to a neon indicator, was placed above the carbon and put in coincidence with the trays which triggered the cloud chambers. The incident energy spectrum was obtained from the work of Mylroi and Wilson.[1] By observing the numbers of protons stopping in the lower cloud chamber after passing through various thicknesses of carbon and correcting for the ionization loss, the ratio of the number stopping to the number incident was calculated, and the mean free path was determined to be $L=167$ g/cm^2 with a lower limit of 136 and an upper of 300. It was also found that about fifty percent of the protons stopping under 44 and 88 g/cm^2 of carbon were produced therein by incident neutral particles, thus confirming the work of Goldwasser and Merkle.[2]

* Assisted by the joint program of the ONR and AEC.
† Now at Princeton University, Princeton, New Jersey.
[1] Mylroi and Wilson, Proc. Phys. Soc. (London) **A64**, 404 (1951).
[2] Goldwasser and Merkle, Phys. Rev. **83**, 43 (1951).

G9. The Disintegration of V-Particles.* C. J. KARZMARK, R. W. THOMPSON, AND HANS O. COHN, *Indiana University*.—The cloud-chamber experiment on penetrating showers previously reported[1] has been continued in order to increase the amount of quantitative data available on V-particles. A 12-inch diameter magnetic cloud chamber under a layer of lead is triggered by an array of counters which responds preferentially to events in which two or more penetrating particles are produced in the lead above the chamber. Certain modifications and improvements of the apparatus have been made in the interest of reproducible accuracy of measurement over an extended period of time. At regular intervals, sets of no-field tracks are taken in order to check that track distortions produced by the chamber are negligible. Up to the present time, a total of 1053 stereoscopic photographs of penetrating showers of multiplicity greater than or equal to 3 have been obtained. Among these, a total of 35 neutral V-particle disintegrations of both types have been found, and also a few examples of the rarer charged V-particle disintegration. In one very energetic penetrating shower, two neutral V-particle disintegrations occur. The experiment is in progress and the results to date on the nature of the disintegration fragments, the disintegration schemes, and the Q-values will be presented.

* Assisted by a grant from the Frederick Gardner Cottrell Fund of the Research Corporation and by the Office of Army Ordnance Research.
[1] Thompson, Cohn, and Flum, Phys. Rev. **83**, 175 (1951).

G10. Nuclear Interaction of Fast μ-Mesons.* H. C. WILKINS† AND R. D. SARD, *Washington University* (Introduced by A. L. Hughes).—Neutron production by the nuclear interaction of fast μ-mesons with Pb has been studied at a depth of 2000 g cm^{-2} underground. An array of G-M counters above and below the absorber registered separately penetration by unaccompanied μ-mesons and those accompanied by one or more other ionizing particles. Neutrons were detected by an array of neutron counters below the absorber. The counting rates for 1, 2, and 3 neutrons detected in delayed coincidence with the penetrating event gave information about the mean multiplicity of neutrons per interaction and the cross section

for the interaction. Upper and lower limits on the inelastic μ-meson-nucleon cross section are given independent of the rather uncertain value of the neutron multiplicity. A discussion will be given of the relationship of these limits to the results previously reported by Cocconi and Tongiorgi; Amaldi and Fidecaro; and Braddick, Nash, and Wolfendale.

* Supported in part by the ONR.
† AEC Predoctoral Fellow.

G11. Production Cross Section and Energy Spectrum of the π_0 Meson (Cosmic-Ray Measurement). G. SALVINI AND Y. KIM, *Princeton University.**—The properties of neutral mesons are studied on the basis of the successive electromagnetic interactions in the closely spaced C and Pb plates of a cloud chamber of dimensions 18×18×8 inches. The nuclear events were detected in an almost unbiased way by sodium iodide crystals.[1] The experiment was performed at Echo Lake, Colorado. The distribution in energy of the π_0's does not differ appreciably from the energy distribution of the charged π-mesons given by the Bristol Group. The table summarizes the cross section for production of π_0's, and the ratio $(\pi_+ + \pi_-)/\pi_0$.

Energy of producing protons (Bev)	0.345	0.8–2	>2
σ_{prod} of the π_0	$1/200\ \sigma_{geo}$†	$0.16\ \sigma_{geo}$	$0.6\ \sigma_{geo}$
Ratio $(\pi^+ + \pi^-)/\pi_0$	...	...	2.8 ± 0.6

The pictures are now being analyzed to estimate the mean free path in C and the cross section for charge exchange in C and Pb of the π-mesons.

* Supported by the joint program of the ONR and AEC.
[1] G. Salvini and George T. Reynolds, Phys. Rev. **83**, 198 (1951); G. Salvini, Nuovo Cimento, **8**, (October, 1951).
† Burton J. Moyer, private communication.

G12. Momentum Spectra of Cosmic-Ray Mesons and Protons at Sea Level and 3.4 km Altitude.* W. L. WHITTEMORE AND R. P. SHUTT, *Brookhaven National Laboratory.*—A cloud-chamber experiment has been performed at sea level and 3.4 km altitude to collect data on the momentum and scattering distributions of 15,000 mesons and protons. Electrons are recognized by the showers they produce in lead inside the chambers and thus can be excluded. The momentum distribution at sea level is in accord with the results of others. A comparison of the sea level and altitude spectra indicates that only few mesons, if any, are produced below 3.4 km up to momenta of 10 Bev/c. The distributions for negative particles have also been used to compute the production spectrum of mesons assuming that production of the fast mesons observed takes place within the top 125 g/cm² of the atmosphere. The resulting differential momentum distribution at production can be represented adequately as a power law with an exponent equal to 2.82 ± 0.07 in good agreement with previous published results. The relative numbers of positive and negative particles agree well with those of other workers at sea level. At altitude this $+/-$ ratio becomes quite large towards the lower momenta (up to 2.4 as against 1.2 at sea level). Assuming that the difference between the sea level and altitude ratios is due to protons, one can compute that above 0.2 Bev/c protons form 20 ± 3 percent of all ionizing particles at 3.4 km. From the $+/-$ ratios the proton momentum spectrum has been calculated.

* Work done at Brookhaven National Laboratory under the auspices of the AEC.

G13. A Redetermination of Mesotron Mean Lifetime as a Function of Momentum. D. W. SEYMOUR AND W. F. G. SWANN, *Bartol Research Foundation* (Introduced by W. F. G. Swann).—Calculations of mesotron mean lifetime were carried out for various momenta by comparing differential lead absorption measurements at two different elevations. An additional lead absorber within the upper counter telescope was used to compensate for the absorption of the air column. The value of the rest mean life thus obtained is 2.3×10^{-6} sec, in reasonable agreement with what has been considered the most precise value of 2.15×10^{-6} sec obtained by Rossi and Nereson by another method.[1]

[1] B. Rossi and N. Nereson, Phys. Rev. **62**, 417 (1942).

G14. Multiplicity of Mesons Produced in Lead.* JOHN LINSLEY† AND E. P. NEY, *University of Minnesota.*—A number of interactions of very energetic particles, presumably primary cosmic-ray protons, have been observed in the lead plates of a counter-controlled cloud chamber at atmospheric depths less than 180 g/cm² (altitudes greater than 40,000 ft). The apparent multiplicity of meson secondaries was greater than 10 in all of 11 events and greater than 20 in 4 of the events, while the corresponding incident proton energies were less than 100 Bev and 200 Bev respectively for the two groups. The data agree with an observation of Hartzler[1] that considerably more mesons are produced in heavy nuclei than Fermi's theory[2] predicts for single nucleon-nucleon collisions. The agreement is interesting since the experimental conditions were quite different. The large multiplicity of mesons supports the opinion that a nucleon-meson cascade develops to a considerable extent within heavy nuclei in such events.

* Research supported by the ONR.
† Now at the University of Virginia.
[1] A. J. Hartzler, Phys. Rev. **82**, 359 (1951).
[2] E. Fermi, Prog. Theor. Phys. **5**, 570 (1950); Phys. Rev. **81**, 683 (1951).

THURSDAY AFTERNOON AT 2:15

Pupin 301

(R. E. MARSHAK presiding)

Scattering of Elementary Particles and Simple Nuclei

H1. Scattering of Gammas by Bound Electrons.* J. S. LEVINGER, *Louisiana State University.*—Knowledge of the amplitude for elastic scattering of gamma-rays (Co^{60}, 1.33 Mev, and ThC″, 2.62 Mev) by bound electrons (Sn and Pb) is essential for the analysis of Wilson's experiment[1] on Delbruck scattering. Franz[2] showed that, subject to many approximations, the coherent electronic scattering amplitude is that given by the form factor calculation. The general expression[3] for the scattering amplitude, subject to the single approximation of a free intermediate state for the electron, is difficult to evaluate. The present author has evaluated this expression by an expansion in q/mc, where q is the photon change of momentum, and m is the electron mass. For $q/mc < 1.8$, the scattering amplitude is slightly larger than that of the form factor calculation and independent of the photon energy. Numerical results for this ratio for scattering of

gammas by K electrons of tin are: ratio = 1.1 for $q/mc = 1$; ratio = 1.2 for $q/mc = 1.8$.

* Assisted by the ONR.
[1] R. R. Wilson, Phys. Rev. **82**, 295 (A), (1951).
[2] W. Franz, Z. Physik **98**, 314 (1936).
[3] Obtained by H. A. Bethe, F. Rohrlich, P. Greifinger, and the present author.

H2. Nuclear Scattering of 17-Mev Gamma-Rays. M. B. STEARNS, *Cornell University*.—Measurements of the elastic and inelastic nuclear scattering of gamma-rays produced by the Li (p, γ) reaction have been made. The gamma-ray detector was a NaI crystal. To reduce backgrounds, an anti-coincidence ring of Geiger counters were placed around the crystal. Scattering from Bi, Pb, Sn, and Cu was measured at an angle of 116°±17°. The following absolute differential cross sections were obtained:

	Bi	Pb	Sn	Cu
I. Elastic ($E>14.4$ Mev)	0.82±0.22	0.53±0.14	0.20±0.049	0.044±0.020
II. Inel. El. ($E>12.3$ Mev)	1.47±0.22	1.21±0.16	0.33±0.049	0.066±0.016

The cross sections in row I are the measured values. The cross sections in row II are lower limits, the upper limits being about 3 times these values. All errors are standard deviations. Bremsstrahlung, from secondary electrons in the scatterers, was negligible in the foregoing measurements. The elastic scattering cross sections varied with Z as $Z^{1.2\pm0.4}$ while the inelastic scattering varied at a rate greater than $Z^{1.2\pm0.3}$. The elastic scattering results combined with observed integrated γ–n cross sections for Cu (about 0.9 Mev-b.) is in agreement with a gamma-ray absorption curve having a width of 4–6 Mev centered near 18 Mev. Appreciable inelastic scattering was observed indicating that narrow one-level theories such as the Goldhaber-Teller theory cannot be correct.

H3. Angular Distribution of Protons Scattered by 1.0 to 3.02-Mev Deuterons.* G. D. FREIER, W. R. STRATTON, R. J. S. BROWN, H. D. HOLMGREN, AND J. L. YARNELL, *University of Minnesota*.—The differential cross section for protons elastically scattered by an incident deuteron beam has been measured in the energy range 1.00 and 3.02 Mev. This corresponds to an extension of the Los Alamos[1] p, d scattering data from 1.51 to 0.50 Mev. An incident deuteron beam from the Minnesota electrostatic generator was passed through a small volume scattering chamber[2] filled with hydrogen. Recoil protons were detected in a proportional counter at laboratory angles less than 90° and scattered deuterons at angles less than 30°. The angular range of data varied with energy. The maximum angle (center of mass system of coordinates) at all energies is 126.4°. The minimum angle at 3.02 Mev is 60° and at 1.00 Mev, 90°. Data at 3.02 Mev agree, within errors, with previous data.[1]

* Supported by the joint program of the ONR and AEC.
[1] Sherr, Blair, Kratz, Bailey, and Taschek, Phys. Rev. **72**, 622 (1947).
[2] Claassen, Brown, Freier, and Stratton, Phys. Rev. **82**, 589 (1951).

H4. Angular Distribution of 1.5 to 3.0-Mev Deuterons Scattered by Tritium Nuclei.* W. R. STRATTON, G. D. FREIER, G. R. KEEPIN, D. RANKIN, AND T. F. STRATTON, *University of Minnesota*.—The differential cross section for deuterons scattered elastically by tritium has been measured in the energy range 1.50 to 3.02 Mev using the Minnesota electrostatic generator as a source of monoenergetic deuterons. The small volume scattering chamber, previously described,[1] has been modified slightly by increasing its volume to about 200 cm³. A proportional counter detected both scattered deuterons and recoil tritons, and measurements of the cross section were obtained between 45° and 125° in the center-of-mass system of coordinates. The cross section as a function of angle displays a typical minimum near 90° in the center-of-mass coordinate system. The cross section at this minimum decreases monotonically with increasing deuteron energy.

* This work is supported by the joint program of ONR and AEC.
[1] Claassen, Brown, Freier, and Stratton, Phys. Rev. **82**, 589 (1951).

H5. Proton-Alpha Particle Scattering Using Photographic Techniques.* W. E. KREGER, R. O. KERMAN,† AND W. K. JENTSCHKE, *University of Illinois*.—The differential cross section of proton-alpha-particle scattering at 5.82±0.06 Mev has been measured using nuclear research plates to detect the scattered protons and the recoil alpha-particles. Values of the differential elastic scattering cross section have been determined for twenty-eight center-of-mass angles between 16° and 154°. The over-all uncertainty in these values is approximately 1.5 percent. A phase-shift analysis of the data has been made following the method of Critchfield and Dodder.[1] No evidence for phase-shifts in collisions with angular momenta greater than that for P-waves has been found. The analysis gives an S-wave phase-shift of −46° 40′, a $P_{\frac{1}{2}}$-wave phase-shift of 34° 42′ and a $P_{\frac{3}{2}}$-wave phase-shift of 180° 47′ on the inverted doublet model.

* Assisted by the joint program of the ONR and AEC.
† Now at Kalamazoo College, Kalamazoo, Michigan.
[1] Critchfield and Dodder, Phys. Rev. **76**, 602 (1949).

H6. Precision Alpha-Alpha Scattering at Low Energies. D. B. COWIE, N. P. HEYDENBURG, G. M. TEMMER,* AND C. A. LITTLE, JR., *Department of Terrestrial Magnetism*.—The differential cross section for the elastic scattering of alpha-particles (He^+) in helium in the energy range 400 kev to 950 kev in 100 kev steps has been measured with the electrostatic generator of the Department of Terrestrial Magnetism over the angular range 10° to 45° (lab). The large currents furnished by a new rf ion source have made this energy range of alpha-particles accessible to experiment. Early work along these lines was confined to the higher energies of natural alpha-emitters and was primarily concerned with the verification of the effects of the identity and boson character of alpha-particles on Coulomb scattering,[1] although some "anomalous" scattering has been observed[2] below 2 Mev. The scattering apparatus used is similar to that of Heydenburg *et al.*[3] with a fixed monitor counter at 15° and helium pressure of 1 mm Hg. The precision attained is about 1 percent. The equipment was tested by scattering from argon gas; pure Rutherford scattering was obtained. At 850 kev the deviations from Mott scattering amount to as much as 8 percent. Phase shift analysis of the results is now in progress. This work is being extended up to 3 Mev with our pressurized electrostatic generator as well as to lower energies in the hope of localizing the ground state of Be^8.

* From the National Bureau of Standards.
[1] Chadwick, Proc. Roy. Soc. (London) **A128**, 114 (1930); Blackett and Champion, Proc. Roy. Soc. (London) **A130**, 380 (1931).
[2] See for instance Mohr and Pringle, Proc. Roy. Soc. (London) **A160**, 190 (1937).
[3] Heydenburg, Hafstad, and Tuve, Phys. Rev. **56**, 1078 (1939).

H7. Neutron-Proton Total Cross Section.* E. M. HAFNER, D. H. FRISCH,† C. E. FALK, T. COOR, AND W. F. HORNYAK, *Brookhaven National Laboratory*.—A precise determination of the total $n-p$ cross section is being carried out with $D-D$ neutrons. Deuterons of 1380 kev enter a gas target of about 100-kev thickness. The exact target thickness, as well as the thickness and nonuniformity of the 0.00005-inch nickel entrance foil, are measured by using the $F^{19}(p, \alpha, \gamma)O^{16}$ resonance at 873.5 kev. The scatterer and detector are located in the forward direction. The detector is a 1-inch diameter button[1] of molded lucite and ZnS at 20 inches from the target. The background with this system is low and consists mostly of $D-D$ neutrons scattered in the room. Cross sections are determined for 16 graphite scatterers and 11 polyethylene scatterers of different diameters. By extrapolating the resulting functions

to zero diameter it is possible to correct $\sigma(n, p)$ for geometrical effects. The scatterers are chemically analyzed and the graphite tested for water vapor absorption. The electronics is continuously checked by using two independent discriminators and scalers on both the monitor and the detector.

* Research carried out under the auspices of the AEC.
† M.I.T.
[1] W. F. Hornyak, Rev. Sci. Instr. (to be published).

H8. Angular Distribution of 215-Mev Neutrons Scattered by Protons.* G. L. GUERNSEY, *University of Rochester.*—The neutron beam obtained by intercepting the circulating protons of the University of Rochester 130-in. synchrocyclotron has been used for neutron-proton scattering experiments. An anthracene scintillation counter telescope has been employed for detection of the scattered protons at laboratory angles of 0° to 50°, with one of the counters serving as a differential energy spectrometer. The angular dependence obtained for the neutron-proton cross section at 215 Mev is in general agreement with the results of the Berkeley 90[1] and 260[2] Mev experiments.

* Supported by the AEC.
[1] Hadley, Kelly, Leith, Segrè, Wiegand, and York. Phys. Rev. **75**, 351 (1949).
[2] Kelly, Leith, Segrè, and Wiegand, Phys. Rev. **79**, 96 (1950).

H9. Total Cross Sections of Carbon and Hydrogen for High Energy Neutrons.* GEORGE R. MOTT, GORDON L. GUERNSEY, AND BRUCE K. NELSON, *University of Rochester.*—Measurements of the total cross sections of carbon and hydrogen have been made at neutron energies of 97±5, 117±5, 140±5, 156±5, 180±7, and 220±10 Mev using a calibrated anthracene crystal as an energy sensitive detector for recoil protons. This proportional crystal was used as the fourth of a quadruple coincidence anthracene scintillation counter telescope which detected protons scattered at 20° from a polyethylene radiator exposed to the collimated high energy neutron beam from the University of Rochester 130-in. cyclotron. The methods used permit the simultaneous measurement of total $n-p$ cross sections over a continuous spectrum of neutron energies. The results obtained are in general agreement with previously reported experimental data, but approximately half the values predicted by Ashkin and Wu[1] ni the 100- to 200-Mev region using tensor force and the symmetrical Rarita-Schwinger exchange model in the rigorous scattering theory.

* Supported by the Joint Program of the AEC and ONR.
[1] J. Ashkin and Ta-You Wu, Phys. Rev. **73**, 973 (1948).

H10. The Total Elastic Scattering Cross Section of Nitrogen for Fast Neutrons.* W. M. PRESTON, P. H. STELSON, AND J. J. HINCHEY, *M. I. T.*—The total cross section of nitrogen has been measured for neutrons in the energy range 200 to 1800 kev, using scatterers of liquid nitrogen and of lithium azide. Eleven resonances were found in the compound nucleus N^{15}, with natural widths of from 3 to 54 kev. Nine of these can be identified with resonances previously known from the reactions $N^{14}(n, p)C^{14}$, $N^{14}(n, \alpha)B^{11}$,[1] or $C^{14}(p, n)N^{14}$.[2] Using the cross sections determined for these reactions, and from the present work, it is possible to assign J-values to many of the excited states of N^{15}. In some cases the parity also can be determined and the effective level spacing D_J computed for the different particles. It must be concluded that the quantities D_J, which contain implicitly the matrix elements for the transition, can vary by a factor of at least one hundred.

* This work was supported by the BuShips and the ONR.
[1] C. H. Johnson and H. H. Barshall, Phys. Rev. **80**, 818 (1950).
[2] Roseborough, McCue, Preston, and Goodman, Phys. Rev. **83**, 1133 1951).

H11. Scattering of Fast Neutrons. E. T. JURNEY AND C. W. ZABEL, *Los Alamos Scientific Laboratory.**—The scattering of fast neutrons by Al, Fe, Ni, Cr, Cu, Ta, Pb, and Bi was investigated by placing samples into the collimated fast neutron beam emerging from the plutonium fast reactor.[1] Small fission ionization chambers containing Np^{237} and U^{238}, respectively, served as neutron detectors. The angular distribution of the scattered neutrons was determined by moving these detectors around the samples. With the same detectors total cross sections were measured in simple transmission experiments. Scattered neutrons detected by the threshold fission counters will be called elastically scattered. If the integral over all angles of the differential elastic scattering cross section is subtracted from the total cross section, an inelastic collision cross section is obtained. Under the assumption that the inelastic scattering is isotropic, transport cross sections were calculated. For all the elements investigated the elastic cross section shows a strong forward maximum, for some elements an additional small maximum occurs near 100°.

* Work performed under the auspices of the AEC.
[1] Rev. Sci. Instr. **18**, 688 (1947).

H12. Inelastic Thermal Neutron Scattering in Lead.* A. W. MCREYNOLDS, *Brookhaven National Laboratory.*—In all crystals the total scattering cross section for neutrons of wavelength $\lambda < 2d$ is dependent on crystalline effects, being the sum of Bragg diffraction and of inelastic and incoherent scattering. The inelastic component of scattering in lead has been studied as a function of temperature and wavelength in the region 2–5.7 angstroms. A beam of neutrons from the reactor was first passed through a mechanical velocity selector consisting of a series of rotating slotted Cd disks, then reflected from the (200) planes of a Pb single crystal to select a monoenergetic beam of high resolution. Measurements were then made of transmission through a Pb single crystal in the symmetry direction 111, 100, and 110, such that Bragg reflection occurs only at certain wavelengths. Between these diffraction regions the inelastic cross section, which varies more smoothly with wavelength, could be determined. Curves of inelastic cross section *vs* λ at 80° and 300°K show increase with decreasing wavelength and a proportionality to temperature in qualitative agreement with theory.

* Research carried out under contract with AEC.

H13. Neutron Energy Distributions from Be, C, and Pb Bombarded by 245-Mev Protons. B. K. NELSON,* *University of Rochester.*—The energy distribution in the forward direction from beryllium, carbon, and lead targets, and at 15° from beryllium and carbon targets, bombarded by 245-Mev protons has been obtained. The neutrons were allowed to bombard a hydrogenous radiator; scattered protons were observed in a scintillation counter relescope. The energy of these protons was determined by measuring the scintillation brilliance in the last crystal of the telescope; neutron energies were then deduced from the kinetics of the $n-p$ scattering. Entire scintillation pulse height spectra were observed at one time by a 24-channel pulse-height analyzer; neutron spectra were deduced from these. All the spectra observed were peaked, the energies at the peaks being about 215, 195, and 180 Mev for Be, C, and Pb, respectively, in the forward direction, and at about 175 and 165 Mev for Be and C at 15°. The carbon and lead spectra were more broadly peaked than the beryllium spectra, and the 15° spectra were broader than the 0° spectra, the full widths at half maximum being about 27 percent, 33 percent, and 49 percent for Be, C, and Pb 0° spectra, and about 40 percent and 42 percent for Be and C at 15°.

* Now at Project Lincoln, M.I.T.

THURSDAY AFTERNOON AT 2:15

Schermerhorn 501

(H. YUKAWA presiding)

Theoretical Physics, I

I1. Interaction between Quantized Electromagnetic Field and Classical Electron. I. R. SENITZKY, *Signal Corps Engineering Laboratories.*—Some quantum-theoretical aspects of the problem of an electron passing through an oscillating cavity have been considered by several authors[1-4] with simplifying assumptions (treating one of the interacting systems classically) and approximate calculations (using first-order perturbation theory or WKB method). The validity of some of the treatments[1,4] is questionable. In the present paper, the Hamiltonian for a quantized field and classical electron with prescribed motion is given. The resulting differential equations of motion are solved exactly by considering the corresponding difference equations. The solution yields some results contrary to those of an earlier theory[1] based on similar assumptions. If the number of photons in the cavity is large and the loss or gain due to the electron is small, the solution reduces to that of another theory[3] in which the field is treated classically and some, but not all, of the wave properties of the electron are considered.

[1] L. P. Smith, Phys. Rev. **69**, 195 (1946).
[2] C. Shulman, Phys. Rev. **82**, 116 (1951).
[3] J. C. Ward, Phys. Rev. **80**, 119 (1950).
[4] D. Gabor, Phil. Mag. **41**, 1180 (1950).

I2. Perturbation Treatment of Electromagnetic Problems. I. Theory. J. R. TERRALL AND BENJAMIN LAX,* *Air Force Cambridge Research Center.*—When inhomogeneous anisotropic media are under consideration, the equations for the electromagnetic field usually cannot be solved exactly in closed form. However, there are cases of practical interest for which the perturbation treatment developed so extensively for the study of quantum-mechanical problems can be profitably applied to the solution of Maxwell's equations. Starting with a complete set of characteristic wave functions of the vector wave equation in a bounded empty space as a basis, we derive expressions for the successive approximations to the electromagnetic field and to the eigenvalues of the wave equation when the perturbing medium, as described by a tensor function of position, is taken into account. We show also how media with the additional complication of time varying properties may be handled. Since the method permits calculation of the field to any order of approximation for generalized media, it is hoped that the usefulness of analysis in experimental applications may be extended. Usually, heretofore, the equivalent of first-order perturbation theory has been used, and this only, in application to isotropic media. Although the theory presented in this paper is specialized to media for which the magnetic permeability is that of empty space, the extension to more general media can be made.

* Now at the Research Laboratory of Electronics, M.I.T.

I3. Perturbation Treatment of Electromagnetic Problems. II. Applications. BENJAMIN LAX* AND J. R. TERRALL, *Air Force Cambridge Research Center.*—Complex inhomogeneous anisotropic media such as plasmas in a magnetic field, dielectrics, semiconductors, and paramagnetic and ferromagnetic materials in resonant microwave cavities have been studied. It is the object of this paper to demonstrate the application of perturbation theory in calculating the effect of these media on the eigenfunctions and eigenvalues of the cavity, i.e., on the electromagnetic field and the resonant frequency and Q of the cavity. A brief discussion of the degenerate perturbation theory as applied to a magneto-ionic plasma will be given, and experimental verification of the theory will be shown. A semiconductor with dielectric properties of large magnitude will be used as an example to demonstrate the need for considering second-order terms. Ferrites with anisotropic magnetic and large magnitude dielectric properties further generalize the application of perturbation theory to Maxwell's equations.

* Now at M.I.T.

I4. Perturbations of Atomic g Values. M. PHILLIPS, *Brooklyn College.*—A further investigation of the perturbation by excited core states of g values of atoms consisting of a single electron outside closed shells takes account of the spin orbit interaction of the excited core. Although the effect vanishes to lower orders than the 4th, and at least the first term in the expansion of the electrostatic interconfiguration interaction cancels even in that order, there is for alkali atoms a residual correction possibly large enough to account for the observed[1] g values for Cs and Rb, which are too large to be attributed to the intrinsic spin anomaly, δ_s. For smaller atomic numbers, however, the effect of perturbations is hardly within the limits of present experimental accuracy. Calculations have also been made for ^2P states: the effect in Ga is negligible, in accord with observed values,[2] but the anomalous observed[3] $g_J(P_{\frac{1}{2}})/g_J(P_{\frac{3}{2}})$ for In may be at least in part due to perturbations of this kind.

[1] P. Kusch and H. Taub, Phys. Rev. **73**, 1477 (1949).
[2] P. Kusch and H. M. Foley, Phys. Rev. **72**, 1256 (1947).
[3] A. K. Mann and P. Kusch, Phys. Rev. **77**, 435 (1950).

I5. On the Magnetic Hyperfine Structure.* R. STERNHEIMER, *Brookhaven National Laboratory.*—Equations have been obtained for the magnetic field at the nucleus due to the current induced in the electron core by an external valence electron. The magnetic field is written as $-4\mu_0(j/j(j+1)) \times\langle r^{-3}\rangle_p(1+R_m)$ where $\langle r^{-3}\rangle_p$ is the average over the valence electron function assumed in a p state, R_m is the correction due to the core, μ_0 = Bohr magneton, j = angular momentum. R_m is of importance in obtaining the nuclear quadrupole moment Q from the value of the magnetic moment μ_I and the ratio b/a of the hfs splittings due to Q and μ_I. The electric field gradient at the nucleus $-(2/5)e\langle r^{-3}\rangle_p(1+R)$ which determines b, contains a similar term R for the distortion of the core by the valence electron. R is the sum of a negative shielding term R_d and an exchange term R_e. It is shown that $R_m \sim R_e$, and that the correction factor for Q is $\sim 1/(1+R_d) \times(>1)$, as predicted by the Thomas-Fermi model.[1] The valence electron interacts with the nuclear moment Q as shielded by the core, so that a greater value of Q is required to give the observed hfs splitting.

* Work performed under the auspices of the AEC.
[1] R. Sternheimer, Phys. Rev. **84**, 244 (1951).

I6. Mass Corrections to the Fine Structure of Hydrogen and Deuterium. E. E. SALPETER, *Cornell University.*—For a hydrogen-like atom with an infinitely heavy nucleus, the Dirac theory gives exact expressions for the fine structure and hyperfine structure. For a nuclear mass M no correction terms of relative order $\alpha(m/M)$ are obtained,[1] if the Breit equation and interaction term (only approximately Lorentz-invariant) is used. It is shown that corrections of relative order $\alpha(m/M)$

are obtained, both for fine structure and hyperfine structure, if a fully relativistic wave equation[3] for two-particle bound states is used. Two of these terms for the fine structure contain $\log\alpha$ as a factor and can also be derived from orthodox perturbation theory. One term is due to recoil energy of the electron in the intermediate state, neglected in the Breit term for the interaction between the electron and nucleus. The other is due to the exchange of *two* transverse quanta between the electron and nucleus, with the electron and nucleonic proton in negative energy intermediate states. These two terms give an energy shift of, very roughly, (m/M) and $(-3m/4M_p)$, respectively, times the Lamb shift.

[1] G. Breit and G. E. Brown, Phys. Rev. **74**, 1278 (1948); Breit, Brown, and Arfken, Phys. Rev. **76**, 1299 (1949).
[2] E. E. Salpeter and H. A. Bethe, Phys. Rev. **85** (to be published).

I7. A Fourth-Order Radiative Correction to Atomic Energy Levels. R. BERSOHN, J. WENESER,* AND N. M. KROLL.—The fourth-order radiative corrections to the elastic scattering of an electron by a specified external potential have been computed using the Dyson S-matrix formalism. Written as a modification in the interaction energy density of the electron with the external potential, the result must be of the form $C_1\bar{\Psi}\sigma_{\mu\nu}\psi F_{\mu\nu}{}^{e}+C_2(-ie\bar{\Psi}\gamma_\mu\psi)\Box^2 A_\mu{}^{e}$ for slowly varying fields. C_1 is a correction to the anomalous moment of the electron and has already been computed.[1] We are concerned here with an evaluation of C_2. The contributions of fourth-order vacuum polarization to C_2 are being calculated elsewhere and therefore have been omitted here. The procedure is similar to that used in the evaluation of C_1. Although the contribution of each diagram diverges in the infrared, the total is finite and equal to $(\alpha^3/2\pi^3K_0^2)$ (0.52 ± 0.21). The indicated uncertainty arises from the fact that certain of the integrals have been estimated by the use of rigorous upper and lower bounds. It is expected that the actual error is considerably less than that indicated. Considered as a perturbing potential the C_2 term contributes to the level of a hydrogenic atom an energy $(2\alpha^6Z^4mc^2)/(n^3\pi^2)\delta_{s0}(0.52\pm0.21)$, which corresponds to 0.24 ± 0.10 megacycles for the $2S$ level in hydrogen.

* AEC Predoctoral Fellow.
[1] R. Karplus and N. M. Kroll, Phys. Rev. **77**, 536 (1950).

I8. Electron Self-Energy. F. J. BELINFANTE, *Purdue University.*—The second-order electron self-energy in quantized Bopp electrodynamics[1] diverges quadratically due to intermediate states with Proca quanta of large negative energy. Pais[2] removed the divergence by subtracting a second-order perturbation through positive-energy Proca quanta (f_+-particles) instead of adding the second-order perturbation through negative-energy Proca quanta. Field-theoretically we obtain Pais' result by introducing an indefinite metric ${}^{\circ}\eta=(-1)^N$, where N is the number of Proca quanta *in interaction representation*. The Proca field (F) is self-adjoint ($F=F^\dagger$) but not hermitian ($F\neq F^*$), and ${}^{\circ}F^{(+)}\Psi_H=0$ replaces ${}^{\circ}F^{(-)}\Psi_H=0$.[1] Thence, ${}^{\circ}\eta\Psi_H=\Psi_H$ and $\Psi_H{}^\dagger=\Psi_H{}^*$. For an observable $\Omega=\Omega^\dagger$ we interpret Ψ_H as a probability distribution for eigenvalues of $({}^{\circ}\eta^H\Omega)$, but the energy can be given by the Hamiltonian in Heisenberg representation ${}^H\mathcal{H}$ itself $(={}^{\circ}\mathcal{H}_0)$, or ${}^H\mathcal{H}_0$ in zeroth-order approximation, with the perturbation causing the electron self-energy $\delta\mathcal{E}$. We thus find[2] $\delta\mathcal{E}=m_e c^2$ for Proca quantum mass $m_+\approx10^{135}m_e$, and $\delta\mathcal{E}\approx0.02\ m_e c^2$ for $m_+=274\ m_e$, for which m_+c^2. Bopp's classical theory gave $\delta\mathcal{E}=m_e c^2$.

[1] F. J. Belinfante, Abstract I9, Chicago meeting Am. Phys. Soc., October, 1951.
[2] A. Pais, Koninkl. Nederland. Akad. Wetenschap. Verh. (1e Sectie), **19**, 1 (1947), particularly pp. 59–60.

I9. On the Definition of the Integral over Paths in Feynman's Formulation of Nonrelativistic Quantum Mechanics. W. H. GUIER* AND A. J. F. SIEGERT, *Northwestern University.*—Feynman[1] defines his integral over all paths $x(t)$ by dividing the time interval t_2-t_1, into small intervals $\Delta t=t_{k+1}-t_k$ and integrating over the variables $x_k=x(t_k)$, with the specification that, inside each interval, $x(t)$ is the path followed by a classical particle between x_k, t_k and x_{k+1}, t_{k+1}. The division of the time interval and the introduction of the classical path into the definition of the integration in function space can be avoided by using the averaging process of random function theory, defining

$$K(x_1,t_1|x_2,t_2)=\langle\chi\{\eta(t);t_1,t_2\}\delta(x_2-x_2-\int_{t_1}^{t_2}\eta(t)dt)\rangle_{Av}.$$

$\chi\{\eta(t);t_1,t_2\}$ is a functional of $\eta(t)$ and a function of t_1 and t_2, and the average over functions $\eta(t)$ is defined by giving the averages of products $\eta(t_1)\eta(t_2)\cdots\eta(t_n)$ as specified in reference 2, Eqs. (41a, b); 42a, b) with $D=i\hbar/2m$, where m is the mass of the particle.

* Now at The Johns Hopkins Applied Physics Laboratory, Silver Spring, Maryland.
[1] R. P. Feynman, Revs. Modern Phys. **20**, 367 (1948).
[2] M. C. Wang and G. E. Uhlenbeck, Revs. Modern Phys. **17**, 323 (1945).

I10. Distribution of the Total Momentum of the Electrons in Pair Production by Photons. A. BORSELLINO, *Cornell University.*—The distribution of the total momentum $\eta=|\vec{p}_++\vec{p}_-|$ of the electrons in pair production by photons on an atom has been calculated in the two limiting cases of a bare nucleus and of complete screening. At high energies the distribution depends only on the quantity $Q^2=\kappa^2-\eta^2$ (where $\kappa=E_++E_-$), which is easy to obtain from measurements of the energies E_+, E_- and the angle ω between the electron and positron. The formulas may be useful in studying, independently of the direction of the photon, the recoil momentum of the nuclei and the distribution of the angle ω. Such an expression, independent of the direction of the primary, is particularly useful in the case of cosmic-ray photons.

I11. Nonlocal Photons. J. S. LOMONT, *North American Aviation, Inc.*—Bloch has pointed out that zero rest mass photons must be local; however, the concept of "heavy photon" (finite rest mass) recently developed by several authors (e.g., Coester) suggests the possibility of a nonlocal heavy photon field. The Fourier expansion of the heavy free-photon potential $A_\mu(X)$ can be obtained by replacing $|\mathbf{k}|$ by $(|\mathbf{k}|^2+\kappa^2)^{\frac{1}{2}}$ in appropriate places in the expansion of the ordinary photon field. The expansion of the nonlocal potential satisfying the usual nonlocal equations can then be obtained by appropriately inserting delta functions containing r in the local heavy photon potential expansion. The nonlocal commutation relations reduce to the local relations as $\lambda\to0$ if $A_\mu(X,r)$ is properly normalized. The total nonlocal Hamiltonian is the same as the local Hamiltonian so nonlocal photons have the same statistics as local photons. The nonlocal photon field interacting with an electron field can then be quantized by the method of "direct quantization" (extension of the Yang-Feldman theory) with the aid of an appropriate nonlocal delta-function. However, the interacting field can be quantized in accordance with either the correspondence principle or the reciprocity principle, so there is some ambiguity.

I12. Subtractive Bosons in a Generalized Theory. ALEX E. S. GREEN, *The University of Cincinnati.*—In a generalized field theory based upon a higher order quadratic Lagrangian, alternate bosons make negative contributions to the total field energy.[1,2] The purpose of this paper is to investigate the possibility that the total field energy will nevertheless be positive definite. We first consider the use of supplementary conditions somewhat analogous to those used in ordinary electrodynamics to suppress negative total energy states. Although suitable for the empty field, this approach appears to lead to difficulties when sources are present. We next consider the use of a perturbation procedure, involving a generalization of the usual occupation number operator concept, which automatically imposes mild restrictions upon the field

eigen states. This more natural approach seems quite promising in several respects. It casts suspicion upon the assumption which has been made in many articles that the various mass components of a generalized field are completely independent. A great many problems remain to be considered, in particular the problem of quantizing the source field and the problem of relating such a mathematical description to the confusing experimental observations.

[1] A. Green, Phys. Rev. **73**, 26, 519 (1948); **75**, 1926 (1949).
[2] A. Pais and G. E. Uhlenbeck, Phys. Rev. **79**, 145 (1950).

I13. Operators and Field Theories.* JAMES L. ANDERSON, *Syracuse University*.—A mathematically rigorous treatment of certain quantum-field-theoretical problems may be achieved with the help of normal-mode representation, which converts the problem into one with a denumerable number of degrees of freedom. Such a decomposition is, however, not readily available in a covariant nonlinear theory, in which the Hamiltonian contains higher than second-degree terms. In any case, an operator is properly defined if it transforms one Hilbert vector into another one. In an attempt to discover approaches circumventing normal modes, we have treated the uniform string of finite length and have cast the Hamiltonian with vanishing zero-point energy into a form free of Fourier coefficients. When we constructed other operators, it was found that only when the corresponding classical variable is the generating functional of a nonsingular canonical transformation, will the quantum analog be a "good" operator. Though this condition obviously is not sufficient, it may be that any operator satisfying it can be turned into a "good" operator merely by the reordering of factors.

* Supported by ONR.

I14. Lower Limits for Interaction Times in Elementary Particle Processes. E. GORA, *Providence College* (Introduced by R. B. Lindsay).—A lower limit for the duration of the interaction between a photon and a charged particle has been obtained in a semiclassical way by assuming correspondence between the photon and a classical wave train of finite length. For spinless particles obeying the equations of motion of Dirac's classical theory of the electron, and photon energies $\hbar\omega \gg mc^2$ (m mass of the scattering particle) this lower limit is $\tau_0(\hbar\omega/mc^2)$ where $\tau_0 = \hbar^3/16me^4c$. This expression resembles formulas for lifetimes of unstable particles both in its dependence upon fundamental constants and in its increase with the energy involved in the process. The transfer of linear momentum to the scattering particle appears to be essentially due to radiation reaction in such a semiclassical theory.[1] An attempt is now made to link these results up with the quantum theory of radiation damping. Different types of interaction processes between elementary particles are taken into consideration.

[1] E. Gora, Phys. Rev. **84**, 1119 (1951).

THURSDAY AFTERNOON AT 2:15

Havemeyer 309

(R. SMOLUCHOWSKI presiding)

Metals and Magnetism

J1. On the Activation Energy for Grain Boundary Viscosity in Metals. A. S. NOWICK, *Yale University*.—The proposal by Kê,[1] that the activation energy for grain boundary viscous slip may be identical with the activation energy for volume diffusion, has aroused much attention. This proposal is based upon very little experimental evidence, nor has there been, as yet, any theoretical justification for it. Recent experiments make possible a direct comparison of the two activation energies in binary alloys which show anelastic effects caused by stress-induced atomic reorientation.[2] For such an alloy a plot of internal friction *versus* temperature shows a double peak. The low temperature peak is a result of the stress-induced reorientation and is therefore controlled by diffusion; the high temperature peak results from grain boundary viscous slip. From the change in resolution of the two peaks with a change in vibration frequency, it is possible to detect small differences in the activation energies for the two processes. Results in α-Ag-Zn and α-brass alloys show that the activation energy for viscous slip is consistently about ten percent *greater* than that for volume diffusion. This result implies that the mechanisms for the two processes are not the same. A tentative mechanism for grain boundary slip is suggested.

[1] T. S. Kê, Phys. Rev. **73**, 267 (1948).
[2] C. Zener, Phys. Rev. **71**, 34 (1947); A. S. Nowick, Phys. Rev. **82**, 340(A) (1951).

J2. Mechanical Properties of Thin Films of Silver.* W. E. WALKER, T. J. TURNER,† AND J. W. BEAMS, *University of Virginia*.—Films of silver of uniform thickness were deposited on small cylindrical steel rotors with rounded ends, and the rotational speeds required to throw them off of the rotors were measured. The films were deposited on the rotors either by electroplating or by evaporation. The rotors were spun in a high vacuum by a method previously described.[1] If N is the rotor speed required to throw off the film, R the radius of the rotor, T the tensile strength, A the adhesion, d the density, and h the thickness of the silver film, then $4\pi^2 dN^2R^2 = T + (AR/h)$. By using rotors of different diameters, both the tensile strength and the adhesion of the films were determined as a function of the thickness. The tensile strength increased markedly as the film thickness was decreased from 10^{-4} to 10^{-6} inch. The adhesion to the rotor was a function of the process of deposition.

* This work was supported by U. S. Navy Bureau of Ordnance under Contract NOrd-7873.
† Now at the University of New Hampshire.
[1] Beams, Young, III, and Moore, J. Appl. Phys. **17**, 886 (1946).

J3. Relations between Thermal Expansion and Chemical Composition of Some Binary Aluminum Alloys. PETER HIDNERT, *National Bureau of Standards*.—Relations between the coefficients of linear thermal expansion and the chemical composition of annealed aluminum-beryllium (about 10 to 70 atomic percent beryllium), aluminum-copper (1 to 18 atomic percent copper), and of aluminum-silicon (5 to 40 atomic percent silicon) alloys were obtained. The relations were derived from data obtained on the coefficients of expansion

of these annealed alloys for several temperature ranges between 20° and 300°C. The addition of beryllium, copper, or silicon to aluminum causes a decrease in the coefficients of expansion. The relations between the coefficients of expansion of these eutectiferous alloys and the chemical composition (atomic percent) are approximately linear, and are therefore in agreement with the theory for the eutectiferous portions of the equilibrium diagrams of the binary alloys. Copper has a greater effect than beryllium, and silicon has the greatest effect of these three alloying elements. The data on these binary alloys will be published in the *Journal of Research* of the National Bureau of Standards.

J4. Influence of Stress on the Temperature of the Diffusionless Transformation in Au–Cd Single Crystals.* J. INTRATER, L. C. CHANG, AND T. A. READ, *Columbia University*.—In the neighborhood of 60°C the alloy of gold containing 47.5 at. % cadmium undergoes a first-order phase change from a high temperature CsCl structure to an orthorhombic structure. The transformation occurs by a shear mechanism, which leads to a change in shape of the sample, with a temperature hysteresis of about 10°C between heating and cooling.[1] In the present work it has been found that an applied shear stress produces a linear shift of the two transformation temperatures, without changing the difference between them. Thus the measured shift is probably equal to that of the thermodynamic equilibrium temperature for the two phases. On this assumption the latent heat of transformation has been calculated from the measured transformation strain and the rate of change of transformation temperature with stress, with the Clausius-Clapeyron equation. A value of 0.40 calories per gram is obtained. This value is now being checked by calorimetric measurements.

* This work was supported by the AEC.
[1] L. C. Chang and T. A. Read, Trans. Am. Inst. Mining Met. Engrs. **189**, 47 (1951).

J5. Grain Boundary Diffusion of Zinc in Copper.* R. SMOLUCHOWSKI AND R. FLANNAGAN, *Carnegie Institute of Technology*.—The depth of penetration of zinc along grain boundaries of columnar copper has been measured as a function of the angle between the two grains. Similarly to the earlier results on diffusion of silver along grain boundaries of columnar copper, the depth of penetration along grain boundaries is greater than volume penetration only for angles greater than about 20° and reaches a maximum at 45°. This critical angle increases with increasing temperature of diffusion in accord with the known fact that at sufficiently high temperatures only volume diffusion is observed. The activation energies have been measured and their dependence on the angle indicates a significant change in the permeability of the grain boundary at the critical angle. These results are in accord with the previously proposed model.[1]

* Sponsored by an AEC contract.
[1] M. R. Achter and R. Smoluchowski, J. Appl. Phys. **22**, 1260 (1951).

J6. Strain Rate, Temperature, and Time Effects in the Ballistic-Speed Deformation of Mild Steel. J. M. KRAFFT, *Naval Research Laboratory*.—Continuous force-time records of the penetration of conical projectiles were obtained from the moving strain pattern introduced into a Hopkinson bar by measuring the strain as a function of time with wire-resistance gages. Penetrations on a fully annealed, low carbon steel have been made with 45° cones at impact velocities ranging from 600 to 2200 ft/sec at temperatures ranging from −100°C to +75°C. The results show that in the strain rate range of 10^4 to 10^5 sec^{-1}, the cone penetration resistance increases linearly with the strain rate at 0.5 $lbs/in.^2/sec^{-1}$. At constant strain rate the penetration resistance decreases linearly with increasing temperature at the rate of 680 $lbs/in.^2/°C$. There is an indication of a "delay time" for plastic yielding of about four microseconds associated with these cone impacts.

J7. Effect of Grain Size on Magnetoresistance of Polycrystalline Copper.* GEORGE B. YNTEMA, *Yale University*.—The magnetoresistance of three samples of copper was measured at liquid helium temperatures, and was found to depend on the grain size of the sample. Such dependence was suggested by MacDonald.[1] The ratio of resistance increment in a magnetic field to the resistance in zero field was 3.5 times as large in the sample with smallest crystal size as in that with the largest crystals. The zero field resistance of the former sample was 0.44 times that of the latter. Samples were wire drawn from Hilger spec-pure copper. The wire was annealed, then cold worked by bending and reannealed to obtain random crystal orientation. The grain size was controlled by the temperature of the second anneal. Similar work is being carried out on other metals.

* Assisted by an AEC Predoctoral Fellowship.
[1] D. K. C. MacDonald, Phil. Mag. **42**, 756 (1951).

J8. Hall Effect in Zinc Crystals at Low Temperatures. JOHN K. LOGAN,* *Northwestern University*.—An experimental study has been made of the Hall effect in single crystals of zinc. For each crystal, one component of the Hall field was measured for a fixed crystallographic orientation of the current density, but for various orientations of the magnetic field in the plane perpendicular to the current density. At 77°K, the Hall field is a linear function of magnetic field which can be characterized by two coefficients. The first coefficient, for the interaction between the field component parallel to the hexagonal axis and current density component in the hexagonal plane, has a value of about 2×10^{-12} ohm cm/gauss. The second coefficient measures the interaction between the field component in the hexagonal plane and the current density component perpendicular to this field component. Its value is about 0.2×10^{-12} ohm cm/gauss. At 20.4°K, the Hall field is no longer linear with magnetic field. For some orientations, the measured component of the Hall field increased with increasing magnetic field. In other cases, the opposite behavior was observed. Between 5 and 10 kilogauss, the Hall effect is of the same order of magnitude at 20.4°K as at 77°K. No correlation was apparent between the Hall effect and either susceptibility or magnetoresistance.

* An AEC Predoctoral Fellow. Now at Naval Research Laboratory.

J9. Multiple Scattering of μ-Mesons in Magnetized Iron. STEPHAN BERKO, *University of Virginia* (introduced by Frank L. Hereford).—Previous experiments[1] on the deflection of μ-mesons in iron employed computed corrections for multiple scattering. The importance of scattering in such experiments has since been discussed theoretically.[2] In the experiment to be described, a beam of μ-mesons was made to penetrate 15 cm of iron, and the angular distribution as a result of multiple scattering was observed with a set of 12 counters located 80 cm below the iron block. Each of these counters was in coincidence with the collimating telescope above the iron. The multiple scattering curve with the iron unmagnetized fitted the theoretical one if the known momentum distribution was assumed. The distribution curve with the iron magnetized was then observed and the two curves compared. The observed effect agrees with the assumption that B is the effective vector inside the ferromagnetic medium. The assymmetry introduced by the magnetic field demonstrates the positive excess of μ-mesons. With increased resolution one will be able to deduce the relative momentum distribution of positive vs negative mesons.

[1] W. F. G. Swann and Danforth, Phys. Rev. **45**, 565 (1934); F. Rasetti, Phys. Rev. **66**, 1 (1944); Bernardini, *et al.*, Phys. Rev. **68**, 109 (1945).
[2] G. Wannier, Phys. Rev. **72**, 304 (1947).

J10. A Theory of Intrinsic Magnetization in Alloys. W. J. CARR.—The intrinsic magnetization of alloys among the iron transition group of metals has been explained using a Heitler-London model for the 3*d* electrons. The magnetic moment associated with each atom is determined by the principle of maximum spin and the sign of the interaction between neighboring pairs from the overlap of the wave functions. It is found that a large number of alloys derive their spontaneous magnetization from an antiparallel arrangement of atomic spins.

J11. Collective Electron Theory of the Saturation Moment of Alloys. J. E. GOLDMAN, *Carnegie Institute of Technology.*—The influence of alloying on the saturation magnetic moment is treated from the collective electron standpoint in a manner analogous to Slater's and James' treatment of impurities in a semiconductor.[1] The method is based on the local distortions in the density of states of an energy band caused by a perturbation in the periodic potential. It is shown that where the solute atom is one that differs from the matrix atom by several atomic numbers (as, for example, chromium in nickel), this perturbation has the effect of causing the occupancy probability for some of the states at the bottom of the 3*d*-band to become very small. Thus some electrons must go into states of higher Fermi energy, but in the 3*d*-band of a ferromagnetic metal the only states available such as these are of negative spin. The net effect is to decrease the magnetic moment of the material provided the perturbation energy is larger than the exchange energy. This suggests a means of explaining the deviations from Pauling's curve in certain alloy systems[2] that differs from the Heitler-London-Neel approach previously proposed.[3]

[1] J. C. Slater, Phys. Rev. **76**, 1592 (1949); H. M. James, Phys. Rev. **76**, 1602 (1949).
[2] R. M. Bozorth, Phys. Rev. **79**, 887 (1950).
[3] J. E. Goldman, J. Appl. Phys. **20**, 1131 (1949).

J12. Domain Structure of Perminvar with a Rectangular Hysteresis Loop. H. J. WILLIAMS AND MATILDA GOERTZ, *Bell Telephone Laboratories.*—Domain patterns obtained with colloidal magnetite on polycrystalline rings of perminvar (43 percent Ni, 34 percent Fe, 23 percent Co), having rectangular hysteresis loops after heat treatment in a magnetic field,[1] showed circular domain boundaries concentric with the rings. An applied magnetic field caused the domain boundaries to either expand or contract so that the relative value of the clockwise and counterclockwise flux circuits changed thus varying the net flux. Nuclei of reversed magnetization were formed by making small notches in the specimens which decreased the coercive force and hysteresis loss by a factor of two. It was found that the change in spin orientations in crossing a 180° domain boundary could be made to have either a right- or left-hand screw relation by the application of a magnetic field of appropriate sign perpendicular to the surface.

[1] J. F. Dillinger and R. M. Bozorth, Physics, 279 (1935).

J13. Neutron Diffraction Studies of Various Transition Elements. C. G. SHULL AND M. K. WILKINSON, *Oak Ridge National Laboratory.*—Powder diffraction patterns have been taken for a series of transition elements, V, Cr, Mn, Cb, Mo, and W in order to establish the presence of possible magnetic structure and to determine the strength of the localized atomic magnetic moments. V, Cb, and W exhibit no observable magnetic scattering effects, either coherent or incoherent, and, hence, from the sensitivity of observation an upper limit of $0.1\mu_B$ for V and $0.3\mu_B$ for W can be set for the maximum strength of the atomic moments, either aligned or unaligned. These materials were studied at temperatures as low as 20°K. Cr, on the other hand, exhibits an antiferromagnetic structure with Curie temperature about 150°C and with an atomic moment of $0.40\mu_B$. From the absence of magnetic diffuse scattering in Cr at low temperatures, a maximum strength of $0.1\mu_B$ can be set for any unaligned moments. The absence of a magnetic moment in V and the presence of a weak moment in Cr agrees rather well with the Slater-Pauling-Shockley curve of magnetic moment *versus* electron concentration when this is extrapolated into the nonferromagnetic region. Studies on Mn are in progress and will be reported.

J14. The Magnetic Properties of the Chromites. W. G. SCHINDLER, T. R. MCGUIRE, LOUIS N. HOWARD, AND J. SAMUEL SMART, *U. S. Naval Ordnance Laboratory.*—The chromites are a series of compounds with the chemical formula MCr_2O_4 where M is a divalent metallic ion. They have the same crystal structure (spinel) and about the same size unit cell as the ferrites.[1] Magnetic susceptibilities over the temperature range 77°K to 1300°K have been measured. The susceptibility curves for Mg and Zn chromites obey a Curie-Weiss law with a negative θ, indicating a negative exchange interaction between magnetic atoms on the octahedral sites. For Mn, Co, Ni, and Cu chromites, the $1/\chi$ *versus* T curve can be represented by a Néel hyperbola.[2] Co and Cu chromites become ferromagnetic at 110°K and 135°K respectively, while Mn and Ni chromites become ferromagnetic somewhere below 77°K. The saturation magnetizations at 4.2°K and 7400 gauss were measured using a ballistic method. Saturation values in Bohr magnetons (μ_B) per molecule are Mn chromite, $1.5\mu_B$; Co chromite, $0.2\mu_B$; Ni chromite, $0.3\mu_B$; and Cu chromite, $0.7\mu_B$. A discussion of the experimental results of this investigation with relation to the Néel theory will be given.

[1] J. W. Verwey and E. L. Heilmann, J. Chem. Phys. **15**, 174 (1947).
[2] L. Néel, Ann. phys. **3**, 137 (1948).

J15. Temperature Dependence of the Magnetic Spectrum of a Ferrite. G. T. RADO, R. W. WRIGHT, W. H. EMERSON, AND A. TERRIS, *Naval Research Laboratory.*—The two natural ferromagnetic resonances previously studied[1] at room temperature have now been observed at 411°K, 195°K, and 77°K in the same sintered material. As the temperature decreases over this range, the mean resonance frequencies ω_0' and ω_0'', which are measured at the absorption peaks and attributed to domain rotations and wall displacements, respectively, both increase by about 500 percent; the total static initial susceptibility, $\chi_0 = \chi_0' + \chi_0''$, decreases substantially; and the two "line" widths change in a complicated way because of partial overlapping. By using single-domain particles of this material embedded in wax, the rotational resonance was observed separately, and χ_0', the rotational static initial susceptibility, found to be independent of temperature below 300°K. By assuming that domain rotations *and* wall displacements are, in this material, determined primarily by crystalline anisotropy and demagnetizing fields rather than by internal stresses, and that (as in molecular field theory) the exchange energy varies as the square of the saturation magnetization, it is shown theoretically that ω_0'/ω_0'' is independent of temperature whenever χ_0' is independent of temperature. This relation is unaffected by the Landé g factor and agrees satisfactorily with the measurements.

[1] Rado, Wright, and Emerson, Phys. Rev. **80**, 273 (1950).

THURSDAY AFTERNOON AT 2:15

McMillin

(G. E. MOORE presiding)

Invited Papers in Electron Physics

K1. Progress in Gaseous Electronics: Report on the Conference of October 1951. W. P. ALLIS, *M.I.T.* (50 min.)

K2. Progress in Electron Physics: Report on the NBS Electron-physics Symposium. L. MARTON, *National Bureau of Standards.* (50 min.)

K3. Surface and Volume Recombination in Germanium. R. N. HALL, *General Electric Company.* (30 min.)

THURSDAY AFTERNOON AT 2:15

Pupin 428

(J. H. MCMILLEN presiding)

Fluid Dynamics

L1. Spalling Produced by Detonation of Explosives in Very Heavy Walled Metal Tubes. L. STARR AND J. SAVITT, *U. S. Naval Ordnance Laboratory.*—In experiments with small, highly confined explosives, it was noted that under some conditions a conical slug of metal was torn from the free end of the metal container. After some speculation, this phenomenon was explained in terms of the convergence of tension waves which had been reflected from free surfaces. Experiments, in which explosives were used and the geometry of the containers were varied, confirm the explanation.

L2. Approximate Analytic Solutions in the Problem of a Spherical Blast. J. A. MCFADDEN, *U. S. Naval Ordnance Laboratory.*—A sphere containing a perfect gas at uniformly high pressure is allowed to expand suddenly into a homogeneous atmosphere. Solutions for short times later are sought by analytic (i.e., not numerical) means. Viscosity and heat conduction are neglected; the particle velocity, sound speed, and entropy are developed in powers of the time, the coefficients depending principally on a slope coordinate $q=(x-R)/t$, where x is the radial coordinate and R is the radius of the original gaseous sphere. (This expansion was also used by Wecken.[1]) The zero-order solution is the plane-wave (shock-tube) solution. The rarefaction zone was discussed in an earlier paper;[2] here the method is extended to the regions between the rarefaction and the outgoing shock. The first-order coefficients are linear in q and also depend weakly on t itself; the pressure is constant spacewise but decreases with time. In the region between the gas-air interface and the outgoing shock, numerical results are given for $\gamma=1.4$, an initial pressure ratio of 13, and a density ratio of 4.

[1] Wecken, Z. angew. Math. Mech. **30**, 270 (1950).
[2] J. A. McFadden, Phys. Rev. **84**, 611 (1951).

L3. Hypersonic Viscous Flow Over a Flat Plate.* L. LEES AND R. F. PROBSTEIN, *Princeton University.*—The steady hypersonic flow of a viscous, heat conducting gas over a semi-infinite flat plate is examined in a region away from the leading edge. As a result of the curvature of the relatively thick boundary layer, variations in pressure are propagated into the main stream along Mach lines, with a subsequent interaction between the "inviscid" field and the boundary layer growth. Solution of this problem shows that the important generating parameter is $M^3/(Re_x)^{\frac{1}{2}}$, where, M is the free stream Mach number and Re_x the Reynolds number based on distance from the leading edge. By successive iterations between the "internal" and "external" fields, asymptotic expansions in terms of $M^3/(Re_x)^{\frac{1}{2}}$ are found for the flow quantities such as pressure, velocity, temperature, etc. The zero-pressure gradient flat-plate boundary layer solution is the first approximation in the expansions. It is shown that there is a wedge-like domain where the "higher order" viscous terms in the x-momentum equation can be neglected. In addition to the horizontal pressure gradient, the gradient normal to the plate is evaluated. From the results, the region of validity of the zero pressure gradient boundary layer solution, as well as the error made in the skin friction and heat transfer rate determined by this solution, can be found. When $M^3/(Re_x)^{\frac{1}{2}}$ is not small, compared to one, the error is considerable.

* This work was supported by the United States Air Force, Air Materiel Command.

L4. Transonic Flow Past a Wedge at Zero Angle of Attack. LEON TRILLING, *Massachusetts Institute of Technology* (Introduced by H. G. Stever).—The steady plane flow of an ideal inviscid nonconducting gas past a thin symmetric diamond wedge at zero angle of attack was investigated theoretically at speeds just below the velocity of sound. The problem was studied in the hodograph plane where the coordinate $y(u, v)$ is a solution of the Tricomi equation, and $x(u, v)$ satisfies a similar equation. The boundary conditions require $y(u, v)$ to have a branch-point singularity $y\sim 1/(u-u_1)^{\frac{1}{2}}$ where u_1 is the free stream velocity; y vanishes along both sides of the cut extended from $u=u_1$ to $u\to-\infty$; along the straight lines $v=\pm v_0$ which represent the wedge surface, and along the downward characteristic through $(0, +v_0)$; forward and rear stagnation points are defined by the condition $\lim_{u\to-\infty} x(u, \pm v)=\pm c$. A solution approximately satisfying these conditions and depending only on the transonic similarity parameter ξ_0 was constructed. The flow was found to be subsonic up to the corner; sonic at the corner, where a local Prandtl Meyer over-expansion followed by a weak oblique shock took place. There followed a decelerating supersonic flow, ending in a normal shock some distance ahead of the rear stagnation point. The pressure drag, the

location, and the strength of the shocks were computed for several values of ξ_0.

L5. On the Recent Development in the Turbulence Theory in Compressible Fluids. M. Z. v. KRZYWOBLOCKI, *University of Illinois* (Introduced by Charles Fletcher).—In his previous paper the author derived the generalized fundamental equations of an isotropic, homogeneous turbulence in compressible viscious fluids. This may be considered to be a generalization of Kármán-Howarth theory. In the present paper the author presents a generalized theory of locally isotropic turbulence which may be considered to be a generalization of Kollmogoroff's theory. Two generalized similarity hypotheses are presented, as well as the conclusions that are derived from these hypotheses.

L6. An Experimental Model of Turbulence.* ROBERT BETCHOV, *University of Maryland*.—An electronic resonant circuit has been built, containing in addition to the usual elements (resistance, capacity and self induction), a particular nonlinear element. When this circuit is excited by a random noise, it responds with another random signal, and in addition, with occasional transients (intermittent pulses). These transients are excited by the random motion, but they correspond to particular trajectories in a suitable phase space. A comparison with real aerodynamical flows showed that in some cases the velocity fluctuation can be considered as the sum of a random signal and of excited transients, corresponding to certain phase trajectories. The basic equation of this nonlinear circuit is somewhat similar to a one-dimensional momentum equation of Navier-Stokes types and the significant parameter could be interpreted in terms of fluid dynamics.

* This work is supported by OAR.

L7. Free-Flight Determination of the Boundary Layer Transition on Cone Cylinders. W. R. WITT, JR., *U. S. Naval Ordnance Laboratory* (Introduced by Albert May).—Investigations are being made to determine the effect of various factors on the transition of the boundary layer from laminar to turbulent flow. At the present time one of the greatest uncertainties in the prediction of skin temperature, skin-friction drag, and base-pressure drag of supersonic missiles is whether the boundary layer is laminar or turbulent. The position of boundary layer transition cannot now be predicted accurately, since it is influenced by a variety of factors such as Mach number, surface roughness, surface temperature, pressure gradient, free-stream turbulence, and surface curvature. The quantitative effect of these factors, either singularly or interrelated is not known. Approximately 35 shots have been analyzed. The models were 20 mm, 25-degree cone cylinders. They were fired in a pressurized ballistics range which is equipped with shadowgraph stations. The transition regions were determined from the appearance of turbulence on the shadowgraph plates. Two degrees of surface finish were employed on different cones. On one group the cone finish was 4- to 10-micro inches and on the other the finish was 35- to 50-micro inches. The boundary layer transition occurred approximately one-half inch nearer the tip of the cones on the rougher models.

L8. Explicit Construction of Large-Amplitude Water Waves in Channels. R. P. SHAW.—A method is given for the construction of the general solution (involving two arbitrary functions) of any homogeneous system of partial differential equations where the coefficients depend only on the two dependent or on the two independent variables. Use is made of an operator involving contour integration, usually around branch points of a Riemann surface. An indication of the utility of the method, as well as some of the difficulties to be expected, is shown in an application to the equations resulting from a hodograph transformation of the equations governing the adiabatic flow of a compressible polytropic fluid with arbitrary adiabatic exponent γ, particularly to the case $\gamma=2$, corresponding to large amplitude water waves in channels. For this case the operator is inverted to give explicit formulas for waves satisfying arbitrarily prescribed initial conditions.

L9. A Preliminary Investigation of a Shock Wave Turbulent Boundary Layer Interaction. S. M. BOGDONOFF AND A. H. SOLARSKI, *Princeton University*.—Preliminary data in the form of static and pitot pressure distributions and shadow and schlieren photographs have been obtained for the interaction of a pressure ratio 2.09 shock wave with a turbulent boundary layer on a flat wall at $M=2.97$. Separation of the boundary layer appears to be incipient and a model of the interaction has been constructed. The model compares closely with that of Bardsley and Mair for turbulent layer-medium strength shocks and resembles as well that obtained by Leipmann for the interaction of weak shocks at low Mach numbers with a laminar layer. Longitudinal static pressure distributions show an upstream influence of approximately three boundary layer thicknesses with an inflection in the curve characteristic of laminar interactions. The entire pressure rise occupies six boundary layer thicknesses and agrees satisfactorily with the theoretically predicted rise. Velocity profiles in the region of the steepest pressure rise, i.e., slightly ahead of the point of impingement of the incident shock, show a behavior that may be associated with imminent separation.

L10. On Shock-Wave Phenomena: Aerothermodynamic Interaction. H. POLACHEK AND R. J. SEEGER, *U. S. Naval Ordnance Laboratory*.—Shock waves accompanied by a gain (or loss) of energy from an external source are a frequent occurrence in nature. A detonation wave is an illustration of such a phenomenon. Another example is a condensation wave, often observed in wind tunnels at high Mach numbers. It is possible to study the resultant equilibrium effects of addition or subtraction of energy immediately behind such shock fronts without detailed information as to the mechanism of the physical process. In the present paper an exploratory numerical analysis has been made of the characteristics of configurations that may result from the interaction of two shock waves of the type described above.

L11. One-Dimensional Theory of Absorption and Amplification of a Plane Shock Wave by a Gaseous Layer. D. BITONDO, I. I. GLASS, AND G. N. PATTERSON, *University of Toronto*.—The problem of gaseous refraction of a plane shock wave at a contact surface is applied to the case where the incident shock wave must pass through a finite layer of gas. The resulting wave system after refraction at a contact surface depends on the ratio of internal energies separated by the contact surface. When the ratio of the internal energies is greater than a certain minimum value, then the resulting wave system is a transmitted shock wave of lower strength than the incident shock wave, and a reflected rarefaction wave. When the internal energy ratio is less than a certain maximum value, then the transmitted shock wave is of higher strength and a shock wave is reflected. In the layer problem, the incident shock wave is refracted at two contact surfaces in succession, and when the emergent shock wave is of a lower strength than the original incident shock wave, then absorption is said to occur. The theory is applied to the practical case where the layer contains a gas which is bounded by air at room temperature at both contact surfaces. Under these conditions the emergent shock wave is always partly absorbed. When the gas in the layer is hydrogen, very significant shock wave absorption occurs even when the hydrogen is at room temperature.

FRIDAY MORNING AT 10:00

Horace Mann Auditorium

(J. STEINBERGER presiding)

Production, Decay and Interactions of Pi-Mesons

M1. Production of Photomesons from Deuterium.* JAMES KECK AND RAPHAEL LITTAUER, *Cornell University*.—The reaction $\gamma+d\rightarrow\pi^-+p+p$ is being investigated by bombarding targets of D_2O and H_2O with bremsstrahlung from the Cornell 310-Mev electron synchrotron. π-mesons emitted at 90° are identified in a counter telescope by specific ionization and range and are counted in coincidence with protons emitted at approximately 30°. The energy and angular distributions of the protons are measured for a known meson energy. These parameters determine the energy of the photon and also the initial momentum of the neutron within the target nucleus. The background due to the oxygen is about 30 percent of the total count. The observed angular distribution of the protons is compatible with reasonable assumptions about the internal momentum of the deuteron. The cross section of the elastic interaction (that in which only one of the residual protons carries away momentum) has been found to be of the order of 10^{-29} cm² sterad^{-1} at a photon energy of 220 Mev. This is comparable to the cross section for $\gamma+p\rightarrow\pi^++n$ at the same energy.[1]

* This work was performed under contract with the ONR.
[1] Bishop, Steinberger, and Cook, Phys. Rev. **80**, 291 (1950).

M2. Dependence of Charged Pion Production on Incident Proton Energy.* S. PASSMAN, M. M. BLOCK, AND W. W. HAVENS, JR., *Columbia University*.—The 90° differential cross section for production of charged pions has been measured for several elements at proton energies of 345, 365, and 380 Mev. The technique, utilizing nuclear emulsions as detectors for mesons produced in targets bombarded by the internal beam of the Nevis cyclotron, has been previously described.[1] The proton energy is varied by changing the distance of the target from the center of the cyclotron magnetic field. Preliminary results for the integrated 90° cross section for π^+ production in hydrogen (by subtraction of carbon from polyethylene) are $(d\sigma)/(d\omega)=(2.9\pm30\%)\times10^{-29}$ cm²/sterad for a proton energy of 345 Mev, and $(d\sigma)/(d\omega)=(3.9\pm30\%)\times10^{-29}$ cm²/sterad for a proton energy of 365 Mev. The total cross sections for meson production in hydrogen are calculated by assuming the reaction $P+P\rightarrow\pi^++D$ with a $\cos^2\theta$ angular dependence in the center-of-mass system.[2] Combined with the previously reported cross section for hydrogen at 381 Mev,[1] the ratios of the production cross sections are: (σ_{total} at 381 Mev):(σ_{total} at 365 Mev):(σ_{total} at 345 Mev)=2.1:1.6:1.

* This research was assisted by the joint program of the AEC and ONR.
[1] Block, Passman, and Havens, Jr., Phys. Rev. **83**, 167 (1951).
[2] Peterson, Iloff, and Sherman, UCRL-1405 (1951); Cartwright, Richman, Whitehead, and Wilcox, UCRL-1278 (1951).

M3. Photoproduction of Mesons on Nuclei. T. R. PALFREY, JR., AND R. R. WILSON, *Cornell University*.*—We are measuring the relative differential meson energy cross sections for the photoproduction of charged mesons from various targets. Preliminary results have been obtained for mesons of energy 40–80 Mev produced from C and Pb at 135° to the 310-Mev synchrotron brehmsstrahlung gamma-ray beam. The detector is a scintillation counter telescope of one NaI(Tl) crystal and one terphenyl-xylene liquid scintillator, each 10 cm in diameter and 1 cm thick. Mesons are identified by their pulse height in the second (NaI) crystal. Their charge and momenta are determined by the magnet system of Camac, *et al.*,[1] use of which also helps minimize corrections for nuclear interaction of the mesons in absorbers. The decay in flight correction is made theoretically, with the aid of a range-measurement estimate of the mu-meson contamination. Work is in progress on other targets. An inhomogeneous 90° sector magnet of the betatron type, with $n=\frac{1}{2}$, is being constructed. After calibration it should permit measurement of absolute cross sections at variable angles and at lower meson energies.

* Work supported by ONR.
[1] Camac, Corson, Littauer, Shapiro, Silverman, Wilson, and Woodward, Phys. Rev. **82**, 745 (1951).

M4. Relative Production of Neutral Mesons by 310-Mev γ-Rays in Hydrogen and Deuterium. A. SILVERMAN AND G. COCCONI, *Cornell University*.—The neutral mesons produced in various targets by 310-Mev bremsstrahlung radiation were detected by observing one of the decay gamma-rays at 90° to the primary beam. This method increases the counting rate by at least a factor of 10 in comparison to detecting the two decay γ-rays in coincidence. This is done at the expense of information concerning the angular distribution. The observed counts have the following characteristics: (a) they are due to γ-rays of energy greater than 40 Mev, (b) the threshold is approximately 150 Mev, (c) the excitation function, as determined by changing the maximum beam energy, is in reasonable agreement with published results for hydrogen,[1] (d) the observed rates correspond to those expected assuming the known cross sections for π^0 production.[1] The targets used were H_2O, D_2O, CH_2, and C. For γ-rays energies of about 300 Mev, the ratio of deuterium to hydrogen cross section for π^0 production is: $\sigma_D/\sigma_H=1.90\pm0.24$. This indicates that the cross sections for production of π^0 by γ-rays on neutrons and protons are approximately equal. The following relative cross sections have also been obtained: $\sigma_C/\sigma_H=10.1\pm1.8$, $\sigma_O/\sigma_H=12.7\pm2.5$.

[1] Panofsky, Steinberger, and Stellar, UCRL, 1495, October, 1951; A. Silverman and M. Stearns, Phys. Rev. **83**, 206 (1951).

M5. Production of 40-Mev π-Mesons by 240-Mev Protons in Seven Elements.* DONALD L. CLARK, *University of Rochester*.—The relative differential cross section for production of 40-Mev π^+ and π^- mesons by 240-Mev protons has been measured in Be, C, Al, Cu, Ag, W, and Pb. The π^+ mesons were observed in the angular range 130° to 150° with respect to the incident protons, and the π^- mesons in the range 30° to 50°. The relative cross section per nucleus was found to vary generally as the geometric cross section, but with significant departures for both positive and negative mesons. The departures from geometric cross section appear to correlate to some extent with the average binding energy per nucleon. The variation of the cross section for π^+ mesons differs significantly from that for π^- mesons. The ratio of the cross section for production of π^+ mesons to that for π^- mesons, at the angles indicated, varies qualitatively as the *a priori* ratio $A+Z/A-Z$ but considerably more strongly.

* This work was sponsored by the AEC.

M6. Measurement of the Production Cross Section of Negative Mesons in Carbon by 341-Mev Protons. WALTER F. DUDZIAK, *University of California, Berkeley*.—Meson production cross sections from carbon ($pC^{12}\rightarrow\pi^-$) in the forward direction to a 341-Mev incident proton-beam, have been measured. The produced charged mesons were magnetically

separated and their number detected in Ilford C-2, (200μ) emulsions. The areas were scanned under 570 diameters magnification. The π^- spectrum is based on more than 450 observed star-forming π^- mesons. A comparison of the π^+ and π^- data shows surprising results which are in complete disagreement with those expected from the relation $\sigma^+/\sigma^- = (A+Z)/(A-Z)$ which results from the assumption that production matrices in $p-n$ and $p-p$ collisions are the same.[1] The peaks of the π^- and π^+ spectra occur at widely separated meson-energies. The σ^- peak occurs at $T_\pi < 25$ Mev, while the σ^+ peak occurs at $T_\pi > 70$ Mev. The σ^+/σ^- ratio of the peaks is approximately 15/1. Within experimental error the integral of the π^- spectrum over energies is the same as obtained at 90° to the proton-beam.[2] This is not true for the σ^+ integral. The marked decrease of σ^- with increasing meson-energy might be explained by the effect of the exclusion principle. The large increase of π^+ production may be the result of the resonance-reaction[3] which accompanies deuteron formation.

[1] E. M. Henley, UCRL-1467, September, 1951.
[2] C. Richman and H. Wilcox, Phys. Rev. **78**, 496 (1950).
[3] This idea has also been advanced by C. Richman.

M7. A Photographic Study of the Muon Range Spectrum from $\pi \to \mu$ Decay.* A. M. Seifert, H. J. Bramson, and W. W. Havens, Jr., *Columbia University.*—The search for anomalous muon ranges from $\pi \to \mu$ decay is being continued.[1] These abnormal muons have been previously reported[1,2] and have been interpreted to indicate a nonhomogeneous decay of the pion. Another interpretation may be the existence of an additional mechanism of energy loss of the muon, other than the usual energy loss by ionization.[3] A muon range spectrum is being compiled to clarify the nature of this anomaly. To date, some 3300 $\pi \to \mu$ decays have been observed where the muon ends in electron sensitive emulsion. A total of six "short" muon decay ranges have been found with lengths: 235, 415, 440, 445, 470, and 485 microns, respectively. A preliminary spectrum of three hundred muon ranges exhibits the expected range straggling of 4–5 percent about the mean. At the low energy end, however, there is a definite indication of an extended non-Gaussian "tail." The shape of the spectrum, especially at the low energy end, is being further studied, and the results of increased statistics will be presented.

* This research is being assisted by the joint program of the ONR and AEC.
[1] Bramson, Seifert, and Havens, Jr., Bull. Am. Phys. Soc. **26**, No. 6, 23 (1951).
[2] W. F. Fry, Phys. Rev. **83**, 1268 (1951).
[3] H. Primakoff, private communication (to be published in Phys. Rev.).

M8. Scattering of Negative Pions by Hydrogen.* A. Lundby, E. Fermi, H. L. Anderson, D. E. Nagle, and G. Yodh, *University of Chicago.*—The scattering of negative pions of energy 115 Mev in liquid hydrogen has been studied using scintillation counter techniques. The beam incident in the hydrogen target is monitored by two 1-in.^{2} scintillators in coincidence, spaced 10 inches apart. The scattering products are observed by quadruple coincidences of these with another pair of scintillators located directly under the scatterer at 90° from the incident beam direction. A $\frac{1}{4}$-in. Pb plate in front of the last pair was used to increase the sensitivity of the equipment to high energy gamma-rays. In a first experiment the ratio of scattered to incident particles without the Pb radiator was found to be $(0.81 \pm 0.05) \times 10^{-4}$ and $(1.21 \pm 0.08) \times 10^{-4}$ without and with liquid hydrogen in the scattering chamber, respectively. With the Pb radiator the corresponding numbers were $(0.71 \pm 0.06) \times 10^{-4}$ and $(1.73 \pm 0.09) \times 10^{-4}$. The net effects of the hydrogen with and without lead radiator are therefore $(0.40 \pm 0.10) \times 10^{-4}$ and $(1.01 \pm 0.11) \times 10^{-4}$. A large contribution because of high energy gamma-rays is apparent, and this is ascribed primarily to the charge exchange scattering with a small addition caused by radiative capture. These intensities are consistent with a total cross section of about 35×10^{-27} cm^2 as observed in the transmission experiments with the charge exchange scattering contribution two or three times as large as that of the ordinary scattering.

* Research supported by the ONR and AEC.

M9. Total Collision Cross Sections of Negative Pions on Protons.* D. E. Nagle, H. L. Anderson, E. Fermi, E. A. Long, and R. L. Martin,† *University of Chicago.*—The transmission of negative pions in liquid hydrogen has been measured using the pion beams of the Chicago synchrocyclotron. Pion beams with energies from 60 to 230 Mev were used. The transmissions were measured using scintillation counting techniques. The total collision cross section increases with energy starting from small values at 50 Mev and rising to the "geometrical" value of about 60×10^{-27} cm^2 at about 160 Mev. Thereafter, up to 220 Mev, the cross section remains close to this value. The steep energy dependence at low energies is consistent with interpretation that the pion is pseudoscalar with a pseudovector interaction.

* Research supported by the ONR and AEC.
† AEC Predoctoral Fellow.

M10. Difference of Hydrogen and Deuterium Total Cross Sections for Charged Pi-Mesons. G. Yodh, H. L. Anderson, D. E. Nagle, and H. Stadler, *University of Chicago.*—Transmission measurements in H_2O and D_2O are reported for negative pi-mesons at several energies. The experimental arrangement is similar to that reported by Martin, Anderson, and Yodh at this meeting. The results indicate that the total scattering cross section ($\sigma_D - \sigma_H$) in the pion energy bands 92–116 Mev and 110–134 Mev is close to the geometrical value of 61 millibarns. In the energy band 41–58 Mev, $\sigma_D - \sigma_H$ has been measured less precisely, but appears to be much smaller.

M11. Slow π^- Meson Reactions in He^3. A. M. L. Messiah,* *University of Rochester.*—The pseudoscalar nature of the π^--meson has been established recently.[1,2] Furthermore, the calculation[1] of the branching ratios for the slow π^- reactions in deuterium using the weak coupling $PS(PV)$ theory and treating the nuclear interaction phenomenologically, gives results in reasonable agreement with experiment. We have investigated the K-capture of π^- mesons by He^3 in the $PS(PV)$ theory using Tamor's method. Comparison with reactions in deuterium and hydrogen should provide a test of the weak coupling approximation. There are six competing processes which fall in three categories: the pure absorption, the γ-absorption and the π^0 absorption. Special attention is given to the γ and π^0 absorptions leading to H^3 because of the similarity with the π^- reactions in hydrogen; using the branching ratio given by the hydrogen experiment, it is possible to eliminate the π^0 coupling constants from the expression for their ratio. We estimate that 80 percent of the absorption events are pure absorption, with formation of deuterium in $\frac{1}{3}$ of the cases. The remaining events are shared almost equally (1.2:1) between γ and π^0 absorption. Numerical results including the shape of the γ-spectrum will be given.

* Work supported by the AEC and The French Direction des Mines.
[1] S. Tamor, Phys. Rev. **82**, 38 (1951).
[2] Clark, Roberts, and Wilson, Phys. Rev. **83**, 649 (1951); Durbin, Loar, and Steinberger, Phys. Rev. **83**, 646 (1951).

M12. Absorption of Negative π-Mesons in Helium Gas.* C. P. Leavitt,† *M.I.T.*—Negative π-mesons produced in a beryllium target by the x-ray beam of the M.I.T. synchrotron entered a high pressure cloud chamber[1] filled with helium gas at 200 atmospheres pressure. Every negative meson that stopped in the gas was observed to give rise to a one-pronged star. By means of their curvature in the magnetic field and

their range in the gas, some of the prong particles could be positively identified and their energy measured. Most of the particles so far identified have proved to be protons, although in at least one case the particle is heavier than a proton. Photographs of typical events will be shown and their analysis discussed.

* This work has been supported in part by the joint program of the ONR and AEC.
† AEC Predoctoral Fellow.
[1] G. E. Valley and J. A. Vitale, Rev. Sci. Instr. **20**, 411 (1949).

M13. Nuclear Cross Sections for Negative Pions of Energy 109 and 133 Mev.* R. L. MARTIN,† H. L. ANDERSON, AND G. YODH, *University of Chicago.*—Measurements of nuclear cross sections for negative pions at 85 Mev have recently been made by Chedester, Isaacs, Sachs, and Steinberger.[1] They studied the attenuation of a 100-Mev pion beam in various absorbing materials using counters in a geometry poor enough to avoid the effects of Coulomb scattering. We have made similar measurements at 109 and 133 Mev with the result that the observed total cross sections have the geometric values, $\pi A^{\frac{1}{3}}(\hbar/\mu c)^2$, within the uncertainties (15 percent) of this technique. With the possible exception of carbon there is no evident energy dependence in the range 85 to 133 Mev.

* Research sponsored by the ONR and AEC.
† AEC Predoctoral Fellow.
[1] Chedester, Isaacs, Sachs, and Steinberger, Phys. Rev. **82**, 958 (1951).

M14. Meson Fission of Mercury. NATHAN SUGARMAN, *University of Chicago.*—Radiochemical studies are in progress on the fission of mercury by 122-Mev π^- mesons from the University of Chicago synchrocyclotron. Activity and yield measurements have been made on the following fission products: 2.4-hr Br^{82}, 36-hr Br^{82}, 9.7-hr Sr^{91}, 2.7-hr Sr^{92}, 3.7-hr Y^{92}, and 4.5-hr Ru^{105}. There was no activity in the mixed rubidium-caesium fraction or in the barium fraction, thus indicating the absence in reasonable yield of 5.5-hr Cs^{137}, 33-min Cs^{138}, and 85-min Ba^{139}. Comparison of the distribution of the fission products of meson fission of mercury with those of high energy neutron (from 450-Mev protons) fission of mercury indicates that the fission products from the meson reaction are less neutron deficient.

FRIDAY MORNING AT 10:00

Havemeyer 309

(G. C. BALDWIN presiding)

Neutrons

N1. Reflection and Refraction of Neutrons from a Beryllium Mirror.* J. A. HARVEY, M. D. GOLDBERG, AND D. J. HUGHES, *Brookhaven National Laboratory.*—Because of spin-dependent scattering the coherent scattering cross section of a nucleus of a monoisotopic element may be less than the bound atom cross section. This spin dependent scattering arises from the difference in the scattering amplitudes of the two possible spin states of the compound nucleus. The difference in the scattering amplitudes arises from the presence of a nearby resonance. The coherent scattering cross section may be determined from a measurement of the critical angle for total reflection of a collimated beam of neutrons. We have measured the coherent cross section of beryllium by both reflection and refraction of neutrons from a beryllium mirror. Using graphite filtered neutrons which have a cut-off wavelength of 6.69A, we find a critical angle of 39.7′. Assuming no spin-dependent scattering and using the best value of 7.42 barns for the bound atom cross section of beryllium, the critical angle would be 40.0′. Therefore, the spin dependent scattering must be small, and a direct measurement is necessary to obtain a quantitative result.[1]

* Research carried out under contract with AEC.
[1] H. Palevsky and R. Smith, following abstract.

N2. Low Energy Cross Section Measurements of Be with the Brookhaven Slow Neutron Chopper.* HARRY PALEVSKY, *Brookhaven National Laboratory,* AND R. R. SMITH, *Columbia University.*—The spin-dependent scattering in Be can be determined from the total cross-section measurements for wavelengths greater than the Bragg cutoff (3.95A). By cooling the sample to liquid air temperatures, the inelastic scattering is reduced to a minimum. The residual cross section minus the capture then gives an upper limit for the spin interaction. Inelastic scattering theory indicates that as the neutron wavelength increases the inelastic cross section approaches a $1/v$ dependence. In this region an extrapolation to zero wavelength will yield the spin dependent cross section. With the slow chopper we have determined the cross section variation with wavelengths, for various temperatures of the sample. The results give a spin-dependent scattering of <0.03 barn. The inelastic scattering cross section from 5A to 18A can be represented accurately, contrary to theory, by the relation $\sigma=a+b\lambda$ where a and b are temperature dependent parameters.

* Research carried out under contract with the AEC.

N3. Total Cross Sections for 400-Mev Neutrons.* V. A. NEDZEL AND JOHN MARSHALL, *University of Chicago.*—The total nuclear cross sections of several elements for neutrons from the Chicago synchrocyclotron were determined in good geometry using a Čerenkov radiation detector. In the arrangement used, the collimated beam from a beryllium target was passed, through absorbers made of the materials studied, onto a hydrogenous radiator. Observations were then made of the recoil protons at an angle of 9° to the neutron beam. Range measurements of the protons actuating the Čerenkov counter indicated that the neutrons studied in this experiment had an energy spectrum centered at about 406 Mev, with a full width, at half-intensity, of 32 Mev. Preliminary results obtained from the cross-section measurements are as follows: carbon, 0.288 ± 0.004; copper, 1.14 ± 0.02; cadmium, 1.70 ± 0.04; lead, 2.69 ± 0.05, the values in barns and the indicated uncertainties the statistical probable errors of the data obtained.

* This work was supported by the joint program of the ONR and AEC.

N4. Slow Neutron Capture Gamma-Rays.* W. A. THORNTON, JR.,† E. DER MATEOSIAN, H. T. MOTZ, AND M. GOLDHABER, *Brookhaven National Laboratory.*—To study low energy γ-rays accompanying the capture of slow neutrons, we have used either a scintillation counter or a lens spectrometer. The 478-kev line emitted in 95 percent of the disintegrations of B^{10} by slow neutrons is used for energy and intensity calibra-

tions. Discrete γ-ray lines were observed for a number of elements. Of particular interest is a 555 ± 5-kev line found to be emitted from $Cd^{113}+n$ with an intensity of 0.9 to 1.0 per neutron captured. This line coincides in energy with a line known from the K-capture decay of In^{114} to Cd^{114} and may therefore indicate that practically each neutron capture leads to the first excited state of Cd^{114}.

* Research carried out under contract with the AEC.
† Graduate student, Yale University.

N5. Measurements of γ-Ray Energies with a Pair Spectrometer. G. A. BARTHOLOMEW AND B. B. KINSEY, *Chalk River.*—The coincidence peak obtained with a pair spectrometer exhibits a sharp linear edge followed by a tail toward high magnetic fields. The end point of the peak or the maximum field at which coincidences are obtained corresponds to the production of pairs at the center of the radiator with the electron and positron having equal energy and following orbits in the median plane which graze the inner edges of the slits. An accurate evaluation of the γ-ray energy depends on a measurement of the distance between the inner edges of the slits and the maximum magnetic field. The end point is, in practice, always obscured by a background caused by scattered electrons, and its position must be obtained by extrapolating the linear slope of the peak to zero counting rate and adding a small correction. The magnitude of the correction and its dependence on the geometry of the spectrometer and the γ-ray energy has been investigated theoretically and experimentally. Neutron binding energies obtained by measuring ground-state neutron-capture γ-rays using this method agree well with those obtained by measuring the Q's of (dp) reactions.

N6. Neutron Capture Cross Sections from (n, γ) Reactions.* E. B. MESERVEY, W. W. HAVENS, AND L. J. RAINWATER, *Columbia University.*—Measurements of neutron capture cross sections have been made by detection of capture-gammas emitted from a sample placed in the slow-neutron beam of a neutron velocity selector. Counting rates in scintillation counters near the sample have been plotted against neutron time-of-flight to give a measure of relative (n, γ) cross sections as a function of neutron energy. Orientation studies on indium and silver showed the well-known resonances in these substances; the silver measurements were carried into the thermal region and showed the characteristic $1/v$ slope. Preliminary measurements have been made in the resonance region on samples of Cd, BaO, and SrF_2. Resonances have been detected in Cd at about 27 ev and 90 ev,[1] in Ba at about 25 ev and 101 ev, and in Sr at 3.5 ev. Comparative studies on Cd and Ag in the thermal region roughly confirm measurements by Muehlhause[2] of the relative capture-gamma multiplicity of these two substances.

* This work was supported in part by the AEC.
[1] This resonance may be the same as that reported previously at 110 ev, Coster, Groendijk, and DeVries, Physica 14, 1.
[2] C. O. Muehlhause, Phys. Rev. 79, 277 (1950).

N7. Slow Neutron Resonances in Cs and Pd. H. H. LANDON, *Rensselaer Polytechnic Institute,* AND V. L. SAILOR, *Brookhaven National Laboratory.*—The neutron cross sections of Cs and Pd have been measured from 0.6 ev to 40 ev with a crystal spectrometer using a beryllium crystal as the monochromator.[1] A strong resonance was found in Cs at 5.70 ev. The strength of this resonance obtained with a thick sample was $\sigma_0\Gamma^2 = 161\pm20$ barns $(ev)^2$. The large thermal cross section of Cs may be attributed to this resonance. Pd has a strong resonance at 31 ev and a weaker one at 12.5 ev. The 31-ev resonance is probably the one previously reported by Goldhaber *et al.*[2] and attributed by them to Pd^{108}. Problems related to the analysis of resonance data will be discussed.

[1] L. B. Borst and V. L. Sailor, Bull. Am. Phys. Soc. 26, No. 6, 15 (1951).
[2] Goldhaber, Lowry, and Sunyar, BNL-C-9, 96 (1949).

N8. Fast Neutron Reaction Cross Sections. E. B. PAUL AND R. L. CLARKE, *Chalk River Laboratories.*—Forty elements have been bombarded with the 14-Mev neutrons from the $T(d, n)He^4$ reaction and the activation cross sections measured. About seventy (n, p), (n, α), and $(n, 2n)$ reactions resulting in known radioactive products with half-lives between a few seconds and a few days have been observed. The counting arrangement has been calibrated using samples containing standardized quantities of radioactive materials. The neutron monitor has been calibrated by counting the α-particles from the $T(d, n)He^4$ reaction. A comparison of the measured cross sections with values predicted by evaporation theory[1] has shown that the charged particle reactions observed for mass number A greater than 100, are from 10 to 1000 times more probable than would be expected from the theory and that the observed $(n, 2n)$ cross sections for A greater than 100 are less than the predicted values by up to a factor of 3. Some possible interpretations of these results are discussed.

[1] Blatt and Weisskopf, M.I.T. Technical Report No. 42 (May, 1950).

N9. Angular and Energy Spectrum of Neutrons Produced in Several Elements Bombarded with 110-Mev Protons. I. Experimental. J. A. HOFMANN* AND K. STRAUCH, *Harvard University.*—A measurement has been made of the angular and energy distribution of neutrons with energies larger than 52 Mev produced in several targets by the internal 110-Mev proton beam of the Harvard cyclotron. The neutrons were collimated by slits cut at 0°, 5°, 10°, 16°, and 28° into a 28-in. deep lead block. The neutrons were detected in the usual way by a recoil proton counter telescope, the proton energies being obtained from a differential range spectrum. To increase counting rates the experiment was carried out close to the cyclotron. The effect of the large background in this position was reduced by using (1) quadruple coincidences between stilbane scintillation counters to define the recoil protons, and (2) fast coincidence circuits (resolving time 2×10^{-8} sec) to reduce accidentals to a negligible amount. Less than 2 percent of the detected neutrons did not come through the lead channel. The energy distribution of the protons striking the internal target will be discussed.

* Central Scientific Company Fellow.

N10. Angular and Energy Spectrum of Neutrons Produced in Several Elements Bombarded with 110-Mev Protons. II. Results. K. STRAUCH* AND J. A. HOFMANN, *Harvard University.*—Considering the energy distribution of neutrons emitted at 0° with respect to the incident protons, the target nuclei fall into two groups: (1) D, Li, and Be each show a pronounced peak at high energies; the width of this peak can be explained by the energy distribution of the primary proton beam as seen by the internal target and the energy resolution of the telescope. (2) C, Al, Cu, and Pb each emit neutrons decreasing in number with higher energies. When comparing the angular dependence of the free neutron-proton scattering at 90 Mev[1] with the angular distribution of high energy neutrons emitted by the various targets, the same two groups appear: (1) the results with Li, Be, and D appear in agreement with free neutron-proton scattering; (2) Al, Cu, Pb, and C give an increasingly less pronounced angular dependence. These results will be discussed with respect to some models for nuclear reactions at this energy.

* Society of Fellows.
[1] Hadley, Kelley, Leith, Segrè, Wiegand, and York, Phys. Rev. 75, 351 (1949).

N11. Angular Distribution of Fast Photoneutrons.* P. T. DEMOS, J. D. FOX, I. HALPERN, AND J. KOCH,† *M.I.T.*—A study of the emission of fast photoneutrons has been begun using the M.I.T. linear electron accelerator. The energies and angular distributions of these neutrons and the de-

pendence of these quantities on photon energy and target element is being investigated by means of threshold detectors.[1] With the accelerator providing a thick target x-ray spectrum of maximum energy 16 Mev, the neutrons from lead were observed with high angular resolution in all 4 quadrants. The $P^{31}(n, p)$ reaction was used as the detector. If it is assumed that the angular distribution of these neutrons with respect to the beam has the form $a+b\sin^2\theta$, then $b/a=0.34\pm0.07$. The effects of neutron scattering, neutron background, and photon absorption in the target were kept negligible. Preliminary runs on other heavy elements give anisotropies of the same order of magnitude but the yield for middle weight elements has so far been too low to permit angular distribution measurements.

* This work was supported in part by the joint program of the ONR and AEC.
† On leave from the Institute of Theoretical Physics, Copenhagen, Denmark.
[1] H. L. Poss, Phys. Rev. **79**, 539 (1950).

N12. The Neutron Source Strength of Granitic Rock. J. PINE AND P. MORRISON, *Cornell University*.—The light isotope He^3 of gas-well helium is expected to come from this set of nuclear reactions in rock:[1] U, Th$\rightarrow\alpha$; Si, Al, etc. (α, n); $Li^6(n, \alpha)H^3$; $H^3(\beta^-)He^3$. We have empirically confirmed the most uncertain of these steps by a direct measurement of the rate of neutron production in igneous rock. The sample was placed in a large neutron counter[2] of measured over-all neutron efficiency about 3 percent, located at a depth underground which eliminated cosmic-ray background. The observed counts gave a number-bias curve appropriate for the B^{10} disintegrations in the BF_3 proportional counters used; gamma-ray pile-up and photoneutrons from the deuterium contained in the paraffin moderator were excluded by direct control experiments; the remaining background had the properties expected from alpha-particle residual contamination of the counters. An alkali granite from the carboniferous of Quincy, Massachusetts, gave a counting rate corresponding to a source strength of 0.5 ± 0.35 neutron per second per ton of rock. To improve the counting rate, an enriched simulated granite was prepared by mixing sand with compounds of the other principal constituents of the rock. Radioactive minerals were finely ground and spread dilutely through the material. When radioactive equilibrium was again reached, the neutron count was made. The results were: 0.028 neutron/second/gram of Th; and 0.066 neutron/second/gram U. Connecting for the effects of alpha-particle self-absorption and neutron absorption, and using the average radioactive content of granitic rock, we find ~0.8 neutron/second/T rock. Such a value is in good agreement with the number calculated for the (α, n) reaction yield, and will give the observed ratio of He^3/He^4.

[1] P. Morrison and D. B. Beard, Phys. Rev. **75**, 1332 (1949).
[2] Kindly lent to us by Professor G. Cocconi and Dr. V. Cocconi Tongiorgi.

Invited Paper

N13. Measurement of the Neutron-Electron Interaction by Mirror Reflection. D. J. HUGHES, *Brookhaven National Laboratory*. (30 min.)

FRIDAY MORNING AT 10:00

Schermerhorn 501

(B. P. DAILEY presiding)

Invited Paper

O1. Significance of Microwave Spectroscopy for the Theory of Magnetism. J. H. VAN VLECK, *Harvard University*. (30 min.)

Microwave Spectroscopy

O2. On Rotational Magnetic Moments. RUTH F. SCHWARZ, *Radcliffe College*.—The following expression has been derived for the rotational magnetic moment m_z of the general polyatomic molecule in the $^1\Sigma$ state,[1]

$$m_z=\tfrac{1}{2}\Sigma_\rho\Sigma_{\rho'}[G_{\rho\rho'}P_{\rho'}\cos(z,\rho)+G^*_{\rho\rho'}\cos(z,\rho)P_{\rho'}].$$

Here, z is an axis fixed in space, P_ρ is the rotational angular momentum along a principal axis ρ of the molecule, and $G_{\rho\rho'}$ is a component of a tensor, independent of the rotational state. Since for $\rho'>\rho$, the expectation value of $P_{\rho'}\cos(z,\rho)$ can be shown to be zero for any asymmetrical top, Zeeman measurements on three rotational lines give sufficient data to compute the diagonal elements of the G tensor. Jen has made Zeeman measurements on one H_2O line and two HDO lines.[2] We have derived a theoretical expression for the relation between the magnetic moments of these isotopic molecules and hence have been able to compute the G tensor for H_2O from Jen's data.

[1] J. R. Eshbach and M. W. P. Strandberg, Research Laboratory of Electronics Technical Report No. 184, M.I.T., January 9, 1951.
[2] C. K. Jen, Phys. Rev. **81**, 197 (1951).

O3. Some Molecular Constants of Li^6F^{19}.* J. C. SWARTZ AND J. W. TRISCHKA, *Syracuse University*.—Radiofrequency spectra of Li^6F^{19} were observed by the electric resonance method. A mass spectrometer was used to separate the ions of the lithium isotopes given off by the hot wire detector. Data were taken on the $(J, m_j)-(J, m_j')$ transitions: $(1, 0)-(1, 1)$ and $(2, 1)-(2, 2)$ at both strong and weak electric fields. The spectra were characteristic of a molecule with a single interaction of the form $cI\cdot J$ associated with the nucleus of spin 1/2 (fluorine). I is the nuclear spin, J the rotational quantum number and c the interaction constant. The constant c/h was measured as 37 ± 1 kc/sec, a value approximately twice that determined from the magnetic resonance data of Nierenberg and Ramsey.[1] Since line widths for a single transition were 12 kc/sec, no fine structure produced by the Li^6 quadrupole[2,3] and $I\cdot J$ interactions[3] was observed. The product μ^2A, where μ is the electric dipole moment of the molecule and A its moment of inertia, was determined to be $747\pm1\times10^{-78}$ cgs units for the vibrational state $v=0$. μ^2A for the

next vibrational state is 4.2±0.1 percent higher than that given above.

* Supported in part by the ONR.
[1] Nierenberg and Ramsey, Phys. Rev. 72, 1075 (1947).
[2] P. Kusch, Phys. Rev. 75, 887 (1949).
[3] Schuster and Pake, Phys. Rev. 81, 157 (1951).

O4. Magnetic Hyperfine Structure in the O_2 Molecule.* S. L. MILLER,† M. KOTANI,‡ AND C. H. TOWNES, *Columbia University*.—Magnetic hyperfine structure has been observed in the microwave spectrum of $O^{16}O^{17}$ in the 5 mm region. The components of the fine structure transitions which fall between 59,250 and 60,300 mc have been identified and are in agreement with the theory of Frosch[1] which predicts a perturbation Hamiltonian $bI\cdot S+cI_zS_z$ for the $^2\Sigma$ state. Both b and c contain terms belonging to the dipole-dipole and the relativistic interactions between the magnetic moments of the O^{17} nucleus and the unpaired electron spins. Values of $b=-101$ mc and $c=140$ mc fit the observed spectrum well, incidentally corroborating the reported value of 5/2 for the O^{17} spin. These values determine the sign and magnitude of the dipole-dipole interaction and show that the unpaired electrons are primarily in $2p\pi$ orbits. The value of $\psi^2(O)$ obtained further shows that they have approximately 1 percent $2s$ character. The data are consistent with unpaired electron wave functions that are about 90 percent $2p\pi$ and 10 percent $2p\sigma$ in character, where the $2p\sigma$ orbit is 10 percent $2s$ hybridized. We wish to thank Professor A. O. Nier for providing a sample of O^{17} enriched to about 1 percent.

* Work supported jointly by the AEC and the Army Signal Corps.
† AEC Predoctoral Fellow.
‡ On leave from Tokyo University.
[1] R. A. Frosch dissertation, December, 1951, Columbia University.

O5. High Temperature Microwave Spectroscopy-Spectrum of KCl, TlCl.* M. L. STITCH, A. HONIG, AND C. H. TOWNES, *Columbia University*.—A microwave stark spectrometer has been successfully developed to operate at high temperatures.[1] Gaseous KCl was examined at approximately 715°C. The $J=2\rightarrow3$ rotational transition was observed for the $K^{39}Cl^{35}$ isotopic species in the $v=0$, 1, 3, and 4 vibrational states. The hyperfine structure of the line was too small to be resolved. Frequencies were determined by wave-meter measurements to facilitate rapid searching, but limited accuracy to ±10 mc.

Transition frequencies seen		expected
$v=0$	23066±10 mc	23067.3±0.2 mc
1	22918±10 mc	22925.1±0.2 mc
3	22646±10 mc	22640.7±0.2 mc
4	22504±10 mc	22498.5±0.2 mc

The expected values are based on $B_e=3856.4$ mc and $\alpha_e=23.7$ mc obtained by molecular beams techniques.[2] An examination of TlCl at approximately 305°C revealed a rich spectra which cannot be the result of diatomic TlCl. This would indicate the presence in the gas of more complex chlorides of thallium.

* Work supported jointly by the Signal Corps and ONR.
[1] Stitch and Townes, Quarterly Report—Columbia Radiation Laboratory, December 31, 1951, and subsequent CRL reports.
[2] Private communication from Lee, Fabricand, and Carlson.

O6. Observation of Rotational Spectra by Molecular Beam Techniques.* C. A. LEE, R. O. CARLSON,† B. P. FABRICAND, I. I. RABI, *Columbia University*.—The molecular beam electrical resonance method has been modified to make possible observation of rotational transitions $J=0\rightarrow J=1$. Because the $J=0$ molecules have a greater polarizability than those of $J>0$, they describe a sigmoid path of greater amplitude than all other molecules in the inhomogeneous fields of the two cylindrical condensers. A suitably disposed stopwire permits passage of a portion of the $J=0$ molecules but excludes almost all the rest. The exciting radiation is introduced through a waveguide into a condenser, permitting observation of the lines in zero field or in a uniform electric field. Because extreme resolution was necessary, one of the chief experimental difficulties lay in achieving sufficient frequency and amplitude stability over long periods of time. To this end automatic frequency regulation of the klystron was employed, using a harmonic of a secondary frequency standard as a reference. The stability achieved made feasible the measurement of spectral lines in KCl, whose width at half maximum was ~18 kc, with an accuracy of >1 part in 3×10^8.

* Supported in part by the ONR.
† AEC Predoctoral Fellow.

O7. The Rotational Spectrum of KCl.* B. P. FABRICAND, R. O. CARLSON,† C. A. LEE, AND I. I. RABI, *Columbia University*.—The molecular beam electrical resonance method has been applied to investigate the structure of the line resulting from the transition $J=0\rightarrow J=1$ in the molecules $K^{39}Cl^{35}$ and $K^{39}Cl^{37}$. This structure resulting from the nuclear quadrupole interactions in the state $J=1$, for different vibrational states, v, was well resolved. The results are

	$K^{39}Cl^{35}$	$K^{39}Cl^{37}$
B_e, mc/sec	3856.352±0.002	3746.565±0.002
α_e, mc/sec	23.680±0.001	22.675±0.003
γ_e, mc/sec	0.050±0.001	0.047±0.001
r_e, cm	2.6665×10^{-8}	

The variations of $(eqQ)_K$, $(eqQ)_{Cl}$, and μ in $K^{39}Cl^{35}$ with vibrational state are shown below.

	$v=0$	1	2	3
$(eqQ)_K$ mc/sec	−5.656	−5.622	−5.571	−5.511
$(eqQ)_{Cl}$ mc/sec	>0.070	−0.080	−0.240	−0.380
μ Debye	10.61		10.82	

The $(eqQ)_{Cl^{37}}$ for $v=0$ is −5.660 mc/sec. The mass ratio of the chlorine isotopes agrees with previous measurements. Attention is drawn to the extraordinary variation of $(eqQ)_{Cl^{35}}$.

* Supported in part by the ONR.
† AEC Predoctoral Fellow.

O8. Lambda-Doubling in a Microwave Spectrum of Nitric Oxide. R. BERINGER AND E. B. RAWSON.—The lambda-doubling in nitric oxide has been observed in the Zeeman levels of the $^2\pi3/2$, $J=3/2$ state. The doubling is observed in a microwave resonance spectrum arising from electric-dipole transitions between the magnetic sublevels. A similar spectrum at somewhat lower resolution has been reported.[1] Because of the level structure the observed line splitting is of the order twice the lambda-doubling. The average splitting (about 1.7 mc/sec) agrees with calculations based on optical band spectrum data. The microwave splitting varies with M_J roughly as indicated by an unpublished theory of M. Karnaugh. The experiments will be described, and correlation with Karnaugh's theory will be discussed.

[1] R. Beringer and J. G. Castle, Jr., Phys. Rev. 78, 581 (1950).

O9. The Zeeman Effect of the Chlorine Nuclear Quadrupole rf Resonance.* CHRISTOPHER DEAN, *Harvard University*.—The first-order Zeeman perturbation of the electric quadrupole energy levels of a nucleus with spin 3/2 interacting with an arbitrary electric field has been computed for all orientations of the magnetic field, and exact solutions have been obtained for special orientations. These results show that the deviation of the electric field gradient tensor from rotational symmetry can be measured and its principal axes located by the Zeeman effect. A superposition of two patterns corresponding to different orientations of the tensor, each having an asymmetry factor $\eta=[\partial^2V/\partial x^2)-(\partial^2V/\partial y^2)]/(\partial^2V/\partial z^2)=0.08$ ±0.02, was found in the Cl^{35} resonance in a crystal of p-dichlorobenzene in the phase stable below 30°C. Taken together, the two sets of principal axes specify a single axis of twofold symmetry, agreeing with the classification of this

crystal as monoclinic, and the two orientations are interpreted as belonging to the two different molecules in the unit cell. The deviation from rotational symmetry can be attributed to the partial double-bond character of the C−Cl bond, and on this assumption the orientation of the molecules can be specified completely.

* This work was partially supported by the joint program of the ONR and AEC.

O10. The Spin and Quadrupole Moment of Se^{79}.* W. A. HARDY, G. SILVEY, AND C. H. TOWNES, *Columbia University.*—Six lines of the quadrupole hyperfine structure of the radioactive nucleus of Se^{79} in the $J=2\rightarrow3$ transition of $O^{16}C^{12}Se^{79}$ have been measured and determine the spin of Se^{79} as 7/2 with a quadrupole coupling constant (eqQ) of 754 ± 3 mc. An estimate of the molecular constant q, gives the Se^{79} quadrupole moment $Q=1.2\times10^{-26}$ cm² with an error probably less than 50 percent. The spectroscopy was done in a recording Stark spectrometer with frequency markers placed directly on the recording trace. One microgram of Se^{79} produced by uranium fission was obtained from the Brookhaven National Laboratory, reduced to elemental Se, and reacted with CO to give OCSe. Nuclear shell structure predicts a $g_{9/2}$ or possibly a $p_{1/2}$ state for the $_{34}Se_{45}^{79}$ nucleus and the observed spin of 7/2 is a clear exception to the single particle, strong spin-orbit coupling model. Goldhaber and Sunyar[1] have, however, predicted the spin of 7/2 for the ground state of Se^{79} from a study of isomeric decay. A nuclear $(g_{9/2})^3$ configuration is indicated in which two particles fail to pair exactly to give zero angular momentum, but give unit angular momentum, instead. The positive quadrupole moment of Se^{79} is consistent with this type of state.

* Work supported by the AEC.
[1] M. Goldhaber and A. W. Sunyar, Phys. Rev. 83, 906 (1951).

O11. The Microwave Spectrum and Structure of Chlorine Trifluoride.* D. F. SMITH, *Carbide and Carbon Chemicals Company.*—The microwave spectrum of ClF_3 is that characteristic of an asymmetric top molecule with a wealth of weak lines which have been observed in the 24 to 31 kilomegacycle region. The lower frequency corresponds to a "band head" of a $K_{-1}=1\rightarrow2$ subgroup. The $J=4$, 5, 6, and 7 of this group, together with the $J=5$ of the $K_{-1}=0\rightarrow1$ subgroup near 21 kilomegacycles have been identified for both $Cl^{35}F_3$ and $Cl^{37}F_3$. These lead to internally consistent values of a-c and κ. Together with the $1_{0,1;-1}\rightarrow2_{1,2;-1}$ transitions these yield preliminary values for the moments of inertia (in atomic mass units angstroms²) of $I_a^{35}=36.764$, $I_b^{35}=109.60$, $I_c^{35}=146.56$ and of $I_a^{37}=37.019$, $I_b^{37}=109.59$, $I_c^{37}=146.81$. Since $I_c\approx I_a+I_b$ as well as $I_b^{35}\approx I_b^{37}$, the molecule is planar, with a C_{2v} axis that is further confirmed by an observed alternation of intensities. These moments of inertia fit an undistorted "T" model with the Cl at the intersection of the two arms. The two similar ClF bonds (1.70A) are longer than the unique ClF bond (1.56A). The FClF angles are 90° within the precision with which this angle is determined. This structure is in fair agreement with the preliminary x-ray structure that had been found by Dr. Burbank of the K-25 Laboratories. The hyperfine structure can be consistently fit to values of $\chi_{aa}(Cl^{35})$ (along the straight FClF line) $=-81$ mc, $\chi_{bb}(Cl^{35})$ (along the unique ClF bond) $=-65$ mc so that $\chi_{cc}(Cl^{35})=146$ mc.

* This document is based on work performed for the AEC by Carbide and Carbon Chemicals Company, at Oak Ridge, Tennessee.

O12. Anomalies in the Hyperfine Structure of ICN.* A. JAVAN AND C. H. TOWNES, *Columbia University.*—Hyperfine components of the $J=3\rightarrow4$ transition of ICN in the excited vibrational state $v_2=1$ apparently show varying amounts of l-type doubling. The variation is proportional to the separation of the particular hyperfine component from the theoretical position of the transition without hyperfine structure, and is as large as 6 mc. This anomaly can be attributed to the fact that the electric field gradients are not symmetric about the axis of the molecule when the molecule is bent because of vibration. The value of the asymmetry parameter

$$\eta=\left(\frac{\partial^2 v}{\partial x^2}-\frac{\partial^2 v}{\partial y^2}\right)\Big/\frac{\partial^2 v}{\partial z^2}$$

is 0.0045. This is about five times larger than the value to be expected from a bending of the molecular bonds with no change in their structure. Its size must in part be the result of an asymmetry of the I—C bond about its axis produced by the bending of the molecule. Other anomalies in the ICN excited states are being studied.

* Work supported jointly by the Signal Corps and ONR.

O13. Anisotropy in Paramagnetic Resonance in Free Radicals.* C. KIKUCHI AND V. W. COHEN, *Brookhaven National Laboratory,* AND JOHN TURKEVICH, *Princeton University.*—We have observed the paramagnetic resonance absorption in Picryl-n-Amino Carbazyl by mounting the specimen at the center of a k band cylindrical cavity. The sample was mounted at the end of an axial quartz rod and could thus be rotated about an axis perpendicular to the applied magnetic field. With samples which appear to be single crystals, the line half width is about 0.5 gauss. For a certain orientation of the crystal with respect to the axis, the position of the line is independent of rotation. For other orientations, the line shifts with respect to rotation by as much as 7 gauss toward the direction of high applied field. The periodicity of this shift is 180°. The g values corresponding to the extremes of the range are 2.0024 and 2.0041 using the value of 2.0036[1] for $\alpha-\alpha$ diphenyl-β-picryl hydrazyl. A similar effect was observed for the hydrazyl but the basic line width was about one gauss with the extremes resulting from rotation of about 5 gauss. These directional effects might be attributed to diamagnetic effect of the molecule.

* Research carried out under contract with the AEC.
[1] C. H. Thomas and J. Turkevich, Phys. Rev. 77, 148 (1950).

FRIDAY MORNING AT 9:45

Pupin 428

(GREGORY BREIT presiding)

Scattering Theory; Nuclear Shell Theory

P1. Nuclear Shell Interactions. KATHARINE WAY AND MARION WOOD, *National Bureau of Standards.*—Neutron and proton binding energies in the region from Tl to Cm have been computed from experimental Q values, α-systematics,[1] and β-decay energies. Interpreted on shell ideas, the results show: (1) For $Z=82$, the shell interaction of the new neutron

shell (starting with 127) is that predicted by the calculation of M. G. Mayer.[3] (2) When both neutrons and protons are put into new shells (protons above 82, neutrons above 126) one finds a strong, quickly saturated, spin dependent $n-p$ interaction with magnitude ≤ 0.8 Mev per pair. This interaction causes neutron binding energies, B_n, to decrease as N_n/N_p increases so that, for Z constant, a plot of $B_n(A)$ near a shell edge is quite different from that found for electrons near an atomic shell edge. Proton binding energies show an added electrostatic repulsion effect. In the course of the study, a new β-systematics was developed which exhibits clearly the shells at $Z=82$ and $N=126$ but no further shells for higher values of Z and N.

[1] Seaborg, Perlman, and Ghiorso, Phys. Rev. **72**, 26 (1950).
[2] M. G. Mayer, Phys. Rev. **78**, 22 (1950).

P2. The Line of Beta-Stability. A. E. S. Green, N. Engler, and N. J. Marucci, *University of Cincinnati.*—We present a chart of the nuclides based upon a transformation involving a simple empirical expression for the line of minimum mass. On this chart beta-stable nuclides are located at points which scatter around the horizontal axis. Our chart is designed to magnify greatly certain trends and irregularities in the tendencies of nuclides. By using it we show (a) the experimental line of β-stability, (b) the effects associated with pairing and magic numbers, (c) the lines of minimum mass according to the semiempirical mass formula with various sets of constants, (d) the limits of β^--, β^+- and K-capture stability according to experiment and the different semiempirical mass formulas, and (e) the relations between the lines of minimum mass and the corresponding lines of maximum binding energy. We conclude with an evaluation of various semiempirical mass equations from several standpoints which are related to beta-stability.

P3. The Hyperfine Structure Anomaly and Models of Nuclear Structure. B. T. Feld, *M.I.T.*—The hyperfine structure anomaly is defined as the difference from 1 of the ratio of the magnetic moments of two isotopes, as determined from their hyperfine structure in atomic s-states by application of the Fermi-Segré formula, divided by the ratio of the moments as observed by nuclear induction. As suggested by Bitter and Kopfermann and demonstrated by A. Bohr and Weisskopf, the hfs anomaly arises from a difference, between the nuclei involved in the distributions of nucleon moments and currents which give rise to the nuclear moments. Anomalies have been observed for $Li^{6,7}$, $K^{39,41}$, $K^{39,40}$, $Rb^{85,87}$, and $Tl^{203,205}$ (atomic ground state $^2p_{\frac{1}{2}}$). These results can be compared with theoretical estimates, based on different nuclear models. In general, reasonable agreement is obtained for models which are, in their essential features, based on the independent particle model with spin-orbit coupling. Particular consideration has been given to the application of the theory to odd-odd nuclei. For the case of K^{40}, unfortunately, all the models which have been investigated (and which are capable of yielding the observed spin and nuclear moment) predict essentially the same anomaly.

P4. Emperical Evaluation of Unpaired Spin Effects for Protons and Neutrons.* Charles D. Coryell and Hans E. Suess, *Massachusetts Institute of Technology and the U. S. Geological Survey.*—By taking as a reference point even-Z and even-N nuclides, the energy of nuclides may conventionally be expressed $E(Z, N)=f(Z, N)+\pi$ (for an unpaired proton) $+\nu$ (for an unpaired neutron). The term δ was introduced by Bohr and Wheeler for either π or ν, so that their δ_A equals $\pi+\nu$. Experiment[1] shows that in some regions π exceeds ν, i.e., for heavy odd-A nuclides, and just above the neutron closed-shells $N=50$ and $N=82$. The $\pi-\nu$ differences in Mev are recorded[1] as 0.2 (Glueckauf), 0.6, and 0.7 (Suess) for the three regions respectively. Consideration of the statistics of Z values of odd-A nuclides shows that $\pi \leq \nu$ in other regions where odd-Z nuclides are favored. For the regions above $Z=14$, $Z=28$, and $Z=50$, ν exceeds π by about 0.5 Mev. As with N-shells other than 126, the $\pi-\nu$ difference fades away with increasing A. These $\pi-\nu$ effects added to considerations[2] of parabolic depth B_A and of stablest charge Z_A, for given A, explain almost quantitatively the instability of A^{97}, the surprisingly low decay energies of Zr isotopes, and the β-energetics of isotopes of Tc, Pm, At, and Fr.

* Supported in part by the AEC.
[1] E. Glueckauf, Proc. Phys. Soc. (London) **61**, 21–33 (1948); L. Kowarski, Phys. Rev. **78**, 477 (1950); H. Suess, Phys. Rev. **81**, 1071 (1951).
[2] Coryell, Brightsen, and Pappas, Bull. Am. Phys. Soc. **26**, No. 6, 36, October, 1950.

P5. First Forbidden Beta-Transitions.* T. Ahrens† and E. Feenberg, *Washington University.*—The general theory of first forbidden beta-transitions involves seven nuclear matrix elements in the nonrelativistic approximation. The number of independent parameters can be reduced to four with the help of the relation, $(W_f-W_i)\langle f|X|i\rangle=\langle f|[H, X]|i\rangle$. Here W is an energy eigenvalue, X a coordinate type first forbidden operator, H the nuclear Hamiltonian [a sum of H_0 (free particles), H_c (Coulomb interaction), and H_σ (specifically nuclear interactions)]. $[H_0, X]$ and $[H_c, X]$ are easily evaluated, but $[H_\sigma, X]$ presents difficulties because H_σ for complex nuclei is essentially unknown. However knowledge of the explicit form of H_σ is not required; the matrix elements of $[H_\sigma, X]$ can be estimated by physical arguments based on the semiempirical nuclear energy surface and the general validity of shell model considerations.

* Supported in part by the joint program of the ONR and AEC.
† AEC Predoctoral Fellow.

P6. Magnetic Moments of Even-Odd Nuclei. Jack P. Davidson,* *Washington University.*—As the ground states of odd-A nuclei are generally considered to be predominantly of the doublet type, one may write for the pure doublet approximation, $\Psi_I=\alpha\Psi_{L=I-\frac{1}{2}}+(1-\alpha^2)^{\frac{1}{2}}\Psi_{L=I+\frac{1}{2}}$, a linear combination of pure $L-S$ coupling states. The deviations of the nuclear magnetic moments from the Schmidt limits are interpreted as the failure of $L-S$ coupling and a simple interpolation procedure which preserves the parity quantum number is applied to compute the statistical weight of the components with $L=I+\frac{1}{2}$ and $L=I-\frac{1}{2}$. The results below odd-N or -$Z=53$ are sufficiently regular to be used to compute the magnetic moment of several odd neutron nuclei.

* Washington University Fellow.

P7. Connection Between Scattering and Derivative Matrices. E. P. Wigner, *Princeton University.*—In problems of simple scattering, both the scattering function S and the derivative function R are analytic. The latter is the ratio of the wave function to its derivative at a fixed point outside the range of the potential; it is a real function of the energy $R(k)=R(-k)=R(k^*)^*$. The connection between the two functions is $S=(1+ikR)(1-ikR)^{-1}\exp(-2ika)$ and S satisfies the relations $S(-k)=S(k^*)^*=S(k)^{-1}$. The poles of S, considered as function of the complex variable k, lie either in the lower half plane or on the imaginary axis; those of R, considered as function of the energy or of k^2, lie on the real axis and their residues are negative. Schutzer and Tiomno have shown that the above properties of S follow from those of R. Although the number of arbitrary constants in both R and S is the same, namely, equal to the number of poles, it can be shown that the constants in the latter have to satisfy certain inequalities if the S is to be derivable from a permissible R. The simplest of these states that the center-of-mass of the poles of S lies in the lower half-plane if their number is even.

P8. Neutron-Proton Scattering with Spin-Orbit Coupling; Formal Theory. JOHN M. BLATT, *University of Illinois* AND L. C. BIEDENHARN, *Oak Ridge National Laboratory.*—Neutron-proton scattering in the triplet spin state is discussed under the following assumptions about the nuclear forces. (1) They are conservative, (2) they allow time-reversal (i.e., the reciprocity law is valid), (3) the spin vectors of the neutron and proton enter in a symmetrical way, so that the total spin of the system is preserved during the collision, and (4) the forces have a finite range. We do *not* assume that the forces can be derived from a potential function. The scattering matrix for the system is expressed in terms of the minimum number of real, independent parameters. These parameters are related to the asymptotic behavior of the solutions of the wave equation for large distances. A general expression is given for the differential scattering cross section in terms of these parameters. The energy dependence of these parameters near zero energy can be predicted uniquely on the basis of assumptions (1) to (4) above. While many of these results are well-known, the derivation given here shows that they hold under much more general assumptions than the usual proofs would indicate.

P9. Nucleon Scattering with Repulsive Core Potentials. M. A. PRESTON, J. R. BIRD, AND J. SHAPIRO, *University of Toronto.*—Interactions of the type proposed by Jastrow[1] but with finite repulsive potentials are considered. Thus for a given "shape" of potential, there are four parameters in the singlet interaction, two ranges and two potential strengths. The scattering data at energies where relativistic effects are assuredly not important are studied to see to what extent these parameters are fixed. The results obtained will be discussed.

[1] R. Jastrow, Phys. Rev. **81**, 165 (1951).

P10. Application of the Variational Method to Scattering by a Square Well Potential.* J. MAYO GREENBERG, *University of Maryland.*—The scattering by a square well potential is calculated by the variational method[1] by using as initial trial functions a plane wave with the appropriate wave number, and an approximate internal wave function obtained[2] by summing the spherical Bessel function expansion of the wave function with the assumption that the well is large compared with the incident wavelength. In order to obtain an expression in closed form for the variational result, one must resort to exactly the same approximation as is used by Hart and Montroll. Use of the approximate internal wave function then leads to the same scattering function. In fact, this result is also obtained by using the approximate internal wave function in the correct integral equation.[3] Comparison of the two results will be made with several exact and experimental values.

* Work supported by the ONR.
[1] W. Kohn, Phys. Rev. **74**, 1763 (1948).
[2] R. W. Hart and E. W. Montroll, J. Appl. Phys. **22**, 376 (1951).
[3] E. W. Montroll and R. W. Hart, J. Appl. Phys. **22**, 1278 (1951).

P11. The Effect of a Singular Triplet Tensor Interaction on $P-P$ Scattering Below 10 Mev. EDWIN A. CROSBIE, *University of Pittsburgh.*—Christian and Noyes[1] have shown that the 32- and 340-Mev $P-P$ scattering data are consistent with the scattering to be expected from the usual singlet square well interaction of the form ∓ 18 Mev $\exp(-r/R)\times(r/R)^{-2}$, $R=1.6\times10^{-13}$ cm. Numerical solution of the differential equations using this interaction gives the following P-wave tensor phase shifts at the indicated energies: $E=8$ Mev, $\delta_{12}=-0.38°$, $\delta_{11}=2.50°$, $\delta_{10}=-3.13°$; $E=6.85$ Mev, δ_{12}: $-0.32°$, $\delta_{11}=2.04°$, $\delta_{10}=-2.61°$. The effect of the P-wave scattering on the apparent S-wave phase shift at these energies is investigated. It is found that an accuracy of about 1 percent in energy plus cross section measurements would be sufficient to detect the singular tensor interaction at energies around 8 Mev. Comparison at 6.85 Mev with the Rouvina[2] nonliquid nitrogen data shows that the calculated apparent S-wave phase shifts as a result of this interaction, as a function of angle is just within the accuracy but does not provide the best fit for the experimental points.

[1] Christian and Noyes, Phys. Rev. **79**, 85 (1950).
[2] Rouvina, Phys. Rev. **81**, 593 (1951).

P12. A Variational Principle for $k\cot\delta$. S. I. RUBINOW AND HERMAN FESHBACH, *M.I.T.*—In the analysis of (n, p) and (p, p) scattering, the quantity $k\cot\delta$, where k is the wave number and δ is the phase shift, is of primary importance for calculating the scattering cross section. Both Schwinger and Hulthen have introduced variational principles for $k\cot\delta$; these, however, suffer from the defect that the trial wave functions contain $k\cot\delta$, the quantity that is sought. While Hulthen has reformulated his method so that this defect is absent, the expression he uses to obtain $k\cot\delta$ is no longer stationary with respect to variations in the wave function. A new variational principle for S-state scattering is introduced which utilizes a stationary expression for $k\cot\delta$ in terms of the "inside" wave function. The latter is independent of $k\cot\delta$. Consequently, the scattering length $1/\alpha$ and the effective range r_0 can be calculated directly. The Born approximation may be obtained by assuming an appropriate trial function. The method is illustrated for the exponential well potential with a simple trial function involving only one parameter. The results obtained for α and r_0 are in very good agreement with the exact solution (given by Blatt and Jackson).

FRIDAY MORNING AT 9:00

McMillin

(C. C. LAURITSEN presiding)

Business Meeting of the American Physical Society

(G. P. HARNWELL presiding)

Invited Papers

Q1. Big Molecules in Biological Systems. R. W. G. WYCKOFF, *National Institutes of Health.* (40 min.)

Q2. Some Recent Experiments with High Centrifugal Fields. J. W. BEAMS, *University of Virginia.* (40 min.)

Q3. Shock Waves and Their Interactions. WALKER BLEAKNEY, *Princeton University.* (40 min.)

FRIDAY MORNING AT 9:45

Pupin 301

(S. C. BROWN presiding)

Business Meeting of the Division of Electron Physics

Symposium of the Division of Electron Physics

R1. Ionization and Recombination Processes in the Afterglow. M. A. BIONDI, *Westinghouse Research Laboratories.* (40 min.)

R2. The Magnetic Moment of the Electron. P. KUSCH, *Columbia University.* (35 min.)

R3. Recent Developments in the Physics of Counters. S. A. KORFF, *New York University.* (35 min.)

FRIDAY AFTERNOON AT 2:15

McMillin

Joint Ceremonial Sessions of APS and AAPT

(J. H. VAN VLECK presiding)

Retiring Presidential Address of the American Physical Society

S1. Some Investigations of Light Nuclei. C. C. LAURITSEN, *California Institute of Technology.*

(M. W. ZEMANSKY presiding)

Presentation of the Oersted Medal of the AAPT

Response by the Oersted Medallist

S2. Opportunities and Rewards in Physics Teaching. ANSEL ALPHONSE KNOWLTON, *Reed College (retired).*

Tenth Richtmyer Memorial Lecture of the AAPT

S3. Large-Cyclotron Research at the University of Chicago. ENRICO FERMI, *University of Chicago.*

FRIDAY AFTERNOON AT 3:20

Schermerhorn 501

(G. E. KIMBALL presiding)

Chemical Physics and Biophysics

SA1. Fourier Transforms and Intensities from Crystalline Proteins.* DOROTHY WRINCH, *Smith College.*—Information is accumulating in published vector maps of crystalline native proteins compatible with the existence, in such crystals, of structures of globular type (and indeed cage structures), as suggested by the writer in 1936. An attempt is therefore being made, by way of Fourier transforms, to derive a structural type, in the first instance spherical, whose transform has turning points at distances from the origin $\sim 1/10A$, $\sim 1/4.7A$, i.e., in the ratio $\sim 1:2.1$. Previous studies[1] show that the ratio is 1:1.58 for the solid sphere and increases for shells, up to 1:1.73 for the spherical surface. This suggests the ratio will be further increased with negative interiors for the shells, a feature which is independently suggested by the fact that our concern is with structures reduced to p, the average electron density in the crystal.[2,3] It has now proved possible to reach

the required ratio with a thin shell, provided only that the density of the interior is sufficiently negative, i.e., far enough below ρ.

* This work is supported by the ONR.
[1] D. Wrinch, *Fourier Transforms and Structure Factors* (1946).
[2] D. Wrinch, Phil. Mag. **27**, 490 (1939).
[3] D. Wrinch, Acta Cryst. **3**, 475 (1950).

SA2. The Effect of Pressure on the Viscosity of Higher Hydrocarbons and Their Mixtures. WAYNE WEBB, EDWARD M. GRIEST, AND ROBERT W. SCHIESSLER.—Using the rolling-ball method, the viscosity of seven pure hydrocarbons (C_{18}–C_{24}) and three binary mixtures has been measured between 15 and 50,000 psi at 100°, 140°, 210°, and 275°F. The hydrocarbons included isoparaffinic, cycloparaffinic, aromatic, and cycloparaffinic-aromatic compounds. The increase in viscosity with pressure was found to be strongly dependent on molecular structure, a 20-fold disparity in relative viscosity existing among the extremes in structure for the same pressure interval. The viscosity-temperature coefficient, $1/u\ (du/dT)$, increases with increasing pressure. Each of the binary mixtures studied, which corresponded in molecular weight and average molecular structure to a single pure compound, was found to exhibit the same behavior as the analogous pure liquid to within 5 percent in spite of a 50–100-fold increase in viscosity with pressure. This remarkable agreement was interpreted as meaning that the viscosity of these high molecular weight compounds is some additive function of their constituent groups, irrespective of whether these groups are combined in the same or different molecules, as long as the basic molecular symmetry is unchanged.

SA3. The Influence of Specific Volume on the Viscosity-Pressure Behavior of Some Hydrocarbon Liquids. EDWARD M. GRIEST, WAYNE WEBB, AND ROBERT W. SCHIESSLER.—It is suggested that the increase of kinematic viscosity with pressure at constant temperature is related to the attendant decrease in specific volume through the Lennard-Jones potential function in the relatively simple equation, $\log Z = \log Z_0 + K/T(-1/v^3 + v_0^3/v^4)$, where the subscript indicates the value at atmospheric pressure. The four hydrocarbons for which experimental density data are available are in good accord with this relation. A correlation exists between the quantity (K/T) and the Eyring activation energy for viscous flow as derived from the viscosity-temperature behavior. Although the relationship is not sufficiently precise to permit a reasonably accurate calculation of the viscosity at any given pressure from the atmospheric viscosity-temperature coefficient and the specific volume, it does constitute a more simple and rigorous proof of the interdependence of the effects of pressure and temperature on viscosity than has been described previously.

SA4. Energy Loss of Deuterons in Hydrocarbons. J. W. PREISS AND ERNEST POLLARD, *Yale University*.*—The use of ionizing radiation to measure the size and shape of large organic molecules requires a knowledge of the rate of energy loss of fast charged particles in material composed of carbon, nitrogen, oxygen, and hydrogen. The effective ionization potential of carbon is not well known. To measure this an absorption cell has been constructed which permits the determination of the range of analyzed deuterons in various gases. Preliminary measurements on ethylene and acetylene as compared to air indicate that the effective ionization potential of carbon is 58 5 ev.

* Assisted by the joint program of the ONR and AEC.

SA5. Effect of Deuteron Bombardment on the Serology of Tobacco Mosaic Virus. E. POLLARD AND A. E. DIMOND, *Yale University** *and Connecticut Agricultural Experiment Station*.—It has previously been shown that deuteron bombardment removes the infectivity of tobacco mosaic virus if a deuteron passes through an area only slightly smaller than the area of the accepted infectious unit of the virus. Further studies have shown that the same cross section per deuteron for inactivation is found when the temperature of the virus is raised while the bombardment takes place. Thus, as regards infectivity the virus appears to act as a single highly sensitive unit. When the ability of the virus to combine with specific antiserum is measured a completely different result is obtained. It proves possible to subject tobacco mosaic virus to bombardment which reduces the infectivity to below one percent without measurable effect on its ability to combine with antibody. It is thus clear that the action of primary ionization in removing infectivity corresponds to some very slight molecular change, which is far less than is needed to alter the surface configurations required for serological combination. If this should prove to be general for all viruses, it offers promise as a method of temporary immunization.

* Assisted by the AEC.

SA6. Electron Inactivation of Enzymes and Viruses. M. SLATER,* *Yale University*.†—The previously reported[1] study of the inactivation of dry preparations of several enzymes and viruses, using a 2-Mev electron beam, has been completed. The molecules studied (catalase, urease, invertase, chymotrypsin, hemoglobin, T-1 bacteriophage, and tobacco mosaic virus) all gave exponential survival curves. Using conventional target theory, the ionization sensitive volume of the molecules can be determined from these curves and compared with the known sizes of the molecules, thus indicating the fraction (between ½ and 1) of the molecule which is sensitive to radiation. These volumes, determined by low ion-density electrons, can also be compared with cross sections measured by high ion-density deuterons.[2] The agreement between them gives good verification of the ion density predictions of the target theory and is experimental evidence that the energy loss per *primary* ionization is the same (110±10 ev) in both gases and solids.

* Now at Oak Ridge National Laboratory, Oak Ridge, Tennessee.
† Assisted by AEC and ONR.
[1] M. Slater, Phys. Rev. **83**, 231 (1951).
[2] E. C. Pollard, American Scientist **39**, 99 (1951).

SA7. Irradiation of *B. subtilis* with Low Voltage Electrons. MARGUERITE DAVIS,* *Yale University* (introduced by Franklin Hutchinson).—The effect of the differential penetration of slow electrons was studied as a means of investigation of the internal organization of living material. Since the energy of the electron is directly related to its depth of penetration, the variation of survival after irradiation can be correlated with the energy of the bombarding particle and its range. As an application of this, low voltage (100–1600 volts) electrons were used to bombard dry *B. subtilis* bacterial spores in vacuum. No effect was seen up to 200 volts; at this point the survival suddenly dropped to a plateau around 50 percent survival extending to 900 volts. Above 900 volts, the survival dropped rapidly to zero by 1600 volts. Dose survival curves were taken at different voltages and with doses of 10^{18} to 10^{17} electrons/cm^2. The slopes of the curves varied with the voltage and a trail off at high doses was seen up to relatively high voltages where the survival goes to zero at high doses. Using Lea's[1] figures for ranges of low voltage electrons in tissue, the position and size of the sensitive volume within the spore can be calculated.

* Assisted by the AEC.
[1] D. E. Lea, *Action of Radiation in Living Cells* (Macmillan Company, New York, 1947).

SA8. The Bombardment of Biological Molecules with Slow Electrons.* FRANKLIN HUTCHINSON, *Yale University*.—In irradiating biological material with the usual types of ionizing

radiations (e.g., x-rays, fast deuterons, etc.) the energy release is the order of 100 ev per primary ionization, which is very large compared to the chemical bonds which hold the material together. Some light might be shed on the mechanism by which biological systems are inactivated by determining this inactivation under irradiation of slow electrons of energies ranging from 0 to 100 volts. This is analogous to the classic Franck-Hertz experiment measuring the excitation potentials of atoms. The target must be only one molecule thick, since very slow electrons cannot penetrate through one molecule to hit another beneath it. Thus it is convenient to irradiate monomolecular layers of protein molecules, using the technique previously described.[1] With monomolecular layers of bovine serum albumin, an inactivation curve has been determined which shows that electrons of less than 16 ev energy are able to inactivate the molecule.

* Assisted by the AEC.
[1] F. Hutchinson, Phys. Rev. 82, 303 (1951).

FRIDAY AFTERNOON AT 3:20

Havemeyer 309

(L. MARTON presiding)

General Physics

SB1. Dynamics of Supernovae. LYLE B. BORST, *University of Utah.*—The light curves of supernovae of type I are characterized by an exponential tail of 55±5 day half-life, experimentally identical to the half-life of non-ionized Be^7 ($T_{\frac{1}{2}}=53d$). This may be quantitatively accounted for by assuming 10^{32} g Be^7 as the energy source in the tenuous expanding gaseous shell observed after explosion. The proposed mechanism for the production of the beryllium involves a nonequilibrium rate controlled endothermic reaction between alpha-particles during the gravitational collapse of the star.

SB2. A New Mutual Inductance Formula. MILAN W. GARRETT, *Swarthmore College.**—For two axially symmetric systems whose axes intersect at angle γ,

$$M=q_0\rho_0+\sum_{n=1}^{\infty} q_n\rho_n(r_2/r_1)^n P_n(\cos\gamma)/n(n+1).$$

Compute central-field constants q_n[1] from primary coordinates, remote-field constants ρ_n from the secondary. Unit radii are, respectively, r_1 and $r_2(<r_1)$. For the coaxial case, choose single or multiple origins for best convergence and to suppress alternate terms. The new expression resembles Maxwell's zonal harmonic formula, with loop constants generalized and zero order added. It includes or replaces in working practice most widely used formulas involving circular filaments, disks, thin or thick solenoids (Gray, Lorenz, Searle-Airey, Roiti, Rosa, Snow, Grover, etc.), but covers also new cases. Suppression of algebraic detail permits simpler and more accurate computation; here, all factors are found and checked, to high orders if needed, by simple recurrent relations. Convergence is accurately foretold by inspection. Study of isolated constants q_n, ρ_n permits new flexibility in system design. A simple extension covers parallel axes.

* Work supported by the ONR and the Research Corporation.
[1] Milan W. Garrett, J. Appl. Phys. 22, 1091 (1951).

SB3. Stress-Induced Noise in Cables.* THOMAS A. PERLS, *National Bureau of Standards.*—Stress-induced cable noise interferes with the transmission of signals in many different types of measurement, control, detection, and communication. The present investigation was undertaken in connection with the design and evaluation of very small barium titanate transducers for acceleration and pressure measurements. A quantitative theory of the mechanism of noise generation predicts a triboelectric separation of charge as a result of intermittent contact between the insulating dielectric and either of a pair of conductors. The necessary redistribution of charge produces a current pulse through the terminating network. Quantitative predictions of this theory are verified by a series of simple experiments. *Stress-induced noise is practically eliminated in cables having conductive coatings both inside and outside of the insulating dielectric.* Comparison of such an experimental, light, flexible, coaxial cable, 0.07 inch o.d., with a standard microphone cable of similar dimensions, shows a reduction in signals caused by twisting and squeezing by a factor of at least 200. There appears to be no limitation on arrangement and number of conductors, or on size and flexibility of cables made by this method. An industrially applicable method of construction will be suggested.

* Work done under a cooperative project on Basic Instrumentation partially sponsored by the ONR, AF, and AEC.

SB4. Noise and Dissipation.* JOHN M. RICHARDSON.†—The connection between noise (producing deviations of observables from their average values) and dissipation (measured by the irreversible part of the drift of these average values toward equilibrium) is investigated in a rigorous and elementary way for any system near equilibrium. In contrast to other work our treatment considers explicitly a large isolated system whose initial nonequilibrium distribution of states is an exponential of a linear combination of the observables. The set of averaged observables, considered as a vector, when operated upon by a suitable impedance matrix, is assumed to vanish except for a correction of short duration. The final result expresses the spectral density matrix of the noise in terms of the Laplace transformed impedance matrix and certain variance matrices of thermodynamic significance. In the classical treatment of voltage fluctuations and resistance, our result agrees completely with the well-known theorem of Nyquist[1] if the impedance is of a restricted type. The connection with the recent work of Callen and Welton[2] will be discussed.

* This research is a part of the work being done at the Bureau of Mines supported by the Air Materiel Command.
† Head, Kinetics Section, Explosives and Physical Sciences Division, Bureau of Mines, Pittsburgh, Pa.
[1] H. Nyquist, Phys. Rev. 32, 110 (1928).
[2] H. B. Callen and T. A. Welton, Phys. Rev. 83, 34 (1951).

SB5. A Constriction Type of Electromechanical Filter Employing a Shear Mode.* SHEPARD BARTNOFF AND CHARLES R. MINGINS, *Tufts College.*—A laminar type of system is considered as the mechanical part of an electromechanical filter with piezoelectric input and output transducers. The different laminae all consist of the same aeolotropic material but have different cross sectional areas. For the transmission of face shear vibrations, it is shown that the system has filter properties analogous to those of a sound filter system consisting

of segments of pipe with varying cross sections. Expressions are derived for the band width, the power transmission coefficient of the filter, and for the nature of the variations of these quantities with changes in the physical dimensions of the system elements and also with changes in the number of laminae.

* This work is sponsored by the U. S. Army Signal Corps.

SB6. Grid Bar Mask Focusing in a Color TV Tube. JENNY E. ROSENTHAL.—Most color TV tubes proposed use the shadow properties of a grid bar mask to keep the electron beam from striking any but the desired phosphor color whether applied in lines or dots. Such shadow effects decrease the effective intensity of the electron beam hitting the phosphor to a small fraction of its value at the electron gun. This loss of efficiency is avoided if the shadow property of the grid bar mask is eliminated by suitable design and replaced by a contraction of the area scanned by the beam after it passes through the mask. This is accomplished by the Deserno effect, which is essentially focusing in a transverse electrostatic field generated, in this case, by maintaining a fixed small potential difference between alternating grid bars. As shown previously,[1] a deflection field applied between the grid bars and the conducting coating on the face plate deflects the beam on the different color phosphor strips. Calculations are given on the magnitude of the potentials and the design of the grid bar mask.

[1] Jenny E. Rosenthal, Phys. Rev. **82**, 325 (1951).

SB7. A Device for Converting a Shaft Rotation to an Input for a Digital Computer. DONALD H. JACOBS AND SEYMOUR SCHOLNICK, *The Jacobs Instrument Company*.—This device comprises an input shaft, a rotating disk with pulses recorded magnetically on its periphery at equal angular intervals, and a magnetic pick-up head for reading these pulses. The output of the pick-up passes through a gate to a counter. The rotating disk is mounted coaxial with, and adjacent to, the input shaft. Electrical means are used to gate pulses from the pick-up to the counter during the interval that a given point on the disk rotates between a reference point and an arm connected to the input shaft. The number in the counter represents the shaft rotation angle in terms of the radix of the arithmetic system employed by the computer. The devise imposes no torque requirements on the input shaft, and permits any desired degree of angular accuracy. A new reading of input angle is obtained for each rotation of the disk, and the accuracy of measurement is not affected by the disk's rotational speed. Readings of the shaft's angular position can be made as frequently as necessary in any practical case. A 3-in. disk gives an accuracy of $\frac{1}{4}°$ when a magnetic pick-up is used, and appears capable of about 1-minute accuracy when an optical pick-off is employed. The devise is capable of indicating angles with either positive or negative signs relative to a given reference point. It can be used in conjunction with either serial or parallel computers.

SB8. Radio Propagation Beyond the Horizon and the Surface Refractive Index. THOMAS J. CARROLL.* *National Bureau of Standards*.—For the bilinear model of the index of refraction of the normal troposphere, Furry's theory shows that the attenuation of all the modes beyond the horizon is a function of the surface index of refraction, not its gradient, as in the conventional linear model of standard refraction. Pickard and Stetson have demonstrated a strong correlation between changes in average observed fields at 92.8 Mc over a 167-mile path and the surface index, which therefore is readily explained by the bilinear model. Similarly, a model on which the index decreases exponentially from its surface value to unity at great heights will likewise have characteristic values giving attenuation rates depending primarily on the surface index, not its gradient. Since the surface index is easily computed from ordinary meteorological data, renewed hope is raised that simple surface index observations may permit normal seasonal field strength changes to be inferred, at least in the absence of ducts. 1940 observations by Englund, Crawford, and Mumford, and the hypothesis of partial internal reflection of the lobe structure by the troposphere also indicate by an independent argument that surface index of refraction not its gradient, is the important meteorological parameter in normal propagation beyond the horizon.

* Now at Massachusetts Institute of Technology.

FRIDAY AFTERNOON AT 3:20

Pupin 301

(K. G. McKAY presiding)

Photoconductivity; Luminescence; Semiconductors

SC1. A Theory of Photoconductivity of Zinc Oxide.* DONALD A. MELNICK AND DOUGLAS M. WARSCHAUER, *University of Pennsylvania*.—The photoconductivity of compressed and sintered zinc oxide has been found to be described by a bimolecular process of time constant of the order of an hour or more, plus a monomolecular process of time constant of the order of minutes. Shorter processes of very small amplitudes also exist. A model has been devised to explain this phenomenon. The minute process is assumed to be a quasi-thermal readjustment between the excited electrons in the conduction band and a band of levels, which also appear in conductivity measurements, about 0.6 or 0.7 ev below the conduction band. The slower process is assumed to be connected with a bimolecular recombination between electrons in the 0.7 ev band and trapped holes, which can have the time constant observed. Since the equations involved are not linear, an approximate method of solution is employed. The equations are set up in such a form that the two processes are separated, with the bimolecular part appearing as a slowly varying term in the faster process. Parameters calculated from the decay curve are then used to calculate the rise curve. The calculated curves give the expected agreement with the experimental data.

* This work was partly supported by the ONR.

SC2. On the Theory of Noise in Photoconductors. RICHARD L. PETRITY, *Catholic University of America*.—The existing theory of the fluctuation in the conductivity of a photoconductor is extended by considering both the number of conduction electrons, $N(t)$, and the number of quanta in the radiation field, $M(t)$, to be random variables, constituting a two-dimensional Markoffian random process. The model used for the photoconductor consists of two energy levels separated by $E=h\nu$ and we assume $h\nu \gg kT$ and neglect effects of the

Pauli principle. The radiation field exchanges energy of $h\nu$ with both the photoconductor and the surrounding heat bath. The power spectrums $S(N)$ and $S(M)$ have been calculated. The results indicate that $S(N)$ depends principally on the lifetime of an electron in the conduction band. $S(M)$ is dependent upon the relative strength of the coupling of the field with the heat bath and with the photoconductor (strong coupling meaning a large transition probability for absorption of a light quantum). In the limit of very weak coupling with the heat bath $S(M)$ has the same character as $S(N)$. In the limit of strong coupling with the heat bath, $S(M)$ differs from $S(N)$ and depends principally on the coupling between the radiation field and heat bath.

SC3. Electron Mobility in CdS. J. W. MacArthur,* *Rensselaer Polytechnic Institute.*—Photoconduction pulses were obtained in CdS by means of α-particle bombardment, and the rise times of these pulses were measured by means of a shorted coaxial stub technique. From the rise times the corresponding mobility values were calculated. The pulses were found to lie in two rough groups: small or normal pulses, corresponding to quantum efficiencies less than 100 percent, and large or amplified pulses showing evidence of current amplification or "secondary photoemission," i.e., quantum efficiencies greater than 100 percent. The normal pulses had a rise time of the order of 4×10^{-8} sec. in the setup used, i.e., the mobility was about $b_n=300$ cm²/volt sec. The amplified pulses had a rise time nearer to 3×10^{-7} sec under the same conditions, i.e., $b_n=40$ cm²/volt sec.

* Now at Marlboro College, Marlboro, Vermont.

SC4. Impedance Measurements on PbS Photoconductive Cells. E. S. Rittner and F. Grace,* *Philips Laboratories.*—It has been postulated[1] that in PbS photoconductive cells the intercrystalline contacts between n- and p-type material constitute a controlling influence on the dark resistance and photosensitivity. The most direct evidence yet advanced in support of this hypothesis is Chasmar's[2] observation that the parallel resistance decreases with increasing frequency, ostensibly due to capacitative shunting of the barriers. However, according to a theory of Howe[3] even a homogeneous resistor should exhibit a decrease in parallel resistance with frequency because of its distributed capacitance. A re-analysis of Chasmar's data in this light indicates that the Howe effect represents an alternative explanation of his results. Moreover, recent impedance measurements of our own on PbS photoconductive cells definitely favor the Howe explanation. Thus, it appears that the frequency dependence of the resistance can no longer be cited as evidence for the existence of barriers in PbS photoconductive cells. However, these results should not be construed as evidence against an n-p barrier picture, as the dispersion due to capacitative shunting of barriers may occur at high frequencies and hence be masked by the lower frequency dispersion due to distributed capacitance.

* Now at International Business Machines Corporation, Poughkeepsie New York.
[1] Sosnowski, Starkiewicz, and Simpson, Nature 158, 28 (1946); 159, 818 (1947).
[2] R. P. Chasmar, Nature 161, 281 (1948).
[3] G. W. O. Howe, Wireless Engineer 12, 291, 413 (1935); 17, 471 (1940).

SC5. Injected Light Emission from Silicon Carbide Crystals. K. Lehovec, C. A. Accardo, and E. Jamgochian, *Signal Corps Engineering Laboratory.*—Previously[1] experiments were described on light emission from a blue silicon carbide crystal when current passes over a p-n-boundary in forward direction ("injected light emission"). We shall report investigations of injected light emission from other silicon carbide crystals, including pale green ones. Spectral distribution and decay time of the emitted light vary considerably, presumably due to presence of various activator impurities. The colors of light emission mainly noticed at room temperature were green and yellow, respectively. Efficiency of green light emission from a pale green crystal increased strongly with decreasing temperature, according to the equation: $2\times10^{-6}\exp(1370/T)$ light quantum emitted per electron passing through the crystal. Light emission from a dark blue silicon carbide crystal was found at voltages ≥1.8 volts at the p-n-barrier. This voltage is slightly less than the $h\nu/e$-value corresponding to the longest wavelength of the emitted light. The current through the barrier of this crystal seems to consist of two parts: one which is not rectified and does not contribute to light emission (conduction on impurity level?) and another which is rectified and leads to light emission (injection over the barrier).

[1] Lehovec, Accardo, and Jamgochian, Phys. Rev. 83, 603 (1941).

SC6. Color Center Formation in Plastically Deformed KCl. E. Burstein, P. L. Smith, and J. W. Davisson, *Naval Research Laboratory.*—The effect of plastic deformation on color center formation in alkali halides, first investigated by Przibram, is being investigated in further detail. In KCl, as is well known, room temperature x-irradiation of annealed crystals yields the F-band, a weak M-band, and the V-band. Optical bleaching of the F-band increases the M-band and leads to the formation of the R- and N-bands. However, a short subsequent x-irradiation removes the R- and N-bands and returns the crystal essentially to its condition before optical bleaching of the F-band. X-irradiation of plastically deformed crystals, on the other hand, forms the R- and N-bands directly as well as new bands at 3400A and 2400A in the ultraviolet. Further, the extent of color center formation is enhanced in moderately deformed crystals, but is decreased in crystals which have been subjected to a strong plastic deformation, as in the case of KCl powder which is highly compressed to produce a transparent body. This investigation is now being extended to other alkali halides and to color center formation at low temperatures.

SC7. Investigation of the Thermoluminescence of Calcium Fluoride Colored by X-Ray Irradiation. John J. Hill and Jack Aron, *Lewis Laboratory, NACA* (introduced by G. Groetzinger).—The bleaching of CaF_2 crystals colored by irradiation with x-rays was studied by observing the spectral distribution of the radiation emitted during heating as a function of time and temperature. The monochromator of a Beckman spectrophotometer was equipped with an automatic scanning device and used in connection with a 5819 photomultiplier tube as a sensitive recording spectrometer. In the spectral range between 320 and 650 mμ, fifteen bands (A to O) were observed with peaks at 343, 365, 371, 379, 381, 415, 427, 437, 457, 478, 489, 522, 535, 543, and 574 mμ, about half of which have not previously been reported, possibly on account of their weak intensity. Consistent with the view that the radiation detected is connected with a decay process, the bands E, F, and H, which show a rather low intensity initially disappear at a slower rate than bands I, J, and K which show at first a much larger intensity.

SC8. Measurement of Diffusion in Germanium by Means of $p-n$ Junctions. W. C. Dunlap, Jr., *General Electric Research Laboratory.*—As pointed out in a recent letter,[1] the formation of a $p-n$ junction by the diffusion of an impurity into a semiconducting crystal can be used to study diffusion. Etched samples of single-crystal germanium were heated with the impurity, usually present as an evaporated film or as a vapor. Amounts of impurity of the order of a few micrograms were used to minimize alloying effects. Samples were ground off at an angle of 5 or 10° and tested for p- or n-type character using a thermoelectric or rectification probe. Diffusion distances ranging from 0.1 to 20 mil were measured. N-type germanium with $\rho<1$ ohm cm was used for the acceptor elements to minimize heat treatment effects. Preliminary values for the diffusion coefficients of six elements were ob-

tained between 600° and 900°C. These are, for 900°C: donors, antimony 2×10^{-10} cm³/sec, arsenic 2×10^{-10}, phosphorus 8×10^{-11}; acceptors, zinc 1×10^{-11}, gallium 3×10^{-13}, indium 2×20^{-13} cm³/sec. The activation energy for antimony is about 2.5 ev. This quantity appears to increase slightly for the more slowly diffusing elements.

[1] R. N. Hall and W. C. Dunlap, Jr., Phys. Rev. **84**, 467 (1950).

SC9. Comparison of $p-n$ Junctions and Radioactive Tracers for Measurement of Diffusion. D. E. Brown and W. C. Dunlap, Jr., *General Electric Research Laboratory.*—Quantitative comparison has been made of the measurement of diffusion by the $p-n$ junction method and by the method of radioactive tracers, using antimony 124. Samples of p-type germanium were prepared by grinding both sides flat to a high precision using a special grinder. A film of antimony was applied by evaporation, and the metal diffused into the germanium a distance of a few mils. Surface layers were ground off on the same grinder used for preparation of the surfaces, and the activity of the powder ground into sheets of emery paper measured with a scintillation counter. The $p-n$ characteristic of each new surface produced was also checked by a thermoelectric probe. The diffusion coefficient for antimony at 900°C from the tracer method was 2.1×10^{-10} cm²/sec, from the $p-n$ junction method 1.6×10^{-10} cm²/sec. The radioactive tracer method is considerably more time-consuming than the $p-n$ junction method for studying diffusion in germanium, but can, unlike the $p-n$ junction method, be used for elements that can be obtained pure in radioactive form but which do not act as donor or acceptor in germanium.

Friday Evening at 7:00

Grand Ballroom, Hotel New Yorker

(C. C. Lauritsen and M. W. Zemansky presiding)

Banquet of the APS and the AAPT

After-dinner speakers: **O. E. Buckley,** *Bell Telephone Laboratories,* and **R. E. Peierls,** *University of Birmingham.*

Saturday Morning at 10:45

Pupin 428

(Arthur Roberts presiding)

Interactions of Mu-Mesons and Electrons

T1. An Improved Technique for μ-Meson Capture Measurements. J. W. Keuffel, F. B. Harrison, T. N. K. Godfrey, and Geo. T. Reynolds, *Princeton University.**—The apparatus previously described[1] for the measurement of mean lifetimes of negative μ-mesons has been modified by using distributed amplifiers, an improved chronotron timing circuit, and a liquid scintillation counter with better light collection. As a result, the timing uncertainty has been reduced to about 2×10^{-9} sec and the counting rates have been improved so that a 10 percent statistical accuracy can be achieved in about a week's run at sea level. When the decay curves of several elements were examined with improved time resolution, a short-lived component ($\tau\sim4-8$ mμsec) was found, which has been identified by a series of auxiliary experiments as caused by neutrons from proton-induced stars; the delays are produced by the time of flight of neutrons of a few mev as they diffuse out of the large (50–100 kg) target or the Pb above it. Errors from this effect, which were present in our earlier results, can be eliminated by rejecting counts delayed less than 30 mμsec, and by using a minimum of Pb in the counter telescope.

* Supported by the joint program of the ONR and AEC.
[1] Harrison, Keuffel, and Reynolds, Phys. Rev. **83**, 680 (1951).

T2. Capture Probabilities of μ-Mesons in Heavy Elements. F. B. Harrison, J. W. Keuffel, T. N. K. Godfrey, and Geo. T. Reynolds, *Princeton University.**—Our latest experimental results for the mean life of negative μ-mesons in heavy elements are: Sb, 80±9 mμsec; Hg, 58±4.7; Pb, 72±5.2; Bi, 63±8. The Wheeler theory, with $Z_0=10.3$ (based on the results for the light elements), gives about 25 mμsec for Hg, Pb, and Bi—a discrepancy of about a factor of three in the case of Pb. Kennedy's modification of the Wheeler theory (see following abstract) predicts 6.1 for the ratio of capture probabilities in Pb and Ca. This gives a mean life ratio of 5.3; the best experimental value is 4.1. The difference between the figures for Hg and Pb, which is thought to be statistically significant, is also qualitatively predicted by Kennedy. The mean life measurement previously reported for μ^--mesons in Sb[1] was affected by a systematic error because of the "short component" discussed in the preceding abstract. We estimate that the Cu value of 122±14 mμsec was not much affected.

* Supported by the joint program of the ONR and AEC.
[1] Harrison, Keuffel, and Reynolds, Phys. Rev. **83**, 680 (1951).

T3. A Theory of μ-Meson Capture. J. M. Kennedy, *Princeton University.**—The rate of absorption of negative μ-mesons in lead and in calcium has been calculated, assuming that the underlying reaction is of the charge exchange type described by Wheeler.[1] A shell model of the nucleus was used in making explicit calculations of the various nuclear matrix elements. The ratio of the absorption rate in lead to that in calcium is 6.1, in contrast to the value 14.3 predicted by Wheeler's theory. Another consequence of the nuclear model is that the absorption rate in mercury should be appreciably larger than that in lead, in spite of its smaller Z. These results are in fair agreement with the measurements of Harrison, Keuffel, Godfrey, and Reynolds, given in the preceding abstract. The coupling constant for the charge exchange reaction is $g\sim3\times10^{-49}$ erg cm³. This is approximately the same as the value of the β-decay coupling constant obtained from the decay of the neutron.

* Supported by the joint program of the ONR and AEC.
[1] J. A. Wheeler, Revs. Modern Phys. **21**, 133 (1949).

T4. An Experiment to Detect Pair-Production by Electrons.* N. S. SHIREN† AND R. F. POST,‡ *Stanford University.*—25-Mev electrons from a linear electron accelerator have been used in an experiment to detect direct pair production by electrons. Care was taken to obtain a beam uncontaminated by x-rays. The targets used were thin enough to make indirect effects negligible. The experimental method consisted of the identification of 511-kev annihilation radiation produced by positrons in a Be stopper placed at various angles with respect to the beam incident on the target. Identification was accomplished by using a "positron counter" described elsewhere,[1] which used NaI scintillation counters and operated by establishing the simultaneity, 180° angular correlation, and energy of the radiation from the stopper. Using a 0.006-inch Al target, measurements at 25° and 35° indicated the presence of positrons, but in an amount not statistically significant compared to background. However, from these data a statistically significant limit on the cross section may be deduced. Depending on the angular distribution assumed for the positrons, an upper limit is found for the total cross section which is equal to or less than theory.[2]

* Work supported by the ONR.
† Now at Columbia University, Hudson Laboratories, Dobbs Ferry, New York.
‡ Now at the University of California, Berkeley, California.
[1] R. F. Post, Phys. Rev. **83**, 886 (1951).
[2] H. J. Bhabha, Proc. Roy. Soc. (London) **A152**, 559 (1935).

T5. Energy Loss of 15-Mev Electrons.* A. O. HANSON, E. L. GOLDWASSER, AND F. E. MILLS, *University of Illinois.*—A 15.7-Mev electron beam from the University of Illinois 22-Mev betatron was incident upon absorbers of Ve, C, Al, Cu, Ag, and Au, each with a thickness of about 1 g/cm². The energy of the electrons after passing through any chosen foil was analyzed by use of a 70° magnetic spectrometer. The resolution of the entire apparatus was limited by the initial beam width and by the regulation of the magnetic field, to 20 kev for 15-Mev electrons. The observed distributions of energy loss for light elements was found to be in good agreement with the calculations of Landau[1] corrected for polarization effects by use of Fermi's expression for extreme relativistic velocities.[2] The most probable energy loss in kev may then be written as $(\Delta E)_\rho = 153.7D(Z/A)[19.43+\ln(D/\rho)]$, where D is the surface density of the foil in g/cm² and ρ is the volume density of the material in g/cm³. The interpretation of the energy losses and struggling in the case of the heavier elements is much more complicated.

* Work supported in part by ONR.
[1] L. Landau, J. Phys. (U.S.S.R.) **8**, 201 (1944).
[2] E. Fermi, Phys. Rev. **57**, 485 (1940).

T6. Energy Loss of 2-Mev Electrons.* F. E. JABLONSKI,† B. WALDMAN, AND W. C. MILLER, *University of Notre Dame.*—The energy distribution of electrons passing through thin aluminum foils has been studied. The source of the 2-Mev electrons was the Notre Dame electrostatic generator. The energy of the incident electrons was constant to within 5 kev. A 90-degree magnetic spectrometer was used to analyze the transmitted beam. The resolution of the spectrometer was approximately 20 kev. Aluminum foils ranging in thickness from 3 to 180 mg/cm² were studied. The most probable energy loss is slightly less than that predicted by Landau.

* This work has been partially supported by the joint program of the ONR and AEC.
† Now at Naval Research Laboratory, Washington, D. C.

T7. Lower Electron Energy Losses in Zinc Oxide. OLIVE G. ENGEL, *National Bureau of Standards.*—A first approximation to the solution of the problem of obtaining cross sections for the energy losses of 30,000-volt electrons on passing through a thin edge of a zinc oxide crystal is made by assuming that scattering takes place from single ions in the lattice. The values of the expected losses are taken from spectroscopic data with the exception of that resulting from the transition of an electron from the oxide ion to the zinc ion. This loss is approximated by a method similar to that used by Seitz, but polarization energy and repulsive potential neglected by Seitz are taken into account. Cross sections for the transitions are found for a small scattering angle. The expression employed is derived by using the scattered amplitude found by Massey for collision of an electron with an atom.

SATURDAY MORNING AT 9:30

Pupin 301

(J. H. VAN VLECK presiding)

Invited Paper

U1. The Determination of Nuclear Masses from Microwave Spectra. STANLEY GESCHWIND, *Columbia University.* (30 min.)

Nuclear Masses; Magnetic Resonance; Radioactive Nuclei

U2. Masses of Pb^{208}, Th^{232}, U^{234}, and U^{238}.* G. S. STANFORD, *Wesleyan University*, H. E. DUCKWORTH, *Wesleyan University and McMaster University*, B. G. HOGG, AND J. S. GEIGER, *McMaster University.*—The following packing fraction differences (all $\times 10^4$) have recently been determined or redetermined, $Pb^{207}-Ba^{138}$: $\Delta f = 5.62 \pm 0.05$, $Th^{230}-Sn^{116}$: $\Delta f = 10.058 \pm 0.03$, $Sn^{116}-Ni^{58}$: $\Delta f = 2.647 \pm 0.015$, $Ni^{58}-Si^{29}$: $\Delta f = 3.07 \pm 0.02$, $U^{234}-Sn^{117}$: $\Delta f = 10.008 \pm 0.025$, $Sn^{118}-Co^{59}$: $\Delta f = 2.99 \pm 0.02$, $U^{238}-Sn^{119}$: $\Delta f = 10.187 \pm 0.025$. Using $H^1 = 1.008142 \pm 3$, $C^{12} = 12.003804 \pm 17$, $Si^{28} = 27.98579 \pm 4$ amu and appropriate transmutation data, one deduces from these and other mass differences previously reported from our laboratory, that $Pb^{208} = 208.0434 \pm 12$ amu, $Th^{232} = 232.1092 \pm 10$ amu, $U^{234} = 234.1133 \pm 11$ amu, and $U^{238} = 238.1234 \pm 10$ amu. Since these masses are related by more or less known disintegration data, they can be considered as a group and the individual values adjusted by imposing upon them the conditions[1] that $U^{238}-Pb^{208} = 30.0834 \pm 15$ amu, $U^{238}-Th^{232} = 6.0148 \pm 6$ amu and $U^{238}-U^{234} = 4.0112 \pm 2$ amu. The adjusted values so obtained are $Pb^{208} = 208.0424$ amu, $Th^{232} = 232.1093$ amu, $U^{234} = 234.1130$ amu, and $U^{238} = 238.1242$ amu, the probable errors being about 1 mMu. Typical mass spectra will be shown and comments will be made regarding the agreement between these and other existing mass data.

* Supported by the AEC, the Research Corporation, and the National Research Council of Canada.
[1] G. T. Seaborg, private communication.

U3. Integral and Rational Numbers in the Nuclear Domain. ENOS E. WITMER, *University of Pennsylvania.*—Some years ago the writer proposed the idea that hc/e^2 is exactly 861, which is $41\times42/2$. From the best and most recent value[1] of α^{-1}, hc/e^2 is slightly less than 861.023, which supports this idea quite well. The nuclear magnetic moments μ appear to be given by the equation $\mu = Ck$, where C is a constant and k is an integer or rational number with a small denominator. k is 1876 for the proton. There is much accurate data to support this statement. The extremely accurate ratios of the nuclear magnetic moments of certain isotopes make possible a very drastic test of this idea. Furthermore, it frequently happens that the k differences of isotopes are integers even when the k values are not integral but only rational. Also the masses of nuclei not subject to beta decay or K-capture appear to be an integral number of prouts. The prout is defined to be one-eleventh of the rest mass of the negative electron. Many of the nuclei subject to beta-decay or K-capture follow the integral rule. There are considerable data to support this.

[1] N. M. Kroll and F. Pollock, Phys. Rev. **84**, 594 (1951).

U4. Nuclear Magnetic Moment of Indium^{115}. YU TING, F. K. BIARD, AND DUDLEY WILLIAMS, *The Ohio State University.*—A nuclear magnetic resonance absorption line attributed to In^{115} has been observed in a saturated solution of indium nitrate in 30 percent nitric acid. Comparison of this line with the Sc^{45} line observed in $ScCl_3$ in the same magnetic field leads to the frequency ratio $\nu_{In}/\nu_{Sc} = 0.902292 \pm 0.000010$, where the indicated uncertainty is a measure of the internal consistency of the data, and the possibility of systematic errors as large as ± 0.000050 cannot be completely excluded. The observed ratio ν_{In}/ν_{Sc} used in conjunction with Lindstrom's value $\nu_{Sc}/\nu_{proton} = 0.242939 \pm 0.000003$ and the recent value $\mu_{proton} = 2.79268 \pm 0.00006$ nm leads to a value $\mu_{In} = 5.50945 \pm 0.00011$ nm when nuclear spin $I = 9/2$ is assumed. This preliminary value for the In^{115} magnetic moment has not been corrected for diamagnetic effects of the extra-nuclear electrons nor for the slight paramagnetic effects of a magnetic catalyst ($Mn(NO_3)_2$) used in the sample. Further work is being done on samples not containing a catalyst. The value obtained in the preliminary work is higher than the value obtained in molecular beam experiments.

U5. The Nuclear Gyromagnetic Ratio of Vanadium 50. H. E. WALCHLI, W. E. LEYSHON, AND F. M. SCHEITLIN, *Oak Ridge National Laboratory.**—The nuclear gyromagnetic ratio of vanadium 50 has been determined in a nuclear induction spectrometer. An electronically regulated electromagnet maintained a field homogeneous to 0.1 gauss over the sample volume. Frequency measurements were made using a BC-221 frequency meter calibrated with an external 100 kc crystal controlled oscillator and checked against WWV. The sample consisted of 271 mg of vanadium as $VOCl_3$ of which 10 percent was V^{50}. Measurements at three values of magnetic field gave the following preliminary ratio:

$$\nu(V^{50})/\nu(D^2) = +0.649530 \pm 0.00007.$$

The sign of the moment was determined to be positive by direct comparison with Rb^{85} and Cl^{35}. Using a value of 2.7926 nm[1] for the proton moment and Levinthal's deuteron-to-proton ratio,[2] the nuclear gyromagnetic ratio for vanadium 50 becomes +0.55707. New frequency ratios, V^{50}/Rb^{85}; V^{50}/Cl^{35}; Rb^{85}/Cl^{35}; Rb^{85}/H^1; and Cl^{35}/H^1 will be reported.

* This paper is based on work performed for the AEC by Carbide and Carbon Chemicals Company, a Division of Union Carbide and Carbon Corporation, Oak Ridge, Tennessee.

[1] Sommer, Thomas, and Hipple, Phys. Rev. **80**, 487 (1950).
[2] E. C. Levinthal, Phys. Rev. **78**, 204 (1950).

U6. High Frequency Lines in the hfs Spectrum of Cesium. J. E. SHERWOOD, HAROLD LYONS, R. H. MCCRACKEN, AND P. KUSCH, *National Bureau of Standards.*—A brief account is given of the atomic beam magnetic resonance apparatus which is being developed at the National Bureau of Standards as a possible time standard in the microwave region.[1] The beam gear is essentially a Rabi[2] type apparatus, except for details. Permanent magnets are used for deflection together with a weak C field of the order of a few oersteds. A quartz oscillator-multiplier system is used as a stable exciting source and for precise frequency measurement. At present, a short path length of approximately one cm is used giving the expected Q of the order of 300,000 at 9192 Mc. Results are confined to experiments with cesium, for which the variation with magnetic field of some of the high frequency lines in the ground state hfs will be given. A new value is obtained for ν_0, the line frequency at zero magnetic field. This directly measured value lies between previously announced[3,4] values and outside their limits of error.

[1] P. Kusch, Phys. Rev. **76**, 161 (1949).
[2] I. M. B. Kellogg and S. Millman, Revs. Modern Phys. **18**, 323 (1946).
[3] P. Kusch and H. Taub, Phys. Rev. **75**, 1477 (1949).
[4] Roberts, Beers, and Hill, Technical Report No. 120, June 6, 1949. Research Lab. of Electronics, M.I.T.; Phys. Rev. **70**, 112 (1946).

U7. Magnetic Moment of Helium in the Metastable $^3S_1$ State by Atomic Beam Method.* G. L. TUCKER, V. W. HUGHES, E. H. RHODERICK, AND G. WEINREICH,† *Columbia University.*—A comparison has been made of the gyromagnetic ratio of the two-electron system in helium in the metastable $^3S_1$ state with that of the one-electron system in the ground state of hydrogen. The atomic beam magnetic resonance method was used and the atoms were made to traverse almost identical paths in the magnetic field.[1] With fields between 400 and 500 gauss the lines $m_J = \pm1 \rightarrow 0$ of helium and F, $m_F = 1$, $0 \leftrightarrow 1$, -1 of hydrogen were measured alternately. Using the Breit-Rabi formula for hydrogen and recent values[2] of g_I and $\Delta\nu$ we find $g_J(\mathrm{He}, {}^3S_1)/g_J(\mathrm{H}, {}^2S_\frac{1}{2}) = 1.000001 \pm 0.000025$. Using $g_J(\mathrm{H}, {}^2S_\frac{1}{2})^3 = 2(1.0011275 \pm 0.000013)$ gives

$$g_J(\mathrm{He}, {}^3S_1) = 2(1.001129 \pm 0.000028).$$

Precision was limited principally by field inhomogeneities and by field drift during approximately 15-minute periods between gases. Further measurements are in progress.

* Supported in part by ONR contract.
† AEC predoctoral fellow.
[1] For production and detection of a beam of metastable helium atoms see V. Hughes and G. Tucker, Phys. Rev. **82**, 322 (1951).
[2] H. Taub and P. Kusch, Phys. Rev. **75**, 1481 (1949); A. G. Prodell and P. Kusch, Phys. Rev. **79**, 1009 (1950). Uncertainties in these numbers do not limit our precision.
[3] Koenig, Prodell, and Kusch, Phys. Rev. **83**, 687 (1951).

U8. Measurement of Short β-Decay Lifetimes. R. N. THORN, R. W. WANIEK AND R. B. HOLT, *Harvard University.*—A method for measuring the lifetimes of isotopes extremely unstable to β-decay is described. These isotopes are produced in the bombardment of light elements by the internal proton beam of the Harvard fm cyclotron. The decay particles are detected by a crystal, Lucite probe, and photomultiplier arrangement. The target is located about four inches directly below the detecting crystal. Because of the focusing action of the magnetic field, most of the decay particles enter a cylindrical shaped anthracene crystal lodged in a slotted hole at the end of the Lucite rod. The Lucite pipe is enclosed in a vacuum-tight tube and transmits the light signal to a photomultiplier outside the cyclotron tank. The signal is fed from the photomultiplier to a cathode follower and from there to a linear amplifier in the control room. The pulses from the discriminator output go into an integrating circuit; the resulting current is registered on linear roll paper by a fast recorder. All circuits are left on continuously. The target is irradiated, the cyclotron is turned off, and the excitation is observed. By this method, lifetimes shorter than one-tenth of a second are measured.

U9. Preliminary Results from the Measurement of Short β-Decay Lifetimes. R. W. WANIEK, R. N. THORN AND R. B. HOLT.—With the arrangement described in the previous communication, measurements were taken by using a carbon plate as a target. Runs were made at 12 different proton energies chosen in the range between 20 and 110 Mev by varying the distance of the target from the center of the cyclotron tank. Due to the occurrence of simple and spallation reactions, a variety of modes of disintegration was observed. By pulse-height analysis and varying the time of irradiation, additional discrimination was obtained. Previously known lifetimes as well as several new ones appeared with great consistency over various bombarding energies. Work is underway to correlate these results with the data obtained using other light elements as targets. preliminary results will be given at the meeting.

U10. Gamma-Radiation of C^{10}.* R. SHERR AND J. GERHART, *Princeton University.*—The gamma-ray spectrum of C^{10} produced by the $B^{10}(p, n)$ reaction has been examined with a NaI scintillation spectrometer. In addition to 511 kev annihilation radiation, gamma-rays of energy 720±15 kev and 1045±20 kev were observed. The photopeak of the 1045-kev radiation is superimposed on a continuous distribution of hard radiation which was found also in C^{11}, Ne^{19}, and A^{38}. Absence of a significant Z dependence on absorbing the positrons in different materials, and the fact that the hardness increases with positron energy suggest that the continuous radiation is to be attributed to annihilation of positrons in motion. The intensities of the 720 kev and 1045 kev lines correspond to (1.0±0.1) and (0.021±0.005) γ-rays per positron of C^{10}. From the known levels of B^{10}, these γ-rays correspond, respectively, to β^+ transitions to the first (713 kev) and second (1740 kev) excited states, the latter reaching the ground state by cascade through the former. The ratio of the intensities expected on the basis of the f-values for allowed transitions is 0.07. The possibility that the existence of the 1045-kev line may be evidence for an allowed $0 \rightarrow 0$ β^+ transition will be discussed.

* Supported by the AEC and Higgins Scientific Trust Fund.

U11. The Nuclear Spectrum of Ge^{77}. ALAN B. SMITH AND ALLAN C. G. MITCHELL, *Indiana University.**—The disintegration of Ge^{77} has been studied with the help of a magnetic lens spectrometer, coincidence counters, and scintillation counters. The beta-ray spectrum of Ge^{77} (12 hr) consists of three groups whose end-point energies are 2.196 Mev, 1.379 Mev, and 0.710 Mev. In addition there are 13 gamma-rays appearing in the product nucleus As^{77}, some of which are internally converted. By coincidence counting techniques it has been shown that the beta-ray of energy 2.196 does not go to the ground state but to an excited state 0.264 Mev above the ground state. The isomeric transition from the 59-sec to the 12-hr states of Ge^{77} has been shown to be accompanied by a gamma-ray of 0.380-Mev energy in competition with the well-known beta-ray transition to the ground state of As^{77}. A disintegration scheme will be proposed.

* Supported by the joint program of the ONR and AEC.

U12. Angular Correlation and Intensity of Inner Bremsstrahlung from P^{32} and RaE. T. B. NOVEY, *Argonne National Laboratory.*—The angular correlation between the beta-particles and co-emitted inner bremsstrahlung has been measured in RaE. As in the similar experiments with P^{32}, the agreement of the correlation with that predicted by the theory of Knipp and Uhlenbeck and Bloch is excellent. Absolute gamma- per beta-intensity measurements have also been made of the continuous gamma-distributions in P^{32} and RaE. The radiation was detected using a NaI(Tl) scintillation-counter arrangement of the type described by Madansky and Rasetti. Problems of escape peak intensities and contributions from Compton distributions at present limit the accuracy of the absolute intensities. Theoretical intensity distributions were calculated using the experimentally obtained beta ray spectra of P^{32} and RaE. The agreement with theory is satisfactory for P^{32}, but is not as good as reported by Rasetti and Madansky for RaE. The theoretical intensity for RaE is about one-third of that for P^{32} due to the abundance of lower energy beta-particles from RaE but the experimental gamma-intensity in RaE is about equal to that in P^{32}. A small amount of $K-x$ radiations was found superimposed upon the RaE gamma spectrum. The x-ray intensity was only a few percent of the continuous gamma-intensity. This is in disagreement with Bruner's value of four conversion electrons per (theoretical) gamma unless the electron emission occurs predominantly from outer shells.

SATURDAY MORNING AT 9:30

Schermerhorn 501

(A. PAIS presiding)

Theoretical Physics, II

V1. One-Three Gamma-Gamma Angular Correlation. G. B. ARFKEN, L. C. BIEDENHARN, AND M. E. ROSE, *Oak Ridge National Laboratory.*—In a nuclear cascade involving three or more gamma-rays it is both desirable and feasible to measure the angular correlation of non-adjacent gammas either to confirm the results of correlating consecutive gammas or to resolve possible ambiguities. The angular correlation functions[1] for the observation of the first and third gammas in a triple cascade have been calculated with the use of Racah coefficients for cases of physical interest.[2] Consideration was limited to dipole and quadrupole radiation. While the anisotropies tend to be somewhat less than those from the correlation of consecutive gamma-rays, they are easily detectable by present experimental techniques. In at least two pairs of hypothetical decay schemes (J values 0, 1, 1, 2 and 0, 2, 1, 1; ½, ½, ½, 5/2 and ½, 5/2, ½, ½) correlation of consecutive gammas can never distinguish between the two possibilities. Correlation of the first and third gammas removes the ambiguity.

[1] Biedenharn, Arfken, and Rose, Phys. Rev. **83**, 586 (1951).
[2] Arfken, Biedenharn, and Rose, Oak Ridge National Laboratory Report No. 1103.

V2. Angular Correlation of the Radiations from Deuteron Stripping Reactions. L. C. BIEDENHARN,* KEITH BOYER,† AND R. A. CHARPIE,* *O.R.N.L.*—The angular distribution from deuteron stripping reactions[1] has proved useful in determining the spin (J) and parity of nuclei formed in the reaction. When the orbital momentum transfer (l_n) is nonzero, however, J is not uniquely determined. If the nucleus emits subsequent radiation (say, a gamma), this radiation should be correlated with the deuteron beam direction. In practice, one would measure coincidences of the gamma-ray and the stripped

protons (say) of measured energy in order to identify the emitting nuclear state.[2] By observing this correlation further information on J might be obtained. The most informative case of this correlation is also the simplest, namely where the target nucleus has zero spin ($j_t=0$), since this eliminates both the channel spin ambiguity and restricts us to a single ln. For this case, we find the rather simple answer that, under the same assumptions as in reference (1), the gamma is correlated with the direction of the (cms) recoil momentum, $\mathbf{k}_d=-\mathbf{k}_p$, precisely as if the residual nucleus were formed by the resonance capture of the neutron from a plane wave directed along this axis, the angular distribution of the proton entering as a multiplicative factor only. The case $j_t\neq 0$ will be discussed.

* Oak Ridge Laboratory.
† Los Alamos Scientific Laboratory.
[1] S. T. Butler, Proc. Roy. Soc. (London), **A208**, 559 (1951).
[2] Experiments of this type, $(d;\ p,\ \gamma)$, were recently reported by G. C. Phillips, N. P. Heydenberg, and D. B. Cowie (Abstract D7, Bull. Am. Phys. Soc. No. 7, 8 (1951)). Isotropy was found in the cases observed, however.

V3. On the Interaction Term in β-Decay Theory. R. H. Good, Jr., *University of California, Berkeley.*—The interaction terms ordinarily discussed are $J_i=-(\psi_P\gamma^4\Omega_i\psi_N)(\psi_e\gamma^4\Omega_i\psi_\nu)$ where i, ranging from 1 to 5, indicates the scalar, vector, tensor, axial vector, or pseudoscalar interaction.[1] Introducing the charge-conjugate descriptions of the proton and electron so as to treat all the particles equivalently, one may also write $J_i=-(\phi_P C\gamma^4\Omega_i\psi_N)(\phi_e C\gamma^4\Omega_i\psi_\nu)$. Since $C\gamma^4\Omega_i C^{-1}$ is the transpose of $\gamma^4\Omega_i$ for the vector and tensor, and the negative of the transpose otherwise, it follows that any linear combination of the vector and tensor interactions is symmetric with respect to an interchange of either the heavy particles or the light particles, and that any linear combination of the other three is correspondingly antisymmetric. The interactions J_i', formed from J_i by interchanging ψ_N and ψ_P, may be expressed linearly in terms of the J_i so that $J_i'=\sum A_{ij}J_j$.[1] By considering the eigenvalue problem for the transpose of this A matrix, one finds that the two-parameter interaction, $(12a+3b)J_1+3aJ_2+(2a+b)J_3+3aJ_4+3bJ_5$, is symmetric with respect to an interchange of either the charged or the uncharged particles and that the three-parameter interaction, $(-2c-e)J_1+(c-d+e)J_2+cJ_3+dJ_4+eJ_5$, is correspondingly antisymmetric. From these two symmetry arguments one may deduce the Wigner-Critchfield interaction.

[1] M. Fierz, Z. Physik **104**, 553 (1937).

V4. On Darling's Theory of Fundamental Length. P. R. Zilsel, *University of Connecticut.*—The infinite-order partial differential equation which in Darling's theory[1] replaces the Dirac-Kemmer equation for a free particle can be transformed into the integral equation,

$$\int[\gamma_\nu(x_\nu-x_\nu')+\omega^2 k]\epsilon(x-x')\psi(x')d^4x'=0, \qquad (1)$$

where $\epsilon(x)=0$ for $x_0^2-r^2\leqq 0$, and

$$\epsilon(x)=(x_0/|x_0|)(16\pi^2\omega^2)^{-1}\delta[2\omega-(x_0^2-r^2)^{\frac{1}{2}}], \quad x_0^2-r^2>0. \qquad (2)$$

This form exhibits clearly the role of the time-like fundamental displacement, ω. It also indicates a connection between Darling's theory and Born's reciprocity principle.[2]

[1] B. T. Darling, Phys. Rev. **80**, 460 (1950).
[2] M. Born, Revs. Modern Phys. **21**, 463 (1949).

V5. Information, Thermodynamics, and Life. Jerome Rothstein, *Signal Corps Engineering Laboratories.*—Complex heat engines with material and energetic intake, and control, sensing, and motor devices forming mechanical analogs of living things, are described in principle. Essential to operation is selection of a subset from the manifold of possible behaviors, i.e., acquisition of information (measurement) and response thereto by virtue of information (constraints) encoded in structural organization. Conventional engines parallel vital chemico-mechanical energy conversion; these parallel reproduction (conventional and novel types), heredity, self-repair, dietary selectivity, food storage, symbiosis, parasitism, disease, poisoning, irritability, attack and defense, possibly learning, and other "vital" or "mental" functions. Cascading structural complexity enhances behavioral complexity, including aggregation into analogs of metazoa or societies. For a finite number of unit designs (cells), aggregates may be limited by internal capacity to transport matter, energy, and information. Adaptability and recuperation apparently depend on internal redundancy. The second law of thermodynamics is not violated notwithstanding "disentropic" behavior; negative entropy of information generating it is balanced by entropy increase accompanying measurement when the information is acquired.

[1] J. Rothstein, Science **114**, 171 (1951).

V6. Theory of Discrimination and Reliability in Crowded Situations. Arthur E. Ruark, *The Johns Hopkins University.*—(1) Garner and Hake, among others, have studied the behavior of observers presented with any one of a number of signals (various loudnesses, in their case), under conditions such that it becomes difficult to distinguish a signal from its neighbors. An "absolute" judgment is involved. Curves can be drawn showing how the frequency of mistakes depends on the spacing between a signal and its neighbors. (Other significant quantities are also measured.) The problem arises, how shall the total body of desired signals, n in number, be spaced along the total range of loudnesses in order to optimize some desired quantity, such as the information rate, or the average reliability per signal? Average reliability is here defined as the sum of (Chance a signal occurs) times (Reliability when that signal occurs). This paper solves the problem, for the case of reliability (for the sake of simplicity), but the method is quite general. (2) Extension to the continuous case yields an equation for designing the actuating mechanism of any scale-instrument, such that the reliability of the readings will be a maximum, when the probability distribution of the input-variable is known.

V7. Super-Potentials in Covariant Theories.* Ralph Schiller and Joshua Goldberg, *Syracuse University.*—In the general theory of relativity, the existence of Bianchi identities permits one to formulate the so-called "strong" conservation laws. These have the form of four-dimensional divergences of the "stress" tensor which vanish identically, even when the field equations are not satisfied. From this relation one can infer that it must be possible to write the "stress tensor" as the divergence of a skew-symmetric form. The Bianchi identities follow from the fact that the field equations are derivable from a variational principle and the general covariance of these equations. The "strong laws" must be similarly related to these properties of the theory. Through explicit use of the infinitesimal transformation law of the Lagrangian density, it has been possible to derive a general expression for these skew-symmetric forms, and for a wider class of theories than the general theory of relativity. We have only assumed that the field equations are derivable from a variational principle. The form of the infinitesimal transformation law for the field variables is general enough to include tensors and spinors.

* Supported by the ONR.

V8. Equations of Motion in a Covariant Field Theory.* Joshua Goldberg and Ralph Schiller, *Syracuse University.*—The only theory known today in which the equations of motion are determined by the field equations is the general theory of relativity.[1] This interrelationship results from the covariance of the theory and more particularly from the so-called Bianchi identities and the nonlinearity of the field

equations, leading to "strong" conservation laws. Because of these strong conservation laws, there exist certain surface integrals, without the need of introducing coordinate conditions or a special power expansion in c^{-1}, which vanish if the field equations are satisfied at least on the surface of integration, regardless of the shape of that surface. In the case of the gravitational theory, plus the Einstein-Infeld expansion, our surface integrals go over into theirs. This result was obtained with the help of the super-potentials discussed in the preceding abstract.

* Supported by the ONR.
[1] A. Einstein and L. Infeld, Can. J. Math. 1, 209 (1949).

V9. Time-Dependent Canonical Transformations.* PETER G. BERGMANN AND RALPH SCHILLER, *Syracuse University.*—A re-examination of the representation of time-dependent coordinate and gauge transformations shows that the corresponding canonical transformations can be set up most conveniently and without logical difficulties in a "parameter" formalism, in which the fourth coordinate appears as a quasi-dynamical variable. Such transformations are meaningful only in a phase space or Hilbert space (in quantum theories) in which the Hamiltonian constraint is satisfied along with any other constraints. We have shown that the so-called secondary constraints[1] (which arise when the commutators or Poisson brackets are formed between the primary constraints and the Hamiltonian) are closely related to the energy-momentum density of such a theory. This whole treatment permits one to tie a consistently four-dimensional representation of a covariant theory together with the canonical approach, which favors one time-like direction.

* Supported by the ONR.
[1] J. L. Anderson and P. G. Bergmann, Phys. Rev. 83, 1018–1025 (1951).

V10. General Relativity and Angular Momentum.* ROBB THOMSON AND PETER G. BERGMANN, *Syracuse University.*—The conservation law of angular momentum, both in non-relativistic and in Lorentz-covariant theories, is based on the invariance of the theory with respect to homogeneous orthogonal (or Lorentz) transformations. In general relativity, such a transformation is meaningless, and what is left of the law of angular momentum must be contained explicitly in the powerful law of conservation of linear momentum density of general relativity. If spinors are introduced into general relativity, we have again the possibility of spin transformations and with them local Lorentz (Bein-) transformations. Examination shows that this transformation group does not lead to a true conservation law. However, the rate of change of the spin angular momentum is determined by an expression which, though not itself a true time derivative, is closely related to what ordinarily would be interpreted as the rate of change of the orbital angular momentum.

* Supported by the ONR.

V11. Statistical Mechanics in General Relativity. J. W. WEINBERG, *University of Minnesota,* AND G. E. TAUBER, *McMaster University, Ontario.*—Relativistic statistical mechanics has been found for particles interacting through gravitation. Canonical momenta p_μ are defined together with an invariant Hamiltonian $m(x, p) = [g^{\mu\nu} p_\mu p_\nu]^{\frac{1}{2}}$ by means of $dx^\mu/ds = (\partial m/\partial p_\mu)_x$. From $dp_\mu/ds = -(\partial m/\partial x^\mu)_p$ and its consequence $dm/ds = 0$, one derives Einstein's geodesic law and the identity of m and the constant rest mass along any trajectory. The space of x^μ, p_ν, a sequence of ordinary phase spaces for each time and mass, admits an invariant n that reduces essentially to the usual density-in-phase near any point and in locally co-moving coordinates. The differential conservation law for the number of systems is expressed by Liouville's theorem $dn/ds = 0$, as a consequence of which the energy density $T_{\mu\nu}(g)^{\frac{1}{2}}$ defined by the integral over p_μ-space of $np_\mu p_\nu$ satisfies the covariant conservation law. This result for $T_{\mu\nu}$ includes a representation of *all* equations of state relating invariant pressure p_0 to density ρ_{00}, that comply with relativistic restrictions on the motion of particles. On comparison, many equations of state proposed in astrophysics prove unacceptable. As a simple example, the case of the spherical cluster possesses in addition to the known $3p_0 \leqq \rho_{00}$, the new relativistic restriction, $4(dp_0/d\rho_{00}) \leqq 1 + (p_0/\rho_{00})$.

V12. Thermal Equilibrium in General Relativity. G. E. TAUBER, *McMaster University, Ontario,* AND J. W. WEINBERG, *University of Minnesota.*—Binary collisions described by an invariant cross section can be introduced into the formalism of the preceding abstract to establish the H-theorem, $\partial S^\mu(-g)^{\frac{1}{2}}/\partial x^\mu \geq 0$ for the entropy S^μ defined as the integral over p_μ-space of $np^\mu \ln(1/n)$. Thermal equilibrium requires detailed balancing which results in $n\alpha \exp(-mq^0 - p_\mu q^\mu)$ for classical statistics. $(q^\mu q_\mu)^{-\frac{1}{2}}$ is essentially the temperature field, while $q^\mu(q^\nu q_\nu)^{-\frac{1}{2}}$ defines a velocity field for the mean motion at every point. Liouville's theorem then requires $q_{\mu,\nu} + q_{\nu,\mu} = 0$. This theory reduces to Tolman's relativistic generalization of thermodynamics in those special cases where Tolman's work is applicable. For example, the limitations on $q^\mu(x)$ reduce to the rule that the temperature $\alpha(g_{44})^{-\frac{1}{2}}$ in the static, spherical cluster; and in nonrelativistic approximation they limit the mean velocity field to that of a rigid motion. For the axially symmetric cluster they describe the generalization of rigid rotation in a simple way permitting the use of integrable co-rotating coordinates for the interior. The field equations then reduce to those of the static case with the limitation that pressure and density depend on g_{44} alone and with the addition of a Coriolis field mixing differentials of angle and time in ds^2. These conclusions remain essentially unaltered in quantum statistics.

V13. Markoff Random Processes and the Statistical Mechanics of Time-Dependent Phenomena. MELVILLE S. GREEN, *University of Maryland.*—An attempt is made to develop the principles of a statistical mechanics of time dependent phenomena. It is asserted that the proper objects of study of such a theory are the grossly observable quantities considered as stationary random processes. The hypothesis suggested by Peirls and Richardson that these random processes are Markoffian is argued for. The Fokker Planck equation for these processes is derived by a generalization of a method of Kirkwood for Brownian motion. If $a_i i = 1 \cdots s$ are the gross variables, $W_0(a_1 \cdots a_s)$, their equilibrium distribution, $W(a_1 \cdots a_s, t)$, their distribution at time t, this equation is

$$\frac{\partial W}{\partial t} = \sum_{ij} \frac{\partial}{\partial a_i}\left\{ -\left[v_i + \xi_{ij}\frac{\partial \log W_0}{\partial a_j} + \frac{\partial}{\partial a_j}\xi_{ij}\right] W + \frac{\partial}{\partial a_j}\xi_{ij} W \right\}.$$

The quantities v_i are the conditional mean rates of change of the a_i for fixed values of the a_i. The ξ_{ij} are related to the conditional auto-correlation of the rates. Reciprocal relations are derived for the ξ_{ij} which are generalizations of the Onsager reciprocal relations. An entropy of the distribution W is defined and shown always to increase.

V14. Brownian Motion Theory as a Tool in Statistical Mechanics. A. J. F. SIEGERT, *Northwestern University.*—The problem of evaluating

$$\rho(\mathbf{q}_0 | \mathbf{q}, \beta) = \sum_\nu \psi_\nu(\mathbf{q}_0) \exp(-\beta H) \psi_\nu(\mathbf{q})$$

for a Boltzmann system of N particles at temperature $T = 1/k\beta$, where the functions $\psi_\nu(\mathbf{q})$ are orthonormal in a region $\Omega = V^N$ of $3N$-dimensional configuration ($\mathbf{q}$) space, and H is the Hamiltonian operator with potential energy $U(\mathbf{q})$, can be formulated as a problem of Brownian motion in $\mathbf{q}$-space, with β interpreted as a time and $|U(\mathbf{q})|\Delta t$ as absorption (or duplica-

tion) probability. This yields

$$\rho(\mathbf{q}_0|\mathbf{q},\beta)=\left\langle \exp\left[-\int_0^\beta U(\mathbf{q}(t))dt\right]\delta(\mathbf{q}(\beta)-\mathbf{q})\right\rangle_{\mathbf{q}_0}$$

averaged over all Brownian motion paths which start at $\mathbf{q}_0$ and do not touch the surface of Ω. From this expression (or from an integral equation deduced by a simple counting argument) one obtains a more convenient form of the Goldberger-Adams[1] series. The average can also in principle be calculated exactly if contributions come only from the neighborhood of a point (solid) or a line in $\mathbf{q}$-space.

[1] M. L. Goldberger and E. N. Adams, II, J. Chem. Phys. (to be published)

SATURDAY MORNING AT 9:30

Havemeyer 309

(M. H. HEBB presiding)

Solid-State Physics (Non-Metals)

W1. Extinction Effects in Neutron Transmission of Polycrystalline Media.* R. J. WEISS, *Watertown Arsenal.*—The effects of primary and secondary extinction are considered for neutron transmission work in the diffraction energy region. It is shown that the grain size is the most important parameter affecting extinction in typical studies with the mosaic block size and the angular spread of the mosaic blocks of secondary importance. Experiments were performed to corroborate the theory, and criteria are set up to avoid extinction effects. It is shown how to determine mosaic block size and the angular spread of the mosaic blocks in large grain substances by using fine resolution near the last Bragg cut-off peak.

* Research carried out at Brookhaven National Laboratory, under contract with the AEC.

W2. The Diffuse Scattering of Neutrons and X-Rays.* DAVID A. KLEINMAN, *Brookhaven.*—It appears that the principal possibility for directly measuring the frequency and polarization of the thermal vibrations (phonons) in a solid is by use of the temperature diffuse scattering of neutrons and x-rays. The important property of the temperature diffuse scattering is that measurements on the scattered radiation can fix the wave vector, frequency, and polarization of the phonons. Although for Bragg scattering of both neutrons and x-rays it is possible to treat the thermal vibrations as merely smearing out the scattering centers, the diffuse scattering should be treated quantum mechanically by considering the creation and annihilation of phonons. Under favorable experimental conditions the diffuse scattering will be due mainly to processes involving a single phonon. Since energy and momentum are conserved in these scattering processes, and since neutrons have very small energies compared to x-rays of the same momentum, there is a considerable difference in the diffuse scattering of neutrons and x-rays. The wave vector of the phonon is determined by the direction and the frequency of the phonon by the intensity of the scattered x-ray. On the other hand both the direction and energy of the scattered neutron must be measured to determine the phonon wave vector, but the frequency is then known from the conservation of energy without a measurement of the scattered intensity.

* Research carried out under contract with the AEC.

W3. Calculation of Energy Bands in Solids by the Integral Iteration Method.* M. DANK AND H. B. CALLEN, *University of Pennsylvania.*—An investigation has been made into the applicability of the Kellogg-Collatz integral iteration method to the calculation of electronic energy levels in solids. Separability of variables is not required, hence the true lattice symmetry need not be sacrificed in favor of a spherical approximation to polyhedral zones. Also, the method is based on integral rather than differential equations, for which numerical calculations are considerably more convenient. A Bloch-type wave function is invariant under the appropriate integral transformations, so that the iterates of an initial approximation function of the Bloch form converge to the true wave function with the same wave vector. The speed of convergence depends on the ratio of the eigenvalues of the two lowest wave functions with the given wave vector in the reduced zone scheme and is therefore quite rapid. The method can be applied in either coordinate or momentum space. The three-dimensional iteration formula in the coordinate space scheme involves a modified Green's function characteristic only of the crystallographic form which is identical to the "lattice sum" of the scattering matrix formalism. A method for treating these sums will be discussed.

* Research supported by the ONR.

W4. Anisotropy of Thermal Expansion and Internal Stresses in Polycrystalline Graphite and Carbons. S. MROZOWSKI, *University of Buffalo.*—The anisotropic thermal expansion of microcrystals has been found to create considerable internal stresses in metals.[1] Much more pronounced effects of this kind are met in polycrystalline carbons, where the extremely large anisotropy of microcrystals is responsible for a number of properties characteristic to these materials. Heating an untreated carbon creates large stresses concentrated at the peripheries of crystallites, where they are attached to their neighbors by C−C valence bonds. These stresses constitute the main driving force promoting the growth of crystallites up to temperatures 2200°C (or even higher). When a heat-treated sample is cooled, the volume of crystallites decreases more than the apparent volume of the sample and as a result an unavoidable internal porosity (up to 8 percent) and internal stresses are formed. Since steady creep is absent (<2200°C),[2] the internal stresses are not relieved by plastic flow and remain locked in the material. The recently observed higher tensile strength of carbons at high temperatures[2] is one of manifestations of the reversible release of these stresses as the material is heated (and vice versa).

[1] F. P. Bowden, "Symposium on Internal Stresses in Metals," Institute of Metals, London, 1948.
[2] Malmstrom, Keen, and Green, Jr., J. Appl. Phys. 22, 593 (1951).

W5. Evidence for a Pressure Effect in Thin Films of LiF. NATHAN SCLAR AND HENRY LEVENSTEIN, *Syracuse University.*—Preliminary studies have been made on the dielectric properties of thin evaporated films. For LiF, the dielectric constant and the break-down field were measured as a function of film thickness. Thin film condensers were prepared by consecutive evaporations of aluminum on glass, dielectric on the aluminum, and finally aluminum on the dielectric. The dielectric constant was calculated from the measured capacitance of the condensers at 1000 c/s, while the thicknesses of the evaporated films were determined by multiple beam interferometry using

white light. Thicknesses ranged from 440–2500A. All the dielectric constant values fall below those of the bulk material. Boswell[1] has recorded a change in lattice constant with crystallite size. He attributed this change to a pressure effect. By combining his data, the compressibility of LiF, and Mayburg's[2] data on the variation of dielectric constant with pressure, we deduce a fractional change in dielectric constant for the thin films which agrees in order of magnitude with the experimental results. This lends credence for the existence of a pressure effect in thin films.

[1] Boswell, Proc. Phys. Soc. (London) **A64**, 465 (1951).
[2] Sumner Mayburg, Phys. Rev. **79**, 375 (1950).

W6. Studies of Self-Diffusion in Graphite Using C^{14} Tracer.* M. FELDMAN, W. GOEDDEL, AND G. J. DIENES.—Self-diffusion in graphite was measured over the temperature range from 1835°C to 2370°C by observing the penetration of C^{14} tracer initially applied to one end of a graphite rod. The experimental data were found to be in agreement with a diffusion mechanism consisting of concurrent volume and grain boundary processes. Activation energies for both processes (E_V and E_B) could not be uniquely obtained from the data, however. An independent determination of either is required in order to evaluate the other. Assuming $E_V = 160$ kcal/mole from recent work, it is calculated from the present experiments that E_B, the activation energy for grain boundary diffusion, is 110 kcal/mole.

* Based on studies conducted for the AEC.

W7. Instability Criteria for the Fracture of Solids. H. L. SMITH, J. A. KIES, AND G. R. IRWIN, *Naval Research Laboratory.*—The development of instability for fast fracturing at the expense of stored elastic energy has been investigated, principally in sheets of transparent plastics, and for geometrically similar specimens has been found to contain a size effect. In fracturing a material one may describe the rate of doing work in terms of the quantity dW/dA where dW is the work increment and dA the increase in fracture area. In a tensile stress field there is a rate of strain energy release accompanying fracturing referred to as dE/dA. The critical point or the point of instability occurs in fast fracturing when $dE/dA \geqq dW/dA$. The use of this instability point permits one to predict a size effect in fracture which agrees with the experimental results obtained. The excess of elastic energy not used in simple fast fracturing can be computed. This is available for other interesting processes, notably shattering.

W8. The Work to Create Fracture Surfaces in Methyl Methacrylate. MARK BOWMAN, JR. AND H. L. SMITH, *Naval Research Laboratory.*—It has been shown that the rate dw/da, the energy absorbed per unit area of fracture surface is of primary importance in determining the stress at fracture in a brittle material. This quantity may be thought of as a combination of surface energy and work expended in plastic deformation of the material very close to the fracture surface. Direct experimental determination of dw/da for fast processes is generally not feasible. Computation of dw/da from the instability criterion used by H. Smith and others in the preceding paper reveals that for methyl methacrylate a value is obtained which is fairly independent of crack length. This is typical of brittle fracture and is contrary to typical results for materials such as aluminum foils. Such a computation permits a more critical evaluation of the embrittling effects of low temperatures than is afforded by standard impact test procedures, for example significant differences were found at 25°C, −10°C, and −40°C in dw/da, whereas Charpy impact tests failed to make distinctions in this range of temperatures.

W9. A Study in the Dynamics of Crystal Growth from a Supersaturated Solution. G. C. KRUEGER, *University of Maine,** AND C. W. MILLER, *Brown University.*—An experimental investigation of the concentration field during crystallization is made using an improved modification of W. F. Berg's interference technique.[1] $Na_2S_2O_3 \cdot 5H_2O$ is crystallized at 23°C, concentrations between 40 percent and 55 percent. Graphing the positions of the growing faces *versus* time indicates, in all cases, a uniform rate of growth with occasional abrupt changes. These discontinuities were in general correlated with changes in the perfection of the growing face, the disappearance of a region of poor growth being associated with a decreased rate, whereas the appearance of an imperfection led to a higher rate. A minimum of concentration is observed near the face center, corroborating previous investigations with $NaClO_3$.[2] A diffusion coefficient of 1.26×10^{-5} cm²/sec was calculated for $Na_2S_2O_3$ corresponding to 0.80×10^{-5} cm²/sec extrapolated from J. D. R. Scheffer's data.[3] There is no strict correlation between maximum, minimum, or average concentration at a crystal face and its rate of growth. It appears that the variations in concentration revealed by interferometer maps are to be interpreted as a consequence of solution depletion occasioned by the crystal's growth.

* The experimental work was done at Brown University.
[1] W. F. Berg, Proc. Roy. Soc. (London) **164A**, 79 (1938); S. P. F. Humphreys-Owen, Proc. Roy. Soc. (London) **197A**, 218 (1949).
[2] J. D. R. Scheffer, Z. physik. Chem. **2**, 397 (1888).

W10. Comparative Elastic Studies of Single Crystals of the NaCl Type.* LEWIS S. COMBES, STANLEY S. BALLARD, AND KATHRYN A. MCCARTHY, *Tufts College.*—Data on Young's modulus, apparent elastic limit, and modulus of rupture have been obtained for five crystals: sodium chloride, silver chloride, lithium fluoride, potassium chloride, and potassium bromide. All measurements were made on bars cut or cleaved from single crystals; each bar was supported as a simple beam and subjected to a flexural stress by loading at its center. Typical load-deflection curves will be shown for each crystal. In addition, measurements were made on a sodium chloride crystal with a silver impurity, Na(Ag)Cl. The apparent elastic limit for this sample was found to be 3.9×10^7 dyne cm^{-2} as compared to a previously reported[1] value of 2.4×10^7 for sodium chloride. The modulus of rupture for this sample was 9.8×10^7 dyne cm^{-2} as compared to 3.9×10^7 for sodium chloride.

* This work has received support from the Permanent Science Fund of the American Academy of Arts and Sciences.
[1] Combes, Ballard, and McCarthy, J. Opt. Soc. Am. **41**, 215–222 (1951).

W11. An Electronic Instrument for the Measurement of Crystal Anelasticity. R. D. LAUGHLIN, *National Bureau of Standards.*—An instrument has been devised which makes it possible to measure the "Q" of a vibrating piezoelectric crystal during its free decay. The principle of operation is that of determining the time interval between any two selected voltage points on the exponentially decaying wave form. The circuit operation is as follows: The specimen is driven at its resonant frequency and then allowed to damp itself in free decay. The decaying vibrations are amplified in a linear amplifier to a level of approximately 100 volts peak and are rectified and filtered. The smoothed replica of the original wave form is fed into two separate Multiar type voltage comparator circuits. The first comparator circuit produces a timing signal to start a bistable multivibrator. The second comparator produces a timing signal to stop the multivibrator. The start and stop voltages are independently controlled by an external source. The rectangle produced by the bistable multivibrator is introduced into an electronic chronoscope to

measure the time interval. The chronoscope gives the interval in milliseconds. A simple relation exists between the time interval, the voltage ratios, and the "Q." "Q's" have been measured as a function of temperature for a quartz bar in torsional oscillation at 36 kc. A preliminary estimate of the accuracy of measurements is 2 percent.

W12. Ferroelectricity in the Ilmenite Structure. H. C. SCHWEINLER, *M.I.T.*—The ferroelectricity of the ilmenite structure minerals lithium tantalate and lithium niobate is studied theoretically, using the method recently introduced by Slater[1] for barium titanate. The metal ions are assumed to move in a potential which has small quartic terms as well as the usual quadratic terms, all satisfying the appropriate crystal symmetry requirements. This results in a slight dependence of the ionic-displacement polarizability of each metal ion on both the temperature and the polarization of the crystal. The local electric field strength is computed exactly for each ion by Ewald's method, and the internal field constants are given for a number of positions in a rhombohedral unit cell of axial angle $\alpha = 56°$. The polarizabilities can be estimated from other crystal polarization data, leading to a spontaneous polarization below the upper Curie temperature T_0 of $2(T_0-T)^{\frac{1}{2}}\mu$ coul cm^{-2} (without electromechanical correction). It is found that (unlike the corresponding case in barium titanate) there are sizeable components of the oxygen dipole moments perpendicular to the total polarization, but these components produce a large field in the direction of the polarization at other ionic positions.

[1] J. C. Slater, Phys. Rev. **78**, 748 (1950)

W13. High Temperature Susceptibility of Permanent Dipolar Lattices.* R. ROSENBERG AND M. LAX, *Syracuse University.*—The spherical approximation yields, for the susceptibility of permanent dipolar materials, a result which is valid at high and low temperatures.[1] For liquids at high temperatures this result agrees perfectly to terms of order T^{-2}, with the Onsager approximation[2] and the Van Vleck[3] exact treatment. In order to judge the success of the spherical approximation, it was therefore necessary to carry the exact treatment at high temperatures to the term of order T^{-4}. The spherialization procedure is found to be more accurate than the Onsager treatment, and underestimates the susceptibility where Onsager overestimates it. In the exact solution for the polarization, the coefficient of T^{-n} is a combination of sums over certain types of dipole clusters which contain n dipoles at most. The clusters of n dipoles are simple open chains, producing essentially all the shape dependence, and therefore cancel out of the susceptibility. In contrast with the exact polarization, which contains all types of clusters, the spherical approximation includes the simple open chains and single-loop clusters only.

* This work supported in part by the ONR.
[1] M. Lax, Bull. Am. Phys. Soc. 26, No. 7, G2 (1951).
[2] J. H. Van Vleck, J. Chem. Phys. 5, 320 (1937).

W14. Multiple Scattering of Waves. II. The Effective Field in Dense Systems.* MELVIN LAX, *Syracuse University.*—The multiple scattering of waves interacting with a system of particles is treated by a self-consistent approach. Scattering processes are described by operators that permit anisotropy, absorption, and creation. The scattering system may be randomly, partially, or completely ordered. The propagation constant k' of the coherent wave in the scatterer medium differs from the vacuum constant k by $(k')^2 = k^2 + 4\pi n c f(\mathbf{k}', \mathbf{k}')$, where n is the scatterer density and f is an operator whose matrix elements $f(\mathbf{b}, \mathbf{a})$ represent the scattering amplitude in direction $\mathbf{b}$ for a wave incident in direction $\mathbf{a}$ on a single scatterer bound by the forces of its neighbors. The parameter c, defined by $cf(k', k') = f \exp(-i\mathbf{k}'\cdot\mathbf{r})\psi_s(\mathbf{r})d\mathbf{r}$, is a measure of the ratio of the effective field $\psi_s(\mathbf{r})$ to the average field. An integral equation is found for $\psi_s(\mathbf{r})$ with the help of a "quasi-crystalline" approximation. A variational expression is then found for c that becomes exact for point scatterers. A comparison is made of finite and infinite scattering systems. The extinction theorem is proven. The macroscopic viewpoint is found to be applicable to small systems whose size is large compared to the scatterer potential range, and the range of scatterer position correlations.

* This work supported in part by the ONR.

W15. Shape of a Two-Dimensional Crystal Minimizing the Surface Energy. JOHN P. NIELSEN, *New York University* AND BORIS GARFINKEL, *Aberdeen.*—A crystal in equilibrium with its surroundings assumes a shape which minimizes the surface energy. For a two-dimensional crystal with a known energy density distribution of the peripheral surface, we may determine the bounding curve by solving an isoperimetric problem in the calculus of variations. If the crystal is isotropic with respect to the surface energy, the curve, of course, is a circle. If the crystal is anisotropic, a more complicated curve results from the solution of the Euler-Lagrange equations. In particular, if $\gamma = 1 + a\cos\phi$, where γ is the energy density, and ϕ the angle made by the tangent to the curve and a symmetry axis in a twofold symmetry crystal, the closed curve consists of a pair of parallel straight lines surmounted by a pair of semicircles. The curve is of class C', i.e., it has no corners. The same solution also holds for the so-called negative crystal, i.e., a hole within a crystal.

SATURDAY MORNING AT 9:30

McMillin

(C. C. LAURITSEN presiding)

Invited Papers in Nuclear Physics

X1. The Nuclear Interactions of Pions of Energy near 70 Mev. J. STEINBERGER AND A. SACHS, *Columbia University.* (30 min.)

X2. Production of Charged Pions by Protons. W. W. HAVENS, JR., *Columbia University.* (30 min.)

X3. Disintegrations Produced by Monoenergetic 14-Mev Neutrons. T. W. BONNER, *Rice Institute.* (30 min.)

X4. Magnetic-Analysis Studies of Nuclear Energy-Levels. W. W. BUECHNER, *M.I.T.* (30 min.)

SATURDAY AFTERNOON AT 2:00

Pupin 301

(R. L. SERBER presiding)

Invited Paper

Y1. Nonlocal Field-Theory. R. E. PEIERLS, *University of Birmingham (England).* (40 min.)

Meson Theory

Y2. Quantization of a Nonlinear Meson Theory. L. I. SCHIFF, *Stanford University.**—Two distinct attempts at quantization of the nonlinear meson theory described earlier[1] have been undertaken. (1) The canonical transformation $\exp[i\int\phi_0(\mathbf{r})\pi(\mathbf{r})d\tau]$, where $\phi_0(\mathbf{r})$ is a c-number function that satisfies the classical field equation, separates the Hamiltonian into static and nonstatic parts that have simple interpretations in some cases. It can be used to treat the scattering of mesons by nuclei (I, Sec. XI), and to show that the result obtained classically in II is also valid in quantum theory if the nonlinear coupling function has a power form ($F=b\phi^m$). (2) The case treated in I can also be quantized approximately by neglecting the $(\nabla\phi)^2$ term in the Hamiltonian, so that the field becomes a set of uncoupled nonlinear oscillators, one for each point in space. This has the advantage that the nonlinearity is explicitly considered in the quantization, and the disadvantages that wave aspects are suppressed and it is difficult to correct for the neglected term. The method is being applied to a finite one-dimensional lattice as an example.

* Assisted in part by the joint program of the ONR and AEC.
[1] Phys. Rev. **84**, 1, 10 (1951); referred to here as I and II, respectively.

Y3. Applications of the Charge Independence Hypothesis to Meson Phenomena. KENNETH M. WATSON, *Indiana University.*—The hypothesis of charge independence for nuclear forces can be generalized to include an extensive class of meson-nucleon phenomena. Application of this principle has previously been made to meson scattering[1] and to meson production in nucleon-nucleon collisions,[2] for which no disagreement is found with presently available experimental results. The principle can also be directly applied to nucleon collisions in which several mesons are produced. Because of the symmetry properties with respect to transformations of charge states of the electric current vectors of mesons and nucleons in field theories, charge independence places certain restrictions on the various cross sections for photomeson production. The restrictions are somewhat complicated, but are nevertheless capable of being subjected to an experimental check. The charge independence principle can also be generalized to include heavy unstable particles, such as V-particles and τ-mesons. Here the theory makes predictions as to the charge states of these particles and to the relative rates of competing decay schemes.

[1] W. Heitler, Proc. Roy. Irish Acad. **51**, 33 (1946).
[2] K. M. Watson and K. A. Brueckner, Phys. Rev. **83**, 1 (1951).

Y4. Some Meson Contributions to the Photodisintegration of the Deuteron. M. H. FRIEDMAN, *University of Illinois.*—One of the difficulties encountered in calculating the cross section for the photodisintegration of the deuteron at high energies is the uncertainty of meson contributions to those channels which involve interaction of the nucleon spins with the electromagnetic field. A calculation has been carried out, treating the nucleons nonrelativistically, and using weak pseudovector coupling pseudoscalar meson theory. Processes in which mesons are exchanged between nucleons are not calculated explicitly. In the case of the electric disintegration, they are taken into account by Siegert's theorem. In the photomagnetic processes they would lead to the interaction momen- effects, which we here assume are small. In the approximation used (which assumes the nucleon kinetic energies are small compared to the meson energies involved) it is found that the only effect of the charge clouds about the nucleons is to make the magnetic moments dependent upon the frequency of the quanta. The static moments were subtracted out and replaced by the experimentally observed ones. The results show that for low energies the magnetic terms are still small compared to the electric. However, for energies of the order of 140 Mev, the magnetic terms become comparable with the electric and contribute appreciably to the cross section.

Y5. Stability of Neutral Scalar Heavy Mesons. H. P. NOYES, *University of Rochester.*—Salam's result[1] that $S(S)$ and $PS(PS)$ meson theories are renormalizable by contact interactions suggests that the calculation of the decay of spin zero heavy mesons into π-mesons and γ-rays should yield finite and unambiguous results. The process (1) $S\rightarrow PS+PS$ is logarithmically divergent but renormalizable by the contact interaction $(\chi+\delta\chi)G_s g_{ps}{}^2\Phi_s\varphi_{ps}{}^*\varphi_{ps}(\chi)$ where $\delta\chi$ cancels the divergence and χ is an empirical constant determinable from this lifetime. This interaction also contributes to (2) $S\rightarrow\gamma+\gamma$ in order $G_s g_{ps}{}^2 e^2$. When χ gives a long lifetime for (1) it also cancels the imaginary part of the matrix element for (2) because of two PS mesons occurring as a real intermediate state. The sum of the remaining fifth order contributions is of opposite sign to the lowest order ($G_s e^2$) matrix element. Consequently there exists a relationship between G_s and g_{ps} for which (2) has a longer lifetime than (1) to fifth order, and an argument will be given to show that this situation probably persists if higher order terms are included. Therefore, heavy neutral scalar mesons could be sufficiently stable against decay through virtual nucleon states into lighter bosons to be observed in cosmic ray experiments.

[1] A. Salam, Phys. Rev. **82**, 217 (1951).

Y6. Multiple Meson Production. H. W. LEWIS, *Institute for Advanced Study.**—The analysis of the effect on the pseudoscalar field theory of multiple-meson production, of the correlations induced by the presumed softness of the internucleon potential, has been carried out along the lines previously mentioned.[1] The results to be discussed include: (1) The mesonic multiplicity, which is reduced by a factor α, approximately equal to $(2\mu/M)^{\frac{1}{2}}$, where μ/M is the mass ratio of meson and nucleon.[2] The factor μ arises from the identification of the range of the force with the meson Compton wavelength —if this identification is not made, α can be varied somewhat. (2) The meson angular distribution, which is no longer spherically symmetric in the center of mass system, but involves cones of angular width $\sim\alpha^{\frac{1}{2}}$. (3) The implications for the theory of the observed symmetric double cone in the center of mass sytem.

* Now at the Bell Telephone Laboratories, Murray Hill, New Jersey.
[1] Proceedings of the Berkeley Statistical Symposium, University of California Press, 1952.
[2] Lewis, Oppenheimer, and Wouthuysen, Phys. Rev. **73**, 127 (1948).

Y7. Intrinsic Properties of the τ-Meson Derived from Conservation Laws.—B. A. JACOBSOHN, *University of Washington.*—Although meson-theoretic studies of the $\tau^+ \rightarrow (3\pi)$ decay have been made, apparently no arguments have been published in which deductions are made solely on the basis of conservation of angular momentum and parity, as in Yang's[1] well-known treatment of two-photon decay. We make the following assumptions: (i) the (π^+, π^0) and (π^+, γ) processes are not observed because they are strictly forbidden, (ii) the π^+ is pseudoscalar and (iii) the π^0 has spin zero. Simple symmetry arguments then show that (i) is true only if the τ has spin zero and the same parity as the π^0. Similar arguments show that $\tau^+ \rightarrow 2\pi^+ + \pi^-$ is forbidden if τ is scalar and allowed if τ is pseudoscalar. Thus, within the framework of our assumptions (which will be discussed), one can deduce that the τ^+ and π^0 are both pseudoscalar without appealing to meson theory.

[1] C. N. Yang, Phys. Rev. **77**, 242 (1950).

Y8. Scattering of Pi-Mesons by the Deuteron. J. S. BLAIR* AND B. SEGALL,† *University of Illinois.*—Exchange and ordinary scattering are considered in the impulse approximation[1] in which the single nucleon amplitudes are those given by the weak coupling theory. For a general type of nucleon-meson coupling, linear in the meson field, the conventional second-order perturbation theory is shown to yield a result that is approximately equal to this impulse approximation. As an illustrative example, numerical results are presented for the case of a pseudoscalar meson with pseudovector coupling. Differential cross sections for the single nucleon and elastic deuteron scattering are computed in a straight forward manner. The summation method of Chew and Placzek is used to obtain the approximate differential cross sections summed over all possible final states.

* Assisted by the joint program of the ONR and AEC.
† University of Illinois Post-Doctoral Fellow.
[1] G. F. Chew, Phys. Rev. **80**, 196 (1950).

Y9. Meson-Nucleon Scattering and Nucleon Isobars. KEITH A. BRUECKNER, *Indiana University.*—The scattering (including charge exchange) of π^- mesons in hydrogen rises from 18 millibarns[1] at 60 Mev to a broad plateau of about 60 millibarns[2] at 200 Mev, and is smaller than the π^+ scattering at 60 Mev in the ratio of 1.58 ± 0.24.[1] The general features of the π^- scattering, except for the high energy plateau, are given qualitatively by pseudoscalar theory with pseudovector coupling in the weak coupling limit; the ratio of π^+ to π^- scattering predicted by this theory is the weak coupling limit is, however, 0.60 which is much lower than the experimental result. A phenomenological theory of the scattering is developed using the methods of Wigner and Eisenbud[3] and imposing the restrictions of charge symmetry. Using the qualitative assignment of the resonance levels parameters as given by weak and strong coupling theory,[4] satisfactory agreement with experiment is obtained. It is concluded that the apparently anomalous features of the scattering can be interpreted to be an indication of a resonant meson-nucleon interaction corresponding to a nucleon isobar with spin $\frac{3}{2}$, isotopic spin $\frac{3}{2}$, and with an excitation of 277 Mev.

[1] Isaacs, Sachs, and Steinberger; post-deadline paper at the Chicago Physical Society meeting, October 27, 1951.
[2] Reported by H. L. Anderson at the Chicago Conference on High Energy Physics, September 15–19, 1951. Bull. Am. Phys. Soc. **26**, No. 6, 33 (1951).
[3] E. P. Wigner and L. Eisenbud, Phys. Rev. **72**, 29 (1947). H. Feshbach, D. C. Peaslee, and V. F. Weisskopf, Phys. Rev. **71**, 145 (1947).
[4] W. Pauli and S. M. Dancoff, Phys. Rev. **62**, 85 (1942).

Y10. The Pseudoscalar Interaction.* L. L. FOLDY, *Case Institute of Technology.*—The problem of a single nucleon (Dirac particle) moving in an external neutral pseudoscalar potential with pseudoscalar coupling is examined by the employment of unitary transformations. A first exact transformation eliminates the pseudoscalar coupling and yields a Hamiltonian describing a Dirac particle, whose rest mass varies with position, coupled to the potential by a nonlinear saturating pseudovector coupling. By a sequence of further transformations to eliminate odd operators, a new Hamiltonian suitable for the investigation of nonrelativistic problems is obtained as an expansion in powers of the ratio of nucleon Compton wavelength to the range of the potential, no assumption being made concerning the smallness of the potential itself. As a rough model of the deuteron, a form for the potential is assumed corresponding to the pseudoscalar meson potential produced by an infinitely heavy nucleon whose spin is also treated as a dynamical variable. It is found that no singlet or triplet bound states exist because of the strong repulsion arising from the dependence of rest mass on position. A strong spin-orbit coupling term is found to be present but of the opposite sign to that required by the Mayer shell model of the nucleus. Indications that the same results may obtain in the pseudoscalar meson theory with pseudoscalar coupling will be discussed.

* Supported by the AEC.

Y11. On the Non-Adiabatic Treatment of the Relativistic Two-Body Problem. MAURICE M. LÉVY, *Institute for Advanced Study.*—The method of Tamm and Dancoff,[1] for the non-adiabatic treatment of the relativistic interaction between two particles, has been generalized to include pair creation and higher order effects in the exchange of field quanta. This generalized form of the Tamm-Dancoff method gives results equivalent to those obtained from the relativistic equation of Bethe and Salpeter.[2] A detailed study has been made of two limiting cases: (a) the maximum number of mesons present at a given time is one, the number of pairs being unrestricted; (b) no pair of interacting particles is created, but an arbitrary number of mesons can be present. This method has been applied to the calculation of the lowest order correction to the scalar meson interaction of two nucleons. The exact correction, which is of the second order in nucleons velocities, is obtained by including the fourth- and sixth-order interaction processes involving, in the corresponding Feynman diagrams, the crossing of the meson lines. The numerical results of the application of this method to the weak coupling treatment of the relativistic pseudoscalar meson theory of the neutron-proton system will be reported.

[1] I. Tamm, J. Phys. U.S.S.R. **9**, 449 (1945); S. M. Dancoff, Phys. Rev. **78**, 382 (1950).
[2] H. A. Bethe and E. Salpeter, Phys. Rev. **82**, 309A (1951); M. Gell-Mann and F. Low, Phys. Rev. **84** (1951).

SATURDAY AFTERNOON AT 2:00

McMillin

(C. H. TOWNES presiding)

Invited Papers in Optical Physics

Z1. 1420-Mc Radiation from Interstellar Hydrogen. H. I. EWEN, *Harvard University.* (30 min.)

Z2. Pure Quadrupole Spectra of Solid Chlorine Compounds. RALPH LIVINGSTON, *Oak Ridge National Laboratory.* (30 min.)

Z3. Optical Hyperfine Structure by Techniques of Atomic Beams. G. K. WOODGATE, *Columbia University.* (30 min.)

SATURDAY AFTERNOON AT 2:00

Pupin 428

(C. F. SQUIRE presiding)

Cryogenics

ZA1. Lattice Oscillations and Superconductivity. M. DRESDEN, *University of Kansas.*—The theories which attempt to explain superconductivity on the basis of a strong interaction between the electrons and the oscillations of a crystal lattice have been criticized by Wentzel and others,[1] who demonstrated that under the conditions required for the existence of the superconductive state, the lattice oscillations would become unstable Because of the conflicting interpretations of this result, the question of the interaction between lattice vibrations and an electron gas has been re-examined for the case of a linear chain. A part of the difficulty stems from the fact that the Hamiltonian used to describe the system cannot be separated in an unambiguous fashion in Hamiltonians referring to the electron-ion system, the lattice vibrations, and the interaction between these systems. In the customary description the frequencies of the normal modes may depend on the strength of the coupling. The treatment was carried out describing the lattice oscillations by the Born and v. Karman method, the electron gas was described using the Tomonaga representation of a non-ideal Fermi gas. Preliminary results indicate that the question of stability or instability depends sensitively on the method of separation and identification of the terms in the original Hamiltonian.

[1] G. Wentzel, Phys. Rev. **83**, 168 (1951).

ZA2. Further Considerations Regarding the Theory of Bose-Einstein Liquids.* J. G. DAUNT, T. S. TSENG, AND C. V. HEER, *Ohio State University.*—Previously Heer and Daunt[1] have shown that a quasi-gaseous model of a Bose-Einstein liquid can be used to explain the properties of dilute solutions of He^3 in liquid He^4. Further calculations, using the same model are reported, extending the results to strong solutions of He^3 in liquid He^4, and comparing them with recent experimental results.[2] It is found that the calculated values for the distribution coefficient are in agreement with experiment over a wide range of He^3 concentrations. At low temperatures (below 1.7°K) the numerical agreement is exact, and at the higher temperatures (above T_λ) the theoretical prediction of values well above those calculable for perfect classical solutions appears to be sustained by the experiments. Detailed calculations for vapor pressures of strong solutions are also given. Finally, a comparison is given with the theory of de Boer and Gorter,[3] for which detailed computations also have been made for strong solutions.

* Assisted by a contract between the AEC and The Ohio State University Research Foundation.
[1] C. V. Heer and J. G. Daunt, Phys. Rev. **81**, 447 (1951).
[2] See reference 1, abstract.
[3] J. de Boer and C. J. Gorter, Physica **16**, 225, 667 (1950).

ZA3. The Solubility of He^3 in Liquid He^4.* J. G. DAUNT AND C. V. HEER, *Ohio State University.*—Measurements are reported of the distribution coefficient for He^3 between solutions of He^3 in liquid He^4 and their saturated vapors in the temperature range 1.4°K to 2.6°K. The results obtained below the λ-temperature give values for C_v/C_L higher than those calculable for perfect classical solutions, but in good agreement with the theory previously proposed by Heer and Daunt.[1] Above 2.18°K, the λ-temperature for pure liquid He^4, the measured C_v/C_L also appears greater than that for perfect classical solutions, as was predicted by Heer and Daunt.[1] A comparison with the theory of de Boer and Gorter[2] is also given.

* Assisted by a contract between the AEC and the Ohio State University Research Foundation.
[1] C. V. Heer and J. G. Daunt, Phys. Rev. **81**, 447 (1951).
[2] J. de Boer and C. J. Gorter, Physica **16**, 225, 667 (1950).

ZA4. Low Temperature Heat Capacity of Niobium. A. BROWN, M. W. ZEMANSKY,* AND H. A. BOORSE,† *Columbia University.*‡—The heat capacity of niobium has been measured in the normal and superconducting states between 2.5° and 20°K. A special type carbon composition resistor was found to be a very satisfactory thermometer.[1] The data confirmed the usual relations, $C_n=\gamma T+464.4(T/\theta_n)^3$, and $C_s=464.4(T/\theta_s)^3$, where $\theta_n=254°$, and $\theta_s=161°$. The coefficient, γ, of the linear term in C_n was found to be 21.0×10^{-4} cal/mole-deg[2]. The Debye characteristic temperature in the normal state, θ_n, is constant at 254° below 12°K, and then increases to approximately 268° at 20°K. In the superconducting state below 3.5°K the specific heat appeared to be significantly smaller than that given by the T^3 relation. The temperature at which $C_n=C_s$ was found to be $T_0/\sqrt{3}$, ($T_0=8.7$°K, the zero field transition temperature), thus indicating that the parabolic relation between the critical field, H, and the absolute temperature holds for niobium. The value of the critical field at absolute zero, H_0, was computed to be 1950 gauss. This value

of H_0 is considerably smaller than any of the previous values determined by magnetic measurements.

* The City College of New York.
† Barnard College, Columbia University.
‡ Assisted in part by the ONR and Linde Air Products Company.
[1] Brown, Zemansky, and Boorse, Phys. Rev. **84**, 1050 (1951).

ZA5. The Specific Heat of Chromium below Room Temperature. J. WEERTMAN, D. BURK, AND J. E. GOLDMAN, *Carnegie Institute of Technology.*—Anomalous properties have been observed in chromium at 121°K.[1] The thermal properties of chromium at other temperatures also show a remarkable behavior. At high temperatures the specific heat is found to be anomalously high,[2] while at liquid helium temperatures the electronic specific heat determined from the linear term in the temperature dependence[3] is particularly low for a transition metal. The suggestion that these properties, and in particular the anomalies observed at 121°K, might be due to an antiferromagnetic transition prompted us to examine the specific heat of chromium at temperatures between liquid helium and room temperature. The experimental technique and thermometry is the same as that used by Estermann and his collaborators.[4] The sample is in the form of very pure electrolytically deposited flakes kindly supplied by the Allegheny-Ludlum Steel Corporation. The results show the usual Debye specific heat curve with no trace of any anomaly in the region of the Fine point. Values of the Debye θ agree well with published values at both extremes of the temperature range.

[1] Fine, Greiner, and Ellis, J. Metals **189**, 56 (1951).
[2] L. D. Armstrong and H. Grayson-Smith, Can. J. Research **28A**, 51 (1950).
[3] Friedberg, Estermann, and Goldman (to be published).
[4] I. Estermann and J. Weertman, Phys. Rev. **83**, 228 (1951).

ZA6. The Specific Heat of Hafnium at 40–190°K. D. BURK AND F. DARNELL, *Carnegie Institute of Technology* (Introduced by I. Estermann).—The anomalous peak in the specific heat of germanium which was found by Cristescu and Simon[1] to occur at 75°K was not found when this experiment was repeated in this laboratory.[2] Since these investigators found a similar peak in hafnium at the same temperature, it was suggested that the measurements on Hf be repeated. A sample of relatively pure metallic hafnium was made available for this purpose by the AEC. The calorimetric technique is similar to that employed by Estermann and Weertman. As in the earlier experiments, temperature measurements were made with a platinum resistance thermometer. The sample is in the form of a solid cylinder $\frac{1}{2}$ in. in diameter and 1 in. in length and consists of solid cast hafnium extremely pure except for approximately 2 percent zirconium. Measurements were carried out in the temperature range of 40°–190°K and give a monotonically increasing Debye curve over the entire range. The anomaly of Cristescu and Simon is completely absent.

* Supported by the ONR.
[1] S. Cristescu and F. Simon, Z. physik. Chem. **25B**, 273 (1934).
[2] I. Estermann and J. Weertman, Phys. Rev. **83**, 228 (1951). J. R. Weertman, thesis, Carnegie Institute of Technology, 1951.

ZA7. On the Superconductivity of a Hafnium-Zirconium alloy. L. D. ROBERTS AND J. W. T. DABBS, *Oak Ridge National Laboratory.*—The magnetic susceptibility of a hafnium-zirconium alloy has been observed between 0.22°K and 4.18°K and no evidence of superconductivity has been found in this temperature region, possibly contrary to the result of Kürti and Simon[1] who reported a transition at 0.35°K. Two hafnium samples, containing about 5 percent zirconium, were used, one prepared by chemical reduction and the other by the "hot wire" method. The latter "crystal bar" sample had a metal volume of 0.87 cc consisting of chips roughly 0.003 cc in volume pressed with 1.14 cc of $CrK(SO_4)_2 \cdot 12H_2O$. Upon demagnetization of this composite to a final $H=0.44$ oersted, the final $T^*=0.22$°K (reciprocal susceptibility) was within 0.002°K of that expected for the pure alum, demonstrating the absence of a superconducting transition. Further, the susceptibility-time curve was linear during the warm up to 1.1°K (usually requiring about 40 minutes). In one experiment the sample was held below 0.25°K for 80 minutes to allow ample time for thermal equilibrium. A duplicate experiment on zirconium gave a very sharp transition at a temperature of 0.63°K. It is planned to extend the hafnium measurements to lower temperatures.

[1] Kürti and Simon, Proc. Roy. Soc. (London) **151**, 610 (1935).

ZA8. The Gyromagnetic Effect in a Superconductor. ROBERT PRY AND ARTHUR L. LATHROP, *Rice Institute.*—Experiments have been completed on measuring the gyromagnetic effect in superconducting tin with results in agreement with Kikoin and Gubar.[1] A tin sphere one inch in diameter was suspended from a torsion fiber and the delicate system driven at resonance by means of reversing a magnetic field (100 gauss and 50 gauss magnitudes). The change of magnetization gave an angular momentum change whose directional sense is that of a positively charged ion lattice under the influence of the Faraday induction of the oscillating magnetic field. The magnetization is caused by the orbital motion of the electrons.

[1] I. Kikoin and S. Gubar, J. Phys. U.S.S.R. **3**, 33 (1940).

ZA9. Spin Paramagnetism of Cr^{+++} at Liquid Helium Temperatures and High Magnetic Fields. WARREN E. HENRY, *Naval Research Laboratory.*—Experimental study of paramagnetism of suitable substances near saturation makes possible a critical examination of existing theories which embrace the ideas of quenching of orbital angular momentum[1] (Lande-g factor 2) and space-quantization[2] of magnetic dipoles. Magnetic moments of potassium chromium alum (containing Cr^{+++} of spin $\frac{3}{2}$) were measured in the liquid helium temperature range and in fields up to 50 kilogauss. For fixed values of magnetic field and temperature, a solid spherical sample of the alum was moved with respect to a double coil system, the resulting deflection of a ballistic galvanometer being proportional to the magnetic moment of the sample. Comparison with theory consisted of taking ratios between measured relative moments of the sample and the calculated magnetic moment for a given H/T. Constancy of these ratios is taken as agreement. The Brillouin space-quantized model[2] gives moments which agree with our experimental values ranging up to 99.5 percent saturation for the largest value of H/T.

[1] H. A. Jahn and E. Teller, Proc. Roy. Soc. (London) **A161**, 220 (1937).
[2] L. Brillouin, J. phys. et radium **8**, 74 (1927).

SATURDAY AFTERNOON AT 2:00

Schermerhorn 501

(L. J. HAWORTH presiding)

Reactions of Transmutation

ZB1. Excitation and Disintegration of Nuclei by Electrons.* J. A. THIE,† C. J. MULLIN, AND E. GUTH, *University of Notre Dame.*—The theory of the excitation and disintegration of nuclei by electrons has been extended and applied to a discussion of the feasibility and theoretical significance of some experiments which could be performed with electron beams.

General expressions have been developed for the cross sections for electron excitation of a nucleus because of the interaction of the electron's field with the electric 2^l-pole moments of the nucleus; unambiguous expressions are obtained for these cross sections because the form of the electric 2^l-pole moment does not depend upon the nuclear interactions.[1] The intimate relation between excitation by photons and by electrons has been developed explicitly. This relation has been exploited, in particular, in a comparison of the theory of the disintegration of the deuteron by high energy electrons with the corresponding photodisintegration theory. Because of the relative precision with which an electron beam can be controlled, electrons may be useful in high energy deuteron disintegration experiments.

* Supported in part by the ONR.
† AEC Predoctoral Fellow, now AEC Postdoctoral Fellow at Cornell University, Ithaca, New York.
[1] R. G. Sachs and N. Austern, Phys. Rev. **81**, 705 (1951).

ZB2. Photodisintegration of the Deuteron.* V. E. KROHN, JR., AND E. F. SHRADER, *Case Institute of Technology*.—The angular distribution of the protons from the $d(\gamma, n)p$ reaction has been investigated for 5–13-Mev gamma-rays by means of the D_2O loaded emulsion technique with the Case betatron serving as gamma-ray source. The results have been compared to a differential cross section of the form $d\sigma = [a + (b + c\cos\vartheta)\sin^2\vartheta]d\Omega$ in the center-of-mass system and the isotropy found consistent with the mean values: $a/b = 0.04 \pm 0.03$ from 5 to 11 Mev and 0.24 ± 0.07 from 11 to 13 Mev. The forward asymmetry was determined for energies above 8 Mev and found to be $c/b = 0.24 \pm 0.09$. Except for the isotropy observed above 11 Mev where the theory predicts $a/b \sim 0.01$ these results are in agreement with the theoretical calculations of Marshall and Guth[1] in which the possible effects of meson exchange currents and tensor forces are neglected.

* Work supported by the AEC.
[1] J. F. Marshall and E. Guth, Phys. Rev. **78**, 738 (1950).

ZB3. High Energy Photodisintegration of the Deuteron. T. S. BENEDICT AND W. M. WOODWARD, *Cornell University*.*—The cross section for the photodisintegration of the deuteron has been measured in the energy range 80 to 150 Mev using 300-Mev synchrotron bremsstrahlung. The experimental arrangement, using a high pressure gas target and scintillation counters for detecting the protons, is essentially that used in a previous photodisintegration experiment[1] on He^4. The geometry of the present experiment has been improved by adding an internal collimator to the pressure chamber and decreasing the solid angles of the counting system. The chamber was filled with deuterium (>99.5 percent H^2) to a pressure of 120 atmospheres and protons were counted at laboratory angles of 60°, 90°, and 120°. The cross section at 80 Mev is in essential agreement with that calculated by Schiff[2] and Marshall and Guth,[3] while at higher energies it is somewhat greater than the theoretical prediction.

* Supported by the joint program of the ONR and AEC.
[1] T. S. Benedict and W. M. Woodward, Phys. Rev. **83**, 1269 (1951).
[2] L. I. Schiff, Phys. Rev. **78**, 733 (1950).
[3] J. F. Marshall and E. Guth, Phys. Rev. **78**, 738 (1950).

ZB4. Excitation Functions for Photoprotons from Carbon. A. M. PERRY AND J. C. KECK, *Cornell University*.—We have measured the yields of 60-, 100-, and 140-Mev protons from a carbon target bombarded by synchrotron γ-ray beams of maximum energy 310, 260, 215, and 180 Mev. The protons were detected by a two-crystal coincidence telescope,[1] at a mean angle of 67° with respect to the γ-rays. Proton energies were determined by copper absorbers in front of the telescope. The energy intervals were determined by discriminator bias on the output of the second crystal and by target thickness. Positive identification of the protons was by their pulse height in the first crystal. Cross sections per γ-ray for producing protons of a given energy were found to be roughly proportional to γ-ray energy above some threshold, which depends on the proton energy, and to decrease rather sharply below this threshold.

[1] J. C. Keck, Cornell thesis (1951); to be published in Phys. Rev.

ZB5. Gamma-Rays from Sodium Bombarded by Protons.* P. H. STELSON, W. M. PRESTON, AND CLARK GOODMAN, *M.I.T.*—The gamma-ray yield from sodium was measured as a function of proton bombarding energy over the range 1.0 to 2.6 Mev using resolutions of 1.5 to 10 kev. Thin targets of metallic sodium were prepared by evaporation in vacuum. Gamma-rays were detected with a NaI(Tl) scintillation counter. Thirty-seven resonances were found, giving an average level spacing of 40 kev at an average excitation energy of 13.5 Mev in the compound nucleus, Mg^{24}. The present results are in general agreement with the earlier work of Burling.[1] The resonances vary in natural width from less than 1.5 kev to 70 kev. The energy spectrum of the gamma-rays from a number of the resonances was investigated with a single crystal NaI(Tl) scintillation spectrometer. Only the very sharp resonance at $E_p = 1.415$ Mev gave appreciable proton capture radiation. The spectra of the other resonances consist mainly of two gamma-rays with energies of 0.45 ± 0.01 and 1.63 ± 0.02 Mev. These are interpreted as resulting from transitions from the first excited states of the residual nuclei formed by the reactions: $Na^{23}(p, p')^*Na^{23}$ and $Na^{23}(p, \alpha)^*Ne^{20}$, respectively.

* Work jointly supported by ONR and BuShips.
[1] R. L. Burling, Phys. Rev. **60**, 340 (1941).

ZB6. Angular Distributions of Photoprotons.* M. A. ROTHMAN, A. K. MANN, AND J. HALPERN, *University of Pennsylvania*.—Targets of Co, Ni, and Cu have been bombarded with bremsstrahlung of maximum energy 23 Mev. The angular distributions of all the emitted protons from each target have been measured with ZnS scintillation counters.[1] Preliminary data indicate that within the precision of the measurements, approximately ±5 percent, protons are emitted isotropically from Ni. The distribution from Cu appears to be peaked in the forward direction with a ratio of 1.17 between the number of protons observed at 45 and at 150 degrees. The distribution from Co is similar to that from Cu. Departures from the assumptions of the statistical theory which might account for the observed angular distributions will be discussed.

* Supported in part by a contract with the Air Force.
[1] A. K. Mann and J. Halpern, Phys. Rev. **82**, 733 (1951).

ZB7. (p, n) Yields from the Light Elements. HARVEY B. WILLARD AND JOE KEAGY BAIR, *Oak Ridge National Laboratory*.—The yields of neutrons from the proton bombardment of T, Li^7, Be^9, B^{11}, and F^{19} have been extended with 0.1 percent resolution to 5.3 Mev. The neutrons produced in the forward direction were measured with a conventional "long" counter and monitored by a beam current integrator. T exhibits a gradual increase up to 4.22 Mev, where it rises more rapidly as though approaching a very broad resonance. New maxima were observed in the yield from Li^7 at 4.90 Mev (broad), from Be^9 at 4.72 Mev (broad), and from B^{11} at 3.17, 3.75, 4.14, and 4.67 Mev (all broad). The $F^{19}(p, n)Ne^{19}$ threshold was determined to be 4.253 ± 0.005 Mev and narrow maxima occur at 4.29, 4.46, 4.49, 4.57, 4.62, 4.71, 4.78, 4.99, 5.07, and 5.20 Mev.

ZB8. Disintegration of Helium by 90-Mev Neutrons. P. TANNENWALD, *University of California, Berkeley*.—90-Mev neutrons produced by stripping 190-Mev deuterons in the 184-inch cyclotron were collimated and sent through a 22-inch Wilson cloud chamber filled with helium gas to a total pressure of 81 cm Hg. The chamber was operated in a pulsed magnetic

field of 21,700 gauss. The possible reaction products are: triton-deuteron, 2 deuterons-neutron, triton-proton-neutron, deuteron-proton-2 neutrons, 2 protons-3 neutrons, He^3-2 neutrons, He^4 recoils. The particles from the two-prong stars are identified by curvature and relative ionization, and the single tracks by characteristic track endings when they end in the chamber. For the first three reactions it is possible to calculate, from measured quantities, the energy of the incident neutron. Of the 90 two-prong stars which have been analyzed so far, there are 18 *dt*, 10 *dd*, 47 *pt*, 14 *pd*, 1 *pp*. 59 He^4 tracks ended in the chamber, and 78 other single tracks were observed which did not end. All these events occurred within an angle of $\pm 30°$ to the horizontal plane containing the neutron beam. Relative cross sections and energy and angular distributions will be presented.

ZB9. The Disintegration of He^3 by Deuterons.* A. B. LILLIE, T. W. BONNER, AND J. P. CONNER, *Rice Institute.*—The reaction $He^3(d, p)He^4$ has been studied, when deuterons of energy 200–1600 kev have bombarded a gaseous thin target of He^3. The absolute number of high energy protons which are produced were observed in the direction of the incident deuterons. The curve of the differential cross section for the reaction at 0° shows a peak at 400-kev deuteron energy and a half-width of 500 kev. The differential cross section is 50 millibarns per unit solid angle at 400 kev and drops to 10 millibarns per unit solid angle at 1600 kev. The results indicate an excited level in Li^5 at 18.5 Mev above the ground state.

* Assisted by the AEC.

ZB10. Angular Distribution of α-Particles from $Li^7(t, \alpha)He^6$. T. P. PEPPER, E. ALMQVIST, AND P. LORRAIN,* *Chalk River Laboratories.*—The angular distribution of the α-particle groups from the reactions[1] $Li^7(t, \alpha)He^6$ and $Li^7(t, \alpha)He^{6*}$ are being studied using two end-window proportional counters filled with A and CO_2. One counter, mounted at 90° to the 240-kev mass-3 beam, monitors the yield of α-particles from the target. The second counter can be set to detect α-particles emitted at chosen angles to the beam. By displaying the pulses from this counter on a 30-channel pulse-height analyzer the yields of the two α-particle groups are observed simultaneously at each angle. Measurements have been made from 75° to 135° to the beam in the center-of-mass system. The angular distribution of the α-group associated with the ground state of He^6 is of the form $1-A\cos^2\theta$ with $A\sim 1$, while that of the α-group associated with the excited state of He^6 is nearly isotropic.

* Permanent address: University of Montreal, Montreal, Quebec.
[1] Pepper, Allen, Almqvist, and Dewan, Phys. Rev. **81**, 315(A) (1951).

ZB11. Reactions of 370-Mev Protons with Cobalt.* E. BELMONT† AND J. M. MILLER, *Columbia University.*—Cross sections have been evaluated for the formation of various products resulting from the irradiation of cobalt with 370-Mev protons in the circulating beam of the Columbia University Nevis cyclotron. The elements from scandium to cobalt are formed in greatest yield; total cross sections of the order of 50–80 millibarns have been found for each of these elements by interpolating values for stable isotopes. On the other hand, nuclei such as carbon and sodium are formed with cross sections of the order of 0.05 millibarn. These results are in accord with the hypothesis of nucleon-nucleon interactions leading to the loss of nucleons from the target by "knock-ons" followed by evaporation of particles from a spectrum of residual nuclei with a spectrum of excitation energy. The cross sections for the more probable events are in qualitative agreement with recent measurements on proton induced stars[1] and with Monte Carlo[2] and evaporation theory[3] calculations.

* Work performed under the auspices of the AEC.
† AEC Predoctoral Fellow.
[1] L. Germain, Phys. Rev. **82**, 596 (1951).
[2] Bernardini, Booth, and Lindenbaum, Phys. Rev. **83**, 669 (1951).
[3] K. Le Couteur, Proc. Phys. Soc. (London) **A63**, 259 (1950).

ZB12. Gamma-Ray Resonances in the Proton Bombardment of Mg^{26}.* WARREN E. TAYLOR, L. N. RUSSELL, JOHN N. COOPER, AND J. C. HARRIS, *Ohio State University.*—Thin targets of Mg^{26} of relatively high purity[1] were formed on a tantalum backing by decomposition of heated MgO in a vacuum. An electrostatic generator provided protons in the energy range between 300 and 1200 kev. Presumably there was induced the reaction $Mg^{26}(p, \gamma)Al^{27}$, which has a calculated Q of approximately 7.5 Mev. The relative yield of gamma-rays per proton indicates well-resolved maxima for incident proton energies of 339, 449, 660, 726, 812, 843, 952, 986, 1011, 1053, and 1183 kev. These values are uncorrected for target thickness, estimated to be 15 kev at one Mev. The error is probably less than 10 kev throughout the range covered. The first two values agree well with two resonances previously reported by Tangen[2] at 336 and 451 kev. There is some evidence for other levels of low intensity in this same region.

* Assisted by a contract between the AEC and the Ohio State University Research Foundation.
[1] Supplied by the Carbide and Carbon Chemical Division, Oak Ridge National Laboratory.
[2] R. Tangen, Kgl Nord. Vid. Selsk. Skr. NR 1 (1946).

ZB13. Excited States of P^{32} from the $P^{31}(d, p)P^{32}$ Reaction.* D. M. VAN PATTER, P. M. ENDT,† A. SPERDUTO, AND W. W. BUECHNER, *M.I.T.*—The $P^{31}(d, p)P^{32}$ reaction has been investigated by means of magnetic analysis of the protons emitted from thin targets containing phosphorus bombarded by 1.8- and 2.0-Mev deuterons. Sixteen of the proton groups observed have been assigned to the $P^{31}(d, p)P^{32}$ reaction, corresponding to the ground state and fifteen excited states of P^{32}, in a region of excitation from zero to 4.3 Mev. The position of the first excited state of P^{32} has been measured as 77.0 ± 1.7 kev. Three other pairs of closely spaced levels were observed. These occurred at 2.2-, 2.7-, and 3.3-Mev excitation with spacings of 50 ± 2, 92 ± 7, and 59 ± 3 kev, respectively. Because of the presence of contaminant groups, it is possible that some $P^{31}(d, p)P^{32}$ groups were missed, corresponding to states in a region of excitation from 3.3 to 4.3 Mev. The nucleus P^{32} appears to have a large number of low-lying states, with the first level very near to the ground state.

* This work has been assisted by the joint program of the ONR and AEC.
† Now at the University of Utrecht, The Netherlands.

ZB14. Neutrons from the Disintegration of Phosphorus by Deuterons.* S. C. SNOWDON, *Bartol Research Foundation.*—The neutron spectrum at 0° and at 90° from the $P^{31}(d, n)S^{32}$ reaction has been investigated using nuclear emulsions. A ground-state Q value of 6.3 ± 0.2 Mev has been found and is in rough agreement with the latest evaluation of the masses of the nuclei involved. The Q values corresponding to the excited states in S^{32} are 5.7, 5.05, 4.2, 3.7, 3.15, 2.5, 1.7, 1.1, 0.5, and 0.05 Mev, each with an uncertainty of about 0.2 Mev.

* Assisted by the joint program of the ONR and AEC.

ZB15. Excited States of Mg^{25} from the $Al^{27}(d, \alpha)Mg^{25}$ and $Mg^{24}(d, p)Mg^{25}$ Reactions.* P. M. ENDT,† H. A. ENGE,‡ J. HAFFNER, AND W. W. BUECHNER, *M.I.T.*—The alpha-particle groups from thin aluminum targets bombarded with 1.8-, 2.0-, and 2.1-Mev deuterons have been studied with the M.I.T. high resolution magnetic spectrograph. Eleven of these groups have been assigned to the $Al^{27}(d, \alpha)Mg^{25}$ reaction, corresponding to the ground state and ten excited states of Mg^{25} in a region of excitation from zero to 4.0 Mev. The proton groups from a thin natural magnesium target were also studied at deuteron bombarding energies of 1.5, 1.8, and 2.0 Mev. Eleven of the observed proton groups could be assigned to the $Mg^{24}(d, p)Mg^{25}$ reaction, corresponding to the transition to the ground state of Mg^{25} and the same ten excited levels found from the $Al^{27}(d, \alpha)Mg^{25}$ reaction. The excited states in Mg^{25}

found from these two reactions are at 0.583, 0.976, 1.611, 1.957, 2.562, 2.736, 2.799, 3.405, 3.898, and 3.969 Mev.

* This work has been assisted by the joint program of the ONR and AEC.
† Now at the University of Utrecht, The Netherlands.
‡ On leave from the University of Bergen, Norway.

ZB16. Energy Levels in Mn^{53} from Scintillation Studies of $Cr^{53}(p, n, \gamma)Mn^{53}$.* CLYDE L. MCCLELLAND, CLARK GOODMAN, AND PAUL H. STELSON, *M.I.T.*—A single crystal NaI(Tl) scintillation spectrometer was used to determine the gamma-spectrum from $Cr^{53}(p, n, \gamma)Mn^{53}$ at several proton energies, $E_p > 1.406$ Mev, the reaction threshold.[1] The instrument was calibrated with the gammas from Cs^{137} (0.669 Mev) and Na^{22} (1.277 and 0.511 Mev). A target of chromium,[2] enriched to 90.06 percent Cr^{53} and approximately 25 kev thick was bombarded with protons from the Rockefeller electrostatic generator. The energies of the gammas observed are:

E_p (Mev)	Gamma-Energy (Mev ±2 percent)
1.75	none
2.00	0.385
2.40	0.385
2.90	0.385, 0.88, 1.27

These gammas are interpreted as resulting from two excited levels in the residual Mn^{53} nucleus, located at 0.385 and 1.27 Mev. Experiments are in progress to determine the relative intensities. Formation of twenty-five minute I^{128} in the crystal from neutron capture is observed at the higher proton energies. This technique supplements the laborious measurements of recoil protons in emulsions to determine the neutron groups.

* Work jointly supported by ORN and BuShips.
[1] Lovington, McCue, and Preston (to be published).
[2] Oak Ridge analysis of enriched Cr^{53}: 90.06 percent Cr^{53}, 0.465 percent Cr^{54}, 0.193 percent Cr^{52}, 9.28 percent Cr^{53}.

SATURDAY AFTERNOON AT 2:00

Havemeyer 309

(M. GOLDHABER presiding)

Radioactive Nuclei

ZC1. *K*-Capture and Positron Emission in Zn^{65}. J. K. MAJOR, *Institut du Radium and Collège de France, Paris.*—The radiations from 250-day Zn^{65} have been studied with a variable-pressure cloud chamber,[1] and Geiger-Müller counters in coincidence, calibrated using standards of RaD+E+F and Fe^{55}, and $\beta\gamma$-coincidences with Na^{22}, Na^{24}, Co^{60}, and Au^{198}. Absorption between source and counters was minimized by evacuating to 10^{-3} mm Hg, and the β, X, and γ-ray components evaluated using a magnetic field and critical absorption in iron foils. $X\gamma$ coincidences show that 55.2±2.1 percent of the K-captures go to the ground state, and absolute counting gives 2.5±0.1 percent for the fraction of all disintegrations by β^+ emission, confirming earlier results.[2] Contrary to other findings,[3] no $\beta\gamma$-coincidences were observed; if the β spectrum is simple, β^+ emission to an excited state is excluded by the energy available for the transition. The branching ratio of K-capture to positron emission (to the ground state only) was 25±10 from cloud-chamber observations and 21.3±1.4 from counting, consistent with other values. Agreement with the Fermi theory is best for a second-forbidden transition ($\Delta J = 1$, $\Delta L = 2$), confirmed by the ft value, but interpretation in terms of the shell model leads to certain difficulties.

[1] F. Joliot, J. phys. et radium (VII) **5**, 216–218 (1934).
[2] W. M. Good and W. C. Peacock, Phys. Rev. **69**, 680 (A) (1946); L. R. Zumwalt, Plut. Proj. Rec. Mon-N-432, 54 (1947).
[3] Watase, Itoh, and Takeda, Proc. Phys.-Math. Soc. Japan **22**, 90–105 (1940); R. A. Cohn and J. D. Kurbatov, Phys. Rev. **78**, 318 (A) (1950).

ZC2. Radioisotopes of Bromine. S. C. FULTZ AND M. L. POOL, *Ohio State University.*—Natural Se and Se enriched with Se^{78} were bombarded with 7.3-Mev protons and 10-Mev deuterons. The radiations of Br^{82}, Br^{80}, Br^{77}, Br^{76}, and Br^{75} have been examined by use of a 180° focusing spectrometer and coincidence methods. Br^{82} emits a simple negatron spectrum with a maximum energy of 0.94±0.02 Mev. The ground state of Br^{80} emits a complex negatron spectrum having components: 1.97±0.03 Mev (82 percent), 0.86 Mev (10 percent), 0.56 Mev (8 percent). The gamma-rays of Br^{77} are associated with the K-capture process. The 17.2-hour activity recently found in bromine and assigned to Br^{76} emits, from its ground state, positrons having a complex spectrum with components 3.57±0.07 Mev (46 percent), 1.66 Mev (10 percent), 1.13 Mev (11 percent), 0.80 Mev (14 percent), 0.63 Mev (19 percent). Gamma-rays identified with Br^{76} have energies of 0.25, 0.33, 0.37, 0.42, 0.68, 0.75, 0.96, and 1.2 Mev. The ground state of Br^{75} decays by emission of positrons having a complex spectrum with components: 1.70±0.02 Mev (46 percent), 0.80 Mev (20 percent), 0.58 Mev (15 percent), 0.33 Mev (19 percent).

ZC3. Characteristic Radiations of Zr^{97} and Nb^{97}.* C. E. MANDEVILLE, E. SHAPIRO, R. I. MENDENHALL, E. R. ZUCKER,† AND G. L. CONKLIN, *Bartol Research Foundation.*—$Zr^{96}O_2$ (isotopic concentration 90 percent) was irradiated by slow neutrons in the Oak Ridge pile. The half-period of the niobium daughter element, chemically separated from zirconium, was found to be 72.1±0.7 minutes and that of Zr^{97} to be 17.0±0.2 hours. By aluminum absorption and Feather analysis, maximum beta-ray energies of 2.50 Mev and 1.40 Mev were measured for parent and daughter element, respectively. Lead adsorption of the quantum radiations of the equilibrium mixture indicated a gamma-ray at 0.74 Mev as well as a softer component. Coincidence absorption yielded a maximum gamma-ray energy of 1.42 Mev. The beta-gamma coincidence rate of Nb^{97} was constant, independent of the beta-ray energy and of such magnitude as to suggest that each beta-ray is followed on the average by 0.7 Mev of gamma-ray energy. The beta-gamma coincidence rate of the equilibrium mixture showed that the hard beta-rays of Zr^{97} proceed directly to the metastable state of Nb^{97}. Very few beta-rays of Zr^{97} are coincident with any gamma-radiation. A disintegration scheme will be proposed.

* Assisted by the joint program of the ONR and AEC.
† Frankford Arsenal.

ZC4. The Beta-Spectrum of Tc^{99}. FRANK WAGNER, JR., AND MELVIN S. FREEDMAN, *Argonne National Laboratory.*—A thin (95 $\mu g/cm^2$) uniform sample, prepared by volatilization of NH_4TcO_4 in vacuum onto a 150 $\mu g/cm^2$ aluminum support, was examined in a double lens spectrometer at 4 percent resolution. The Kurie plot, corrected by C_{FT}[1] with $|A_{ij}|^2/|T_{ij}|^2 = 6.60$ and with $|\int \sigma \cdot r|^2 = 0$ is quite straight from $E_0 = 296$ kev down to 60 kev, and definitely does not fit

the α-shape.[2] The contribution of backscattering from the aluminum foil was assayed by a comparison of the spectrum of Pm^{147}, also prepared by a vacuum volatilization technique using the trifluoro-acetyl acetonate, onto a 10 $\mu g/cm^2$ LC-600 film, with an added aluminum foil backscatterer. Without backscatterer present the Pm spectrum is linear from $E_0 = 227$ kev to 10 kev; with backscatterer, to 60 kev, deviating upwards by 6 percent at 30 kev. Application of the ratio as a correction to Tc^{99} extends the straight line to ~35 kev. These results are in agreement with the shell model[3] assignment for this transition, $g_{9/2} - d_{5/2}$, and furnish, together with the high energy transition in Cs^{137},[4] a second confirmation for a predominantly tensor interaction on the basis of spectral shape.

[1] Nakamura, Umezawa, and Takebe, Phys. Rev. **83**, 1273 (1951).
[2] S. I. Taimuty, Phys. Rev. **81**, 461 (1951); Wu and Feldman, Phys. Rev. **82**, 332 (1951).
[3] Mayer, Moszkowski, and Nordheim, ANL-4626 (May, 1951).
[4] Langer and Moffat, Phys. Rev. **82**, 635 (1951); also confirmed by the authors (to be published).

ZC5. The Angular Correlation of the Pd^{106} Gamma-Rays.* ROLF M. STEFFEN, *Purdue University*.—A possible explanation of the observed angular correlation of the Pd^{106} gamma-rays is the reduction of the correlation because of the magnetic field of the atomic shell. The ground state of the Pd^{106} atom however is a $^1S_0$-state, hence the atom must be highly excited or ionized in order to disturb appreciably the orientation of the nucleus during the rather short lifetime (~10^{-11} sec) of the intermediate state. By embedding the decaying atoms in metals and in ionic crystals, it should be possible to change the correlation reducing effects in Pd^{106}.[1] Rh^{106} "metal sources" were prepared by electroplating the parent Ru^{106} with and without excess of Ag. In both cases the angular correlation was found to be the same within 2 percent as the one measured with a $RuCl_3$ source, whereas In^{111} sources prepared in exactly the same way exhibited both a maximum anisotropy of (18 ± 2) percent as compared to (7 ± 2) percent measured with $InCl_3$ sources. Sources in which the Rh^{106} formed a lattice defect in ionic crystals (AgCl, NaCl) showed no change in angular correlation, whereas with In^{111} sources prepared in a similar way a maximum anisotropy of (2 ± 2) percent was found. The results obtained with the In^{111} sources confirm the correlation measurements reported by Frauenfelder *et al.*[1]

* Work supported by the AEC.
[1] Frauenfelder *et al.*, Phys. Rev. **82**, 549 and 550 (1951).

ZC6. Excitation of Metastable Cd^{111} by Inelastic Scattering of Neutrons.* J. J. G. MCCUE, A. E. FRANCIS, AND CLARK GOODMAN, *Massachusetts Institute of Technology*.—We have studied the formation of metastable Cd^{111}, with 49-minute half-life,[1] by inelastic scattering of nearly monoergic neutrons. The plot of cross section *vs* neutron energy is concave toward the energy axis. The threshold is at 400 ± 20 kev; at 720 ± 20 kev, and 1150 ± 20 kev, there are cusps indicating excitation of higher levels. The threshold agrees with the excitation energy of the metastable state, known from conversion-electron spectra to be 396 kev.[2] The level at 1150 is perhaps the one reported at 1250 kev by Wiedenbeck[1] on the basis of electron bombardment; the 720-kev level is new. At 1350 kev, the cross section is 13.0 times as large as it is at 580 kev, where it has a local maximum. A preliminary measurement shows that the cross section at 1350 kev is roughly 0.4 barns, with a probable error estimated as a factor 2. A more precise measurement of the absolute cross section is in progress.

* Work jointly supported by the ONR and BuShips.
[1] M. L. Wiedenbeck, Phys. Rev. **67**, 92 (1945).
[2] Helmholz, Hayward, and McGinnis, Phys. Rev. **75**, 1469 (1949).

ZC7. The Spins of the Excited States of Cd^{114}.* M. W. JOHNS, C. D. COX, AND C. C. MCMULLEN, *McMaster University*.—The gamma-gamma angular correlation function for the 552- and 722-kev gamma-rays of In^{114} has been determined using anthracene crystals with a coincidence circuit of resolution 5×10^{-9} sec.[1] The data are well represented by the equation $W(\theta)/W(\pi/2) = 1 - 0.005\cos^2\theta + 0.197\cos^4\theta$. This function, which is quite similar to the 0-2-4 correlation[2] can be uniquely described in terms of a 0-2-2 cascade in which the 2-2 transition is a mixture of M.D. (86 percent) and E.Q. (14 percent) radiation together with a 66° phase shift. By studying the photoelectrons ejected from a lead radiator, the relative intensity of the 1.27-Mev crossover transition has been measured as 3 percent of the cascade gammas. This intensity is consistent with the 0-2-2 but not with the 0-2-4 spin assignment. From the number of coincidences at the 180° position, it is possible to set an upper limit to the number of positrons at 5×10^{-6} per β^- disintegration.[3]

* Assisted by the National Research Council of Canada.
[1] Petch and Johns, Phys. Rev. **80**, 478 (1950).
[2] Steffen, Phys. Rev. **83**, 166 (1951).
[3] Boehm and Preiswerk, Helv. Phys. Acta, **22**, No. 3, 331 (1949).

ZC8. The Decay of the Metastable State in In^{115}.* L. M. LANGER, R. D. MOFFAT AND G. A. GRAVES, *Indiana University*.—Using the large high resolution magnetic spectrometer, a precise measurement was made on the internal conversion electrons in the transition from the 4.5 hour metastable state of In^{115}. For this purpose, the activity was grown and extracted from the 54.0 hour Cd^{115} parent, which had been produced by deuteron bombardment in the cyclotron. The energy of the transition is 333.7 kev. The $K/L+M$ conversion ratio was found to be 3.76. This value is somewhat less than one might expect from the empirical curve[1] for a $M4$ transition. From spectrometer measurements made with a source in secular equilibrium with the 54-hour Cd^{115}, prepared by neutron capture† in enriched (94.2 percent) Cd^{114}, the total internal conversion coefficient is found to be 0.98 and the K conversion coefficient is 0.64. The 0.84-Mev beta-branch to Sn^{115} accounts for 5.5 percent of the transitions. The 54.0-hour Cd^{115} feeds the metastable level of In^{115} via two beta-groups with end points of 1.11 Mev (58 percent) and 0.58 Mev (42 percent).

* Assisted by a grant from the Frederick Gardner Cottrell Fund of the Research Corporation and by the joint program of the ONR and AEC.
[1] M. Goldhaber and A. W. Sunyar, Phys. Rev. **83**, 906 (1951).
† In the Los Alamos nuclear reactor.

ZC9. The Beta-Spectrum of 2.3-Year Cs^{134}. F. H. SCHMIDT AND G. L. KEISTER, *University of Washington*.—The electron radiations resulting from the decay of Cs^{134} have been studied in a high resolution solenoidal spectrometer. Conversion electrons have been observed from seven gamma-rays; *viz.*, 561.5 ± 1.0, 566.5 ± 0.8, 601.2 ± 0.5, 793.1 ± 0.7, 1037.2 ± 2.6, 1164.4 ± 2.9, and 1365.7 ± 3.3 kev. The two lowest energy gammas, whose ratio of K electron intensities is ~0.5, correspond to the single gamma-ray found by other workers.[1] The three high energy lines are very weak; the measured K-L differences do not exclude conversion in Xe, but indicate that conversion is more probably occurring in Ba. There is no evidence of a contaminant. The continuous spectrum shows some indication of two high energy components whose end points differ by 30–40 Kev. The end point of the low energy branch (~24 percent) is ~79 kev. On the basis of these energies and other data,[2] a fairly consistent scheme for Ba^{134} can be constructed with levels at 793, 1359, 1394, and 1955 kev. The K internal conversion coefficients for the 793 and 601 gammas can be found with reasonable certainty; *viz.*, 2.1 ± 0.2 and $5.7 \pm 0.5 \times 10^{-4}$, respectively. Coefficients for the 561 and 566 depend strongly upon which is associated with the low energy beta-branch. The role of the 1037 gamma is very uncertain. Partial support of the AEC is acknowledged.

[1] Waggoner, Moon, and Roberts, Phys. Rev. **80**, 420 (1950).
[2] Elliot and Bell, Phys. Rev. **72**, 979 (1947).

ZC10. Beta-Spectra of Ce^{144} and Pr^{144}. CHENG, LIN-SHENG, G. JOHN, AND J. D. KURBATOV, *Ohio State University*.—Ce^{144},

$T_{\frac{1}{2}}$~275 day, carrier free fission product, was aged and purified partly without addition of carrier and partly with addition of carrier. The beta-spectra of these two samples were studied with a solenoidal spectrometer. Three beta-spectra were identified in Pr^{144} and two beta-spectra in Ce^{144}. The beta spectra of Pr^{144} are with upper energy limits 3.00±0.06 Mev, 1.30±0.02 Mev and 605±8 kev. Their relative intensities have been estimated to be 85±5 percent, 12±2 percent, 3±1 percent. The beta-spectra of Ce^{144} have upper energy limits 446±8 kev, 307±6 kev and relative intensities 3±1 percent, 97±1 percent. The partial half-lives calculated from the relative intensities are compatible with the *ft* values estimated from degree of forbiddenness, except in the case of the 605-kev beta-spectrum. The conversion lines of low energy gamma-rays were observed. They were identified as the *L*-line of 54.7±0.5 kev, *K* and *L* lines of 79.4±0.8 kev, 134±1 kev, and 231±2 kev gamma-rays. The *K*/*L* ratios of the latter three were estimated to be 6.3±0.7, 8.3±0.6, 1.7±0.3, respectively.

ZC11. The Decay Scheme and Angular Correlation of Pr^{144}.* D. E. Alburger and J. Kraushaar, *Brookhaven National Laboratory.*—Beta-rays of maximum energy 2.965±0.015 Mev (90 percent), 2.3±0.1 Mev (~5 percent), and 0.86±0.1 Mev (~5 percent) have been found in the decay of 17-min Pr^{144} with a lens spectrometer. Gamma-rays of 0.695±0.005 Mev, 1.48±0.01 Mev, and a cross-over of 2.185±0.015 Mev with relative intensities of 1:0.4:1.1, respectively, are associated with this activity. Coincidences between gamma-rays are present and exhibit an angular correlation of the form $1-0.33\cos^2\vartheta$ characteristic of either a 1-1-0 or a 1-2-0 cascade. A decay scheme is proposed in which the first excited state of Nd^{144} is at 0.695 Mev and has spin 2 and even parity. The second level at 2.185 Mev has spin 1 and even parity. All beta-transitions are allowed by selection rules if Pr^{144} is assigned spin 1 and even parity. The 300-kev beta-spectrum and internal conversion lines of a 135-kev gamma-ray in the decay of the mother 282-day Ce^{144} have been observed. This high yield fission-product isotope is suggested as a useful reasonably long-lived source of homogeneous photo-neutrons from Be in which the gamma-ray occurs in about 3 percent of beta-decays.[1] The authors are indebted to S. Katcoff for chemical purification of the beta-source.

* Research carried out under contract with the AEC.

[1] Alburger, der Mateosian, Goldhaber, and Katcoff, Phys. Rev. **82**, 332(A) (1951).

ZC12. Europium 148 and 150. Rex C. Mack, Donald I. Prickett, and M. L. Pool, *Ohio State University.*—Bombardments of the enriched isotopes of Sm^{148}, Sm^{149}, and Sm^{150} have given rise to two new and well-defined activities, one with half-life of 13.1-hours, and one with half-life of 58.6-days. The 13.1-hour activity was shown to be a negative beta-activity with complex spectrum, the main component of the spectrum having an end point of approximately 0.85 Mev. This activity is assigned to Eu^{150} and the assignment leads to the prediction that Gd^{150} has a half-life of 10^4 years or longer. The 58.6-day activity, which consisted primarily of electromagnetic radiation, decayed by *K*-electron capture. This activity is assigned to Eu^{148}. Gamma-rays of 0.69 Mev and internal conversion electrons were observed in connection with the activity.

ZC13. Experimental Determination of *K*/*L* Ratios for $_{71}Lu^{173}$ and $_{21}Sc^{48m}$ (20 Seconds). S. B. Burson and W. C. Rutledge, *Argonne National Laboratory.*—Neutron activation of $_{72}Hf^{174}$ produces 70-day $_{72}Hf^{173}$, which decays by *K*-capture to $_{71}Lu^{173}$. In addition to the four γ-rays of 0.089, 0.113, 0.228, and 0.342 Mev reported,[1] two more of 0.318 and 0.431 Mev are found to be associated with $_{71}Lu^{173}$. These are shown to be consistent with the proposed energy level scheme. By use of both the 180° β-ray spectrometer and the photographic spectrograph, *K*/*L* ratios were measured for most of the lines. The type of radiation is suggested for each γ-ray, and spin and parity changes are assigned. To compare the two methods of measurement, the highly converted 0.342 Mev γ-ray was used. A *K*/*L* ratio of 4.95±0.25 was determined from area measurements of photodensitometer traces of the plates and found to be in good agreement with a value of 4.93±0.20 determined from the spectrometer momentum plot. Thus, the photographic method, when properly calibrated, provides a reliable means of *K*/*L* ratio determination for activities too short-lived to be measured by other methods. The isomeric transition in $_{21}Sc^{48m}$ (20 seconds) was measured as 0.142 Mev. A *K*/*L* ratio of 10±3 is determined from the plate.

[1] Burson, Blair, Keller, and Wexler, Phys. Rev. **83**, 62 (1951).

ZC14. Radiations of Th^{231}(UY). M. S. Freedman, F. Wagner, Jr., A. H. Jaffey, and J. May, *Argonne National Laboratory.*—The electron spectrum of Th^{231}(UY) was examined on our double lens spectrometer with a resolution of 3 percent. The samples were separated carrier-free from isotopically pure U^{235} by solvent extraction. Sample thickness in order of 50 $\mu g/cm^2$ mounted on about 10 $\mu g/cm^2$ film was employed. We find three β-components with maximum energies 302 kev (44 percent), 216 kev (11 percent), and 93 kev (45 percent) and 19 conversion lines assignable to gammas of 208, 167, 107, 85, 63, 59, and 22 kev. Each of these gammas was directly observed on a scintillation spectrometer using thalliated sodium iodide. The less intense gammas were emphasized experimentally with respect to the strong 59-, 63-, and 85-kev gammas by the use of absorbers. An additional gamma of 122 kev was observed only in the scintillation spectrometer. A decay scheme will be presented.

SUPPLEMENTARY PROGRAMME

SP1. Theory as Organization of Observation. JEROME ROTHSTEIN, *Signal Corps Engineering Laboratories.**—Define organization for elements individually associated with characteristic sets of alternatives as the excess in entropy of the ensemble of distinguishable alternatives of the composite system computed for independent elements over the entropy of the set of alternatives when the correlations (constraints, interactions, controls, instructions) characterizing the organized system are operative. Define organizational redundancy as the excess of maximal organization consistent with the alternatives required of the system over actual organization present. Organization is then information (as in communication) or negative entropy (as in physics), and provides a rational basis for system engineering design. Measurement yields an ensemble of alternative possible results for which an entropy can be defined.[1] A theoretical law or relationship is a correlation between ensembles corresponding individually to various measurements and therefore constitutes organization of the system consisting of these ensembles according to the above definition. Theory strives to maximize organization of observation. Of two theories giving equally good representations of a given ensemble of observations the "simpler" is preferred, i.e., the one which is less redundant.

* To be called for at the end of Session V if the Chairman rules that time permits.
[1] J. Rothstein, Science **114**, 171 (1951).

SP2. Information, Thermodynamics, and Time. JEROME ROTHSTEIN, *Signal Corps Engineering Laboratories.**—The communication-measurement analogy[1] yields an informational conception of the first law leading to Caratheodory's form of the second law and interpretation of entropy as missing information without appeal to statistical concepts. The third law is trivially true. Irreversibility of measurement is equivalent to the second law. The positive time direction is distinguished as that permitting information to be acquired (measurements made) about a system of interest (e.g., clock) or equivalently as characterized by entropy increase (information loss) in the wider totality of system of interest plus means of observation. At equilibrium entropy is maximum, no information can be obtained, and symmetry obtains between past and future. For a pure case entropy is zero, no nonredundant information is obtainable without converting the pure case to a mixture, and perfect reversibility again holds; similarly for classical mechanics. Time direction is well defined only for nonequilibrium. Irreversibility of measurement is fundamentally phenomenological rather than quantal in origin.

* To be called for at the end of Session V if the Chairman rules that time permits.
[1] J. Rothstein, Science **114**, 171 (1951).

SP3. On the Boundary Layer Theory in Hypersonic Flow in Rarefied Gases. M. Z. v. KRZYWOBLOCKI, *University of Illinois* (Introduced by Charles Fletcher).*—Equations of motion consisting of the first three approximations developed by the kinetic theory of nonuniform gases are assumed to correctly describe the motion in hypersonic flow in rarefied gases. The kinetic theory of gases gives in addition to known terms in Navier-Stokes equations higher order terms which represent complicated additional stresses and heat flux in the equations of motion and energy. The paper analyses the boundary layer equations in a two-dimensional flow under the assumption that higher order terms should be considered. A new method of solving the complicated system of partial differential equations is derived. By a suitable transformation the foregoing set is transformed into a set of ordinary differential equations with the preservation of a quasi-one-to-one relation. In the final step differential analog must be used.

* To be called for at the end of Session L if the Chairman rules that time permits.

Author Index to Papers Presented at the Annual Meeting

Adams, R. V., Dorothy Montgomery Hirshfelder, J. A. Northrop, and N. R. Whetten—F4
Ahrens, T. and E. Feenberg—P5
Alburger, D. E. and J. Kraushaar—ZC11
Allis, W. P.—K1
Anderson, James L.—I13
Annis, M. and H. S. Bridge—F8
Annis, Martin, Herbert S. Bridge, and Stanislaw Olbert—F10
Anslow, Gladys A. and Irene S. White—E9
Antonoff, G., A. Yakimac, A. Urmancry, and R. Madrazo, Jr.—D9
Arfken, G. B., L. C. Biedenharn, and M. E. Rose—V1
Bainbridge, K. T.—A1
Ballam, J.—G8
Barbour, Ian—G7
Bartholomew, G. A. and B. B. Kinsey—N5
Bartnoff, Shepard and Charles R. Mingins—SB5
Beach, W. H., W. J. Childs, P. V. C. Hough, J. S. King, and W. C. Parkinson—B2
Beams, J. W.—Q2
Beiser, Arthur—F7
Belinfante, F. J.—I8
Belmont, E. and J. M. Miller—ZB11
Benedict, T. S. and W. M. Woodward—ZB3
Bergmann, Peter G. and Ralph Schiller—V9
Beringer, R. and E. B. Rawson—O8
Berko, Stephan—J9
Bernstein, W., R. L. Chase, M. Slavin, J. Garfield, and A. W. Schardt—B13
Bersohn, R., J. Weneser, and N. M. Kroll—I7
Betchov, Robert—L6
Biedenharn, L. C., Keith Boyer, and R. A. Charpie—V2
Biondi, M. A.—R1
Bitondo, D., I. I. Glass, and G. N. Patterson—L11
Blair, J. S. and B. Segall—Y8
Blatt, John M.—P8
Bleakney, Walker—Q3
Block, M. M., W. W. Brown, and G. G. Slaughter—B7
Bogdonoff, S. M. and A. H. Solarski—L9
Bonner, T. W.—X3
Borkowski, C. J. and R. L. Clark—B8
Borsellino, A.—I10
Borst, Lyle B.—SB1
Bowman, Mark, Jr., and H. L. Smith—W8
Branscomb, Lewis M.—E6
Brown, A., M. W. Zemansky, and H. A. Boorse—ZA4
Brown, D. E. and W. C. Dunlap, Jr.—SC9
Brown, Fielding, R. Ronald Rau, George T. Reynolds—G6
Brueckner, Keith A.—Y9
Buechner, W. W.—X4
Burk, D. and F. Darnell—ZA6
Burson, S. B. and W. C. Rutledge—ZC13
Burstein, E., P. L. Smith, and J. W. Davisson—SC6
Carr, W. J.—J10
Carroll, Thomas J.—SB8
Cheng, Lin-sheng, G. John, and J. D. Kurbatov—ZC10
Clark, Donald L.—M5
Clark, M. A.—F5
Cleland, M. R. and H. W. Koch—E12
Combes, Lewis S., Stanley S. Ballard, and Kathryn A. McCarthy—W10
Coryell, Charles D. and Hans E. Suess—P4
Cowie, D. B., N. P. Heydenburg, G. M. Temmer, and C. A. Little, Jr.—H6
Crocco, L. and L. Lees—C1
Crosbie, Edwin A.—P11
Dank, M. and H. B. Callen—W3
Daunt, J. G. and C. V. Heer—ZA3
Daunt, J. G., T. S. Tseng, and C. V. Heer—ZA2
Davidson, Jack P.—P6
Davis, Marguerite—SA7
Dean, Christopher—O9
Demos, P. T., J. D. Fox, I. Halpern, and J. Koch—N11
Dresden, M.—ZA1
Dudziak, Walter F.—M6
Dunlap, W. C., Jr.—SC8
Endt, P. M., H. A. Enge, J. Haffner, and W. W. Buechner—ZB15
Engel, Olive G.—T7
Ewen, H. I.—Z1
Fabricand, B. P., R. O. Carlson, C. A. Lee, and I. I. Rabi—O7
Feld, B. T.—P3
Feldman, M., W. Goeddel, and G. J. Dienes—W6
Fermi, Enrico—S3
Ferri, A.—C2
Feshbach, H.—A3
Foldy, L. L.—Y10
Freier, G. D., W. R. Stratton, R. J. S. Brown, H. D. Holmgren, and J. L. Yarnell—H3
Friedman, M. H.—Y4
Freedman, M. S., F. Wagner, Jr., A. H. Jaffey, and J. May—ZC14
Fultz, S. C. and M. L. Pool—ZC2
Gallar, Norman M. and Earle K. Plyler—E4
Garrett, Milan W.—SB2
George, E. P.—F11
Geschwind, Stanley—U1
Goldberg, Joshua and Ralph Schiller—V8
Goldgraber, Howard D.—E8
Goldman, J. E.—J11
Good, R. H., Jr.—V3
Gora, E.—I14
Green, A. E. S., N. Engler, and N. J. Marucci—P2
Green, Alex E. S.—I12
Green, Melville S.—V13
Greenberg, J. Mayo—P10
Griest, Edward M., Wayne Webb, and Robert W. Schiessler—SA3
Guderley, G.—C3
Guernsey, G. L.—H8
Guier, W. H. and A. J. F. Seigert—I9
Hafner, E. M., D. H. Frisch, C. E. Falk, T. Coor, and W. F. Hornyak—H7
Hall, R. N.—K3
Hanson, A. O., E. L. Goldwasser, and F. E. Mills—T5
Hardy, W. A., G. Silvey, and C. H. Townes—O10
Harrison, F. B., J. W. Keuffel, T. N. K. Godfrey, and Geo. T. Reynolds—T2
Harth, E. M., F. E. Froehlich, and K. Sitte—G1
Harvey, J. A., M. D. Goldberg, and D. J. Hughes—N1
Havens, W. W., Jr.—X2
Henderson, R. E. and N. S. Gingrich—D6
Henry, Warren E.—ZA9
Herzberg, G. and D. A. Ramsay—E5
Hidnert, Peter—J3
Hill, John J. and Jack Aron—SC7
Hofmann, J. A. and K. Strauch—N9
Hoffman, R. E.—D7
Hough, P. V. C.—B1
Hughes, D. J.—N13
Hults, M. and S. Mrozowski—E7
Hutchinson, Franklin—SA8
Intrater, J., L. C. Chang, and T. A. Read—J4
Jablonski, F. E., B. Waldman, and W. C. Miller—T6
Jacobs, Donald H. and Seymour Scholnick—SB7
Jacobs, Harold and John Freely—D2
Jacobsohn, B. A.—Y7
Javan, A. and C. H. Townes—O12
Johns, M. W., C. D. Cox, and C. C. McMullen—ZC7
Johnston, R. W. and D. H. Tomboulian—E10
Jurney, E. T. and C. W. Zabel—H11
Karp, Samuel N.—E2
Karzmark, C. J., R. W. Thompson, and Hans O. Cohn—G9
Keck, James and Raphael Littauer—M1
Kennedy, J. M.—T3
Keuffel, J. W., F. B. Harrison, T. N. K. Godfrey, and Geo. T. Reynolds—T1
Kikuchi, C., V. W. Cohen, and John Turkevich—O13
King, Gilbert W. and A. G. Emslie—E1
Kleinman, David A.—W2
Knowlton, Ansel Alphonse—S2
Korff, S. A.—R3
Krafft, J. M.—J6
Kraybill, Henry L.—G3
Kreger, W. E., R. O. Kerman, and W. K. Jentschke—H5
Krohn, V. E., Jr., and E. F. Shrader—ZB2
Krueger, G. C. and C. W. Miller—W9
Kusch, P.—R2
Landon, H. H. and V. L. Sailor—N7
Langer, L. M., R. D. Moffat, and G. A. Graves—ZC8
Laughlin, R. D.—W11
Lauritsen, C. C.—S1
Lax, Benjamin and J. R. Terrall—I3
Lax, Melvin—W14
Leavitt, C. P.—M12
Lee, C. A., R. O. Carlson, B. P. Fabricand, and I. I. Rabi—O6
Lees, L. and R. F. Probstein—L3
Lehovec, K., C. A. Accardo, and E. Jamgochian—SC5
Levinger, J. S.—H1
Lévy, Maurice M.—V11
Lewis, H. W.—Y6
Lillie, A. B., T. W. Bonner, and J. P. Conner—ZB9
Linsley, John and E. P. Ney—G14
Livingston, Ralph—Z2
Logan, John K.—J8
Lomont, J. S.—I11
Lundby, A., E. Fermi, H. L. Anderson, D. E. Nagle, and G. Yodh—M8
MacArthur, J. W.—SC3
Mack, Rex C., Donald I. Prickett, and M. L. Pool—ZC12
Major, J. K.—ZC1
Malkin, M. S.—D5
Mandeville, C. E., E. Shapiro, R. I. Mendenhall, E. R. Zucker, and G. L. Conklin—ZC3
Marshall, John—B5
Martin, Jack—D1

Martin, R. L., H. L. Anderson, and G. Yodh—M13
Marton, L.—D3, K2
McClelland, Clyde L., Clark Goodman, and Paul H. Stelson—ZB16
McCue, J. J. G., A. E. Francis, and Clark Goodman—ZC6
McFadden, J. A.—L2
McReynolds, A. W.—H12
Melnick, Donald A. and Douglas M. Warschauer—SC1
Meservey, E. B., W. W. Havens, and L. J. Rainwater—N6
Messiah, A. M. L.—M11
Miller, S. L., M. Kotani, and C. H. Townes—O4
Mott, George R., Gordon L. Guernsey, and Bruce K. Nelson—H9
Motz, J. W., William Miller, and H. O. Wyckoff—B11
Mrozowski, S.—W4
Nagle, D. E., H. L. Anderson, E. Fermi, E. A. Long, and R. L. Martin—M9
Nedzel, V. A. and John Marshall—N3
Nelson, B. K.—H13
Nielsen, John P. and Boris Garfinkel—W15
Novey, T. B.—U12
Nowick, A. S.—J1
Noyes, H. P.—V5
Olbert, Stanislaw—F9
Palevsky, Harry and R. R. Smith—N2
Palfrey, T. R., Jr., and R. R. Wilson—M3
Passman, S., M. M. Block, and W. W. Havens, Jr.—M2
Paul, E. B. and R. L. Clarke—N8
Peierls, R. E.—Y1
Pepper, T. P., E. Almqvist, and P. Lorrain—ZB10
Perls, Thomas A.—SB3
Perry, A. M. and J. C. Keck—ZB4
Petrity, Richard L.—SC2
Phillips, M.—I4
Pine, J. and P. Morrison—N12
Placzek, G.—E11
Polachek, H. and R. J. Seeger—L10
Pollard, E. and A. E. Dimond—SA5
Pomerantz, Martin A. and Gordon W. McClure—F3
Preiss, J. W. and Ernest Pollard—SA4
Preston, M. A., J. R. Bird, and J. Shapiro—P9
Preston, W. M., P. H. Stelson, and J. J. Hinchey—H10
Pry, Robert and Arthur L. Lathrop—ZA8
Rado, G. T., R. W. Wright, W. H. Emerson, and A. Terris—J15
Richardson, John M.—SB4
Rittner, E. S. and F. Grace—SC4
Roberts, L. D. and J. W. T. Dabbs—ZA7
Rosenberg, R. and M. Lax—W13
Rosenthal, Jenny E.—SB6
Rothman, M. A., A. K. Mann, and J. Halpern—ZB6
Rothstein, Jerome—SP2, SP1, V5
Ruark, Arthur E.—V6
Rubinow, S. I. and Herman Feshbach—P12
Salpeter, E. E.—I6
Salvini, G. and Y. Kim—G11
Sawyer, G. A., W. R. Arnold, J. A. Phillips, E. J. Stovall, Jr., and J. L. Tuck—B6
Schardt, A. W. and W. Bernstein—B9
Schiff, L. I.—V2
Schiller, Ralph and Joshua Goldberg—V7
Schindler, W. G., T. R McGuire, Louis N. Howard, and J. Samuel Smart—J14
Schmidt, F. H. and G. L. Keister—ZC9
Schwarz, Ruth F.—O2
Schweinler, H. C.—W12
Sclar, Nathan and Henry Levenstein—W5
Scott, W. T.—G5
Seifert, A. M., H. J. Bramson, and W. W. Havens, Jr.—M7
Senitzky, I. R.—I1
Seymour, D. W. and W. F. G. Swann—G13
Shaw, R. P.—L8
Sherr, R. and J. Gerhart—U10
Sherwood, J. E., Harold Lyons, R. H. McCracken, and P. Kusch—U6
Shiren, N. S. and R. F. Post—T4
Shoemaker, F. C., R. J. Britten, and B. C. Carlson—B3
Shull, C. G. and M. K. Wilkinson—J13
Siegert, A. J. F.—V14
Silverman, A. and G. Cocconi—M4
Simpson, J. Arol—D4
Sitte, K.—G2
Slater, M.—SA6
Smith, Alan B. and Allan C. G. Mitchell—U11
Smith, D. F.—O11
Smith, H. L., J. A. Kies, and G. R. Irwin—W7
Smoluchowski, R. and R. Flannagan—J5
Snowdon, S. C.—ZB14
Soberman, R. K. and S. A. Korff—B12
Stanford, G. S., H. E. Duckworth, B. G. Hogg, and J. S. Geiger—U2
Starr, L. and J. Savitt—L1
Stearns, M. B.—H2
Steffen, Rolf M.—ZC5
Steinberger, J. and A. Sachs—X1
Stelson, P. H., W. M. Preston, and Clark Goodman—ZB5
Sternheimer, R.—I5
Stitch, M. L., A. Honig, and C. H. Townes—O5
Stratton, W. R., G. D. Freier, G. R. Keepin, D. Rankin, and T. F. Stratton—H4
Strauch, K. and J. A. Hofmann—N10
Strickler, Thomas D. and W. G. Wadey—B10
Sugarman, Nathan—M14
Swann, W. F. G. and D. W. Seymour—F2
Swartz, J. C. and J. W. Trischka—O3
Swetnick, M. J., H. A. C. Neuburg, and S. A. Korff—F6
Tannenwald, P.—ZB8
Tauber, G. E. and J. W. Weinberg—V12
Taylor, Warren E., L. N. Russell, John N. Cooper, and J. C. Harris—ZB12
Terrall, J. R. and Benjamin Lax—I2
Thie, J. A., C. J. Mullin, and E. Guth—ZB1
Thomson, Robb and Peter G. Bergmann—V10
Thorn, R. N., R. W. Waniek, and R. B. Holt—U8
Thornton, W. A., Jr., E. der Mateosian, H. T. Motz, and M. Goldhaber—N4
Ting, Yu, F. K. Biard, and Dudley Williams—U4
Trilling, Leon—L4
Tucker, G. L., V. W. Hughes, E. H. Rhoderick, and G. Weinreich—U7
Twersky, Vic—E3
Van Patter, D. M., P. M. Endt, A. Sperduto, and W. W. Buechner—ZB13
Van Vleck, J. H.—O1
v. Krzywoblocki, M. Z.—L5
v. Krzywoblocki, M. Z.—SP3
Wagner, Frank, Jr., and Melvin S. Freedman—ZC4
Walker, W. E., T. J. Turner, and J. W. Beams—J2
Walchli, H. E., W. E. Leyshon, and F. M. Scheitlin—U5
Waniek, R. W., R. N. Thorn, and R. B. Holt—U9
Warren, Dana T.—F1
Watson, Kenneth M.—Y3
Way, Katharine and Marion Wood—P1
Webb, Wayne, Edward M. Griest, and Robert W. Schiessler—SA2
Weertman, J., D. Burk, and J. E. Goldman—ZA5
Weil, J. W. and B. D. McDaniel—B4
Weinberg, J. W. and G. E. Tauber—V11
Weiss, R. J.—W1
Weisskopf, V. F.—A2
Whittemore, W. L. and R. P. Shutt—G12
Wigner, E. P.—P7
Wilkins, H. C. and R. D. Sard—G10
Willard, Harvey B. and Joe Keagy Bair—ZB7
Williams, H. J. and Matilda Goertz—J12
Wilson, Robert R.—G4
Witmer, Enos E.—U3
Witt, W. R., Jr.—L7
Woodgate, G. K.—Z3
Wrinch, Dorothy—SA1
Wyckoff, R. W. G.—Q1
Yadoff, Oleg—D8
Yntema, George B.—J7
Yodh, G., H. L. Anderson, D. E. Nagle, and H. Stadler—M10
Zilsel, P. R.—V4

Proceedings of the American Physical Society

MINUTES OF THE 1952 MARCH MEETING AT COLUMBUS, MARCH 20–22, 1952

(*Bulletin of the American Physical Society*, Volume 27, number 2)

THE 1952 March meeting of the American Physical Society was held in Columbus, Ohio, in the buildings of the Ohio State University, on Thursday, Friday, and Saturday, March 20, 21, and 22, 1952. As usual, this meeting included the Annual Meeting of our Division of Solid-State Physics, and even the most casual inspection of the subjoined programme will show that this Division provided most of the invited papers and its members most of the ten-minute papers. Our March meeting has thus become the principal convention of American solid-state physicists, and this is a good tradition. By exception, our Division of High-Polymer Physics also included with ours its 1952 Annual Meeting, providing three symposia and an unusual number of contributed papers. Cryogenics was also stressed in the programme, and invited papers were bespoken from other fields of physics so as to round out the meeting. Owing to all of these circumstances together , the meeting swelled to a size hitherto unprecedented for March, and actually exceeded—with its 758 registrants—every one of the past Chicago meetings except the very latest. Our March convention now figures among the *big* meetings of our calendar.

The banquet of the Society was held on the Friday evening in the Deshler-Wallick Hotel, President Van Vleck presiding. The after-dinner speakers were H. H. Nielsen representing the Department of Physics of the Ohio State University, W. James Lyons representing the Division of High-Polymer Physics, and J. C. Slater representing the Division of Solid-State Physics.

The Council met on the Friday afternoon. It elected to Fellowship two candidates and to Membership 144 candidates; their names are appended.

Reports reaching the office of the Society indicate that we have lost through death Felix Ehrenhaft and P. F. Nemenyi.

Elected to Fellowship: F. E. Borgnis, J. H. Webb.

Elected to Membership: George Adomian, Orson LaMar Anderson, Petros Nicholaos Argyres, J. R. Bannister, Thomas Walter Bauer, Norman Paul Baumann, Bradley Frederick Bennett, Walter Betteridge, Sydney Doree Black, Arthur M. Bolsterli, Irby Gerald Bowen, Leo Raymond Boyd, Wilbur L. Bunch, William Merle Carey, Jr., James Curtis Carlson, Edward Elmer Carroll, Jr., William Andrew Chupka, Robert Jay Coates, Jerrold Cohen, George Arthur Cowan, Richard Timothy Daly, Jr., Robert Houser Davis, Charles Jarchow Delbeco, Gerald de Montmollin, Amos De-Shalit, Fernand Marcel Devienne, Richard Talbot Dolloff, Alvin Ralph Eaton, Jr., Thomas Harvey Edwards, Frederick Robert Eisler, Gilbert Elliot, Jr., Hal Frederick Fruth, Lawrence J. Gallaher, Kantilal Mohanlal Gatha, Henrique Alexander Gerardo, Alberto Gigli, Frank Stafford Greenwald, William Howard Guier, Douglas Weir Hall, Daniel L. Harmon, Leonard O. Hayden, Juergen W. Heberle, Warren Heckrotte, Robert Edwin Heineman, David Gordon Henshaw, Thomas Ward Hickmott, Robert Gordon Hires, Marvin Morrison Hoffman, John Garrett Holt, Robert Lynn Hopkins, John Kenneth Hulm, Dennis Bryan James, Louis Koehler Jensen, Walter John, Jr., Robert William Jones, Harold H. Kanter, Paul Kaplan, Frank Charles Karal, Jr., Samuel N. Karp, Horst H. Kedesdy, Clement Joseph Kevane, Young B. Kim, David T. King, Daniel Kivelson, Erik Klokholm, Hans Werner Kohler, Leo Gen Komai, Herman Joseph Kopineck, Wulf Bernard Kunkel, Rodger Gustave Larson, Herbert Lashinsky, Edwin Bryce Lee, Erastus Henry Lee, Edward Clarence Lerner, David R. Lide, Jr., Frederick W. Lipps, Jr., Walter Edward Lotz, Jr., George Maenchen, John Holmes Malmberg, John Carter Marinace, Frank Fausten Mark, Robert Henry Martin, Ronald Lavern Martin, Charles Cameron McDonald, Paul R. McGee, Harlan C. Meal, John Ralph Messera, Mary Louise Meurk, H. J. G. Meyer, Clement Moritz, Richard Carl Nelson, James Barker Niday, Yoshiko Nisida, Eugene LeRoy Nooker, Joseph Francis O'Brien, Raymond Clifford O'Rourke, Billy Ray Pagel, Rudolph Pariser, Charles R. Pearce, Thomas E. Petriken, Harvey Picker, William Dale Ploughe, Harry Polachek, William Cedric Porter, Francis Ware Prosser, Jr., Milton Earl Pugh, Carol Haines Purdy, Edwin Louis Resler, Jr., Joseph Abraham Saloom, Peter J. Sandiford, Leo Sartori, Morton Jefferson Saunders, Anton Sawatzky, Charles W. Scherr, Alan Hugh Schoen, Seymour Alan Scholnick, Roald Amudsen Schrack, Bertram Daniel Schurin, Ephraim Segerman, Albert Shadowitz, Irwin Ira Shapiro, Leo M. Silber, Brendan Patrick Smith, Thorvald Arthur Solberg, Folden Burt Stumpf, Toshio Tasaka, Raymond Jerome Thome, William John Toulis, John Robert Townsend, Antoine Visconti, Thomas P. Vogl, Richard Alden Walker, John L. Walsh, Charles Seabury Ward, Robert Louis Wehrli, Lewis Bernard Wetzel, Horace Frederick White, David B. Wittry, Leland A. Wooenk, William Francis Wraga, Arthur H. Youmans, Jiro Yukawa, Arvid Vernon Zuber, and Joseph Zucker.

KARL K. DARROW, *Secretary*
American Physical Society
Columbia University
New York 27, N. Y.

(Errata on page 638.)

Errata Pertaining to Papers C2, D15, E7, M7, N3, N5, and N6

C2, by Paul Molmud. In line 8, $1/(r^2+a^2)^4$ should read $1/(r^2+a^2)^4$.

D15, by I. G. Geib and R. E. Grace. In lines 11 and 13, 4.7 and 5.1 μamp-hr should read 6.2 and 6.7 μamp-hr per cm^2, respectively.

E7, by John D. Ferry and Edwin R. Fitzgerald. In line 4, $G^*=G'=iG$ should read $G^*=G'+iG$.

M7, by G. J. Dienes. The second paragraph should read: Comparison of the total activation energies for self-diffusion via vacancies, direct interchange, and interstitial atoms indicates that direct interchange is the preferred mechanism. The activation energy for self-diffusion by means of direct interchange is estimated to be 90 kcal/mole. The present theoretical treatment is not applicable to diffusion along grain boundaries or pores.

N3, by T. G. Fox. In the last line of the footnote to the abstract, Office of Rubber Reserve, Reconstruction Finance Corporation should read, Synthetic Rubber Division, Reconstruction Finance Corporation.

N5, by R. J. Derenthal, F. P. Baldwin, and R. L. Anthony and **N6,** by Herbert Bauss and R. F. Boyer. The last four sentences of abstract **N5** belong with abstract **N6**.

PROGRAMME

THURSDAY MORNING AT 10:15

Chemistry 100

(J. H. VAN VLECK presiding)

Opening Session

Welcome by the Chairman of the Department of Physics of The Ohio State University.
Response by the President of the American Physical Society.

Invited Papers

A1. The Low Temperature Properties of Helium 3. J. G. DAUNT, *Ohio State University.* (45 min.)
A2. Polymer Research as a Branch of Solid-State Physics. E. GUTH, *University of Notre Dame.* (45 min.)
A3. Recent Work on Magnetic Resonance, and Relaxation Effects in Ferromagnetic Resonance. N. BLOEMBERGEN, *Harvard University.* (45 min.)

THURSDAY AFTERNOON AT 2:30

Chemistry 100

(DUDLEY WILLIAMS presiding)

Invited Papers of the DSSP

B1. Nuclear Magnetic Resonance in Metallic Sodium. R. E. NORBERG, *University of Illinois.* (30 min.)
B2. Relaxation of Nuclear Spins by Diffusion. H. C. TORREY, *Rutgers University.* (30 min.)
B3. Hyperfine Structure in Free-Radical Paramagnetic Resonance. G. E. PAKE, *Washington University.* (30 min.)
B4. Paramagnetic Resonance Absorption in a Single Crystal of Manganese Fluoride. C. A. HUTCHINSON, *University of Chicago.* (30 min.)
B5. Pure Quadrupole Spectra of Solid Chlorine Compounds. RALPH LIVINGSTON, *Oak Ridge National Laboratory.* (30 min.)

THURSDAY AFTERNOON AT 2:30

Physics 110

(H. H. NIELSEN presiding)

General Physics

C1. On the Theory of the Electron. WALTER WESSEL, *USAF Institute of Technology.*—The mass operator proposed recently[1] is shown to lead to an additional magnetic moment of the electron of the order of 1/137 Bohr magneton. The exact determination still meets with the difficulties of handling the infinite matrices. By insertion of a simple finite and not wholly equivalent representation of the underlying commutator algebra, one obtains a moment which is too large by a factor 16/3 as compared with Schwinger's well-known value.[2] For analytical purposes the difference operator representation, introduced in a foregoing paper,[3] has been fully developed with the use of the model of the spinning electron of Rosen,[4] which is shown to be kinematically equivalent to the author's. Besides, for reasons of interpretation, the theory has slightly been modified by exchange of the vectors ϵ_3 and ϵ_4 in the Hamiltonian.

[1] W. Wessel, Phys. Rev. **83**, 1031 (1951); Z. Naturforsch. **6a**, 478 (1951)
[2] J. Schwinger, Phys. Rev. **73**, 416 (1948); **76**, 790 (1949).
[3] W. Wessel, Z. Naturforsch. **6a**, 473 (1951).
[4] N. Rosen, Phys. Rev. **82**, 621 (1951).

C2. On the Order of Magnitude of the Signal Radius of the Electron. PAUL MOLMUD, *Clarkson College of Technology.*—According to Landé's theory of the electron,[1] the stationary electron has a potential $e/(r^3+a^3)^{\frac{1}{3}}$ and a field $er/(r^3+a^3)^{\frac{1}{3}}$ where a is the signal radius. To get some idea of the magnitude of this factor a, the following computations were performed: (1) The Hamiltonian for a hydrogen-like atom was perturbed by $H'=Ze^2(1/r-1/(r^3+a^3)^{\frac{1}{3}})$. The shifts in the $2S_{\frac{1}{2}}$ and $2P_{\frac{1}{2}}$

energy levels were computed by the methods of perturbation theory and the separation of these perturbed levels was equated to the experimentally observed Lamb-Retherford shift. This equation is satisfied when a is assigned the value of six classical electron radii.[3] (2) The electron is assumed to have an intrinsic magnetic moment of one Bohr magneton. The resultant magnetic field and the classical electric field bear an angular momentum which can readily be computed.[3] The gyromagnetic ratio of the electron can have the correct ratio only when a is assigned the value $\frac{2}{3}e^2/mc^2$, two-thirds of the classical electronic radius.

[1] A. Landé, Phys. Rev. **76**, 1176–79 (1949).
[2] See author's dissertation, Appendix IV (Ohio State University, 1951). Cf. E. David, Z. Physik. 125 (1948–49).
[3] F. A. Kaempffer, Can. J. Research **A28**, 336 (1950).

C3. The Semiclassical Franck-Condon Principle and Its Application to Complex Systems. MELVIN LAX, *Syracuse University and the Naval Research Laboratory.*—The semiclassical Franck-Condon principle follows from the more rigorous quantum-mechanical transition probability if a mean-value theorem approximation and closure are applied to the sum over final and average over initial vibrational states. In order to provide a test of the accuracy of the semiclassical formula as well as to lay the ground work for a number of applications, the following problem was considered: Absorption or emission by a complex system whose vibrational states are describable by normal modes, such that the configurational energy difference between two electronic states can be approximated by a linear expression in the normal coordinates. The absorption and emission spectrum are then found to be Gaussian curves with displaced peaks. Another problem investigated is the extent to which a complex system can, as is customary in Franck-Condon calculations, be replaced by a one-parameter system. It was established that if the electronic energy *difference* (whether linear in the vibrational coordinates or not) is a function only of a single parameter, then a one-parameter *description* is possible. However, this *description* is in general equivalent to a one-parameter *system* (harmonic oscillator) only if the resonant frequency of the oscillator is made temperature dependent.

C4. Phenomenological Quantum Electrodynamics with Magnetic Poles. M. AVRAMY MELVIN,* *Eastsound, Washington.*—Electrodynamics is here developed with the following generalizations: (A) The flux fields **B** and **D** are distinguished from the force fields **H** and **E**. (B) The usual restriction to the absence of free magnetic poles is *not* made. The treatment differs from that given by Dirac, in which the generalization (B) has been made, in that generalized symmetry and covariance requirements (including independence of a metric) are here met.[1] It differs from the phenomenological quantum electrodynamics of Jauch and Watson, in which the generalization (A) has been made, in the addition of (B) as well as in the consistent satisfaction of the generalized covariance requirements mentioned above. The theory is also covariant, with *invariant ponderomotive phenomena*, under a transformation from "electric" to "magnetic" quantities. The possible physical significance of this covariance will be discussed. One can do without the singular "strings," attached to the poles in Dirac's theory, by introducing an independent "magnetic" 4-vector potential in addition to the usual "electric" potential. Generalized gauge invariance holds. Lagrangian and Hamiltonian formulations are given. The theory is then quantized, and inferences drawn.

* Guggenheim Fellow, 1951–1952.
[1] M. Avramy Melvin, "Symmetry and affinity of electromagnetic fields, charges, and poles," Proc. Second Can. Math. Congress (Vancouver, 1949).

C5. On Thermal Expansion of Propylalcohol. GEORGE ANTONOFF.—All liquids expand with temperature following the same pattern.[1] They all show "kinks" at intervals in densities, vapor pressures, and allied properties. The kinks are perfectly reproducible in standard conditions, and conditions under which they are not reproducible are known. I worked so that my results dublicate substantially those of Sydney Young. In a recent paper[2] Kretschmer disputes my results. The case is quite analogous to that of the kink in benzene at 45 or 46°C, about which it is known that it can be well reproduced, and yet it disappears in conditions of work of Cohen and Buy.[3]

[1] Compt. rend. 3/XII (1951).
[2] C. B. Kretschner, J. Phys. Coll. Chem. **55**, 1351 (1951).
[3] Cohen and Buy, Z. physik. Chem. **B35**, 270 (1937).

C6. An Improved "Lock-In" Amplifier.* HENRY L. COX, JR., *The Ohio State University.*—A phase-detector or "lock-in" amplifier has been completed recently which offers linear response, simplicity of circuitry and adjustment, and a high degree of independence from variations of the reference signal amplitude and of vacuum-tube parameters. A square-wave reference voltage is used to minimize the undesired effects of nonlinearity of the detecting diode characteristic curves. While the basic instrument has unwanted response to noise components which are odd harmonics of the reference frequency, suitable filtering removes this minor defect. The instrument to be described was designed to operate at audio-frequencies but could be adapted for the lower radiofrequency range.

* Supported in part by a contract between the Geophysical Division of the Air Force Research Center and the Ohio State University Research Foundation.

C7. A Phenomenological Uncertainty Principle. JEROME ROTHSTEIN, *Signal Corps Engineering Laboratories.*—The existence of a thermodynamic limit to the precision of any measurement follows from the facts that: (a) information is conveyed by making choices from an ensemble of alternatives for which an "entropy" is definable measuring initial freedom of choice and hence quantity of information when choices are made; (b) measurement chooses from an ensemble of possible results, thus yielding "physical" information; (c) either the informational entropy of physical information multiplied by Boltzmann's constant must be a lower bound to the thermodynamic entropy generated in acquiring it or the second law can be violated. Example: A quantity equiprobably between o and u is measured to fall within Δu. Then choice from $u/\Delta u$ alternatives was made at entropy cost ΔS not less than $k \ln(u/\Delta u)$. For preassigned experimental conditions maximum ΔS is well defined and $\Delta u \geq u \exp(-\Delta S/k)$. Individually sharp p or q is then undefined operationally on phenomenological grounds rather than quantal as for simultaneously sharp p and q. Speculation: Divergencies may originate in ascribing theoretically sharp values to operationally uncertain parameters.

C8. Relative Variation of DC and Pulse Emission from Mixtures of Rare-Earth Oxides.* E. N. WYLER AND F. C. TODD, *Battelle Memorial Institute.*—Coomes observed that good dc emitters are usually good pulse emitters, but the reverse is not necessarily true.[1] The resistance of an interface when present, electrolytic flow of barium, and gas bombardment of the cathode surface "can contribute" to the pulse decay of oxide-coated cathodes.[2] From experiments on mixtures of rare-earth oxides of the $4f$ series and from published results for oxide-coated cathodes, a correlation has been observed between the ratio of pulse to dc emission and the formation of solid solution of the components of a binary mixture in each other and in new phases of the two components. The nature of the mixtures has been analyzed by x-ray diffraction patterns. The dc and pulse emission currents from each mixture were checked and rechecked by alternate measurements in a diode with a platinum anode. Measurements were made on mixtures

for the full range of proportions of neodymium oxide with gadolinium oxide, and in some proportions on mixtures of dysprosium oxide with gadolinium oxide, and of terbium oxide with gadolinum oxide.

* This work was sponsored by Evans Signal Laboratory and Wright-Patterson Air Force Base.
[1] E. A. Coomes, J. Appl. Phys. 17, 647–654 (1946).
[2] D. A. Wright, *Semi-Conductors* (John Wiley and Sons, Inc., New York, 1950), p. 119.

C9. Cathode Effects in Dielectric Breakdown. R. W. CROWE, A. H. SHARBAUGH, AND J. K. BRAGG, *General Electric Research Laboratory.*—The electron emission characteristics of the surface of the cathode used in the study of the electric breakdown of insulators have a fundamental bearing of electric strength observed. It has been suggested that formation of a negative space charge is the mechanism through which this influence is exerted.[1] This space charge is assumed to be supplied by field emission from the cathode. It distorts the field in the dielectric and causes breakdown at lower applied voltages than would be indicated by a knowledge of the intrinsic electric strength. These suggestions lead to a semi-quantitative account of the influence of certain properties of the cathode: for example, its vacuum work function and, in case of an aqueous electrolyte cathode, the concentration of the negative ion. They also provide for the time required for the breakdown process. These considerations indicate the sort of experiment which must be done to measure the intrinsic electric strength of condensed dielectrics.

[1] A. von Hippel and R. S. Alger, Phys. Rev. 76, 127 (1949).

C10. $L\alpha_{1,2}$ and $L\beta_1$ Emission Lines of Copper and Zinc.* C. H. SHAW AND NATHAN SPIELBERG,† *The Ohio State University.*—Preliminary measurements of the shapes of the Cu and Zn $L\alpha_{1,2}$ and $L\beta_1$ emission lines, representing transitions from d bands to the L_{III} and L_{II} levels, respectively, have been completed on a new two-crystal vacuum x-ray spectrometer. Beryl crystals, cut along the $(10\bar{1}0)$ planes ($d=7.96$A), ground, polished, and etched, and having a $(1, -1)$ width of 0.34 volt at 13.3A were used in conjunction with an Allen type photomultiplier[1] as detector. Comparisons with the corresponding $K\beta_{1,3}$ lines and with earlier photographic work bring out some interesting points. Certain operating data of the spectrometer will be presented.

* Supported in part by ONR.
† DuPont Fellow, 1950–1951.
[1] J. S. Allen, Rev. Sci. Instr. 18, 739 (1947).

THURSDAY AFTERNOON AT 2:30

Physics 100

(F. SEITZ presiding)

Effects of Nuclear Irradiation upon Solids

D1. Fading Characteristics of Gamma-Induced Coloration in High Density Glass. ROBERT H. KERNOHAN AND GRACE M. MCCAMMON, *Oak Ridge National Laboratory.*—Specimens of a high density lead silicate glass suitable for gamma-shielding were measured for optical transmission characteristics. The specimens were then given varying dosages from a 300 Curie cobalt 60-gamma-source. Color centers were readily introduced. Transmission characteristics were measured as a function of time following irradiation. The gamma-induced coloration faded at room temperature, and this fading could be greatly accelerated by illuminating the specimens. All specimens nearly recovered their original transmission characteristics. The glass specimens were furnished by the Penberthy Instrument Company.

D2. Energy Levels in Ge Produced by Nucleon Bombardment. J. H. CRAWFORD, JR. AND J. W. CLELAND, *Oak Ridge National Laboratory.*—In an attempt to determine the precise nature and position of energy levels associated with nucleon bombardment produced lattice defects, the results of the phenomenological model of James and Lehman[1] have been reexpressed in a form more amenable for calculation of readily measured experimental quantities, namely, hole concentration and initial rate of change of hole concentration with trap introduction in P-type Ge. These calculations are compared with experiment. Equilibrium carrier concentrations are calculated from the law of chemical equilibrium and the condition of electrical neutrality under the assumptions (1) all chemical impurity levels are completely ionized, (2) classical statistics are valid throughout, and (3) annealing of lattice disorder is negligible. These calculations have been extended to include other ideas of energy level situation, notably those of James and Lark-Horovitz.[2] These models are used to calculate bombardment curves for N-type material and ratios of N-type slope to P-type slope in order to compare these models with experimental results.

[1] K. Lark-Horovitz, Reading Conference on properties of Semiconducting Materials, Appendix II, by C. W. Lehman and H. M. James.
[2] H. M. James and K. Lark-Horovitz, Z. physik Chem. 198, 107 (1951).

D3. Slip Lines in Pile Irradiated Copper Single Crystals. R. E. JAMISON AND T. H. BLEWITT.—Single crystals of high purity (99.999 percent) copper were grown with random orientations (in vacua by the Bridgman method) in the form of tensile bars. These were individually irradiated in a pile with the fast neutron flux varied from 5×10^{17} to 8×10^{18} neutrons/cm^2. The slip lines formed by subsequent cold working were then studied. Pronounced differences in these lines and those in nonirradiated crystals were observed. For small strains the lines were found to occur in clusters and in some cases cross-slip lines appeared. For larger strains, a similar clustering of slip lines was observed with the initiation of slip in the latent system. The load-extension curves show a reduction in stress with the activation of the latent slip system, suggesting that the latent system hardens at a faster rate than the active system. All of these slip characteristics are similar to those observed in alpha-brass.[1,2]

[1] Maddin, Mathewson, and Hibbard, Jr., *Unpredicted Cross-slip in Single Crystals of Alpha-Brass*, Metals Tech. February (1948), T. P. 2331.
[2] V. Göler and G. Sachs, Z. Physik 55, 581 (1929).

D4. The Effect of Neutron Irradiation of Metallic Diffusion. R. R. COLTMAN AND T. H. BLEWITT.—It has been previously reported[1] that neutron irradiation will substantially increase the rate of metallic diffusion owing to an increase in the number of Frenkel defects. The disordered system Cu_3Au was used as a tool in these studies as each atomic motion tended toward ordering. Electrical resistance was used as a criterion for measuring the ordering process. Observations showed that

the relaxation time for ordering was substantially decreased as a result of the irradiation. Further measurements have been made. X-ray Debye-Scherrer patterns were made of the irradiated sample and the size of the ordered domains were deduced from the half-breadth of the super lattice lines indicating an average value of 125A. This domain size indicates that the Frenkel defects have an appreciable path before anihilation.

[1] T. H. Blewitt and R. R. Coltman, Phys. Rev. 85, 384 (1952).

D5. Comparison of Thermally Induced Lattice Defects in Germanium and Silicon with Defects Produced by Nucleon Bombardment.* W. E. TAYLOR, *Oak Ridge National Laboratory.*—Quenching high purity germanium from elevated temperatures induces large changes in the room-temperature conductivity. The changes, which were noted by earlier investigators,[1,2] are similar to the changes induced by nucleon bombardment[3] and are sufficiently large to require a change in the number of carriers for their explanation. Similar large changes were observed with silicon, again the changes were analogous to those resulting from nucleon bombardment. In germanium only electron traps were observed. The density of traps was proportional to $\exp(-W/kT_q)$, where T_q is the quenching temperature. Both hole and electron traps were observed in silicon. The traps are believed to be associated with Frenkel and possibly Schottky type defects which are in equilibrium at the elevated temperatures, and are retained at room-temperature on quenching. These are the same type of defects to which nucleon bombardment effects are attributed.[3] The energy of formation of the defects in germanium was found to be $W=(42{,}700-12.5T)$ cal/mole.

* Experiments done at Purdue University under a Signal Corps Contract.

[1] Lark-Horovitz, NDRC Report 14-585, November 1945.
[2] Theuerer and Scaff, J. Metal Tech. 191, 51 (1951).
[3] Cleland, Crawford, Lark-Horovitz, Pigg, and Young, Phys. Rev. 83, 312 (1951).

D6. Neutron Bombardment of a Copper-Beryllium Alloy. G. T. MURRAY AND W. E. TAYLOR, *Oak Ridge National Laboratory.*—The effect of bombarding a supersaturated solid solution of beryllium in copper with neutrons was investigated and compared with the effect of similar irradiation of unsaturated solid solutions. The hardness increased approximately 45 DPH and the electrical resistance increased approximately 10 percent in the copper-beryllium alloy after a bombardment of 2.3×10^{18} n/cm^2. For comparable exposures a hardness increase of 20 DPH and a resistance increase of 0.5 percent was observed in unsaturated copper solid solutions. The behavior of the copper-beryllium alloy specimens during bombardment and subsequent thermal aging indicated that clustering or nucleation of a precipitate phase had occurred during irradiation. Evidence is presented which, for this alloy, supports Mott's[1] hypothesis that the increase in electrical resistance during the early stages of thermal aging at low temperatures is the result of coherent scattering of the electrons by precipitate particles rather than a strain effect. The resistance increase resulting from neutron bombardment is also attributed to scattering of the electrons by precipitate particles.

[1] N. F. Mott, Discussion of Paper by Gayler, J. Inst. Metals 60, 267 (1937).

D7. Diffusion Effects of Cobalt when Bombarded with Neutrons. GEORGE W. CALLENDINE, JR.,* VIRGINIA C. RIDOLFO, AND M. L. POOL, *Ohio State University.*—Cobalt 59 cylinders were irradiated in the nuclear reactor at the Oak Ridge National Laboratories. These cylinders were given a thin gold plate before irradiation. After plating, the cylinders were positioned in layers between 0.18-inch thick carbon disks. These disks after irradiation were found to be radioactive with Co-60. This activity decreases rapidly by a factor of about 4000 from the surface of the disk to the center. It is suggested that this Co-60 activity in the carbon results from a diffusion type of mass transfer of cobalt atoms caused by collisions between high energy neutrons and cobalt. One would anticipate a similar type of mass transfer for other materials irradiated with high energy neutrons. It would therefore appear advisable to electroplate the gold onto the cobalt cylinders after irradiation if one desires to eliminate Co-60 activity in the gold layer.

* Research supported by the AEC.

D8. A Technique for Self-Diffusion Measurements. DAVID B. LANGMUIR,* *National Research Council of Canada, Chalk River.*—By allowing neutrons in the N.R.X. thermal column to fall upon a tantalum strip through a slit in a block of cadmium, a sharply defined region of activity can be produced. The variation of activity A with distance x along the strip in the shielded region can be computed to be $A=A_0\exp(-\mu x/\theta)+(\mu x/\theta)Ei(-\mu x/\theta)$, where μ is the absorption coefficient of cadmium for neutrons and θ is the angle of collimation throughout which neutrons strike the cadmium. With $\theta=0.15$ radian, the activity drops by a factor of 10 in about .018 mm. After suitable heat treatment the edges of the active spot become fuzzy because of diffusion. The effect has been observed qualitatively by autoradiography, and quantitatively by grinding off sections on 4/0-metallographic emery paper, which can be inserted in a counter. The above formula has been quantitatively confirmed for unheated samples. After heat treatment the measured distribution follows the error function, as predicted by theory.

* USAEC Liaison Officer, Chalk River.

D9. Experiments in Silver Self-Diffusion.* R. D. JOHNSON AND A. B. MARTIN, *North American Aviation, Inc.*—The rate of self-diffusion in silver has been measured in polycrystalline and single crystal solvents using radioactive tracer techniques. Measurements have been made in polycrystalline solvents diffused at temperatures as low as 497°C, at which point grain-boundary diffusion appears to be the predominant process. Analysis of experiments with both type solvents in the temperature range 903°C to 640°C have yielded the expression $D=0.11e^{-40,800/RT}$ for the volume diffusion process. The use of single crystal solvents has enabled the extension of the volume diffusion results to temperatures as low as 545°C, although the relatively short time anneals used at these low temperatures have resulted in D values which are somewhat higher than the extrapolated high temperature data. Results will also be given for specimens diffused in the presence of intense proton bombardment at 715°C and 555°C, and compared with the results of other irradiation-diffusion studies.

* This paper is based on work performed under Contract for the AEC.

D10. Analysis of the Resistivity Changes Produced by Deuteron Irradiation of Copper, Silver, and Gold.* J. W. HENDERSON, H. G. COOPER, J. W. MARX, *University of Illinois.*—It is assumed that the resistivity increase which results from deuteron bombardment of metallic foils is proportional to the concentration, N, of interstitial-vacancy pairs produced; i.e., $\Delta\rho=KN$. The production of such pairs is described by the equation $dN=Adm-BNdn-C(N,T)dt$, where n is the number of incident deuterons per unit area; A is the number of pairs produced in unit volume per incident particle; B is the probability that a given pair is annihilated by the action of any one incident particle; and $C(N,T)$ represents a process of thermal recovery. If it is further assumed that the bombardment was carried out at such low temperatures that $C(N,T)$ is negligible, the resistivity increase may be described by the integrated expression $\Delta\rho=KA/B\times(1-e^{-Bn})$. This expression gives excellent agreement with

the data obtained by deuteron bombardment of foils of 99.95 percent Au, Ag, and Cu at −140°C, in the University of Illinois cyclotron. It is suggested that the phenomenological saturation value KA/B, given by this equation, may provide a significant reference point for determining low temperature radiation damage.

* Supported by AEC Contract AT (11-1) 182.

D11. Effect of Cyclotron Irradiation on Some Thermocouple Materials. A. ANDREW, M. R. JEPPSON, AND H. P. YOCKEY.—The effect of irradiation on the thermoelectric power of iron, constantan, chromel, alumel, platinum, and 10 percent rhodium platinum thermocouple wires has been measured at temperatures up to 500°C using the 40-Mev alpha-beam of the Crocker Laboratory Cyclotron. One section of a loop of wire was subjected to a temperature gradient while being irradiated. Measurement of the emf produced in this loop showed that the emf resulting from the irradiation was less than 3×10^{-7} volt per degree centigrade, the limit of measurement of the equipment. Two other experiments involving direct exposure of a thermocouple junction showed no measurable effect with changing irradiation intensities. Work is continuing on this problem at lower temperatures.

D12. Radiation Damage in Sodium Chloride.* DONALD WESTERVELT, *North American Aviation, Inc.*—The properties of sodium chloride crystals which have been irradiated with high energy alpha-particles or electrons are compared with those of crystals penetrated by x-rays, or additively colored. While regions penetrated by fast particles at first appear to contain only a high density of *F*-centers, after optical bleaching they develop a deep purple color similar to that of crystals slowly cooled after heating in sodium vapor. A purple color after electron irradiation was reported elsewhere,[1] and was attributed to the presence of colloidal sodium. The purple irradiated crystals can be completely bleached by warming, however, and this, combined with their chemical neutrality, clearly differentiates them from crystals containing excess sodium. It is suggested that the new lattice defects introduced are the result of displaced sodium in interstitial sites, thermal annealing then proceeding through recombination with positive vacancies. The annealing process is accompanied by blue luminescence similar to that which accompanies thermal annealing of photochemically produced *F*-centers. Some effects are discussed of these lattice defects on other properties of the crystal.

* Work carried out under contract with the AEC.
[1] D. E. McLennan, Can. J. Phys. **29**, 122 (1951).

D13. Effect of Deuteron Bombardment on the Electrical Resistivity of Copper, Silver, and Gold.* J. MARX, J. KOEHLER, AND C. WERT, *University of Illinois.*—Three-mil foils of 99.5 percent copper, silver, and gold were bombarded by 12-Mev deuterons from the University of Illinois cyclotron. The foils were maintained at an average temperature of −150°C; their temperature never exceeded −140°C during irradiation. The deuteron flux as determined by copper monitor wires was uniform to 10 percent over the target area. The resistivity was determined at −172°C for silver and gold, and at −174°C for copper after various amounts of irradiation up to 11.4 microampere hours per cm². The initial slope of the resistivity *versus* irradiation curve for gold was 2.5 times the initial slope for silver, and 3.0 times that for copper. Total resistivity changes were Cu, 1.2×10^{-7}; Ag, 1.7×10^{-7}; Au 4.8×10^{-7} ohm cm. The total percentage changes were: Cu 23.5 percent, Ag 31 percent, Au 47.2 percent. After bombardment, the foils were maintained for 40 hours at −171°C±3°C, during which time the resistivity decreased less than 1.0 percent for any specimen. We would like to thank R. D. Erickson, H. G. Cooper, and J. W. Henderson for their help.

* Supported by the AEC contract AT (11-1) 182.

D14. Conductivity of Deuteron Irradiated Germanium and Silicon.* J. H. FORSTER, H. Y. FAN, AND K. LARK-HOROVITZ, *Purdue University.*—The conductivity, σ, of low resistivity n and p-type germanium and p-type silicon has been followed during irradiation with 10-Mev deuterons under controlled conditions (known flux and temperature). *P*-type material with a carrier density of 9.8×10^{17}/cm³ shows a decrease in conductivity with a gradual decrease in slope, the conductivity approaching a limiting value. *P*-type material with a carrier density of 7.8×10^{16}/cm³ shows an increase in conductivity after irradiation. The conductivity of n-type germanium with a carrier density of 3.3×10^{17}/cm³ changes with deuteron irradiation as with neutron irradiation.[1] The initial rate of change in carrier concentration per incident deuteron per unit volume, $\Delta n/\Delta n_D$, as determined from the σ *vs* flux curve was about −11 for n-type germanium and about −4 for low resistivity p-type germanium. *P*-type silicon of initial carrier concentration $n=2.4\times10^{16}$/cm³ at 0°C showed an initial value of $\Delta n/\Delta n_D=-31$, and the conductivity decreases in the early stages at an exponential rate. These results will be discussed in terms of the model of James and Lark-Horovitz.[2]

* Supported by a Signal Corps Contract.
[1] Cleland, Crawford, Lark-Horovitz, Pigg, and Young, Phys. Rev. **83**, 312 (1951); Cleland, Crawford, Lark-Horovitz, Pigg, and Young, Phys. Rev. **84**, 861 (1951).
[2] James and K. Lark-Horovitz, Z. physik Chem. **198**, 222 (1951).

D15. Hardness of Deuteron Irradiated Molybdenum.* I. G. GEIB AND R. E. GRACE, *Purdue University.*—The hardness of Mo sheets, 0.005 inch thick, has been measured before and after annealing and before and after bombardment with 10-Mev deuterons of either unannealed or annealed specimens. Hardness numbers were obtained using a Tukon tester with Knoop indenter and 1-kg load. Annealing a cold rolled specimen 3 hours at 2250°F gives a decrease in Knoop hardness number from 269 to 158. Photomicrographs and x-ray diffraction patterns show recrystallization and grain growth resulting from this annealing. 4.7μ amp-hr deuteron bombardment gives no change in the hardness of a cold rolled specimen. 5.1μ amp-hr bombardment increases the hardness number of an annealed specimen about 12 percent. X-ray transmission and back reflection patterns of annealed specimens before and after bombardment show no difference in structure.

* Supported by AEC Contract.

D16. Displacements Produced by Electron Bombardment of Germanium.* E. E. KLONTZ AND K. LARK-HOROVITZ, *Purdue University.*—The threshold energy for removal of Ge atoms from their lattice sites by electron bombardment is about .63 Mev.[1] Irradiation[2] at 1.5 Mev of several *N*-type samples having resistivities from 10^{-3} to 10 ohm cm indicates that about 1 carrier is trapped per incident electron at liquid nitrogen temperatures. For higher temperatures the number of trapped electrons is smaller because of healing out accompanying the bombardment. At lower incident energies the number of trapped electrons is smaller because of smaller cross sections for displacement. Investigation into the healing process has been carried out by observation of changes in Hall and resistivity curves while heat treating after bombardment.

* Supported by AEC Contract.
[1] E. E. Klontz and K. Lark-Horovitz, Phys. Rev. **82**, 763 (1951).
[2] We are indebted to Professor Burton and Charles Scholer of the Notre Dame Radiation Chemistry group for these irradiations.

THURSDAY AFTERNOON AT 2:30

Chemistry 161

(J. B. NICHOLS presiding)

Contributed Papers of the DHPP

E1. A New Approximate Conversion Method for Relating Stress Relaxation and Dynamic Modulus. ROBERT S. MARVIN, *National Bureau of Standards.*—It is of interest to relate the results of transient and dynamic measurements of the mechanical properties of matter, both as a check on the results and to permit a unified presentation of mechanical behavior over a wide range of frequencies. The difference between the real part of the dynamic modulus at a radian frequency $1/t$, $G'(1/t)$, and the stress relaxation function at a time t, $\Psi(t)$, may be written

$$G'(1/t)-\Psi(t)=\int_0^\infty\left[\frac{\tau^2/t^2}{1-\tau^2/t^2}-e^{-t/\tau}\right]g(\tau)d\tau,$$

where $g(\tau)$ is the Maxwell distribution of relaxation times which can be evaluated approximately from either type of measurement by graphical differentiation. Since the terms on the left are nearly equal, the transformation from one to the other can be effected with a high degree of precision and with relative ease. Data on a high molecular weight polyisobutylene taken by a number of investigators as part of a cooperative program are used to illustrate the method.

E2. Correlation of Dynamic and Static Measurements on Rubber-Like Materials. II. R. D. ANDREWS, *Dow Chemical Company.*—Static modulus (relaxation of stress), dynamic modulus and dynamic loss measurements on rubber-like materials can all be correlated in terms of the relaxation time distribution which characterizes the particular material under consideration. In carrying out calculations to relate these properties to the relaxation time distribution or to one another, it is very convenient to have approximate relationships which can be conveniently used. The present paper extends the investigation of approximate relations begun in the first paper of this series. More general derivations are given of some of the specific results derived previously. Second approximation expressions are derived which differ from those obtained in the preceding paper. The distribution of relaxation times for a polyisobutylene sample is calculated from relaxation of stress data to illustrate the application of the second approximation expression for the static modulus case. Static modulus measured by creep experiments is related to a distribution function of retardation (or orientation) times. First and second approximation expressions which can be used in this case are derived.

E3. Viscoelastic Properties of Polymers by Phase Angle Measurements. R. D. SPANGLER.—Equipment has been devised to measure the mechanical phase angle of polymers. Specimens are subjected to forced vibrations of 20 or 30 cycles per second at stress levels up to the ultimate strength of the materials. Measurements can be made on molded plastic specimens, on polymer melts, and on monofilaments and cords. From phase angle measurements the viscous and elastic components can be calculated. The elastic component of some polymer melts has been shown to be approximately equal to the viscous component. Data will be presented for a number of plastics including FM 10001 Nylon, FM 3001 Nylon, "Lucite" acrylic resin, and "Alathon" polythene resin.

E4. Investigations on Plastics in a Large Range of Mechanical Frequencies. W. PHILIPPOFF, *Franklin Institute Laboratories.*—Shear experiments have been made on some plastics, including National Bureau of Standards polyisobutylene, at mechanical frequencies ranging from 10 cycles per second up to 12 hours per cycle, and the measurements of the properties in this range correlate well with measurements made in other ranges by the laboratories cooperating in the test program of the National Bureau of Standards on polyisobutylene. These results, obtained by the extension of the frequency range, contribute to the further understanding of the properties of plastics. Tests on filled rubber containing carbon show that the "box distribution" formula applies throughout the range investigated, which leads to further conclusions as to the mechanical behavior of rubber.

E5. Dielectric Properties of Liquids, Gels, and Solids at Audiofrequencies. II. Polyvinylchloride Plasticized by Di-2-Ethylhexylphthalate and Dimethylthianthrene. R. F. MILLER, E. R. FITZGERALD,* J. M. DAVIES,† AND W. C. SEARS,‡ *B. F. Goodrich Company.*—In order to provide a useful range of hardness-temperature characteristics, polyvinylchloride is plasticized by such polar liquids as di-2-ethylhexylphthaate and dimethylthianthrene. Pure polyvinylchloride has a 60-cps dipole maximum near 100°C, while these plasticizers behave similarly at −70°C and −20°C, respectively. Plasticized polyvinylchloride exhibits essentially a merger of these to a lower and broader maximum at an intermediate temperature depending on the amount and type of plasticizer. The maximum shifts to lower temperature with increase in plasticizer or decrease in frequency. Ionic loss, which becomes appreciable at temperatures above the dipole maxima, is reduced by stabilizers such as lead oxide and lead silicate. In studying these properties for improvement in electrical insulating applications, additional information has been obtained about the structure of polyvinylchloride and the method of plasticization. Measurements cover the range from 0 to 100 percent plasticizer, from −75 to +150°C, and dc through 15, 60, 1000, and 10,000 cps. Essentially static measurements of hardness show a relatively small variation at the temperature of the dipole maximum with considerable change in plasticizer content. Individual dipoles are closely associated with their neighbors so that a considerable number probably move together in response to either electrical or mechanical forces.

* Now employed at University of Wisconsin, Madison, Wisconsin.
† Now employed at Army Quartermasters Corps, Philadelphia, Pennsylvania.
‡ Now employed at University of Georgia, Athens, Georgia.

E6. Method for Determining Dynamic Mechanical Properties of Gels and Solids at Audiofrequencies; Comparison of Mechanical and Electrical Properties. EDWIN R. FITZGERALD AND JOHN D. FERRY, *University of Wisconsin.*—A method has been developed for measurements of complex shear modulus on samples ranging from soft gels to stiff solids at −50 to +150°C over the frequency range 25 to 5000 cps. A rigid tube with coils around the ends is suspended so that the coils are in radial magnetic fields. Alternating currents are passed through the coils and the consequent motion is modified by introducing a sample between the tube and a heavy inner core. From determinations of the mechanical impedance of the system with and without a sample the impedance of the sample alone is found. One transducer coil is placed in the arm of a bridge where it acts as an electrical impedance, Z_1', while the other parallels the bridge circuit. Z_2' is found for two current ratios in the coils and the mechanical impedance from the difference in electrical impedance values. By a proper

choice of sample dimensions a precision of ±2 percent is obtained. Experimental results are given for a National Bureau of Standards polyisobutylene sample and for a polyvinyl chloride-dimethylthianthrene gel (10 percent polymer by volume). The temperature and frequency variation of the complex shear modulus of the gel is compared with that of the complex dielectric constant at the same temperatures and frequencies, previously reported for this gel by Fitzgerald and Miller.[1]

[1] Paper presented at the 305th meeting of the American Physical Society at Washington, D. C. (April 27, 1951).

E7. Dynamic Mechanical and Electrical Properties of the System Polyvinyl Chloride-Dimethylthianthrene. JOHN D. FERRY AND EDWIN R. FITZGERALD, *University of Wisconsin.*—The complex shear modulus, $G^* = G' = iG''$, measured at different temperatures and frequencies, is reduced to a single reference temperature T_0 by plotting $G'T\rho_0/T\rho$ and $G''T\rho_0/T\rho$ against ωa_T, a_T being a reduction factor which expresses the temperature dependence of the mechanical relaxation times.[1] The complex dielectric constant ϵ^* is treated similarly by plotting $\sigma' T\rho/T\rho_0$ and $\sigma'' T\rho/T\rho_0$ against ωb_T, where the relative nonoptical elastivity, $\sigma^* = \sigma' + i\sigma''$, is taken as $1/(\epsilon^* - n^2)$, and b_T expresses the temperature dependence of the electrical relaxation times. For a polyvinyl chloride-dimethyl thianthrene gel, 10 percent by volume, a single curve is obtained for each component of G^* and σ^*, and the factors a_T and b_T are found to be identical over a wide range of time scale. The reduced dispersion functions are quite different, however. The distribution function of mechanical relaxation times may be calculated from either component of the reduced modulus, and the two results agree. A similar concurrence is found for the distribution function of electrical relaxation times, but the electrical and mechanical functions differ. The treatment is also applied to compositions of other concentrations.

[1] Ferry, Fitzgerald, Johnson, and Grandine, J. Appl. Phys. **22**, 717 (1951).

E8. The Relaxation Distribution Function in Polyisobutylene and Polyisobutylene-Decalin Solutions. LESTER D. GRANDINE, JR., EDWIN R. FITZGERALD, IVO JORDAN, AND JOHN D. FERRY, *University of Wisconsin.*—Measurements of the complex shear modulus of a sample of polyisobutylene distributed by the National Bureau of Standards have been made by the double transducer apparatus described in a previous abstract, from 25 to 5000 cps and over a wide range of temperatures. The results are reduced to a reference temperature by the use of reduced variables and the distribution function of relaxation times is calculated from both real and imaginary components. The relaxation distribution function is compared with that derived for solutions in decalin at various concentrations, from measurements of wave propagation, the single transducer, and stress relaxation following cessation of steady-state flow.

E9. Ultrasonic Investigation of Plasticized Polymethyl Methacrylate. R. G. CHEATHAM AND ALBERT G. H. DIETZ, *M.I.T.*—Polymethyl methacrylate of varying plasticizer content was examined by pulsing bursts of ultrasound through flat specimens of varying thickness over a wide range of frequencies and temperatures. It is fairly well known that the mechanical properties of various states of matter are related to the attenuation and velocity of transmission of ultrasound. Perhaps the least understood concepts are the relationships involved in attenuation measurements. The purpose of this research was to investigate the relationships between the velocity and attenuation of ultrasound and the mechanical properties. It was found that increased plasticizer content resulted in an increase in attenuation and a decrease in velocity of transmission. The plasticizer content varied in steps of 0, 5, 10, 20, and 30 percent. The plasticizer used was dibutyl phthalate. The frequency range covered was 0.414 mc to 4.85 mc, and the temperature range from −40°C to +85°C. The velocity decreases with increased temperature along a straight line, whereas the attenuation passes through maxima and minima while exhibiting a general rise in value with increase in temperature. The velocity generally increases with increase in frequency, but again the attenuation passes through maxima and minima while exhibiting a general rise with increased frequency. There are possible indications of hydrogen bonding. The ultrasonic measurements have been correlated with dielectric measurements over the same temperature range.

E10. Acoustic Properties of Rubber as a Function of Chemical Composition. WILLIAM S. CRAMER AND IRVING SILVER, *Naval Ordnance Laboratory.*—An experimental study was made of the bulk and Young's moduli of elasticity at selected audiofrequencies for various natural and synthetic rubber compositions. Both results are expressed in the form of a complex modulus, $E(1+i\eta)$, where η is the loss factor or loss tangent. The bulk data were obtained with a resonant water column at 30°C and 1530 cps. Observations were made of the change in Q and shift in resonant frequency when the sample is inserted in a pressure antinode of the column. The Young's modulus was calculated from measurements on the velocity and attenuation of progressive waves in thin rubber rods. These measurements were carried out at 30°C over the frequency range 1 kc/s to kc/s. Graphs are presented showing variations of acoustic properties as functions of type and amount of filler or plasticizer. Special attention was given to carbon black fillers ranging in size from 30 to 200 microns and to nonreinforcing fillers such as titanium dioxide and diatomaceous earth. In general, the real part of both moduli increased and the loss factors decreased with loading. The variations of the moduli with loading changed substantially with types of filler and of rubber.

FRIDAY MORNING AT 9:30

Physics 100

(E. GUTH presiding)

Invited Papers of the DHPP

F1. Explicit Light-Scattering Functions for Colloidal Solutions of Spheres. W. HELLER AND W. J. PANGONIS, *Wayne University.* (30 min.)

F2. The Small-Angle Scattering of X-Rays by Solutions of Macromolecules. W. W. BEEMAN, *University of Wisconsin.* (30 min.)

F3. Infrared Analysis of the Structure of High Polymers: Recent Developments. G. B. B. M. SUTHERLAND, *University of Michigan.* (30 min.)

F4. Studies of Rapid Crystallization in Polymers. W. H. COBBS, JR. AND R. L. BURTON, *DuPont Company.* (30 min.)

FRIDAY MORNING AT 9:30

Chemistry 161

(CYRIL SMITH presiding)

Invited Papers of the DSSP: Radiation Effects

G1. Introduction to Irradiation Effects in Solids. F. SEITZ, *University of Illinois.* (15 min.)
G2. Radiation Effects in Copper Single Crystals. T. H. BLEWITT, *Oak Ridge National Laboratory.* (30 min.)
G3. Optical Properties of Irradiated Semiconductors. H. Y. FAN AND K. LARK-HOROVITZ, *Purdue University.* (30 min.)
G4. Changes Produced by Irradiation in the Steady-State and the Kinetic Properties of Metals. W. H. PARKINS, *North American Aviation.* (30 min.)
G5. The Thermal Conductivity of Non-Metals at Low Temperatures. W. W. TYLER, *General Electric.* (20 min.)
G6. Heat Conductivity of Quartz. R. BOWERS, *University of Chicago.* (20 min.)

FRIDAY MORNING AT 10:00

Chemistry 100

(J. G. DAUNT presiding)

Invited Papers in Cryogenics

H1. First and Second Sound in Liquid Helium. K. R. ATKINS, *University of Toronto.* (30 min.)
H2. Research of the Cryogenics Branch at the Naval Research Laboratory. R. L. DOLECEK, *Naval Research Laboratory.* (30 min.)

Invited Paper in Nuclear Physics

H3. The Electron-Neutron Interaction. L. L. FOLDY, *Case Institute of Technology.* (30 min.)

FRIDAY MORNING AT 10:00

Physics 110

(L. R. APKER presiding)

Magnetic Resonance: Semiconductors and Rectifiers

I1. Magnetic Resonance in a System Containing Two Magnetic Sublattices.* ROALD K. WANGSNESS, *U. S. Naval Ordnance Laboratory.*—A classical calculation has been made of the normal precession frequencies of a system comprising the magnetizations of the two sublattices. Demagnetizing fields and the effects of anisotropy were included, the latter being described by effective demagnetizing factors which were separately defined for each sublattice. Weiss molecular fields were used to represent the inter- and intralattice interactions which can be of either ferromagnetic or an antiferromagnetic character. The general result thus obtained includes the known special cases of ferromagnetic and antiferromagnetic resonance conditions.[1,2] In the ferromagnetic case, an additional high frequency resonance is predicted which corresponds to a precession in the exchange field where the magnetizations do not precess in phase. The application of these results to resonance experiments is considered.

* Supported in part by the ONR.
[1] C. Kittel, Phys. Rev. **73**, 155 (1948).
[2] T. Nagamiya, Prog. Theoret. Phys. **6**, 350 (1951); C. Kittel, Phys. Rev. **82**, 565 (1951); F. Keffer and C. Kittel (private communication).

I2. Paramagnetic Relaxation in Metals. ALBERT W. OVERHAUSER,* *University of California, Berkeley.*—The paramagnetic relaxation effects of electron spins in metals have been studied. A description for the spin relaxation of a degenerate electron gas was developed, and five interactions which contribute to this relaxation were considered in detail. The relaxation times to be associated with the following processes were calculated: (a) interaction with magnetic fields arising from lattice vibrations, (b) interaction with electric fields arising from lattice vibrations, (c) interaction with nuclear spins, (d) interaction with the spins of other electrons, and (e) interaction with the fields due to the translational motion of other electrons. Only first-order transitions caused by the above perturbations were considered, and with the exception of process (c), the electrons were treated by means of plane waves, corresponding to independent motion in a potential well of constant depth. The most important process is that due to (e). This relaxation time was found to be approximately inversely proportional to temperature and to have a value of one microsecond at room temperature. The influence of exchange and correlation energies on the relaxation times, and the energy absorption, line width, and saturation effects that would be expected in a resonance absorption experiment were also treated.

* Now at the University of Illinois, Urbana, Illinois.

I3. Radiation Produced in Germanium and Silicon by Electron-Hole Recombination. J. R. HAYNES AND H. B. BRIGGS, *Bell Telephone Laboratories.*—Radiation has been obtained by carrier injection in both germanium and silicon. Analysis shows that at room temperature the radiation intensity is sharply peaked at a wavelength which corresponds so closely to the best estimates of the energy gap that there is little doubt that it is due to the direct recombination of excess electrons and holes. The wavelength of the maximum of the radiant energy from germanium was found to decrease with decreasing temperature from room temperature to that of liquid hydrogen. This decrease is in quantitive accord with the temperature coefficient of the energy gap deduced from electrical resistivity and Hall measurements[1] ($\mathcal{E}_0 - 0.72 = 10^{-4}T$ electron volts). The value of the half-intensity width of the radiation from germanium may be expressed by the emperical formula $W = 0.022 + 3kT$ electron volts over the temperature range investigated.

W. Shockley, *Electrons and Holes in Semiconductors* (D. Van Nostrand Company, Inc., New York, 1950), p. 335.

I4. Test of Transistor Equations. M. B. PRINCE AND F. S. GOUCHER, *Bell Telephone Laboratories.*—By measuring five parameters in a *n-p-n* junction transistor, *viz.*, the conductivities and diffusion lengths for minority carriers in the emitter and base regions and the width of the base region, an α for the transistor can be computed from theory.[1] Previous to this investigation two of the parameters associated with the thin *p*-layer had not been measured. We have been able to measure these parameters and thus to calculate an α. The quantity α was also obtained independently in two ways: (1) by measuring the collector current—emitter current characteristic, and (2) by measuring the apparent quantum efficiency of the transistor as a two-electrode device with the base floating.[1] Five experimental samples with significant variations in the five parameters were examined. The three values of α for each sample were found to agree within the experimental error.

[1] Shockley, Sparks, and Teal, Phys. Rev. 83, 151–162 (1951).

I5. Probing the Space-Charge Layer in a *p-n* Junction. G. L. PEARSON, W. T. READ, AND W. SHOCKLEY, *Bell Telephone Laboratories, Inc.*—The potential distribution in the space-charge region in a germanium *p-n* junction was determined by measuring the zero-current potential of a pointed tungsten probe pressed against the space-charge layer where it comes to the surface of the specimen. The space-charge layer is wide compared to the area of contact of the point and may be thought of as a region of dielectric. When the point is at the natural potential of the dielectric, no current flows. When the point has a potential applied to it externally, a current flows which consists of injected carriers. The point was moved by dragging it with light pressure, using a Hilger interferometer movement and the zero-current potential measured as a function of distance for different reverse biases from 20 to 90 volts. The relationship $4\pi C = \kappa W$ between the capacity per unit area C and the width of the space-charge layer W was found to hold within experimental error over the measured range of voltages for a dielectric constant κ of 16.1. It was found that C varied as $1/V^{\frac{1}{2}}$ at low reverse voltages and as $1/V^{\frac{1}{3}}$ at large reverse voltages indicating a linear concentration gradient in the center merging into constant concentration regions at each side.

I6. High Temperature Reduced-TiO_2 Rectifiers.* A. E. MIDDLETON, C. S. PEET, O. J. MENGALI, AND R. C. SIRRINE.—Work on high temperature semiconductor rectifiers has been in progress for 2½ years at Battelle. An analysis of the relationship between properties of materials in rectifiers and obtainment of rectification, in addition to a point-contact rectification survey of selected semiconductors, was initially conducted. Subsequently, selected semiconductors were purified and made in semicontrolled impurity states. Resistivity, thermoelectric power, and rectification tests were used to classify the semiconductors. Reduced TiO_2 showed early promise for use in an area rectifier. Reduced-TiO_2 rectifiers have been prepared by (a) oxidizing titanium sheet in oxygen and in water vapor, and (b) preparing ceramic TiO_2, followed by reduction in vacuum (also hydrogen) and applying vaporized, electroplated, and metal wire counterelectrodes. Rectifiers with counterelectrode areas ranging from 0.0028 to 0.2 square inch were successfully made. The influence of the work function and type of counterelectrode in the dc characteristic have been studied up to 250°C. Thirty-six-volt reverses and 0.8-volt forwards at room temperature have been observed. Rectification persists up to 300°C. A comparison of Se, Cu_2O, and TiO_2 rectifiers reveals that the TiO_2 rectifier may satisfy the practical need for high temperature rectifiers.

* This work has been supported by Wright-Patterson Air Force Base.

I7. Analysis of High Temperature Reduced-TiO_2 Rectifier Characteristics.* C. S. PEET and A. E. MIDDLETON.—Analysis of typical high temperature reduced-TiO_2 rectifier characteristics indicates that the Schottky diffusion theory of rectification applies. The current-voltage characteristics and behavior of the barrier-layer capacity were studied as a function of temperature, applied voltage, and work function of the counterelectrode. The contact resistance was found by extrapolation of the current-voltage characteristic through zero voltage. The height of the potential barrier was calculated from the slope of the contact resistance *versus* temperature curve between room temperature and 200°C. The height of the potential barrier varies directly with the work function of the counterelectrode, indicating that the rectifying junction is at the interface between the reduced TiO_2 and the counterelectrode. Alpha, the experimental value of e/kT in the Schottky diffusion equation, was found to vary between 0.4 and 0.8 per volt, instead of being 40 per volt at room temperature. Analysis of the capacitive characteristics of the barrier as a function of voltage and temperature gave information regarding the barrier thickness and the number of current carriers in the barrier region. The occurrence of rectification at high temperatures is apparently due to a high Schottky diffusion potential.

* This work has been supported by Wright-Patterson Air Force Base.

I8. Thermoelectric Effects in Germanium at Low Temperatures.* H. P. R. FREDERIKSE, *Purdue University.*—The thermoelectric power of germanium (against lead) was measured in the temperature region between 10° and 85°K. The apparatus was designed in accordance with Borelius' method[1] (with three junctions of which two are at the same temperature). The sample was soldered between two copper blocks; one block was in thermal contact with the refrigerant bath, the other block could be heated. The temperatures of both junctions were measured by means of resistance thermometers (lead wires or carbon resistors). Two (*n*-type) antimony-doped germanium single crystals were investigated. The thermoelectric power was found to be several hundred microvolts per degree and could be described by $Q = aT$ in the impurity range ($T < 30$°K). Above this temperature the dependence is more complicated. The behavior is very similar to that observed in SiC, CoO, and V_2O_3.[2] The theory predicts for the thermoelectric emf of semiconductors the following expression: $Q = (k/e)(\ln RT^{\frac{3}{2}} - 5.32)$, in which R is the Hall coefficient. This formula gives good agreement down to $T \sim 150$°K,[3] but seems to break down at very low temperatures.

* Supported by Signal Corps Contract.
[1] G. Borelius, Ann. Phys. (4) 66, 73 (1921).
[2] B. M. Hochberg and M. S. Sominskl, Phys. Z. Sowjet 13, 198 (1938).
[3] K. Lark-Horovitz, W. Scanlon, *et al.*, N.D.R.C. report 14, 385.

I9. Calculation of Magnetic Field Effect upon the Hall Coefficient of Impurity Semiconductors.* W. J. WHITESELL, II, AND V. A. JOHNSON, *Purdue University.*—A number of investigations have demonstrated the dependence of the Hall coefficient R of semiconductors upon magnetic field H. The theoretical treatment of this effect by Harding[1] employs the Lorentz solution of the Boltzmann equation and assumes that the mean-free-path l of conduction electrons is independent of energy. However, these electrons are subject to various types of scattering, particularly lattice scattering with an energy-independent mean-free-path and Rutherford scattering with a mean-free-path proportional to the square of the energy. Upon this basis, the integrals giving the dependence of R upon H have been evaluated with $l=l_I l_L/(l_L+l_I)$, where l_L is constant and l_I is proportional to E^2. The dependence of R upon H has been found as the proportion of impurity scattering rises from 0 to 100 percent. Generally, R decreases with increasing H, but the rate of decrease is dependent on the proportion of impurity scattering.[2] For the most part, the computed change of R with H is too small to agree with observation.

* Supported in part by Signal Corps Contract.
[1] J. W. Harding, Proc. Roy. Soc. (London) **A140**, 205 (1933).
[2] Case $l = l_I$ discussed in V. A. Johnson and K. Lark-Horovitz, Phys. Rev. 79, 176 (1950).

I10. Infrared Absorption Band in Germanium.* R. J. COLLINS AND H. Y. FAN, *Purdue University.*—Infrared transmission of bulk germanium was measured up to 38 microns. The absorption coefficient of a high resistivity sample (39 ohm-cm) up to 15 microns was so low that it could not be reliably determined, it then begins to rise steeply with increasing wavelength showing a sharp maximum of 25 cm^{-1} at 29 microns. A sample with ~600 times higher carrier concentration gives a similar absorption coefficient curve, the values being only slightly higher. The curve for a sample with still higher carrier concentration and much higher absorption coefficient can be analyzed into two parts; a smooth curve of increasing absorption coefficient with increasing wavelength plus the curve for the high resistivity sample. This indicates that the curve for the high resistivity sample corresponds to an absorption band independent of the carriers and characteristic of lattice. The limiting frequency of the lattice vibration for a diamond type lattice is related to the elastic constants by an expression given by Born.[1] This relation is well satisfied by the frequency of the absorption peak.

* Work supported by Signal Corps Contract.
[1] M. Born, Nature 582 (1946).

FRIDAY AFTERNOON AT 1:45

Physics 100

(R. BUCHDAHL presiding)

Invited Papers of the DHPP

J1. Structure of Solid Solutions. R. SMOLUCHOWSKI, *Carnegie Institute of Technology.* (35 min.)

J2. Structure of Solids by Neutron-Diffraction. C. G. SHULL, *Oak Ridge National Laboratory.* (40 min.)

J3. Structure and Mechanical Properties of Glasses. W. A. WEYL, *Pennsylvania State College.* (45 min.)

Business Meeting of the Division of High-Polymer Physics

FRIDAY AFTERNOON AT 2:30

Chemistry 100

(J. H. VAN VLECK presiding)

Invited Papers of the DSSP: Recent Theory

K1. Electronic Wave Functions for Magnetism and Chemical Binding. J. C. SLATER, *M.I.T.* (30 min.)

K2. A Collective Description of Electron Interactions. D. PINES, *University of Pennsylvania.* (30 min.)

K3. The Physical Basis of Ferromagnetism. C. ZENER, *Westinghouse Research Laboratories.* (30 min.)

K4. Recent Calculations on the Alkali Metals. H. BROOKS, *Harvard University.* (30 min.)

K5. Theory of Antiferromagnetic Resonance. C. E. KITTEL, *University of California, Berkeley.* (30 min.)

FRIDAY AFTERNOON AT 3:15

Physics 110

(W. V. HOUSTON presiding)

Cryogenics

L1. Energy Levels of a One-Dimensional Bose Solid. H. W. LEWIS, *Bell Telephone Laboratories.*—A study has been made of the effects of anharmonicity and statistics on the energy-level structure of a one-dimensional solid whose atoms obey Bose statistics and are treated as point particles. (The same procedure applies to Fermi statistics, with a few changes of sign.) In order to study the effect of statistics, it is essential to introduce an anharmonicity into the interatomic force, thus to go beyond the usual description of the Debye waves. This is clear, since a solid composed of indistinguishable particles, interacting through attractive harmonic forces, will obviously collapse. One must therefore choose a potential with a finite range; for this work, Gaussian potentials were used, largely because one can then do all the integrals that occur. Using a Gaussian repulsion centered at the origin, plus a Gaussian attraction centered at some optimum interatomic distance, we then make a variational fit of wave functions of the usual Debye type, expressed in terms of their configuration space variables. We then symmetrize these wave functions to study the effect of statistics. The results will be discussed with reference in particular, to the anomaly in the specific heat of solid helium at very low temperatures.

L2. Relativistic Quantum Statistics of Thermal Excitations and Its Application to Condensed Systems at Very Low Temperatures. C. V. HEER AND J. G. DAUNT.—In systems of short range order for which quantum mechanics are applicable, i.e., for fluids at very low temperatures, the thermal excitations are energetically of magnitude $h\mu s$, where s is the velocity of sound and μ a parameter expressing the range of ordering. The quantum statistics of these thermal excitations are treated relativistically, using field theory methods analogous to those employed by Scheidegger and McKay,[1] but in which statistics the energy for the "creation" of excitations may be equal to or *less* than kT. It is shown that this treatment leads: (a) to a transition phenomena analogous to the degeneracies in Bose-Einstein and in Fermi-Dirac statistics; and (b), to the result that for long range order (e.g., in solids or in liquids helium II near 0°K), where $\mu \to 0$, the well-known phonon excitations are arrived at as a limiting case, both for field representations which commute and anti-commute. A parallel treatment is given for relativistic systems in which the "particular" nature of the system is stressed, and it is found that the degeneracy temperatures of such systems correspond to the transition temperatures of the previous models. Tentative applications are made to transitional phenomena in liquid He^4 and in liquid He^3, and to other phenomena occuring in such liquids very close to the absolute zero.

[1] A. E. Scheidegger and C. D. McKay, Phys. Rev. **83**, 125 (1951).

L3. Design and Performance of a New Type Heat Interchanger for Large Helium Liquefiers. J. NICOL, T. S. SMITH, C. V. HEER, AND J. G. DAUNT, *Ohio State University.*—A counterflow heat interchanger for exchanging between high pressure and low pressure helium gas flows at temperatures between 10°K and 90°K is described. The design is such that the low pressure flow is at right angles to the tubes carrying the high pressure gas, and is canalized through spaces formed by threading the high pressure tubes. A comparison is given of the computed performance with the observed results. Observations of the efficiency of the interchanger were made by incorporating it in a large helium liquefier in use in the Physics Department. This liquefier, constructed in the laboratory, is of the Kapitza type,[1] using as in the Collins machine[2] two reciprocating expansion engines, and has a production rate of 4 liters of liquid helium per hour.

[1] P. L. Kapitza, Proc. Roy. Soc. (London) **A147**, 189 (1934).
[2] S. C. Collins, Rev. Sci. Instr. **18**, 157 (1947).

L4. The NBS Liquid Level Indicator for Condensed Gases. W. E. WILLIAMS, JR. AND E. MAXWELL, *National Bureau of Standards.*—This instrument indicates the liquid level inside of a closed vessel and is especially designed for use at low temperatures with liquefied gases such as nitrogen, oxygen, hydrogen, and helium. It operates on a capacitance principle, and makes use of the difference in dielectric constants of the liquid and vapor. The sensing element is a cylindrical capacitor, whose capacitance is a function of the height of the liquid column. The sensing capacitor is one element of an automatically balanced bridge which both indicates and records the liquid level. An over-all accuracy of ±1 percent has been obtained. The sensitivity is adequate for use where the difference in dielectric constants of the liquid and vapor is 0.05 or greater. The instrument also incorporates a control function, and supplies a controlled air pressure to a pneumatically operated value for maintaining the level at a predetermined point.

L5. Superconductivity of Thallium Isotopes. E. MAXWELL AND O. S. LUTES, JR., *National Bureau of Standards.*—The isotope effect has been observed in the superconductivity of thallium samples of mass 203.3 and 205.0. The difference in transition temperatures is 0.012°±.003°. This would correspond to a mass temperature relation of the form $_M 0.61 \pm .15 T_c = \text{constant}$. $(dH/dT)T_c = 126$ oersteds/°K. The specimens were prepared by chemical reduction of isotopically enriched samples of Tl_2O_3 loaned by the Atomic Energy Commission. Measurements were made on duplicate samples by a magnetic method.

L6. Experiments with a Rotating Cylinder Viscometer in Liquid Helium. II. A. C. HOLLIS-HALLETT, *University of Toronto* (Introduced by M. F. Crawford).—In the experimental arrangement, the inner cylinder was suspended by a torsion fiber while the outer cylinder was rotated at various constant velocities in the range 0.1 to 3 cm/sec. Unlike the results obtained with ordinary fluids, the torque, produced by the rotating helium II upon the inner cylinder, was not found to be directly proportional to the velocity of rotation at any temperature between the lambda-point and 1.15°K. It has been found necessary to postulate the existence of a new type of frictional force in liquid helium II in order to explain the results; the force of mutual friction proposed by Gorter and Mellink is inadequate. Extrapolation of the results to zero velocity has given values of the viscosity of the normal component. These agree with the oscillating disk results between the lambda-point and about 1.6°K; but, at lower temperatures, the present results are significantly lower, suggesting, perhaps, that the accuracy of the existing data for the density of the normal component is less than has been supposed below 1.6°K.

L7. Free Energies and Phase Transition of a Cylindrical Superconductor.* PAUL M. MARCUS, *University of Illinois.*—The definitions of, and distinctions between the Helmholtz

and the appropriate Gibbs free energies for a cylindrical superconductor in a uniform longitudinal magnetic field, (field lines straight, arbitrary cross section) have been carefully discussed, taking account of the exact form of the field penetration according to the London equations. Free energy density formulas are derived, which are used to obtain the condition for the first breakdown of the superconducting phase and formation of a normal region, by considering the change of the total Gibbs free energy of the specimen. Full account is taken of the modification of the field distribution as the phase boundary pushes into the specimen. The condition found is, that the current density at some point on the surface must attain the same value as that at which a massive superconductor undergoes transition. For a thin specimen of convex cross section, this occurs at higher critical fields than for a massive specimen. This condition is definitely not that for complete transformation to the normal state, which occurs at still higher fields. The condition may also be expressed by saying that the Gibbs free energy density is spatially continuous through the phase boundary.

* Work supported by the ONR.

L8. Low Temperature Dielectric Behavior of Potassium Niobate.* R. PEPINSKY, R. THAKUR, AND C. MCCARTY, *The Pennsylvania State College.*—Dielectric measurements of $KNbO_3$ by Matthias and co-workers[1,2] revealed the ferroelectric Curie point at 420°C and a further transition at 228°C. These investigators reported finding no significant variation in dielectric constant at temperatures below the latter point. Measurements in this laboratory at 10 Kc/sec on single crystals of $KNbO_3$, prepared without flux, do show a sharp peak in dielectric constant at about −50°C, as the temperature is dropped. The peak is observable in crystals of high purity and consequent low conductivity, and corresponds to an increase in dielectric constant from about 500 to nearly 1000. Between −50°C and −100°C the dielectric constant drops slowly, and from −100°C to −190°C it falls more rapidly to a value of about 100. The coercive field shows an increase as the temperature drops toward −50°C, becomes very large at that temperature, and then falls slowly as the temperature falls. The dielectric change is less pronounced and shifted upward by about 15° for measurements made from −190°C upward. The nature of this lower transition is under x-ray examination.

* Development supported by Office of Air Research.
[1] B. T. Matthias, Phys. **75**, 1771 (1949).
[2] B. T. Matthias and J. P. Remeika, Phys. Rev. **82**, 727 (1951).

L9. The De Haas-Van Alphen Effect in Tin.* G. T. CROFT, W. F. LOVE, F. C. NIX, *University of Pennsylvania.*—The de Haas-van Alphen effect has been observed in a spherical single crystal of tin $\frac{1}{16}''$ D at 1.81°K. The torsional method was used where the difference in susceptibilities along the tetragonal Z-axis and the X-axis is measured. The angle between the tetragonal axis and the magnetic field was 45°. In order to remove the effects due to eddy currents, the galavnometer coil in the torsional suspension was made part of a negative feedback split photocell-amplifier circuit. The magnetic field was carefully regulated by a current control circuit utilizing a *Brown Converter*, permitting the period of the oscillations in tin to be resolved. Results are in fair agreement with data published by Shoenberg.[1] The period of the oscillations goes from approximately 26 gauss in the neighborhood of 6.3 kg, to approximately 50 gauss at 8.6 kg, while the amplitude of the oscillations increases by a factor of 5 over the same interval. A plot of $1/H$ at successive maxima in $x_s - x_s$ *versus* a set of consecutive intergers yields a linear relationship indicating that the oscillations contain a factor of the form $\sin[(\alpha/H)-\beta]$.

* Supported by the AEC.
[1] Shoenberg, Nature **8162**, 225 (1949).

L10. Magnetic Properties of Superconducting Tin-Bismuth Alloys.* W. F. LOVE, *University of Pennsylvania.*—Magnetization curves for spherically shaped superconducting alloys of Sn and Bi have been measured as a function of temperature and Bi content. The Bi is kept in solid solution at 135°C and quenched in liquid air just before taking measurements. With increasing Bi content (up to 12 at. percent Bi) the magnetic transition from superconducting to normal state becomes broader and the transition temperature increases uniformly. Alloys through 8 percent Bi show a better than 70 percent Meissner effect. A plot of the field at which penetration begins as well as that for which penetration is complete *versus* T^2 yields a straight line. In the former case the slope of this line decreases with increasing Bi content while in the latter case it rises rapidly.

* Supported by the AEC.

FRIDAY AFTERNOON AT 3:15

Chemistry 161

(F. SEITZ presiding)

Nonmetallic Crystals

M1. Electron Microscopic and Diffraction Studies of Some Paraffinic Sodium Soaps.* MORTON L. E. CHWALOW,† *Temple University.*—Electron microscopic investigations of the crystalline structures formed by the paraffinic sodium soaps, from sodium butyrate ($NaC_4H_7O_2$) through sodium stearate ($NaC_{18}H_{35}O_2$), show these to consist primarily of ribbon-like fibers which in the higher molecular weight soaps occasionally form closed rings. The maximum widths of these fibers decrease as the molecular weights of the soaps increase. As is known, sodium soap molecules align themselves parallel the long axes of their hydrocarbon chains and with their ionic ends adjacent to each other, thus forming bimolecular laminae. Present electron diffraction studies substantiate this and demonstrate that the long axes of the hydrocarbon chains are oriented essentially normal to the planes of the above noted ribbon-like fibers. Knowledge of this plus analysis of the van der Waals forces acting between the adjacent hydrocarbon chains and the forces prevailing in the ionic layer, lead to a direct explanation of the structures and structural changes observed electron microscopically.

* Materials and equipment (RCA) were provided by Socony Vacuum Laboratories.
† Present address: Frankford Arsenal Philadelphia, Pennsylvania.

M2. Effect of Lattice Imperfections upon X-Ray Diffraction and Linear Dimensions of Crystals.* P. H. MILLER, JR., AND B. R. RUSSELL, *University of Pennsylvania.*—Assuming radial distortion of a symmetric cubic crystal around a vacancy (or interstitial atom) at the origin, the relative change

in lattice parameter calculated from the shift in the x-ray diffraction maxima is of the general form $\Delta d/d = \{(\Sigma l)(\Sigma lf(r)) - N(\Sigma l^2 f(r))\} + \{(\Sigma l)^2 - N(\Sigma l^2)\}$, where $f(r)$ is the relative change in length of the lattice vector $r = a(l^2+m^2+n^2)^{\frac{1}{2}}$, and the summations are over lmn of the N lattice points. When $f(r)$ is taken as Aa^3r^{-3} and n, such defects occur in the crystal. It is found that $\Delta d/d = 2.0(4/3\pi A)n/N$, allowing a 30 percent reduction as a result of the random distribution of the defects.[1] The macroscopic crystal expansion for this case, however, is only one-half as great so that the observations of Berry[2] and Strelkow on AgBr cannot be explained as a result of a predominance of Frenkel defects.

* This work supported by ONR.
[1] This equation corrects an error in the abstract previously submitted, Am. Phys. Soc. Bulletin 26, No. 6, D4.
[2] C. R. Berry, Phys. Rev. 82, 422 (1951).

M3. Structure of Ordered Phase of Ag_2HgI_4.* C. E. OLSEN AND P. M. HARRIS, *The Ohio State University*.—As a result of the development of a suitable technique, single crystals of $\beta-Ag_2HgI_4$ have been grown. As a result of interest in the well-known transformation at 52°C observed by Ketelaar[1] and in the structure proposed by him for the temperature (β) modification of this substance, its structure has been reinvestigated. Powder x-ray diffraction data for this β-phase show only lines assignable to a cell of cubic dimensions, even at liquid air temperatures. However, a number of weak lines (correspond to a cell with a_0 twice that of Ketelaar. Some of these have been reported by Frevel.[2] Single crystals of the β-phase exhibit $D_{2d}(\bar{4}\,2m)$ symmetry. Weissenburg x-ray goniometric measurements appear to require a body-centered tetragonal cell with $a_0 = 6.32$A° and $c_0 = 12.64$A°. This corresponds to a cell with just twice the c_0 reported by Ketelaar. The structure will be discussed.

* Assisted by funds from ONR.
[1] Ketelaar, Trans. Faraday Soc. 34, 874 (1938).
[2] L. K. Frevel and P. P. North, J. Appl. Phys. 21, 1038 (1950).

M4. Crystal Structure of Cesium Monoxide.* KHI-RUEY TSAI AND P. M. HARRIS, *The Ohio State University*.—Single crystals of cesium monoxide (Cs_2O) have been prepared for the first time. The anti-$CdCl_2$ layer structure (D_{3d}^5) of the monoxide previously suggested by Helms and Klemm[1] from powder data has been confirmed from single crystal x-ray diffraction work. The cell constants (hexagonal indexing) and interionic distances have been found to be: $a = 4.256$A, $c = 18.99$A, $u = 0.242$, $Cs^+ - O^= 3.01$A, and $Cs^+ - Cs^+ = 3.77$A, respectively, compared with $a = 4.27$A, $c = 18.8$A, $u = 0.25$, $Cs^+ - O^= 2.91$A, and $Cs^+ - Cs^+ = 3.99$A as observed by Helms and Klemm. The orange-yellow crystals of the monoxide tend to develop the basal planes and exhibit shearing disorder when freshly pulverized. The structures and characteristics of some of the suboxides of cesium will also be discussed. Interest in this substance arose due to its possible occurrence in the Ag−O−Cs photocathode.

* Work supported in part by a fellowship grant from The Ohio State University Research Foundation to the University for Aid in Fundamental Research and under contract with the Engineer Research and Development Laboratory, Fort Belvoir, Virginia.
[1] A. Helms and W. Klemm, Z. anorg. u. allgem. Chem. 242, 33 (1939).

M5. Charge Distribution and Vibration Amplitudes in LiH and Li D. C. K. STAMBAUGH* AND P. M. HARRIS, *The Ohio State University*.—Intensities of Laue-Bragg scattering of CuK alpha x-rays from powder samples of LiH and LiD have been made from 20°K to room temperature. From the temperature coefficient of scattering the amplitudes of vibration have been evaluated. The corresponding characteristic temperatures are 851°K and 638°K for LiH and LiD, respectively. Charge distributions in the ions have been evaluated and compared with those calculated by Ewing and Seitz.[1] The variation of the charge distribution with temperature will be discussed.

* Major, USAF, Los Alamos Scientific Laboratory.
[1] D. H. Ewing and F. Seitz, Phys. Rev. 50, 772 (1936).

M6. Structure of Graphitized Carbon Blacks. EDWARD A. KMETKO, *University of Buffalo*.—Previous electron microscopic studies of a carbon black (Thermax) showed that the particles lose their spheroidal forms during graphitization and assume shapes exhibiting polygonal outlines.[1] In this paper more detailed investigations of such structures are reported. Thermax carbon black (particle size ~3000A), heat treated to 3000°C in an atmosphere of nitrogen, was dispersed in a thermosetting resin. Formvar replicas of fracture surfaces were made by a variation of the usual procedure. Electron micrographs of these replicas show partial view of polyhedra which appear to have a high degree of symmetry and whose facets appear consistent with the symmetry of the aromatic lattice. All the projected views of the graphitized particles can be generated from a single type of polyhedron. Therefore, it seems probable that all carbon black particles during graphitization crystallize into a single form. In the case of another black of somewhat smaller size (*P*-33) direct views of the particles themselves show not only the same general features, but indicate clearly that the polyhedral structure extends throughout the body of the particle.

[1] Ragoss, Hoffman, and Holst, Kolloid-Z. 105, 118 (1943).

M7. Mechanism for Self-Diffusion in Graphite.* G. J. DIENES,† *North American Aviation, Inc.*—The mechanism for self-diffusion in single crystals of graphite has been examined theoretically. Calculations for vacancy and direct interchange mechanisms are based on atomic interactions within the graphite hexagonal layers. These interactions are obtained from the known systematic change of carbon-carbon bond strength with interatomic distance. In order to be able to calculate the energy of formation of an interstitial carbon atom a potential function has been devised to account for interaction between the planes. This potential function consists of two terms, a Van der Waals' attraction and an exponential type repulsion. The adjustable constants have been evaluated from known physical data.

Comparison of the total activation energies for self-diffusion via vacancies, direct interchange, and interstitial atoms shows clearly that vacancy diffusion is the preferred mechanism. The activation energy for self-diffusion by means of vacancies is estimated to be 160 kcal/mole with 90k cal/mole required for the formation and 70 kcal/mole for the motion of vacancy. The present theoretical treatment is not applicable to diffusion along grain boundaries or pores.

* This work was supported by the AEC under contract AT-11-1-GEN-8.
† Now at Brookhaven National Laboratory, Upton, Long Island, New York.

M8. The Electrical Conductivities of Natural Graphite Crystals. W. PRIMAK AND L. FUCHS, *Argonne National Laboratory*.—General agreement exists in the literature concerning the value of the "*a*" axis conductivity of graphite. However, measurements and estimates of the "*c*" to "*a*" axis conductivity ratio ranging from 10^{-2} to 10^{-4} have been reported. Graphite crystals (which are somewhat imperfect) have been separated from graphite-bearing crystalline limestones from northeastern North America. Measurements of potential drops and potential distributions on the surfaces of these graphite crystals carrying electric current show their "*c*" to "*a*" axis conductivity ratio to be approximately 10^{-2} and in no case less than 1.7×10^{-3}.

M9. Development of the Korringa Method for Energy Band Calculations. R. J. HARRISON, *Battelle Memorial Institute*.—The Korringa method for determining electronic energy levels in crystals, which we have restated in terms of a scattering matrix formalism,[1] has the computational advantage that the part of the calculation which is concerned with meeting the periodic boundary conditions implied by the Bloch theorem may be performed once and for all for a given lattice type. For this purpose one evaluates the components

of a certain matrix $\mathbf{S}_B$, which is a function of the Bloch wave vector $\mathbf{k}$ and the energy E. In the other part of the calculation, which depends on the particular potential, V, within an atomic polyhedron, one determines $E(\mathbf{k})$ from a matrix equation connecting $\mathbf{S}_B(\mathbf{k}, E)$ and the scattering matrix $\mathbf{S}_V(E)$. In preparation for the specific application of this method, besides computing the elements of $\mathbf{S}_B$ for cubic lattices we have been exploring the formalism itself by considering certain special cases in detail. In particular we have examined the extreme cases of the "tight binding" and the "nearly free" electron approximations. These show features which are of intrinsic interest as well as relevant in testing the general method.

[1] R. J. Harrison, Phys. Rev. **84**, 377 (1951).

M10. Optical Polarization in Single Crystals of Tellurium.* JOSEPH J. LOFERSKI AND PARK HAYS MILLER, JR., *University of Pennsylvania.*—The transmission of polished single crystals of tellurium has been observed as a function of the polarization of the incident radiation. The position of the absorption edge and the amount of radiation transmitted differ with the direction of polarization. For radiation polarized with the E vector perpendicular to the C-axis of the crystal, the absorption edge lies at 3.7μ and the transmission beyond the edge is about 34 percent for a sample 0.034 cm thick; if the E vector is parallel to the C-axis of the crystal, the edge has shifted to 3.3μ and the transmission has dropped to 18 percent. The index of refraction of the material, which varies between 5.0 and 7.0 in the region from 4.0μ to 8.0μ, was determined by measuring the deviation of a beam of unpolarized light occurring in a small angle prism. Computation of the refractive index from the reflected radiation yields a value of about 5.

* This work supported by the ONR.

FRIDAY EVENING AT 7:00
Deshler-WALLICK HOTEL
(J. H. VAN VLECK presiding)

Banquet of the American Physical Society

After-dinner speakers: W. J. Lyons, H. H. Nielsen, and J. C. Slater

---

SATURDAY MORNING AT 9:30
Chemistry 161
(L. M. DANNIS presiding)

Invited Paper of the DHPP

N1. The Viscosity of Concentrated Macromolecular Solutions. R. SIMHA, *New York University.* (30 min.)

Contributed Papers

N2. Self-Diffusion and Bulk Viscosity of High Polymers.* F. BUECHE, *Cornell University.*—In spite of its fundamental importance for an understanding of the physical properties of solid polymers, little is known about the rate of molecular diffusion in such systems. This paper will outline some results obtained from radioactive tracer measurements of the self diffusion constant, D, in polystyrene and poly n-butyl acrylate. A theoretical treatment of its relation to η, the bulk viscosity, will also be given. The experiments confirm a theoretically derived relation that $D \times \eta$ equals a constant composed of known quantities. Moreover, simple considerations have led to a relation for the bulk viscosity of solid polymers which agrees with experimental data available for polystyrene and polyisobutylene. Some success has been achieved in evaluating the segmental jumping frequency from a knowledge of bulk viscosity. The values thus found are in substantial agreement with those inferred from dielectric data—at least at the so-called second-order transition temperature.

* This work was supported by a contract with the R.F.C., Office of Rubber Reserve in connection with the U. S. Government's synthetic rubber program.

N3. The Effect of Diluents on the Second-Order Transition and Flow Properties of Polystyrene.* T. G. FOX, *Rohm and Haas Company.*—Volume dilatometric data on polystyrene mixed with each of thirteen low molecular weight diluents differing widely in their chemical nature have been obtained over broad ranges in temperature and composition. Viscometric measurements over the entire composition range have also been made for mixtures with dibenzyl ether. Up to about 30 percent of diluent, the second-order transition temperature (T_g) is depressed by an amount that is approximately proportional to the *volume fraction* of diluent added. When the data are represented in this way, the effects of the various diluents employed here are indistinguishable. At higher concentrations of diluent, the depression of T_g is much less than the above-mentioned linear relationship would predict. The dependence of T_g on composition closely parallels corresponding data on the lowering of the viscosity-temperature coefficient for polystyrene-dibenzyl ether mixtures. No correlation exists between the T_g-composition relationship and the S-shaped curves obtained in plots of the logarithm of the viscosity at a given temperature *vs* the composition for polystyrene-dibenzyl ether mixtures.

* This work was carried out at Cornell University, in connection with the Government Research Program on Synthetic Rubber under contract with the Office of Rubber Reserve, Reconstruction Finance Corporation.

N4. The Effect of Cross Linking on the Second-Order Transition Temperature of Polymethyl Methacrylate. S. LOSHAEK, *Rohm and Haas Company.*—The second-order transition temperature (T_g) of methyl methacrylate copolymerized with zero to 100 percent of (1) ethylene glycol dimethacrylate, (2) decamethylene glycol dimethacrylate, (3) 2,2-dimethyl-propanediol-1,3 dimethacrylate, and (4) 2-ethyl-2-butyl-propanediol-1,3 dimethacrylate have been determined by volume dilatometric measurements. The foregoing cross linkers were chosen to demonstrate first, the effect of increasing the length of the carbon chain between functional groups and second, the length of the side chain. There is a marked dependence of T_g on the structure of the cross linker molecule for a given concentration of the latter. Since T_g of the polymers formed from 100 percent of (2) and (4) is lower than that of pure polymethyl methacrylate, the possibility of a maximum T_g at some composition appears. The results can be rationalized if it is assumed that T_g is raised by the presence of cross

links and is at the same time lowered by an internal plasticization effect, the latter being dependent on the average composition and structure of the comonomer.

N5. Strain-Temperature Studies of Transitions in Rubbers.* R. J. DERENTHAL, F. P. BALDWIN, AND R. L. ANTHONY, *University of Notre Dame.*—Previously reported studies of the apparent second-order transition in rubbers by the length-temperature method (constant stretching load on sample) indicated an unusual dependence of the transition temperature, T_L, upon the initial tension strain, ϵ_0, of the sample. T_L was found to first increase as ϵ_0 was increased from zero to the thermoelastic inversion extension (about 7 percent), then to decrease with further increase in ϵ_0; finally, for some rubbers, T_L appeared to level off at higher extensions. These studies have been continued. In addition, a study of the dependence of the transition temperature upon shearing strain was undertaken. Results for several rubbers indicate no dependence of the transition temperature upon initial shearing strain for strains ranging from 0 percent to about 13 percent, in sharp contrast to the behavior observed in length temperature studies. The experimental methods employed in this work will be described, and the results obtained from both types of measurements will be discussed. It is not yet possible to specify the frequency spectrum for any of the materials studied (Cellophane, Nylon, and vinylidene chloride copolymers) because many of the patterns exhibit multiple effects. While the amplitude is generally decreasing with frequency secondary maxima appear in various parts of the record. These results are consistent with our earlier interpretation of this noise as arising from the motion of clusters of ions.

* Supported in part by the ONR.

N6. Random Noise in Dielectrics, II. HERBERT BAUSS AND R. F. BOYER, *The Dow Chemical Company.*—The fluctuating currents previously observed on applying a steady voltage to a number of polar polymers have been investigated further, both as regards temperature dependence and frequency spectrum of the noise. The effect diminishes with temperature but does not disappear on going through the second-order transition temperature. In the case of Nylon and a vinylidene chloride—vinyl cyanide copolymer, the noise almost vanishes at −75°C but reappears when the specimen is warmed to room temperature. Thus far, the frequency spectrum has been studied in various wave bands up to 3000 cycles per second. The random current from the sample was recorded on a tape recorder so that the same sequence of signals could be studied over various frequency intervals by using a band pass filter. This was considered necessary because the character of the noise appears to change with time.

N7. Dielectric Breakdown of Polymers Under Prolonged Stress. CARL G. BRODHUN.—The life of electrical insulation subjected to continuous electrical stress depends on the magnitude of the stress. Plots of electrical stress *vs* time to rupture resemble mechanical endurance curves. When corona is present, its effects are superposed on the effects caused by the dielectric stress and thus causes an inflection on the endurance curve. It is shown experimentally that breakdown because of corona attack is progressive, and apparently universal for solid dielectrics. Polymeric materials studied included "Alathon" polythene resin, "Teflon" tetrafluoroethylene resin. Other insulating materials included mica and glass. The endurance curves for all materials investigated leveled off only with the disappearance of corona. When corona is prevented, e.g., by excluding gases from the test region, the endurance curve is essentially flat in less than one hour. A theory to explain this behavior is proposed.

N8. A Zirconium Concentrated-Arc Infrared Source for Infrared Spectroscopy. M. B. HALL AND R. G. NESTER, *E. I. du Pont de Nemours & Company.*—Zirconium oxide concentrated-arc lamps have been enclosed in argon-filled, water-cooled jackets provided with rocksalt or thallium bromide-iodide windows. The arcs, so altered, have operated troublefree for thousands of hours as highly satisfactory infrared spot sources, particularly useful in infrared microspectroscopy. Since the sources are isolated in cool jackets, they can be placed near to mirrors, etc., when desired, for example, to provide magnified images of the same intrinsic brilliance. Examples are given illustrating applications in the infrared microspectroscopy of polymers.

SATURDAY MORNING AT 10:00

Chemistry 100

(JOHN BARDEEN presiding)

Invited Papers of the DSSP: Low Temperature Phenomena

O1. Supercurrents and Mean Free Paths. A. B. PIPPARD, *Cambridge University.* (40 min.)
O2. Experiments on Supraconducting Spheres. W. V. HOUSTON, *Rice Institute.* (30 min.)
O3. New Supraconducting Compounds. B. T. MATTHIAS, *Bell Telephone Laboratories.* (20 min.)
O4. Meissner Effect in Alloys. J. W. STOUT, *University of Chicago.* (30 min.)

Business Meeting of the Division of Solid-State Physics

SATURDAY MORNING AT 10:30

Physics 110

(M. L. POOL presiding)

Nuclear and Molecular Physics

P1. Positron Activity Arising from the Proton Bombardment of $^{25}Mg^{26}$.* LEONARD N. RUSSELL, WARREN E. TAYLOR, AND JOHN N. COOPER, *The Ohio State University.*—Thin targets of electromagnetically separated[1] Mg^{26} were deposited on a 0.0005-in. tantalum foil by vacuum evaporation. They were bombarded with protons from an electrostatic generator

for 45 seconds. The beam was then cut off and the positron activity measured over a period of 25 seconds, which corresponds to four half-lives of Al^{26} formed by proton capture in Mg^{25}. The yield of positrons per proton over the range 300 to 1050 kev indicates well-resolved maxima at 386, 489, 508, 560, 586, 650, 680, 722, 777, 812, 880, 924, 980, and 1043 kev. The 489, 560–586, and 812 resonances can be correlated with the early work of Curran and Strothers,[3] who used relatively thick targets. The values 386, 489, and 508 agree well with the later work of Tangen.[4] The other levels have not been previously reported.

* Assisted by a contract between the AEC and The Ohio State University Research Foundation.
† Supplied by the Carbide and Carbon Chemical Division, Oak Ridge National Laboratory.
[3] Curran and Strothers, Proc. Roy. Soc. (London) **A172**, 72 (1939).
[4] R. Tangen, Kgl. Norske. Videnskab. Selskabs. Skrifter No. 1 (1946).

P2. Technetium 98 and 100. R. A. HOUSE, R. L. COLLIGAN, D. N. KUNDU, AND M. L. POOL, *The Ohio State University.*—Bombardments of all the enriched isotopes of molybdenum were made with 6.3 and 7.4-Mev protons. An activity of 42 ± 2 minutes produced from Mo^{97} and more strongly from Mo^{98} is assigned to Tc^{98}. The decay characteristics are 2.1 ± 0.1-Mev positrons by aluminum absorption, K-capture, β^+/K-cap.~1, two gamma-rays of energies 0.86 and 0.2 Mev by lead absorption and conversion electrons from the latter gamma-ray. The reported 2.8-day β^- activity is not confirmed to be Tc^{98} and is suspected to be chemical contamination of Mo^{99} which is produced with a very large yield from $Mo^{98}+d$ and $Ru+n$. A 17.5 ± 1-second activity was produced from Mo^{100} as also the known 14-minute Tc^{101} with a yield ratio~1. The former half-life characterized by negatrons of 2.4 ± 0.3 Mev and some gamma-rays is presumably assignable to $Tc.^{100}$ Very short bombardments of Mo^{100} on internal probe targets failed to confirm the 1.3-minute Tc^{100}, whereas similar targets exposed to an external beam in the atmosphere showed an activity~1.3 minutes apparently caused by $N+p$ activities.

P3. Radiations of Niobium 96. D. R. JONES,* S. C. FULTZ,† AND M. L. POOL, *The Ohio State University.*—Nb^{96} was obtained by bombarding enriched $Zr^{96}O_2$ with protons. The beta-spectrum, internal conversion peaks, and photoelectron peaks were examined in a 180° spectrometer. The beta-spectrum was found to be complex, having two components, 0.686 (±0.005) Mev (92 percent) and 0.37 Mev (8 percent). Gamma-rays found by examining peaks from a uranium radiator have energies of 0.455, 0.545, 0.745, 0.9, and 1.045 Mev. Gamma-rays identified by internal conversion peaks are 0.745, 1.045, and 1.1 Mev. Coincidence measurements have been made on a scintillation spectrometer. A tentative decay scheme has been drawn up.

* Major, USAF.
† Fellow, National Cancer Institute.

P4. An Empirical Mass Surface. ALEX E. S. GREEN, *The University of Cincinnati.*—Atomic masses for $A>10$, may be computed quite accurately by the use of the simple equation

$$M-A=\Delta_m(A)+\delta H(A)+\theta^2 J(A)$$
$$=100(\mathbf{A}-1)^2-62+\delta/\mathbf{A}^{\frac{1}{2}}+\theta^2/4\mathbf{A}\ (\text{in } mmu),$$

where $\mathbf{A}=A/100$, $\delta=+1, 0, -1$ according to nuclear type, $\theta=N-Z-D_m$ and $D_m=40\mathbf{A}^2/\mathbf{A}+2$. This empirical surface, which is an outgrowth and improvement of a nuclear energy surface previously used,[1] is useful for predicting unknown nuclear masses and Q values, for charting the irregularities of experimental masses in connection with studies of shell structure, for evaluating the accuracy of various semiempirical mass equations, and for simplifying computations based upon various semiempirical mass equations.

[1] A. Green, Phys. Rev. **83**, 1248 (1951).

P5. The Experimental Mass Surface. R. B. MINOGUE, R. OPPENHEIM AND A. E. S. GREEN.—We develop a set of parameters to characterize the deviations of experimental masses from our empirical masses. The experimental mass data is then used to evaluate some of these parameters. The pairing functions $H(A)=36/A^{\frac{1}{2}}$ and $H(A)=10/A^{\frac{1}{2}}$ (in *mmu*) are examined and compared in the light of the experimental evidence. The experimental-empirical neutron binding energy residuals and the experimental-empirical proton binding energy residuals are examined, and an effort is made to interpret these residuals in terms of nuclear shell structure.

P6. The Mass Surface and Radioactivity. J. S. NADER, N. J. MARUCCI AND A. E. S. GREEN, *The University of Cincinnati.*—Beta-decay energies may be used to evaluate some of the parameters which characterize the deviations of the experimental mass surface and the empirical mass surface. We first develop the formulas needed for such calculations. The results of an analysis of the experimental data are then given. The mass surface may be used to predict radioactive decay sequences involving alpha- and beta-particle emission. We compare various predicted chains with actual chains. The significance of the discrepancies is discussed.

P7. Semiempirical Mass Surfaces. N. ENGLER AND A. E. S. GREEN, *The University of Cincinnati.*—The functions which characterize the differences between the semiempirical mass surface and our empirical mass surface are developed. These functions have been computed for seven different sets of constants which have appeared in the literature. These functions are then compared with the functions which characterize the differences between the experimental mass surface and the empirical mass surface. In this way we subject the semiempirical mass surfaces to microscopic examinations. We also present in graphical form the correction factors needed for the rapid computation of semiempirical mass values and Q values.

P8. Nuclear Quadrupole Interactions in the Microwave Spectrum of Hydrogen Azide.* JOHN D. ROGERS AND DUDLEY WILLIAMS, *The Ohio State University.*—The rotational transition $J=0$ to $J=1$ in N_3H has been re-examined with a view to obtaining further information concerning the effects of nuclear quadrupole interactions. Although the problem of quadrupole effects in a molecule containing three nuclei with equal quadrupole moments has not yet been solved, it is found that in the case of N_3H all major features of the $J=0$ to $J=1$ transition can be explained in terms of the effects produced by a single N^{14} nucleus. The nucleus involved is presumably that of the end nitrogen atom and the interaction term $eQq=-4.67\pm0.04$ mc/sec as compared with -4.7 mc/sec in HCN and -4.67 mc/sec in CH_3CN. On the basis of a single quadrupole interaction, the ratio of frequency separations of the hyperfine structure components should be 1.50, whereas the observed value is 1.52 ± 0.04. If the present analysis is valid, the frequency of the unperturbed transition leads to a value $B+C=23{,}815.56\pm0.05$ mc/sec, which is in fair agreement with the value of Amble and Dailey, who obtained the value 23,815.7 mc/sec from the center of the incompletely resolved pattern but differs from our earlier value based on measurements of the Stark pattern.

* Supported in part by a contract between the Geophysical Division of the Air Force Cambridge Research Center and The Ohio State University Research Foundation.

P9. Absorption Bands of Atmospheric Carbon Monoxide.* J. H. SHAW AND J. N. HOWARD, *The Ohio State University.*—Several investigators[1] have identified strong lines in the 4.7μ region of the solar spectrum with the fundamental band of atmospheric CO. For such an intensity of the fundamental band, laboratory measurements show appreciable absorption

in the overtone band.[2] However, lines of this expected intensity in the overtone region are not present in spectra taken at Lake Angelus, Michigan or Mt. Wilson.[3] Preliminary solar observations taken at Columbus, Ohio, in the overtone region also fail to show lines of the expected intensity. These results may be indicative of an anomalous intensity distribution between the fundamental and overtone bands under the conditions prevailing in the earth's atmosphere. Solar and laboratory data will be presented and discussed.

* Supported in part by a contract between the Geophysics Research Division of the Air Force Cambridge Research Center and The Ohio State University Research Foundation.

[1] M. V. Migeotte, Phys. Rev. **76**, 1108 (1949); M. V. Migeotte and L. Neven, Physica **16**, 123 (1950); Shaw, Chapman, Howard, and Oxholm, Astrophys. J. **113**, 268 (1951).
[2] S. S. Penner and D. Weber, J. Chem. Phys. **19**, 807 (1951).
[3] Mohler, Pierce, McMath, and Goldberg, *Photometric Atlas of the Near Infrared Solar Spectrum* (University of Michigan Press, Ann Arbor, 1951).

P10. Theory of the Ozone Molecule.* B. T. DARLING AND J. A. WEISS, *The Ohio State University.*—In the theory of the ozone molecule the three isomeric forms may be treated by the use of an angular coordinate x such that $x \rightarrow x+2\pi/3$ corresponds to cyclic permutation of the nuclei. The potential energy must be an even function of x and have the period $2\pi/3$ similarly to the case of methyl alcohol. Here however, this potential leads to only a twofold degeneracy of the vibrational levels, described by periodic and "anti-periodic" wave functions; the former is associated with the even-K, the latter with the odd-K, where K is the component of angular momentum perpendicular to the plane of the nuclei. There are no interaction terms in the Hamiltonian connecting these two classes of states. If the equilibrium configuration is isosceles, the barrier against inversions is too high to produce observable splitting of the levels. We are analyzing the 1040 cm^{-1} band of the solar ozone spectrum, as observed by Howard and Shaw,[1] in the assumption of isosceles form such as that proposed by Hughes.[2] We are also investigating the possibility of a nearly-isosceles form (threefold double minimum) which may account for the presence of lines that would otherwise not appear in the spectrum.

* Supported in part by a contract between the Geophysical Division of the Air Force Research Center and The Ohio State University Research Foundation.

[1] J. N. Howard and J. H. Shaw, private communication.
[2] Richard H. Hughes, Am. Phys. Soc. Bulletin, Vol. 26 No. 6 (1951), abstract G 12.

SATURDAY MORNING AT 9:30

Physics 100

(R. SMOLUCHOWSKI presiding)

Metals

Q1. The Elastic Constants of a Cu-Si Alloy.* CHARLES S. SMITH AND J. W. BURNS, *Case Institute of Technology.*—The elastic constants of a Cu−4 atom percent Si single crystal have been determined by the pulsed ultrasonic method. The crystal† was in the form of a cylinder with end faces normal to [110]. Measurement of the two transverse wave velocities in this direction yields directly the two fundamental shear constants $C=c_{44}$ and $C'=(c_{11}-c_{12})/2$, and these when combined with the measured longitudinal velocity yield the compressibility K. The constants C and C' are significantly lower than those for pure Cu.[1] The differences ΔC and $\Delta C'$ have been considered, starting from Fuchs' theoretical calculation of the elastic constants of copper. Simple assumptions about the composition dependence of the important contributions to the elastic constants lead to reasonable conclusions. Similar considerations applied to the only previously measured face centered copper base alloy, Cu−28 percent Zn are consistent.

* Work supported by ONR.
† Furnished and prepared by B. L. Averbach, MIT.
[1] D. Lazarus, Phys. Rev. **76**, 545–553 (1949).

Q2. A Study of the Hafnium-Hydrogen System. S. S. SIDHU AND JOSEPH C. MCGUIRE, *Argonne National Laboratory.*—A series of hafnium samples containing 2 to 66 atomic percent hydrogen was prepared and studied by the x-ray diffraction and the microscopic methods. The limit of solubility of hydrogen in hafnium, the number of stable hydrides formed, and their x-ray diffraction data and densities were determined. The lattice parameters and the number of molecules per unit cell of each hydride were calculated, and tentative crystal structures are proposed. The limits of compositions within which each phase exists are given.

Q3. Atomic Arrangements in Gold-Nickel Solid Solutions.* P. A. FLINN AND B. L. AVERBACH, *M.I.T.*—Absolute measurements of the diffuse x-ray scattering from polycrystalline single phase gold-nickel alloys have been made using a Geiger counter spectrometer. The observed intensity distribution, anomalous in terms of simple short range order theory, has been satisfactorily interpreted as a combination of short range order and a "size effect." A modification of the usual Fourier transform procedure has been developed which permits separate evaluation of the short range order coefficients and of the size effect coefficients, which are a measure of the actual atomic sizes in the solid solution. Since the observed short range order is of the copper-gold type opposite to that predicted for this system by the quasi-chemical theory, this type of theory is inapplicable, and an interpretation of the thermodynamic properties of the system in terms of elastic energies appears necessary.

* Research sponsored by AEC.

Q4. Order Disorder Theory.* DWAIN BOWEN, *North American Aviation, Inc.*—An equilibrium theory of order disorder has been formulated that includes the effect of lattice oscillations on the ordering process. The order parameter is defined in terms of long range order. The usual assumption of linearity of ordering energy on order parameter has been abandoned in favor of an empirical determination from internal energy measurements. This new ordering energy is related to short range ordering forces. Detailed calculations on $AuCu_3$ indicate that the contributions to ordering from lattice oscillations arise from a change in Debye temperature with order of approximately five percent. This small change, however, contributes appreciably to the ordering, particularly in the region near zero order where the persistance of order above the critical temperature may be explained. A theory of the rate of ordering or disordering has been formulated that is consistent with the equilibrium theory discussed above. (The Bragg relaxation equation is not consistent with equilibrium requirements for disordering.) The anomalies of order-

ing rates in $AuCu_3$ find at least qualitative explanation in this formulation. The absence of order in Au_3Cu and the inability to quench in disorder in β-brass will be discussed.

* Work carried out under contract with the AEC.

Q5. Short Range Order Diffuse Scattering in Al-Zn.* PETER S. RUDMAN, PAUL A. FLINN, AND B. L. AVERBACH, *M.I.T.*—Measurements have been made of the x-ray diffuse scattering from polycrystalline samples of Al-Zn alloys at temperatures above the solubility gap in the alpha FCC region. The experimental technique combines data from a Geiger counter spectrometer with film data obtained from transmission samples. The diffuse scattering shows a large small angle component which can be interpreted in terms of clusters of like atoms within the solid solution. A Fourier transform method is used to evaluate the x-ray data, and the results indicate an excess over random of like nearest neighbors. This preference for like neighbors is believed to arise from clusters of like atoms in the solid solution. This tendency toward clustering is in agreement with predictions of the quasi-chemical theory. Similar effects have been observed in Al-Ag alloys.

* Research sponsored by AEC.

Q6. Neutron Diffraction Studies of Cold-Worked Brass. R. J. WEISS, *Watertown Arsenal*, J. R. CLARK, *U. S. Naval Postgraduate School*, J. HASTINGS AND L. CORLISS, *Brookhaven National Laboratory**.—Recent x-ray studies of cold-worked aluminum by Hall and Williamson and of cold-worked brass by Warren and Averbach are in disagreement as to the type of extinction causing variations in intensity of the low index peaks in annealed and cold-worked samples, the former postulating secondary extinction, the latter primary. Since thermal neutrons exhibit negligible extinction effects for powdered metals, powder patterns have been taken of the 111 and 200 peaks in cold-worked and annealed brass. The intensities of the peaks are found to agree to within 1 percent in support of Averbach and Warren. In addition, a new technique of examining the Bragg discontinuities which occur in neutron transmission studies at long wavelengths has substantiated the nature of the broadening to be mostly lattice distortion. A second point of disagreement, though, between the above authors is that Averbach and Warren have found no change in the diffuse background whereas Hall and Williamson find an increase in the cold-worked samples. To resolve this difference, transmission studies are being made with very long wavelength neutrons beyond the Bragg region. Any difference in transmission between cold-worked and annealed specimens is then directly attributable to diffuse scattering.

* Research carried out under contract with AEC.

Q7. Effect of a Low Absorption Coefficient on X-Ray Spectrometer Measurements.* D. T. KEATING AND B. E. WARREN, *M.I.T.*—In x-ray spectrometer measurements with a flat sample, if the absorption coefficient is low, diffraction takes place in the interior of the sample as well as in the surface layer, resulting in an asymmetric broadening and displacement of the measured peak. The effect can be corrected by a simple expression involving only the measured peak shape and its derivative. The effect can also be corrected by the Stokes method of Fourier analysis, and values of the Fourier coefficients for the low absorption effect are presented by plots covering a suitable range of experimental conditions.

* Sponsored by AEC under Contract.

Q8. Effect of Cold Work on X-Ray Patterns of Aluminum.* M. MCKEEHAM, B. L. AVERBACH, AND B. E. WARREN, *M.I.T.*—X-ray studies of cold-worked and annealed filings of aluminum have been reported[1] which indicate a background level for the cold-worked sample about 15 percent higher than that for the annealed material. Measurements have been made with crystal monochromated $CuK\alpha$ on annealed and nonannealed flat pressed compacts of aluminum filings without binder. There is a small broadening of the peaks from the nonannealed sample, but except in the immediate vicinity of the peaks there is no measurable difference in background level for the annealed and nonannealed samples. The same absence of any difference in background has been found with single crystals of aluminum in the initial state and after cold work.

* Sponsored by AEC under Contracts.
[1] W. H. Hall and G. K. Williamson, Proc. Phys. Soc. (London) **64B**, 946 (1951).

Q9. The Separation of Cold Work Distortion and Particle Size Broadening in X-Ray Patterns.* B. E. WARREN AND B. L. AVERBACH, *M.I.T.*—For an x-ray reflection in which there is both particle size and distortion broadening, the shape can be represented by a Fourier series whose coefficients are the product of two coefficients, one relating to particle size only and the other to distortion. The distortion coefficient depends upon the order of the reflection, while the particle size coefficient is independent of order. The two effects can be separated by measuring at least two orders of a reflection, and plotting $ln\ A_n(l)$ *vs* l^2 where l is the order of the reflection. The intercept at $l^2=0$ gives the coefficient for particle size only. This method of separation is completely general in that it does not involve any assumption about the peak shape. A single crystal of Cu−2 percent Si rolled to 50 percent reduction gives intercepts corresponding to an average particle dimension $\bar{L}=1000$A. The major part of the broadening is due to distortion, the particle size broadening is small but not small enough to neglect.

* Sponsored by AEC under Contracts.

Q10. Elastic and Plastic Properties of Very Small Metal Specimens. J. K. GALT AND CONYERS HERRING, *Bell Telephone Laboratories*.—Very thin whiskers of tin ($r=0.9\times10^{-4}$ cm) often grow from tin platings.[1] We have examined the elastic and plastic properties of these whiskers and find them to show properties very near those to be expected from theoretically perfect crystals. Strain of 1 percent has been produced in these whiskers without plastic deformation. A strain of 1/2 percent was held in one whisker for a week and, it also recovered elastically. At strains of 2 or 3 percent deformation occurs. This plastic deformation consists of a bend which is quite sharp. Slides will be shown.

[1] Compton, Mendizza, and Arnold, Corrosion **7**, 327 (1951).

Q11. Kinetics of Grain Boundary Diffusion. R. SMOLUCHOWSKI, *Carnegie Institute of Technology*.—According to the proposed model of a grain boundary the more or less regular array of dislocations applicable at small angles of disorientation changes with increasing angle into rod-like bunches of dislocations which eventually transform into islands of fit and misfit. An approximate solution of the diffusion equation is obtained for the various ranges of the disorientation angle, and it is shown that the apparent activation energy for grain boundary diffusion can be expressed in terms of E_B and E_V which are respectively activation energies for diffusion in the grain boundary material itself and in the grains. For the rod-like bunches one obtains very low, or even negative, apparent activation energies which increase with increasing angle. These results are in good agreement with data obtained on grain boundary diffusion of zink in copper.

Q12. Diffusion of Silver and Antimony in Silver.* L. SLIFKIN, D. LAZARUS, AND T. TOMIZUKA, *University of Illinois*.—Measurements of self-diffusion of silver 110 in pure polycrystalline silver are described. The results are compared with those of Hoffman and Turnbull.[1] The activation energy

for grain boundary diffusion obtained by these investigators is very close to reported activation energies for the diffusion of many metals into polycrystalline silver. It is therefore of value to study the diffusion of these metals into single crystals of silver. Some preliminary results of the diffusion of antimony 124, at extremely low concentrations, into single crystal silver are presented.

* Supported in part by the AEC.
[1] R. E. Hoffman and D. Turnbull, J. Appl. Phys. 22, 634 (1951).

Q13. The Optical Properties of Evaporated Antimony Films. CALVIN TILLER AND HENRY LEVINSTEIN, *Syracuse University.*—The optical properties of evaporated antimony films at various wavelengths have been studied as a function of rate of evaporation and film thickness. The dependance of the structure of antimony films on the rate of evaporation has been studied by Levinstein.[1] Reflectivity and transmissivity for the various types of films have now been measured. Antimony is evaporated in a high vacuum onto a quartz substrate. All optical measurements are made first in the vacuum system immediately after evaporation and are repeated later in air. Film thickness is measured by multiple beam interferometry. Below 100A films are always amorphous, between 100 and 400A films are crystalline for rapid evaporation rates and amorphous for slow evaporation. Above 400A films are always crystalline. Amorphous films are brown while crystalline films have a grey, metallic luster. Amorphous films show greater transmissivity but smaller reflectivity than crystalline films. Very slowly evaporated amorphous films have a greater transmissivity and smaller reflectivity than amorphous films evaporated more rapidly. The optical properties of crystalline films are not influenced by their rate of formation. Both reflectivity and transmissivity vary more rapidly with wavelength for amorphous than for crystalline films.

[1] H. Levinstein, J. Appl. Phys. 20, 306 (1949).

Q14. Effect of Thickness of Thin Metal Films on the Mean Free Path of Conduction Electrons.* E. C. CRITTENDEN, JR., E. H. LAYER, AND R. W. HOFFMAN, *Case Institute of Technology.*—Measurements of the temperature coefficient of resistance of evaporated films of nickel and copper indicate that the mean free path l of the conduction electrons is a function of thickness t. A simple theoretical model predicts $l=\gamma l_\infty^2/t$, where l_∞ is the mean free path for a thick slab, and γ is an adjustable parameter. Theoretical values of the temperature coefficient of resistance predicted on this basis fit the experimental data well. The usual assumption of constant mean free path[1,2] gives serious disagreement. In contrast, values of the resistivity, ρ, predicted on the basis of constant mean free path, agree approximately with experimental values, as others have also reported.[1,3] The introduction of variable mean free path alters the theoretical curves for ρ very little and accounts for the previous apparent agreement.

* Supported by the ONR.
[1] Klaus Fuchs, Proc. Cambridge Phil. Soc. 34, 100 (1938).
[2] E. H. Sondheimer, Phys. Rev. 80, 401 (1950).
[3] P. G. Wilkinson, Jour. Appl. Phys. 22, 419, (1951).

SATURDAY AFTERNOON AT 2:00

Physics 110

(R. BUCHDAHL presiding)

Contributed Papers of the DHPP

R1. Structure and Properties of Polyamides. R. BRILL, *Polytechnic Institute of Brooklyn.*—The structure of polyamides will be discussed as a result of new x-ray investigations. The importance of the hydrogen bond will be illustrated by means of the thermal behavior, the tensile strength, and the interaction of water with polyamides.

R2. The Specific Heat and Degree of Crystallinity of Polychlorotrifluoroethylene. JOHN D. HOFFMAN, *General Electric.*—The specific heats of slow-cooled and air-quenched samples of polychlorotrifluoroethylene (mp~210–212°C) have been measured between 0°C and 250°C in a differential calorimeter. The calorimeter is described. By comparison of the experimental heat of fusion with the heat of fusion of the pure crystalline polymer obtained from Flory's theory by Bueche, the degree of crystallinity at 0°C was found to be 0.82 ± 0.07 for the slow-cooled sample, and 0.35 ± 0.03 for the air-quenched sample. The enthalpies of the pure crystals and supercooled liquid polymer were obtained as functions of temperature by a simple interpolation procedure. Comparison of these enthalpies with the observed enthalpies permitted the degree of crystallinity of both the air-quenched and slow-cooled polymer to be calculated as a function of temperature. The results for the slow-cooled sample were in good agreement with those obtained by Price by a volume method. The quenched sample showed a distinct tendency to crystallize on warming. Reasons were advanced for believing that the glass transformation temperature for this polymer is below −80°C.

R3. Sedimentation and Diffusion of Polyelectrolytes. B. ROSEN AND F. R. EIRICH, *Polytechnic Institute of Brooklyn.*—The interpretation of the sedimentation and diffusion rates of flexible particles is complicated by the simultaneous influences of charge and shape. Although there are theories of these two effects separately, there is no instance where work of the combined effect is reported. Experimentally, there is the difficulty that charge and shape cannot be varied independently. Measurements were carried out on a fraction of polyvinyl *N-n* butyl pyridinium bromide as a function of *p*H and ion concentration. The combination of sedimentation and diffusion data with values obtained from electrophoretic measurements, together with a knowledge of the molecular weight, permit the calculation of the effective charge as well as of the frictional constant. The axis ratios obtained from the latter by means of a modified equation is in agreement with the axial ratio obtained from viscosity measurements.

R4. Relations Between Viscosity and Flow Birefringence of Polyelectrolytes. P. M. KAMATH, B. ROSEN, AND F. R. EIRICH, *Polytechnic Institute of Brooklyn.*—The intrinsic viscosities, dilution curves, the extinction angles, and the flow birefringence were measured as a function of concentration on a high molecular weight fraction of poly-4-vinyl *N-n* butyl pyridinium bromide. The observed concentration dependence is so strong as to render the calculation of a rotary diffusion constant impossible. The form of the viscosity concentration curves indicates that in dilution experiments one might never reach the concentration range for independent

particles, within the experimental accuracy attainable. The inference from this data is that present views on the behavior of polyelectrolytes may as yet not distinguish clearly between concentration effects and the behavior of individual particles.

R5. Polystyrene Molecular Weight Distribution by Turbidity Titration and the Effect on This Distribution of Variations in the Preparation of the Polymers. ARTHUR F. ROCHE, JR., *Dow Chemical Co.*—A turbidimetric method for determining the molecular weight distribution of polystyrene is described. The solvent is ethyl benzene; the precipitant is amyl alcohol. The calibration of the equipment and a discussion of some of the possible errors are considered. Calculation of the results is explained, including the use of IBM machines. A useful method for graphing distribution curves to show relative sharpness is a feature of the method. The effects of temperature of polymerization and percent conversion on the molecular weights are shown, as well as correlations of calculated number and weight average molecular weights, with osmotic and light scattering molecular weights, respectively. The curves are compared with those obtained with other solvents as well as with those obtained by standard fractionation procedures.

R6. A New Molecular Weight Distribution Technique for Polystyrene. Part II. Experimental Results. R. F. BOYER, *Dow Chemical Company.*—The molecular weight distribution curve of a polymer-homologous soluble polystyrene can be obtained by observing the cumulative volume of precipitate, which corresponds to increasing additions of nonsolvent to a dilute solution of polymer.[1] Two general experimental techniques will be described. In one case, daily increments of nonsolvent are added to a single container of the polymer solution; in the second method, varying amounts of nonsolvent are added simultaneously to 12 containers of polymer solution. The latter method is much more rapid, but also less likely to represent equilibrium data. The two methods are in substantial agreement if the initial concentration of polystyrene is around 0.1 percent. Most of the polystyrene samples examined thus far are showing multiple peaks in their molecular weight distribution curves, essentially confirming the earlier results of Gralén and Lagermalm.[2]

[1] R. F. Boyer, J. Polymer Sci. **8** (January, 1952).
[2] N. Gralén and G. Lagermalm, Chem. Abstracts **42**, 5257 (1948).

R7. Configuration Distribution of a Chain Molecule with Correlations. C. M. TCHEN, *National Bureau of Standards.*—We consider first, a correlation covering the whole chain of the type $c^{|i-j|}$ between the ith and jth links, where c is a partial correlation between the neighbor links. Thus, the configurations of the chain are controlled by Markoff processes. If r is the end-to-end distance of the chain, the high order moments of r can be studied by the theory of combinations. The moments show that the distribution is Gaussian for an infinite number of links and not extremely large values of r. From this result, we can show also the validity of the central limit theorem in its extension to Markoff processes. Next we take the random walk as a model of the chain configurations, and extend the concept of correlation to long range effects and non-Markoff processes. For this purpose, we consider a random walk with restricted occupancy: a directional preference occurs in regions of excessive accumulation of density. If, in the one dimensional problem of random walk, we allow a limit of accumulation of density at any spot, a large number of "pockets" will be isolated between hindrances, inaccessible to the development of the random walk. The expansion of the configurations is studied by the correlation which exists between the paths at the hindrance points.

SATURDAY AFTERNOON AT 2:00

Physics 100

(P. W. ANDERSON presiding)

Invited Papers of the DSSP: Second-Order Phase Changes

S1. Progress in Computing the Statistics of Cooperative Assemblies. G. H. WANNIER, *Bell Telephone Laboratories.* (40 min.)

S2. The Thermodynamics of Phase Transitions. L. TISZA, *M.I.T.* (30 min.)

S3. Phase Transitions in the Ammonium Halides. H. A. LEVY, *Oak Ridge National Laboratory.* (30 min.)

S4. Influence of Pressure on Some Electron Phenomena in Solids. A. MICHELS, *University of Amsterdam.* (30 min.)

S5. Cooperative Effects in Paramagnetic Crystals Having Low Critical Temperatures. C. G. B. GARRETT, *Harvard University.* (30 min.)

SATURDAY AFTERNOON AT 2:00

Chemistry 100

(A. LANDE presiding)

Invited Papers in Molecular Spectroscopy

T1. Survey of the Spectrum of Water-Vapor. D. M. DENNISON, *University of Michigan.* (45 min.)

T2. The Infrared Spectra and the Molecular Structure of Pyramidal Molecules. H. H. NIELSEN. *The Ohio State University.* (45 min.)

Post-Deadline Papers, if Any

SATURDAY AFTERNOON AT 2:00

Chemistry 161

(R. S. SHANKLAND presiding)

Transactions of Crystals and Light

U1. Optical and Electrical Properties of Edge Emission in Cadmium Sulfide. CLIFFORD C. KLICK, *Naval Research Laboratory.*—Measurements of optical transmission, photoconductive response, luminescent edge emission, and excitation spectrum for edge emission have been made on single crystal specimens of CdS at 77K° and 4K°. At the lowest temperature there is an energy gap between the absorption edge and the onset of emission of more than 0.1 electron volt. The excitation spectrum shows three peaks of which two also appear in the photoconductive measurements. The third excitation peak occurs at 0.1 electron volt to the low energy side of the main excitation and photoconductive peak. This may be compared with the rough theoretical prediction of an energy gap of 0.2 electron volt between the lowest exciton level and the bottom of the conduction band.

U2. An Interpretation of the Absence of *F'* Centers in KCl and KBr X-Rayed at 4°K. JORDAN J. MARKHAM, *Johns Hopkins University.**—Recent data by Dutton, Heller, and Maurer[1] indicated that *F'* centers in KCl do not form during x-radiation at liquid helium temperature. This is also true for KBr.[2] *F'* centers form at liquid nitrogen temperature during x-radiation in both crystals. These conclusions have have prompted a re-examination of Peck's[3] earlier data on the formation of *F'* centers in additively colored crystals. These data indicate that *F'* centers should form at liquid helium as well as at liquid nitrogen temperature. The absence of these centers at liquid helium temperature seems to indicate that negative ion vacancies are formed during the x-raying process. If this interpretation is correct, we may conclude that the x-rays produce negative ion vacancies as well as free electrons.

* This research was supported by the Bureau of Ordnance, U. S. Navy.
[1] Dutton, Heller, and Maurer, Phys. Rev. **84**, 363 (1951).
[2] W. Duerig and J. J. Markham, Conference on the Electrical and Optical Properties of Ionic Crystals, Urbana, Illinios (1951).
[3] H. Pick, Ann. Physik **37**, 421 (1940).

U3. An Experimental Search for Self-Trapped Electrons in the Alkali Halides.* WILLIAM H. DUERIG, *University of Maryland and Johns Hopkins University.*—Calculations for NaCl of self-trapped electrons, first proposed by Landau, indicate that to a first approximation, these electrons should be thermally stable at liquid helium temperatures. NaCl, KCl, and KBr were x-rayed at these temperatures and their optical absorption spectra examined from the *F* band in the visible to the infrared absorption limits of the crystals. The 1- to 3.5-micron region was measured on a rapid scanning spectrometer[1] to preclude the bleaching of any centers before the measurement was completed. The rest of the spectrum was obtained with conventional Beckman and Perkin-Elmer spectrophotometers. No optical absorption bands were found. Hence one can conclude that stable self-trapping centers do not exist in sufficient quantities at temperatures down to liquid helium to be detected by the sensitivity of our instruments. If these centers do exist, it may be only at lower temperatures, or they may rapidly diffuse through the crystal during x-raying until they form a more stable center, e.g., *F* center.

* This research was supported by the Bureau of Ordnance, U. S. Navy.
[1] B. W. Bullock and S. Silverman, J. Opt. Soc. Am. **40**, 608 (1950).

U4. Preparation and Properties of Indium Sulfide Phosphors.* D. C. REYNOLDS, C. S. PEET, AND A. E. MIDDLETON. —Indian sulfide phosphors have been prepared from In_2S_3, made by direct combination of indian and sulfur and also by wet chemical methods. The In_2S_3 powders have a deficit-type spinel structure. Extra x-ray diffraction lines were observed; these have been attributed to free sulfur in the samples. A single crystal of In_2S_3 was grown; this sample also gave a deficit-type spinel structure. However, in this case, extra diffraction lines were not observed. The unit cell size a_0 for the single crystal was 10.790±0.002A; for the powdered samples, a_0 was 10.75A. Phosphors were prepared from the In_2S_3 samples by firing with NaCl+MgF flux materials and an activator. The firing was done in a vacuum at approximately 900°C. The powdered material sublimed at this temperature and the luminescent material condensed in a region at approximately 550°C. Material condensing in regions at different temperatures was not luminescent. The luminescent material is excitable by both ultraviolet radiation and particle bombardment. The copper-activated material has an emission peak at 5850A. This phosphor contains two phases, one being the β-phase described above, the other a nonisotropic phase that has not been identified.

* This work was supported by Consolidated Mining and Smelting Company of Trail, British Columbia.

U5. Electrical and Optical Properties of Single Crystals of Zinc Sulfide. WM. W. PIPER AND FERD E. WILLIAMS, *General Electric Research Laboratory.*—Single crystals of zink sulfide have been grown by a modification of the technique described by Reynolds and Czyzak.[1] Zink sulfide powder is sublimed at 1185°C, and single crystals 1×1×3 mm have been grown from the vapor phase on a quartz wall at 1080°C. The crystals are essentially the Wurtzite-structure with some stacking disorders. The room temperature dark conductivity of a typical crystal previously exposed to room light is 10^{-11} mho/cm. After heating such a crystal to 300°C in the dark to empty traps, measurements of conductivity from 200 to 500°C indicate intrinsic semiconductor characteristics with a thermal band gap of (3.75±0.1) ev. The optical absorption edge of these crystals is at (3.67±0.03) ev. The photoconductivity spectrum has been measured and a peak is observed at 3.68 ev with a 0.069 ev half-width. Single crystals of copper-activated zink sulfide prepared by this technique luminesce upon application of ac or dc fields. Brightnesses up to 50 millilamberts have been measured at 60 cps and 10^4 v/cm. Variation of the light output as a function of voltage, current, and frequency will be discussed. A mechanism for electroluminescence will be proposed.

[1] D. C. Reynolds and S. J. Czyzak, Phys. Rev. **79**, 543L (1950).

U6. Multiple Time Constants in Photoconductivity. W. W. SCANLON, R. L. PETRITZ, AND F. L. LUMMIS, *U. S. Naval Ordnance Laboratory.*—The response time characteristics for photoconductivity in semiconductors of the PbS and PbTe type have been studied using both frequency and transient methods. The results, interpreted in terms of a numbers theory indicate that the response time in PbS may be characterized by a single time constant obeying a monomolecular law (exponential decay). In PbTe the response is best described by two time constants, one obeying a monomolecular law and the other obeying a bimolecular law (hyperbolic decay). A simple model leading to two time constants of the above type

consists of a conduction band and two lower energy states, one of which may be the normally filled band. The bimolecular law results from transitions between the normally filled band and the conduction band. The monomolecular law results from transitions between the conduction band and localized impurity states, a large number of which are unoccupied. While the experiments described here can be adequately interpreted in terms of a numbers theory, further experiments are required in order to reach conclusions regarding the relative merits of the barrier theory and the numbers theory of photoconductivity.

U7. The Relation between Noise and Response Time in Photoconductors: I. Theory. R. L. PETRITZ,* *U. S. Naval Ordnance Laboratory.*—Changes in the average intensity of illumination falling on a photoconductive cell produce corresponding changes in the equilibrium member of conduction electrons. The rate of approach to the new equilibrium state depends upon the cross section for photon absorption and the cross sections for electron recombinations. Fluctuations in the number of conduction electrons occur in a photoconductor in equilibrium with the radiation field. The rate at which these fluctuations occur depends on the same cross sections mentioned above. These considerations from the basis of our claim that the power spectrum of the current noise associated with fluctuations in the number of conduction electrons should be of the same form as the frequency response of a photoconductor to a light signal. This correspondence is proved for the general case where the radiation field interacts with a heat bath and with the photoconductor by use of the recombination equations of the theory of photoconductivity and the equations of the theory of current noise. The equation of the current noise power spectrum contains explictly the mobility and time constants; therefore from noise measurements it should be possible to obtain numerical values for these quantities.

* Also Catholic University, Washington, D. C.

U8. The Relation Between Noise and Response Time in Photoconductors: II. Experiment. F. L. LUMMIS AND R. L. PETRITZ,* *U. S. Naval Ordnance Laboratory.*—Response time and noise characteristics have been measured at temperatures from liquid air to room temperature on PbS cells. Response time studies show an increase of time constant, τ_R, with decreasing temperature. The noise measurements were made with two systems: a visual short-time average of a fluctuating meter deflection and a recorded long-time average involving a thermocouple as the noise power sensitive device. The noise spectrum has been found to be similar in form to the frequency response curve for photoconductivity. At the low frequency end, there is a slope much less than indicated by a $1/f$ law. This is followed at higher frequencies by a horizontal region which then goes smoothly through a 3 db per octave slope to a slope which is greater than a $1/f$ law. This limiting slope has not been accurately determined. A time constant, $\tau_N = 1/2\pi f_0$, has been calculated directly from the noise curve where f_0 is the frequency at which the slope is 3 db/octave. τ_N was found to increase with decreasing temperature and agrees in magnitude with τ_R. The mobility has been calculated using the theoretical expression for the noise and is in the range of 2–3 cm²/volt-sec.

* Also Catholic University

U9. The Impedance of Semiconducting Films. J. N. HUMPHREY, F. L. LUMMIS AND W. W. SCANLON, *U. S. Naval Ordnance Laboratory.*—The determination of activation energy values of semiconductors by the method of dc resistance measurements on thin films is discussed. Evaporated films 10^{-3} to 10^{-4} mm thick are known to consist of microcrystallites in partial disorder. This structure produces relatively high contact resistance between crystallites, together with an intercrystalline capacitance. An equivalent electrical circuit based on the above structure was used to calculate the resistance as a function of frequency. Impedance measurements from dc to 200 mc are presented for films of tellurium, lead telluride, and lead sulfide. The intercrystalline capacitance was found to be of the order of 0.5 mmfd per square. Resistance-temperature data obtained from both dc and ac measurements will be presented for Te. Dc resistance measurements, which gave a $\log R$ *vs* $1/T$ curve linear over three decades of resistance indicated an intrinsic activation energy of 0.43 ev. Over this same temperature range, however, measurements of resistance at 10 mc show that the film was not in the intrinsic region. It is concluded that the usual dc resistance measurement is a questionable method for determining activation energy in thin films of semiconductors.

SUPPLEMENTARY PROGRAMME

SP1. Application of the Quantum-Mechanical Franck-Condon Principle to Complex Systems. MELVIN LAX, *Syracuse University and the Naval Research Laboratory.**—Many vibrational systems—crystals, molecules—are adequately described by normal modes and a quadratic Hamiltonian. If, in addition, the energy difference between two electronic states is a linear function of the vibrational coordinates, then the calculation of the absorption or emission spectrum can be calculated in an all quantum-mechanical fashion. The summation over all possible final states (involving emission or absorption of large numbers of phonons) *consistent* with conservation of energy is performed *exactly* with the help of an integral representation for the energy conservation delta-function. The quantum-mechanical absorptoin or emission spectrum is found to have the same peak (mean-value) and breadth (second moment) as the corresponding semiclassical spectrum discussed in an earlier abstract. However, the quantum-mechanical spectrum is not Gaussian but possesses odd moments of all orders and higher order even moments that do not quite agree with a Gaussian curve. The skewness (third moment) is positive for absorption and negative for emission (i.e., the high frequency tail is longer on absorption). And the kurtosis (fourth moment) is larger than that of the semiclassical Gaussian curve. Thus for the *same* rms width, the quantum-mechanical curve is flatter and longer tailed.

* To be given after Session C if the Chairman rules that time permits.

SP2. On Thermal Expansion of Water. GEORGE ANTONOFF.*—In thermal expansion of water, changes of curvature can be observed at intervals just as in other liquids.[1] They transpire in figures of all authors (on this subject a paper will soon appear exploring the whole field). Kretschmer disputes the kink at 50°C, which can be put into evidence by three or four independent methods and is supported by Magat in an indirect way, indicating an anomaly in this region. In every sense this case is analogous to that of benzene, and in standard conditions the kinks are reproducible. Kretschmer obviously worked in conditions which could give only indefinite results; but even he gives a curve with a noticeable disturbance at 50°C.

* To be given after Session C if the Chairman rules that time permits.
[1] Compt. rend, December 3, 1951.

Author Index to Papers Presented at the Columbus Meeting

Andrew, A., M. R. Jeppson, and H. P. Yockey—D11
Andrews, R. D.—E2
Antonoff, George—C5, SP2
Atkins, K. R.—H1
Bauss, Herbert and R. F. Boyer—N6
Beeman, W. W.—F2
Blewitt, T. H.—G2
Bloembergen, N.—A3
Bowen, Dwain—Q4
Bowers, R.—G6
Boyer, R. F.—R6
Brill, R.—R1
Brodhun, Carl G.—N7
Brooks, H.—K4
Bueche, F.—N2
Callendine, George W., Jr., Virginia C. Ridolfo, and M. L. Pool—D7
Cheatham, R. G. and Albert G. H. Dietz—E9
Chwalow, Morton L. E.—M1
Cobbs, W. H., Jr., and R. L. Burton—F4
Collins, R. J. and H. Y. Fan—I10
Coltman, R. R. and T. H. Blewitt—D4
Cox, Henry L., Jr.—C6
Cramer, William S. and Irving Silver—E10
Crawford, J. H., Jr., and J. W. Cleland—D2
Crittenden, E. C., Jr., E. H. Layer, and R. W. Hoffman—Q14
Croft, G. T., W. F. Love, and F. C. Nix—L9
Crowe, R. W., A. H. Sharbaugh, and J. K. Bragg—C9
Darling, B. T. and J. A. Weiss—P10
Daunt, J. G.—A1
Dennison, D. M.—T1
Derenthal, R. J., F. P. Baldwin, and R. L. Anthony—N5
Dienes, G. J.—M7
Dolecek, R. L.—H2
Duerig, William H.—U3
Engler, N. and A. E. S. Green—P7
Fan, H. Y. and K. Lark-Horovitz—G3
Ferry, John D. and Edwin R. Fitzgerald—E7
Fitzgerald, Edwin R. and John D. Ferry—E6
Flinn, P. A. and B. L. Averbach—Q3
Foldy, L. L.—H3
Forster, J. H., H. Y. Fan, and K. Lark-Horovitz—D14
Fox, T. G.—N3
Frederikse, H. P. R.—I8
Galt, J. K. and Conyers Herring—Q10
Garrett, C. G. B.—S5
Geib, I. G. and R. E. Grace—D15
Grandine, Lester D., Jr., Edwin R. Fitzgerald, Ivo Jordan, and John D. Ferry—E8
Green, Alex E. S.—P4
Guth, E.—A2
Hall, M. B. and R. G. Nester—N8
Harrison, R. J.—M9
Haynes, J. R. and H. B. Briggs—I3
Heer, C. V. and J. G. Daunt—L2
Heller, W. and W. J. Pangonis—F1
Henderson, J. W., H. G. Cooper, and J. W. Marx—D10
Hoffman, John D.—R2
Hollis-Hallett, A. C.—L6
House, R. A., R. L. Colligan, D. N. Kundu, and M. L. Pool—P2
Houston, W. V.—O2
Humphrey, J. N., F. L. Lummis, and W. W. Scanlon—U9
Hutchinson, C. A.—B4
Jamison, R. E. and T. H. Blewitt—D3
Johnson, R. D. and A. B. Martin—D9
Jones, D. R., S. C. Fultz, and M. L. Pool—P3
Kamath, P. M., B. Rosen, and F. R. Eirich—R4
Keating, D. T. and B. E. Warren—Q7
Kernohan, Robert H. and Grace M. McCammon—D1
Kittel, C. E.—K5
Klick, Clifford C.—U1
Klontz, E. E. and K. Lark-Horovitz—D16
Kmetko, Edward A.—M6
Langmuir, David B.—D8
Lax, Melvin—C3, SP1
Levy, H. A.—S3
Lewis, H. W.—L1
Livingston, Ralph—B5
Loferski, Joseph J. and Park Hays Miller, Jr.—M10
Loshaek, S.—N4
Love, W. F.—L10
Lummis, F. L. and R. L. Petritz—U8
Marcus, Paul M.—L7
Markham, Jordan J.—U2
Marvin, Robert S.—E1
Marx, J., J. Koehler, and C. Wert—D13
Matthias, B. T.—O3
Maxwell, E. and O. S. Lutes, Jr.—L5
McKeehan, M., B. L. Averbach, and B. E. Warren—Q8
Melvin, M. Avramy—C4
Michels, A.—S4
Middleton, A. E., C. S. Peet, O. J. Mengali, and R. C. Sirrine—I6
Miller, P. H., Jr., and B. R. Russell—M2
Miller, R. F., E. R. Fitzgerald, J. M. Davies, and W. C. Sears—E5
Minogue, R. B., R. Oppenheim, and A. E. S. Green—P5
Molmud, Paul—C2
Murray, G. T. and W. E. Taylor—D6
Nader, J. S., N. J. Marucci, and A. E. S. Green—P6
Nicol, J., T. S. Smith, C. V. Heer, and J. G. Daunt—L3
Nielsen, H. H.—T2
Norberg, R. E.—B1
Olsen, C. E. and P. M. Harris, M3
Overhauser, Albert W.—I2
Pake, G. E.—B3
Parkins, W. H.—G4
Pearson, G. L., W. T. Read, and W. Shockley—I5
Peet, C. S. and A. E. Middleton—I7
Pepinsky, R., R. Thakur, and C. McCarty—L8
Petritz, R. L.—U7
Philippoff, W.—E4
Pines, D.—K2
Piper, Wm. W. and Ferd E. Williams—U5
Pippard, A. B.—O1
Primak, W. and L. Fuchs—M8
Prince, M. B. and F. S. Goucher—I4
Reynolds, D. C., C. S. Peet, and A. E. Middleton—U4
Roche, Arthur F., Jr.—R5
Rogers, John D. and Dudley Williams—P8
Rosen, B. and F. R. Eirich—R3
Rothstein, Jerome—C7
Rudman, Peter S., Paul A. Flinn, and B. L. Averbach—Q5
Russell, Leonard N., Warren E. Taylor, and John N. Cooper—P1
Scanlon, W. W., R. L. Petritz, and F. L. Lummis—U6
Seitz, F.—G1
Shaw, C. H. and Nathan Spielberg—C10
Shaw, J. H. and J. N. Howard—P9
Shull, C. G.—J2
Sidhu, S. S. and Joseph C. McGuire—Q2
Simha, R.—N1
Slater, J. C.—K1
Slifkin, L., D. Lazarus, and T. Tomizuka—Q12
Smith, Charles S. and J. W. Burns—Q1

Smoluchowski, R.—J1, Q11
Spangler, R. D.—E3
Stambaugh, C. K. and P. M. Harris—M5
Stout, J. W.—O4
Sutherland, G. B. B. M.—F3
Taylor, W. E.—D5
Tchen, C. M.—R7
Tiller, Calvin, and Henry Levinstein—Q13
Tisza, L.—S2
Torrey, H. C.—B2
Tsai, Khi-Ruey and P. M. Harris—M4
Tyler, W. W.—G5
Wangsness, Roald K.—I1
Wannier, G. H.—S1
Warren, B. E. and B. L. Averbach—Q9
Weiss, R. J., J. R. Clark, J. Hastings, and L. Corliss—Q6
Wessel, Walter—C1
Westervelt, Donald—D12
Weyl, W. A.—J3
Whitesell, W. J., II, and V. A. Johnson—I9
Williams, W. E., Jr., and E. Maxwell—L4
Wyler, E. N. and F. C. Todd—C8
Zener, C.—K3